Title
Improving Therapeutic Properties of Small Molecules and Proteins Through Strategic Covalent Modification

Author
Tamshen, Kyle

Publication Date
2020

Peer reviewed|Thesis/dissertation

UNIVERSITY OF CALIFORNIA

Los Angeles

Improving Therapeutic Properties of Small Molecules and Proteins Through Strategic Covalent Modification

A dissertation submitted in partial satisfaction of the

requirements for the degree Doctor of Philosophy

in Chemistry

by

Kyle Tamshen

2020

ABSTRACT OF THE DISSERTATION

Improving Therapeutic Properties of Small Molecules and Proteins

Through Strategic Covalent Modification

by

Kyle Tamshen

Doctor of Philosophy in Chemistry

University of California, Los Angeles, 2020

Professor Heather D. Maynard, Chair

Therapeutic agents including small molecules and proteins compose the majority of marketed pharmaceutics and are indispensible to modern medicine. Although many of these therapeutic agents have proven to be excellent drug products, others possess limitations that have detracted their full potential. In such cases, strategic covalent modification can be employed to reversibly or irreversibly modify a known drug substance in order to improve one or more of its therapeutic properties. Due to the broad variability and availability of functional handles on any given therapeutic molecule, covalent modification strategies vary substantially from one drug to another and must be rationally tailored to meet the needs of the desired application. This dissertation provides several unique examples in which strategic bioconjugation was employed with the goal of enhancing the therapeutic potential of small molecules and proteins to address unmet challenges in diverse therapeutic areas.

Biomacromolecules such as proteins, peptides, and nucleic acids represent important therapeutic agents that have become indispensable for the treatment of a broad array of diseases ranging from hemophilia to cancer. The practice of covalently attaching the polymer polyethylene glycol (PEG) to these biologics, known as PEGylation, has further enabled the development and regulatory approval of at least 15 distinct biotherapeutics by extending circulation time and reducing immunogenicity. Despite its overwhelming success over the last 40 years, evidence from a number of independent research groups has revealed that antibodies can be generated in animals and humans that specifically bind to PEG and can compromise the safety and efficacy of PEGylated therapeutics. More concerning are the increasingly frequent reports of high incidences of pre-existing anti-PEG antibodies in healthy individuals who have never received PEGylated medicines. Chapter 1 discusses the clinical reports of immune responses against PEGylated biomolecules, how anti-PEG antibodies can affect the safety and efficacy of these therapeutics, as well as the incidences and effects of pre-existing antibodies. Additionally, Chapter 1 examines what is known about the induction of antibodies against PEG, factors that may contribute to this immune stimulation, and methods for the detection of anti-PEG antibodies. Finally, possible strategies for overcoming PEG immunogenicity are considered and perspectives are offered on the future of PEGylated biotherapeutics.

Human vault nanoparticles are naturally occurring, uniform, barrel-shaped protein nanostructures that have demonstrated aptitude as drug delivery vehicles due to their large size, abundant and easily modifiable side chains, and biocompatibility. Vaults are readily internalized by over 90% of $CD4^+$ T-cells, which are the key immune cells targeted by Human Immunodeficiency Virus (HIV). Chapter 2 explores the utility of these protein nanoparticles as a targeting vehicle for the delivery of three covalently attached antiretroviral drugs to vulnerable

cell populations. Drugs were conjugated to vault lysine residues, by first modifying each drug with a protein reactive group in such a way that the active drug could be released in its unmodified form following hydrolytic or enzymatic cleavage of an ester linkage between the protein and drug. Good drug loading was achieved, and the conjugation efficiencies were found to correlate with the hydrophobicity of each drug. All vault-drug conjugates performed similarly to free drug in *in vitro* infection assays, and are expected to demonstrate enhanced targeting to $CD4^+$ T-cells *in vivo*.

Prescription opioids, though often necessary for pain management, are highly addictive and are consequently abused with increasing frequency. Over the last 20 years, deaths involving opioids have increased dramatically. There are few FDA approved abuse deterrent opioid formulations available, and even fewer are robust enough to deter motivated users. Chapter 3 outlines the design and synthesis of a dual enzyme responsive prodrug platform for oxycodone. This prodrug is designed to only release the active drug upon ingestion and yields no active drug following injection, snorting, nor when these methods of administration are preceded by physical tampering such as acidification, grinding, microwaving, etc. Various chemistries were investigated to provide relevant and stable, but reversible covalent linkages. These linkages were assessed for hydrolytic stability over a broad pH range to simulate accelerated release conditions that could be employed by drug users. The prodrugs showed resistance to hydrolytic degradation and were determined to release only in the presence of gastric enzymes trypsin and chymotrypsin. Synthetic efforts and observation of unexpected side-products are also discussed.

Regulation of human growth hormone (GH) signaling has important applications in the remediation of several diseases including acromegaly and cancer. Growth hormone receptor (GHR) antagonists currently provide effective means for suppression of GH signaling. However,

these small 22 kDa recombinantly engineered GH analogs exhibit short plasma circulation times. To improve clinical viability, between 4-6 molecules of 5 kDa PEG are nonspecifically conjugated to the 9 amines of the GHR antagonist designated as B2036 in the FDA-approved therapeutic pegvisomant. PEGylation increases the molecular weight of B2036 and considerably extends its circulation time, but also dramatically reduces its bioactivity, contributing to high dosing requirements and increased cost. As an alternative to nonspecific PEGylation, Chapter 4 reports the use of genetic code expansion technology to site-specifically incorporate the unnatural amino acid propargyl tyrosine (pglY) into B2036 with the goal of producing site-specific protein-polymer conjugates. Substitution of tyrosine 35 with pglY yielded a B2036 variant containing an alkyne functional group without compromising bioactivity, as verified by a cellular assay. Subsequent conjugation of 5, 10, and 20 kDa azide-containing PEGs via the copper catalyzed click reaction yielded high purity, site-specific conjugates with >89% conjugation efficiencies. Site-specific attachment of PEG to B2036 is associated with substantially improved *in vitro* bioactivity values compared to pegvisomant, with an inverse relationship between polymer size and activity observed. Notably, the B2036-20 kDa PEG conjugate has a comparable molecular weight to pegvisomant, while exhibiting a 12.5 fold improvement in half-maximal inhibitory concentration in GHR-expressing Ba/F3 cells (103.3 nM vs. 1289 nM). This straightforward route to achieve site-specific GHR antagonists is expected to be useful for GH signal regulation.

Given the potential issues associated with the use of PEG in protein-polymer conjugates as outlined in Chapter 1, there is significant interest in the development of structural analogs to PEG that offer added functionality while retaining the beneficial properties of the polymer. In addition to its immunogenic concerns, PEG is not biodegradable and can also exhibit significant

heterogeneity in molecular weight. Lack of biodegradability has been linked with safety concerns such as vacuole formation in liver and kidney tissue following repeated dosing. Additionally, the heterogeneity inherent to the molecular weight of PEG could potentially lead to variability in efficacy when conjugated to therapeutic proteins. Chapter 5 details efforts to overcome these obstacles by exploring the synthesis of degradable and uniform PEG analogs. Degradable PEG analogs were synthesized from unsaturated crown-ether monomers by ring-opening metathesis polymerization (ROMP) and found to readily depolymerize in aqueous conditions in the presence of Grubbs III catalyst. These polymers contained aldehyde end groups that were conjugated to the model enzyme lysozyme. Depolymerization of the polymer from the protein was demonstrated and the effect of the reaction on the activity of the conjugate was evaluated. Chapter 5 also outlines and discussed efforts toward the synthesis of high molecular weight, uniform PEG analogs prepared by iterative monomer addition of heterobifunctional thiol-vinyl ether PEG oligomers.

The dissertation of Kyle Tamshen is approved.

Leonard H. Rome

Timothy J. Deming

Craig A. Merlic

Heather D. Maynard, Committee Chair

University of California, Los Angeles

2020

This dissertation is dedicated to my wife Maria

for her unwavering love, support, patience, and words of

encouragement; she has always brought out the best in me,

and I am truly blessed to have her in my life.

Table of Contents

List of Figures

List of Tables

List of Schemes

List of Abbreviations

ABC	Accelerated Blood Clearance
ADA	Adenosine Deaminase
ADTs	Abuse-Deterrent Technologies
AGC	Automated Gain Control
AIDS	Acquired Immunodeficiency Syndrome
ANOVA	Analysis of Variance
APC	Antigen Presenting Cells
ATR	Attenuated Total Reflectance
AZT	Zidovudine
BCA	Bicinchoninic Acid
BSA	Bovine Serum Albumin
BTTAA	2-(4-((Bis((1-(*tert*-butyl)-1*H*-1,2,3-triazol-4-yl)methyl)amino)methyl)-1*H*-1,2,3-triazol-1-yl)acetic acid
CuAAC	Copper Catalyzed Azide Alkyne Cycloaddition
DCC	Dicyclohexylcarbodiimide
DCM	Dichloromethane
DDM	n-dodecyl-beta-D-maltoside
DIAD	Diisopropyl Azodicarboxylate
DIPEA	Diisopropylethylamine
DMAP	Dimethylaminopyridine
DME	Dimethoxyethane

DMF	Dimethylformamide
DMPA	Dimethoxyphenylacetophenone
DMSO	Dimethylsulfoxide
DPBS	Dulbecco's Phosphate-buffered Saline
DTG	Dolutegravir
DTT	Dithiothreitol
EDC	Ethyl(dimethylaminopropyl)carbodiimide
EDTA	Ethylenediaminetetraacetic Acid
EGVE	Ethylene Glycol Vinyl Ether
ELISA	Enzyme-Linked Immunosorbant Assay
ESI	Electrospray Ionization
EVG	Elvitegravir
FBS	Fetal Bovine Serum
FDA	Food and Drug Administration
FPLC	Fast Protein Liquid Chromatography
FT-IR	Fourier Transformed Infrared Spectroscopy
GH	Growth Hormone
GHR	Growth Hormone Receptor
GPC	Gel-Permeation Chromatography
GRAS	Generally Regarded as Safe
HCD	Higher-Energy Collisional Dissociation
HCV	Naive Hepatitis C
HES	Hydroxyethyl Starch

HIV	Human Immunodeficiency Virus
HLA	Human Leukocyte Antigen
HMDS	Hexamethyldisilylamide
HPLC	High Performance Liquid Chromatography
HPMA	poly(N-(2-Hydroxypropyl)(Methacrylamide)
HRMS	High Resolution Mass Spectrometry
IGF-1	Insulin-Like Growth Factor 1
IMAC	Immobilized Metal Affinity Chromatography
IPTG	Isopropyl-β-D-thiogalactopyranoside
KHMDS	Potassium Hexamethyldisilylamide
LCMS	Liquid Chromatography-Mass Spectrometry
LiHMDS	Lithium Hexamethyldisilylamide
Lyz	Lysozyme
MALDI	Matrix-Assisted Laser Desorption/Ionization
MHC	Major Histocompatibility Complex
mPEG	methoxy-poly(ethylene glycol)
MVP	Major Vault Protein
MWCO	Molecular Weight Cutoff
NaHMDS	Sodium Hexamethyldisilylamide
NASH	Non-Alcoholic-Steato-Hepatitis
NHS	N-hydroxysuccinimide
Ni-NTA	Nickel-Nitrilotriacetic Acid
NMR	Nuclear Magnetic Resonance

OPA	o-phthaldialdehyde
OVA	Ovalbumin
PBMC	Peripheral Blood Mononuclear Cells
PBS	Phosphate Buffered Saline
PCB	Poly(carboxybetaine)
PDB	Protein Data Bank
PEG	Polyethylene Glycol
PEG-INF-α	PEGylated Interferon-α2a
PEG-INF-λ	PEGylated Interferon-λ-1a
PEG12	Dodecylpoly(ethylene glycol)
PEG4	Tetraethylene glycol
PFP	Pentafluorophenol
PG	Poly(Glycerol)
PMMA	poly(methyl methacrylate)
pNAcM	Poly(N-Acryloylmorpholine)
POZ	Poly(2-Oxazoline)
pPEGMA	Poly(Poly(Ethylene Glycol) Methyl Ether Methacrylate
PrEP	Pre-Exposure Prophylaxis
PSA	Polysialic Acid
PVP	Poly(vinylpyrrolidone)
QTOF	Quadrupole-Time-of-Flight
rAvPAL	Recombinant A. variabilis Phenylalanine Ammonia Lysase
RID	Refractive Index Detector

ROMP	Ring-Opening Metathesis Polymerization
SCID	Severe Combined Immunodeficiency
SDS-PAGE	Sodium Dodecyl Sulfate-Polyacrylamide Gel Electrophoresis
SLE	systemic-lupus-erythe-matous
SPOS	Solid-Phase Organic Synthesis
TAF	Tenofovir Alafenamide Fumarate
TCEP	Tris(2-carboxyethyl)phosphine
TDF	Tenofovir Disoproxil Fumarate
TEA	Triethylamine
TEP1	Telomerase-Associated Protein 1
TEV	Tobacco Etch Virus
TFA	Trifluoroacetic Acid
TFV	Tenofovir
THF	Tetrahydrofuran
TIC	Total-ion Chromatogram
TIPS	Triisopropylsilane
TLC	Thin-layer Chromatography
TMEDA	Tetramethylethylenediamine
TNFα	Tumor Necrosis Factor alpha
TRX	Thioredoxin
UAA	Unnatural Amino Acid
VEGF	Vascular Endothelial Growth Factor
VPARP	Vault Poly(ADPribose) Polymerase

Acknowledgements

Over the last five years, I have been privileged to work with some of the finest scientists, mentors, and friends I could have imagined. Without the guidance, support, and encouragement from many of these people, this dissertation would not have been possible. I am truly indebted to those in this section that have helped me time and again, and especially to those who convinced me to keep going even when I was ready to give up. Each person in this section has helped shape me into the scientist I have become.

First and foremost, I must acknowledge the continued support of my advisor, Heather Maynard, whom I have learned so much from over the last five years. She has always pushed me to the limits of my abilities, and I doubt I would have learned so much so quickly otherwise. Most of all, however, I must thank her for the opportunity to work with so many talented scientists both in the Maynard Lab and elsewhere, as these collaborations have most wholly defined my graduate experiences. Beginning with the members of the Maynard Lab, I would especially like to thank Natalie Boehnke, Sam Raftery, Emma Pelegri-O'Day, and Jacquelin Woodford for their outstanding mentorship, encouragement, and friendship. I am also incredibly grateful to Priera Panescu, Doug Rose, Neil Forsythe, Arvind Bhattacharya, Jane Yang, and Mikayla Tan for their support, friendship, and ability to make everyday lab work enjoyable. Though we only overlapped briefly, I also thank Grace Kunkel for her invaluable help with aspects of Chapter 1 in this dissertation. I also thank all of the other Maynard Lab members, past and present, who contributed to my successes and consoled me in my failures.

My collaborators outside the Maynard Lab have also played an instrumental part in my graduate career, and I begin by thanking my doctoral committee, Timothy Deming, Craig Merlic, and Leonard Rome, for their helpful guidance and feedback during the course of my dissertation

work. Additionally, I thank Leonard Rome, Valerie Kickhoefer, Jan Mrazek, Otto Yang, Peter Anton, Jennifer Fulcher, Julie Elliot, Javier Ibarrondo, Timothy Deming, and Alex Wollenberg with whom I worked on the Vault/HIV project. I would also be remiss not to thank Mark Arbing for his endless patience and good humor; he has genuinely been one of the most knowledgeable and helpful people I have worked with at UCLA. Outside of UCLA, I thank Yue Wang, Stephen Jamieson, Ries Langley, and Jo Perry for the invaluable materials and advice they provided as well as their welcoming and accommodating collaboration during my visit.

In addition to my scientific peers, I also thank my family as well as my wife's family for their support and kindness. I thank my wife Maria for her endless patience, love, and encouragement over the last seven and a half years, but especially over the last five. I have also been fortunate to have so many close friends that have always rooted for me throughout this process and helped me get through the late nights and stressful moments.

The work outlined in this dissertation was funded predominantly by the National Institutes of Health and various facets of UCLA, including the UCLA Department of Chemistry and Biochemistry. I thank the SG Fellowship for funding during the Winter 2020 quarter.

[†]Chapter 1 is in preparation for publication as: Tamshen, K.; Kunkel, G.E.; Maynard, H.D. "Clinical Observations of Antibodies against Polyethylene Glycol and Implications for Biotherapeutics." *In preparation.* Figures in Chapter 1 were created using BioRender.com. Portions of chapter 2 have been reproduced with permission from Fulcher, J. A.; Tamshen, K.; Wollenberg, A.; Kickhoefer, V. A.; Mrazek, J.; Elliott, J.; Ibarrondo, F. J.; Anton, P. A.; Rome, L. H.; Maynard, H. D.; Deming, T. J.; Yang, O. O. "Human Vault Nanoparticle Targeted Delivery of Antiretroviral Drugs to Inhibit Human Immunodeficiency Virus Type 1 Infection." *Bioconjugate Chemistry* **2019**, 30, 2216-2227. Portions of Chapter 3 are in preparation for

publication as: Rose, D.A.; Tamshen, K.; Boehnke, N.B.; Maynard, H.D. “A Dual-Enzyme Responsive Prodrug for Abuse-Deterrent Opioid Formulations.” *In preparation*. Chapter 4 has been reproduced with permission from Tamshen, K.; Wang, Y.; Jamieson, S.M.F.; Perry, J.K.; Maynard, H.D. “Genetic Code Expansion Enables Site-Specific PEGylation of a Human Growth Hormone Receptor Antagonist through Click Chemistry.” *Bioconjugate Chemistry* **Article ASAP** DOI: 10.1021/acs.bioconjchem.0c00365. Portions of Chapter 5 are reproduced with permission from Pelegri-O’Day, E. M.; Matsumoto, N.M.; Tamshen, K.; Raftery, E.D.; Lau, U.Y.; Maynard, H.D. “PEG Analogs Synthesized by Ring-Opening Metathesis Polymerization for Reversible Bioconjugation.” *Bioconjugate Chemistry* **2018**, *29*, 3739-3745.

Vita

Education:

University of California, Los Angeles, Department of Chemistry, Los Angeles, CA

Ph. D. in Chemistry, Expected Fall 2020

Santa Clara University, Santa Clara, CA

Bachelor of Science in Biochemistry, June 2015

Publications (*Denotes equal contribution):

1. Tamshen, K.; Kunkel, G.E.; Maynard, H.D. "Clinical Observations of Antibodies against Polyethylene Glycol and Implications for Biotherapeutics." *In preparation.*
2. Rose, D.A.; Tamshen, K.; Boehnke, N.B.; Maynard, H.D. A Dual-Enzyme Responsive Prodrug for Abuse-Deterrent Opioid Formulations. *In preparation*.
3. Wang, Y.; Langley, R.J.; Tamshen, K.; Harms, J.; Maynard, H.D.; Jamieson, S.M.; Perry, J.K. Enhanced bioactivity of a human GHR antagonist by solid-phase site-specific PEGylation. *In revision.*
4. Tamshen, K.; Wang, Y.; Jamieson, S.M.F.; Perry, J.K.; Maynard, H.D. Genetic Code Expansion Enables Site-Specific PEGylation of a Human Growth Hormone Receptor Antagonist through Click Chemistry. *Bioconjugate Chemistry*, **Articles ASAP 2020**, DOI: 10.1021/acs.bioconjchem.0c00365.
5. Wang, Y.; Langley, R.J.; Tamshen, K.; Jamieson, S.M.; Lu, M. Maynard, H.D.; Perry, J.K. Long-Acting Human Growth Hormone Receptor Antagonists Produced in E. coli and Conjugated with Polyethylene Glycol. *Bioconjugate Chemistry*, **2020** *31*, 1651-1660.
6. Fulcher, J. A.*; Tamshen, K.*; Wollenberg, A.*; Kickhoefer, V. A.; Mrazek, J.; Elliott, J.; Ibarrondo, F. J.; Anton, P. A.; Rome, L. H.; Maynard, H. D.; Deming, T. J.; Yang, O.

O. Human Vault Nanoparticle Targeted Delivery of Antiretroviral Drugs to Inhibit Human Immunodeficiency Virus Type 1 Infection. *Bioconjugate Chemistry* **2019**, *30*, 2216-2227.

7. Pelegri-O'Day, E. M.; Matsumoto, N.M.; Tamshen, K.; Raftery, E.D.; Lau, U.Y.; Maynard, H.D. PEG Analogs Synthesized by Ring-Opening Metathesis Polymerization for Reversible Bioconjugation. *Bioconjugate Chemistry* **2018**, *29*, 3739-3745.

Presentations:

1. Tamshen, K.; Fulcher, J. A.; Wollenberg, A.; Kickhoefer, V. A.; Mrazek, J.; Elliott, J.; Ibarrondo, F. J.; Anton, P. A.; Rome, L. H.; Maynard, H. D.; Deming, T. J.; Yang, O. O. *Human Vault Nanoparticle Targeted Delivery of Antiretroviral Drugs to Inhibit Human Immunodeficiency Virus Type 1 Infection*. ACS Fall 2019 International Meeting, San Diego, CA; August 25, 2019; Poster Presentation.
2. Tamshen, K.; Kousnetsov, R.; Miller, L. *Promoter Bashing of a Hox Gene Involved in C. elegans Cell Fate Determination*. 40th Annual West Coast Biological Sciences Undergraduate Research Conference, Pointe Loma, CA; April 25, 2015; Poster Presentation.

Selected Honors and Awards:

University of California, Los Angeles

SG Fellowship (2020)

UCLA Research Showcase Travel Grant (2019)

Santa Clara University

American Institute of Chemists Student Award (2015)

ALZA Corporation Science Scholar Award (2013-2015)

Chapter 1

Clinical Observations of Antibodies against Polyethylene Glycol and Implications for Biotherapeutics[†]

1.1 Introduction

Biological therapeutics such as peptides, proteins, and nucleic acids comprise a diverse and important class of pharmaceuticals that possess distinct advantages over small molecule therapeutics due to their specific and well-tolerated interactions with complex biological systems.[1] With well over 200 marketed biotherapeutics currently available, these molecules have enabled advancements in a broad range of areas including replacement therapies and targeted drug delivery.[2,3] Despite the widespread clinical successes of these complex macromolecules, many native biomolecules do not make optimal drug candidates due to challenges inherently associated with their administration and delivery. For example, many biologics are prone to physical or chemical degradation as a result of environmental or biological stressors.[2,4] Most also exhibit short *in vivo* half-lives, and therefore require intervention to improve therapeutic efficacy and minimize dosing amount and frequency. Addition of exogenous biomolecules for disease treatment is also accompanied by risk of immune responses that can lead to accelerated blood clearance of the therapeutic, requiring increased dosing, as well as other more severe detrimental events such as hypersensitivity and infusion reactions, and in rare instances, anaphylaxis.[4–6]

Numerous strategies have been pursued to overcome these challenges, including formulation of proteins or peptides with stabilizing agents,[2] development of fusion constructs to extend half-lives *in vivo*,[7] and, in some cases, protein engineering to reduce immunogenicity of antigenic proteins.[8,9] One of the most widely employed strategies for overcoming these obstacles has been the covalent conjugation of polyethylene glycol (PEG) to biomolecules, known as PEGylation. PEG is a water soluble, chemically inert, synthetic polymer consisting of ethylene glycol subunits ($-CH_2-CH_2-O-$). Several important physical properties make PEG well suited for addressing the challenges of delivering therapeutic biomolecules.

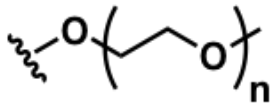

Figure 1.1. Chemical structure of methoxy-terminated polyethylene glycol (PEG).

First, PEG exhibits a large hydration sphere with 2-3 water molecules per ethylene glycol subunit for free PEG and up to 4.6 water molecules for PEG-coated liposomes where the conformation is shifted from a random coil to a brush.[10] As the molecular weight of PEG increases, its hydration sphere, or hydrodynamic radius, also increases; however as temperature increases, its overall hydration sphere decreases in size.[11] This large hydration sphere also contributes to the characteristic of PEG as a non-fouling polymer that is preferentially excluded from the surface of proteins,[12] DNA,[13] and liposomes.[14] The mechanism of preferential exclusion results from steric exclusion of the PEG from the protein domains, which are preferentially hydrated in the presence of PEG.[12,15] Second, PEG possesses a high degree of conformational flexibility, and adopts a random-coil conformation in aqueous solutions.[16] Limitation of the conformational freedom of PEG molecules is thermodynamically unfavorable and PEG therefore resists displacement by intruding molecules, acting as a steric blocking group. In this way, PEG confers stealth properties onto attached biomolecules. Third, PEGylated biomolecules therefore demonstrate resistance to proteolysis as well as reduced opsonization.[17] Fourth, in addition to shielding attached biomolecules from biological stressors, the ability of PEG to act as a soluble, inert, bulking agent can also effectively increase the hydrodynamic radius of PEGylated biomolecules above the renal filtration threshold, which can reduce renal clearance and extend circulation time.[18] Fifth, due to its stealth properties and inert polyether backbone, PEG has historically been regarded as non-immunogenic and non-antigenic,[19] and is also generally regarded as safe (GRAS) by the FDA.

The first reports of PEGylation by the Davis group in 1977 demonstrated that nonspecific amine-PEGylation of both bovine serum albumin and bovine liver catalase attenuated immunogenicity, prolonged circulation time, and conferred resistance to proteolytic degradation.[20,21] Since these initial reports, PEGylation has become one of the leading approaches for overcoming the limitations of biotherapeutics with 15 distinct PEGylated biologics and numerous biosimilars on the market (see Table 1.1). However, despite the broadly successful application of this technology toward biotherapeutics, more and more reports over the last two decades have emerged with evidence of antibodies against PEG. Clinical outcomes of these anti-PEG antibodies have varied substantially. In some cases, these anti-PEG antibodies have no apparent effect on the pharmacokinetic or pharmacodynamic parameters of a given PEGylated drug, but in other cases, repeated administration has been associated with accelerated blood clearance of PEGylated species. In rare cases, severe allergic reactions have been reported following injection of a PEGylated drug. As an added complication, a growing body of evidence has confirmed the existence of anti-PEG antibodies in healthy individuals who have never before received PEGylated therapeutics. The contemporary incidence of these pre-existing anti-PEG antibodies varies widely with estimates ranging from 4.3% to 97.5% over the last decade, but generally this incidence appears to have increased substantially from the seminal report in 1984 of 0.2%.[22–24] Understanding the incidence, mechanism, implications, and factors affecting PEG immunogenicity is therefore critical to predicting the immunogenic potential of future PEG-containing therapeutics.

The topic of PEG immunogenicity extends to all PEGylated molecules, and while we have limited our focus in this chapter to PEGylated biomolecules, which represent the majority of PEGylated therapeutics on the market, we include key mechanistic studies using PEGylated

nanocarriers such as liposomes as necessary. For more focused overviews on immune responses to specific nanocarriers, we recommend the recent reviews on the immunogenicity of PEGylated liposomes,[25,26] micelles,[27] and nanoparticles.[28] Herein, we discuss the immunogenicity of PEGylated biomolecules in humans, the possible reasons for anti-PEG antibody generation, and the effects of anti-PEG antibodies on the safety and efficacy of PEGylated therapeutics. Additionally, we review the incidence of clinical and pre-existing anti-PEG antibodies, methods for their detection, and factors affecting PEG immunogenicity. Finally, we consider potential solutions for circumventing PEG immunogenicity and offer perspectives on promising new technologies. Our objective in writing this review is not only to provide chemists with a guide for understanding PEG immunogenicity, but also to encourage and enable more researchers to enter into this important area of investigation. Given the breadth and depth of research performed to interrogate this topic over the past few decades, we have therefore tailored this review to cover key discoveries and developments in technology that can enable other researchers to enter and further probe this field. Though complex, the challenge of overcoming the immunogenicity of PEG is rife with opportunity for the development of next-generation biotherapeutics.

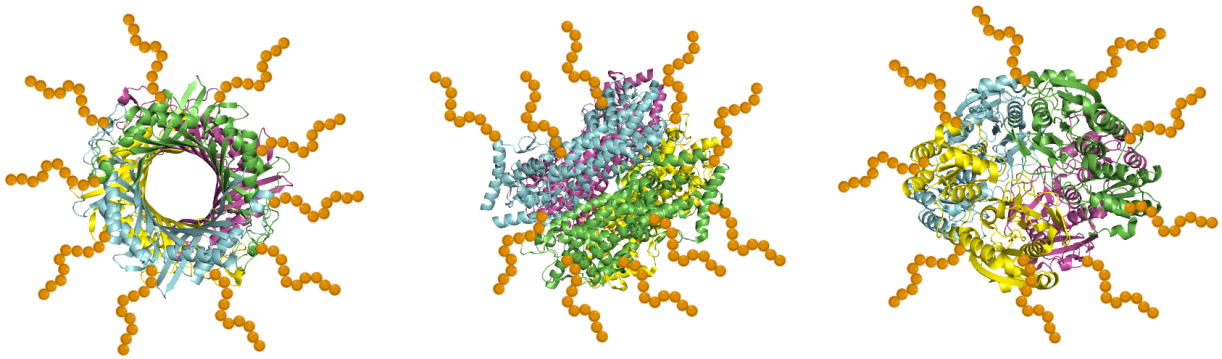

Figure 1.2. Schematic representations of various protein-polymer conjugates. Protein structures were generated from PDB structures 3ECA, 4MB8, and 2NYN using PyMol v.1.8.6.0. Chains of orange spheres represent PEG polymer chains.

1.2 Preclinical Evidence for PEG as a Hapten

Since the early investigations of PEGylation by the Davis group in 1977 showing that PEGylation of bovine serum albumin and bovine liver catalase inhibited immune responses in rabbits,[20,21] PEG has become widely accepted as a non-immunogenic, non-antigenic polymer. In most cases, this observation has generally held true with PEGylation enabling administration of otherwise immunogenic exogenous proteins. Shortly after developing the technology, the Davis group applied it to the therapeutically relevant protein, bovine adenosine deaminase (ADA). In 1981, the group reported that nonspecific PEGylation of ADA with 5 kDa methoxy-polyethyleneglycol (mPEG) increased the half-life of the protein in mice from 30 minutes to >28 hours and also eliminated observable antibodies against the protein as evaluated by immunodiffusion studies.[29] After alteration of the conjugation chemistry from cyanuric chloride to the more robust succinimidyl ester PEG, PEGylated ADA (pegademase) was investigated for clinical use in patients with severe combined immunodeficiency (SCID) and eventually received FDA approval in 1990.[30,31] In the years immediately following, a similar strategy was employed

to facilitate the administration of *E. coli* derived L-asparaginase to treat acute lymphoblastic leukemia. Similar to PEG-ADA, nonspecific PEGylation of L-asparaginase with 5 kDa succinimidyl mPEG significantly increased circulation half-life in rabbits and mice while simultaneously reducing immune responses.[32,33] FDA-approval was subsequently granted for pegaspargase following clinical investigations in 1994. With strong precedent from these early examples, PEGylation has successfully been applied to a variety of important biotherapeutics over the past few decades (see Table 1.1). However, especially in the recent years, a variety of preclinical and clinical studies have documented the production of anti-PEG antibodies, which can be associated with negative outcomes such as reduced efficacy and hypersensitivity.

The first instance of an anti-PEG antibody response in animals was reported by Richter and Åkerblom in 1983 in which the authors induced anti-PEG antibodies in rabbits by administering PEGylated ovalbumin, superoxide dismutase, or ragweed pollen extracts with Freund's complete adjuvant.[34] In total, 18 of 34 rabbits produced anti-PEG antibodies. Antibody production was dependent on protein, with ovalbumin conjugates generating the majority of the immune responses. Additionally, the extent to which each protein was PEGylated affected the observed immune response, with more heavily modified proteins exhibiting lower immune responses. Importantly, repeated administration of free 10 and 100 kDa PEGs with Freund's complete adjuvant failed to exhibit any immune response, and even 5.9 MDa PEG proved only poorly immunogenic in mice.[34] Based on these results, the authors concluded that PEG acts as a polyvalent hapten, or a molecule that elicits an immune response only when attached to an immunogenic biomolecule. In such cases, the immunogenic potential of PEG results directly from the immunogenic potential of the attached biomolecule. Since this initial study, considerable evidence for the haptogenic nature of PEG has been accumulated.

Over the past few decades, anti-PEG antibodies have been induced in numerous animal species following administration of PEGylated proteins,[34–40] aptamers,[41] liposomes,[25,26] micelles,[27] nanoparticles,[28] and red blood cells.[42] In each of these cases, PEG elicited an immune response only when conjugated to other immunogenic agents. In most instances, the conditions under which anti-PEG antibodies were generated were relatively severe. For example, anti-PEG antibodies have been observed upon conjugation to highly immunogenic proteins such as ovalbumin[34,38] and uricase,[37,43] or in the presence of adjuvants such as plasmid DNA in PEGylated liposomes.[44] However, several scattered reports also indicate that it may be possible for free PEGs to trigger immune responses, but this may be attributable to the high concentrations of PEG employed in these studies.[45–47] Several groups have also intentionally elicited production of anti-PEG antibodies, which has provided further insight into the conditions required for immune stimulation. In 1999, the Roffler group described production of the first anti-PEG IgM monoclonal antibody after repeated injection of PEGylated β-glucuronidase conjugated to a monoclonal antibody into mice.[35] Several years later, the group reported the development of an anti-PEG IgG_1 monoclonal antibody following a similar procedure with addition of Freund's complete adjuvant.[36] In their second report, the authors commented that it was difficult to induce an antibody response against PEG and that robust anti-PEG antibody response in mice required repeated injections.[36] Compared to other polymers investigated for bioconjugation to reduce immunogenicity, PEG does not possess a strong proclivity for evoking an immune response. Upon immunization of mice with uricase conjugated to either poly(*N*-vinylpyrrolidone), poly(*N*-acriloylmorpholone), or PEG, it was found that PEGylated uricase induced significantly lower production of both anti-uricase antibodies as well as anti-polymer antibodies compared to the other conjugates.[37]

The Ishida group also induced and isolated anti-PEG IgM monoclonal antibodies following repeated immunizations of mice with PEGylated ovalbumin and complete Freund's adjuvant. Interestingly, PEGylated liposomes were able to generate an antibody response following only a single injection, suggesting potential mechanistic differences between immune stimulation for PEGylated proteins and nanoparticles.[38] Further support for the haptogenic properties of PEG was demonstrated by van Helden et al. with the assessment of a PEGylated human Factor VIII in both a transgenic and conventional hemophilic mouse model. When challenged with PEGylated human Factor VIII, the conventional hemophilic mice developed anti-PEG antibodies against the foreign protein whereas the transgenic mice that expressed human Factor VIII recognized exogenous PEGylated Factor VIII as self-protein and did not mount an immune response.[48] As described below, this phenomenon has also held true for clinical investigations, with biomolecules derived from other organisms with foreign proteins generally yielding more negative outcomes.

1.3 Clinical Induction of Anti-PEG Antibodies in Humans

PEGylation remains a successful strategy for mitigating the immunogenicity of therapeutic biomolecules and has enabled their development for a variety of clinical indications. There are currently 15 FDA-approved PEGylated biotherapeutics, most of which consist of recombinantly expressed proteins conjugated to one or more PEG chains. PEGylation has historically facilitated extension of serum half-life of attached proteins while simultaneously shielding them from immune detection, and has consequently enabled development of the first FDA-approved PEGylated proteins bovine-derived ADA[30,31] and *E. coli*-derived L-asparaginase.[49,50] In the years following approval of these therapeutics, PEGylation was successfully applied to a variety of

recombinantly expressed proteins with low reported incidences of immunogenicity as shown in Table 1.1. For most of these PEGylated biomolecules, induced anti-drug antibodies did not appear to be associated with reduced efficacy or safety profiles, but particularly with proteins derived from other organisms, anti-drug antibodies as well as anti-PEG antibodies have been more frequently observed. Though the clinical implications of these antibodies appear to be largely protein dependent, foreign proteins also tend to be associated with more significant immune responses, supporting the theory that PEG acts as a polyvalent hapten.

The first report of anti-PEG antibody induction in humans was recorded in 1984 by Richter and Åkerblom based on a clinical trial investigating the use of PEGylated allergens for hyposensitization treatment.[24] In this study, 50% of allergy patients developed anti-PEG antibodies following 1 year of treatment, but these antibodies did not elicit further immune responses and after two years of treatment, the incidence dropped to 28.5%.[24] Though the impact of these antibodies on the efficacy of treatment was not reported for this study, later clinical reports have shown that anti-drug antibodies do not necessarily predict diminished safety or efficacy. For instance, in a phase I study for PEG-ADA where 59% of patients generated antibodies, all of the observed antibodies were formed against ADA, but the efficacy of PEG-ADA was not impacted.[51] This observation was also supported by a follow up study that evaluated treatment outcomes after 8.5 years.[52] Various PEGylated interferons have also elicited antibody responses against PEG, but in several studies these antibodies were not correlated with negative patient outcomes.[53,54] In fact, the majority of significant negative outcomes resulting from anti-PEG antibodies, such as reduced efficacy due to accelerated clearance or allergic responses, have been limited to just a few biotherapeutics. This section will briefly summarize these cases.

Anti-PEG antibodies have been correlated with significant reduced therapeutic efficacy for only three PEGylated proteins: asparaginase, uricase, and, to a lesser extent, phenylalanine ammonia lyase. PEGylated asparaginase was developed in an effort to mask the antigenic epitopes of the *E. coli* derived protein and consequently reduce immune responses to the protein so that it could be used to treat acute lymphoblastic leukemia, which successfully lowered incidences of hypersensitivity compared to the unmodified protein.[49] The drug received FDA approval in 1994, but was later discovered by Armstrong and coworkers to induce anti-PEG antibodies, which led to accelerated clearance and diminished efficacy.[55] By serological testing, 32% of pediatric patients treated with PEGylated asparaginase exhibited anti-PEG antibodies, and all patients with detectable antibody titers showed no measurable asparaginase activity. The authors further confirmed these results using a flow cytometry assay and found 46% of patients tested positive for anti-PEG IgM antibodies, with 12 out of 13 of these patients showing undetectable asparaginase activity.[55] A strong correlation was observed between anti-PEG antibody incidence and low serum asparaginase activity in patients treated with PEGylated asparaginase. Interestingly, the authors found that patients treated with unmodified asparaginase also tested positive for anti-PEG antibodies by serological testing (13%) and flow cytometry (38%), suggesting that antibody occurrence in patients treated with the PEGylated protein may have been pre-existing.[55] A later, comprehensive study that monitored 615 pediatric acute lymphoblastic leukemia patients who received PEGylated asparaginase for 30 weeks found that 79 patients (13.2%) developed an allergy to the treatment and discontinued therapy for that reason;[50] however, whether the allergic responses were related to anti-PEG antibodies was not determined.

Another protein that has received significant attention due to its ability to induce anti-PEG antibodies is uricase. Uricase has been investigated extensively for treatment of gout; however, because humans do not express uricase, enzymes from other organisms have been recombinantly expressed for administration to patients.[56,57] In a phase I clinical trial in which patients were subcutaneously administered a single dose of PEGylated uricase (pegloticase), 8 of 13 patients demonstrated detectable plasma uricase concentrations 21 days following injection, but the other 5 (38%) patients showed no detectable concentration.[58] Further investigation revealed the presence of low-titer anti-PEG antibodies in all 5 of these low-responders, with IgM and IgG antibodies developing 3-7 and 7-14 days after exposure to pegloticase, respectively. Additionally, 3 of these 5 patients' allergic reactions began at injection sites 8-9 days post injection, with one patient experiencing cellulitis, and the other two experiencing uticaria that began at the injection site and became widespread within 1-2 days.[58] A similar, follow-up phase I study mitigated allergic reactions by employed intravenous dosing of pegloticase, but anti-PEG antibodies were still observed in 9 of 24 patients (38%), and antibody positive patients cleared pegloticase significantly faster.[59] Further evidence of antibody-mediated clearance was obtained after an antibody-positive patient was given a second injection of pegloticase one year after the initial dose. Before the second dose, the patient's anti-PEG antibody titer had declined below the limit of detection, but became strongly positive 7 days after the second dose and coincided with complete clearance of pegloticase after 7 days. Notably, no allergic responses were reported in this study, illustrating how the route of administration can affect immunogenicity of PEGylated biomolecules.[59] In phase II clinical trials, 30 patients were treated with up to five infusions of pegloticase in three week intervals and patients were classified as either persistent, transient, or non-responders. In total, 17 persistent responders (57%) showed sustained pegloticase plasma

concentration with minimal observation of antibodies against pegloticase, all 12 transient responders (40%) showed diminished pegloticase plasma concentrations and tested positive for anti-PEG antibodies, and 1 non-responder was withdrawn due to a syncopal reaction during the first infusion and was found to have the highest antibody titers against pegloticase.[60] Antibody positive patients experienced the majority of infusion reactions, which occurred during 24% of all infusions, and 5 withdrew from the trial as a result of these reactions. During the course of this investigation authors additionally confirmed the specificity of induced anti-PEG antibodies for the polyether backbone of PEG through competition ELISA experiments with free PEG.[60]

Pegloticase has also been evaluated in several long-term safety studies from 6 months to 3 years.[61,62] In a 6 month study, 40% of all patients developed anti-PEG antibodies, and non-responders possessed significantly higher anti-PEG antibody titers than responders. Interestingly, pre-existing anti-pegloticase antibodies were observed in 15% of patients at baseline, but these antibodies did not predict loss of response to treatment. However, diminished response to pegloticase preceded infusion reactions in 79% of patients.[61] Similar results were observed in a follow-up 3 year study with 31% of patients developing anti-pegloticase antibodies and these antibodies were correlated with reduced responses to treatment.[62] Over this extended timeframe, 34% of patients recorded at least one serious adverse event, with 25% of these patients discontinuing treatment.[62] In each of these studies, anti-PEG antibodies were correlated to diminished efficacy and higher risk of adverse reactions.

While most clinical data surrounding the immunogenicity of PEGylated biologics pertains to uricase and asparaginase, more recent studies also report that PEGylated phenylalanine ammonia lyase (rAvPAL-PEG) may be an even more potent inducer of anti-PEG antibodies. In a phase I dose escalation study for rAvPAL-PEG, 100% of patients developed anti-rAvPAL-PEG

antibodies after a single dose, but no relationship between antibody presence and dose or adverse events were observed.[63] However, a phase II investigation revealed that upon administration of multiple doses of rAvPAL-PEG, antibody mediated clearance was observed, but could be compensated for by titrating dosing of rAvPAL-PEG accordingly. All participants developed antibodies directed against rAvPAL and most also developed transient anti-PEG antibodies, but interestingly anti-PEG antibody titers declined over the course of the study.[64] Similar trends were also observed following assessments from a phase III study with anti-PEG IgM and IgG returning to near baseline levels by the end of the study timeframe. Adverse events also decreased over the course of the study, and 99% were non-severe and 96% were resolved without dose interruption or reduction.[65]

While it is clear from these clinical examples that the immunogenicity of PEG can impact the efficacy and safety of biotherapeutics, it is important to understand the nuances in immunogenicity risk assessment. Immunogenicity of PEG remains a concern for many therapeutics, but in most cases the associated risks have been insufficient to justify removing these drugs as treatment options as evidenced by their continued prescription. Consideration must be given to a variety of factors when evaluating the therapeutic benefits of a given biologic, and each must be evaluated on a case-by-case basis. For instance, while biologics like FVIII variants that regularly stimulate production of neutralizing antibodies in 20-30% of patients have continued to be approved, others may be denied approval or withdrawn even with lower incidence if, for example, antibodies are developed against the endogenous biomolecule as was the case with the FVIIa mutant vatreptacog alpha.[66] This principle is also applicable to PEGylated biologics. Omontys (peginesatide), an erythropoiesis stimulating peptide, was FDA-approved in 2012 to treat anemia in dialysis patients, but was voluntarily recalled in 2013 after it

was found that 0.2% of patients developed allergic reactions, and fatal reactions were observed in 0.02% of patients within 30 minutes of the first dose.[67,68] Despite the small proportion of patients, Omontys was withdrawn due to the large number of potential users and because of the established safety profile of erythropoietin agents.[66,68,69] More recently, a similar observation halted development of the PEGylated RNA aptamer pegnivacogin when 0.5% of patients experienced serious allergic reactions immediately following the first injection in a phase II trial.[70,71] The finding that immunogenicity was raised against the PEG portion of pegnivacogin raised significant concerns that pre-existing anti-PEG antibodies might not only be associated with severe adverse events, but also might affect the safety and efficacy of other PEGylated molecules. These concerns subsequently spurred swift investigation by a number of groups.

Table 1.1. FDA-approved PEGylated biotherapeutics (excluding biosimilars and generics).

Year Approved	Trade Name (Brand Name)	Protein/ Biologic Description	Number of PEG Chains per Protein, [Chain MW (kDa)], Site of Attachment	Indication	Patient Dose, Duration of Treatment	Route of Administration	Antibody Induction (% Incidence)	Ref
1990	Pegadamase bovine (Adagen)	Purified bovine adenosine deaminase	11-17, [5], nonspecific amines	Severe combined immuno-deficiency	15 U/kg/week, chronic	IV	8.3% against adenosine deaminase	72
1994	Pegaspargase (Oncaspar)	*E. coli* L-asparaginase	69-82, [5], nonspecific amines	Acute Lympho-blastic Leukemia	2500 IU/m^2	IV/IM	11%	73
2001	PEG-interferon-alpha 2b (PegIntron)	Recombinant human interferon-alpha 2a	1, [12], multiple residues	Chronic hepatitis C	1.0 µg/kg/week for 1 year	SC	2% neutralizing antibodies	74
2002	Pegfilgrastim (Neulasta)	Recombinant human granulocyte colony-stimulating factor	1, [20], N-terminus	Chemo-therapy induced neutropenia	6 mg every 3 weeks	SC	6% pre-existing anti-PEG antibodies, <1% induced, no neutralizing antibodies detected	75
2002	PEG-interferon alpha 2a (Pegasys)	Recombinant human interferon-alpha 2a	1, [2 x 20], lysine	Chronic hepatitis B, C	2.7 and 3.6 µg/kg/week for 48 weeks	SC	29% low titer neutralizing antibodies for Hepatitis B 9% low titer neutralizing antibodies for Hepatitis C	76

2003	Pegvisomant (Somavert)	Recombinant engineered growth hormone receptor antagonist	4-6, [5], nonspecific amines	Acromegaly	40 mg loading dose, then 10-30 mg/day	SC	17% low titer non-neutralizing	77
2004	Pegatinib-sodium (Macugen)	Anti-VEGF aptamer	1, [2 x 20], 3' phosphate	Age-related macular degeneration	0.3 mg every 6 weeks	Intravitreous	Not reported	78
2007	PEG-epoetin beta (Mircera)	Epoetin beta	1, [30], lysine	Anemia due to Chronic Kidney Disease	0.6 µg/kg every 2 weeks	SC/IV	0%	79
2008	Certolizumab pegol (Cimzia)	Antibody Fab' fragment specific for human tumor necrosis factor alpha (TNFα)	1, [2 x 20], C-terminal cystein	Crohn's Disease, Rheumatoid Arthritis, Psoriatic Arthritis, Ankylosing Spondylitis	Loading dose followed by up to one 400 mg dose per month	SC	8-23% for Crohn's patients, 6% neutralizing antibodies 7% rheumatoid arthritis patients, 3% neutralizing antibodies 8-19% for psoriasis patients, 5% neutralizing antibodies	80
2010	Pegloticase (Krystexxa)	Recombinant porcine uricase	9-11, [10], nonspecific amines	Chronic gout	8 mg every 2 weeks	IV	92% anti-pegloticase antibodies, 42% anti-PEG antibodies	81
2012*	Peginesatide (Omontys)	Erythro-poiesis-stimulating agent	1, [2 x 20], C-termini	Anemia due to chronic kidney disease	0.04 mg/kg once monthly	SC/IV	1.2% overall; 0.7% and 1.9% anti-peginesatide antibodies for IV and SC, respectively, 0.9% neutralizing antibodies	82
2014	Peginterferon beta-1a (Plegridy)	Recombinant interferon beta-1a	1, [20], N-terminus	Multiple Sclerosis	0.125 mg every 14 days	SC	<1% neutralizing antibodies, 7% anti-PEG antibodies	83
2015	Antihemo-philic factor (Adynovate)	Recombinant antihemophilic factor VIII	1+, [20], lysines	Hemophilia A	1 U/kg/ episode	IV	2% antibodies overall, 1.2% pre-existing anti-PEG antibodies	84
2017	Coagulation Factor IX, GlycoPEGylated (Rebinyn)	Recombinant coagulation factor IX	1, [40], glycoPEGylated	Hemophilia B	40 IU/kg or 80 IU/kg	IV	Not reported	85
2018	Pegvaliase-pqpz (Palynziq)	Recombinant *A. variabilis* phenylalanine ammonia lyase	~36, [20], nonspecific amines	Phenyl-ketonuria	2.5 mg once weekly for 4 weeks	SC	98% anti-phenylalanine ammonia lyase antibodies, 98% anti-PEG antibodies, 88% neutralizing antibodies	86

*Voluntarily withdrawn from market in 2013

1.4 Pre-existing anti-PEG Antibodies

Safety and efficacy concerns surrounding the immunogenic potential of PEG have grown considerably in recent years given the abundance of preclinical and clinical evidence that exposure to PEGylated therapeutics may lead to negative patient outcomes such as reduced efficacy and hypersensitivity. While these concerns may have been anticipated given the highly immunogenic nature of certain therapeutic biomolecules, the discovery that individuals who have never been treated with a PEGylated therapeutic can exhibited pre-existing anti-PEG antibodies presented an unexpected obstacle that has sparked significant investigation, particularly in the past 5 years. Table 1.2 chronologically summarizes the prevalence of pre-existing anti-PEG antibodies in humans and provides information pertaining to antibody subtypes as well as demographic trends. As evident from the wide variation in sample populations, data reporting, and assay types, no standardized approach to study this phenomenon has yet been adopted. While this phenomenon warrants continued investigation, several key takeaways can be extracted from the available information.

Despite substantial variation in estimates of pre-existing anti-PEG antibodies in the general population, it is clear that the incidence has increased over the last four decades. In 1984, one year after their discovery that anti-PEG antibodies could be induced in animals, Richter and Åkerblom published the first report of human anti-PEG antibodies in naive, healthy donors as well as naive allergy donors. The authors observed a low incidence of just 0.2% in healthy donors and 3.3% in allergy patient donors using a semi-quantitative hemagglutination assay. They further observed that the vast majority of these antibodies were likely IgM since near complete abolition of hemagglutination was observed following treatment with 2-mercaptoethanol, however no further subtyping experiments were performed.[24] Based on the

very low incidence of anti-PEG antibodies observed in healthy donors, the authors concluded that such an antibody response would not likely interfere with the clinical usefulness of PEGylated biologics. The authors' conclusions on the non-immunogenic nature of PEG were reasonable based on the available data and persisted for many years as the sole report of this phenomenon. In fact, it was twenty years later in 2004 when this issue was revisited by Armstrong and coworkers amidst investigations of PEGylated red blood cells. Whereas Richter and Åkerblom observed low incidences of anti-PEG antibodies among healthy donors, Armstrong and coworkers found using the same hemagglutination method that about 27% of naive healthy donors exhibited measurable anti-PEG antibodies, and most of these antibodies were determined to be IgG by flow cytometry.[87,88] Further evidence for the increasing prevalence of pre-existing anti-PEG antibodies was recently presented by Yang et al. in which 72% of contemporary samples (from 2015) versus 56% of historic samples (from 1970-1999) from healthy donors tested positive for antibodies against PEG.[89] Despite the variability in incidence reports over the past 15 years, even the lowest values are well above those recorded in the original 1984 studies, suggesting that these pre-existing antibodies are becoming a common occurrence.

The prevailing theory for the rise in pre-existing anti-PEG antibodies in the naive, general population is that PEG and PEG-containing products have become more and more commonplace in everyday consumer goods, resulting in greater exposure over the past decades. PEG is widely used in a variety of products such as cosmetics, foods, pharmaceuticals, and many others.[90] Although PEG itself generally does not appear to be able to elicit an immune response, Yang and Lai have speculated that introduction of PEG or PEGylated molecules into sites of inflammation (e.g. treatment of a minor abrasion with a PEG-containing soap) may allow highly active

immune cells to induce anti-PEG antibodies.[25] Although the mechanism of PEG immunogenicity is not yet fully understood, this theory is consistent with the view that PEG is a hapten and requires some type of adjuvant to stimulate an immune response. Though further studies are needed to clearly elucidate the mechanism of immunogenicity, it is clear from a survey of the literature that the occurrences of antibodies against PEG have become more common over time. It is therefore desirable to understand the factors influencing the prevalence of pre-existing anti-PEG antibodies, especially given their well-documented potential to alter the therapeutic safety and efficacy profiles of biopharmaceuticals.

Clinically, these antibodies can prove either deleterious or benign. As expected, the effects of these antibodies appear directly related to the attached biomolecule. For instance, Tillmann et al. found that although anti-PEG antibodies in individuals with Hepatitis C (HCV) were significantly higher than in healthy patients (44% versus 6.9%), there was no evidence that these antibodies led to impaired response to treatment with PEGylated interferon-α2a or interferon-α2b. Interestingly, antibody levels actually declined over the course of treatment for both treatment groups.[53] In another example, in a phase II clinical trial, Myler et al. quantified anti-PEG antibodies before, during, and after treatment with either PEGylated interferon-α2a (PEG-INF-α) or interferon-λ-1a (PEG-INF-λ). The authors found that 9.1% of 83 PEG-INF-α patients and 6.3% of 80 PEG-INF-λ patients possessed pre-existing anti-PEG antibodies, but that these antibodies were not associated with negative outcomes and no hypersensitivity events were reported. Additionally, these antibody levels were generally low, did not increase upon treatment, and were predominantly transient with only 7.4% of patients exhibiting persistent antibodies.[54] It was therefore concluded that for these therapeutics, pre-existing antibodies were likely to have little to no clinical impact. Interestingly, in a phase I clinical trial for phenylalanine

ammonia lyase in patients with phenylketonuria, 16% of subjects exhibited pre-existing anti-PEG antibodies and 100% developed anti-PEG antibodies after a single dose, yet these antibodies did not appear to influence the efficacy of the therapeutic.[63]

In contrast, several clinical studies with more immunogenic PEGylated biomolecules have demonstrated association of anti-PEG antibodies with more severe clinical outcomes. Especially in the case of PEGylated uricase (pegloticase), pre-existing anti-PEG antibodies have been associated with accelerated blood clearance resulting in attenuated efficacy as well as increased risk of infusion reactions.[58–60] In a phase II clinical trial of pegloticase for refractory gout, pre-existing anti-PEG antibodies were detected in 19% of patients, and patients with higher levels of antibodies had more frequent and severe infusion reactions.[61] In rare cases, these pre-existing antibodies can be associated with severe adverse events such as allergic reactions and anaphylaxis. In fact, a recent phase II trial for the use of a PEGylated RNA aptamer was terminated after 3 of 640 patients experienced serious allergic reactions immediately following the first injection, with 2 patients meeting the criteria for anaphylaxis. It was determined that pre-existing anti-PEG antibodies were a major (but not sole) contributor since each patient with severe reactions demonstrated high antibody levels.[70,71] While a major factor, the authors note that these responses are complex and may also have been affected by the high dosing requirement for this therapeutic (1 mg/kg) as well as individual differences in anti-PEG antibodies, as allergic responses were not triggered in other patients with high antibody titers. These cases underscore the complex biological relationship between pre-existing anti-PEG antibodies and their effects on the safety and efficacy of PEGylated therapeutics.

In addition to understanding the clinical ramifications of anti-PEG antibodies, it is also useful to understand the demographic prevalence of these antibodies as it may offer insight into

their induction and also help predict risk for adverse responses. Because investigations into demographic incidences of this nature have only recently been initiated, the data is somewhat limited and variable for these studies, but nevertheless offers insight for future work in this area. Based on our review of these reports, we propose that the differences in observed incidences of pre-existing anti-PEG antibodies are primarily due to two factors: subject demographics and assay technique. Particularly with regard to demographics, several factors have been correlated with antibody incidence including geographic location, health condition, sex, and age. Lubich et al. tested donor plasma samples from Australia as well as 5 US cities and found significant differences in observed anti-PEG IgG antibodies across cities, although IgM titers were similar.[91] While most studies used slightly different assay formats and therefore cannot be directly compared, it is possible that part of the variability in incidences of antibodies in healthy individuals may stem from the geographic location of the plasma donors sampled, as few studies reported sampling from multiple regions. In several studies, plasma donors with known diseases also had antibody titers different from healthy subjects in the same study. These conditions have included donors with allergies,[24] Hepatitis C and other liver diseases,[53] and hemophilia.[91] Reasons for these differences are unclear, but likely reflect the nuanced interplay between these diseases and immune responses.

Three reports also address differences in antibody incidence between males and females. While Lubich et al. reported no difference in antibody frequency between sexes,[91] Chen et al. recorded higher IgM rates and IgG rates for females,[92] and Yang et al. noted that females were more likely to contain IgM but not IgG anti-PEG antibodies.[89] Each of these groups thoroughly validated their detection assays, so it is unlikely that these differences reflect variations in assay format. This may more likely be the result of regional variations in antibody prevalence, as the

three groups primarily sampled subjects from Australia, Taiwan, and the United States, respectively. Just as region may affect exposure to PEG, sex may also impact exposures to PEG-containing products. For example, females may be more likely to use consumer products or medications containing PEG than males. Following administration of PEGylated phenylalanine ammonia lyase in a phase I clinical study to treat phenylketonuria, 2 of 25 participants developed hypersensitivity reactions to an incidentally prescribed birth control medication formulated with PEG.[63] This example highlights not only differences in sources of exposure to PEG for males and females, but also how each may be affected differently by anti-PEG antibodies. One factor correlated to the incidence of pre-existing anti-PEG antibodies that was supported by data from all three of these studies was age. In each report, younger plasma donors were more likely to exhibit antibodies than older donors. Interestingly, the frequency of antibody-positive patients generally appeared to decrease with age.[89,91,92]

While the studies in Table 1.2 provide valuable insight into factors affecting the incidence and clinical outcomes of pre-existing anti-PEG antibodies in naive individuals, many aspects of these antibodies remain a mystery. For instance, several studies report that these antibodies can be transient or persistent,[1–3] but it is unclear why this is and how they may be correlated to patient outcomes. It has been found that these pre-existing antibodies can effectively bind to PEGylated therapeutics and effect efficacy,[39,40,92,93] but their effect on safety appears to vary from one therapeutic to another. Each novel therapeutic should therefore be evaluated on a case-by-case basis. As this field is further developed, we also expect that the assays used to detect these antibodies will need to be standardized to improve consistency and translatability across studies.

Table 1.2. Prevalence of pre-existing anti-PEG antibodies across different studies.

Year	Sample Population (Location)	Sample Number	Female /Male	Anti-PEG Antibody Positive	Anti-PEG IgM Positive	Anti-PEG IgG Positive	Anti-PEG IgM and IgG Positive	Correlations between Antibody and Demographic Characteristics	Assay Method	Ref
1984	Naive healthy donors (Japan, Germany, Italy)	453 (Japan: 142; Germany: 151; Italy: 160)	NR	0.2%	NR	NR	NR	NR	Hema-gglutination	24
1984	Naive allergy donors	92	NR	3.3%	NR	NR	NR	NR	Hema-gglutination	24
2004	Naive healthy donors	350	NR	Hema-gglutination: 26.9% Flow cytometry: 27.7%	5.1%	19.1%	3.4%	NR	Hema-gglutination Flow cytometry (for subtyping)	88
2006	Naive gout patients	13	3/10	38.5%	NR	NR	NR	Subjects with pre-existing antibodies cleared drug faster	Direct ELISA against PEG-uricase + competition ELISA with PEG-uricase	58
2007	Naive gout patients	24	4/20	NR	NR	8.3%	NR	Subjects with pre-existing Abs cleared drug faster	Direct ELISA against 10 kDa PEG-glycine	59
2007	Naive pediatric acute lymphoblastic leukemia patients	16	6/10	Hemagglu-tination: 13% Flow cytometry 38%	38%	NR	NR	Anti-PEG antibodies were correlated with faster clearance of PEGylated asparaginase	Hema-gglutination Flow cytometry (for subtyping)	55
2010	Naive hepatitis C (HCV), non-alcoholic-steato-hepatitis (NASH), and systemic-lupus-erythe-matous (SLE) patients and naive healthy donors	Naive HCV: 68 NASH: 30 SLE: 40 Healthy: 30	NR	Naive HCV: 44% NASH: 6.6% SLE: 7.5% Healthy: 6.9%	NR	NR	NR	HCV patients exhibited higher incidence of anti-PEG antibodies Antibodies did not impair therapeutic efficacy Antibody titers declined over course of treatment	Direct ELISA against PEG-uricase + competition ELISA with PEG-uricase and 10 kDa PEG	53
2011	Naive Healthy Donors	350	NR	4.3%	NR	NR	NR	NR	Bridge assay against 40 kDa PEG using hapten-PEG-40 kDa	22
2014	Naive severe gout patients	30 (3/30 were not naive)	8/22	19%	NR	NR	NR	3/30 non-naive patients exhibited anti-	Direct ELISA against PEG-uricase +	60

								PEG antibodies 5/10 non- or transient responders exhibited pre-existing anti-PEG antibodies	competition ELISA with 10 kDa PEG-diol	
2014	Naive phenyl-ketonuria patients	25	10/15	16%	4%	12%	NR	Neither pre-existing nor induced antibodies appeared to be related to any negative outcomes All subjects exhibited anti-PEG antibodies after receiving rAvPAL-PEG	NR	63
2015	2 cohorts of naive chronic hepatitis B infected HBeAg+ subjects (Cohort 1 received interferon lambda-20 kDa PEG; Cohort 2 received interferon-alpha-20 kDa PEG)	Cohort 1: 32 Cohort 2: 22	NR	Cohort 1: 6.3% Cohort 2: 9.1%	NR	NR	NR	All subjects who had at least one positive sample for anti-PEG antibodies also displayed anti-interferon antibodies Anti-PEG antibodies could be transient or persistent (only 7.4% persistent) Anti-interferon antibodies were more frequent, persistent, and higher titer than anti-PEG antibodies	Bridge electro-luminescent assay using biotinylated and ruthen-ylated Interferon-(lambda or alpha)-PEG-20 kDa against streptavidin + competition with 40 kDa branched PEG Direct electro-luminescent assay using biotinylated interferon-(lambda or alpha)-20 kDa PEG against streptavidin	54
2016	Naive acute coronary syndrome patients	354	NR	36%	NR	NR	NR	Pre-existing anti-PEG antibodies were determined to be a major (but not sole) contributor for triggering first-exposure allergic reaction to pegnivacogen; 3 serious allergic reactions caused termination of phase 2b clinical trial	Direct ELISA against PEG-uricase + competition ELISA with 10 kDa PEG-diol	70

2016	2 cohorts of naive healthy donors (Cohort 1: Austria; Cohort 2: Austria and US)	Cohort 1: 710 Cohort 2: 600 (100 from Austria and each of 5 US cities)	NR	Cohort 1: 23% Cohort 2: 24%	Cohort 1: 13% Cohort 2: 14%	Cohort 1: 15% Cohort 2: 12%	Cohort 1: 5% Cohort 2: 2%	No reported difference between male/female Higher incidence for younger subjects Significant variation was observed between locations for IgG, but not for IgM	Cohort 1: Flow cytometry Cohort 2: Direct ELISA against HSA-20 kDa-PEG + competition ELISA using 20 kDa mPEG 95.8% agreement was found between the two approaches	91
2016	Naive hemophilia patients (Austria; naive to PEGylated drugs)	110 (Hemophilia A: 93; Hemophilia B: 17)	NR	6%	NR	6%	NR	NR	Direct ELISA against HSA-20 kDa-PEG + competition ELISA using 20 kDa mPEG	91
2016	Naive healthy donors (Austria; longitudinal screen over 14 months)	38	NR	NR	18.4% (7/38) confirmed positive for at least one time point 71.4% (5/7) exhibited persistent antibody expression	28.9% (11/38) confirmed positive for at least one time point 72.7% (8/11) exhibited persistent antibody expression	NR	Anti-PEG antibodies in healthy individuals could be transient or persistent No pathology was associated with transient or persistent antibodies Anti-PEG antibodies did not bind any of 36 human tissues	Direct ELISA against HSA-20 kDa-PEG + competition ELISA using 20 kDa mPEG	91
2016	Naive healthy donors (Taiwan)	1504	748/756	44.3%	27.1%	25.7%	8.4%	Higher IgM and IgG for females than males (IgM: 32.0% vs 22.2%; IgG 28.3% vs 23.0%). Higher incidence for younger subjects (up to 60% for 20 year olds vs 20% for >50 year olds)	Direct ELISA against 10 kDa H_2N-PEG-NH_2 + competition ELISA using PEG-liposomes	92
2016	Naive healthy donors (US)	Contemporary: 377 1970s: 30 1980s: 30 1990s: 19	Contemporary: 151/226 1970s: 15/15	Contemporary: 72% 1970-1999: 56%	Contemporary: 25% IgG_1: 26% IgG_2: 57% IgG_3:	Contemporary: 18% 1970-1999: 20%	Contemporary: 30% 1970-1999: 16%	No correlation between antibodies and race observed Females were more likely to possess anti-PEG IgM, but	Direct ELISA against 5 kDa PEG-diglyceride + competition ELISA using 8 kDa PEG-diol or 40 kDa PEG-	89

			1980s: 15/15 1990s: 6/13		1% IgG_4: 1% 1970-1999: 19%			not IgG Small correlation between age and antibody prevalence and concentration with higher incidence observed for younger subjects	myoglobin	
2019	Naive donors (US)	100 healthy 50 obese 50 Type 2 diabetes	NR	97.5%	NR	NR	NR	NR	Direct ELISA against BSA-20 kDa-PEG + competition ELISA using BSA-20 kDa-PEG Immuno-depletion, kinetic binding, immuno-precipitation, western blot validating experiments	23

NR, not reported.

1.5 Methods of Anti-PEG Antibody Detection

Detection assays have evolved and converged significantly over the years. Early efforts to detect antibodies were carried out using the method of hemagglutination whereby PEG-coated red blood cells were incubated with serial dilutions of sera and settling patterns were observed and used to estimate antibody titers.[24,34,87] As these assays were qualitative in nature, secondary techniques were required to verify the results such as radial gel immunodiffusion[24,34] and flow cytometry.[87] A number of additional antibody detection methods have since been developed and evaluated including western blotting,[94] an acoustic membrane microparticle assay,[95] surface plasmon resonance,[96] electrochemiluminescent assays,[54] and enzyme-linked immunosorbent assays (ELISA).[97] Several of these assays have been briefly reviewed[98] as well as related techniques to assess PEGylated molecules.[99] Despite the variety of available methods for detecting anti-PEG antibodies, by far the most common are ELISAs as they are robust, sensitive,

modular, and do not usually require complex equipment. The remainder of this section will therefore discuss various assay formats and best practices when implementing these assays.

Though most anti-PEG antibodies are detected by ELISA, the assay formats vary considerably from one report to another, and while some are thoroughly validated, others are problematic and have incited controversy.[100] While there are some reports of bridging assays for detection of anti-PEG antibodies in serum,[22,54] most immune studies rely on direct ELISA formats. As shown in Figure 1.3, a direct ELISA is performed by first coating an antigen onto the wells of a microtiter plate, then excess antigen is washed away and the remainder of each well is blocked, often with bovine serum albumin. After washing and drying, diluted sera samples are plated and incubated to allow serum antibodies to bind to the antigen, then wells are washed and dried again and finally a labeled capture antibody is added and used to visualize the serum antibody concentration in each well. Visualization is often colorimetric, fluorescent, or chemiluminescent. Several factors make the detection of anti-PEG antibodies challenging to measure compared to other serum antibodies.

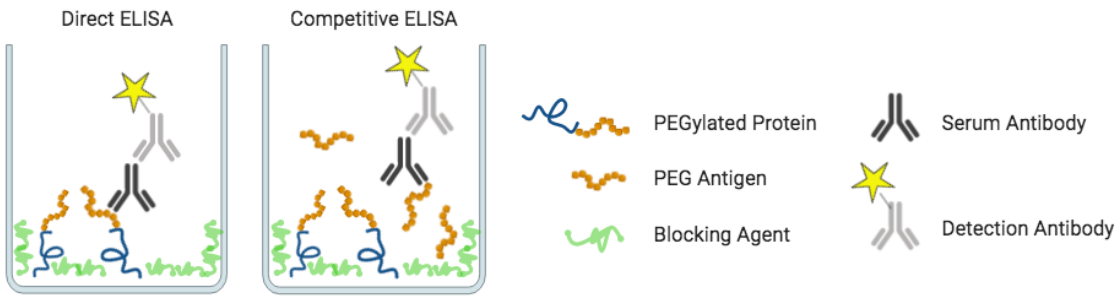

Figure 1.3. Direct and competitive ELISAs are commonly used to detect anti-PEG antibodies. Direct ELISAs establish antibody titer while competitive ELISAs can confirm the specificity of antibodies to PEG and to control for nonspecific adsorption. Choice of detergent, antigen, and blocking agent are also important for achieving good assay sensitivity and reproducibility.

First and foremost, because anti-PEG antibodies are cross-reactive with different PEGylated molecules, it is imperative that PEG-containing detergents like Tween be omitted from these assays as they have been shown to artificially lower antibody signal.[23,100] One solution to this challenge is to simply omit PEGylated detergents and this strategy has been employed by a number of groups.[38,89,92,101] However without detergents, nonspecific adsorption can become problematic, leading to artificially high assay signals. An alternative option is to replace PEGylated detergents with other nonionic surfactants such as n-dodecyl-beta-D-maltoside (DDM), which, along with other similar detergents, can minimize nonspecific adsorption while also not attenuating serum antibody signal.[23] However, the high cost of these alternative nonionic surfactants relative to their PEGylated counterparts can be a deterrent.

A second challenge surrounds the choice of which PEGylated molecules to use as antigens in ELISAs. Since PEG itself is a highly hydrophilic, nonfouling polymer, its direct use to coat the wells of microtiter plates can be a concern.[27] While free PEG has been used in direct ELISAs with apparent success,[92] most of the time PEG is conjugated to a more hydrophobic moiety such as a lipid[89] or protein.[23] This practice has been infrequently addressed in the

literature and warrants further investigation. It is clear that the nature of the antigen used to coat a microtiter plate can affect the results of the assay. Shiraishi et al. found that when equivalent amounts of two polymers were used to coat microtiter plate wells, a diblock copolymer containing a hydrophilic PEG block and a hydrophobic block versus a triblock copolymer with an anionic block between PEG and the hydrophobic block, longer anionic segments of the triblock copolymer more effectively suppressed anti-PEG IgM binding.[102] The authors also showed that this principle was applicable to PEGylated micellar drug delivery vehicles,[103,104] and in these reports suggest that the anti-PEG antibody binding epitope may require some hydrophobic component in addition to the PEG backbone. While this hypothesis provides insight into how the differences in antigen polarity can affect antibody binding, especially in the context of immunoassays, further investigation is required to determine effects of hydrophobicity on epitope recognition. Earlier this year, Roffler and coworkers reported the first crystal structure of an antibody Fab fragment with PEG and confirmed that the binding epitope for their previously developed anti-PEG antibodies is the PEG backbone ($-CH_2-CH_2-O$)[105] The most commonly observed binding mode did not require hydrophobic contacts beyond those provided by free PEG, however, these observations were made under crystallographic conditions, and epitope binding could change in different environments.

In addition to considerations surrounding the choice of detergents and PEGylated antigens used for these assays, researchers must also employ necessary controls and validation techniques to ensure assay reliability, reproducibility, and relevance. Regardless of ELISA format, all assays should include positive and negative controls. Negative controls typically consist of naive serum prior to administration of PEGylated molecules and are used to correct for

background adsorption. Immunodepletion of serum samples can also be implemented as a negative control to confirm that anti-PEG signals are due to anti-PEG antibody binding.[23]

Most studies report the use of negative controls, but positive controls can be less common. Positive controls are most frequently incorporated by substituting known amounts of commercially available monoclonal anti-PEG antibodies (either IgM or IgG) in place of serum samples. Serial dilutions of these antibodies can also be evaluated to generate a standard curve. The major limitation of this approach is that the standard curve can only give an approximation of the assay sensitivity and dynamic range and cannot be used to directly quantify antibody concentration from serum samples because these antibodies could be different from those induced in study subjects. Because these antibodies provide only an approximation, assay signal is often reported in terms of absorbance units or as a titer. Nevertheless, these positive controls are paramount for assay reliability.

Crucial in these assays are also controls that confirm that antibodies are bound to PEG itself versus an attached biomolecule or nonspecific adsorption. To ensure specificity against PEG, each sample analyzed by direct ELISA should also be analyzed via competitive ELISA wherein free PEG or another PEGylated antigen is incubated with the serum samples and allowed to compete for binding of serum antibodies with the coated antigen. Samples that generate a high anti-PEG antibody signal in a direct ELISA will show diminished signal in a competitive ELISA if the epitope is PEG specific. This secondary assay can thereby confirm the specificity of serum antibodies for PEG. This technique has proven useful in clinical studies to identify antibodies specific to PEG for PEGylated interferons,[54] uricase,[58,60,61] and for the PEGylated aptamer pegnivacogin.[70]

In summary, there are many factors to consider when developing an immunogenicity assessment for a PEGylated biomolecule. We expect that the lack of assay uniformity across the literature reflects the different needs and requirements for each study. Regardless of the assay format, however, ELISA-based serum antibody concentration assessments should at minimum be designed and implemented with suitable positive and negative controls. Additionally, if detectable antibody signal is acquired, specificity of the serum antibody to PEG should subsequently be confirmed via a competition assay. A number of reported assays have received criticism for lack of procedural detail and incorporation of necessary controls,[100,106] and many such examples have since been published. We have therefore included this section to offer guidance to researchers investigating the immunogenicity of PEGylated biomolecules. While we have discussed a number of important considerations for ELISA-based immunogenicity assessments, this section is by no means comprehensive on the topic. For additional resources, we recommend helpful reviews that consolidate and summarize various guidance documents.[5,66,107]

1.6 Mechanism of Anti-PEG Antibody Induction

The mechanism of anti-PEG antibody induction for PEGylated therapeutics has been investigated several times in the recent past, but is not yet fully understood. Most research in this area has focused on PEGylated liposomes, and while many aspects overlap with PEGylated biomolecules, minor differences have also been observed. Especially with regard to the accelerated blood clearance phenomenon observed for PEGylated liposomes, considerable progress has been made, which, despite some conflicting observations, has led to the proposal of a reasonable mechanism. After the first injection of PEGylated liposomes, anti-PEG IgM is

produced and secreted by the spleen.[108] While most B-cells are compartmentalized in the follicle zone of the spleen, PEGylated liposomes have been determined to primarily bind B-cells within the marginal zone, which then cross-link in a multivalent fashion (Figure 1.4B).[109] Crosslinking occurs when 10-20 antigen receptors are clustered on the membrane of B-cells, which recruits Btk (Bruton's tyrosine kinase) molecules to the membrane.[110] This process mobilizes intracellular calcium, leading to upregulation of transcription factors and ultimately to T-cell independent proliferation of B-cells. PEGylated liposomes are considered a type two T-cell independent (TI-2) antigen because there are no peptide sequences to present to T-cells and the surface contains a highly repetitive structure. Upon a second injection of PEGylated liposomes, these antibodies bind to the liposome and cause rapid activation of the complement system and clearance by Kupffer cells in the liver.[111]

Fewer studies have focused on antibody induction of PEGylated proteins. In rats that underwent a splenectomy, an injection of PEG-BSA resulted in suppressed anti-PEG IgM induction.[112] This observation supports the hypothesis that anti-PEG antibodies for PEGylated proteins originate within the spleen, similar to PEGylated liposomes. Furthermore, Kiwada and coworkers found that an initial PEGylated ovalbumin (PEG-OVA) injection was sufficient to cause accelerated clearance of a secondary PEGylated liposome injection.[113] Together these studies potentially suggest that the anti-PEG IgM induced by both a PEGylated liposome and PEGylated protein react similarly against both therapeutic classes with respect to the PEG antigen, with both induction mechanisms acting independently of T-cells. However, the opposite induction scheme was not observed: the IgM induced by PEGylated liposomes did not cause accelerated clearance of PEG-OVA.[113] Additionally, this study also revealed that athymic rats, which lack T-cells, were unable to produce anti-PEG IgM against PEG-OVA, suggesting that

antibody induction against PEGylated proteins may in fact be T-cell dependent.[113] Consequently, evidence also exists that the IgM of these therapeutic classes may not fully cross-react or may act within different immunogenicity pathways altogether. Moreover, T-cell independent immunogenicity usually does not cause antibody class switching. In direct contrast to this trend, the class switching phenomenon was observed by Judge et al., where an initial IgM response to PEGylated liposomes was replaced by an IgG response.[114] This may have been caused by excessive B-cell stimulation, or by induction of antibodies by a different immunogenicity pathway.[115] Overall, the dependency of immunogenicity on T-cells for both PEGylated liposomes and proteins have yet to be elucidated fully, and warrants further investigation.

For the case of T-cell dependent immunogenicity, the established clearance mechanism has been well-summarized by Rosenberg and Sauna (Figure 1.4A).[116] First, an antigenic PEGylated protein is taken up by antigen presenting cells (APC), such as dendritic cells or B-cells. The therapeutic protein is then cleaved into smaller peptides by proteolysis. Next, HLA-II (human leukocyte antigen) molecules bind to these peptides, and the resulting complex is presented on the cell surface. In humans, HLA-II are major histocompatibility complex cells that have specialized antigen recognition. $CD4^+$ T-cells with specific receptors for this complex can recognize the peptide-HLA-II species on the cell surface, causing upregulation of APC, T-cells, and cytokines. Ultimately this leads to proliferation and increased immune response to continued exposure to the antigenic therapeutic. T-cell independent antigens are also susceptible to this pathway. For example, marginal zone splenic B-cells may capture an APC complex that was induced by an IgM T-cell independent process and present the complex to T-cells.[117] T-cell independent antigens that form complexes with splenic B-cells can also be cleared by macropinocytosis, phagocytosis, or receptor-mediated endocytosis into immature dendritic

cells.[117] This may explain why subcutaneous injections are often more immunogenic when compared to other administration routes; Langerhans Cells (LC), or skin tissue-resident dendritic cells, are in close proximity and available to immediately participate in endocytosis. Finally, the immunogenic complex can also be opsonized with the complement system through uptake by CR-1 and CR-2 receptors.[117] The induction of anti-PEG antibodies and subsequent accelerated blood clearance is observed to occur in a wave pattern: after an initial injection, anti-PEG antibodies increase on day 3, peak at day 5, and decrease until their elimination by day 28.[118,119] This was further demonstrated by Li et al. wherein an immunogenic response was observed if a PEGylated therapeutic was administered within the first week of an initial injection, but was absent if the interval time was prolonged to four weeks.[120] The duration of dosage intervals may be critical for the increased efficacy of PEGylated therapeutics, which is a modular variable in prescription regiments.

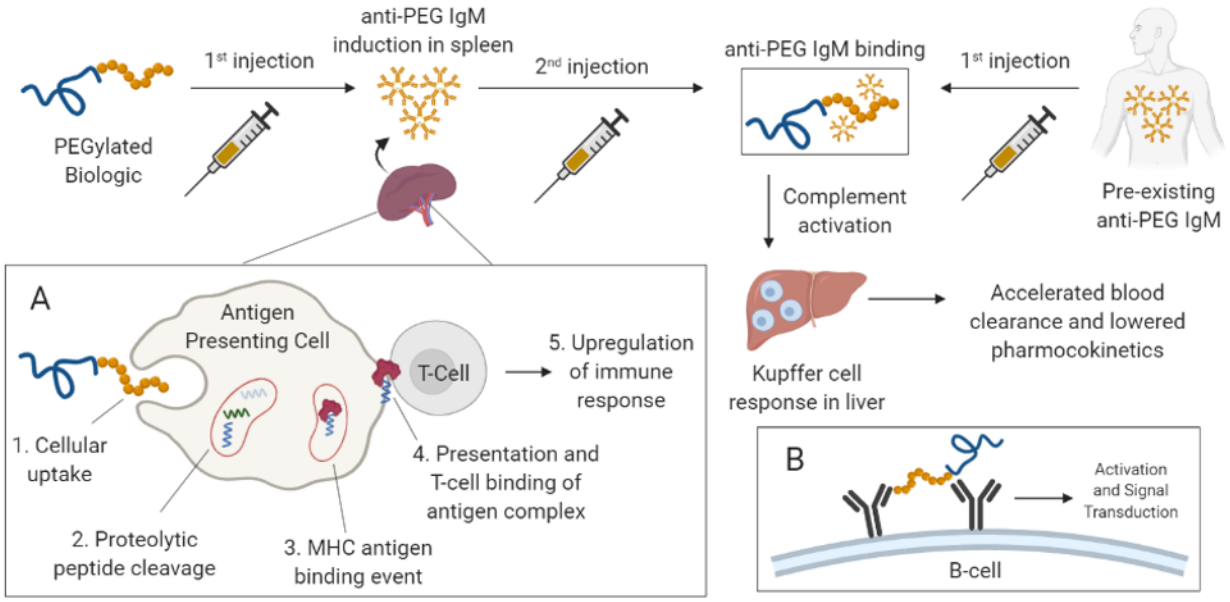

Figure 1.4. Induction of anti-PEG antibodies against PEGylated biologics. Upon the first injection, anti-PEG is induced within the spleen either (A) via a T-cell dependent involving MHC antigen binding and presentation to T-cells, or (B) T-cell independent mechanism involving B-cell antigen receptor cross-linking. Upon a second injection,

anti-PEG antibodies bind and activate the complement system, leading to Kupffer cell activation in the liver and accelerated blood clearance. Alternatively, accelerated blood clearance can occur upon a single injection in the presence of pre-existing anti-PEG antibodies.

PEGylated liposomes and proteins can activate similar complement activation pathways in order to facilitate accelerated clearance. For both systems, splenic B-cells recognize either the PEG sequence or PEG conjugation site and cross-link to produce anti-PEG IgM.[121] However, IgM cannot itself induce phagocytosis because there are no Fc receptors for IgM on macrophage surfaces. Instead, the IgM for both PEGylated liposomes and PEGylated proteins, such as PEGylated BSA, have been observed to activate complement factors and hepatic Kupffer cells to facilitate opsonization.[119] This process is known as the classical pathway for complement activation, which has been determined to be the primary pathway for liposomes.[122] In the case of PEGylated proteins, as was observed for PEGylated BSA, complement activation was dependent on molecular weight as 30 kDa PEG-BSA induced greater complement activation than 2 kDa PEG-BSA.[112] Similar complement activation pathways among PEGylated liposomes and proteins may indicate that opsonization is fully dependent on recognition of either the PEG chain or the conjugation site rather than the therapeutic type.

In contrast to the classical complement activation described above, both PEGylated liposomes and PEGylated proteins have also been observed to activate the complement system using either the mannose-binding lectin or alternative pathway. These pathways are not mediated by the presence of antibodies and can therefore be activated by a single dose of PEGylated therapeutics. For example, PEGylated liposomes carrying chemotherapy payloads, such as Doxil and AmBisome, cause complement activation after a single dose.[123] It is speculated that this may also be the case for PEGylated proteins, such as the PEGylated erythropoietin therapeutic known

as Peginesatide. This therapeutic has been removed from the market due to deaths resulting from anaphylaxis. As previously noted, antibody induction occurs over the course of multiple days, and only reaches a maximum at the fifth day.[118,119,120] In the case of peginesatide, clinical symptoms were observed within 30 minutes of the first administration, indicating that the immune response may have occurred in a complement pathway that was antibody-independent.[121,124] This observation is notable in that it suggests that elimination of antibody induction may not fully resolve the issue of PEG immunogenicity.

Pre-existing anti-PEG antibodies can also lead to accelerated blood clearance for PEGylated liposomes as well as PEGylated proteins. For instance, after mice were immunized with a single dose of PEGylated liposomes, a second dose can lead to lower blood circulation times relative to the first dose due to accelerated blood clearance.[125] While in many cases liposomes demonstrate accelerated blood clearance after a single dose, PEGylated proteins vary in their ability to generate an immune response. As noted in previous sections, proteins like asparaginase, uricase, and phenylalanine ammonia lyase can induce anti-PEG antibody production following a single dose, but this is not always the case. As an example, a negligible IgM response was observed in mice that received a single dose of Pegasys (peginterferon alfa-2a), and the first dose had little effect on the pharmacokinetics of the second dose. This pattern remained true even after four sequential clinically-relevant doses.[126] However, when the authors immunized mice with PEGylated ovalbumin before dosing Pegasys, the authors observed low concentrations of Pegasys at all time points, suggesting that pre-existing anti-PEG IgM antibodies facilitated clearance of Pegasys.[126] While the antibody response produced in mice following injection with PEGylated ovalbumin may not perfectly reflect clinically relevant anti-PEG antibody titers, it nevertheless demonstrates the potential for pre-existing anti-PEG

antibodies to facilitate accelerated blood clearance of PEGylated proteins in a manner similar to that observed for PEGylated liposomes. The increasing incidence of pre-existing anti-PEG antibodies in the naïve general population is therefore concerning, especially given the possibility that antibodies from other sources can affect the efficacy of a drug more than repeated injections of the drug itself. With the increased pervasiveness of PEG in consumer goods, further studies will need to be conducted to better understand the acquisition of pre-existing anti-PEG antibodies and their effects on PEGylated therapeutics.

1.7 Factors Affecting Anti-PEG Antibody Response

Before devising strategies to avoid or overcome the challenges associated with induction of anti-PEG antibodies, it is important to first consider some of the factors that affect the immunogenic potential of PEG. Many of these factors and their effects on immunogenic outcomes have already been alluded to in prior sections including effects of dose, route of administration, and carrier protein as well as demographic characteristics like age, sex, geographic location, and health status. It has also been noted that there may be a genetic predisposition toward production of anti-PEG IgM antibodies.[127] Most of these represent dispositional or environmental factors whose influences on immune responses may be difficult to predict or control. Rather than reiterate how these influences can impact the safety and efficacy of biotherapeutics, we will instead discuss how modulation of the chemical properties of PEGylated biomolecules can affect immune responses. Due to the simple chemical structure of PEG, chemical modification of PEGylated biomolecules is limited to only a few key parameters: the molecular weights of conjugated PEG chains and of the entire conjugate, surface coverage density, and the hydrophobicity of PEG end groups.

As discussed previously, the immunogenic potential of PEG is usually directly related to the immunogenic potential of the attached biomolecule. Accordingly, it is desirable to implement PEGylation strategies in ways that most effectively mask antigenic epitopes in surface-exposed regions of biomolecules. Ideally, the surface of a therapeutic agent of interest could be completely covered with high molecular weight PEG in order to fully shield the agent from immune system recognition. While this approach may be practical for liposomes[128] or red blood cells[42] that rely primarily on diffusion to exert their effects, therapeutic biomolecules typically rely on specific interactions (e.g. with receptors) to affect biological outcomes, which may be hindered by excessive PEGylation. Especially for known immunogenic proteins, PEG size and surface coverage must often be tuned to balance suppression of immune responses and pharmacokinetics with pharmacodynamics.[129]

In their seminal work, Abuchowski et al. illustrated the effect of PEG molecular weight on the suppression of immune responses against antigenic proteins by showing that 5 kDa PEG was more effective than 1.9 kDa PEG in preventing antibody production against nonspecifically PEGylated bovine serum albumin, even when 5 kDa conjugates contained fewer overall conjugated PEG chains.[20] A similar finding was observed for the difference in immunogenicity of uricase conjugated to equivalent numbers of either 5 kDa or 10 kDa PEG chains.[37] Increased PEG surface coverage has also been shown to reduce antibody production against antigenic proteins. In another report, Abuchowski et al. demonstrated that antibody response against PEGylated catalase was related to the extent of PEGylation, as conjugates with 13% of all amino groups modified showed significant immune response compared to conjugates with 19%, 27%, and 43% modification showing progressively lower responses.[21] Richter and Åkerblom later observed that ovalbumin conjugated to 6 PEG chains of 11 kDa elicited antibody production in

rabbits, but when the number of conjugated PEG chains was increased to 20, no such response was observed.[34] As a result, a number of FDA-approved PEGylated proteins are heavily modified, especially those proteins derived from non-human sources.

In addition to the molecular weight of PEG, the molecular weight of the PEGylated biomolecule can also affect the likeliness of immune stimulation. While this observation has mostly been used to explain the accelerated clearance of liposomes, micelles, and other nanoparticles,[130–133] high molecular weight PEGylated proteins can also enter similar size regimes and may therefore be subject to similar immunostimulatory mechanisms as these nanoparticles. Though the immunogenicity associated with PEGylated asparaginase, uricase, and phenylalanine ammonia lyase are likely primarily due to their derivation from other organisms, the high molecular weight of each PEGylated tetrameric protein (~516 kDa, ~540 kDa, and ~1000 kDa, respectively) may also be a contributing factor.

Interestingly, whereas higher degrees of PEGylation and higher molecular weight PEG chains can dampen or prevent immune responses against immunogenic biomolecules, if anti-PEG antibodies are induced, these antibodies actually demonstrate improved binding to larger PEG chains than smaller ones. When comparing relative binding affinities of anti-PEG antibodies to PEGs of various molecular weights ranging from 0.3-6,000 kDa, antibodies were generally found to bind to higher molecular weight PEGs with 40 kDa PEG demonstrating binding at the lowest antibody concentration assessed by gel diffusion assays.[34] These antibody binding observations have also been corroborated by several other studies. For example, Saifer et. al also found that the binding affinities of anti-PEG antibodies depended more on the backbone length of PEG than on other factors. In another instance, Cheng et. al found that sensitivity of an ELISA assay using a monoclonal anti-PEG antibody was dependent on the

length of the protein-conjugated PEG chain, with longer PEGs providing dramatically improved assay sensitivity.[134] This observation further complicates the choice PEGylation strategies. PEG chains attached to a biotherapeutic must be large and abundant enough to deter stimulation of immune responses, but these same factors will likely increase the rate of clearance if anti-PEG antibodies are induced.

Another minor contributor to PEG's immunogenicity is the hydrophobicity of its end groups. In a study intended to elucidate the effect of the methoxy end group on the immunogenicity of PEG, Sherman et. al reported that methoxy terminated PEG conjugates for several proteins consistently yielded higher anti-PEG antibody titers than their alcohol terminated counterparts. The authors further found that a tert-butyloxy terminated PEG-albumin conjugate generated an approximately 8-fold higher antibody titer than the corresponding alcohol terminated conjugate, and approximately 5-fold higher titer than the corresponding methoxy terminated conjugate.[135] A follow up study by the same group with the objective of narrowing the epitope to which anti-PEG antibodies bind was reported. After inducing anti-PEG antibodies in rabbits with either methoxy or alcohol terminated PEG conjugates of three unrelated proteins, the authors performed competitive ELISAs with a variety of PEG-based reagents and found that while none of the monoclonal or polyclonal antibodies tested were absolutely specific to methoxy end groups or backbone epitopes, distinct relative selectivities were observed. During this work, it was also found that binding affinities depended more on the length of the PEG polymers than the hydrophobicity of the end group.[136]

On the opposite end of the polymer, the hydrophobicity of the linkage between PEG and its conjugation partner have also been implicated in the resulting immunogenicity of PEG. Previously noted studies have investigated the *in vitro* and *in vivo* immunogenicity against

PEGylated micelles resulting from conjugation of PEG to hydrophobic polymers and have suggested that a significant portion of the immunogenicity may result from this linkage.[102–104] However, because free PEG (without this linkage) can inhibit binding of anti-PEG antibodies to PEGylated antigens in competitive ELISAs, this proposal does not provide a complete explanation for the epitope of anti-PEG antibodies. Hydrophobicity may still play a role in antibody selectivity, but the end group may not necessarily need to be the source of this interaction. In a screen of 6 commercially available and 2 recombinantly expressed anti-PEG IgM and IgG antibodies, McCallen et al. discovered that 5 of the 8 could bind polymers with similar structural motifs to PEG including poly(propylene glycol), poly(tetramethylene ether glycol), and poly(1,4-butylene adipate).[137] As expected, the common binding epitope was suggested to be the iterative oxyethylene (-CH_2-CH_2-O) motif, common to each of the noted polymers. Though this study did not uncover the precise antigenic epitope recognized by anti-PEG, it did demonstrate the potential for cross-reactivity of anti-PEG antibodies with other oxyethylene-containing polymers, which may have implications for immune responses against polymers with structural similarities to PEG.

A number of groups have studied the specific epitope binding requirements for PEG, and although the hypothesized binding mechanisms have not yet been universally explained, significant strides over the past few years have provided new insights. The epitope of anti-PEG antibodies has primarily been investigated through competitive ELISA or other immunoassays, with various types of PEG polymers, oligomers, and macrocycles being used as competitive binders. Richter and Åkerblom were the first to investigate the epitope and found that 300 Da PEG could inhibit hemagglutination of PEGylated red blood cells, suggesting that the antigenic epitope could comprise as few as 6-7 oxyethylene units.[34] A later study by Saifer et al. reported

that anti-PEG antibodies raised in rabbits bound to and could distinguish as few as 3 oxyethylene units.[136] Notably, it is very likely that this number differs among antibodies produced across studies due to individual and species differences. For example, monoclonal mouse anti-PEG IgM and IgG antibodies produced by the Roffler group and available commercially require at least 16 oxyethylene subunits to bind to PEG.[36] The Roffler group also recently reported the crystal structure of the Fab fragments of these antibodies with PEG that supports their previous observation that binding requires ~16 oxyethylene units and interestingly found that one molecule of PEG could actually allow two Fab molecules to dimerize around an S-shaped PEG.[105] As the authors note, the structures provided may not necessarily apply to the other anti-PEG antibodies, but these results provide the first example of such an interaction and will likely be used in the near future to further explore the binding modes of other anti-PEG antibodies as well as other forms of PEG.

While the majority of this section has focused on how chemical properties can affect the immunogenicity of PEGylated biotherapeutics, there are numerous factors that contribute to individual responses. It should also be noted that the chemical properties discussed above pertain predominantly to PEGylated biomolecules, and factors affecting the immunogenicity of other PEGylated particles such as nanoparticles, micelles, liposomes, etc. may differ. For an excellent overview of these considerations, we recommend the prominent review from the Ishida group.[133] Although the mechanisms and factors surrounding the induction of anti-PEG antibodies remain incompletely understood, many recent observations and key advances have provided sufficient insight, allowing researchers to not only better understand the issues associated with PEG immunogenicity, but also to begin addressing these issues with creative solutions.

1.8 Strategies for Overcoming Anti-PEG Antibody Responses

Even with the extensive investigation in recent years, many details regarding the mechanism and factors contributing to the immunogenicity of PEG remain unclear, making it difficult to predict not only the extent to which a given therapeutic may induce anti-PEG antibodies, but also how this issue may be circumvented. Given the clear and growing body of evidence that specific antibody responses can be raised against PEG and contribute to decreased safety and efficacy for PEGylated biologics, strategies to overcome these obstacles are highly desirable. One approach that has not been systematically explored, but has been occasionally referenced in clinical reports is to co-administer immunosuppressive agents alongside PEGylated therapeutics to subside antibody production or responses.[60,61,138,139] However, immunosuppressive agents can be associated with side effects and increased risks that could be unadvisable depending on existing illnesses of a given patient. Additionally, this would likely be at the discretion of a patient's attending physician and this option would also need to be assessed on a case-by-case basis.

Another strategy that may offer more universal utility consists of saturating circulating anti-PEG antibodies with a sacrificial source of PEG prior to injection of a PEGylated therapeutic. McSweeney et al. recently employed this strategy by intravenously injecting into mice that had been passively immunized with anti-PEG antibodies either 2200 mg/kg of 10 kDa PEG-diol or 550 mg/kg of 20 kDa or 40 kDa PEG-diol 30 minutes prior to injection of PEGylated liposomes. The authors found that pre-infusions of 20 kDa and 40 kDa PEG could effectively restore prolonged circulation of PEGylated liposomes to that of non-immunized mice, but 10 kDa PEG could only partially rescue exposure levels.[140] As the authors note, this strategy could potentially restore safe and effective use of PEGylated therapeutics in patients exhibiting

high anti-PEG antibody titers without the need for reformulation, although the high concentrations of free PEG used for these studies may present alternative concerns, especially given reports of hypersensitivity reactions to drug formulations containing PEG as an excipient.[46] A related example was also recently published by Chang et al. in which the authors determined that higher doses of PEGylated erythropoietin beta could be administered in mice to compensate for and overcome the accelerated clearance effects caused by pre-existing anti-PEG antibodies.[141] The authors termed this strategy "dosing through," which also effectively depletes serum anti-PEG antibodies to the point where circulation times return to expected profiles. While the practicality of these approaches requires further validation, these strategies nevertheless offer creative solutions that may eventually become useful for restoring the efficacy and safety profiles of PEGylated therapeutics.

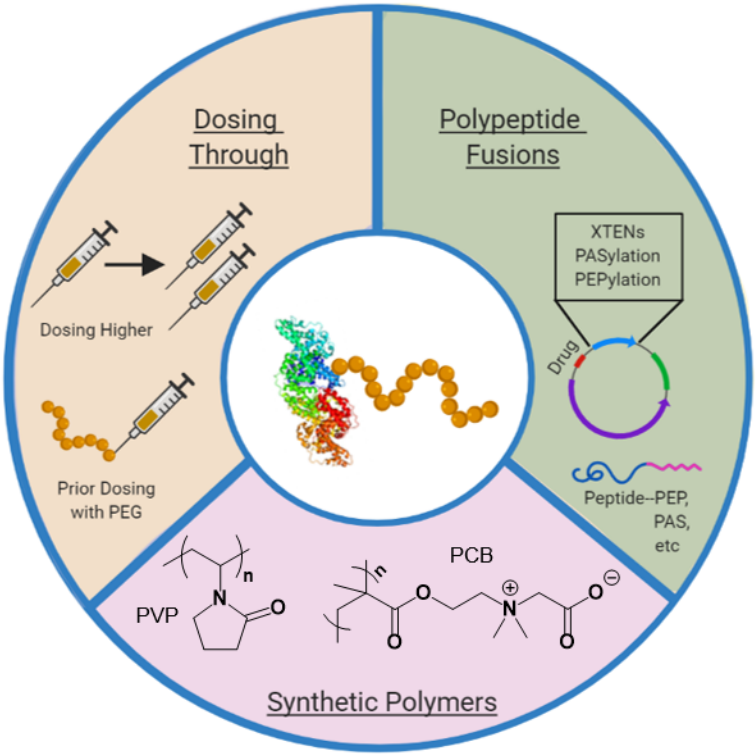

Figure 1.5. Strategies to overcome PEG immunogenicity. Dosing through involves increasing therapeutic doses to overcome losses of efficacy, or prior dosing with PEG to bind with existing anti-PEG antibodies. Polypeptide

fusions such as XTENs, PASylation, or PEPylation or synthetic polymers such as PVP and PCB can be used as alternative conjugates.

When it comes to addressing the challenges associated with anti-PEG antibody responses, the overwhelming majority of the literature has focused on the development of alternative polymers that provide opportunities beyond PEGylation. Especially with the increasing awareness of immunogenic potential associated with PEG over the past decade, the topic of alternatives to PEG has been reviewed by a number of groups, including ours.[7,17,98,142–145] Given the abundance of excellent reviews available, we will therefore limit our discussion of this topic to several recently developed technologies that have demonstrated promising results specifically with regard to immunological outcomes. Of the studied alternatives, most polymers fall into three distinct categories: biologically derived polymers, synthetic polymers, and polypeptide fusions. Biologically derived polymers such as hydroxyethyl starch (HES), dextran, and polysialic acid (PSA) have been extensively investigated and some have shown significant promise, but concerns in recent years pertaining to their immunogenicity and safety profiles has limited their development, especially for HES and dextran.[145]

Like PEG, the majority of synthetic polymers investigated as PEG alternatives have also been neutral, nonionic, water-soluble polymers. Examples of these polymers include poly((*N*-hydroxypropyl)methacrylamide) (HPMA), poly(vinylpyrrolidone) (PVP), poly(2-oxazoline) (POZ), poly(*N*-acrolylmorpholine) (pNAcM), poly(glycerol) (PG), and poly(poly(ethylene glycol) methyl ether methacrylate) (pPEGMA). Several of these polymers have also been directly compared to PEG under conditions known to induce anti-PEG antibodies. For example, in a study comparing the immune responses of uricase-polymer conjugates, both PVP and pNAcM uricase conjugates generated anti-polymer antibodies after the first dose while PEG-

uricase conjugates produced low levels of anti-polymer antibodies only after the second dose.[37] Like PEG, these polymers proved haptogenic when conjugated to a highly antigenic biotherapeutic, which emphasizes the challenges associated with development of alternative polymers. In spite of these challenges, there have been several reports of synthetic polymers that have successfully reduced immunogenicity of a carrier molecule when used to replace PEG.

Using prior knowledge of typical anti-PEG antibody binding epitopes, Qi et al. demonstrated that pPEGMA polymers could be effectively employed as PEG alternatives via tuning of the length of the oligo-ethylene glycol side chain length.[146] Bottlebrush pPEGMA polymers with side chains comprising 9 oxyethylene units were conjugated to the therapeutic peptide extendin-4 and exhibited significantly lower reactivity toward anti-PEG antibodies derived from clinical studies than FDA-approved PEGylated adenosine deaminase and uricase. Further reduction of the side chain length from 9 to 2 oxyethylene units completely abolished reactivity while maintaining the efficacy of the extendin-4 conjugate.[146] In a follow up study from the same group, these polymers were investigated as blocking agents for analysis of anti-PEG antibodies and it was determined that 2-3 oxyethylene units were optimal for reducing nonspecific adsorption of anti-PEG antibodies onto surfaces.[147] Although this strategy may provide relief from anti-PEG specific antibodies, neither study investigated antibody induction against pPEGMA via immunization, so it is unclear whether or not these polymers will induce anti-pPEGMA antibodies. However, a conceptually similar study that used on a poly(L-glutamic acid) backbone with pendant triethylene glycol side-chains showed that, at least for polypeptide backbones, antibody induction against the polymer could be reduced compared to PEG by using shorter oxyethylene segments.[148] This strategy, referred to as "PEPylation," may provide a promising platform for development of polypeptide-based PEG alternatives. Polypeptides are

biologically ubiquitous and may therefore provide improved biocompatibility compared to other synthetic polymers, however, these backbones have only recently been explored for the purpose of reducing immunogenicity and require further investigation. PG has also been investigated as a potential alternative to PEG for coating liposomes and was found to mitigate the accelerated blood clearance observed for PEGylated liposomes, even after repeated injections.[149] This may be in part due to the increased hydrophilicity of PG compared to PEG.

In addition to neutral, nonionic synthetic polymers, a number of zwitterionic polymers have been investigated as potential PEG alternatives. Like PEG, these polymers are nonfouling, possess large hydration spheres, and resist nonspecific protein adsorption when used to coat surfaces.[150] Though a number of groups have reported on the various applications of zwitterionic polymers and materials, the Jiang group in particular has made significant contributions towards the development of novel zwitterionic polymers for bioconjugation, with several recent examples that have effectively reduced antibody production when directly compared to PEG.[96,101,151–155] Specifically, the group has shown that polymers containing various backbones such as methacrylates, acrylamides, and amino acids consistently outperform PEG in terms of reducing the immunogenicity of an antigenic carrier protein, usually uricase. Most of these studies have focused on polymers with carboxybetaine side chains, as these appear to have the optimal balance of low cationic charge density and high anionic charge density that provides strong hydration, which is required to repel protein adsorption, but that also simultaneously limits self-association.[156] However, more recently other biomimetic side chains based on trimethylamine *N*-oxides and phosphoserine have been explored, expanding the scope of potential PEG alternatives. While these zwitterionic polymers have shown promise, one potential limitation may be the more complex synthesis as compared to PEG, which could increase costs and limit

the scalability of these polymers. Additionally, these polymers may not provide a universal solution, as it was recently reported that liposomes coated with polycarboxybetaines were able to induce an anti-polymer IgM in mice, leading to accelerated clearance.[157] Nevertheless, these studies and considerations underscore both the importance and opportunities in polymer chemistry for design and evaluation of novel polymers to address the unmet needs in bioconjugation.

Beyond synthetic polymers, polypeptide fusions have demonstrated tremendous success in extending the circulation half-lives of a wide variety of protein therapeutics, and have also been examined for their protective properties against immune stimulation. A number of technologies that consist of genetic fusions with unstructured polypeptides of specific amino acid compositions have been previously described in the excellent review by Strohl and include XTENylation, PASylation, ELPylation, HAPylation, and others.[7] These fusion constructs have several distinct advantages over synthetic or biologically derived polymers. First, they can be directly connected to proteins as genetic N- or C-terminal fusions, which can simplify production and manufacturing of the therapeutic by bypassing the conjugation step and potentially assist purification. Additionally, because these molecules are recombinantly expressed, they are biodegradable and have precisely defined sequences and molecular weights. Due to precise sequence control, these molecules are highly modular. For example, XTENs, which are engineered, nonimmunogenic polypeptides containing only six hydrophilic amino acids (A, E, G, P, S, and T) in random sequence, can be expressed as fusion proteins or independently.[158] If expressed independently, each XTEN polymer will have only one amino group, which can be selectively modified with a protein reactive group for subsequent bioconjugation. Alternatively, one or more cysteine residues can be introduced into the XTEN sequence, providing two

orthogonal handles for chemical modification. In this way, these molecules can be used not only as half-life extenders, but also as polymeric vehicles to which drugs, probes, or peptides can be appended via cysteine functionalization.[159] As with all expressed polypeptides, there are some production drawbacks when compared to synthetic polymers such as increased burden of purification, cost, and limitation to amino acid monomer units; however, these issues are relatively minor obstacles. These and other engineered polypeptides therefore provide exceptionally modular and promising alternatives to PEGylation.

1.9 Conclusions and Future Perspectives

From its debut in 1977, PEGylation rapidly became a mainstay in the field of biotherapeutics due to its proclivity for enhancing the pharmacokinetic properties of biomolecules while simultaneously reducing their immunogenicity. Its success is evidenced by the 15 distinct FDA-approved biologics that rely on this technology. As an FDA GRAS compound, PEG has also seen increased use in a variety of medications as well as consumer products, which has also likely increased the general populations exposure to PEG. In most cases, PEGylation has continued to be an asset, but especially in more recent years the limitations of this technology have become apparent as evidenced by the concerns surrounding its safety and efficacy when conjugated to antigenic biomolecules. After reviewing the literature discussed herein, we have identified several key takeaways pertaining to the immunogenicity of PEG.

(1) There is significant evidence that PEG is a hapten, and can only elicit an immune response upon conjugation to an immunogenic agent. We therefore expect that in most cases not involving particularly immunogenic agents that PEG will remain useful, however,

immunogenicity should always be evaluated on a case-by-case basis. (2) Pre-existing anti-PEG antibodies in the general population have become more common over time and can affect the safety and efficacy of PEGylated biotherapeutics. While much remains unknown about how these antibodies are acquired or how they will interact with specific drugs, they must be taken into consideration when evaluating new PEGylated therapeutics. (3) Assays used to detect antibodies against PEG should be validated and appropriate controls employed. Reports of detection assay format vary widely in the literature, and although development of a standard method may not be practical for all circumstances, each assay should, at minimum, implement positive and negative controls to establish assay limits as well as competitive binding experiments to confirm antibody specificity. (4) Many factors affect the immunogenicity of PEG. Induction of anti-PEG antibodies depends on a variety of factors ranging from chemical properties like PEG molecular weight and surface coverage density to demographic factors that affect the prevalence of pre-existing antibodies. The large number of potential factors and the complex interplay between them has not yet been fully elucidated and requires further investigation.

Although it is clear from the evidence presented throughout this review that there are serious concerns surrounding the continued use of PEG in the context of biotherapeutics, it should also be noted that PEGylation has enabled the development of many therapeutics that may not have been otherwise successful. Additionally, for biotherapeutics, the majority of issues stem from the use of this technology with large, foreign, highly antigenic proteins like asparaginase, uricase, and phenylalanine ammonia lyase, which could be a limitation for any alternative polymer. Regardless of the polymer used, the immunological risks and safety profile will always need to be evaluated for each novel biotherapeutic, which may bias future drugs

toward using PEGylation instead of new technologies given its extensive precedence and established safety profile. We therefore expect that PEG will continue to be a mainstay for pharmacokinetic extension of biotherapeutics. Nevertheless, we also expect to see continued exploration and advancement of promising, alternative technologies, particularly if the polymers can offer some other advantage like enhanced protein stability.

Looking forward, we expect and hope to see other technologies join PEG at the forefront. Especially in the area of synthetic polymers, there remains significant space for exploration. In addition to providing reduced immunogenicity, these novel polymers will also likely benefit from lack of anti-polymer pre-existing antibodies due to the unlikely use of these polymers in consumer goods. Furthermore, the specific parameters surrounding what components of hydrophilic polymers contribute to production of anti-polymer antibodies have been insufficiently studied, presenting an excellent opportunity for further investigation in this area. While formidable, the task of overcoming PEG immunogenicity is rich with opportunity for discovery in fields ranging from immunology to chemistry, and we believe that this review will provide researchers with the necessary background to address this challenge.

1.10 References

(1) Leader, B.; Baca, Q. J.; Golan, D. E. (2008) Protein Therapeutics: A Summary and Pharmacological Classification. *Nat. Rev. Drug Discov. 7*, 21–39.

(2) Mitragotri, S.; Burke, P. A.; Langer, R. (2014) Overcoming the Challenges in Administering Biopharmaceuticals: Formulation and Delivery Strategies. *Nat. Rev. Drug Discov. 13*, 655–672.

(3) Usmani, S. S.; Bedi, G.; Samuel, J. S.; Singh, S.; Kalra, S.; Kumar, P.; Ahuja, A. A.; Sharma, M.; Gautam, A.; Raghava, G. P. S. (2017) THPdb: Database of FDA-Approved Peptide and Protein Therapeutics. *PLOS ONE 12*, e0181748.

(4) Kimchi-Sarfaty, C.; Schiller, T.; Hamasaki-Katagiri, N.; Khan, M. A.; Yanover, C.; Sauna, Z. E. (2013) Building Better Drugs: Developing and Regulating Engineered Therapeutic Proteins. *Trends Pharmacol. Sci. 34*, 534–548.

(5) Shankar, G.; Shores, E.; Wagner, C.; Mire-Sluis, A. (2006) Scientific and Regulatory Considerations on the Immunogenicity of Biologics. *Trends Biotechnol. 24*, 274–280.

(6) Shankar, G.; Pendley, C.; Stein, K. E. (2007) A Risk-Based Bioanalytical Strategy for the Assessment of Antibody Immune Responses against Biological Drugs. *Nat. Biotechnol. 25*, 555–561.

(7) Strohl, W. R. (2015) Fusion Proteins for Half-Life Extension of Biologics as a Strategy to Make Biobetters. *BioDrugs 29*, 215–239.

(8) Carter, P. J. (2011) Introduction to Current and Future Protein Therapeutics: A Protein Engineering Perspective. *Exp. Cell Res. 317*, 1261–1269.

(9) Mazor, R.; Eberle, J. A.; Hu, X.; Vassall, A. N.; Onda, M.; Beers, R.; Lee, E. C.; Kreitman, R. J.; Lee, B.; Baker, D.; King, C.; Hassan, R.; Benhar, I.; Pastan, I. (2014) Recombinant Immunotoxin for Cancer Treatment with Low Immunogenicity by Identification and Silencing of Human T-Cell Epitopes. *Proc. Natl. Acad. Sci. 111*, 8571–8576.

(10) Tirosh, O.; Barenholz, Y.; Katzhendler, J.; Priev, A. (1998) Hydration of Polyethylene Glycol-Grafted Liposomes. *Biophys. J. 74*, 1371–1379.

(11) Branca, C.; Magazù, S.; Maisano, G.; Migliardo, F.; Migliardo, P.; Romeo, G. (2002) Hydration Study of PEG/Water Mixtures by Quasi Elastic Light Scattering, Acoustic and Rheological Measurements. *J. Phys. Chem. B 106*, 10272–10276.

(12) Arakawa, T.; Timasheff, S. N. (1985) Mechanism of Polyethylene Glycol Interaction with Proteins. *Biochemistry 24*, 6756–6762.

(13) Jordan, C. F.; Lerman, L. S.; Venable, J. H. (1972) Structure and Circular Dichroism of DNA in Concentrated Polymer Solutions. *Nature. New Biol. 236*, 67–70.

(14) Arnold, K.; Zschoernig, O.; Barthel, D.; Herold, W. (1990) Exclusion of Poly(Ethylene Glycol) from Liposome Surfaces. *Biochim. Biophys. Acta BBA - Biomembr. 1022*, 303–310.

(15) Bhat, R.; Timasheff, S. N. (1992) Steric Exclusion Is the Principal Source of the Preferential Hydration of Proteins in the Presence of Polyethylene Glycols. *Protein Sci. 1*, 1133–1143.

(16) Alessi, M. L.; Norman, A. I.; Knowlton, S. E.; Ho, D. L.; Greer, S. C. (2005) Helical and Coil Conformations of Poly(Ethylene Glycol) in Isobutyric Acid and Water. *Macromolecules 38*, 9333–9340.

(17) Knop, K.; Hoogenboom, R.; Fischer, D.; Schubert, U. S. (2010) Poly(Ethylene Glycol) in Drug Delivery: Pros and Cons as Well as Potential Alternatives. *Angew. Chem. - Int. Ed. 49*, 6288–6308.

(18) Pasut, G.; Veronese, F. M. (2012) State of the Art in PEGylation: The Great Versatility Achieved after Forty Years of Research. *J. Controlled Release 161*, 461–472.

(19) Harris, J. M.; Chess, R. B. (2003) Effect of Pegylation on Pharmaceuticals. *Nat. Rev. Drug Discov. 2*, 214–221.

(20) Abuchowski, A.; Es, T. van; Palczuk, N. C.; Davis, F. F. (1977) Alteration of Immunological Properties of Bovine Serum Albumin by Covalent Attachment of Polyethylene Glycol. *J. Biol. Chem. 252*, 3578–3581.

(21) Abuchowski, A.; McCoy, J. R.; Palczuk, N. C.; Es, T. van; Davis, F. F. (1977) Effect of Covalent Attachment of Polyethylene Glycol on Immunogenicity and Circulating Life of Bovine Liver Catalase. *J. Biol. Chem. 252*, 3582–3586.

(22) Liu, Y.; Reidler, H.; Pan, J.; Milunic, D.; Qin, D.; Chen, D.; Vallejo, Y. R.; Yin, R. (2011) A Double Antigen Bridging Immunogenicity ELISA for the Detection of Antibodies to Polyethylene Glycol Polymers. *J. Pharmacol. Toxicol. Methods 64*, 238–245.

(23) Ehlinger, C.; Spear, N.; Doddareddy, R.; Shankar, G.; Schantz, A. (2019) A Generic Method for the Detection of Polyethylene Glycol Specific IgG and IgM Antibodies in Human Serum. *J. Immunol. Methods 474*, 112669.

(24) Richter, A. W.; Åkerblom, E. (1984) Polyethylene Glycol Reactive Antibodies in Man: Titer Distribution in Allergic Patients Treated with Monomethoxy Polyethylene Glycol Modified Allergens or Placebo, and in Healthy Blood Donors. *Int. Arch. Allergy Immunol. 74*, 36–39.

(25) Yang, Q.; Lai, S. K. (2015) Anti-PEG Immunity: Emergence, Characteristics, and Unaddressed Questions. *WIREs Nanomedicine Nanobiotechnology 7*, 655–677.

(26) Mohamed, M.; Lila, A. S. A.; Shimizu, T.; Alaaeldin, E.; Hussein, A.; Sarhan, H. A.; Szebeni, J.; Ishida, T. (2019) PEGylated Liposomes: Immunological Responses. *Sci. Technol. Adv. Mater. 20*, 710–724.

(27) Shiraishi, K.; Yokoyama, M. (2019) Toxicity and Immunogenicity Concerns Related to PEGylated-Micelle Carrier Systems: A Review. *Sci. Technol. Adv. Mater. 20*, 324–336.

(28) Gabizon, A.; Szebeni, J. (2020) Complement Activation: A Potential Threat on the Safety of Poly(Ethylene Glycol)-Coated Nanomedicines. *ACS Nano*.

(29) Davis, S.; Abuchowski, A.; Park, Y. K.; Davis, F. F. (1981) Alteration of the Circulating Life and Antigenic Properties of Bovine Adenosine Deaminase in Mice by Attachment of Polyethylene Glycol. *Clin. Exp. Immunol. 46*, 649–652.

(30) Hershfield, M. S.; Buckley, R. H.; Greenberg, M. L.; Melton, A. L.; Schiff, R.; Hatem, C.; Kurtzberg, J.; Markert, M. L.; Kobayashi, R. H.; Kobayashi, A. L.; Abuchowski, A. (1987) Treatment of Adenosine Deaminase Deficiency with Polyethylene Glycol–Modified Adenosine Deaminase. *N. Engl. J. Med. 316*, 589–596.

(31) Levy, Y.; Hershfield, M. S.; Fernandez-Mejia, C.; Polmar, S. H.; Scudiery, D.; Berger, M.; Sorensen, R. U. (1988) Adenosine Deaminase Deficiency with Late Onset of Recurrent Infections: Response to Treatment with Polyethylene Glycol-Modified Adenosine Deaminase. *J. Pediatr. 113*, 312–317.

(32) Abuchowski, A.; Kazo, G. M.; Verhoest, C. R.; Van Es, T.; Kafkewitz, D.; Nucci, M. L.; Viau, A. T.; Davis, F. F. (1984) Cancer Therapy with Chemically Modified Enzymes. I. Antitumor Properties of Polyethylene Glycol-Asparaginase Conjugates. *Cancer Biochem. Biophys. 7*, 175–186.

(33) Ho, D. H.; Wang, C. Y.; Lin, J. R.; Brown, N.; Newman, R. A.; Krakoff, I. H. (1988) Polyethylene Glycol-L-Asparaginase and L-Asparaginase Studies in Rabbits. *Drug Metab. Dispos. 16*, 27–29.

(34) Richter, A. W.; Åkerblom, E. (1983) Antibodies against Polyethylene Glycol Produced in Animals by Immunization with Monomethoxy Polyethylene Glycol Modified Proteins. *Int. Arch. Allergy Immunol. 70*, 124–131.

(35) Cheng, T.-L.; Wu, P.-Y.; Wu, M.-F.; Chern, J.-W.; Roffler, S. R. (1999) Accelerated Clearance of Polyethylene Glycol-Modified Proteins by Anti-Polyethylene Glycol IgM. *Bioconjug. Chem. 10*, 520–528.

(36) Cheng, T.-L.; Cheng, C.-M.; Chen, B.-M.; Tsao, D.-A.; Chuang, K.-H.; Hsiao, S.-W.; Lin, Y.-H.; Roffler, S. R. (2005) Monoclonal Antibody-Based Quantitation of Poly(Ethylene Glycol)-Derivatized Proteins, Liposomes, and Nanoparticles. *Bioconjug. Chem. 16*, 1225–1231.

(37) Caliceti, P.; Schiavon, O.; Veronese, F. M. (2001) Immunological Properties of Uricase Conjugated to Neutral Soluble Polymers. *Bioconjug. Chem. 12*, 515–522.

(38) Hashimoto, Y.; Shimizu, T.; Mima, Y.; Abu Lila, A. S.; Ishida, T.; Kiwada, H. (2014) Generation, Characterization and in Vivo Biological Activity of Two Distinct Monoclonal Anti-PEG IgMs. *Toxicol. Appl. Pharmacol. 277*, 30–38.

(39) Mima, Y.; Hashimoto, Y.; Shimizu, T.; Kiwada, H.; Ishida, T. (2015) Anti-PEG IgM Is a Major Contributor to the Accelerated Blood Clearance of Polyethylene Glycol-Conjugated Protein. *Mol. Pharm. 12*, 2429–2435.

(40) Elsadek, N. E.; Hondo, E.; Shimizu, T.; Takata, H.; Abu Lila, A. S.; Emam, S. E.; Ando, H.; Ishima, Y.; Ishida, T. (2020) Impact of Pre-Existing or Induced Anti-PEG IgM on the Pharmacokinetics of Peginterferon Alfa-2a (Pegasys) in Mice. *Mol. Pharm.*

(41) Moreno, A.; Pitoc, G. A.; Ganson, N. J.; Layzer, J. M.; Hershfield, M. S.; Tarantal, A. F.; Sullenger, B. A. (2019) Anti-PEG Antibodies Inhibit the Anticoagulant Activity of PEGylated Aptamers. *Cell Chem. Biol. 26*, 634-644.e3.

(42) Garratty, G. (2008) Modulating the Red Cell Membrane to Produce Universal/Stealth Donor Red Cells Suitable for Transfusion. *Vox Sang. 94*, 87–95.

(43) Tsuji, J.; Hirose, K.; Kasahara, E.; Naitoh, M.; Yamamoto, I. (1985) Studies on Antigenicity of the Polyethylene Glycol (PEG)-Modified Uricase. *Int. J. Immunopharmacol. 7*, 725–730.

(44) Judge, A.; McClintock, K.; Phelps, J. R.; MacLachlan, I. (2006) Hypersensitivity and Loss of Disease Site Targeting Caused by Antibody Responses to PEGylated Liposomes. *Mol. Ther. 13*, 328–337.

(45) Hamad, I.; Hunter, A. C.; Szebeni, J.; Moghimi, S. M. (2008) Poly(Ethylene Glycol)s Generate Complement Activation Products in Human Serum through Increased Alternative Pathway Turnover and a MASP-2-Dependent Process. *Mol. Immunol. 46*, 225–232.

(46) Wenande, E.; Garvey, L. H. (2016) Immediate-Type Hypersensitivity to Polyethylene Glycols: A Review. *Clin. Exp. Allergy 46*, 907–922.

(47) Poppenborg, S. M.; Wittmann, J.; Walther, W.; Brandenburg, G.; Krähmer, R.; Baumgart, J.; Leenders, F. (2016) Impact of Anti-PEG IgM Antibodies on the Pharmacokinetics of Pegylated Asparaginase Preparations in Mice. *Eur. J. Pharm. Sci. 91*, 122–130.

(48) van Helden, P. M.; Unterthurner, S.; Hermann, C.; Schuster, M.; Ahmad, R. U.; Schiviz, A. N.; Weiller, M.; Antoine, G.; Turecek, P. L.; Muchitsch, E. M.; Schwarz, H. P.; Reipert, B. M. (2011) Maintenance and Break of Immune Tolerance against Human Factor VIII in a New Transgenic Hemophilic Mouse Model. *Blood 118*, 3698–3707.

(49) Müller, H.-J.; Löning, L.; Horn, A.; Schwabe, D.; Gunkel, M.; Schrappe, M.; Schütz, V. V.; Henze, G.; Palma, J. C. da; Ritter, J.; Pinheiro, J. P. V.; Winkelhorst, M.; Boos, J. (2000) Pegylated Asparaginase (OncasparTM) in Children with ALL: Drug Monitoring in

Reinduction According to the ALL/NHL-BFM 95 Protocols. *Br. J. Haematol. 110*, 379–384.

(50) Henriksen, L. T.; Harila-Saari, A.; Ruud, E.; Abrahamsson, J.; Pruunsild, K.; Vaitkeviciene, G.; Jónsson, Ó. G.; Schmiegelow, K.; Heyman, M.; Schrøder, H.; Albertsen, B. K. (2015) PEG-Asparaginase Allergy in Children with Acute Lymphoblastic Leukemia in the NOPHO ALL2008 Protocol. *Pediatr. Blood Cancer 62*, 427–433.

(51) Chaffee, S.; Mary, A.; Stiehm, E. R.; Girault, D.; Fischer, A.; Hershfield, M. S. (1992) IgG Antibody Response to Polyethylene Glycol-Modified Adenosine Deaminase in Patients with Adenosine Deaminase Deficiency. *J. Clin. Invest. 89*, 1643–1651.

(52) Hershfield, M. S. (1995) PEG-ADA Replacement Therapy for Adenosine Deaminase Deficiency: An Update after 8.5 Years. *Clin. Immunol. Immunopathol. 76*, S228–S232.

(53) Tillmann, H.; Ganson, N. J.; Patel, K.; Thompson, A. J.; Abdelmalek, M.; Moody, T.; McHutchison, J. G.; Hershfield, M. S. (2010) High Prevalence of Pre-Existing Antibodies against Polyethylene Glycol (PEG) in Hepatitis C (HCV) Patients Which Is Not Associated with Impaired Response to PEG-Interferon. *J. Hepatol. 52*, S129.

(54) Myler, H.; Hruska, M. W.; Srinivasan, S.; Cooney, E.; Kong, G.; Dodge, R.; Krishna, M.; Zhu, J.; Felix, T.; Gleason, C.; Piccoli, S. P.; DeSilva, B. (2015) Anti-PEG Antibody Bioanalysis: A Clinical Case Study with PEG-IFN-λ-1a and PEG-IFN-A2a in Naive Patients. *Bioanalysis 7*, 1093–1106.

(55) Armstrong, J. K.; Hempel, G.; Koling, S.; Chan, L. S.; Fisher, T.; Meiselman, H. J.; Garratty, G. (2007) Antibody against Poly(Ethylene Glycol) Adversely Affects PEG-Asparaginase Therapy in Acute Lymphoblastic Leukemia Patients. *Cancer 110*, 103–111.

(56) Sherman, M. R.; Saifer, M. G. P.; Perez-Ruiz, F. (2008) PEG-Uricase in the Management of Treatment-Resistant Gout and Hyperuricemia. *Adv. Drug Deliv. Rev. 60*, 59–68.

(57) Dalbeth, N.; Choi, H. K.; Joosten, L. A. B.; Khanna, P. P.; Matsuo, H.; Perez-Ruiz, F.; Stamp, L. K. (2019) Gout. *Nat. Rev. Dis. Primer 5*, 1–17.

(58) Ganson, N. J.; Kelly, S. J.; Scarlett, E.; Sundy, J. S.; Hershfield, M. S. (2006) Control of Hyperuricemia in Subjects with Refractory Gout, and Induction of Antibody against Poly(Ethylene Glycol) (PEG), in a Phase I Trial of Subcutaneous PEGylated Urate Oxidase. *Arthritis Res. Ther. 8*, R12.

(59) Sundy, J. S.; Ganson, N. J.; Kelly, S. J.; Scarlett, E. L.; Rehrig, C. D.; Huang, W.; Hershfield, M. S. (2007) Pharmacokinetics and Pharmacodynamics of Intravenous PEGylated Recombinant Mammalian Urate Oxidase in Patients with Refractory Gout. *Arthritis Rheum. 56*, 1021–1028.

(60) Hershfield, M. S.; Ganson, N. J.; Kelly, S. J.; Scarlett, E. L.; Jaggers, D. A.; Sundy, J. S. (2014) Induced and Pre-Existing Anti-Polyethylene Glycol Antibody in a Trial of Every 3-Week Dosing of Pegloticase for Refractory Gout, Including in Organ Transplant Recipients. *Arthritis Res. Ther. 16*, R63.

(61) Lipsky, P. E.; Calabrese, L. H.; Kavanaugh, A.; Sundy, J. S.; Wright, D.; Wolfson, M.; Becker, M. A. (2014) Pegloticase Immunogenicity: The Relationship between Efficacy and Antibody Development in Patients Treated for Refractory Chronic Gout. *Arthritis Res. Ther. 16*, R60.

(62) Becker, M. A.; Baraf, H. S. B.; Yood, R. A.; Dillon, A.; Vázquez-Mellado, J.; Ottery, F. D.; Khanna, D.; Sundy, J. S. (2013) Long-Term Safety of Pegloticase in Chronic Gout Refractory to Conventional Treatment. *Ann. Rheum. Dis. 72*, 1469–1474.

(63) Longo, N.; Harding, C. O.; Burton, B. K.; Grange, D. K.; Vockley, J.; Wasserstein, M.; Rice, G. M.; Dorenbaum, A.; Neuenburg, J. K.; Musson, D. G.; Gu, Z.; Sile, S. (2014) Single-Dose, Subcutaneous Recombinant Phenylalanine Ammonia Lyase Conjugated with Polyethylene Glycol in Adult Patients with Phenylketonuria: An Open-Label, Multicentre, Phase 1 Dose-Escalation Trial. *The Lancet 384*, 37–44.

(64) Zori, R.; Thomas, J. A.; Shur, N.; Rizzo, W. B.; Decker, C.; Rosen, O.; Li, M.; Schweighardt, B.; Larimore, K.; Longo, N. (2018) Induction, Titration, and Maintenance Dosing Regimen in a Phase 2 Study of Pegvaliase for Control of Blood Phenylalanine in Adults with Phenylketonuria. *Mol. Genet. Metab. 125*, 217–227.

(65) Thomas, J.; Levy, H.; Amato, S.; Vockley, J.; Zori, R.; Dimmock, D.; Harding, C. O.; Bilder, D. A.; Weng, H. H.; Olbertz, J.; Merilainen, M.; Jiang, J.; Larimore, K.; Gupta, S.; Gu, Z.; Northrup, H. (2018) Pegvaliase for the Treatment of Phenylketonuria: Results of a Long-Term Phase 3 Clinical Trial Program (PRISM). *Mol. Genet. Metab. 124*, 27–38.

(66) Rosenberg, A. S.; Sauna, Z. E. (2018) Immunogenicity Assessment during the Development of Protein Therapeutics. *J. Pharm. Pharmacol. 70*, 584–594.

(67) Eckardt, K.-U. (2013) The Safety and Efficacy of Peginesatide in Patients with CKD. *Nat. Rev. Nephrol. 9*, 192–193.

(68) DeFrancesco, L. (2013) Three Deaths Sink Affymax. *Nat. Biotechnol. 31*, 270–270.

(69) Hermanson, T.; Bennett, C. L.; Macdougall, I. C. (2016) Peginesatide for the Treatment of Anemia Due to Chronic Kidney Disease – an Unfulfilled Promise. *Expert Opin. Drug Saf. 15*, 1421–1426.

(70) Ganson, N. J.; Povsic, T. J.; Sullenger, B. A.; Alexander, J. H.; Zelenkofske, S. L.; Sailstad, J. M.; Rusconi, C. P.; Hershfield, M. S. (2016) Pre-Existing Anti–Polyethylene

Glycol Antibody Linked to First-Exposure Allergic Reactions to Pegnivacogin, a PEGylated RNA Aptamer. *J. Allergy Clin. Immunol. 137*, 1610-1613.e7.

(71) Povsic, T. J.; Lawrence, M. G.; Lincoff, A. M.; Mehran, R.; Rusconi, C. P.; Zelenkofske, S. L.; Huang, Z.; Sailstad, J.; Armstrong, P. W.; Steg, P. G.; Bode, C.; Becker, R. C.; Alexander, J. H.; Adkinson, N. F.; Levinson, A. I. (2016) Pre-Existing Anti-PEG Antibodies Are Associated with Severe Immediate Allergic Reactions to Pegnivacogin, a PEGylated Aptamer. *J. Allergy Clin. Immunol. 138*, 1712–1715.

(72) Adagen® prescribing information. 2014 [cited 2020]; Available from: https://www.accessdata.fda.gov/drugsatfda_docs/label/ 2014/019818s053lbl.pdf. (accessed Aug 21, 2020).

(73) Oncaspar® (pegaspargase) prescribing information. Baxalta US Inc. (subsidiary of Shire plc.), Lexington, MA 024212019 [cited 2020]; Available from: https://www.accessdata.fda.gov/ drugsatfda_docs/label/2019/193411s5196lbl.pdf (accessed Aug 21, 2020).

(74) PegIntron® (peginterferon alfa-2b) prescribing information. Merck Sharp & Dohme Corp., a subsidiary of Merck & Co., Inc., Whitehouse Station, NJ 08889, USA 2019 [cited 2020]; Available from: https://www.accessdata.fda.gov/drugsatfda_docs/label/ 2019/103949s5313lbl.pdf (accessed Aug 21, 2020).

(75) Neulasta® (pegfilgrastim) prescribing information. Amgen Inc. One Amgen Center Drive, Thousand Oaks, California 91320–1799 2019 [cited 2020]; Available from: https:// www.accessdata.fda.gov/drugsatfda_docs/label/2019/125031s198lbl.pdf. (accessed Aug 21, 2020).

(76) Pegasys® (peginterferon alfa-2a) prescribing information. Genentech, Inc. South San Francisco, CA 94080–49902017 [cited 2020]; Available from: https://www.accessdata.fda.gov/drugsatfda_docs/label/2017/103964s5270lbl.pdf (accessed Aug 21, 2020).

(77) Somavert® (pegvisomant) prescribing information. Pfizer Inc, NY, NY 100172019 [cited 2020]; Available from: https:// www.accessdata.fda.gov/drugsatfda_docs/label/2013/021106s064lbl.pdf (accessed Aug 21, 2020).

(78) Macugen® (Pegaptanib Sodium) prescribing information. Pfizer Inc, NY, NY 100172019. 2004 [cited 2020] https://www.accessdata.fda.gov/drugsatfda_docs/nda/2004/21-756_Macugen.cfm (accessed Sep 1, 2020). (accessed Sep 2, 2020).

(79) Mircera® (methoxy polyethylene glycol-epoetin beta) prescribing information. Vifor (International) Inc. Rechenstrasse 37, 9014 St. Gallen, Switzerland 2018 [cited 2020]; Available from: https://www.accessdata.fda.gov/drugsatfda_docs/label/2018/125164s078lbl.pdf (accessed Aug 21, 2020).

(80) Cimzia® (certolizumab pegol) prescribing information. UCB, Inc. 1950 Lake Park Drive, Smyrna, GA 300802019 [cited 2020]; Available from: https://www.accessdata.fda.gov/drugsatfda_docs/label/2019/125160s293lbl.pdf (accessed Aug 21, 2020).

(81) Krystexxa® prescribing information. 2010 [cited 2020]; Available from: https://www.accessdata.fda.gov/drugsatfda_docs/label/2010/125293s0000lbl.pdf

https://www.accessdata.fda.gov/drugsatfda_docs/label/2010/125293s0000lbl.pdf (accessed Aug 21, 2020).

(82) Omontys® (peginesatide) prescribing information. 2012 [cited 2020]; Available from: https://www.accessdata.fda.gov/ drugsatfda_docs/label/2012/202799s001lbl.pdf (accessed Aug 21, 2020).

(83) Plegridy® (peginterferon beta-1a) prescribing information. Biogen Idec, Inc. Cambridge, MA 02142 [cited 2020] Available from: https://www.accessdata.fda.gov/drugsatfda_docs/label/2014/125499lbl.pdf https://www.accessdata.fda.gov/drugsatfda_docs/label/2014/125499lbl.pdf (accessed Aug 21, 2020).

(84) Adynovate® (antihemophilic factor) prescribing information. Baxalta US Inc. (subsidiary of Shire plc.), Lexington, MA 024212019 [cited 2020]; Available from: https://www.fda.gov/media/94470/download (accessed Sep 3, 2020).

(85) Rebinyn® (Recombinant Coagulation Factor IX, GlycoPEGylated) prescribing information. Novo Nordisk Inc., Plainsboro, NJ [cited 2020]; Available from: https://www.fda.gov/media/105491/download https://www.fda.gov/media/105491/download (accessed Aug 24, 2020).

(86) Palynziq® (pegvaliase-pqpz) Prescribing Information. BioMarin San Rafael, Ca [Cited 2020]; Available from: https://www.accessdata.fda.gov/drugsatfda_docs/nda/2018/761079Orig1s000lbl.pdf https://www.accessdata.fda.gov/drugsatfda_docs/nda/2018/761079Orig1s000lbl.pdf (accessed Aug 21, 2020).

(87) Armstrong, J. K.; Leger, R.; Wenby, R. B.; Meiselman, H. J.; Garratty, G.; Fisher, T. C. (2003) Occurrence of an Antibody to Poly(Ethylene Glycol) in Normal Donors. *Blood 102*, 556A.

(88) Armstrong, J. K. The Occurrence, Induction, Specificity and Potential Effect of Antibodies against Poly(Ethylene Glycol). In *PEGylated Protein Drugs: Basic Science and Clinical Applications*; Veronese, F. M., Ed.; Milestones in Drug Therapy; Birkhäuser: Basel, 2009; pp 147–168.

(89) Yang, Q.; Jacobs, T. M.; McCallen, J. D.; Moore, D. T.; Huckaby, J. T.; Edelstein, J. N.; Lai, S. K. (2016) Analysis of Pre-Existing IgG and IgM Antibodies against Polyethylene Glycol (PEG) in the General Population. *Anal. Chem. 88*, 11804–11812.

(90) Fruijtier-Pölloth, C. (2005) Safety Assessment on Polyethylene Glycols (PEGs) and Their Derivatives as Used in Cosmetic Products. *Toxicology 214*, 1–38.

(91) Lubich, C.; Allacher, P.; de la Rosa, M.; Bauer, A.; Prenninger, T.; Horling, F. M.; Siekmann, J.; Oldenburg, J.; Scheiflinger, F.; Reipert, B. M. (2016) The Mystery of Antibodies Against Polyethylene Glycol (PEG) - What Do We Know? *Pharm. Res. 33*, 2239–2249.

(92) Chen, B. M.; Su, Y. C.; Chang, C. J.; Burnouf, P. A.; Chuang, K. H.; Chen, C. H.; Cheng, T. L.; Chen, Y. T.; Wu, J. Y.; Roffler, S. R. (2016) Measurement of Pre-Existing IgG and IgM Antibodies against Polyethylene Glycol in Healthy Individuals. *Anal. Chem. 88*, 10661–10666.

(93) Elsadek, N. E.; Lila, A. S. A.; Emam, S. E.; Shimizu, T.; Takata, H.; Ando, H.; Ishima, Y.; Ishida, T. (2020) Pegfilgrastim (PEG-G-CSF) Induces Anti-PEG IgM in a Dose

Dependent Manner and Causes the Accelerated Blood Clearance (ABC) Phenomenon upon Repeated Administration in Mice. *Eur. J. Pharm. Biopharm. 152*, 56–62.

(94) Sroda, K.; Rydlewski, J.; Langner, M.; Kozubek, A.; Grzybek, M.; Sikorski, A. F. (2005) Repeated Injections of PEG-PE Liposomes Generate Anti-PEG Antibodies. *Cell. Mol. Biol. Lett. 10*, 11.

(95) Dong, H.; Mora, J. R.; Brockus, C.; Chilewski, S. D.; Dodge, R.; Merrifield, C.; Dickerson, W. M.; DeSilva, B. (2015) Development of a Generic Anti-PEG Antibody Assay Using BioScale's Acoustic Membrane MicroParticle Technology. *AAPS J. 17*, 1511–1516.

(96) Zhang, P.; Sun, F.; Tsao, C.; Liu, S.; Jain, P.; Sinclair, A.; Hung, H.-C.; Bai, T.; Wu, K.; Jiang, S. (2015) Zwitterionic Gel Encapsulation Promotes Protein Stability, Enhances Pharmacokinetics, and Reduces Immunogenicity. *Proc. Natl. Acad. Sci. 112*, 12046–12051.

(97) Tsai, N.; Cheng, T.-L.; Roffler, S. R. (2001) Sensitive Measurement of Polyethylene Glycol-Modified Proteins. *BioTechniques 30*, 396–402.

(98) Zhang, P.; Sun, F.; Liu, S.; Jiang, S. (2016) Anti-PEG Antibodies in the Clinic: Current Issues and beyond PEGylation. *J. Controlled Release 244*, 184–193.

(99) Cheng, T.-L.; Chuang, K.-H.; Chen, B.-M.; Roffler, S. R. (2012) Analytical Measurement of PEGylated Molecules. *Bioconjug. Chem. 23*, 881–899.

(100) Schellekens, H.; Hennink, W. E.; Brinks, V. (2013) The Immunogenicity of Polyethylene Glycol: Facts and Fiction. *Pharm. Res. 30*, 1729–1734.

(101) Li, B.; Jain, P.; Ma, J.; Smith, J. K.; Yuan, Z.; Hung, H.-C.; He, Y.; Lin, X.; Wu, K.; Pfaendtner, J.; Jiang, S. (2019) Trimethylamine N-Oxide–Derived Zwitterionic Polymers: A New Class of Ultralow Fouling Bioinspired Materials. *Sci. Adv. 5*, eaaw9562.

(102) Shiraishi, K.; Kawano, K.; Maitani, Y.; Aoshi, T.; Ishii, K. J.; Sanada, Y.; Mochizuki, S.; Sakurai, K.; Yokoyama, M. (2016) Exploring the Relationship between Anti-PEG IgM Behaviors and PEGylated Nanoparticles and Its Significance for Accelerated Blood Clearance. *J. Controlled Release 234*, 59–67.

(103) Shiraishi, K.; Hamano, M.; Ma, H.; Kawano, K.; Maitani, Y.; Aoshi, T.; Ishii, K. J.; Yokoyama, M. (2013) Hydrophobic Blocks of PEG-Conjugates Play a Significant Role in the Accelerated Blood Clearance (ABC) Phenomenon. *J. Controlled Release 165*, 183–190.

(104) Shiraishi, K.; Yokoyama, M. (2013) Polymeric Micelles Possessing Polyethyleneglycol as Outer Shell and Their Unique Behaviors in Accelerated Blood Clearance Phenomenon. *Biol. Pharm. Bull. 36*, 878–882.

(105) Lee, C.-C.; Su, Y.-C.; Ko, T.-P.; Lin, L.-L.; Yang, C.-Y.; Chang, S. S.-C.; Roffler, S. R.; Wang, A. H.-J. (2020) Structural Basis of Polyethylene Glycol Recognition by Antibody. *J. Biomed. Sci. 27*, 12.

(106) Verhoef, J. J. F.; Anchordoquy, T. J. (2013) Questioning the Use of PEGylation for Drug Delivery. *Drug Deliv. Transl. Res. 3*, 499–503.

(107) Wadhwa, M.; Knezevic, I.; Kang, H.-N.; Thorpe, R. (2015) Immunogenicity Assessment of Biotherapeutic Products: An Overview of Assays and Their Utility. *Biologicals 43*, 298–306.

(108) Ishida, T.; Ichihara, M.; Wang, X.; Kiwada, H. (2006) Spleen Plays an Important Role in the Induction of Accelerated Blood Clearance of PEGylated Liposomes. *J. Controlled Release 115*, 243–250.

(109) Shimizu, T.; Ishida, T.; Kiwada, H. (2013) Transport of PEGylated Liposomes from the Splenic Marginal Zone to the Follicle in the Induction Phase of the Accelerated Blood Clearance Phenomenon. *Immunobiology 218*, 725–732.

(110) Vos, Q.; Lees, A.; Wu, Z. Q.; Snapper, C. M.; Mond, J. J. (2000) B-Cell Activation by T-Cell-Independent Type 2 Antigens as an Integral Part of the Humoral Immune Response to Pathogenic Microorganisms. *Immunol. Rev. 176*, 154–170.

(111) Ishida, T.; Harada, M.; Wang, X. Y.; Ichihara, M.; Irimura, K.; Kiwada, H. (2005) Accelerated Blood Clearance of PEGylated Liposomes Following Preceding Liposome Injection: Effects of Lipid Dose and PEG Surface-Density and Chain Length of the First-Dose Liposomes. *J. Controlled Release 105*, 305–317.

(112) Shimizu, T.; Ichihara, M.; Yoshioka, Y.; Ishida, T.; Nakagawa, S.; Kiwada, H. (2012) Intravenous Administration of Polyethylene Glycol-Coated (PEGylated) Proteins and PEGylated Adenovirus Elicits an Anti-PEG Immunoglobulin M Response. *Biol. Pharm. Bull. 35*, 1336–1342.

(113) Mima, Y.; Hashimoto, Y.; Shimizu, T.; Kiwada, H.; Ishida, T. (2015) Anti-PEG IgM Is a Major Contributor to the Accelerated Blood Clearance of Polyethylene Glycol-Conjugated Protein. *Mol. Pharm. 12*, 2429–2435.

(114) Judge, A.; McClintock, K.; Phelps, J. R.; Maclachlan, I. (2006) Hypersensitivity and Loss of Disease Site Targeting Caused by Antibody Responses to PEGylated Liposomes. *Mol. Ther. J. Am. Soc. Gene Ther. 13*, 328–337.

(115) Yang, Q.; Lai, S. K. (2015) Anti-PEG Immunity: Emergence, Characteristics, and Unaddressed Questions. *Wiley Interdiscip. Rev. Nanomed. Nanobiotechnol. 7*, 655–677.

(116) Rosenberg, A. S.; Sauna, Z. E. (2018) Immunogenicity Assessment during the Development of Protein Therapeutics. *J. Pharm. Pharmacol. 70*, 584–594.

(117) Krishna, M.; Nadler, S. G. (2016) Immunogenicity to Biotherapeutics – The Role of Anti-Drug Immune Complexes. *Front. Immunol. 7*.

(118) Koide, H.; Asai, T.; Hatanaka, K.; Akai, S.; Ishii, T.; Kenjo, E.; Ishida, T.; Kiwada, H.; Tsukada, H.; Oku, N. (2010) T Cell-Independent B Cell Response Is Responsible for ABC Phenomenon Induced by Repeated Injection of PEGylated Liposomes. *Int. J. Pharm. 392*, 218–223.

(119) Shimizu, T.; Ichihara, M.; Yoshioka, Y.; Ishida, T.; Nakagawa, S.; Kiwada, H. (2012) Intravenous Administration of Polyethylene Glycol-Coated (PEGylated) Proteins and PEGylated Adenovirus Elicits an Anti-PEG Immunoglobulin M Response. *Biol. Pharm. Bull. 35*, 1336–1342.

(120) Li, C.; Zhao, X.; Wang, Y.; Yang, H.; Li, H.; Li, H.; Tian, W.; Yang, J.; Cui, J. (2013) Prolongation of Time Interval between Doses Could Eliminate Accelerated Blood Clearance Phenomenon Induced by Pegylated Liposomal Topotecan. *Int. J. Pharm. 443*, 17–25.

(121) Verhoef, J. J. F.; Carpenter, J. F.; Anchordoquy, T. J.; Schellekens, H. (2014) Potential Induction of Anti-PEG Antibodies and Complement Activation toward PEGylated Therapeutics. *Drug Discov. Today 19*, 1945–1952.

(122) Kawanishi, M.; Hashimoto, Y.; Shimizu, T.; Sagawa, I.; Ishida, T.; Kiwada, H. (2015) Comprehensive Analysis of PEGylated Liposome-Associated Proteins Relating to the

Accelerated Blood Clearance Phenomenon by Combination with Shotgun Analysis and Conventional Methods. *Biotechnol. Appl. Biochem. 62*, 547–555.

(123) Szebeni, J.; Bedőcs, P.; Rozsnyay, Z.; Weiszhár, Z.; Urbanics, R.; Rosivall, L.; Cohen, R.; Garbuzenko, O.; Báthori, G.; Tóth, M.; Bünger, R.; Barenholz, Y. (2012) Liposome-Induced Complement Activation and Related Cardiopulmonary Distress in Pigs: Factors Promoting Reactogenicity of Doxil and AmBisome. *Nanomedicine Nanotechnol. Biol. Med. 8*, 176–184.

(124) Mikhail, A. (2012) Profile of Peginesatide and Its Potential for the Treatment of Anemia in Adults with Chronic Kidney Disease Who Are on Dialysis. *J. Blood Med. 3*, 25–31.

(125) Ishida, T.; Ichihara, M.; Wang, X.; Yamamoto, K.; Kimura, J.; Majima, E.; Kiwada, H. (2006) Injection of PEGylated Liposomes in Rats Elicits PEG-Specific IgM, Which Is Responsible for Rapid Elimination of a Second Dose of PEGylated Liposomes. *J. Controlled Release 112*, 15–25.

(126) Elsadek, N. E.; Hondo, E.; Shimizu, T.; Takata, H.; Abu Lila, A. S.; Emam, S. E.; Ando, H.; Ishima, Y.; Ishida, T. (2020) Impact of Pre-Existing or Induced Anti-PEG IgM on the Pharmacokinetics of Peginterferon Alfa-2a (Pegasys) in Mice. *Mol. Pharm.*

(127) Chang, C. J.; Chen, C. H.; Chen, B. M.; Su, Y. C.; Chen, Y. T.; Hershfield, M. S.; Lee, M. T. M.; Cheng, T. L.; Chen, Y. T.; Roffler, S. R.; Wu, J. Y. (2017) A Genome-Wide Association Study Identifies a Novel Susceptibility Locus for the Immunogenicity of Polyethylene Glycol. *Nat. Commun. 8*, 1–7.

(128) Yang, Q.; Jones, S. W.; Parker, C. L.; Zamboni, W. C.; Bear, J. E.; Lai, S. K. (2014) Evading Immune Cell Uptake and Clearance Requires PEG Grafting at Densities

Substantially Exceeding the Minimum for Brush Conformation. *Mol. Pharm. 11*, 1250–1258.

(129) Fishburn, C. S. (2008) The Pharmacology of PEGylation: Balancing PD with PK to Generate Novel Therapeutics. *J. Pharm. Sci. 97*, 4167–4183.

(130) Koide, H.; Asai, T.; Hatanaka, K.; Urakami, T.; Ishii, T.; Kenjo, E.; Nishihara, M.; Yokoyama, M.; Ishida, T.; Kiwada, H.; Oku, N. (2008) Particle Size-Dependent Triggering of Accelerated Blood Clearance Phenomenon. *Int. J. Pharm. 362*, 197–200.

(131) Koide, H.; Asai, T.; Kato, H.; Ando, H.; Shiraishi, K.; Yokoyama, M.; Oku, N. (2012) Size-Dependent Induction of Accelerated Blood Clearance Phenomenon by Repeated Injections of Polymeric Micelles. *Int. J. Pharm. 432*, 75–79.

(132) Kaminskas, L. M.; Mcleod, V. M.; Porter, C. J. H.; Boyd, B. J. (2011) Differences in Colloidal Structure of PEGylated Nanomaterials Dictate the Likelihood of Accelerated Blood Clearance. *J. Pharm. Sci. 100*, 5069–5077.

(133) Abu Lila, A. S.; Kiwada, H.; Ishida, T. (2013) The Accelerated Blood Clearance (ABC) Phenomenon: Clinical Challenge and Approaches to Manage. *J. Controlled Release 172*, 38–47.

(134) Cheng, T.-C.; Chuang, K.-H.; Chen, M.; Wang, H.-E.; Tzou, S.-C.; Su, Y.-C.; Chuang, C.-H.; Kao, C.-H.; Chen, B.-M.; Chang, L.-S.; Roffler, S. R.; Cheng, T.-L. (2013) Sensitivity of PEGylated Interferon Detection by Anti-Polyethylene Glycol (PEG) Antibodies Depends on PEG Length. *Bioconjug. Chem. 24*, 1408–1413.

(135) Sherman, M. R.; Williams, L. D.; Sobczyk, M. A.; Michaels, S. J.; Saifer, M. G. P. (2012) Role of the Methoxy Group in Immune Responses to MPEG-Protein Conjugates. *Bioconjug. Chem. 23*, 485–499.

(136) Saifer, M. G. P.; Williams, L. D.; Sobczyk, M. A.; Michaels, S. J.; Sherman, M. R. (2014) Selectivity of Binding of PEGs and PEG-like Oligomers to Anti-PEG Antibodies Induced by MethoxyPEG-Proteins. *Mol. Immunol. 57*, 236–246.

(137) McCallen, J.; Prybylski, J.; Yang, Q.; Lai, S. K. (2017) Cross-Reactivity of Select PEG-Binding Antibodies to Other Polymers Containing a C-C-O Backbone. *ACS Biomater. Sci. Eng. 3*, 1605–1615.

(138) Abeles, A. M. (2014) PEG-Ing down (and Preventing?) The Cause of Pegloticase Failure. *Arthritis Res. Ther. 16*, 112.

(139) Bavli, Y.; Chen, B.-M.; Roffler, S. R.; Dobrovolskaia, M. A.; Elnekave, E.; Ash, S.; Barenholz, Y.; Turjeman, K. (2020) PEGylated Liposomal Methyl Prednisolone Succinate Does Not Induce Infusion Reactions in Patients: A Correlation Between in Vitro Immunological and in Vivo Clinical Studies. *Molecules 25*, 558.

(140) McSweeney, M. D.; Versfeld, Z. C.; Carpenter, D. M.; Lai, S. K. (2018) Physician Awareness of Immune Responses to Polyethylene Glycol-Drug Conjugates. *Clin. Transl. Sci. 11*, 162–165.

(141) Chang, T.-C.; Chen, B.-M.; Lin, W.-W.; Yu, P.-H.; Chiu, Y.-W.; Chen, Y.-T.; Wu, J.-Y.; Cheng, T.-L.; Hwang, D.-Y.; Roffler, S. (2020) Both IgM and IgG Antibodies against Polyethylene Glycol Can Alter the Biological Activity of Methoxy Polyethylene Glycol-Epoetin Beta in Mice. *Pharmaceutics 12*, 15.

(142) Pelegri-O'Day, E. M.; Lin, E.-W.; Maynard, H. D. (2014) Therapeutic Protein–Polymer Conjugates: Advancing Beyond PEGylation. *J. Am. Chem. Soc. 136*, 14323–14332.

(143) Qi, Y.; Chilkoti, A. (2015) Protein-Polymer Conjugation-Moving beyond PEGylation. *Curr. Opin. Chem. Biol. 28*, 181–193.

(144) Zaman, R.; Islam, R. A.; Ibnat, N.; Othman, I.; Zaini, A.; Lee, C. Y.; Chowdhury, E. H. (2019) Current Strategies in Extending Half-Lives of Therapeutic Proteins. *J. Controlled Release 301*, 176–189.

(145) van Witteloostuijn, S. B.; Pedersen, S. L.; Jensen, K. J. (2016) Half-Life Extension of Biopharmaceuticals Using Chemical Methods: Alternatives to PEGylation. *ChemMedChem 11*, 2474–2495.

(146) Qi, Y.; Simakova, A.; Ganson, N. J.; Li, X.; Luginbuhl, K. M.; Ozer, I.; Liu, W.; Hershfield, M. S.; Matyjaszewski, K.; Chilkoti, A. (2016) A Brush-Polymer/Exendin-4 Conjugate Reduces Blood Glucose Levels for up to Five Days and Eliminates Poly(Ethylene Glycol) Antigenicity. *Nat. Biomed. Eng. 1*, 1–12.

(147) Joh, D. Y.; Zimmers, Z.; Avlani, M.; Heggestad, J. T.; Aydin, H. B.; Ganson, N.; Kumar, S.; Fontes, C. M.; Achar, R. K.; Hershfield, M. S.; Hucknall, A. M.; Chilkoti, A. (2019) Architectural Modification of Conformal PEG-Bottlebrush Coatings Minimizes Anti-PEG Antigenicity While Preserving Stealth Properties. *Adv. Healthc. Mater. 8*, 1801177.

(148) Hou, Y.; Zhou, Y.; Wang, H.; Sun, J.; Wang, R.; Sheng, K.; Yuan, J.; Hu, Y.; Chao, Y.; Liu, Z.; Lu, H. (2019) Therapeutic Protein PEPylation: The Helix of Nonfouling Synthetic Polypeptides Minimizes Antidrug Antibody Generation. *ACS Cent. Sci. 5*, 229–236.

(149) Abu Lila, A. S.; Nawata, K.; Shimizu, T.; Ishida, T.; Kiwada, H. (2013) Use of Polyglycerol (PG), Instead of Polyethylene Glycol (PEG), Prevents Induction of the Accelerated Blood Clearance Phenomenon against Long-Circulating Liposomes upon Repeated Administration. *Int. J. Pharm. 456*, 235–242.

(150) Jiang, S.; Cao, Z. (2010) Ultralow-Fouling, Functionalizable, and Hydrolyzable Zwitterionic Materials and Their Derivatives for Biological Applications. *Adv. Mater. 22*, 920–932.

(151) Yang, W.; Liu, S.; Bai, T.; Keefe, A. J.; Zhang, L.; Ella-Menye, J.-R.; Li, Y.; Jiang, S. (2014) Poly(Carboxybetaine) Nanomaterials Enable Long Circulation and Prevent Polymer-Specific Antibody Production. *Nano Today 9*, 10–16.

(152) Liu, S.; Jiang, S. (2016) Zwitterionic Polymer-Protein Conjugates Reduce Polymer-Specific Antibody Response. *Nano Today 11*, 285–291.

(153) Li, B.; Yuan, Z.; Hung, H. C.; Ma, J.; Jain, P.; Tsao, C.; Xie, J.; Zhang, P.; Lin, X.; Wu, K.; Jiang, S. (2018) Revealing the Immunogenic Risk of Polymers. *Angew. Chem. - Int. Ed. 57*, 13873–13876.

(154) Zhang, P.; Jain, P.; Tsao, C.; Yuan, Z.; Li, W.; Li, B.; Wu, K.; Hung, H.-C.; Lin, X.; Jiang, S. (2018) Polypeptides with High Zwitterion Density for Safe and Effective Therapeutics. *Angew. Chem. Int. Ed. 57*, 7743–7747.

(155) Li, B.; Yuan, Z.; Jain, P.; Hung, H.-C.; He, Y.; Lin, X.; McMullen, P.; Jiang, S. (2020) De Novo Design of Functional Zwitterionic Biomimetic Material for Immunomodulation. *Sci. Adv. 6*, eaba0754.

(156) Shao, Q.; Jiang, S. (2015) Molecular Understanding and Design of Zwitterionic Materials. *Adv. Mater. 27*, 15–26.

(157) Ryujin, T.; Shimizu, T.; Miyahara, R.; Shimazui, R.; Yoshikawa, T.; Kishimura, A.; Mori, T.; Ishida, T.; Katayama, Y. (2020) Blood Retention and Antigenicity of Polycarboxybetaine-Modified Liposomes.

(158) Schellenberger, V.; Wang, C.; Geething, N. C.; Spink, B. J.; Campbell, A.; To, W.; Scholle, M. D.; Yin, Y.; Yao, Y.; Bogin, O.; Cleland, J. L.; Silverman, J.; Stemmer, W. P. C. (2009) A Recombinant Polypeptide Extends the in Vivo Half-Life of Peptides and Proteins in a Tunable Manner. *Nat. Biotechnol. 27*, 1186–1190.

(159) Podust, V. N.; Balan, S.; Sim, B.-C.; Coyle, M. P.; Ernst, U.; Peters, R. T.; Schellenberger, V. (2016) Extension of in Vivo Half-Life of Biologically Active Molecules by XTEN Protein Polymers. *J. Controlled Release 240*, 52–66.

Chapter 2

Human Vault Nanoparticle Targeted Delivery of Antiretroviral Drugs to Inhibit Human Immunodeficiency Virus Type 1 Infection[†]

2.1 Introduction

In 2018, approximately 38 million people worldwide were living with HIV-1 and an estimated 1.7 million were newly infected.[1] Antiretroviral therapy is currently the frontline treatment for HIV-1 infection, and although highly effective, prevention strategies remain key in mitigating the spread of the disease. Pre-exposure prophylaxis (PrEP), or systemic administration of antiretrovival agents to uninfected individuals to prevent infection, is highly effective; however effectiveness is predicated on user compliance to the prescribed dosage regimen as well as tissue penetration of the drugs.[2–4] Because PrEP agents are administered systemically, they can elicit significant side effects as well as long-term toxicity. One strategy that aims to mitigate these side-effects while maintaining efficacy is to employ targeted drug delivery platforms. Delivery of drugs to specific sites and/or cells involved in disease can reduce systemic and increase local exposure, which in turn helps minimize deleterious off-target effects, improve efficacy, and increase user compliance. Targeted delivery approaches have proven useful in cancer chemotherapy and immunotherapy[5] and are likewise promising for anti-HIV-1 microbicide development.

Activated CD4+ T cells are the primary cells targeted and infected by HIV-1. These cells primarily reside in the gastrointestinal mucosa with mucosal HIV-1 transmission accounting for the majority of transmission and infection events.[6] To prevent infection, adequate drug levels must be achieved and maintained in these cells; however, oral administration of antiretrovirals is associated with substantial variation in penetration of vaginal and rectal mucosal tissues because of the systemic distribution of the drugs.[7] Targeting antiretroviral drugs specifically to these vulnerable cells would improve efficacy while simultaneously decreasing dosing. Topical microbicides are the most common targeting strategy for HIV-1 infection prevention. These

microbicides are attractive drug delivery platforms because they can be applied locally (rectally and/or vaginally) and have the potential to be applied during sexual intercourse to prevent infection. However, topical microbicides often suffer from insufficient tissue bioavailabilty leading to lack of efficacy as well as poor tolerability and therefore lowering user compliance.[8] In short, even when employing local delivery of antiretrovirals with topical microbicides, limitations similar to systemic delivery are often encountered.

Improvement of bioavailablity and reduction of off-target effects requires a targeted drug delivery strategy that maximizes dosing in only the most vulnerable cell populations while minimally perturbing adjacent cells. Nanoparticle drug delivery vehicles have been investigated extensively for applications in treatment and prevention of HIV-1 infection and may provide platforms for overcoming these limitations.[9] Examples include dendrimers,[10,11] polymeric nanoparticles composed of poly(lactic-co-glycolic acid),[12–17] and lipid-based nanoparticles or liposomes.[18–20] The small size of the particles in these formulations provides enhanced mucosal penetration and consequently increases distribution and retention[16] as well as intracellular uptake of drug-loaded particles.[21,22] Mucosal penetration can also be enhanced following covalent attachment of polyethylene glycol (PEG) to the surface of the nanoparticle though a process known as PEGylation.[23] For these reasons, nanoparticles have become attractive vehicles for antiretroviral delivery.

Most research using nanoparticle-based drug delivery vehicles has focused on delivery of tenofovir (TFV), which is a reverse transcriptase inhibitor.[14,17,18,24,25] Currently, oral tenofovir disoproxil fumarate/emtricitabine and tenofovir alafenamide/emtricitabine are the only FDA-approved drug formulations for PrEP use. TFV was the first effective topical drug for HIV-1 prevention,[26] but has been associated with symptoms of renal toxicity and decreased bone

mineral density.[27–30] Therefore, local, targeted delivery of TFV has become a topic of significant interest. Beyond TFV, other drugs have also been explored including other reverse transcriptase inhibitors including protease inhibitors like indivavir[31] and saquinavir[17,21], non-nucleoside reverse transcriptase inhibitors like efavirenz[16,17] and dapivirine[12,13], and other nucleoside reverse transcriptase inhibitors like zidovudine (AZT)[32–36]. As the first drug FDA-approved to treat HIV-1 infection, AZT was highly effective, it is no longer used due to systemic toxicities such as macrocytic anemia, granulocytopenia, myopathy, and mitochondrial toxicity.[37,38] Integrase strand transfer inhibitors such as elvitegravir (EVG)[14] and bictegravir[15] have also been examined. EVG is well tolerated, but experiences rapid hepatic metabolism and accordingly requires coadministration with an additional drug such as cobicistat to inhibit its metabolism. In each of these works, noncovalent encapsulation was employed using polymeric or lipid nanoparticles for drug delivery, with only one exception that used covalent conjugation for drug loading onto a dendrimer.[11] Additionally, both polymeric and lipid nanoparticles inherently possess a high degree of heterogeneity, which can lead to variability in efficacy. Homogeneous, highly uniform nanostructures are therefore appealing alternatives.

Initially reported in 1986 by Rome and Kedersha, vault nanoparticles are highly conserved ribonucleoprotein particles that are expressed in most eukaryotic cells.[39,40] These uniform 13 MDa barrel-shaped particles predominantly consist of 78 copies of the major vault protein (MVP) that are aligned C- to N-terminus and assemble noncovalently to form the overall vault structure (Figure 2.1). Endogenous vaults also contain several other components including two other proteins, vault poly(ADPribose) polymerase (VPARP) and telomerase-associated protein 1 (TEP1), as well as several copies of short, untranslated vault associated RNAs;[41–45] however, recombinant expression of MVP alone is sufficient to produce intact vaults that can

subsequently be functionalized with various molecules.[46–48] Although their biological role remains unclear, vaults have been engineered and used for a variety of applications including vaccination,[49,50] enzyme delivery,[51,52] cellular receptor targeting,[53] immunotherapeutic delivery,[47] and cellular uptake and labeling.[48] Additionally, vaults can also be engineered with cysteine rich regions to provide additional bioconjugation handles,[51,54] which are designated as CP-MVP vaults. In most of these applications, vaults were investigated as potential delivery vehicles for either large or small molecules. Protein packaging into recombinant vaults can be facilitated via fusion with a VPARP interaction domain that binds in the vault interior,[55] however, noncovalent packaging of small molecules has proven more challenging. Highly hydrophobic molecules can be noncovalently loaded into vaults engineered with internal hydrophobic domains,[46] but size, polarity, and solubility limit drug loadings. Instead of relying on noncovalent encapsulation, we aimed to use vaults to deliver covalently bound small molecules.

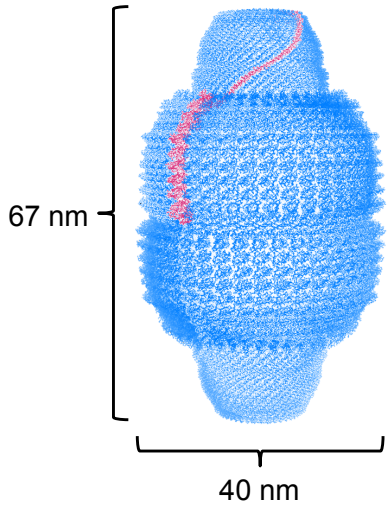

Figure 2.1. Crystal structure of vault protein nanoparticle (PDB 4V60) with a single MVP subunit highlighted in red.

Previous work demonstrated that vaults could be taken up by certain cell types,[56] but the specific cells that naturally take up vaults had not been clarified prior to this work. We assessed

the propensity of peripheral blood mononuclear cells (PBMC) to internalize vaults and it was found that approximately 23% of all PBMC internalized vaults and maximal uptake occurred after 10 minutes. Of these PBMC, approximately 16% were B cells, 2% were T cells, and 82% were a mixture of other cell types consisting mostly of dendritic cells (77%). Among B cells that internalized vaults, 74% were naïve B cells. Among T cells that internalized vaults, 65% were activated CD4+ T cells, and >90% of activated T cells internalized vaults.[57] Having established that vaults were internalized rapidly and selectively by the most vulnerable immune cells to HIV-1, we envisioned the utility of vaults as drug delivery vehicles for HIV-1 infection inhibition.

In this work, we investigated the use of recombinant human vault nanoparticles as delivery vehicles for small molecule antiretroviral drugs to inhibit HIV-1 infection. We describe strategies to stably, yet reversibly conjugate multiple drugs to vaults for targeted cellular uptake and release in cell types relevant to the pathogenesis of HIV-1 infection and transmission and demonstrate inhibition levels comparable to free drug (Figure 2.2). Additionally, we report a procedure for facile PEGylation and fluorescent tagging of vaults that has the potential to enhance mucosal penetration and increase bioavailability of conjugated drug molecules.

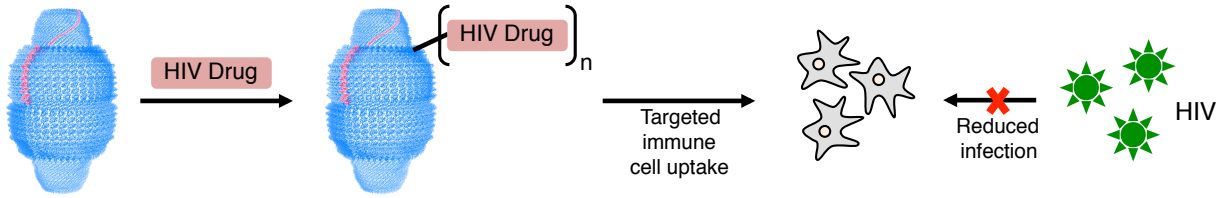

Figure 2.2. Vault nanoparticles can be used to target delivery of small molecule antiretrovirals to vulnerable immune cells, consequently inhibiting HIV infection.

2.2 Results and Discussion

2.2.1 Selection of Antiretroviral Drugs for Direct Conjugation to Recombinant Vault Nanoparticles

The subsets of PBMC to which vaults naturally target are also the key target cells for HIV-1 infection. As such, we tested the utility of recombinant vaults for antiretroviral drug delivery. While vaults have been engineered to package highly hydrophobic molecules,[46] available antiretroviral drugs against HIV-1 were not sufficiently hydrophobic to employ this method. Alternatively, we selected drugs that were amenable to conjugation to vaults, based on having reactive groups that would be either easily modifiable or directly available for protein conjugation using high-efficiency coupling methods. These included FDA-approved drugs from two clinically relevant antiretroviral drug classes: the nucleoside reverse transcriptase inhibitors and integrase strand transfer inhibitors. Specifically, the drugs chosen were zidovudine (AZT), tenofovir (TFV), dolutegravir (DTG) and elvitegravir (EVG) (Figure 2.3), for which we employed ester-, carbonate-, ester-, and carbamate-based conjugation strategies, respectively. These chemistries were chosen to provide stability until hydrolytic and/or enzymatic cleavage, which we hypothesized would occur mostly intracellularly after vault uptake, allowing slow and sustained release of the active drug at the site of action, and offering the potential advantage of better regulating release kinetics compared to typical non-covalent encapsulation strategies. Additionally, this approach provided a direct route to modify the limited functional handles available on the selected drugs.

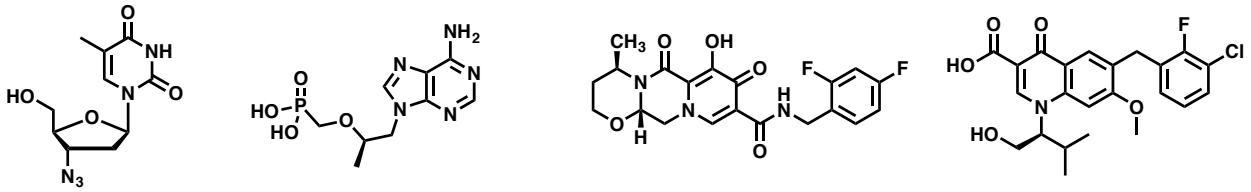

Figure 2.3. Drugs investigated for this work. From the nucleoside reverse transcriptase inhibitors were selected zidovudine and tenofovir, and from the integrase inhibitors were selected dolutegravir and elvitegravir.

2.2.2 Modification and Conjugation of Zidovudine to Recombinant Human Vault Nanoparticles

AZT was suitable for vault conjugation due to the presence of a single hydroxyl group at the 5′ position of the nucleoside, facilitating modifications without unwanted side products. We first added a succinate group through an ester linkage by reacting the 5′ hydroxyl group with succinic anhydride[58] (Scheme 2.1). This linkage provided relative stability while allowing susceptibility to hydrolysis under acidic conditions or by esterases or nucleases, conditions present in the endosome and cytoplasm of cells,[59,60] to regenerate the 5′ hydroxyl group in the active form of AZT. This modified drug molecule was then conjugated to the 3432 free amine groups on each vault (43 lysine amine groups and an unmodified N-terminal amine per MVP, and 78 MVPs per vault).[48] The carboxyl end of the functionalized AZT succinate was converted to an N-hydroxysuccinimide ester (AZT-NHS) using N,N′-dicyclo-hexylcarbodiimide (DCC) and N-hydroxysuccinimide (NHS;[58] Scheme 2.1).

Scheme 2.1. Synthesis of AZT-NHS.

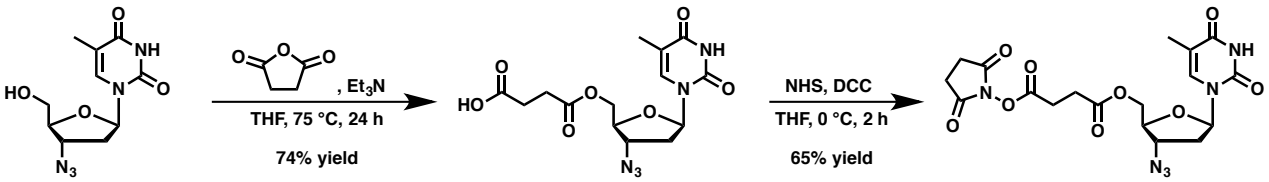

This NHS ester was then reacted with free amino groups on lysine (ε-amino) or N-termini (Scheme 2.2) using 3.28 molar equivalents of AZT−NHS with respect to vault amines, resulting in an average of 1296 ± 3 AZT molecules per vault (37.8% derivatization of the 3432 vault amines; Table 2.1) conjugated through amide linkages. This efficiency exceeded a prior estimate that 9−16% of these vault amines are available for reactivity by NHS coupling.[48] High performance liquid chromatography (HPLC) studies showed that the ester linkage between the AZT and vault was stable in Dulbecco's phosphate-buffered saline (DPBS) over 24 h at ambient temperature (data not shown).

Scheme 2.2. Conjugation of AZT-NHS to vaults.

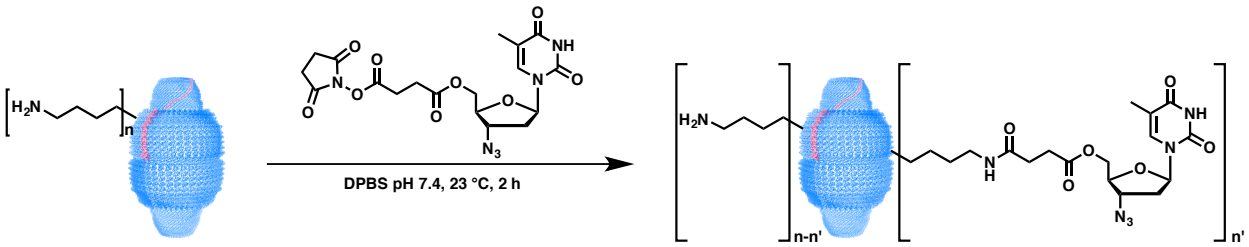

Table 2.1. Loading and efficiency of antiretroviral drug conjugation to vaults.

Drug	Equivalents/Lysine	Drugs/Vault	% Derivatization
Zidovudine	3.28	1296 ± 3.19	37.8
Tenofovir	2.25 (linker)/ 5 (drug)	640 ± 3.74	18.8
Elvitegravir	0.3	67 ± 4.81	1.9

2.2.3 Modification and Conjugation of Tenofovir to Recombinant Human Vault Nanoparticles

Due to limited oral bioavailability, tenofovir is administered as a prodrug, either tenofovir disoproxil fumarate (TDF) or tenofovir alafenamide fumarate (TAF).[61] Initial attempts were made to conjugate cleavable linkers to the exocyclic amine of TDF or TAF but were unsuccessful due to the limited options of cleavable linkers that could be added to this amine. To circumvent this problem, we designed a novel tenofovir prodrug containing an oxycarbonyloxymethyl linker, similar to the linker found on TDF (Scheme 2.3) In place of the inert terminal isopropyl groups on TDF, we used norbornene, providing a stable and orthogonal functional handle for conjugation of the prodrug to vaults. This was accomplished by alkylative esterification of TFV using norbornene methyl- (chloromethyl) carbonate to yield tenofovir-dimethylcarbonatemethlynorbornene (TFV−Nor; Scheme 2.3) to create a prodrug that can undergo esterase hydrolysis in a manner similar to TDF.

Scheme 2.3. Synthesis of TFV-Nor.

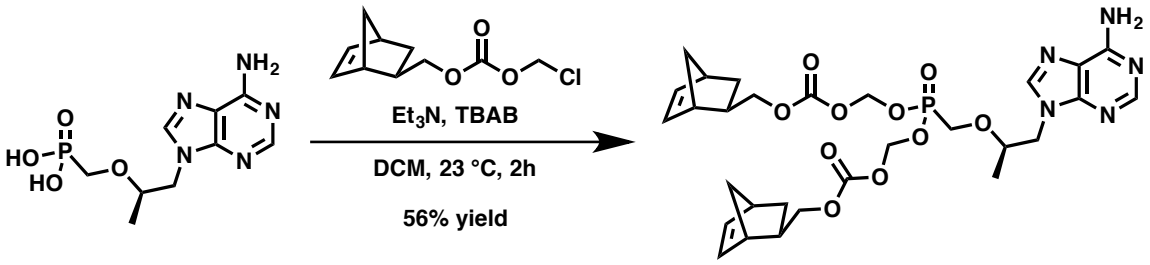

A methyltetrazine-PEG_4-NHS ester linker was used to conjugate TFV-Nor to vaults, requiring a two-part reaction. First, the linker was attached to vault proteins by reacting the NHS ester of the linker with free amines of the vault. This yielded vaults that were heavily decorated with methyltetrazine for selective reactivity with the norbornene of TFV-Nor through an irreversible inverse-electron-demand Diels-Alder reaction (Scheme 2.4; only one isomer is

shown for cycloaddition).[62,63] Vault conjugation was then performed using 5 mol equivalents of TFV-Nor with respect to vault amines, resulting in an average of 640 ± 4 TFV molecules per vault (18.8% derivatization of vault amines; Table 2.1).

Scheme 2.4. Conjugation of tenofovir-norbornene to vaults. Unfunctionalized vault amines are likely present in addition to the noted modifications but are omitted for clarity.

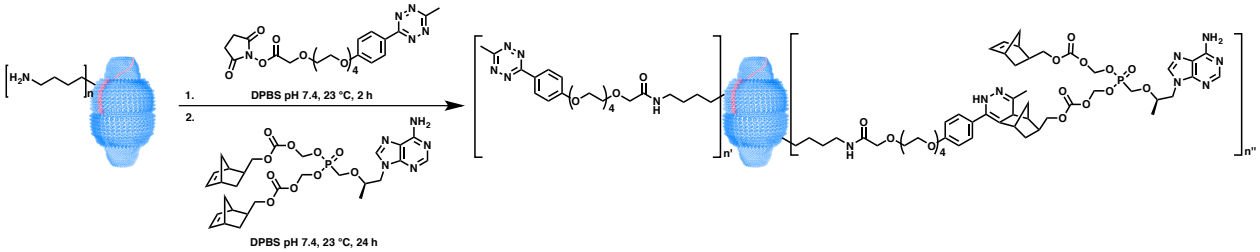

This conjugation efficiency was lower than that of AZT for two potential reasons. First, TFV-Nor is significantly more hydrophobic than AZT-NHS, which likely led to increased aggregation of vault proteins when higher conjugation efficiencies were achieved. Second, having two tetrazine reactive norbornene groups per molecule of TFV may have cross-linked vaults, leading to a loss of some vault particles. Despite these potential challenges, our TFV conjugation strategy still resulted in reasonable conjugation efficiency.

2.2.4 Efforts toward Modification of Dolutegravir for Conjugation to Recombinant Human Vault Nanoparticles

In addition to the previous reverse transcriptase inhibitor drugs, we selected the integrase strand transfer inhibitor DTG, which contains a pyridinone hydroxyl group that could be possible to reversibly modify. Realizing that this particular hydroxyl group likely had a low pK_a value and was accordingly likely to be a good leaving group, we investigated only relatively hydrophobic ester linkages in an effort to ensure stability of the resulting linkage to aqueous conditions. We first attempted to acylate the hydroxyl group via reaction with succinyl chloride to effectively

convert the available hydroxyl group into a carboxylic acid that could subsequently be transformed into an activated ester for lysine bioconjugation, similar to our synthesis of AZT-NHS. Interestingly, reaction of DTG with succinyl chloride followed by mild hydrolysis under aqueous conditions only returned starting material; however, hydrolysis in the presence of methanol yielded DTG-succinate methyl ester in good yield (Scheme 2.5). We therefore hypothesized that hydrolysis of the acid chloride was occurring, but was quickly followed by cyclization of the 4 carbon linker to produce succinic anhydride while simultaneously regenerating dolutegravir. Reaction of the acid chloride with methanol formed the corresponding methyl ester and effectively blocked this cyclization. Replacement of methanol with NHS or 4-nitrophenol in attempt to make the activated ester were unsuccessful, likely due to faster hydrolysis rates of the less stable linkages.

Scheme 2.5. Attempted synthesis of DTG-succinate with observed hydrolytic byproducts.

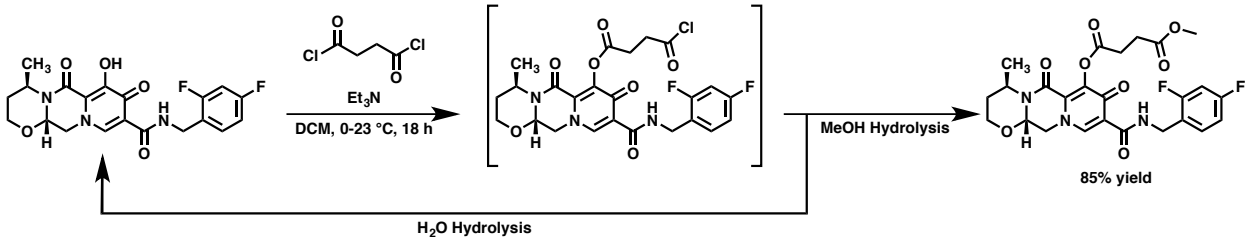

Scheme 2.6. Synthesis of DTG-fumarate.

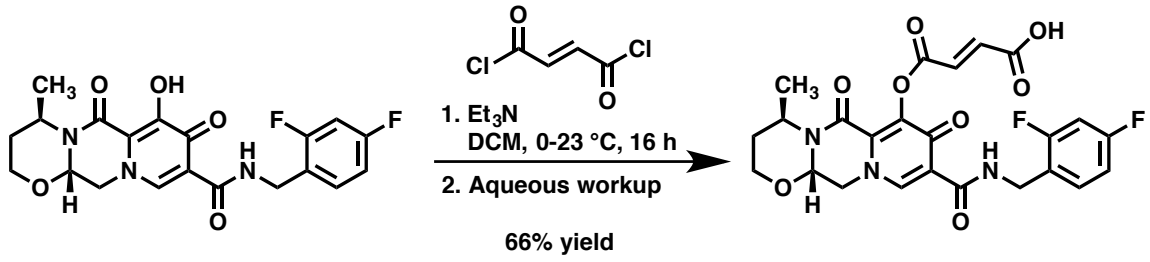

To prevent this unproductive cyclization, we replaced succinyl chloride with fumaryl chloride, which is a trans-2,3-unsaturated diacid chloride that cannot cyclize (Scheme 2.6).

Gratifyingly, we were able to isolate the desired product, DTG-fumarate; however, efforts to produce the corresponding activated ester were again unsuccessful and returned unmodified dolutegravir. This observation suggested that the newly installed ester linkage was unstable either due to the increased hydrophilicity of the newly installed carboxylic acid or due to the leaving group potential of dolutegravir. We decided to test the former hypothesis by coupling 4-maleimide butyric acid to dolutegravir using 1-ethyl-3-(3-dimethylaminopropyl)carbodiimide (EDC) and 4-dimethylaminopyridine (DMAP) (DTG-maleimide; Scheme 2.7). Although the desired pure product was obtained in reasonable yield, it became clear upon assessing stability by HPLC that even this hydrophobic ester was unstable in solution due to the leaving group potential of DTG, as the newly formed linkage was unstable even to acetonitrile over 18 hours (Figure 2.4). Although successful acylation of dolutegravir was later reported using myristoyl chloride,[64] conjugation of such a hydrophobic moiety to vaults would have likely experienced significant precipitation.

Scheme 2.7. Synthesis of DTG-maleimide.

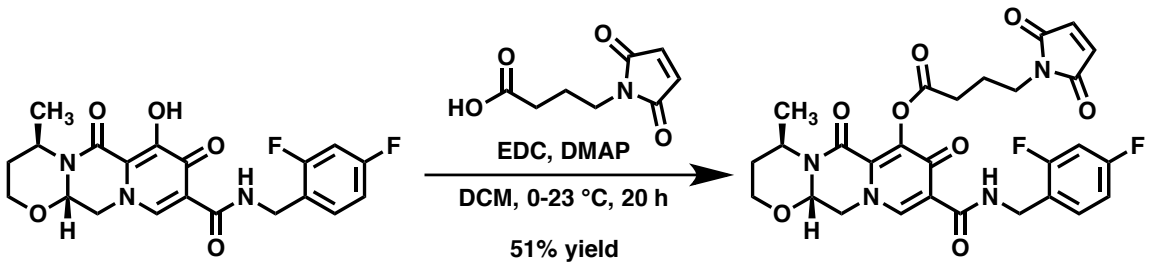

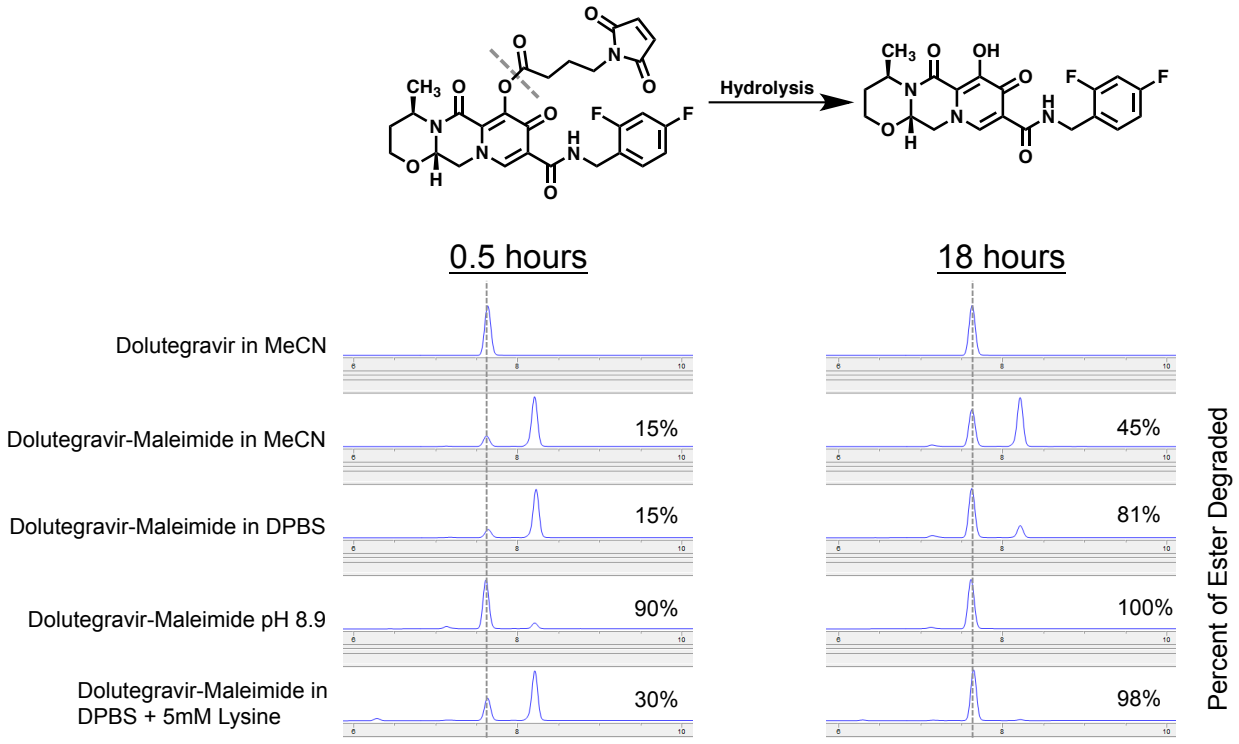

Figure 2.4. Hydrolysis of dolutegravir-maleimide monitored over time by HPLC. Upper scheme depicts the hydrolysis reaction being monitored with a dashed line indicating the site of hydrolysis. The vertical dashed line in the HPLC chromatograms marks the elution time of unmodified dolutegravir while the later eluting peak is dolutegravir-maleimide. Percentages to the right refer to the percentage of total ester linkage degraded by the indicated time of measurement.

2.2.5 Modification and Conjugation of Elvitegravir to Recombinant Human Vault Nanoparticles

Due to stability concerns pertaining to the linkages used for DTG, we shifted our focus to the integrase inhibitor EVG, which contains a readily modifiable primary hydroxyl group. We initially modified EVG in a manner similar to DTG-MAL to install a thiol reactive maleimide for conjugation to vault cysteine residues (EVG-MAL; Scheme 2.8). Each MVP subunit of the vaults possessed 5 cysteine residues (390 per vault), however it was unclear whether they were

free cysteines or engaged in disulfide bonds and to what extent these residues were surface-exposed and available for conjugation.

Scheme 2.8. Synthesis of EVG-MAL.

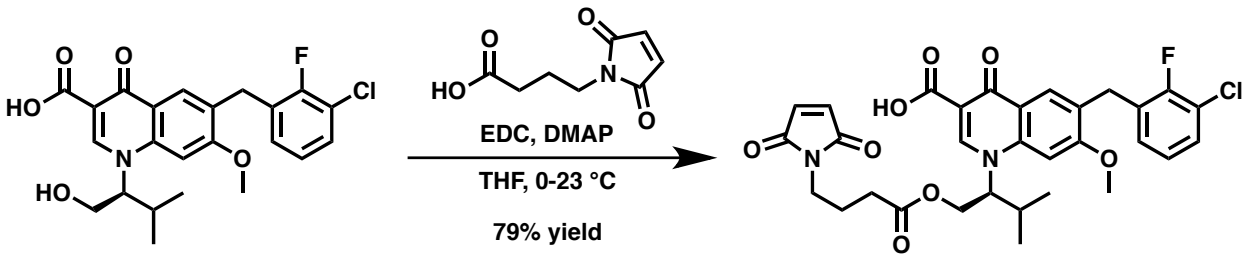

Scheme 2.9. Colorimetric quantification of free thiols using Ellman's Reagent.

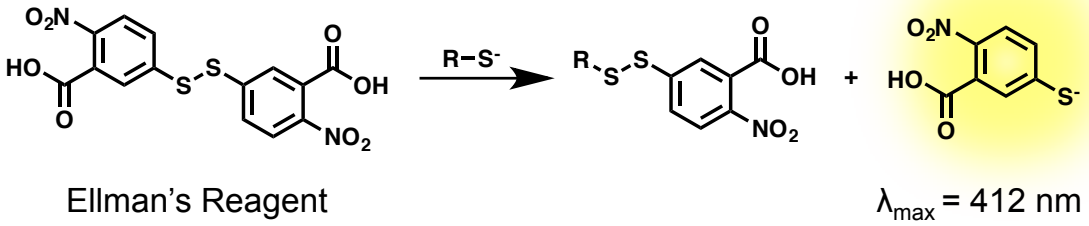

To determine the number of free thiols per MVP subunit, Ellman's Assay was performed (Scheme 2.9) and it was found that approximately 1 sulfhydryl per vault was available to react with small molecules. EVG-MAL was then conjugated to vault cysteines using 1 molar equivalent of EVG-MAL per cysteine residue under mildly reducing conditions in order to increase sulfhydryl availability (Scheme 2.10). This conjugation resulted in approximately 17 ± 3 molecules per vault (4.4% derivatization of the 390 vault thiols). To increase the drug loading, more drug equivalents were added, but this lowered vault recovery, most likely due to precipitation. Additionally, we attempted to increase the number of thiols per vault by using Traut's reagent (2-iminothiolane) to convert vault amines into reactive thiols, but due to the abundance of vault amines, this strategy lead to extensive crosslinking and precipitated nearly all

of the vaults from solution. Since free thiols were not abundant on the vaults and installation of additional thiols lead to crosslinking, we elected to instead develop an amine reactive linker to take advantage of the abundant vault amines.

Scheme 2.10. Conjugation of EVG-MAL to vaults.

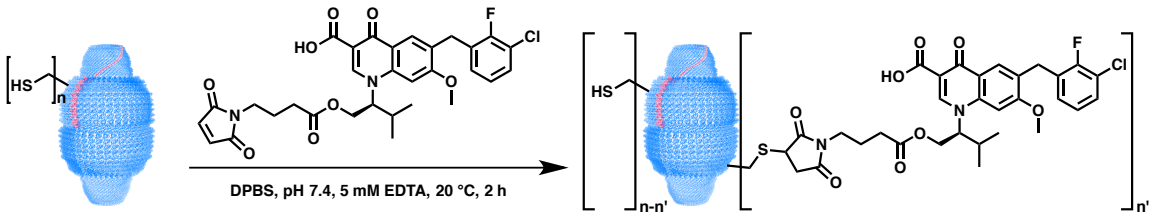

To install an amine-reactive functional group on EVG, the drug was reacted with N,N′-disuccinimidyl carbonate to create the N-hydroxysuccinimidyl carbonate of EVG (EVG-NHS, Scheme 2.11). Vault conjugation through carbamate linkages was then performed using 0.3 molar equivalents of EVG−NHS with respect to vault amines (Scheme 2.12), resulting in 67 ± 5 EVG molecules per vault (1.9% derivatization of vault amines, Table 2.1). Being a more hydrophobic drug compared to AZT and TFV, EVG demonstrated the lowest conjugation efficiency as expected. Titration experiments showed that as the drug to amine ratio increased, overall vault recovery decreased, suggesting that increased hydrophobicity imparted by EVG conjugation to the vaults caused them to precipitate (Table 2.2). By plotting protein recovery against conjugation efficiency versus the molar equivalents of drug used in each conjugation, an optimal compromise between drug loading and protein recovery was achieved (Figure 2.5). This phenomenon has similarly been reported for antibody-drug conjugates.[65–67]

Scheme 2.11. Synthesis of EVG-NHS.

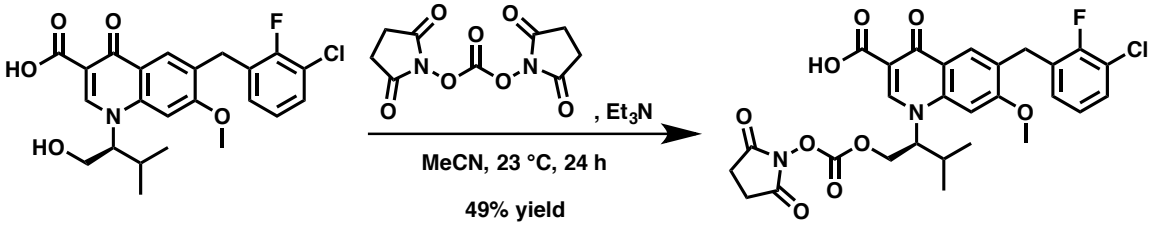

Scheme 2.12. Conjugation of EVG-NHS to vaults.

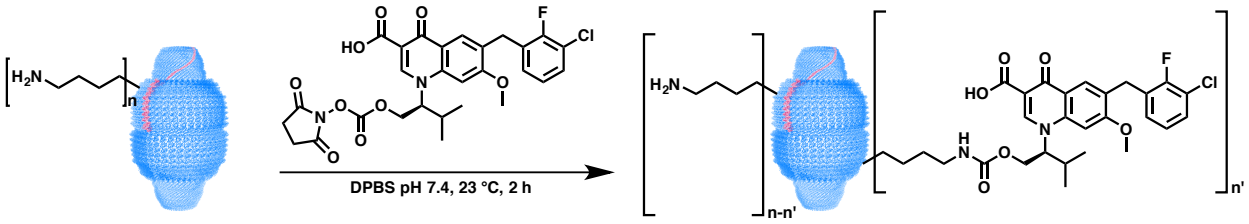

Table 2.2. Optimization of conjugation reaction between EVG-NHS and vaults. ND indicates not determined.

Entry	Vault Conc. (μg/ml)	% DMSO (v/v)	Equiv. Drug/Lysine	% Protein Yield	Drugs/Vault
1	667	8.5	5	0	ND
2	196	10	2	0	ND
3	200	5	0.500	8.2 ± 19.8	ND
4	200	5	0.250	41 ± 6.3	119 ± 5.6
5	200	5	0.125	56 ± 6.9	54 ± 2.9
6	200	5	0.050	60 ± 2.7	18 ± 4.2

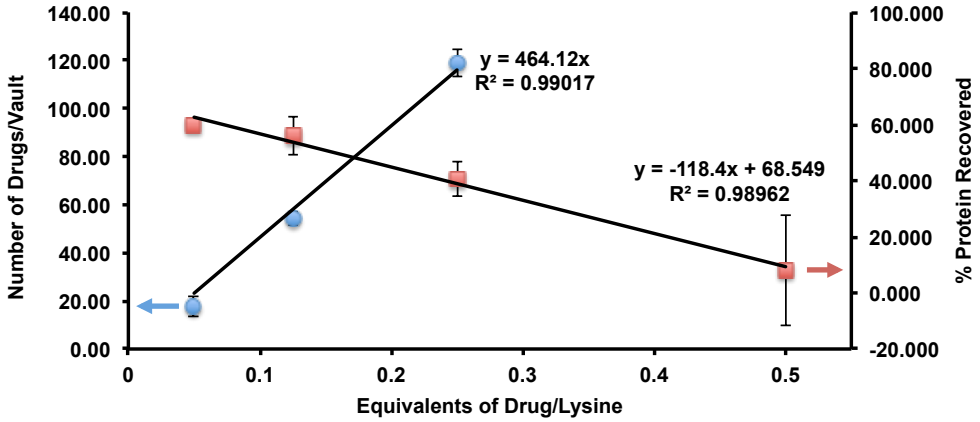

Figure 2.5. Relationship between drug loading and protein recovery in conjugation of EVG-NHS to vaults. Data plotted from Table 2.2.

2.2.6 Antiretroviral Drug-Conjugated Vaults Effectively Inhibit HIV-1 Infection in Human PBMC

To evaluate whether our drug-conjugated vaults access the intracellular compartment and release the active drug at the relevant site for antiviral activity, we compared equivalent titrated amounts of each drug in vault-conjugated versus free forms for the inhibition of in vitro HIV-1 infection of human PBMC. All drug-vault conjugates were similarly effective compared to the free drug,[57] indicating that vaults taken up intracellularly released the active form of the drug for access to the cytoplasm. These results were not due to any residual free drug in our vault conjugates, as multiple purification steps were performed and none was detectable by HPLC analyses (Figure 2.6).

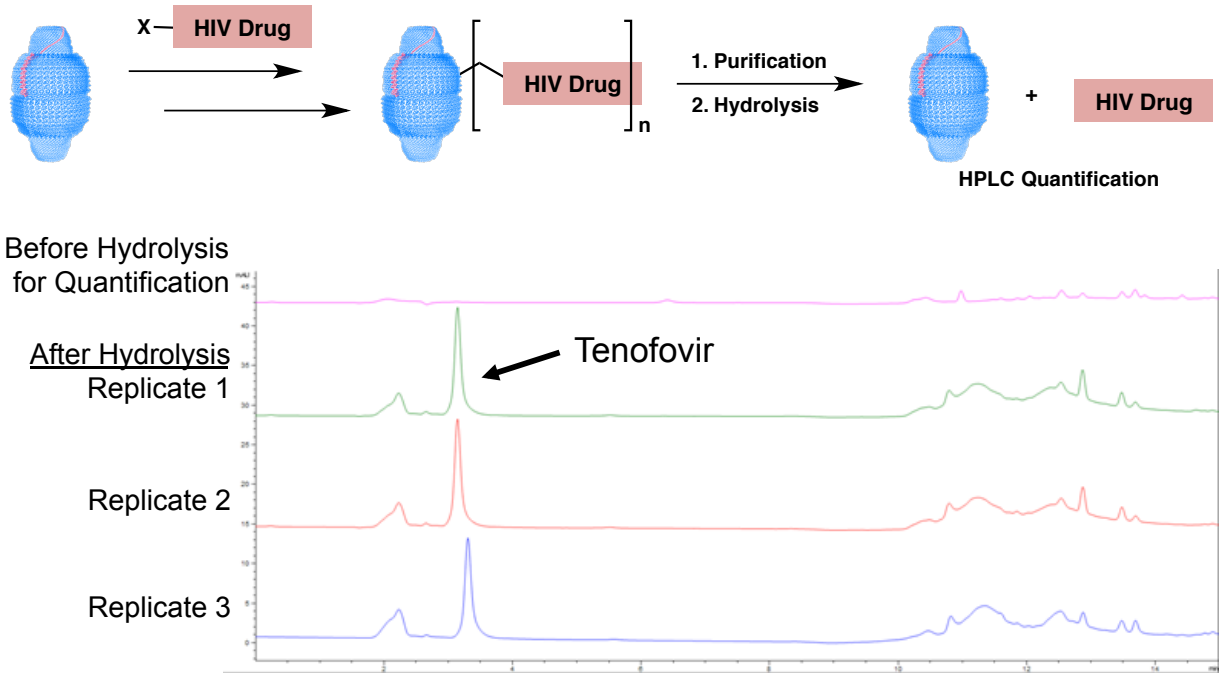

Figure 2.6. Schematic of drug loading quantification procedure with sample HPLC chromatograms of vault-tenofovir conjugates before and after alkaline hydrolysis. Following conjugation of antiretroviral drugs to vaults, conjugates were purified via sucrose gradient then the labile linkages between drugs and vaults were hydrolyzed with 1 M NaOH and the released drug was quantified via HPLC (≥3 replicates; bottom three chromatograms). A portion of the unhydrolyzed conjugate was also analyzed via HPLC as a control to ensure no background release (top chromatogram).

While the targeted drug-vault conjugates might have been predicted to have higher potency compared to the free drug, the similar observed potency may be related to the assay, where direct exposure of PBMC to free drug in vitro would minimize any comparative advantage of vault targeting. Drug targeting via vault conjugation could be advantageous in vivo where the key cells for HIV-1 infection are found in lower concentrations within tissues. A possible caveat is that drug conjugation may have interfered with vault uptake into the relevant target cells for HIV-1 infection, but this seems unlikely for two reasons. First, the experiments showing intracellular uptake of vaults utilized similar chemistry for fluorescent dye conjugation. Second,

drug conjugation to the vaults should have been relatively stable extracellularly, yet the active site of the drugs is intracellular, suggesting uptake. Although the precise mechanism of drug release for these conjugates remains unknown, drug release likely is facilitated by endosomal degradation of vaults and enzymatic or pH-dependent hydrolysis, or some combination thereof after uptake into cells. It has also been demonstrated in the context of other protein-drug conjugates (such as some antibody−drug conjugates) that release of the drug is not always required for full drug activity,[68] so it is possible that the antiretroviral drugs are active as conjugates or peptide adducts. Overall, comparison of drug-conjugated vaults to free drug antiviral activity allowed a functionally relevant assessment of active drug release from vaults.

A prior study showed that enhanced activity was only seen for targeted delivery of specific drug combinations, but not for single drugs.[22] We initially focused on single drugs since targeted drug delivery will most likely have immediate clinical utility in HIV-1 prevention (for which single agents may suffice, as in the case of a TFV gel rectal microbicide). Vaults conjugated with different drugs could be combined as needed for therapy or prevention. Conjugating multiple drugs simultaneously onto vaults would be problematic due to competition for lysine side chain reactive sites, making it difficult or impossible to control the relative ratios of drugs. Finally, vault nanoparticles can be engineered to have antibody-specific targeting,[53] and engineering CD4-targeted vaults could further improve targeting to HIV-1-susceptible cells. Others have used CD4 targeting strategies to improve nanodelivery of indinavir for HIV-1 infection.[31] Overall, our data have shown that functional drugs can be effectively delivered via conjugation to recombinant human vault nanoparticles, which are naturally self-targeted to the key cells involved in HIV-1 infection, potentially improving efficacy and minimizing systemic toxicity.

2.2.7 PEGylation and Fluorescent Labeling of Recombinant Vault Nanoparticles

These vault-drug conjugates demonstrated excellent drug loading and proved effective for inhibition of HIV-1 infection *in vitro*; however, *in vivo* delivery requires not only effective targeting and release, but also sufficient bioavailability to achieve adequate drug levels in vulnerable cells. Anticipating that vault-drug conjugates might have difficulty penetrating the colorectal mucosa, we investigated PEGylation of vaults as a means to increase diffusion through this layer, as coverage of nanoparticles with short PEG chains is known to enhance nanoparticle diffusion in mucus.[23] We investigated PEGylation of both cysteine and lysine vault residues using maleimide and NHS functionalized PEGs, respectively. Once conjugation conditions were optimized, vaults were further fluorescently tagged to demonstrate their amenability to loading of both large and small molecules and also for detection in eventual mucosal diffusion assays.

Scheme 2.13. General synthesis of mPEG-maleimide reagents.

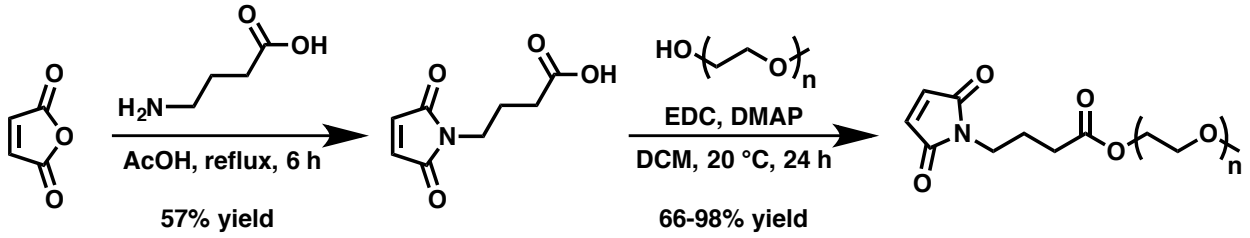

To generate a maleimide-containing functional group that could be used to easily functionalize commercial PEG reagents, 4-maleimide butyric acid was prepared by refluxing γ-amino butyric acid with maleic anhydride in acetic acid. Synthesis of methyl ether PEG-maleimide (mPEG-MAL) was then carried out in good yields via reaction of hydroxyl-terminated 2, 5, and 20 kDa mPEG with EDC, DMAP, and 4-maleimide butyric acid (Scheme 2.13). Conjugation of these maleimide-functionalized polymers was then attempted under a variety of conditions using 7800 molar equivalents of polymer per vault (approximately 20 molar

equivalents per cysteine residue) in the presence of 10 mM TCEP to maximize the availability of free thiols on human recombinant vault nanoparticles (Figure 2.7A). However, conjugation to human vault cysteine residues was ultimately unsuccessful for all lengths of mPEG-MAL due to limited availability of cysteine residues (approximately 78 free thiols per vault) and limited accessibility of these residues to macromolecules (Figure 2.7B).

Interestingly, conjugation of mPEG-MAL with cysteine-enriched, recombinant rat vault nanoparticles (CP-MVP vaults) under the same conditions yielded conjugates with all mPEG-MAL polymers (Figure 2.7C). This result further supports the hypothesis that there are few accessible thiols in recombinant human vaults for conjugation, which was also noted in EVG-MAL conjugation reactions. Although conjugate bands were observed in the SDS-PAGE analysis for CP-MVP vaults, these bands were faint and only a few polymers per MVP subunit were observed, implying a low-efficiency conjugation. Again, this is most likely attributed to low accessibility of the polymers to the engineered free thiols as CP-MVP vaults still only contain 9 cysteine residues per MVP subunit compared to 5 residues for human vaults. Key to these 4 additional residues is their accessibility, which confers a significant improvement in conjugation efficiency with no conjugation observed for human vaults whereas CP-MVP vaults exhibited higher molecular weight conjugate bands. Even with conjugate bands observed, conjugation efficiency was still low and could not be accurately measured due to the close proximity of the bands observed by SDS-PAGE as well as the faintness of the conjugate bands compared to background staining. Typically, a much higher degree of surface functionalization is required for enhanced mucosal penetration, so we adjusted our conjugation strategy accordingly to target the more plentiful lysine residues.

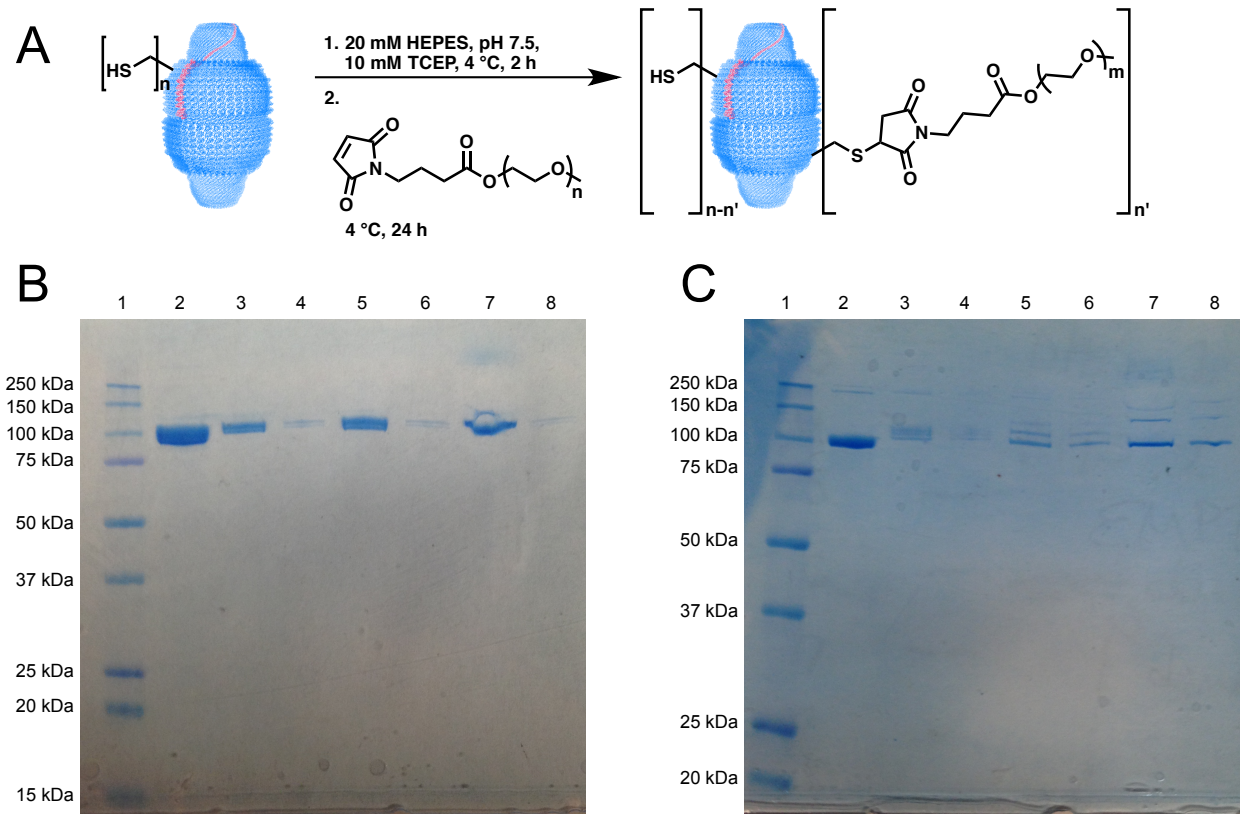

Figure 2.7. Conjugation of mPEG-maleimide to vault nanoparticles. (**A**) Conjugation reaction conditions of 2, 5, and 20 kDa mPEG-maleimide polymers to (**B**) human vaults and (**C**) recombinantly engineered, cysteine enriched rat vaults analyzed by SDS-PAGE stained with Coomassie Brilliant Blue. Gel images in (B) and (C) were prepared identically except for the species of vaults used as noted. Lane 1: protein standards; lane 2: vault protein standard; lanes 3-8 were loaded with 10 and 2 µl aliquots from conjugation reactions of vaults with 2 kDa (lanes 3-4), 5 kDa (lanes 5-6), and 20 kDa (lanes 7-8) mPEG-maleimide, respectively.

Recombinant human vault amines were modified using a short 2 kDa methyl ether PEG succinimidyl ester (mPEG-NHS) with 30 molar equivalents per lysine residue (100,620 molar equivalents per vault). Following PEGylation, the vaults were immediately tagged with AlexaFluor 594-NHS using 0.47 molar equivalents per lysine (1560 molar equivalents per vault) to fluorescently label the particles for mucosal diffusion assays (Figure 2.8A). As expected, functionalization of vault amines proceeded more efficiently than thiol modifications as was

evident from SDS-PAGE analysis followed by differential visualization (Figure 2.8B-D). Quantification of conjugation efficiency was determined by measuring the amount of free amines before and after PEGylation and fluorescent tagging, respectively, using the amine-reactive ortho-phthaldialdehyde (OPA) assay (Scheme 2.14). PEGylation of recombinant human vault nanoparticles (before fluorescent tagging) resulted in a conjugation efficiency of 36.0 ± 5.0%, or approximately 1236 ± 172 molecules of 2 kDa mPEG per vault. Fluorescent tagging increased the conjugation efficiency by 12.3% and added about 422 molecules of AlexaFluor 594 for a final conjugation efficiency of 48.3 ± 2.9%, or approximately 1658 ± 100 total molecules of 2k mPEG and AlexaFluor 594 per vault.

These results also follow the same trend observed for vault-drug conjugates with the highly soluble, hydrophilic 2k mPEG and AlexaFluor 594 demonstrating excellent conjugation efficiencies compared to the more hydrophobic drugs. We expect that not only will PEGylation of the vaults enhance mucosal penetration and therefore increase bioavailability, but also that PEGylation may be useful for increasing conjugation efficiencies of other small molecules by preventing vault precipitation due to increased particle hydrophilicity following PEGylation.

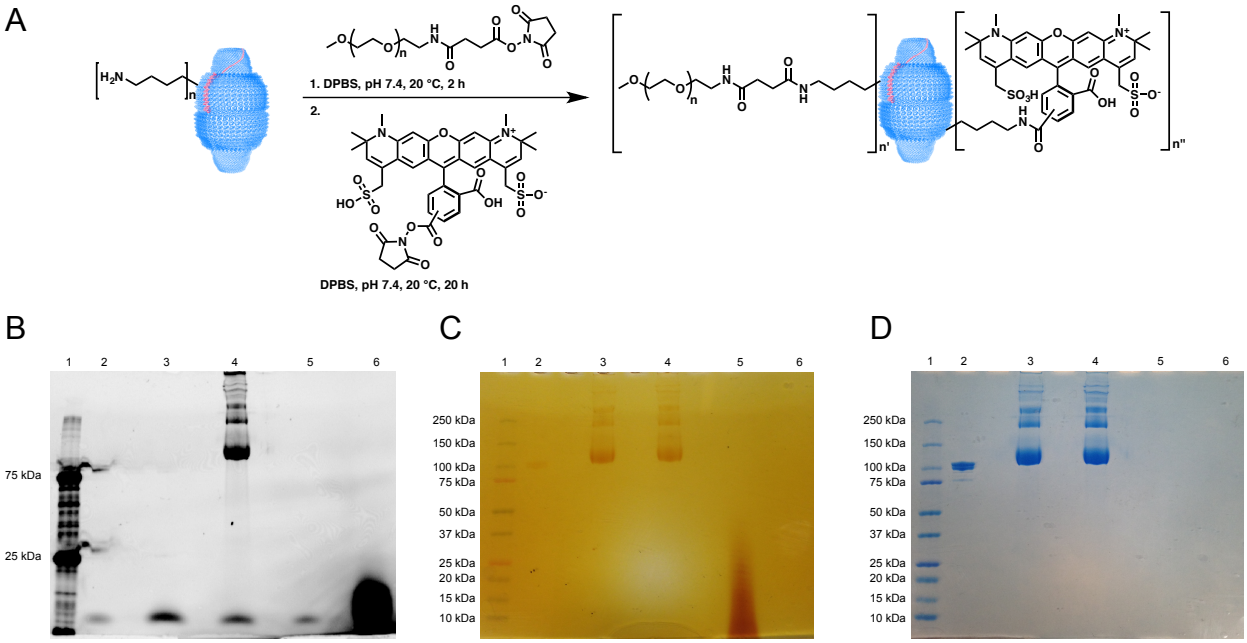

Figure 2.8. PEGylation and fluorescent tagging of amino groups on human vault nanoparticles. (**A**) Conjugation reaction conditions of 2 kDa mPEG-NHS and AlexaFluor 594 to vaults followed by SDS-PAGE analysis and visualization with (**B**) fluorescence imaging, (**C**) 0.1 N iodine solution, and (**D**) Coomassie Brilliant Blue to confirm presence of fluorescent tags, PEG, and protein, respectively. Unfunctionalized vault amines are likely present in addition to the noted modifications but are omitted for clarity. SDS-PAGE images (B-D) were captured from the same gel using different imaging techniques. Lane 1: protein standards; lane 2: vault protein standard; lane 3: PEGylated vaults without AlexaFluor 594; lane 4: PEGylated and fluorescently tagged vaults; lane 5: 2 kDa mPEG only; lane 6: AlexaFluor 594 only.

Scheme 2.14. Fluorescent quantification of primary amines using *o*-phthaldialdehyde (OPA).

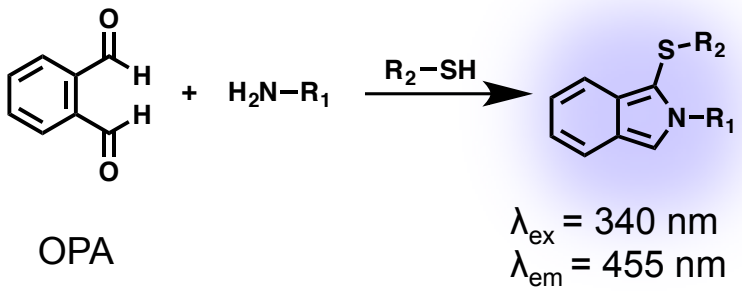

2.3 Conclusions

Specific subsets of immune cells were identified that readily take up human vault nanoparticles, predominantly antigen presenting cells (dendritic cells, monocytes/macrophages) and activated T cells. Because these are the key cell types infected by HIV-1, this suggests that vault targeting could be harnessed for antiretroviral drug delivery for HIV-1 prevention or treatment strategies to maximize efficacy while minimizing systemic toxicity. As a proof of concept, three anti-HIV-1 drugs were each directly conjugated to recombinant human vault nanoparticles. These vault-conjugated drugs retained antiviral activity against HIV-1 infection of PBMC, indicating intracellular access and release of active drug. Furthermore, vault nanoparticles were highly amenable to PEGylation and could also be co-loaded with other small molecules such as a fluorescent dye, which has implications for enhanced mucosal penetration. This delivery system has the potential to facilitate targeted drug delivery for HIV-1 prevention (e.g., microbicides) or enhanced treatment strategies.

2.4 Experimental

2.4.1 Materials

Tetrahydrofuran (THF), acetonitrile (MeCN), and dichloromethane (DCM) were dried by purging with nitrogen and passage through activated alumina columns prior to use. Zidovudine and tenofovir were purchased from Combi-Blocks, elvitegravir from eNovation Chemicals, dolutegravir from MedChem Express, and the methyltetrazine-PEG_4-NHS ester linker from Click Chemistry Tools. All other chemicals were used as purchased unless otherwise noted from Acros, Alfa Aesar, Sigma Aldrich, Chem-Impex, or Fisher Scientific. All reactions were performed using dry solvents under an inert Argon atmosphere unless otherwise noted. Vault

nanoparticles were expressed and purified as described previously[69] by Dr. Valerie Kickhoefer and Dr. Leonard Rome. The synthesis of AZT-NHS and TFV-Nor was performed by Dr. Alex Wollenberg based on the published procedures.[57,58]

2.4.2 Analytical Techniques

NMR spectra were obtained using either Bruker AV400, AV500, or DRX500 spectrometers. ESI mass spectra were obtained using either a Waters Acquity LCT Premier XE equipped with an autosampler and direct injection port or an Agilent 6530 QTOF-ESI with a 1260 Infinity LC with autosampler. Infrared absorption spectra were obtained using a PerkinElmer FT-IR equipped with an ATR accessory. Normal phase flash column chromatography was carried out using a Biotage Isolera One Flash Purification Chromatography system. Analytical reverse phase high performance liquid chromatography (HPLC) was carried out on a Agilent 1260 Infinity II HPLC system equipped with an autosampler and a UV detector using a Poroshell 120 2.7 μm C18 120 Å column (analytical: 2.7 μm, 4.6 × 100 mm) with monitoring at λ = 220 and 280 nm and with a flow rate of 0.8 mL/min. Preparatory reverse phase HPLC was carried out on a Shimadzu high performance liquid chromatography system equipped with a UV detector using a Luna 5 μm C18 100 Å column (preparatory: 5 μm, 250 × 21.2 mm) with monitoring at λ = 215 and 254 nm and with a flow rate of 20 mL/min. UV/Vis spectra were obtained using a JASCO V-770 UV-Visible/NIR spectrophotometer. Microplate absorbance and fluorescence measurements were recorded using a Tecan Infinite M1000 Pro automated plate reader system. SDS-PAGE was performed using Bio-Rad Any kD Mini-PROTEAN-TGX gels and gels were stained with Coomassie for visualization of protein or 0.1 N iodine for visualization of PEG. SDS-PAGE protein standards were obtained from Bio-Rad (Precision Plus Protein Pre-stained Standards).

General procedure for quantification of drug-vault conjugates via HPLC

An HPLC standard curve for each antiretroviral was generated by measuring the peak area (280 nm absorbance) after injecting, in triplicate, 1, 5, 10, 50, 100, 500, and 1000 ng of each drug and plotting the corresponding peak areas against the amount of drug injected. After generating these standard curves, the average number of drugs per vault was determined for each conjugate via basic hydrolysis of the labile linkages (either ester or carbamate) between drug molecules to release the native drug. The area under the peak corresponding to the retention time of each drug was then used to determine the amount of drug injected, which was then used to calculate the number of drugs attached to each vault. Additionally, a negative control consisting of the conjugate with no NaOH added was used to determine the amount of free drug before basic hydrolysis, and this amount was subtracted from the amount of calculated conjugated drug. A sample set of HPLC chromatograms is provided in Figure 2.6.

Analytical HPLC

Zidovudine was analyzed using a mobile phase consisting of 10-100% MeCN + 0.1% TFA in water beginning with a 1 min isocratic at 10%, then up to 100% over 10 min in a linear gradient, followed by an isocratic hold at 100% MeCN + 0.1% TFA for 4 min (total time was 15 min; product eluted at 5.9 min). Tenofovir was analyzed using a mobile phase consisting of 5-100% MeCN + 0.1% TFA in water beginning with 5 min isocratic at 5%, then up to 100% over 6 min in a linear gradient, followed by an isocratic hold at 100% MeCN + 0.1% TFA for 4 min (total time was 15 min; product eluted at 3.1 min). Dolutegravir was analyzed using a mobile phase consisting of 10-100% MeCN + 0.1% TFA in water beginning with a 1 min isocratic at 10%, then up to 100% over 10 min in a linear gradient, followed by an isocratic hold at 100% MeCN + 0.1% TFA for 4 min (total time was 15 min; product eluted at 7.6 min). Elvitegravir

was analyzed using a mobile phase consisting of 10-100% MeCN + 0.1% TFA in water beginning with a 1 min isocratic at 10%, then up to 100% over 10 min in a linear gradient, followed by an isocratic hold at 100% MeCN + 0.1% TFA for 4 min (total time was 15 min; product eluted at 11.0 min).

Preparative HPLC

AZT-NHS was purified using a mobile phase consisting of 10-95% MeCN + 0.1% trifluoroacetic acid (TFA) in water beginning with 1 min isocratic at 10%, then up to 95% over 15 min in a linear gradient, followed by an isocratic hold at 95% MeCN + 0.1% TFA for 4 min (total time was 20 min; product eluted at 13.5 min). TFV-Nor was purified using a mobile phase consisting of 40-95% MeCN + 0.1% TFA in water beginning with 1 min isocratic at 40%, then up to 95% over 15 min in a linear gradient, followed by an isocratic hold at 95% MeCN + 0.1% TFA for 4 min (total time was 20 min; product eluted at 12.0 min). EVG-NHS was purified using a mobile phase consisting of 50-95% MeCN + 0.1% TFA in water beginning with 1 min isocratic at 50%, then up to 95% over 15 min in a linear gradient, followed by an isocratic hold at 95% MeCN + 0.1% TFA for 4 min (total time was 20 min; product eluted at 15.8 min).

2.4.3 Methods

Ellman's Assay

Quantification of free sulfhydryl groups on both human and engineered rat vaults were determined using Ellman's Reagent according to the manufacturer's procedure (Thermo Scientific).

Synthesis of 4-maleimide butyric acid

Synthesis of 4-maleimide butyric acid was based on the reported procedure.[70] To a previously oven dried 1-neck 100 mL round bottom flask equipped with a stir bar and water

condenser was added γ-amino butyric acid (2.00 g, 19.4 mmol, 1 eq), maleic anhydride (2.28 g, 23.3 mmol, 1.2 eq), and 60 mL of glacial acetic acid. The mixture was heated to 120 °C in an oil bath for 6 hours, then cooled to ambient temperature before pouring into water and extracting with 4 times with ethyl acetate. The combined organics were then washed once with brine, dried over anhydrous magnesium sulfate, and the solvent removed under vacuum to yield a yellowish solid. The resultant solid was further purified on silica gel via flash column chromatography using a gradient of 2-20% MeOH in DCM (R_f = 0.71; 9:1 DCM:MeOH). Fractions containing pure product were combined and dried under vacuum to yield a white crystalline solid (2.021 g, 56.9% yield). See Figure 2.9 for ^{1}H NMR (400 MHz, $CDCl_3$, 25 °C): δ 11.01 (s, 1H), 6.71 (s, 2H), 3.60 (t, J = 6.8 Hz, 2H), 2.38 (t, J = 7.4 Hz, 2H), 1.93 (q, J = 7.1 Hz, 2H). See Figure 2.10 for ^{13}C NMR (100 MHz, $CDCl_3$, 25 °C): δ 178.06, 170.76, 134.16, 36.98, 31.08, 23.55.

Synthesis of mPEG-maleimide

Representative procedure: To a previously oven dried 2-neck 25 mL round bottom flask was added 20 kDa mPEG (0.500 g, 0.025 mmol, 1 eq) followed by 25 mL DCM. Once dissolved, 4-malemide butyric acid (0.046 g, 0.250 mmol, 10 eq) was added to the flask and stirred for several minutes until dissolved. Next, 1-ethyl-3-(3-dimethylaminopropyl)carbodiimide (EDC; 0.039 g, 0.250 mmol, 10 eq) and 4-dimethylaminopyridine (DMAP; 0.002 g, 0.013 mmol, 0.5 eq) were added to the flask and stirred for 24 hours at 20 °C. Solvent was then removed under vacuum and the crude material was redissolved in minimal MeOH and purified via dialysis over 36 hours beginning with 100% MeOH, then 50% MeOH in H_2O, then 100% H_2O with solvent changes performed every 12 hours. Lyophilization of the resulting solution yielded a white solid (0.497 g, 98.4% yield). See Figure 2.11 for 2 kDa mPEG-maleimide ^{1}H NMR (400 MHz, $CDCl_3$, 25 °C): δ 6.70 (s, 2H), 4.23 (t, J = 4.8 Hz, 2H), 3.83-3.38 (m, 182H), 3.38 (s, 3H),

2.35 (t, J = 7.4 Hz, 2H), 1.93 (q, J = 7.2 Hz, 2H). See Figure 2.12 for 5 kDa mPEG-maleimide ^{1}H NMR (400 MHz, $CDCl_3$, 25 °C): δ 6.69 (s, 2H), 4.22 (t, J = 4.8 Hz, 2H), 3.82-3.37 (m, 477H), 3.37 (s, 3H), 2.34 (t, J = 7.4 Hz, 2H), 1.92 (q, J = 7.2 Hz, 2H). See Figure 2.13 for 20 kDa mPEG-maleimide ^{1}H NMR (400 MHz, $CDCl_3$, 25 °C): δ 6.70 (s, 2H), 4.22 (t, J = 4.8 Hz, 2H), 3.82-3.46 (m, 1948H), 3.38 (s, 3H), 2.35 (t, J = 7.4 Hz, 2H), 1.93 (q, J = 7.1 Hz, 2H).

Conjugation of mPEG-maleimide to vaults

To a 0.5 mL LoBind tube was added 12.5 µl of a 2 mg/mL stock solution of either recombinant human vaults or CP-2 MVP engineered rat vaults followed by 12.5 µl of 20 mM HEPES buffer, pH 7.5 with 10 mM TCEP and the solutions were incubated at 4 °C for 2 hours. 25 µl solutions containing either 2, 5, or 20 kDa mPEG-maleimide in 20 mM HEPES buffer, pH 7.5 were then prepared at concentrations of 2.01 mM, and each solution was added to a separate tube containing the aforementioned reduced vault solutions; the molar ratio of mPEG-maleimide to vaults in each condition was 7800:1, respectively. The reactions were gently mixed, then incubated at 4 °C for 24 hours before being transferred to 0.5 mL 30kDa cutoff Centriprep tubes and centrifuged at 14,000 rcf to remove excess polymer and to concentrated samples (5 x 500 µl 20 mM HEPES, pH 7.5). The resulting protein-polymer conjugates were then analyzed by SDS-PAGE under reducing conditions.

Conjugation of 2 kDa mPEG-NHS and AlexaFluor 594 to vaults

To a 1.5 mL LoBind tube was added 200 µl of a 1 mg/mL solution of recombinant human vaults followed by 582.4 µl of a 10 mg/mL solution of 2k mPEG-NHS (30 molar equivalents mPEG-NHS per vault lysine residue) and 16 µl of buffer to bring the total volume up to 800 µl; all solutions were prepared using DPBS, pH 7.4. The reaction was then incubated at 20 °C for 2 hours with gentle rocking. Next, 160 µl of this reaction solution was removed for use as a

control, and 1.32 µl of a 20 mg/mL AlexaFluor 594 carboxylic acid succinimidyl ester solution (1560 molar equivalents per vault) was added to the remaining solution and the reaction was protected from light and rocked at 20 °C for an additional 20 hours. After 22 hours total, the reactions were transferred to 0.5 mL 30kDa cutoff Centriprep tubes and centrifuged at 14,000 rcf to remove excess polymer and dye and to concentrate samples (5 x 500 µl DPBS, pH 7.4). The resulting PEGylated, dye-labeled vaults were then analyzed by SDS-PAGE under reducing conditions. Protein concentration was determined via a standard BCA Assay according to the manufacturer's recommended procedure (ThermoFisher Scientific). At least 3 replicates were used for all samples and standards.

OPA Assay for quantification of vault amines to determine conjugation efficiency

Quantification of conjugation efficiency was carried out via a fluorescent assay using o-phthaldialdehyde (OPA) as an amine-reactive reporter. The OPA assay was carried out based on the previously reported procedure.[71] Briefly, the OPA reagent working solution was prepared fresh and consisted of 0.1 M borate buffer, pH 10 with 6 mM OPA reagent (previously dissolved in 1% of the total solution volume of ethanol), 28 mM 2-mercaptoethanol, and 0.05% Triton X-100. 10 µl of each sample and standard were added to microplate wells, then 300 µl of OPA reagent working solution was added to each well. Incubation with moderate shaking was carried out for 5 minutes at 20 °C, then average fluorescence was measured with excitation and emission wavelengths of 340 and 455 nm, respectively. Unmodified vaults were used as standards and relative fluorescence values were compared to modified vaults to determine approximate conjugation efficiency. At least 3 replicates were used for all samples and standards.

Synthesis of AZT-NHS

The synthesis of AZT-NHS was performed by Dr. Alex Wollenberg by modifying a preexisting procedure.[57,58]

Synthesis of TFV-Nor

The synthesis of TFV-Nor was performed by Dr. Alex Wollenberg according to the published procedure.[57]

Synthesis of DTG-succinate

To an oven dried 2-neck 25 mL round bottom flask was added DTG (50.0 mg, 0.120 mmol, 1 eq). Next, DTG was dissolved in 10 mL of DCM and cooled to 0 °C in an ice bath, then allowed to stir for 5 minutes before adding succinyl chloride (106 µl, 0.960 mmol; 8 eq) dropwise over one minute. The reaction was stirred for several minutes, then triethylamine (33 µl, 0.240 mmol, 2 eq) was added. The reaction was stirred at 0 °C for an additional 5 minutes, then the water bath was removed and the reaction was allowed to stir for 18 hours overnight at 20 °C. The solution was then concentrated under vacuum and dissolved in 40% MeOH in water and purified by preparative HPLC. DTG-succinate was purified using a mobile phase consisting of 40-95% MeOH in water beginning with 2 min isocratic at 40%, then up to 95% over 19 min in a linear gradient, followed by an isocratic hold at 95% MeOH for 4 min (total time was 20 min; product eluted at 18.5 min). Fractions containing product were concentrated under vacuum to yield the pure product as a white solid (52.8 mg, 85.2% yield). See Figure 2.14 for ^{1}H NMR (400 MHz, $CDCl_3$, 25 °C): δ 10.15 (t, *J* = 5.7 Hz, 1H), 8.43 (s, 1H), 7.32 (q, *J* = 5.9 Hz, 1H), 6.79 (ddd, *J* =4.1 Hz, 2H), 5.22 (q, *J* = 3.2 Hz, 1H), 4.92 (t, *J* = 6.0 Hz, 1H), 4.62 (m, 2H), 4.28 (dd, *J* = 13.3, 3.8 Hz, 1H), 4.15 (dd, *J* = 13.3, 6.0 Hz, 1H), 3.97 (d, *J* = 6.7 Hz, 2H), 3.71 (s, 3H), 3.07 (t, *J* = 7.3 Hz, 2H), 2.79 (t, *J* = 7.3 Hz, 2H), 2.17 (m, 1H), 1.51 (dd, *J* = 14.1, 2.0 Hz, 1H), 1.33

(d, J = 7.0 Hz, 3H). HRMS: $C_{25}H_{26}F_2N_3O_8$ Calc. $[M+H]^+$ = 534.1688 Da; Obs. $[M+H]^+$ = 534.2159.

Synthesis of DTG-fumarate

To an oven dried 2-neck 25 mL round bottom flask was added DTG (50.0 mg, 0.120 mmol, 1 eq). Next, DTG was dissolved in 10 mL of MeCN and cooled to 0 °C in an ice bath, then allowed to stir for 5 minutes before adding fumaryl chloride (129 µl, 1.19 mmol; 10 eq). The reaction was stirred at 0 °C for an additional 30 minutes, then the water bath was removed and the reaction was allowed to stir for 16 hours overnight at 20 °C. The solution was then concentrated under vacuum and dissolved in 50% MeOH in water and purified by preparative HPLC. DTG-succinate was purified using a mobile phase consisting of 30-95% MeCN + 0.1% TFA in water beginning with 2 min isocratic at 30%, then up to 95% over 19 min in a linear gradient, followed by an isocratic hold at 95% MeCN + 0.1% TFA for 4 min (total time was 25 min; product eluted at 12.6 min). Fractions containing pure product were concentrated under vacuum to yield the product as a white solid (40.9 mg, 66.0% yield). See Figure 2.15 for ^{1}H NMR (400 MHz, DMSO-d_6, 25 °C): δ 13.37 (s, 1H), 10.08 (t, J = 5.9 Hz, 1H), 8.68 (s, 1H), 7.36 (m, 1H), 7.19 (m, 1H), 7.02 (m, 1H), 6.86 (d, J = 2.0 Hz, 2H), 5.38 (dd, J = 3.9, 5.5 Hz, 1H), 4.66 (t, J = 6.0 Hz, 1H), 4.60 (dd, J = 13.6, 3.7 Hz, 1H), 4.50 (d, 5.8 Hz, 2H), 4.42 (d, 12.8 Hz, 1H), 3.94 (t, 11.1 Hz, 1H), 3.82 (dt, J = 9.3, 2.4 Hz, 1H), 1.90 (m, 1H), 1.47 (dd, J = 13.7, 2.1 Hz), 1.22 (d, J = 7.0 Hz, 3H).

Synthesis of DTG-MAL

To a 25mL 2-neck round bottom flask was added 10 mL DCM followed by DTG (40.0 mg, 0.100 mmol, 1 eq). Next, 4-maleimidobutyric acid (35.0 mg, 0.190 mmol, 2 eq) was added and the reaction mixture was cooled to 0 °C in an ice bath and stirred for 5 minutes before

adding DMAP (2.0 mg, 0.020 mmol, 0.2 eq) and EDC (37.0 mg, 0.190 mmol, 2 eq). The reaction was stirred for 30 min at 0 °C, then the ice bath was removed and the reaction proceeded for a total of 20 hours. The entire mixture was then concentrated under vacuum and redissolved in 30% MeCN in H_2O before purification by preparative HPLC. DTG-MAL was purified using a mobile phase consisting of 20-95% MeCN + 0.1% TFA in water beginning with 2 min isocratic at 20%, then up to 95% over 19 min in a linear gradient, followed by an isocratic hold at 95% MeCN + 0.1% TFA for 4 min (total time was 25 min; product eluted at 20.5 min). Fractions containing pure product were concentrated under vacuum to yield the product as a white solid (28.4 mg, 50.7% yield). See Figure 2.16 for ^{1}H NMR (400 MHz, $CDCl_3$, 25 °C): δ 10.31 (t, J = 5.7 Hz, 1H), 8.54 (s, 1H), 7.31 (m, 1H), 6.79 (m, 2H), 6.68 (s, 2H), 5.23 (dd, J = 3.9, 5.7 Hz, 1H), 4.90 (t, J = 5.8 Hz, 1H), 4.59 (d, J = 5.3 Hz, 1H), 4.34 (dd, J = 13.5, 5.8 Hz, 1H), 4.19 (dd, J = 13.5, 5.7 Hz, 1H), 3.96 (d, J = 7.8 Hz, 2H), 3.65 (t, J = 7.1 Hz, 2H), 2.73 (t, J = 7.6 Hz, 2H), 2.15 (m, 1H), 2.06 (m, 1H), 1.51 (dd, J = 14.0, 1.9 Hz, 1H), 1.32 (d, J = 7.0 Hz, 3H). See Figure 2.17 for ^{13}C NMR (125 MHz, $CDCl_3$, 25 °C): δ 171.85, 170.69, 170.00, 163.27, 162.51 (dd, J = 189.1, 11.9 Hz), 160.53 (dd, J = 190.4, 11.9 Hz), 154.95, 144.97, 143.19, 134.12, 130.64 (dd, J = 5.8, 9.6 Hz), 129.17, 121.22 (dd, J = 15.2, 3.8 Hz), 119.70, 111.22 (dd, J = 21.1, 3.7 Hz), 103.81 (t, J = 25.4 Hz), 76.14, 62.59, 53.13, 44.85, 37.07, 36.58 (d, J = 3.9 Hz), 31.27, 29.31, 23.71, 15.88. See Figure 2.18 for UV-Vis absorption spectra of DTG and DTG-maleimide.

Synthesis of EVG-MAL

To a 25 mL 2-neck round bottom flask was added 10 mL MeCN followed by EVG (50.0 mg, 0.112 mmol, 1 eq). Next, 4-maleimidobutyric acid (102.0 mg, 0.558 mmol, 5 eq) was added and the reaction mixture was cooled to 0 °C in an ice bath and stirred for 5 minutes before adding DMAP (2.7 mg, 0.022 mmol, 0.2 eq) and EDC (42.8 mg, 0.223 mmol, 2 eq). The

reaction was stirred for 30 min at 0 °C, then the ice bath was removed and the reaction proceeded for a total of 16 hours. The entire mixture was then concentrated under vacuum and redissolved in 60% MeCN in H_2O before purification by preparative HPLC. EVG-MAL was purified using a mobile phase consisting of 60-95% MeCN + 0.1% TFA in water beginning with 1 min isocratic at 60%, then up to 95% over 14 min in a linear gradient, followed by an isocratic hold at 95% MeCN + 0.1% TFA for 5 min (total time was 20 min; product eluted at 14.4 min). Fractions containing pure product were concentrated under vacuum to yield the product as a white solid (53.82 mg, 79.1% yield). See Figure 2.19 for ^{1}H NMR (500 MHz, $CDCl_3$, 25 °C): δ 8.80 (s, 1H), 8.26 (s, 1H), 7.28 (t, J = 6.6 Hz, 1H), 7.06 (t, J = 6.3 Hz, 1H), 7.00 (dt, J = 0.9, 7.9 Hz, 1H), 6.94 (s, 1H), 6.65 (s, 1H), 4.63 (dd, J = 4.1, 9.4 Hz, 2H), 4.47 (dd, J = 8.2, 13.2 Hz, 1H), 4.11 (s, 2H), 4.00 (s, 3H), 3.44 (J = 6.7 Hz, 2H), 2.50 (m, 1H), 2.17 (m, 2H), 1.74 (q, J = 6.8 Hz, 2H), 1.24 (d, J = 6.4 Hz, 3H), 0.86 (d, J = 6.6 Hz, 3H). See Figure 2.20 for ^{13}C NMR (125 MHz, $CDCl_3$, 25 °C): δ 176.65, 172.34, 170.87, 163.10, 157.50, 155.33, 144.63, 142.34, 134.12, 129.52, 129.40 (d, 3.7 Hz), 129.14, 128.19, 127.51 (d, 15.5 Hz), 124.49 (d, 4.6 Hz), 121.21 (d, 18.1 Hz), 119.16, 95.83, 64.87, 63.37, 56.27, 36.42, 30.64, 30.49, 29.15 (d, 2.8 Hz), 23.28, 19.59, 19.56. HRMS: $C_{31}H_{31}ClFN_2O_8$ Calc. $[M+H]^+$ = 613.1753 Da; Obs. $[M+H]^+$ = 613.1751.

Synthesis of EVG-NHS

To a previously oven dried 2-neck 25 mL round bottom flask under Argon was added *N,N′*-disuccinimidyl carbonate (0.143 g, 0.53 mmol, 5 eq) and 4 mL dry MeCN. In a separate vial was dissolved EVG (0.050 g, 0.11 mmol, 1 eq) in 3 mL dry MeCN and TEA (0.047 mL, 0.33 mmol, 3 eq) while under Argon. This solution of EVG was briefly mixed and then added dropwise via syringe into the solution of *N,N′*-disuccinimidyl carbonate. The reaction was stirred at 20 °C for 5 hours, then the solvent was completely removed under vacuum. The crude material

was purified using preparative HPLC followed by removal of solvent under vacuum to yield a yellow solid (30.93 mg, 46.9% yield). See Figure 2.21 for ^{1}H NMR (500 MHz, $CDCl_3$, 25 °C): δ 8.73 (s, 1H), 8.25 (s, 1H), 7.25 (dd, *J* = 14.8, 1.4 Hz, 1H), 7.06 (t, *J* =7.1 Hz, 1H), 6.98 (t, *J* = 7.8 Hz, 1H), 6.94 (s, 1H), 4.89 (d, *J* = 9.8 Hz, 1H), 4.73 (m, 2H), 4.10 (q, *J* = 12.9 Hz, 2H), 3.99 (s, 3H), 2.73 (s, 4H), 2.42 (m, 1H), 1.25 (d, *J* = 6.3 Hz, 3H), 0.83 (d, *J* = 6.5 Hz, 3H). See Figure 2.22 for ^{13}C NMR (126 MHz, $CDCl_3$, 25 °C): δ 177.2, 168.2, 167.9, 163.0, 157.5, 151.3, 143.5, 142.4, 129.42, 129.41, 129.38, 128.96, 128.90, 128.47, 127.83, 127.71, 124.44, 124.40, 121.17, 121.03, 119.7, 109.3, 95.6, 70.0, 64.4, 56.2, 30.8, 29.05, 29.03, 25.4, 19.8, 19.5. FTIR: ν = 2957, 2920, 1814, 1789, 1739, 1613, 1456, 1374, 1305, 1257, 1195, 1152, 1095, 1047, 1012, 991, 923, 878, 810, 790, 753, 732 cm^{-1}. HRMS: Calc. [M+1] = 589.1389 Da; Obs. [M+1] = 589.1391 Da.

Conjugation of AZT-NHS to vaults

0.5 mg of lyophilized human MVP (hMVP) vaults was resuspended in 125 µl 1x DPBS. 1 µl of 200 µg/µl AZT-NHS stock solution in DMSO was added to 74 µl of 4 µg/µl hMVP vaults in 1 x DPBS. The reaction was incubated at room temperature for 2 hours. AZT conjugated vaults were purified from unconjugated AZT-NHS by gel exclusion chromatography using Bio-Gel® P polyacrylamide P-6 Columns. To further eliminate any potential contamination of the AZT conjugated vaults with free AZT-NHS, a stepwise sucrose gradient (sucrose fractions of 20%, 30%, 40%, 45%, 50% and 60%) was performed. The sucrose gradient was spun at 25K, 16 hours, 4 °C, ω^2t=3.95E11 in a sw41 rotor. Sucrose fractions (40% and 45%) containing AZT conjugated vaults were collected, diluted in 1 x DPBS and spun at 40K for 2 hours, 4 °C in a Ti 70.1 rotor. The resulting AZT-vault pellet was washed with 6.5 mL of 1x DPBS and centrifuged at 40K for 1 h, 4 °C in a Ti70.1 rotor. The wash step was repeated 2x to ensure the complete removal of any residual sucrose. Subsequently, the washed pellet was

resuspended in 150 µl of 1x DPBS, filtered via 0.2 µm syringe filter and the protein concentration determined by BCA assay.

Conjugation of TFV-Nor to vaults

1 mg of lyophilized recombinant human vaults was added 1375 µl DPBS and the lyophilized cake was dissolved by gentle shaking. NHS-TEG-tetrazine linker was then added (125 µl of a 4 µg/µl stock solution prepared in DMSO; 0.50 mg; 0.562 µmol; 2.25 eq./lysine). The reaction was then mixed on a rocker table at 20 °C for 2 hours. The unreacted linker was then removed by centrifugal filtration using a pre-equilibrated 30 kDa MW cutoff filters. The contents were centriprepped 5 times and the products collected by inverse centrifugation. This material was diluted in 1407 µl of DPBS in a new 1.5 mL tube and TFV-Nor was added (93 µl of a 15 µg/µl stock solution prepared in DMSO; 1.40 mg; 2.16 µmol; 5 eq./lysine). Some drug precipitated, but the conjugation was continued on the rocker for 24 hours followed by purification by sucrose gradient as described above. The vaults eluted in the 40 and 45% fractions and were collected and their concentration measured via standard BCA Assay.

Conjugation of EVG-MAL to vaults

To a 1.5 mL LoBind tube was added 51.2 µl of a 1 mg/mL solution of recombinant human vaults followed by 11.0 µl of a 3 mg/mL solution of EVG-MAL in DMF (7800 molar equivalents EVG-MAL per vault) and 437.8 µl of buffer to bring the total volume up to 500 µl; all solutions were prepared using DPBS, pH 7.4 with 5 mM EDTA. The conjugation was gently mixed on a rocker table for 2 hours at 20 °C followed by purification by sucrose gradient as described above. The conjugate eluted in the 40 and 45% fractions and was collected and its concentration determined via standard BCA Assay.

Conjugation of EVG-NHS to vaults

1 mg of lyophilized recombinant human vaults was added 950 μl DPBS, then transferred to a 2 mL LoBind tube. Another 950 μl DPBS was used to wash the tube and also transferred to the 2 mL tube for a total volume of 1900 μl. 23.5 μl DMSO was then added to the 2 mL tube. Then, EVG-NHS was added (76.5 μl of 1 μg/μl stock solution prepared in DMSO; 0.076 mg; 0.13 μmol; 0.3 eq./lysine). The conjugation was gently mixed on a rocker table for 4 hours at 20 °C followed by purification by sucrose gradient as described above. The conjugate eluted in the 40 and 45% fractions and was collected and its concentration determined via standard BCA Assay. Optimization for this conjugation reaction was carried out by varying the molar equivalents of EVG-NHS while keeping all other variables constant.

2.5 Appendix A

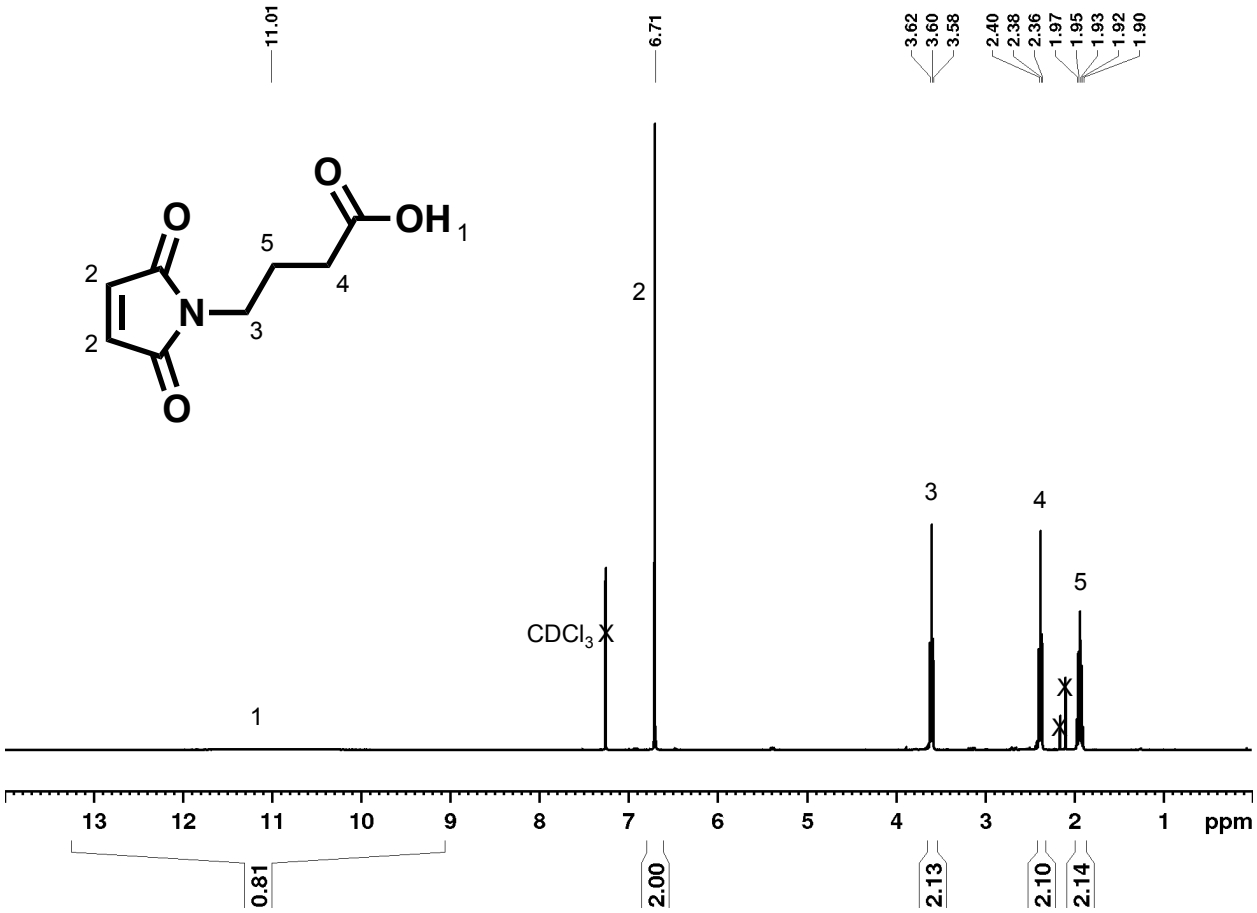

Figure 2.9. ^{1}H NMR spectrum of 4-maleimide butyric acid in $CDCl_3$.

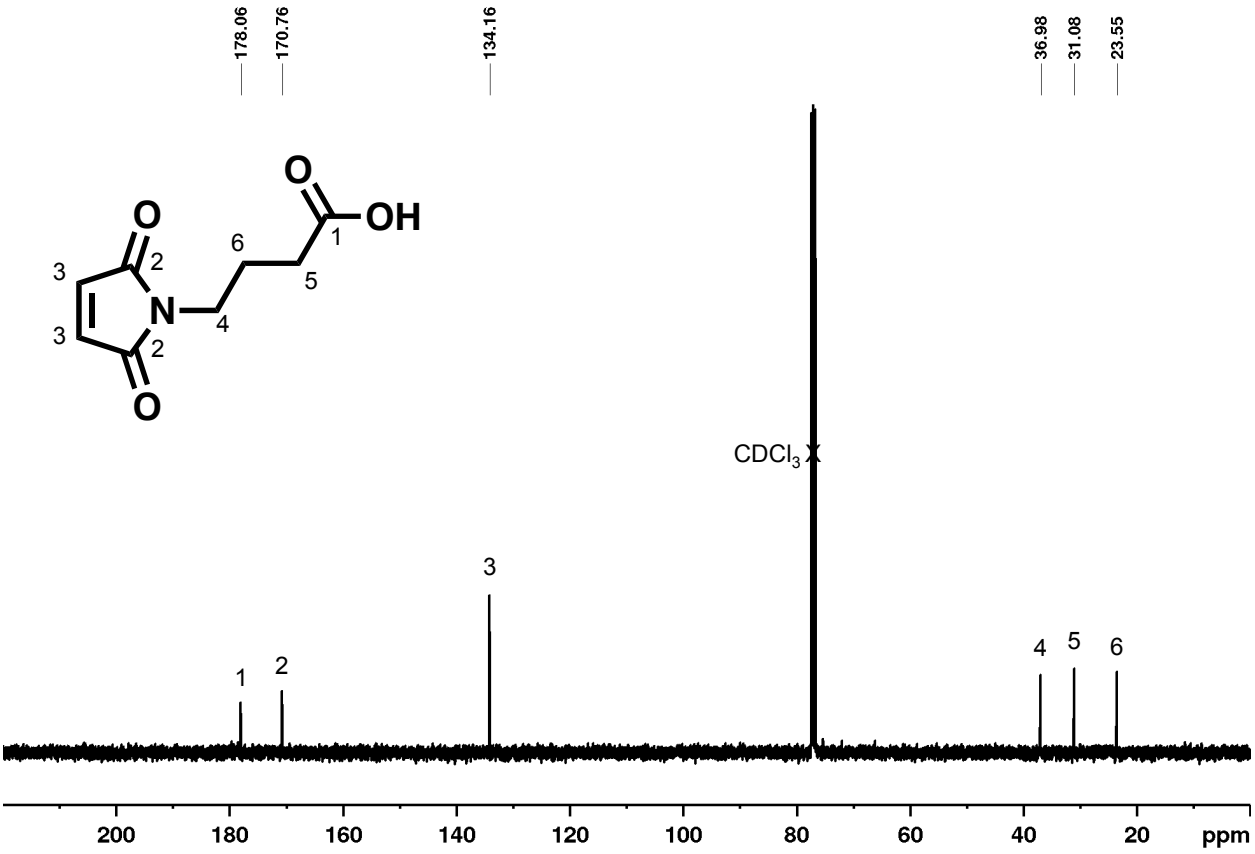

Figure 2.10. ^{13}C NMR spectrum of 4-maleimide butyric acid in $CDCl_3$.

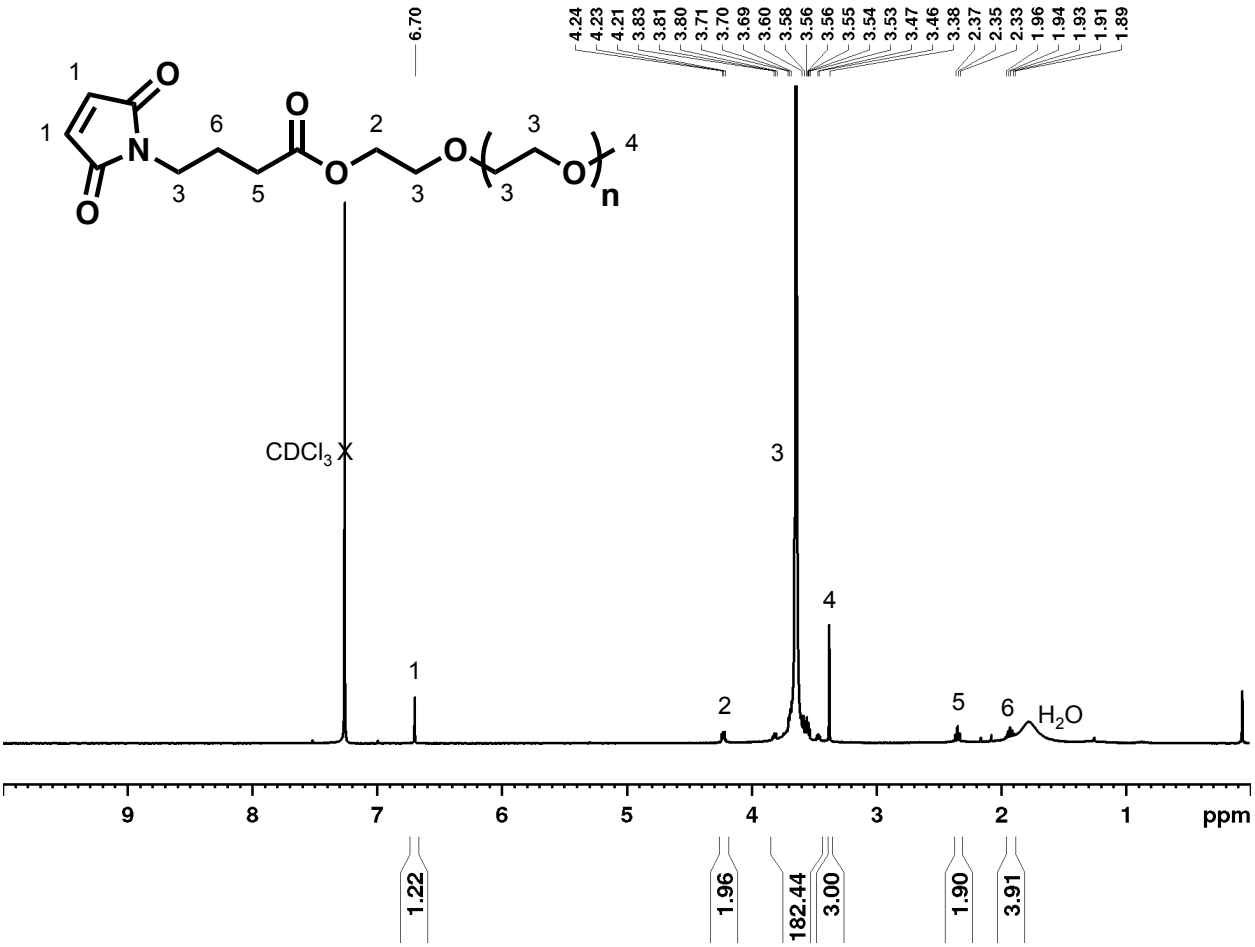

Figure 2.11. ^{1}H NMR spectrum of 2 kDa mPEG-maleimide in $CDCl_3$.

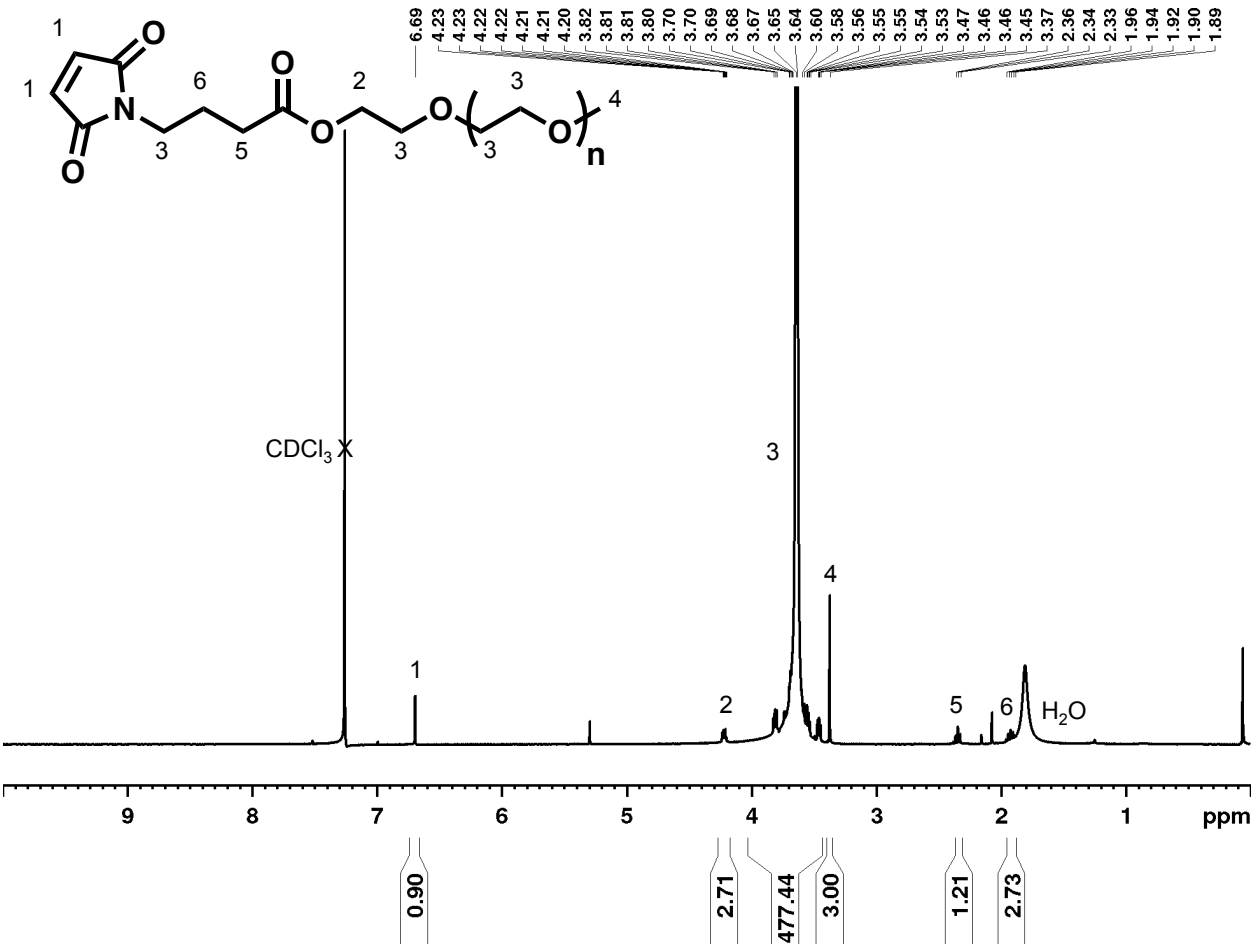

Figure 2.12. ^{1}H NMR spectrum of 5 kDa mPEG-maleimide in $CDCl_3$.

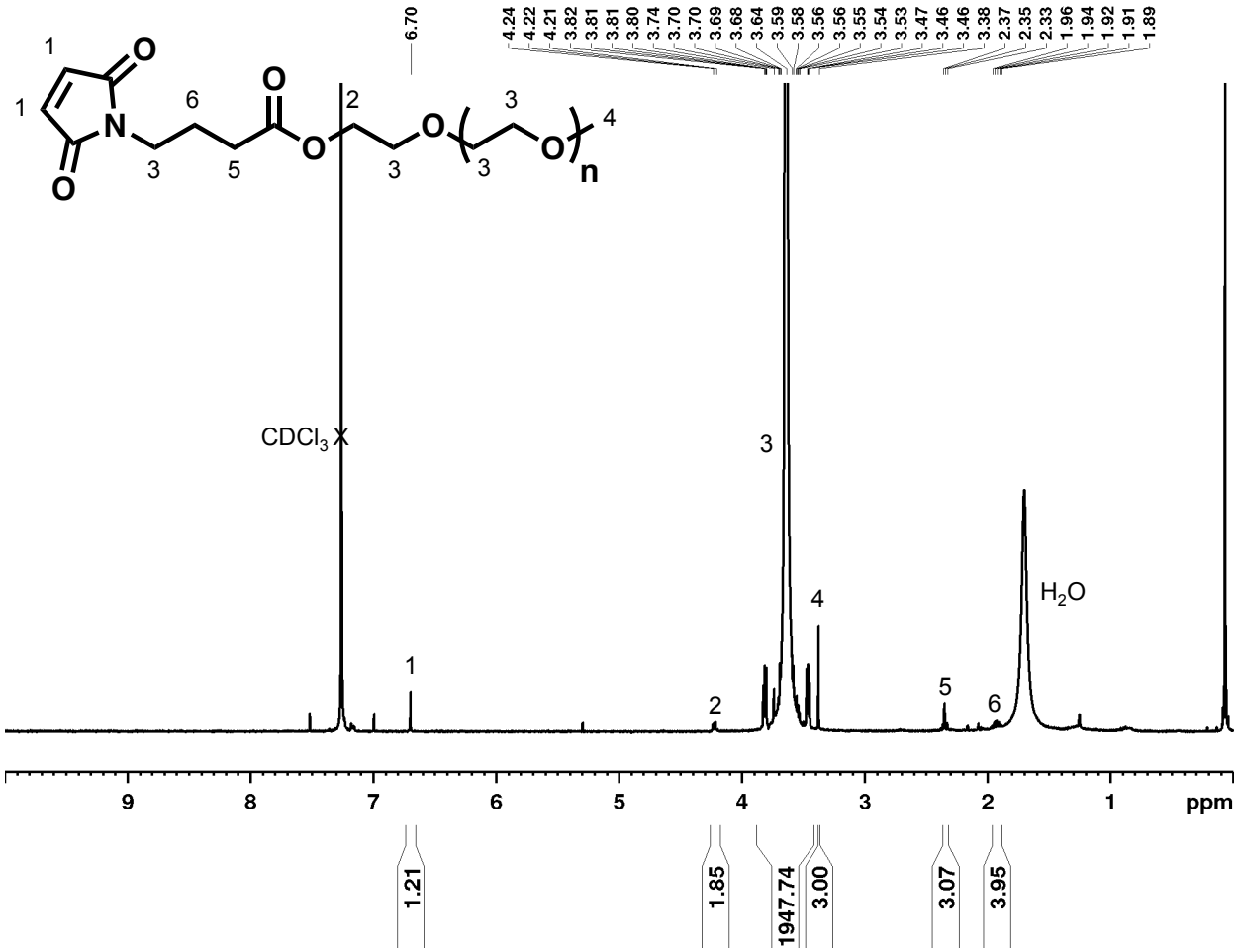

Figure 2.13. ^{1}H NMR spectrum of 20 kDa mPEG-maleimide in $CDCl_3$.

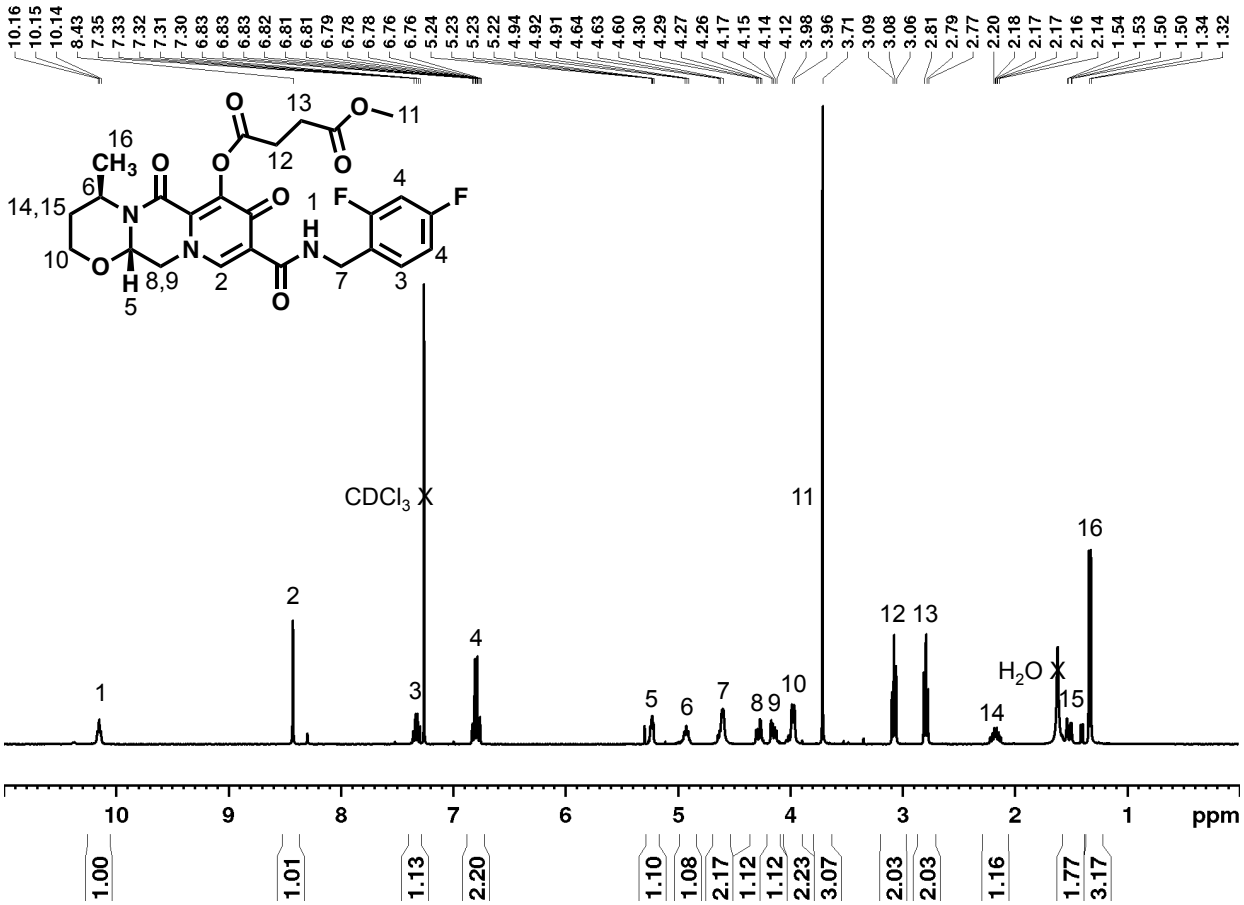

Figure 2.14. ^{1}H NMR spectrum of DTG-succinate methyl ester in $CDCl_3$.

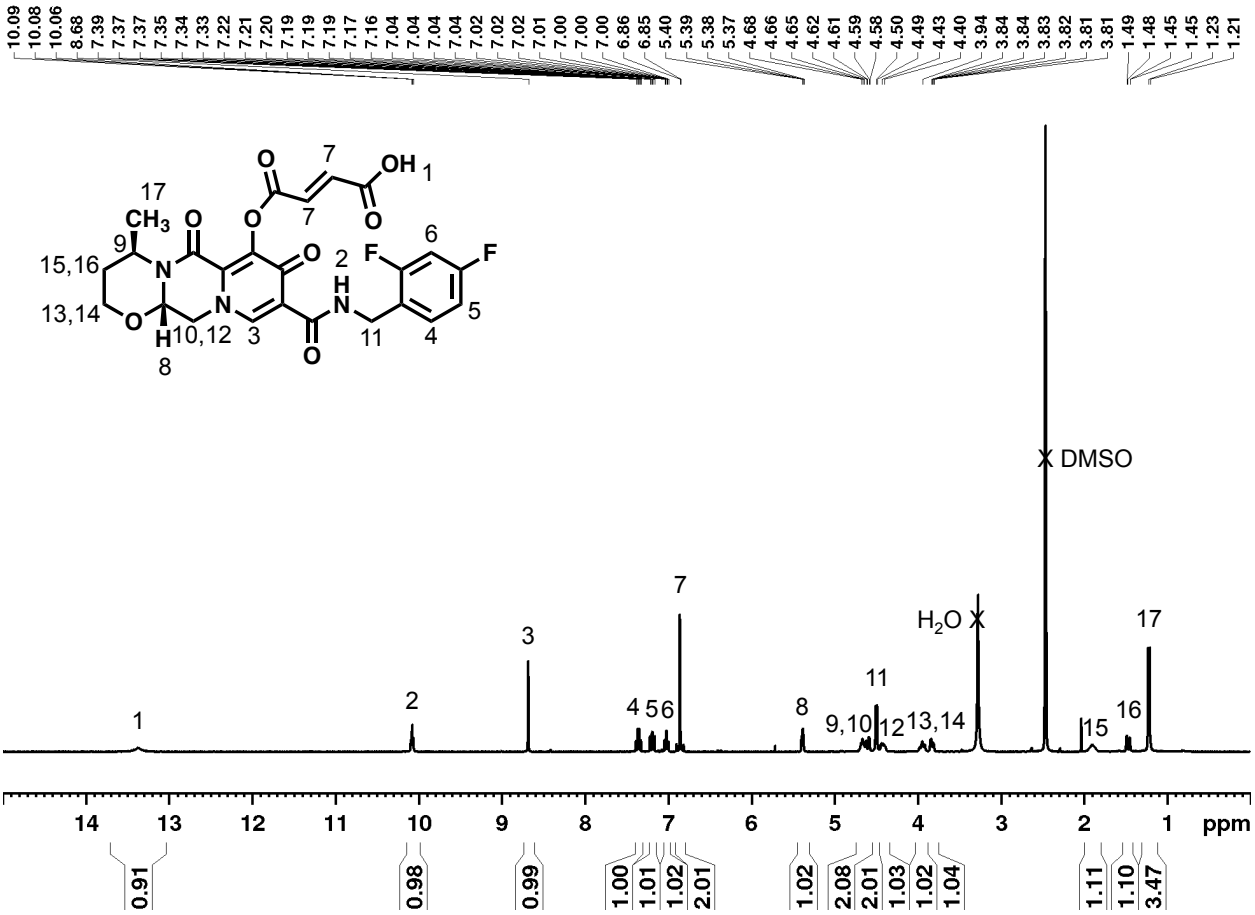

Figure 2.15. ^{1}H NMR spectrum of DTG-fumarate in DMSO-d_6.

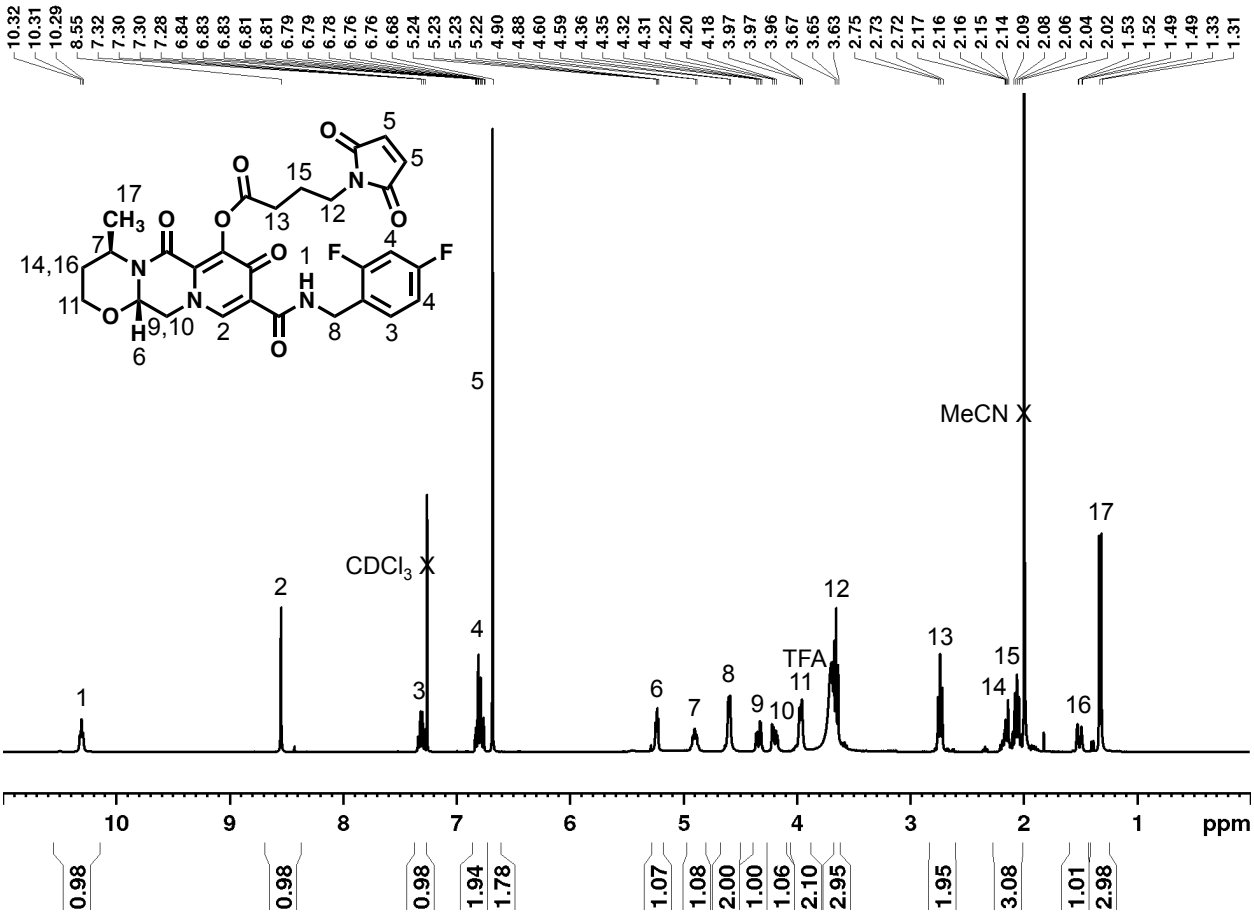

Figure 2.16. ^{1}H NMR spectrum of DTG-maleimide in $CDCl_3$.

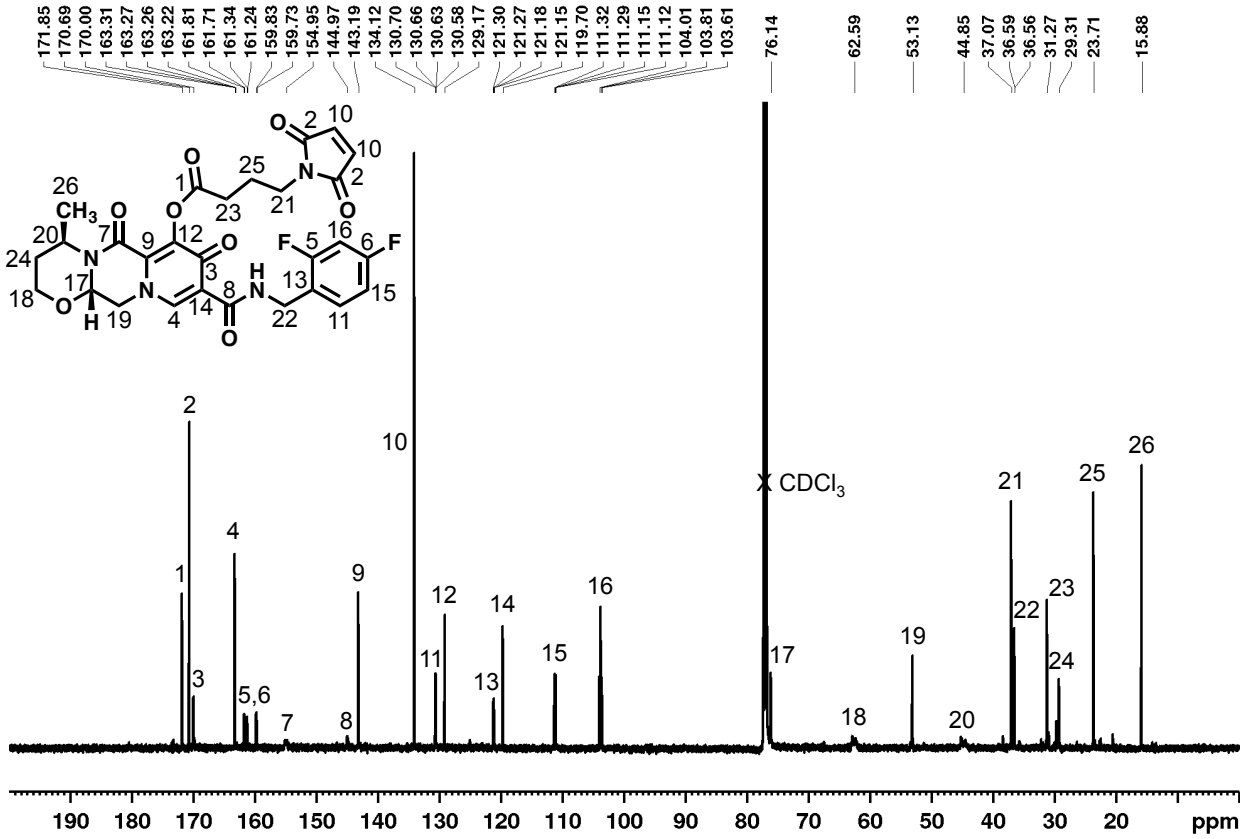

Figure 2.17. ^{13}C NMR spectrum of DTG-maleimide in $CDCl_3$.

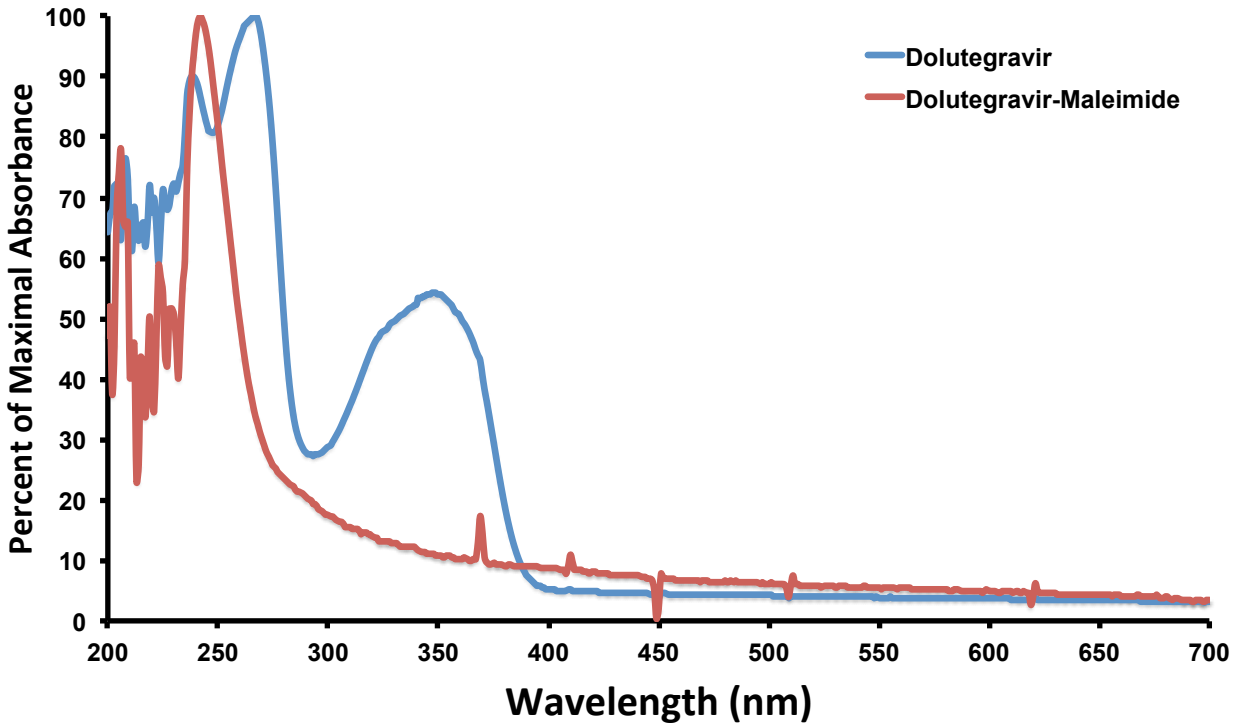

Figure 2.18. UV-Vis absorption spectra of DTG and DTG-maleimide shows significant shift in absorbance profiles following coupling with 4-maleimide butyric acid.

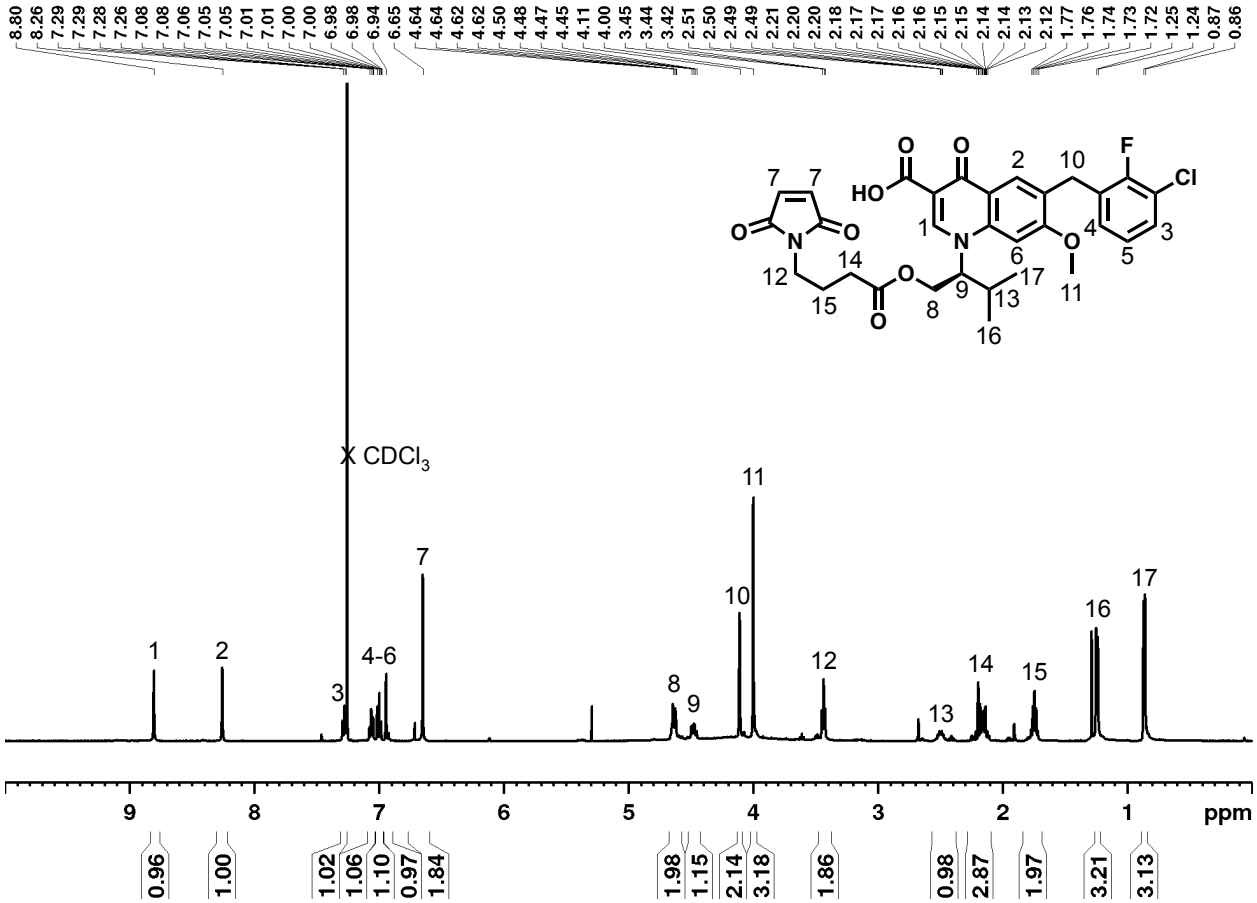

Figure 2.19. ^{1}H NMR spectrum of EVG-MAL in $CDCl_3$.

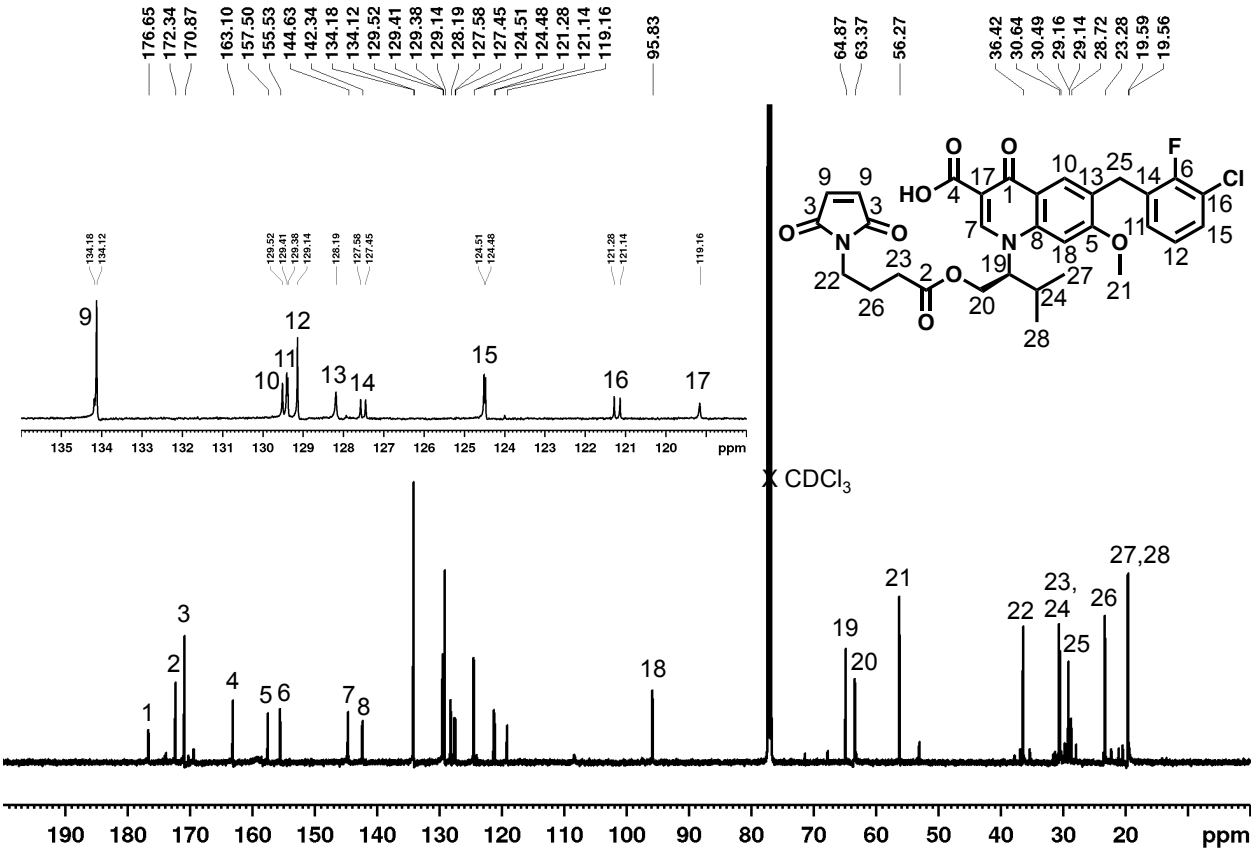

Figure 2.20. ^{13}C NMR spectrum of EVG-MAL in $CDCl_3$.

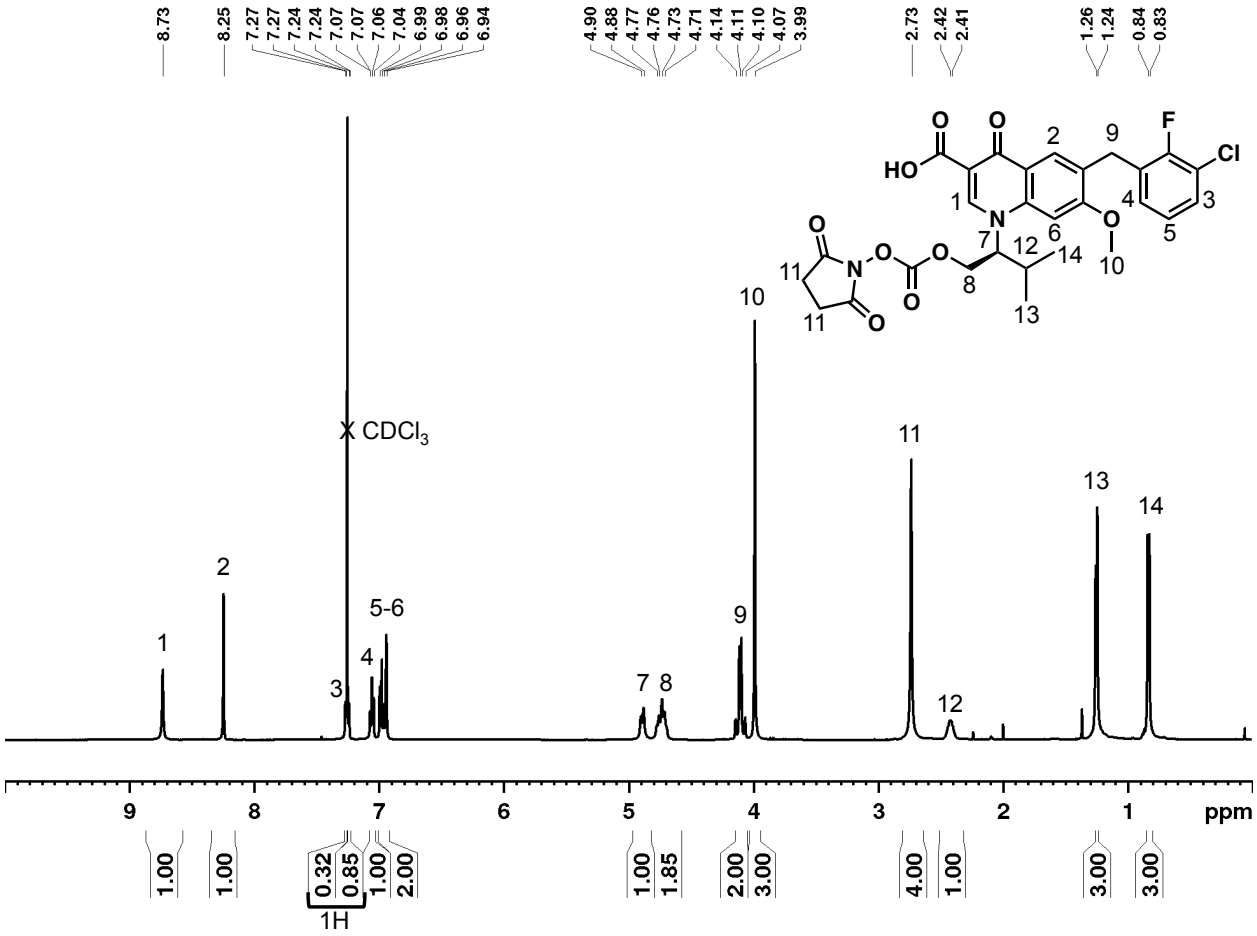

Figure 2.21. ^{1}H NMR of EVG-NHS in $CDCl_3$.

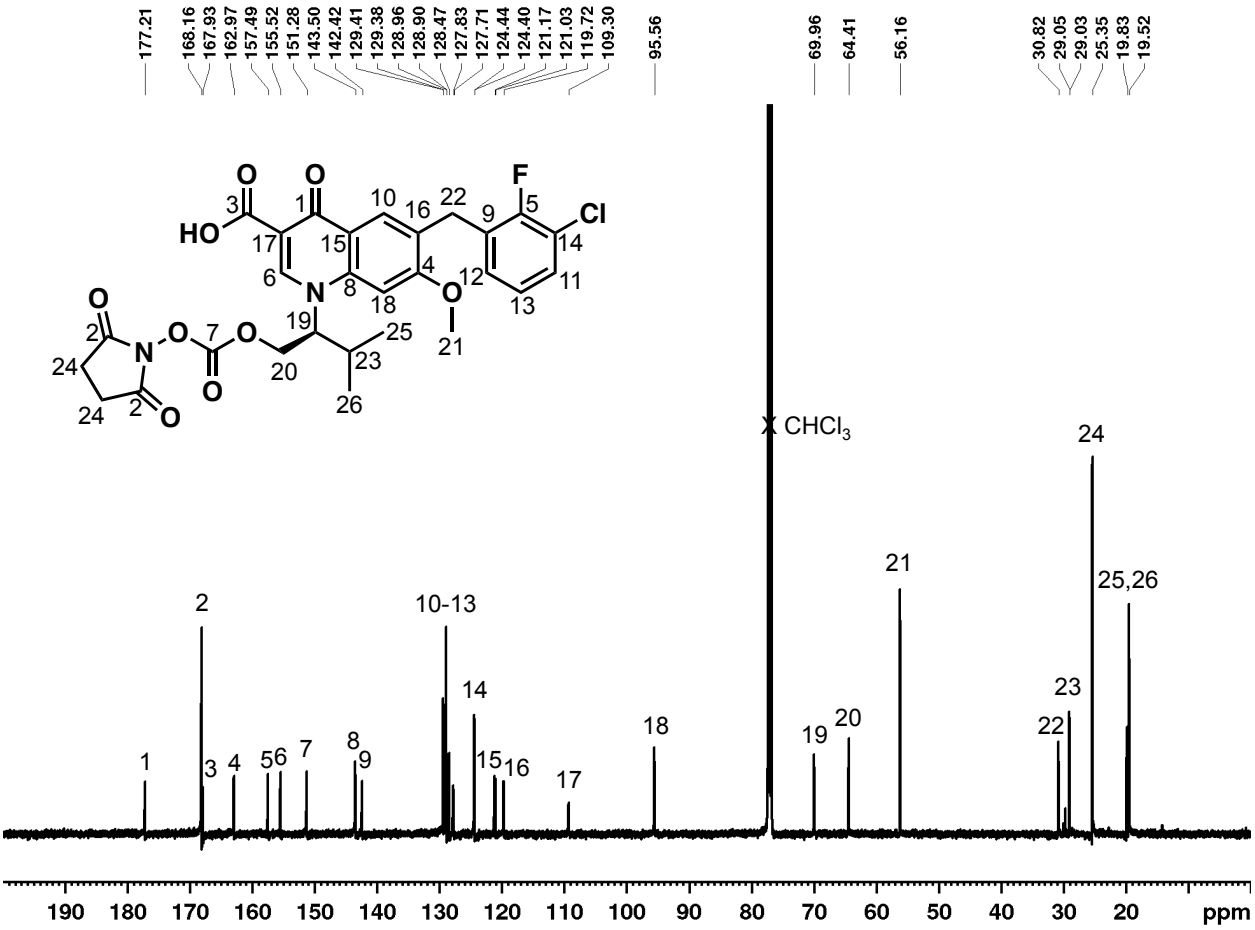

Figure 2.22. ^{13}C NMR of EVG-NHS in $CDCl_3$.

2.6 References

(1) World Health Organization. Global Health Observatory Data Repository http://apps.who.int/gho/data/view.main.HIVINCIDENCEREGIONv?lang=en (accessed Jun 24, 2019).

(2) Baeten, J. M.; Donnell, D.; Ndase, P.; Mugo, N. R.; Campbell, J. D.; Wangisi, J.; Tappero, J. W.; Bukusi, E. A.; Cohen, C. R.; Katabira, E.; Ronald, A.; Tumwesigye, E.; Were, E.; Fife, K. H.; Kiarie, J.; Farquhar, C.; John-Stewart, G.; Kakia, A.; Odoyo, J.; Mucunguzi, A.; Nakku-Joloba, E.; Twesigye, R.; Ngure, K.; Apaka, C.; Tamooh, H.; Gabona, F.; Mujugira, A.; Panteleeff, D.; Thomas, K. K.; Kidoguchi, L.; Krows, M.; Revall, J.; Morrison, S.; Haugen, H.; Emmanuel-Ogier, M.; Ondrejcek, L.; Coombs, R. W.; Frenkel, L.; Hendrix, C.; Bumpus, N. N.; Bangsberg, D.; Haberer, J. E.; Stevens, W. S.; Lingappa, J. R.; Celum, C. (2012) Antiretroviral Prophylaxis for HIV Prevention in Heterosexual Men and Women. *N. Engl. J. Med. 367*, 399–410.

(3) Grant, R. M.; Lama, J. R.; Anderson, P. L.; McMahan, V.; Liu, A. Y.; Vargas, L.; Goicochea, P.; Casapía, M.; Guanira-Carranza, J. V.; Ramirez-Cardich, M. E.; Montoya-Herrera, O.; Fernández, T.; Veloso, V. G.; Buchbinder, S. P.; Chariyalertsak, S.; Schechter, M.; Bekker, L.-G.; Mayer, K. H.; Kallás, E. G.; Amico, K. R.; Mulligan, K.; Bushman, L. R.; Hance, R. J.; Ganoza, C.; Defechereux, P.; Postle, B.; Wang, F.; McConnell, J. J.; Zheng, J.-H.; Lee, J.; Rooney, J. F.; Jaffe, H. S.; Martinez, A. I.; Burns, D. N.; Glidden, D. V. (2010) Preexposure Chemoprophylaxis for HIV Prevention in Men Who Have Sex with Men. *N. Engl. J. Med. 363*, 2587–2599.

(4) Thigpen, M. C.; Kebaabetswe, P. M.; Paxton, L. A.; Smith, D. K.; Rose, C. E.; Segolodi, T. M.; Henderson, F. L.; Pathak, S. R.; Soud, F. A.; Chillag, K. L.; Mutanhaurwa, R.;

Chirwa, L. I.; Kasonde, M.; Abebe, D.; Buliva, E.; Gvetadze, R. J.; Johnson, S.; Sukalac, T.; Thomas, V. T.; Hart, C.; Johnson, J. A.; Malotte, C. K.; Hendrix, C. W.; Brooks, J. T. (2012) Antiretroviral Preexposure Prophylaxis for Heterosexual HIV Transmission in Botswana. *N. Engl. J. Med. 367*, 423–434.

(5) Gotwals, P.; Cameron, S.; Cipolletta, D.; Cremasco, V.; Crystal, A.; Hewes, B.; Mueller, B.; Quaratino, S.; Sabatos-Peyton, C.; Petruzzelli, L.; Engelman, J. A.; Dranoff, G. (2017) Prospects for Combining Targeted and Conventional Cancer Therapy with Immunotherapy. *Nat. Rev. Cancer 17*, 286–301.

(6) Zhang, Z.-Q.; Schuler, T.; Zupancic, M.; Wietgrefe, S.; Staskus, K. A.; Reimann, K. A.; Reinhart, T. A.; Rogan, M.; Cavert, W.; Miller, C. J.; Veazey, R. S.; Notermans, D.; Little, S.; Danner, S. A.; Richman, D. D.; Havlir, D.; Wong, J.; Jordan, H. L.; Schacker, T. W.; Racz, P.; Tenner-Racz, K.; Letvin, N. L.; Wolinsky, S.; Haase, A. T. (1999) Sexual Transmission and Propagation of SIV and HIV in Resting and Activated $CD4^+$ T Cells. *Science 286*, 1353.

(7) Patterson, K. B.; Prince, H. A.; Kraft, E.; Jenkins, A. J.; Shaheen, N. J.; Rooney, J. F.; Cohen, M. S.; Kashuba, A. D. M. (2011) Penetration of Tenofovir and Emtricitabine in Mucosal Tissues: Implications for Prevention of HIV-1 Transmission. *Sci. Transl. Med. 3*, 112re4.

(8) Traore, Y. L.; Chen, Y.; Ho, E. A. (2018) Current State of Microbicide Development. *Clin. Pharmacol. Ther. 104*, 1074–1081.

(9) Mamo, T.; Moseman, E. A.; Kolishetti, N.; Salvador-Morales, C.; Shi, J.; Kuritzkes, D. R.; Langer, R.; von Andrian, U.; Farokhzad, O. C. (2010) Emerging Nanotechnology Approaches for HIV/AIDS Treatment and Prevention. *Nanomed. 5*, 269–285.

(10) Telwatte, S.; Moore, K.; Johnson, A.; Tyssen, D.; Sterjovski, J.; Aldunate, M.; Gorry, P. R.; Ramsland, P. A.; Lewis, G. R.; Paull, J. R. A.; Sonza, S.; Tachedjian, G. (2011) Virucidal Activity of the Dendrimer Microbicide SPL7013 against HIV-1. *Antiviral Res. 90*, 195–199.

(11) Arnáiz, E.; Vacas-Córdoba, E.; Galán, M.; Pion, M.; Gómez, R.; Muñoz-Fernández, M. Á.; Mata, F. J. de la. (2014) Synthesis of Anionic Carbosilane Dendrimers via "Click Chemistry" and Their Antiviral Properties against HIV. *J. Polym. Sci. Part Polym. Chem. 52*, 1099–1112.

(12) das Neves, J.; Michiels, J.; Ariën, K. K.; Vanham, G.; Amiji, M.; Bahia, M. F.; Sarmento, B. (2012) Polymeric Nanoparticles Affect the Intracellular Delivery, Antiretroviral Activity and Cytotoxicity of the Microbicide Drug Candidate Dapivirine. *Pharm. Res. 29*, 1468–1484.

(13) das Neves, J.; Araújo, F.; Andrade, F.; Michiels, J.; Ariën, K. K.; Vanham, G.; Amiji, M.; Bahia, M. F.; Sarmento, B. (2013) In Vitro and Ex Vivo Evaluation of Polymeric Nanoparticles for Vaginal and Rectal Delivery of the Anti-HIV Drug Dapivirine. *Mol. Pharm. 10*, 2793–2807.

(14) Mandal, S.; Prathipati, P.; Kang, G.; Zhou, Y.; Yuan, Z.; Fan, W.; Li, Q.; Destache, C. (2017) Tenofovir Alafenamide and Elvitegravir Loaded Nanoparticles for Long-Acting Prevention of HIV-1 Vaginal Transmission. *Aids 31*, 469–476.

(15) Mandal, S.; Prathipati, P. K.; Belshan, M.; Destache, C. J. (2019) A Potential Long-Acting Bictegravir Loaded Nano-Drug Delivery System for HIV-1 Infection: A Proof-of-Concept Study. *Antiviral Res. 167*, 83–88.

(16) Nunes, R.; Araújo, F.; Barreiros, L.; Bártolo, I.; Segundo, M. A.; Taveira, N.; Sarmento, B.; das Neves, J. (2018) Noncovalent PEG Coating of Nanoparticle Drug Carriers Improves the Local Pharmacokinetics of Rectal Anti-HIV Microbicides. *ACS Appl. Mater. Interfaces 10*, 34942–34953.

(17) Chaowanachan, T.; Krogstad, E.; Ball, C.; Woodrow, K. A. (2013) Drug Synergy of Tenofovir and Nanoparticle-Based Antiretrovirals for HIV Prophylaxis. *PLOS ONE 8*, e61416.

(18) Perazzolo, S.; Shireman, L. M.; Koehn, J.; McConnachie, L. A.; Kraft, J. C.; Shen, D. D.; Ho, R. J. Y. (2018) Three HIV Drugs, Atazanavir, Ritonavir, and Tenofovir, Coformulated in Drug-Combination Nanoparticles Exhibit Long-Acting and Lymphocyte-Targeting Properties in Nonhuman Primates. *J. Pharm. Sci. 107*, 3153–3162.

(19) Alukda, D.; Sturgis, T.; Youan, B.-B. C. (2011) Formulation of Tenofovir-Loaded Functionalized Solid Lipid Nanoparticles Intended for HIV Prevention. *J. Pharm. Sci. 100*, 3345–3356.

(20) Caron, M.; Besson, G.; Etenna, S. L.-D.; Mintsa-Ndong, A.; Mourtas, S.; Radaelli, A.; Morghen, C. D. G.; Loddo, R.; La Colla, P.; Antimisiaris, S. G.; Kazanji, M. (2010) Protective Properties of Non-Nucleoside Reverse Transcriptase Inhibitor (MC1220) Incorporated into Liposome against Intravaginal Challenge of Rhesus Macaques with RT-SHIV. *Virology 405*, 225–233.

(21) Shah, L. K.; Amiji, M. M. (2006) Intracellular Delivery of Saquinavir in Biodegradable Polymeric Nanoparticles for HIV/AIDS. *Pharm. Res. 23*, 2638–2645.

(22) Jiang, Y.; Cao, S.; Bright, D. K.; Bever, A. M.; Blakney, A. K.; Suydam, I. T.; Woodrow, K. A. (2015) Nanoparticle-Based ARV Drug Combinations for Synergistic Inhibition of Cell-Free and Cell–Cell HIV Transmission. *Mol. Pharm. 12*, 4363–4374.

(23) Huckaby, J. T.; Lai, S. K. (2018) PEGylation for Enhancing Nanoparticle Diffusion in Mucus. *Adv. Drug Deliv. Rev. 124*, 125–139.

(24) Meng, J.; Agrahari, V.; Ezoulin, M. J.; Zhang, C.; Purohit, S. S.; Molteni, A.; Dim, D.; Oyler, N. A.; Youan, B.-B. C. (2016) Tenofovir Containing Thiolated Chitosan Core/Shell Nanofibers: In Vitro and in Vivo Evaluations. *Mol. Pharm. 13*, 4129–4140.

(25) Destache, C. J.; Mandal, S.; Yuan, Z.; Kang, G.; Date, A. A.; Lu, W.; Shibata, A.; Pham, R.; Bruck, P.; Rezich, M.; Zhou, Y.; Vivekanandan, R.; Fletcher, C. V.; Li, Q. (2016) Topical Tenofovir Disoproxil Fumarate Nanoparticles Prevent HIV-1 Vaginal Transmission in a Humanized Mouse Model. *Antimicrob. Agents Chemother. 60*, 3633–3639.

(26) Karim, Q. A.; Karim, S. S. A.; Frohlich, J. A.; Grobler, A. C.; Baxter, C.; Mansoor, L. E.; Kharsany, A. B. M.; Sibeko, S.; Mlisana, K. P.; Omar, Z.; Gengiah, T. N.; Maarschalk, S.; Arulappan, N.; Mlotshwa, M.; Morris, L.; Taylor, D.; Group, on behalf of the C. 004 T. (2010) Effectiveness and Safety of Tenofovir Gel, an Antiretroviral Microbicide, for the Prevention of HIV Infection in Women. *Science 329*, 1168–1174.

(27) Tang, E.; Vittinghoff, E.; Anderson, P.; Cohen, S.; Doblecki-Lewis, S.; Bacon, O.; Coleman, M.; Buchbinder, S.; Chege, W.; Kolber, M.; Elion, R.; Shlipak, M.; Liu, A. (2018) Changes in Kidney Function Associated With Daily Tenofovir Disoproxil Fumarate/Emtricitabine for HIV Preexposure Prophylaxis Use in the United States Demonstration Project. *Jaids J. Acquir. Immune Defic. Syndr. 77*, 193–198.

(28) Gandhi, M.; Glidden, D. V.; Mayer, K.; Schechter, M.; Buchbinder, S.; Grinsztejn, B.; Hosek, S.; Casapia, M.; Guanira, J.; Bekker, L.-G.; Louie, A.; Horng, H.; Benet, L. Z.; Liu, A.; Grant, R. M. (2016) Association of Age, Baseline Kidney Function, and Medication Exposure with Declines in Creatinine Clearance on Pre-Exposure Prophylaxis: An Observational Cohort Study. *Lancet HIV 3*, e521–e528.

(29) Kasonde, M.; Niska, R. W.; Rose, C.; Henderson, F. L.; Segolodi, T. M.; Turner, K.; Smith, D. K.; Thigpen, M. C.; Paxton, L. A. (2014) Bone Mineral Density Changes among HIV-Uninfected Young Adults in a Randomised Trial of Pre-Exposure Prophylaxis with Tenofovir-Emtricitabine or Placebo in Botswana. *PLOS ONE 9*, e90111.

(30) Mulligan, K.; Glidden, D. V.; Anderson, P. L.; Liu, A.; McMahan, V.; Gonzales, P.; Ramirez-Cardich, M. E.; Namwongprom, S.; Chodacki, P.; de Mendonca, L. M. C.; Wang, F.; Lama, J. R.; Chariyalertsak, S.; Guanira, J. V.; Buchbinder, S.; Bekker, L.-G.; Schechter, M.; Veloso, V. G.; Grant, R. M.; Vargas, L.; Sanchez, J.; Mai, C.; Saokhieo, P.; Murphy, K.; Gilmore, H.; Holland, S.; Faber, E.; Duda, J.; Bewerunge, L.; Batist, E.; Hoskin, C.; Brown, B.; de Janeiro, R.; Beppu-Yoshida, C.; da Costa, M. D.; Assis de Jesus, S. C.; Grangeiro da Silva, J. R.; Millan, R.; de Siqueira Hoagland, B. R.; Martinez Fernandes, N.; da Silva Freitas, L.; Grinsztejn, B.; Pilotto, J.; Bushman, L.; Zheng, J.-H.; Anthony Guida, L.; Kline, B.; Goicochea, P.; Manzo, J.; Hance, R.; McConnell, J.; Defechereux, P.; Levy, V.; Robles, M.; Postle, B.; Burns, D.; Rooney, J. (2015) Effects of Emtricitabine/Tenofovir on Bone Mineral Density in HIV-Negative Persons in a Randomized, Double-Blind, Placebo-Controlled Trial. *Clin. Infect. Dis. 61*, 572–580.

(31) Endsley, A.; Ho, R. (2012) Enhanced Anti-HIV Efficacy of Indinavir After Inclusion in CD4-Targeted Lipid Nanoparticles. *Jaids J. Acquir. Immune Defic. Syndr. 61*, 417–424.

(32) Joshy, K. S.; Susan, M. A.; Snigdha, S.; Nandakumar, K.; Laly, A. P.; Sabu, T. (2018) Encapsulation of Zidovudine in PF-68 Coated Alginate Conjugate Nanoparticles for Anti-HIV Drug Delivery. *Int. J. Biol. Macromol. 107*, 929–937.

(33) Pedreiro, L. N.; Stringhetti, B.; Cury, F.; Gremião, M. P. D. (2016) Mucoadhesive Nanostructured Polyelectrolyte Complexes as Potential Carrier to Improve Zidovudine Permeability. *J. Nanosci. Nanotechnol. 16*, 1248–1256.

(34) Dalpiaz, A.; Contado, C.; Mari, L.; Perrone, D.; Pavan, B.; Paganetto, G.; Hanuskovà, M.; Vighi, E.; Leo, E. (2014) Development and Characterization of PLGA Nanoparticles as Delivery Systems of a Prodrug of Zidovudine Obtained by Its Conjugation with Ursodeoxycholic Acid. *Drug Deliv. 21*, 221–232.

(35) Mainardes, R. M.; Gremião, M. P. D.; Brunetti, I. L.; da Fonseca, L. M.; Khalil, N. M. (2009) Zidovudine-Loaded PLA and PLA–PEG Blend Nanoparticles: Influence of Polymer Type on Phagocytic Uptake by Polymorphonuclear Cells. *J. Pharm. Sci. 98*, 257–267.

(36) Aykaç, A.; Noiray, M.; Malanga, M.; Agostoni, V.; Casas-Solvas, J. M.; Fenyvesi, É.; Gref, R.; Vargas-Berenguel, A. (2017) A Non-Covalent "Click Chemistry" Strategy to Efficiently Coat Highly Porous MOF Nanoparticles with a Stable Polymeric Shell. *Biochim. Biophys. Acta BBA - Gen. Subj. 1861*, 1606–1616.

(37) Richman, D. D.; Fischl, M. A.; Grieco, M. H.; Gottlieb, M. S.; Volberding, P. A.; Laskin, O. L.; Leedom, J. M.; Groopman, J. E.; Mildvan, D.; Hirsch, M. S.; Jackson, G. G.; Durack, D. T.; Nusinoff-Lehrman, S. (1987) The Toxicity of Azidothymidine (AZT) in the Treatment of Patients with AIDS and AIDS-Related Complex. *N. Engl. J. Med. 317*, 192–197.

(38) Barry, M.; Howe, J. L.; Back, D. J.; Swart, A. M.; Breckenridge, A. M.; Weller, I. V.; Beeching, N.; Nye, F. (1994) Zidovudine Pharmacokinetics in Zidovudine-Induced Bone Marrow Toxicity. *Br. J. Clin. Pharmacol. 37*, 7–12.

(39) Kedersha, N. L.; Rome, L. H. (1986) Isolation and Characterization of a Novel Ribonucleoprotein Particle : Large Structures Contain a Single Species of Small RNA. *J Cell Biol 103*, 699–709.

(40) Kedersha, N. L.; Miquel, M. C.; Bittner, D.; Rome, L. H. (1990) Vaults. II. Ribonucleoprotein Structures Are Highly Conserved among Higher and Lower Eukaryotes. *J. Cell Biol. 110*, 895–901.

(41) Kong, L. B.; Siva, A. C.; Rome, L. H.; Stewart, P. L. (1999) Structure of the Vault, a Ubiquitous Cellular Component. *Structure 7*, 371–379.

(42) Tanaka, H.; Kato, K.; Yamashita, E.; Sumizawa, T.; Zhou, Y.; Yao, M.; Iwasaki, K.; Yoshimura, M.; Tsukihara, T. (2009) The Structure of Rat Liver Vault at 3.5 Angstrom Resolution. *Science 323*, 384–388.

(43) Kickhoefer, V. A.; Siva, A. C.; Kedersha, N. L.; Inman, E. M.; Ruland, C.; Streuli, M.; Rome, L. H. (1999) The 193-Kd Vault Protein, Vparp, Is a Novel Poly(Adp-Ribose) Polymerase. *J. Cell Biol. 146*, 917–928.

(44) Kickhoefer, V. A.; Liu, Y.; Kong, L. B.; Snow, B. E.; Stewart, P. L.; Harrington, L.; Rome, L. H. (2001) The Telomerase/Vault-Associated Protein Tep1 Is Required for Vault RNA Stability and Its Association with the Vault Particle. *J. Cell Biol. 152*, 157–164.

(45) Kickhoefer, V. A.; Stephen, A. G.; Harrington, L.; Robinson, M. O.; Rome, L. H. (1999) Vaults and Telomerase Share a Common Subunit, TEP1. *J. Biol. Chem. 274*, 32712–32717.

(46) Buehler, D. C.; Marsden, M. D.; Shen, S.; Toso, D. B.; Wu, X.; Loo, J. A.; Zhou, Z. H.; Kickhoefer, V. A.; Wender, P. A.; Zack, J. A.; Rome, L. H. (2014) Bioengineered Vaults: Self-Assembling Protein Shell–Lipophilic Core Nanoparticles for Drug Delivery. *ACS Nano 8*, 7723–7732.

(47) Kar, U. K.; Srivastava, M. K.; Andersson, Å.; Baratelli, F.; Huang, M.; Kickhoefer, V. A.; Dubinett, S. M.; Rome, L. H.; Sharma, S. (2011) Novel CCL21-Vault Nanocapsule Intratumoral Delivery Inhibits Lung Cancer Growth. *PLOS ONE 6*, e18758.

(48) Benner, N. L.; Zang, X.; Buehler, D. C.; Kickhoefer, V. A.; Rome, M. E.; Rome, L. H.; Wender, P. A. (2017) Vault Nanoparticles: Chemical Modifications for Imaging and Enhanced Delivery. *ACS Nano 11*, 872–881.

(49) Kar, U. K.; Jiang, J.; Champion, C. I.; Salehi, S.; Srivastava, M.; Sharma, S.; Rabizadeh, S.; Niazi, K.; Kickhoefer, V.; Rome, L. H.; Kelly, K. A. (2012) Vault Nanocapsules as Adjuvants Favor Cell-Mediated over Antibody-Mediated Immune Responses Following Immunization of Mice. *PLOS ONE 7*, e38553.

(50) Champion, C. I.; Kickhoefer, V. A.; Liu, G.; Moniz, R. J.; Freed, A. S.; Bergmann, L. L.; Vaccari, D.; Raval-Fernandes, S.; Chan, A. M.; Rome, L. H.; Kelly, K. A. (2009) A Vault Nanoparticle Vaccine Induces Protective Mucosal Immunity. *PLOS ONE 4*, e5409.

(51) Kickhoefer, V. A.; Garcia, Y.; Mikyas, Y.; Johansson, E.; Zhou, J. C.; Raval-Fernandes, S.; Minoofar, P.; Zink, J. I.; Dunn, B.; Stewart, P. L.; Rome, L. H. (2005) Engineering of Vault Nanocapsules with Enzymatic and Fluorescent Properties. *Proc. Natl. Acad. Sci. 102*, 4348–4352.

(52) Wang, M.; Abad, D.; Kickhoefer, V. A.; Rome, L. H.; Mahendra, S. (2015) Vault Nanoparticles Packaged with Enzymes as an Efficient Pollutant Biodegradation Technology. *ACS Nano 9*, 10931–10940.

(53) Kickhoefer, V. A.; Han, M.; Raval-Fernandes, S.; Poderycki, M. J.; Moniz, R. J.; Vaccari, D.; Silvestry, M.; Stewart, P. L.; Kelly, K. A.; Rome, L. H. (2009) Targeting Vault Nanoparticles to Specific Cell Surface Receptors. *ACS Nano 3*, 27–36.

(54) Matsumoto, N. M.; Prabhakaran, P.; Rome, L. H.; Maynard, H. D. (2013) Smart Vaults: Thermally-Responsive Protein Nanocapsules. *ACS Nano 7*, 867–874.

(55) Rome, L. H.; Kickhoefer, V. A. (2013) Development of the Vault Particle as a Platform Technology. *ACS Nano 7*, 889–902.

(56) Zhu, Y.; Jiang, J.; Said-Sadier, N.; Boxx, G.; Champion, C.; Tetlow, A.; Kickhoefer, V. A.; Rome, L. H.; Ojcius, D. M.; Kelly, K. A. (2015) Activation of the NLRP3 Inflammasome by Vault Nanoparticles Expressing a Chlamydial Epitope. *Vaccine 33*, 298–306.

(57) Fulcher, J. A.; Tamshen, K.; Wollenberg, A. L.; Kickhoefer, V. A.; Mrazek, J.; Elliott, J.; Ibarrondo, F. J.; Anton, P. A.; Rome, L. H.; Maynard, H. D.; Deming, T.; Yang, O. O. (2019) Human Vault Nanoparticle Targeted Delivery of Antiretroviral Drugs to Inhibit Human Immunodeficiency Virus Type 1 Infection. *Bioconjug. Chem.*

(58) Tadayoni, B. M.; Friden, P. M.; Walus, L. R.; Musso, G. F. (1993) Synthesis, in Vitro Kinetics and in Vivo Studies on Protein Conjugates of AZT: Evaluation as a Transport System to Increase Brain Delivery. *Bioconjug. Chem. 4*, 139–145.

(59) Giammona, G.; Cavallaro, G.; Fontana, G.; Pitarresi, G.; Carlisi, B. (1998) Coupling of the Antiviral Agent Zidovudine to Polyaspartamide and in Vitro Drug Release Studies. *J. Controlled Release 54*, 321–331.

(60) Wannachaiyasit, S.; Chanvorachote, P.; Nimmannit, U. (2008) A Novel Anti-HIV Dextrin–Zidovudine Conjugate Improving the Pharmacokinetics of Zidovudine in Rats. *AAPS PharmSciTech 9*, 840.

(61) Ray, A. S.; Fordyce, M. W.; Hitchcock, M. J. M. (2016) Tenofovir Alafenamide: A Novel Prodrug of Tenofovir for the Treatment of Human Immunodeficiency Virus. *Antiviral Res. 125*, 63–70.

(62) Schoch, J.; Wiessler, M.; Jäschke, A. (2010) Post-Synthetic Modification of DNA by Inverse-Electron-Demand Diels−Alder Reaction. *J. Am. Chem. Soc. 132*, 8846–8847.

(63) Blackman, M. L.; Royzen, M.; Fox, J. M. (2008) Tetrazine Ligation: Fast Bioconjugation Based on Inverse-Electron-Demand Diels−Alder Reactivity. *J. Am. Chem. Soc. 130*, 13518–13519.

(64) Sillman, B.; Bade, A. N.; Dash, P. K.; Bhargavan, B.; Kocher, T.; Mathews, S.; Su, H.; Kanmogne, G. D.; Poluektova, L. Y.; Gorantla, S.; McMillan, J.; Gautam, N.; Alnouti, Y.; Edagwa, B.; Gendelman, H. E. (2018) Creation of a Long-Acting Nanoformulated Dolutegravir. *Nat. Commun. 9*.

(65) Jain, N.; Smith, S. W.; Ghone, S.; Tomczuk, B. (2015) Current ADC Linker Chemistry. *Pharm. Res. 32*, 3526–3540.

(66) King, H. D.; Dubowchik, G. M.; Mastalerz, H.; Willner, D.; Hofstead, S. J.; Firestone, R. A.; Lasch, S. J.; Trail, P. A. (2002) Monoclonal Antibody Conjugates of Doxorubicin

Prepared with Branched Peptide Linkers: Inhibition of Aggregation by Methoxytriethyleneglycol Chains. *J. Med. Chem. 45*, 4336–4343.

(67) Hollander, I.; Kunz, A.; Hamann, Philip. R. (2008) Selection of Reaction Additives Used in the Preparation of Monomeric Antibody−Calicheamicin Conjugates. *Bioconjug. Chem. 19*, 358–361.

(68) Doronina, S. O.; Mendelsohn, B. A.; Bovee, T. D.; Cerveny, C. G.; Alley, S. C.; Meyer, D. L.; Oflazoglu, E.; Toki, B. E.; Sanderson, R. J.; Zabinski, R. F.; Wahl, A. F.; Senter, P. D. (2006) Enhanced Activity of Monomethylauristatin F through Monoclonal Antibody Delivery: Effects of Linker Technology on Efficacy and Toxicity. *Bioconjug. Chem. 17*, 114–124.

(69) Stephen, A. G.; Raval-Fernandes, S.; Huynh, T.; Torres, M.; Kickhoefer, V. A.; Rome, L. H. (2001) Assembly of Vault-like Particles in Insect Cells Expressing Only the Major Vault Protein. *J. Biol. Chem. 276*, 23217–23220.

(70) Han, J.; Sun, L.; Chu, Y.; Li, Z.; Huang, D.; Zhu, X.; Qian, H.; Huang, W. (2013) Design, Synthesis, and Biological Activity of Novel Dicoumarol Glucagon-like Peptide 1 Conjugates. *J Med Chem 56*, 9955–9968.

(71) Benson, J. R.; Hare, P. E. (1975) O-Phthalaldehyde: Fluorogenic Detection of Primary Amines in the Picomole Range. Comparison with Fluorescamine and Ninhydrin. *Proc. Natl. Acad. Sci. U. S. A. 72*, 619–622.

Chapter 3

Development of a Dual-Enzyme Responsive Opioid Prodrug for Abuse-Deterrence[†]

3.1 Introduction

Pain management is an important part of modern healthcare with over 30% of Americans reporting some form of chronic pain.[1] Chronic pain can be debilitating and often requires medical intervention to be alleviated or corrected. The most commonly prescribed drugs for treatment of acute and chronic pain are opioid analgesics. Opioids accounted for 168 million (2.9%) of 5.8 billion total prescriptions with 51.4 prescriptions per 100 individuals in 2018 in the United States.[2] It has been widely recognized that despite their effectiveness for reducing both acute and chronic pain, these highly addictive opioids have been heavily overprescribed.[3–8] Not only is the number of prescriptions excessive, but the majority of patients receive a higher quantity of pills than are needed for their treatment, and patients overwhelmingly keep these extra pills after they have completed their dosing regimen.[9] There is also evidence that a significant portion of these leftover pills are disseminated into the community and subsequently abused.[10,11] A variety of studies have also linked dependence on prescription opioids with heroin use, with many individuals first becoming addicted to prescription opioids before transitioning to heroin.[12–14]

A combination of these and other factors have led to a dramatic increase in opioid consumption and abuse, the consequences of which have proven devastating across all demographics and communities.[6,15,16] To put the scope of this epidemic in perspective, in 2018, 10.3 million Americans (3.7%) reported misusing or abusing opioids.[17] Prevalence of abuse has also substantially increased over the past twenty years.[18] This excessive reliance on opioids has consequently led to a dramatic increase in opioid-related deaths over the past 20 years as is evident by the steeply increasing rates shown in Figure 3.1. At its peak in 2017, opioids were responsible for the deaths of over 130 Americans per day.[16] Despite numerous efforts, the

negative impacts of the opioid epidemic remain pronounced and poised to continue unless new strategies are developed to mitigate these drugs' potential for abuse.

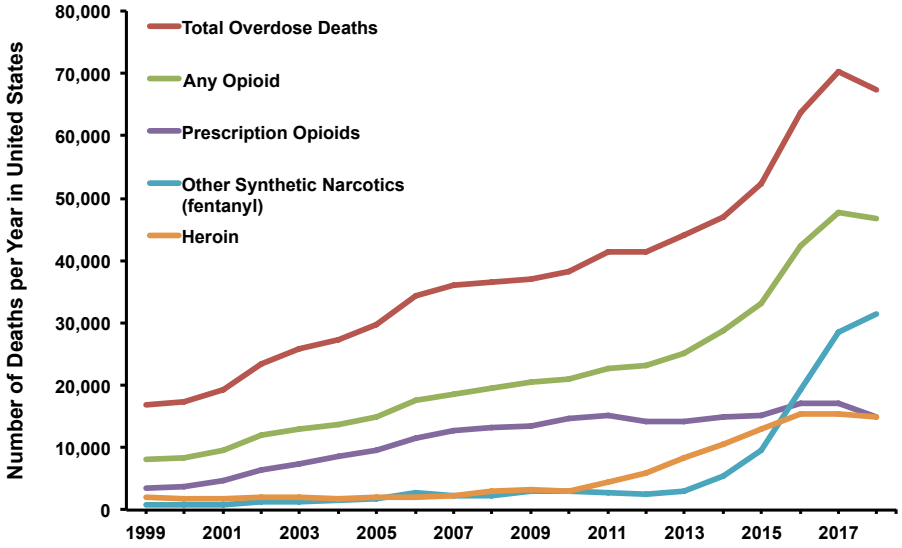

Figure 3.1. Number of deaths per year in the United States attributed to drug overdose. Chart plotted from data made available from the National Institute on Drug Abuse.[16]

Although many intervention strategies will undoubtedly be required to synergistically curb the opioid epidemic, one strategy has been the development of engineering controls that can reduce an opioid's potential for abuse. These abuse-deterrent formulations have been developed to make manipulation of a formulated drug more difficult, or abuse of the manipulated drug less rewarding.[19] Prescription opioids are most commonly abused by ingestion of a larger dose than prescribed, which results in a euphoric sensation. While orally ingesting more than a prescribed dose will provide a rewarding euphoric sensation, alternative routes of administration such as snorting or injection elicit the same effects faster and with higher euphoria.[20] Drugs without engineered safeguards against these routes of administration are therefore associated with greater abuse potential, highlighting the need for abuse-deterrent formulations.[21–23]

The FDA has recognized several forms of abuse-deterrent technologies (ADTs) that fall under the umbrella of abuse-deterrence.[24] The most common type of formulation uses physical or chemical barriers that are formulated specifically to resist mechanical or chemical manipulation and prevent burst release.[25] Seven of the ten FDA-approved drugs with abuse-deterrent labeling fall into this category. These products contain oxycodone, hydrocodone, or morphine as the active ingredient formulated in a polymeric matrix that resists mechanical deformation and are therefore difficult to crush or break. These formulations also demonstrate resistance to extraction with solvents like water or ethanol, and form viscous gels that cannot be injected if extraction is attempted.[19,26] The remaining three FDA-approved drugs with abuse-deterrent labeling are formulated as an agonist/antagonist pair wherein manipulation of the product causes the release of a potent antagonist that inhibits euphoria associated with the active ingredient. These products contain either naltrexone or naloxone as the antagonist, which is sequestered within the core of a microsphere capsule (see Figure 3.2). Physical or chemical manipulation of the capsule disrupts the inner core and releases the sequestered antagonist.[19,25,26]

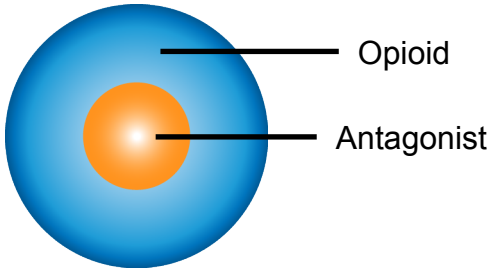

Figure 3.2. Schematic of an agonist antagonist formulation. When administered orally, the opioid active ingredient is slowly released while the antagonist core remains intact. Upon physical or chemical manipulation, the protective layer surrounding the antagonist core is ruptured and antagonist is released to inhibit euphoria.

Although these ten FDA-approved drugs received abuse-deterrent labeling, there is mixed evidence as to whether or not these drugs effectively mitigate abuse.[19,26] It is important to

note that in order to receive abuse-deterrent labeling, evidence must be provided that a drug *deters* abuse, but it is not necessary that it completely *prevents* abuse.[24] As can be imagined, determined individuals can maneuver around these engineered safeguards to achieve burst release of an opioid. Additionally, there are no currently available opioid formulations that cannot be abused by orally ingesting more than the prescribed dose.

A promising alternative to these noncovalent abuse-deterrent strategies is to employ covalent modification to control the release parameters of a drug. This can be implemented through the design of a prodrug that limits release of the active opioid to within the gastrointestinal tract so that improper administration, such as by intravenous or intranasal routes, does not induce euphoria.[23] An abuse-deterrent prodrug should also be resistant to physical and chemical manipulations so that determined users cannot release the active drug then ingest it at its full potency. Ideally, this prodrug will also facilitate slow release of the active compound so that even if an excessive dosage is administered orally, the release will be sufficiently slow so as to alleviate pain, but mitigate euphoria. It may also be possible that the delayed release of the euphoric agent decouples association with the opioid due to temporal differences between dosing and rewarding sensations, which may further help reduce the addiction potential of these formulations. Several opioid prodrugs have been investigated, and although various prodrugs have been shown to successfully release active opioids in response to gastrointestinal stimuli, none have sufficiently prevented chemical manipulation of the formulation.[23,27–29]

In this chapter, we report the design and synthesis of a dual-enzyme responsive opioid prodrug that addresses the shortcomings of currently available abuse-deterrent formulations. This prodrug was developed based on our group's previously reported dual-enzyme responsive peptide that effectively released a small molecule reporter upon incubation with digestive

enzymes trypsin and chymotrypsin.[30] First, chymotrypsin is required to cleave the isopeptide bond between a phenylalanine residue and the ε-amine of a lysine residue. Once cleaved, the lysine residue is unmasked and can further be processed by trypsin, which subsequently cleaves the lysine C-terminally and releases a primary amine. This primary amine can then rapidly cyclize and release an attached, active opioid, forming 1-methylimidazolidine-2-thione as a nontoxic byproduct.[31]

Scheme 3.1. Design of a dual-enzyme responsive opioid prodrug for abuse deterrence.

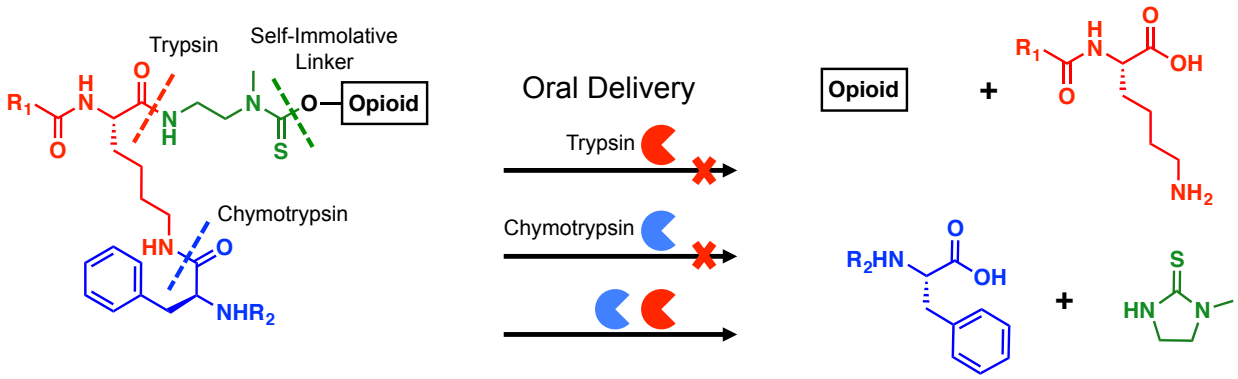

Our prodrug design possesses several layers of protection against unintentional release. First, two separate digestive enzymes are required to release the active opioid, making it significantly more difficult for individuals to chemically or biochemically manipulate the formulation and achieve burst release. Additionally, since these enzymes are only present in the gastrointestinal tract, administration by other routes will be ineffectual to release active drug. Second, our prodrug is composed of stable, but reversible linkages that are resistant to unintended release that is most commonly facilitated by hydrolysis. Third, because enzymes control release of the opioid from the prodrug scaffold, the release rate may be sufficiently slow that even if the prodrug is orally overdosed, only a limited amount of the prodrug may be enzymatically processed, thereby further mitigating burst release. We expect that this platform

will therefore offer significant improvements to the currently available abuse-deterrent formulations.

In the following sections, we report the development of chemistry to activate functional groups common to most opioids for conjugation to our dual-enzyme responsive peptide platform in order to synthesize abuse-deterrent opioid prodrugs. We then describe the application of this chemistry to the commonly prescribed opioid oxycodone, and evaluate the stability of the prodrug to a broad pH range. Finally, we describe optimization of this chemistry, elucidation of possible reaction side products, and reaction conditions to mitigate them.

3.2 Results and Discussion

3.2.1 Evaluation of Common Opioids for Reversible Modification

There are many FDA-approved opioid analgesics commercially available for pain management.[19,32,33] Our aim in this study was to design a prodrug scaffold that would not only provide effective release of the active drug, but also to develop a strategy with broad utility that could be applied to the majority of marketed opioids. We therefore evaluated the structures of each of the most commonly prescribed opioids, especially those involved in deaths caused by drug overdose. These drugs include oxycodone, hydrocodone, morphine, and methadone, and the structures of these molecules are shown in Figure 3.3A.[34,35] Most prescription opioids such as oxycodone and hydrocodone share common structural motifs with morphine, although it is also common for purely synthetic opioids like methadone to contain similar functional groups.

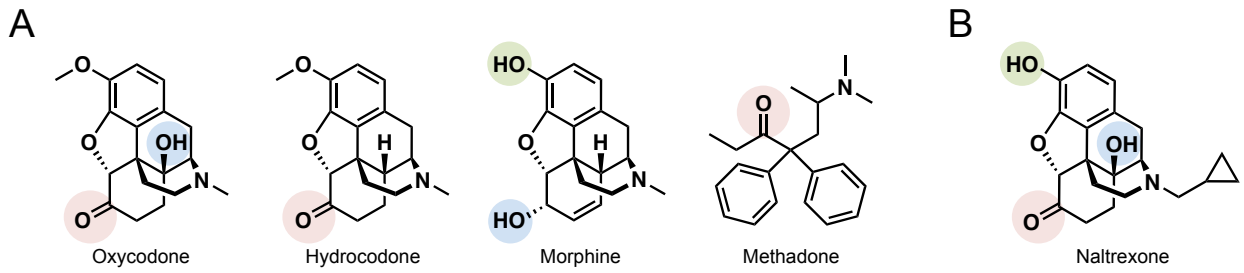

Figure 3.3. Overview of (A) common opioids with highlighted reversibly modifiable functional groups, and (B) selection of naltrexone as a suitable model compound.

Generally, opioids contain one or more of four possible functional groups that can be used for reversible modification: a tertiary amine, a phenol, a tertiary alcohol, or a ketone (Figure 3.3A). Tertiary amines can be reversibly quaternized through reaction with a benzyl halide to form the corresponding quaternary ammonium salt as reported by Staben, et al.[36] However, yields for these reactions were generally low, and side reactions with other functional groups presented a concern for opioid modification. As an alternative strategy, we envisioned that both phenols and alcohols could be reversibly modified in high yield through the reaction with chloroformates or chlorothionoformates to provide the corresponding carbonates or thionocarbonates. We also recognized the possibility of implementing a similar approach for ketone modification by trapping the corresponding enolate as an enol carbonate or thionocarbonate. These carbonates or thionocarbonates could then be reacted with a variant of our previously reported dual-enzyme responsive peptide[30] to provide opioid prodrugs with stable carbamate and thionocarbamate linkages that could only release active drug upon oral administration (Scheme 3.2). We initially investigated both carbamate and thionocarbamate chemistries in order to determine which linkage would demonstrate the greater stability against release under unintended conditions and therefore minimize potential for abuse of the linked

drug. Phenol, alcohol, and ketone modifications each provided promising functional handles to implement this chemistry for the development of abuse-deterrent prodrugs.

Scheme 3.2. Synthetic route to access naltrexone-peptide conjugates.

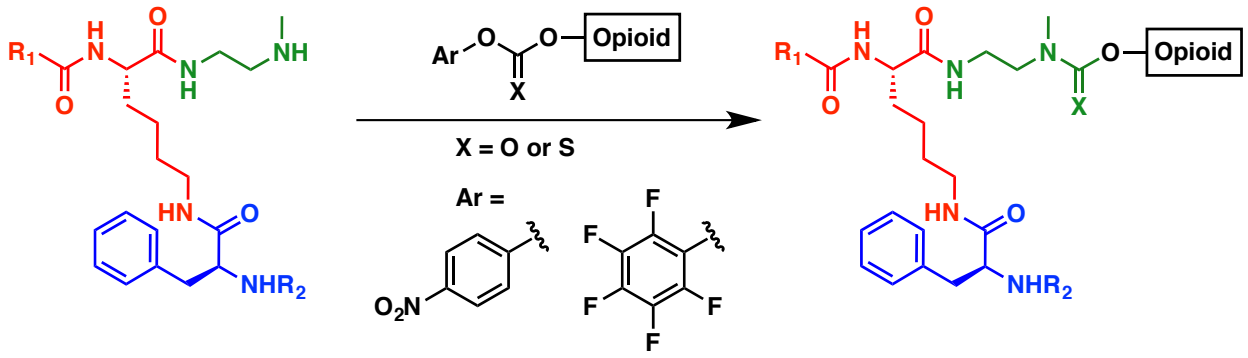

With these three promising modification strategies in mind, we began preliminary studies using naltrexone as a model compound. Naltrexone is a commercially available μ-opioid receptor antagonist and was an attractive model compound because it contains a phenol (like morphine), a tertiary alcohol (like oxycodone), and a ketone (like oxycodone, hydrocodone, and methadone) while sharing many other structural features associated with these drugs (Figure 3.3B). Unlike the opioids in Figure 3.3A, naltrexone is not a controlled substance and does not share the same toxicity as these compounds, making it easier to obtain and safer to work with for preliminary studies. After establishing reaction conditions to create the desired linkages and subsequently evaluating their stabilities, we applied our findings toward modification of oxycodone. We selected oxycodone because it is one of the most commonly prescribed opioids and shares the majority of its structure with naltrexone, which we hypothesized would make our findings with naltrexone as translatable as possible.

3.2.2 Reversible Phenol Modification of Naltrexone

We began our investigation of reversible modification with the phenol of naltrexone. We hypothesized that this would offer the most straightforward strategy to reversibly modify the drug in high yield and this methodology would be directly applicable to morphine. Naltrexone was reacted with diisopropylethylamine (DIPEA) and either 4-nitrophenylchloroformate or pentafluorophenylchlorothionoformate to provide the corresponding carbonate (Naltrexone-phenol-NPC) and thionocarbonate (Naltrexone-phenol-PFPTC) linkages, respectively (Scheme 3.3). Both reactions provided products in good yields (83-87%) and purification was carried out via straightforward flash column chromatography. The two activated naltrexone species were then coupled to the dual-enzyme responsive, protected peptide CAAK(F), which was prepared with a C-terminal secondary amine by Doug Rose (University of California, Los Angeles). This secondary amine was coupled directly with the activated naltrexone compounds in the presence of DIPEA to yield the corresponding CAAK(F)-Naltrexone-phenol conjugates. Protected peptide-naltrexone conjugates were then purified by HPLC, deprotected with trifluoroacetic acid (TFA), and precipitated to provide the peptide-naltrexone conjugates in sufficient yields for stability testing.

Scheme 3.3. Synthesis of activated naltrexone species (A) Naltrexone-phenol-NPC, (B) Naltrexone-phenol-PFPTC, and conjugation of activated naltrexone species to dual-enzyme responsive peptide CAAK(F) to give (C) CAAK(F)-Naltrexone-phenol peptide conjugates.

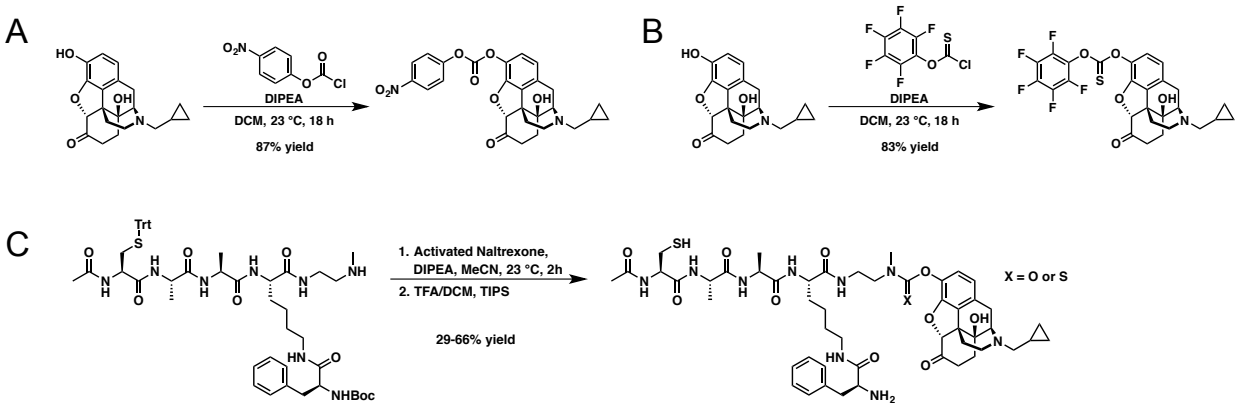

Table 3.1. Hydrolytic stability assessment of CAAK(F)-Naltrexone-phenol peptide conjugates. X = O indicates analysis of carbamate peptide-naltrexone linkage; X = S indicates analysis of thionocarbamate peptide-naltrexone linkage.

	% Degraded after 24 hours	
Condition	**X = O**	**X = S**
pH 2	12.3%	4.1%
pH 4	2.9%	2.0%
pH 7	3.6%	3.6%
pH 9	5.2%	3.4%
pH 12	6.9%	6.7%

Hydrolytic stability of the resulting carbamate and thionocarbamate linkages was assessed by HPLC following incubation of the deprotected peptide-naltrexone conjugates in phosphate buffer pH 2-12 for 24 hours (Table 3.1). Peak areas for the conjugates after 24 hours were compared to initial values to determine percent degradation of the carbamate and thionocarbamate linkages. The resulting values were also checked against peak area ratios between peptide-drug conjugate and released drug to confirm that differences in peak areas were

due to hydrolysis mediated drug release. Based on the results of this study as presented in Table 3.1, the thionocarbamate linkage proved slightly more stable than the corresponding carbamate across all pH conditions tested, but was substantially (3-fold) more stable at pH 2. We hypothesize that these differences are a result of the diminished electrophilicity at the carbon atom of the thionocarbamate as a result of the significantly less electronegative sulfur atom versus the highly electronegative oxygen atom of the carbamate. The less electrophilic carbon is consequently less susceptible to hydrolysis. Given that a number of readily available household products can have low pH values such as lemon juice and cola beverages, the thionocarbamate linkage offers more suitable protection against these agents.

Concurrent to these stability studies, we additionally investigated the extent to which the N-methyl substituent of the carbamate linkage impacted its stability compared to the corresponding N-H substituted carbamate. Synthetically, preparation of the dual-enzyme responsive peptide could be carried out more easily if the symmetric 1,2-diaminoethane could be coupled to the protected CAAK(F) peptide rather than the asymmetric N-methylethylenediamine, which required more elaborate protection/deprotection strategies. It was therefore more desirable to form the N-H carbamate, but only if the resulting linkage demonstrated a comparable stability profile to the N-methyl carbamate. To test this, Naltrexone-phenol-NPC was coupled with n-butylamine in the presence of triethylamine (TEA) to give Naltrexone-n-butyl-phenylcarbamate in 53% yield after HPLC purification (Scheme 3.4). Stability of the compound was assessed similarly to the peptide-naltrexone conjugates (Table 3.2). Interestingly, whereas CAAK(F)-Naltrexone-phenol-carbamate exhibited minimal degradation except for at pH 2, Naltrexone-n-butyl-phenylcarbamate displayed significant hydrolysis across all pH conditions and degradation of the carbamate linkage increased with pH.

Scheme 3.4. Synthesis of Naltrexone-n-butyl-phenylcarbamate.

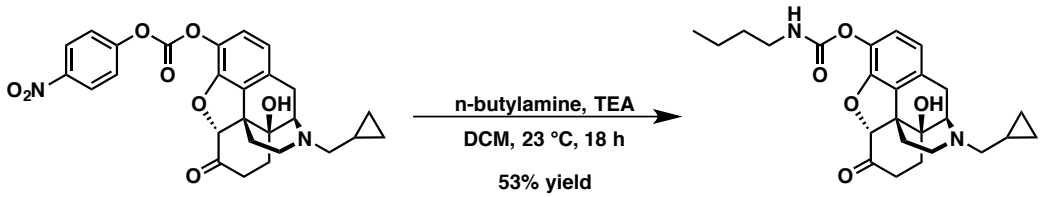

Table 3.2. Hydrolytic stability assessment of Naltrexone-n-butyl-phenylcarbamate.

Condition	% Degraded after 16 hours
pH 2	8.5%
pH 4	10.6%
pH 7	32.2%
pH 9	94.0%
pH 12	100%

We hypothesized that hydrolytic degradation increased with elevated pH conditions for two reasons. First, the N-H carbamate may undergo equilibrium elimination to form isocyanates under basic conditions, which can then be hydrolyzed to release n-butylamine. During the course of this work, we observed some evidence that this transformation may have occurred, but we were unable to confirm it (data not shown). Second, once n-butylamine is released, it may act as a nucleophile and react with other carbamate linkages to release further naltrexone and produce bis(n-butyl)urea. Addition of excess n-butylamine to Naltrexone-n-butylcarbamate in a follow up experiment validated this part of the hypothesis, as significant urea byproduct and released naltrexone were observed (data not shown). Taken together, these findings revealed that the N-methyl carbamate imparted substantial resistance to hydrolytic degradation compared to the N-H carbamate and would therefore provide better stability when incorporated into an abuse-deterrent opioid prodrug. We expected analogous findings for the corresponding thionocarbonate linkage. Since the N-methyl thionocarbamate peptide-naltrexone conjugate demonstrated the best overall

resistance to hydrolytic degradation with < 7% degradation observed from pH 2-12, we designed our synthetic efforts for other functional groups around this stable linkage.

3.2.3 Efforts toward Reversible Alcohol Modification of Naltrexone

Due to the presence of other functional groups, functionalization of the alcohol first required protection of the phenol and ketone of naltrexone. Because alcohol modifications are most applicable to oxycodone, which possesses a phenyl methyl ether, reversible protection of the phenol of naltrexone was not required. Therefore, the phenol of naltrexone was first protected as a methyl ether in quantitative yield to give O-Me Naltrexone based on the reported procedure using methyl iodide and potassium carbonate (Scheme 3.5).[37] O-Me Naltrexone was then refluxed in methanol (MeOH) in the presence of excess trimethyl orthoformate and catalytic sulfuric acid to protect the ketone as a dimethyl ketal in 49% yield after HPLC purification. The protected O-Me Naltrexone-dimethyl ketal was then subjected to a variety of reaction conditions in attempt to acylate the tertiary alcohol.

Scheme 3.5. Synthetic route towards functionalization of the tertiary alcohol of Naltrexone.

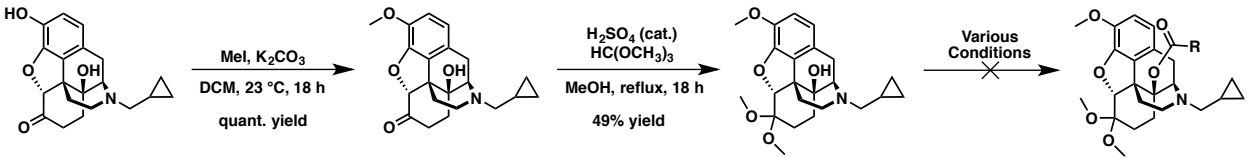

Reactions were mostly carried out using pentafluorophenylchlorothionoformate as the electrophile, but the less bulky acylating reagent acetyl chloride was also used. Initially relatively weak tertiary amine bases such as TEA were used, but only starting materials were observed under the conditions tested. Stronger bases like sodium hydride were also unsuccessful in yielding the desired acylated product, again yielding only the O-Me Naltrexone-dimethyl ketal

starting material. Despite a variety of reaction conditions surveyed, no alcohol modification products were ever observed (data not shown).

This lack of reactivity was somewhat expected at the outset of these efforts given the especially hindered nature of this alcohol as a result of its position in the molecule. More specifically, the alcohol is tertiary and adjacent to quaternary and tertiary carbon centers that are both bridgeheads to three and two 6-membered rings, respectively. Additionally, we are not aware of any literature reports that functionalize the alcohol of naltrexone, although acetylation has been reported for the N-methyl variant.[37] This suggests that the added bulk of the N-methyl cyclopropane substituent in combination with other steric constraints may be sufficient to impair the reactivity of this alcohol. To better visualize these steric constraints, we modeled naltrexone using Spartan software (Figure 3.4). Although the generated structures to not conclusively confirm that sterics prohibit reactivity of the alcohol, the alcohol does appear to be in a relatively crowded local environment. It should be noted that these images are static renderings and are therefore not necessarily reflective of the molecule's dynamic motion in solution. However, the accumulated evidence suggests that the alcohol of naltrexone is sufficiently sterically hindered so as not to allow reaction with acylating reagents. Such a reaction may be possible with other molecules like oxycodone, but due to the feasibility of other approaches, we did not pursue this modification strategy further.

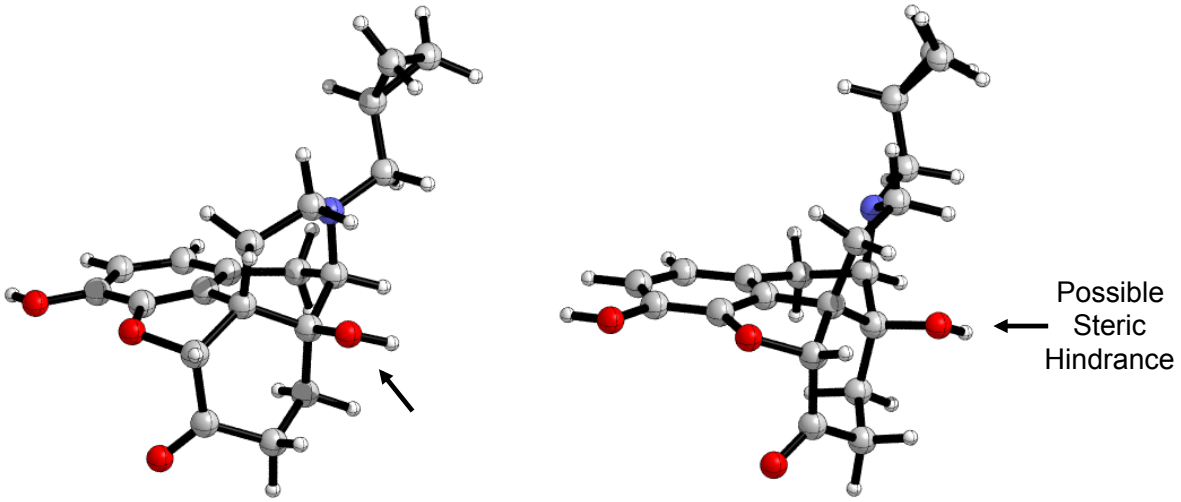

Figure 3.4. Three-dimensional modeling of naltrexone generated in Spartan with B3LYP/6-31G(d) level of theory in the gas phase. Two slightly rotated views of the same structure are provided for clarity. Modeling suggests possible steric hindrance around tertiary alcohol, which is indicated with arrows.

3.2.4 Reversible Ketone Modification of Naltrexone

Modification of the ketone of naltrexone was accomplished by treatment with strong base to generate the ketone enolate, which was then trapped with an acylating reagent in a strategy similar to other functional group modifications. The lack of reactivity demonstrated by the alcohol of naltrexone proved fortuitous for selective ketone modification. Since efforts to directly acylate the alcohol were unsuccessful, we did not expect to observe any such side products resulting from indirect acylation during ketone modification reactions. Accordingly, we were also able to carry out these reactions without protecting the tertiary alcohol. The phenol of naltrexone was first protected as a methyl ether using the procedure noted in the previous section to provide O-Me Naltrexone.

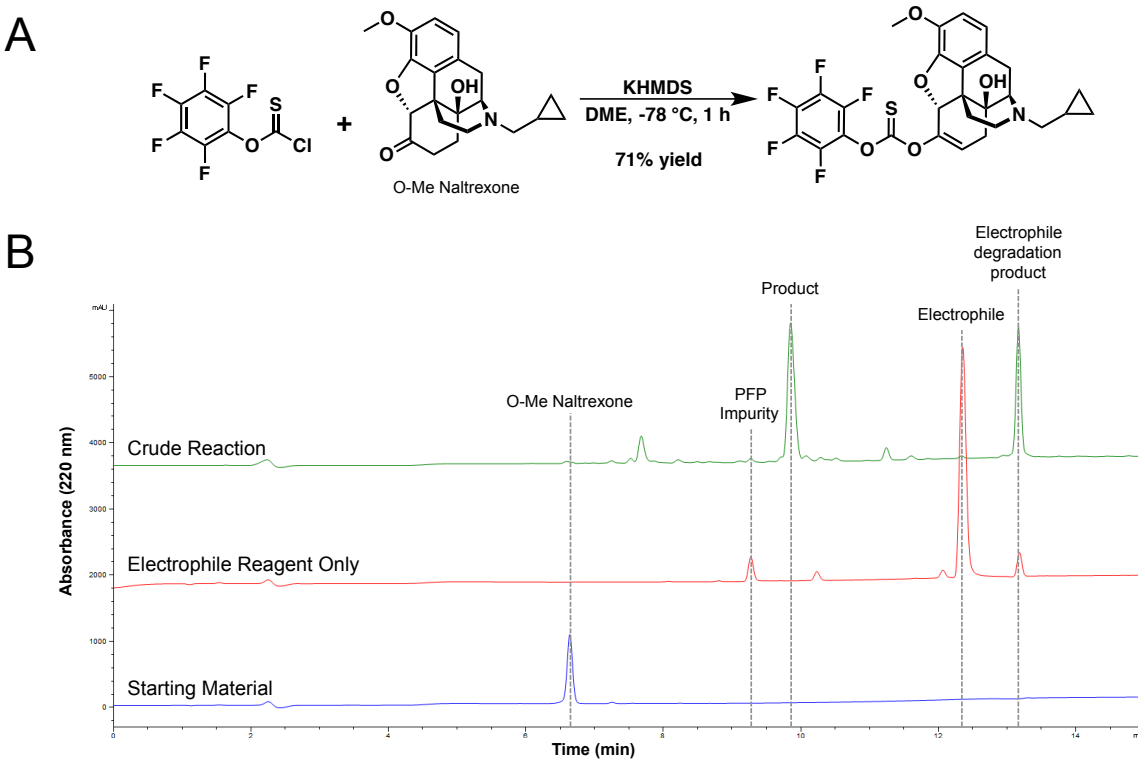

Figure 3.5. Synthesis of O-Me Naltrexone-enol-PFPTC. (A) Reaction scheme of enolate trapping of O-Me Naltrexone with pentafluorophenylchlorothionoformate. (B) Overlay of analytical HPLC chromatograms for O-Me Naltrexone (bottom), pentafluorophenylchlorothionoformate (middle), and the crude reaction (top). A small portion of pentafluorophenol (PFP) was observed in the electrophile starting material, but did not significantly affect the reaction.

The enolate of O-Me Naltrexone was generated by treatment with 2 molar equivalents of potassium hexamethyldisilylamide (KHMDS) at -78 °C in dimethoxyethane (DME). The solution of enolate was then cannulated slowly into a separately prepared solution of 3 molar equivalents of pentafluorophenylchlorothionoformate at -78 °C in DME to ensure that the electrophile remained in excess throughout the reaction. The combination of the solvent-separated ion pair (potassium enolate salt) as well as use of a coordinating solvent like DME are thought to favor O-acylation of enolates over the corresponding C-acylation products, especially in combination with hard electrophiles like anhydrides and formyl halides.[38–42] The reaction was

monitored by HPLC with a representative chromatogram shown in Figure 3.5. As indicated by the chromatogram, the reaction proceeded to high conversion with only minor impurities present in the crude reaction mixture, most of which were identified as degradation products of the electrophile. The activated O-Me Naltrexone-enol-pentafluorophenylthionocarbamate (O-Me-Naltrexone-enol-PFPTC) was obtained in 71% yield following HPLC purification. Characterization by high-resolution mass spectrometry (HRMS), ^{1}H, ^{13}C, ^{19}F, COSY, and HSQC NMR was used to confirm the product structure. As expected, no alcohol modification products were observed.

The activated O-Me-Naltrexone-enol-PFPTC was reacted with the protected CAAK(F) peptide then purified and deprotected using the same conditions mentioned previously, providing the CAAK(F)-Naltrexone-enol-thionocarbamate conjugate in 55% yield (Scheme 3.6). Stability of the formed linkage was again evaluated over a pH range of 2-12 with < 9% degradation observed for each condition over 24 hours. These values were slightly higher than for the phenol linkage, which may be reflective of a slightly less stable linkage; but since both generated low percent degradation values across the entire pH range, we attributed these slight differences to variations in measurement. This linkage was also stable at pH 2 as well as the other pH conditions assessed, which provides protection from possible household hydrolytic agents. Taken together, the combination of this high-yielding, short synthesis and the stable, yet enzymatically reversible formed linkage in this model compound provided an ideal foundation for application to opioid drugs such as the structurally analogous oxycodone.

Scheme 3.6. Conjugation of activated Naltrexone-enol-PFPTC to dual-enzyme responsive peptide CAAK(F) to give CAAK(F)-Naltrexone-enol-thionocarbamate.

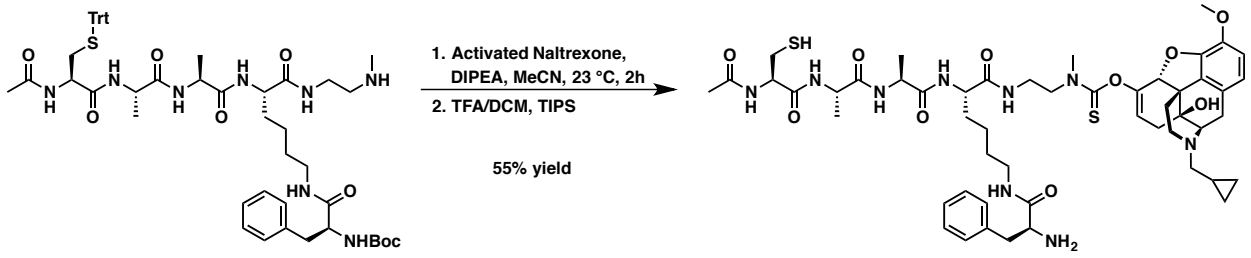

Table 3.3. Hydrolytic stability assessment of CAAK(F)-Naltrexone-enol-thionocarbamate peptide conjugate.

Condition	% Degraded after 24 hours
pH 2	6.8%
pH 4	3.3%
pH 7	4.4%
pH 9	8.3%
pH 12	7.1%

3.2.5 Reversible Ketone Modification of Oxycodone

Unlike naltrexone, oxycodone was provided as the HCl salt, and we found that reaction yields were substantially reduced if the salt was used directly in the enolate trapping reaction, likely due to the low solubility of the salt. Therefore, we obtained oxycodone as the free base by dissolving the oxycodone HCl salt in water, then precipitating the free base via addition of aqueous 1 M potassium carbonate. Multiple strategies were used to recover the precipitated drug, but ultimately extraction with chloroform proved to be the most straightforward and oxycodone was recovered as the free base in good yield (77-100%) (Scheme 3.7A). Using the reaction conditions established for modification of the ketone of O-Me Naltrexone, we proceeded to trap the enolate of oxycodone to activate the opioid for conjugation to the dual-enzyme responsive

peptide. Surprisingly, the yields of this reaction were consistently low (18-53%) compared to those of O-Me Naltrexone despite using the same reaction conditions (Scheme 3.7A). Characterization by high-resolution mass spectrometry (HRMS), ^{1}H, ^{13}C, ^{19}F, COSY, and HSQC NMR was used to confirm the product structure.

Scheme 3.7. Synthesis of activated oxycodone species (A) Oxycodone-enol-PFPTC, and conjugation of activated oxycodone species to dual-enzyme responsive peptide CAAK(F) to give (B) CAAK(F)-Oxycodone-enol-thionocarbamate peptide conjugate.

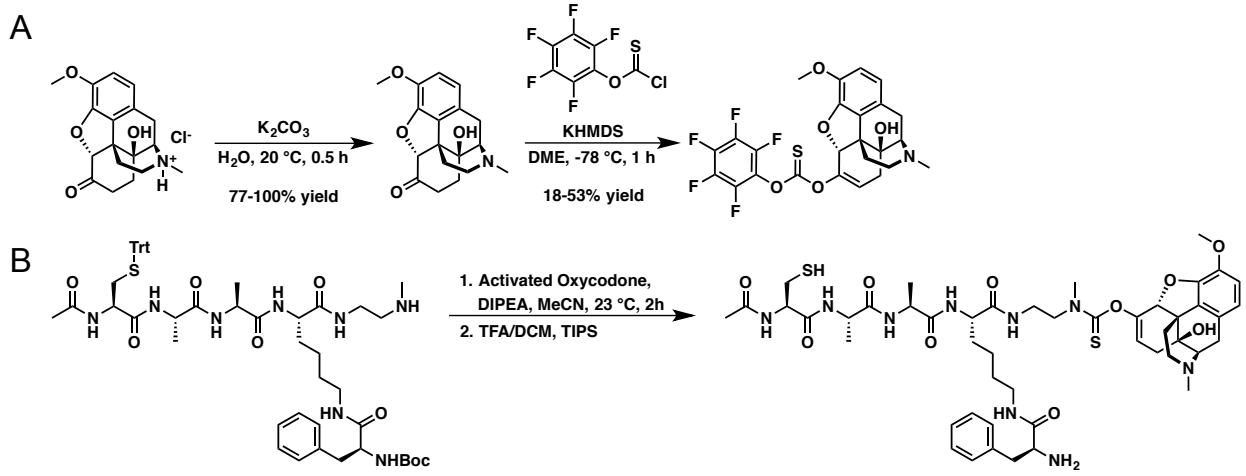

To understand this, we followed the reaction by HPLC and LCMS. A representative LCMS chromatogram of the crude reaction intended to form Oxycodone enol-pentafluorophenylthionocarbamate (Oxycodone-enol-PFPTP) is shown in Figure 3.6. As shown in the chromatogram, three distinct oxycodone products were observed in addition to the three electrophile-related peaks that are typically observed in these reactions. Residual unreacted oxycodone was observed in the chromatogram, indicating the reaction did not proceed to full conversion. The desired product, Oxycodone-enol-PFPTP, eluted later as one of the major product peaks. This left one final peak that eluted after the desired product peak, suggesting that it was more hydrophobic than the desired product. As noted in Figure 3.6, this unidentified peak

also possessed a mass difference equal to the difference between Oxycodone-enol-PFPTF and oxycodone starting material, strongly suggesting that this observed product was the result of oxycodone addition to two electrophile molecules.

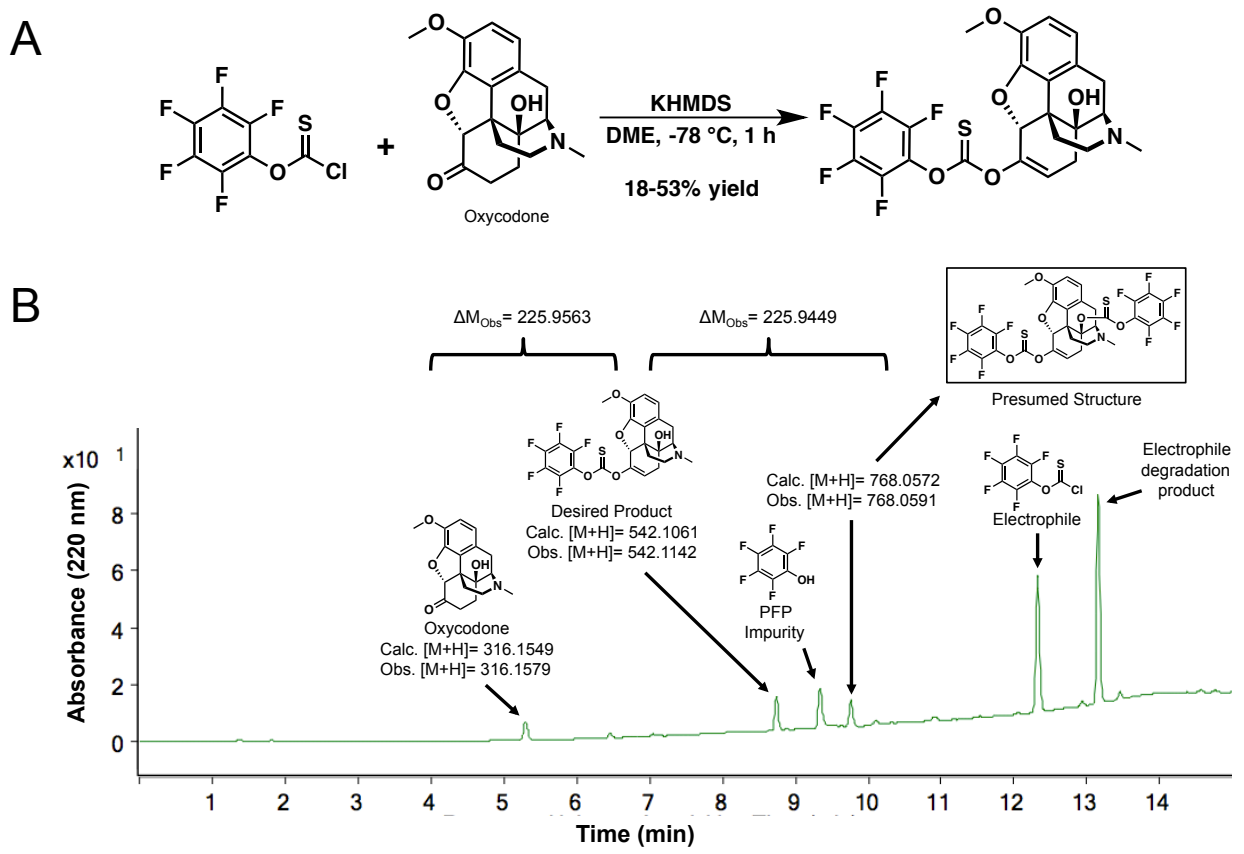

Figure 3.6. Synthesis of Oxycodone-enol-PFPTC. (A) Reaction scheme of enolate trapping of Oxycodone with pentafluorophenylchlorothionoformate with a representative yield range reflective of minor adjustments to reaction conditions. (B) Annotated LCMS chromatogram of crude reaction mixture. The mass difference between oxycodone and the desired single addition product matched the mass difference between the desired product and a side product, indicating double addition of the electrophile to oxycodone. The putative structure of the double addition product is boxed.

Based on the structure of oxycodone, we deduced that this double addition product could be one of two possible isomers. The first possible isomer could have been formed from double

addition of the oxycodone enolate to the electrophile first by C-acylation, then by O-acylation (for a more detailed description of this reaction mechanism, see the following section, specifically Scheme 3.8). However, given that we had never observed this reaction for O-Me Naltrexone, which is structurally identical to oxycodone in the region of the molecule surrounding the ketone, this reaction pathway seemed unlikely. The second possible isomer could have been formed from a second addition of the desired product to the electrophile via reaction with the alcohol of oxycodone. Though surprising, this explanation actually fit well with our observations for reactions with O-Me Naltrexone. As noted in Section 3.2.3, we hypothesized that the steric bulk surrounding the tertiary alcohol likely prevented its reaction for O-Me Naltrexone and also noted that acylation of the N-methyl variant had been reported. This suggests that steric hindrance of the tertiary alcohol may actually be the result of the N-methylcyclopropane substituent instead of the alcohol's proximity to other structural features. Although we were unable to obtain enough of this material to confirm which of the two isomers it was, we believe the available evidence strongly suggests that it is the enolate and alcohol double addition product.

Despite the reduction in yield of this reaction due to double addition side product formation, we were still able to prepare sufficient material for conjugation to the dual-enzyme responsive peptide (Scheme 3.7). This conjugation was performed by Doug Rose (University of California, Los Angeles) using the same methodology as noted in previous sections. Stability of the resulting conjugate was likewise assessed as described previously (Table 3.4). The CAAK(F)-oxycodone-enol-thionocarbamate conjugate demonstrated excellent stability, with < 2% linkage degradation observed after 24 hours. Follow up studies and further stability testing revealed this and subsequent conjugates based on this chemistry to be stable to a wide variety of

household reagents. We therefore expect that conjugates of this nature will provide an excellent platform for abuse-deterrent opioid formulations.

Table 3.4. Hydrolytic stability assessment of CAAK(F)-Oxycodone-enol-thionocarbamate peptide conjugate

Condition	% Degraded after 24 hours
pH 2	1.2%
pH 4	1.1%
pH 7	1.1%
pH 9	1.5%
pH 12	0.9%

Interested in improving the yield of the oxycodone ketone functionalization reaction to generate more material, we designed and performed a reaction screen to identify the optimal reaction conditions that would maximize the yield of the desired Oxycodone-enol-PFPTC while simultaneously minimizing side-product formation. Twenty individual 1 mg oxycodone reactions were performed simultaneously in a combinatorial manner so that each combination of base and electrophile was reacted at the same concentration using the same molar ratios of oxycodone, base, and electrophile (see Figure 3.7A). Bases used in the reaction screen were lithium hexamethyldisilylamide (LiHMDS) with tetramethylethylenediamine (TMEDA), LiHMDS, sodium hexamethyldisilylamide (NaHMDS), and KHMDS. Electrophiles used in the reaction screen were acetyl chloride, pentafluorophenylchlorothionoformate, phenylthionochloroformate, thiophosgene, and thionocarbonyldiimidazole with $BF_3 \cdot OEt_2$. Reactions were carried out in oven-dried dram vials suspended in a -78 °C cold bath (acetone/dry ice) and kept under argon using an argon splitter (see Figure 3.7B). After adding all components to each reaction vessel, all reactions were allowed to stir for 30 minutes, and then samples were filtered and prepared for

HPLC/LCMS analysis. Reaction conversion was assessed by measuring the ratio of oxycodone to product peaks, and these conversions were used to construct a heat map (Figure 3.7C). Reactions with the highest conversions and minimal side products were further analyzed by LCMS using a similar method, with optimal conditions displayed in see Figure 3.7D.

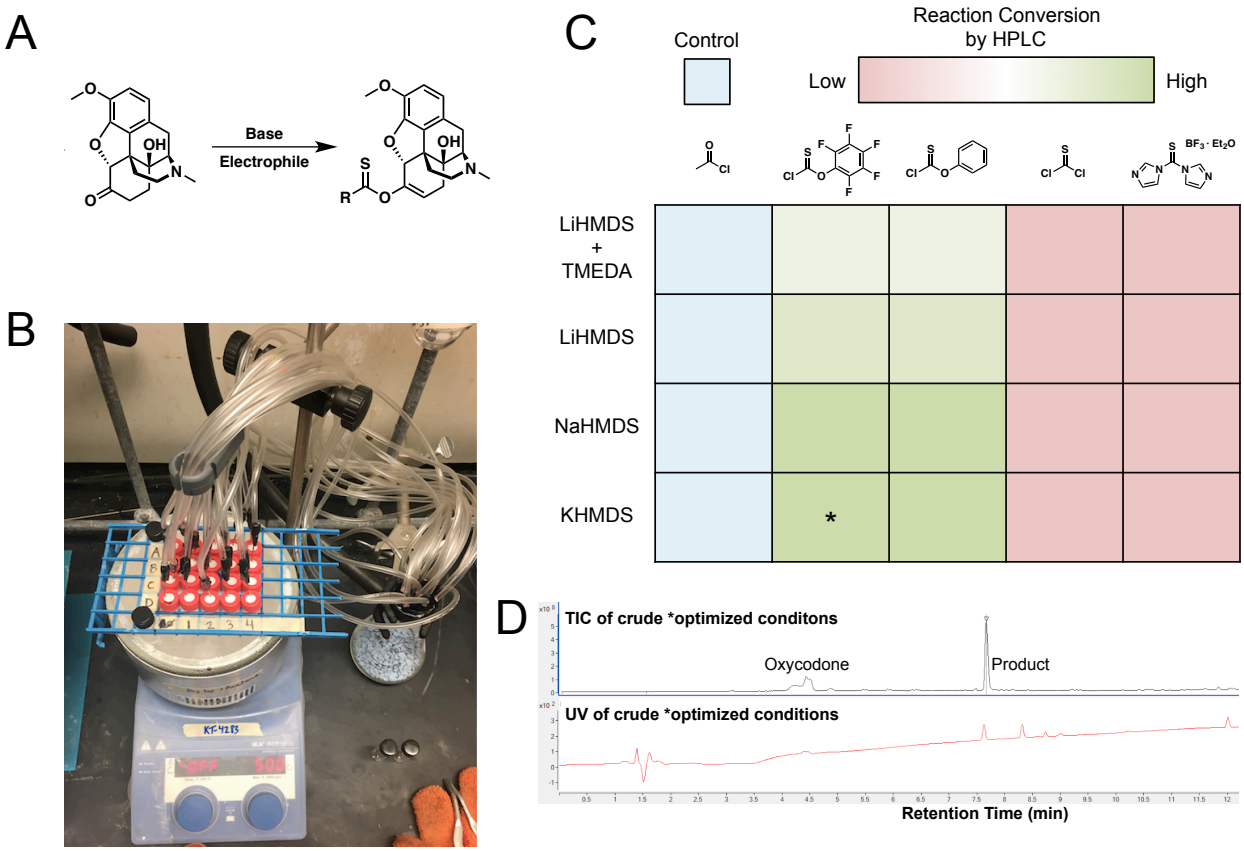

Figure 3.7. Optimization of oxycodone enolate trapping reaction. (A) General reaction scheme. (B) Photo of the reaction screen set up. Reactions were carried out in 1 mL glass vials under an inert argon atmosphere with stirring at -78 °C in a dry ice and acetone bath. (C) Reaction screen heat map. Reactions were carried out via combinatorial variation of base and electrophile as indicated by the row and column labels around the color-coded grid. Conversion was assessed for each reaction combination via comparison by HPLC of oxycodone and product peak intensities and color-coded accordingly on the heat map. Reactions with the highest observed relative conversion were further analyzed by LCMS. *Indicates reaction conditions with highest observed conversion. (D) Overlaid total-ion (top) and ultraviolet (bottom; 220 nm) chromatograms for highest conversion reaction conditions as

indicated in (C) with an asterisk. No significant peaks for oxycodone side-products or double addition products were observed in the total-ion chromatogram (TIC). Outside of starting material and product, the ultraviolet (UV) chromatogram displayed only peaks associated with the electrophile and its degradation products.

Interestingly, the combination of pentafluorophenylchlorothionoformate and KHMDS was determined to provide the highest reaction conversion with no significant side products as indicated by the single major product peak observed in the total ion chromatogram (TIC). The combination of KHMDS and phenylthionochloroformate also yielded similar results, but it was later found that the phenol led to side-product formation during the peptide-drug conjugations, likely due to its higher nucleophilicity compared to pentafluorophenol. These results generally make sense in the context of enolate reactions. For example, potassium is the largest cation in the HMDS base series, and solvent-separated cation-enolate ion pairs tend to be more reactive and favor O-acylation.[39,41] Acetyl chloride was used as a control to facilitate observation of double addition products. As expected, the small electrophile led to considerable double addition for all base conditions. Reactions with thiophosgene and thionocarbonyldiimidazole yielded negligible product, likely due to their proclivity for crosslinking. In summary, conditions initially utilized for ketone modifications of naltrexone and oxycodone provided the best reaction conditions. Future replication of these conditions is therefore expected to yield Oxycodone-enol-PFPTC in good yields, providing a succinct and efficient route to preparation of dual-enzyme responsive opioid prodrugs for abuse-deterrence. We expect that the previous reaction yields may have been low due to purification challenges. While Oxycodone-phenol-PFPTC could be purified in good yield via silica gel flash chromatography, Oxycodone-enol-PFPTC could not be purified in this manner despite extensive solvent system screening. The purification therefore relied on preparative HPLC, which exposed the crude reaction mixture to aqueous conditions in the

presence of bases and nucleophiles that may have enhanced the rate of degradation. As noted previously, side-product formation appeared to compete with the desired product under certain conditions and may also have partially contributed to modest yields in some reactions. Improved methods of purification will therefore need to be assessed to improve future yields. While the yields of these reactions proved somewhat variable, we were nevertheless able to produce sufficient material for our applications.

3.2.6 Griseofulvin Case Study: Ketone Modification of Griseofulvin and Identification of a Double Addition Side Product

Inspired by our success in developing naltrexone and oxycodone-based prodrugs, we envisioned that this chemistry might be useful for synthesizing prodrugs from other ketone-containing drugs beyond opioids. Although several factors ultimately led us to discontinue this work, we thought it prudent to disclose an example of particular interest that we encountered during our efforts to modify other ketone-containing drugs that also provided insight into the double addition side reaction discussed in the previous section. In this section we briefly shift our focus from opioids to griseofulvin, an FDA-approved antifungal agent. We became interested in griseofulvin purely for structural reasons, as it contained only one enolizable ketone moiety and few other functional groups likely to interfere with modification of this ketone.

We modified griseofulvin using our established enolate trapping reaction conditions described in previous sections, and found that the reaction proceeded with high conversion with minimal unreacted griseofulvin observed by thin-layer chromatography (TLC) and HPLC (Figure 3.1A). Purification of the resulting products was attempted by flash column chromatography, but LCMS analysis revealed the presence of non-product impurities. The annotated LCMS chromatogram in Figure 3.1B revealed an early-eluting impurity to be

unreacted griseofulvin starting material, and the second impurity that eluted after the desired product was determined to have the same mass difference from the desired product as the desired product had from griseofulvin, indicating this impurity to be a double addition product. Unlike oxycodone, griseofulvin did not possess an additional nucleophilic moiety that could react with additional electrophile, so the second addition must have stemmed from the formation and addition of a second enolate to the electrophile. The double addition product could therefore be only one of two possible isomers, the C-,O-acylation product (Isomer 1) or the C-,C-acylation product (Isomer 2) (Figure 3.1C). The single and double addition griseofulvin products were further purified by preparative HPLC and analyzed by ^{1}H, ^{13}C,and ^{19}F NMR to elucidate their structures. The single addition product was recovered in 58% yield and the double addition product comprised 21% yield.

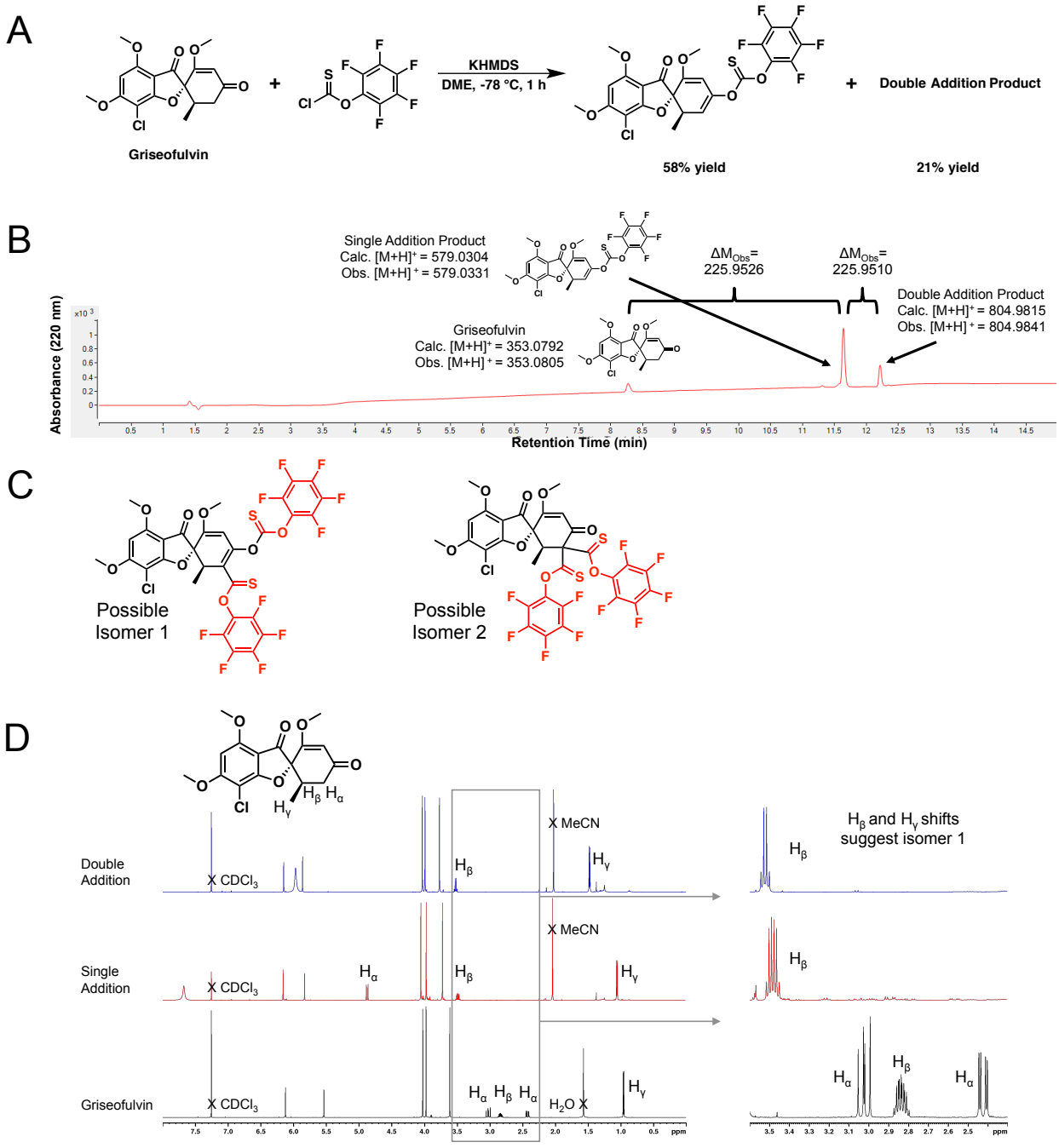

Figure 3.8. Synthesis of Griseofulvin-enol-PFPTC and observation of double addition product. (A) Reaction scheme of enolate trapping of griseofulvin with pentafluorophenylchlorothionoformate using the same reaction conditions as for oxycodone. (B) Annotated LCMS chromatogram of the semi-purified reaction mixture. The mass difference between griseofulvin and the desired single addition product matched the mass difference between the desired product and a side product, indicating double addition of the electrophile to griseofulvin. (C) Structures of

the two possible double addition product isomers. (D) Overlaid ^{1}H NMR analyses of unmodified griseofulvin (black), Griseofulvin-enol-PFPTC single addition product (red), and the double addition product (blue). An enlarged spectral window from 3.6-2.3 ppm is provided to the right to highlight the changes in chemical shifts and multiplicities of select protons among each isolated product.

Overlaid ^{1}H NMR spectra are presented in Figure 3.8D for griseofulvin, the single addition product, and the double addition product. Unmodified griseofulvin exhibited two distinct alpha-protons (H_α), each possessing an integration of 1.00 and appearing as a doublet-of-doublets. Upon addition of griseofulvin to a single electrophile molecule, loss of one of the two protons at this position was observed with the total number of protons in the molecule dropping by 1.00, confirming formation of an enolate product. The remaining H_α shifted from 3.02 ppm to 4.87 ppm and became a doublet, which was consistent with expectations for the O-acylated, trapped enolate. This structural assignment was also confirmed by the downfield shift of the beta- (H_β) and gamma-protons (H_γ) as well as reduction in the multiplicity of H_β. As expected for the double addition product, no H_α were observed, confirming that the second addition of griseofulvin to the electrophile was via an enolate nucleophile. Again, this structural assignment was corroborated by the H_β and H_γ chemical shifts and multiplicities. Specifically, H_β did not shift significantly, indicating that its chemical environment was insignificantly changed following a second electrophile addition and implying that it was still adjacent to an alkene, which is more consistent with Isomer 1. Additionally, H_γ shifted significantly more downfield following the second electrophile addition compared to the first, implying that the second addition was much more proximal, and different than the first, which also provides support for Isomer 1.

Similar analysis was carried out for ^{19}F and ^{13}C NMR. Two sets of distinct pentafluorophenyl peaks were observed by ^{19}F NMR, confirming griseofulvin addition to two molecules of electrophile. In all analyses, it was clear from the change in chemical shifts between the single and double addition products that the second electrophile unit added to griseofulvin was present in a chemical environment distinct from the first, as evidenced by the large separations between corresponding peaks of each. If double addition product were Isomer 2, these peak separations would be expected to be significantly smaller since the two electrophile units would be in very similar chemical environments. Taken together, this body of spectral evidence supports the structure of Isomer 1 as the product of the double addition reaction.

Intrigued by this finding, we hypothesized a mechanism that would not only explain the formation of the double addition product, but might also elucidate the ratio of products for the reaction. The single addition product was purified in 58% yield while the double addition product was recovered in 21% yield. O-acylation of griseofulvin to form the single addition product effectively prevents further enolate formation since the resultant alpha-proton is no longer sufficiently acidic to be deprotonated by KHMDS. Because the majority of the product formed was the single addition product, and this reaction pathway effectively terminated further reactions, we concluded that the double addition product must proceed through an alternate, less favorable pathway. We present our proposed reaction mechanism in Scheme 3.8.

We propose that the initially formed griseofulvin enolate can undergo two distinct reaction pathways. The primary reaction pathway proceeds via O-acylation of the griseofulvin enolate to give the single addition product as the major product. Alternatively, this enolate can also proceed through a C-acylation pathway to form the double addition product as the minor product. No C-acylation single addition products were observed during this reaction or other

similar reactions. This is most likely because once the C-acylation single addition product is formed, the alpha-proton of the formed β-keto thionoester becomes significantly more acidic and is therefore immediately deprotonated by KHMDS. This second enolate can then proceed through a second O- or C- acylation pathway, but preferentially proceeds through O-acylation as these are favored by the reaction conditions. We believe this rational mechanism not only offers an explanation for the product distribution, but also supports the spectral evidence for Isomer 1 as the double addition product.

Scheme 3.8. Proposed mechanism of double addition to electrophile during griseofulvin enolate trapping reaction.

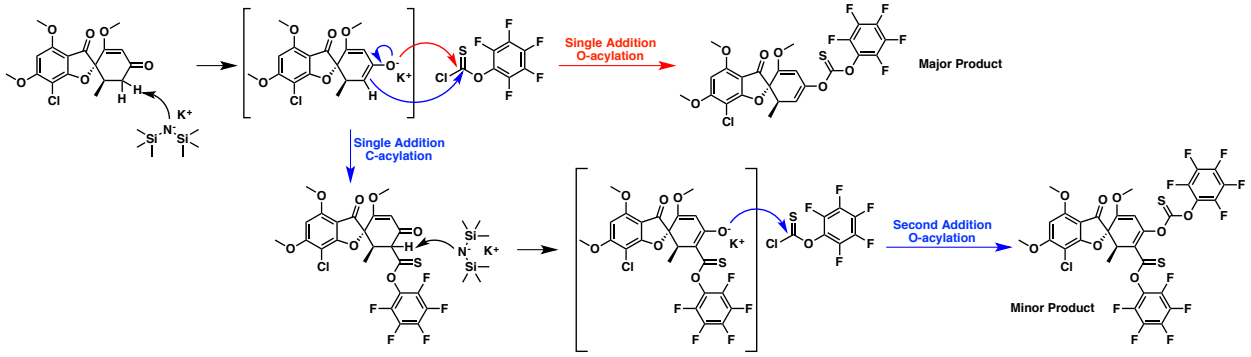

Despite their evident utility in this chapter, enol carbonates and enol carbamates remain relatively underexplored linkages in organic chemistry. We expect that our work in this area will garner interest in this area not only for applications in prodrug synthesis, but also as synthetically interesting functionalities with many potential uses. The ability to transform a simple ketone into an enolate-trapped, double addition product such as the one we have elucidated in this section presents an attractive and potentially useful avenue for rapid access to complex structures. We expect that further investigation of these moieties will undoubtedly deliver worthwhile results.

3.3 Conclusions

With the ongoing opioid epidemic claiming thousands of lives in the United States each year, development of technologies to mitigate the abuse of these necessary, but highly addictive analgesic agents has become a high priority of paramount importance. In this chapter, we report the development of chemistry to activate functional groups common to most opioids for conjugation to dual-enzyme responsive peptides. This chemistry was then applied to the commonly prescribed opioid oxycodone, and the resulting prodrug demonstrated excellent stability to a broad pH range and could be obtained in reasonable yields. We further explored side product formation for this chemistry and successfully screened and identified reaction conditions that minimized side product formation and maximized product conversion. During this process we also encountered an interesting reaction pathway that may offer novel synthetic utility and may provide interesting chemistry applicable to other pharmaceutically relevant molecules. We expect and sincerely hope that the chemistry and abuse-deterrent opioid prodrug that we have developed in this chapter will contribute to efforts in combating the opioid epidemic.

3.4 Experimental

3.4.1 Materials

Naltrexone was purchased from MedChem Express, oxycodone (hydrochloride salt) was supplied by Prof. Chris Evans (University of California, Los Angeles), and all peptides were prepared by Doug Rose (University of California, Los Angeles). Griseofulvin was purchased from TCI America. All other chemicals were used as purchased unless otherwise noted from Acros, Alfa Aesar, Sigma Aldrich, Chem-Impex, or Fisher Scientific. All reactions were

performed using dry solvents under an inert argon atmosphere unless otherwise noted. Dichloromethane (DCM) was distilled over CaH_2 and stored under argon. Tetrahydrofuran (THF) was distilled over sodium/benzophenone and stored under argon. 1,2-dimethoxyethane, methanol, acetonitrile (MeCN) and other dry solvents were dried by purging with nitrogen and passage through activated alumina columns prior to use. TMEDA was freshly distilled and stored over 3Å molecular sieves prior to use. LiHMDS was purchased from Acros Organics as a 1.0 M solution in THF. NaHMDS and KHMDS were stored in a Vacuum Atmospheres Genesis stainless steel glove box under nitrogen atmosphere. Representative procedures are provided for each reaction.

3.4.2 Analytical Techniques

NMR spectra were obtained using either Bruker AV400, AV500, DRX500, or AV600 spectrometers. ESI mass spectra were obtained using either a Waters Acquity LCT Premier XE equipped with an autosampler and direct injection port or an Agilent 6530 QTOF-ESI with a 1260 Infinity LC with autosampler. Infrared absorption spectra were obtained using a PerkinElmer FT-IR equipped with an ATR accessory. Normal phase flash column chromatography was carried out using a Biotage Isolera One Flash Purification Chromatography system. Analytical reverse phase high performance liquid chromatography (HPLC) was carried out on a Agilent 1260 Infinity II HPLC system equipped with an autosampler and a UV detector using a Poroshell 120 2.7 μm C18 120 Å column (analytical: 2.7 μm, 4.6 × 100 mm) with monitoring at λ = 220 and 280 nm and with a flow rate of 0.8 mL/min. Peptide-drug conjugates were analyzed using a mobile phase consisting of 10-100% MeCN + 0.1% TFA in water beginning with a 1 min isocratic at 10%, then up to 100% over 10 min in a linear gradient, followed by an isocratic hold at 100% MeCN + 0.1% TFA for 4 min (total time was 15 min).

Purification was carried out on the same system using a Zorbax SB-C18 5.0 μm C18 120 Å column (semi-preparative: 5.0 μm, 9.4 × 250 mm) with monitoring at λ = 220 and 280 nm and with a flow rate of 3.0 mL/min. Peptide-drug conjugates were purified using a mobile phase consisting of 10-100% MeCN + 0.1% TFA in water beginning with a 3 min isocratic at 10%, then up to 100% over 15 min in a linear gradient, followed by an isocratic hold at 100% MeCN + 0.1% TFA for 4 min (total time was 22 min). Preparatory reverse phase HPLC was carried out on a Shimadzu high performance liquid chromatography system equipped with a UV detector using a Luna 5 μm C18 100 Å column (preparatory: 5 μm, 250 × 21.2 mm) with monitoring at λ = 215 and 254 nm and with a flow rate of 20 mL/min. Enolate trapped drug products were purified using a mobile phase consisting of 40-95% MeCN + 0.1% trifluoroacetic acid (TFA) in water beginning with 1 min isocratic at 10%, then up to 95% over 15 min in a linear gradient, followed by an isocratic hold at 95% MeCN + 0.1% TFA for 4 min (total time was 20 min).

General procedure for quantification of peptide-drug conjugate stability via HPLC

Peptide-drug conjugate samples were dissolved to final concentrations of 0.2-1.0 mg/mL in a 10 mM solution of either phosphate buffer or citrate-phosphate buffer at the indicated pH range from 2-12. Immediately after dissolution, samples were injected and analyzed via analytical HPLC and the peak area corresponding to the retention time of the peptide-drug conjugate was recorded as a baseline. Percent degradation of the hydrolytically susceptible carbamate linkage was calculated by comparison of subsequent injection time points to the peak area of the initial injection. The ratio of peak areas between the intact peptide-drug conjugate and the released free drug was assessed as an additional confirmation of degradation. Data is expressed as the percent of total peptide-drug conjugate degraded over the given time interval to give free peptide and drug. A negative control consisting of the conjugate dissolved in

acetonitrile was used to confirm that degradation of the carbamate linkage resulted from hydrolysis. Each degradation percentage value was obtained following a single, independent experiment.

3.4.3 Methods

Synthesis of Naltrexone-phenol-NPC

To an oven dried 2-neck 25 mL round bottom flask was added 10 mL DCM and Naltrexone-HCl salt (100 mg, 0.26 mmol, 1 eq). Diisopropylethylamine (DIPEA; 115 μL, 0.66 mmol, 2.5 eq) was then added and stirred for several minutes until all material had visibly dissolved. 4-nitrophenyl chloroformate (107 mg, 0.53 mmol, 2 eq) was then added and the reaction was stirred at 20 °C for 18 hours. The crude reaction mixture was concentrated under vacuum and purified using a 10 g SNAP KP-SIL Biotage column with a solvent system of 2-20% DCM in acetone. Fractions containing the desired product were isolated and solvent was removed under vacuum to give a pale yellow solid (117 mg, 87.2% yield). R_f = 0.6 (9:1 DCM:Acetone). See Figure 3.9 for ^{1}H NMR (500 MHz, $CDCl_3$): δ 8.30 (d, *J* = 9.2 Hz, 2H), 7.52 (d, *J* = 9.2 Hz, 2H), 7.00 (d, *J* = 8.3 Hz, 1H), 6.73 (d, *J* = 8.3 Hz, 1H), 4.76 (s, 1H), 3.23 (d, *J* = 5.8 Hz, 1H), 3.12 (d, *J* = 18.8 Hz, 1H), 3.05 (td, *J* = 14.6, 5.1 Hz, 1H), 2.73 (dd, *J* = 12.1, 4.7 Hz, 1H), 2.64 (dd, *J* = 18.8, 6.0 Hz, 1H), 2.47 (td, *J* = 12.6, 5.3 Hz, 1H), 2.42 (d, *J* = 6.7 Hz, 2H), 2.34 (dt, *J* = 14.5, 3.1 Hz, 1H), 2.13 (td, *J* = 12.2, 3.8 Hz, 1H), 1.92 (dq, *J* = 13.4, 2.6 Hz, 1H), 1.64 (dd, *J* = 14.1, 3.3 Hz, 1H), 1.59 (m, 1H), 0.88 (m, 1H), 0.57 (m, 2H), 0.15 (m, 2H). See Figure 3.10 for ^{13}C NMR (100 MHz, $CDCl_3$): δ 207.45, 155.45, 150.27, 147.36, 145.55, 132.65, 131.51, 130.84, 125.33, 122.10, 121.76, 119.62, 91.08, 69.98, 61.85, 59.23, 50.84, 43.40, 36.09, 31.30, 30.80, 23.04, 9.37, 4.03, 3.85. HRMS: $C_{27}H_{27}N_2O_8$ calc. $[M+H]^+$ = 507.1767 Da; obsd. $[M+H]^+$ = 507.1524 Da.

Synthesis of Naltrexone-phenol-PFPTC

To an oven dried 2-neck 25 mL round bottom flask was added 10 mL DCM and Naltrexone (100 mg, 0.29 mmol, 1 eq). DIPEA (128 µl, 0.73 mmol, 2.5 eq) was then added and stirred for several minutes until all material had visibly dissolved. Pentafluorophenylchlorothionoformate (94 µl, 0.59 mmol, 2 eq) was added and the reaction was stirred at 20 °C for 20 hours. The crude reaction mixture was concentrated under vacuum and purified using a 10 g SNAP KP-SIL Biotage column with a solvent system of 2-20% DCM in acetone. Fractions containing the desired product were isolated and solvent was removed under vacuum to give a pale yellow solid (139 mg, 83.4% yield). R_f = 0.6 (9:1 DCM:Acetone). See Figure 3.11 for ^{1}H NMR (500 MHz, $CDCl_3$): δ 6.95 (d, *J* = 8.3 Hz, 1H), 6.75 (d, *J* = 8.3 Hz, 1H), 5.20 (s, 1H), 4.76 (s, 1H), 3.22 (d, *J* = 5.8 Hz, 1H), 3.12 (d, *J* = 18.8 Hz, 1H), 3.03 (td, *J* = 14.5, 5.1 Hz, 1H), 2.73 (dd, *J* = 12.2, 4.8 Hz, 1H), 2.65 (dd, *J* = 18.8, 6.0 Hz, 1H), 2.45 (td, *J* = 12.6, 5.3 Hz, 1H), 2.41 (d, *J* = 6.6 Hz, 2H), 2.33 (dt, *J* = 14.6, 3.1 Hz, 1H), 2.14 (td, *J* = 12.3, 3.8 Hz, 1H), 1.92 (dq, *J* = 13.4, 2.6 Hz, 1H), 1.65 (td, *J* = 14.0, 3.5 Hz, 1H), 1.56 (dd, *J* = 12.8, 2.6 Hz, 1H), 0.88 (m, 1H), 0.57 (m, 2H), 0.15 (m, 2H). See Figure 3.12 for ^{13}C NMR (125 MHz, $CDCl_3$): δ 207.01, 190.29, 147.18, 142.17, 140.17, 139.13, 137.01, 135.40, 132.03, 131.17, 122.24, 119.63, 91.03, 69.98, 61.85, 59.87, 43.37, 36.07, 31.34, 30.76, 23.09, 9.38, 3.99, 3.89. See Figure 3.13 for ^{19}F NMR (375 MHz, $CDCl_3$): δ -151.18 (d, *J* = 17.6 Hz, 2H), -156.57 (t, *J* = 21.8 Hz, 1H), -161.87 (dd, *J* = 21.7, 17.4 Hz, 2H). HRMS: $C_{27}H_{23}F_5NO_5S$ calc. $[M+H]^+$ = 568.1217 Da; obsd. $[M+H]^+$ = 568.1055 Da.

Synthesis of CAAK(F)-Naltrexone-phenol-carbamate

To a 3 mL glass vial equipped with a stir bar was dissolved the protected peptide CAAK(F) (5.0 mg, 5.1 µmol, 1 eq) in 1.5 mL MeCN. DIPEA (2.2 µl, 12.8 µmol, 2.5 eq) was

then added to the vial followed by Naltrexone-phenol-NPC (5.2 mg, 10.2 μmol, 2 eq) and the reaction was stirred at 20 °C for 18 hours. The crude reaction mixture was then concentrated under vacuum, redissolved in minimal MeCN, filtered, and purified by semi-preparative HPLC using a method of 30-100% MeCN + 0.1% TFA. Fractions containing the desired product were isolated and lyophilized to yield a white solid (2.0 mg, 29.1% yield). HRMS: $C_{74}H_{91}N_9O_{13}SNa$ calc. $[M+Na]^+$ = 1368.6355 Da; obsd. $[M+Na]^+$ = 1368.6036 Da. Deprotection was carried out by dissolving the purified peptide in 1 mL of approximately 45:45:5:5 TFA:DCM:triisopropylsilane (TIPS):H_2O with stirring for 30 minutes. The reaction was concentrated under vacuum, then precipitated into cold 1:1 hexane:diethyl ether to yield a white solid (1.5 mg, quant. yield). HRMS: $C_{50}H_{69}N_9O_{11}SNa$ calc. $[M+Na]^+$ = 1026.4735 Da; obsd. $[M+Na]^+$ = 1026.4547 Da.

Synthesis of CAAK(F)-Naltrexone-phenol-thionocarbamate

To a 20 mL glass vial equipped with a stir bar was dissolved the protected peptide CAAK(F) (15.0 mg, 15.3 μmol, 1 eq) in 5 mL MeCN. DIPEA (6.7 μl, 38.3 μmol, 2.5 eq) was then added to the vial followed by Naltrexone-phenol-PFPTC (17.4 mg, 30.6 μmol, 2 eq) and the reaction was stirred at 20 °C for 24 hours. The crude reaction mixture was then concentrated under vacuum, redissolved in a 30% MeCN in H_2O, filtered, and purified by preparative HPLC using a method of 30-95% MeCN + 0.1% TFA. Fractions containing the desired product were isolated and lyophilized to yield a white solid (14.9 mg, 71.4% yield). HRMS: $C_{74}H_{91}N_9O_{12}S_2Na$ calc. $[M+Na]^+$ = 1384.6126 Da; obsd. $[M+Na]^+$ = 1384.5886 Da. Deprotection was carried out by dissolving the purified peptide in 2 mL of approximately 45:45:5:5 TFA:DCM:triisopropylsilane (TIPS):H_2O with stirring for 30 minutes. The reaction was concentrated under vacuum, then precipitated into cold 1:1 hexane:diethyl ether to yield a white

solid (11.4 mg, quant. yield). HRMS: $C_{50}H_{69}N_9O_{10}S_2Na$ calc. $[M+Na]^+$ = 1042.4507 Da; obsd. $[M+Na]^+$ = 1042.4312 Da.

Synthesis of Naltrexone-n-butyl-phenylcarbamate

To a 3 mL glass vial equipped with a stir bar was dissolved the Naltrexone-phenol-NPC (20.0 mg, 39.5 μmol, 1 eq) in 2 mL DCM. Triethylamine (6.5 μl, 47.4 μmol, 1.2 eq) was then added to the vial followed by n-butylamine (4.7 μl, 47.4 μmol, 1.2 eq) and the reaction was stirred at 20 °C for 18 hours. The crude reaction mixture was then concentrated under vacuum, redissolved in minimal MeCN, filtered, and purified by preparative HPLC using a method of 10-95% MeCN + 0.1% TFA. Fractions containing the desired product were isolated and lyophilized to yield a white solid (9.3 mg, 53.2% yield). For ^{1}H NMR see Figure 3.14 (500 MHz, $CDCl_3$): δ 6.93 (d, *J* = 8.2 Hz, 1H), 6.65 (d, *J* = 8.2 Hz, 1H), 5.15 (s, 1H), 4.71 (s, 1H), 3.26 (m, 2H), 3.22 (m, 1H), 3.08 (d, *J* = 18.7 Hz, 1H), 3.02 (dd, *J* = 14.5, 5.1 Hz, 1H), 2.70 (dd, *J* = 12.1, 4.6 Hz, 1H), 2.60 (dd, *J* = 18.6, 6.0 Hz, 1H), 2.43 (m, 1H), 2.41 (m, 2H), 2.31 (dt, *J* = 14.4, 3.0 Hz, 1H), 2.14 (m, 1H), 1.89 (dq, *J* = 13.3, 2.6 Hz, 1H), 1.63 (m, 2H), 1.54 (p, *J* = 7.4 Hz, 2H), 1.38 (s, *J* = 7.4 Hz, 2H), 0.93 (t, *J* = 7.3 Hz, 3H), 0.87 (m, 1H), 0.56 (m, 2H), 0.15 (m, 2H). HRMS: $C_{25}H_{33}N_2O_5$ calc. $[M+Na]^+$ = 441.2389 Da; obsd. $[M+Na]^+$ = 441.2231 Da.

Synthesis of O-Me Naltrexone

The synthesis of O-Me Naltrexone was performed based on the reported procedure.[37] To a 20 mL glass vial was dissolved naltrexone (0.500 g, 1.46 mmol, 1 eq) in 10 mL DCM. Anhydrous potassium carbonate (1.012 g, 7.32 mmol, 5 eq) was then added to the vial followed by methyl iodide (1.823 mL, 29.29 mmol, 20 eq) and the reaction was stirred at 20 °C for 18 hours. The reaction was then diluted with DCM and washed four times with a mixture of water and saturated bicarbonate solution. The organic layer was then dried over anhydrous magnesium

sulfate, filtered, and concentrated under vacuum to yield a tan solid (0.527 g, quant. yield). For ^{1}H NMR see Figure 3.16 (400 MHz, $CDCl_3$): δ 6.69 (d, *J* = 8.2 Hz, 1H), 6.60 (d, *J* = 8.2 Hz, 1H), 5.20 (s, 1H), 4.66 (s, 1H), 3.89 (s, 3H), 3.17 (d, *J* = 5.9 Hz, 1H), 3.05 (d, *J* = 17.5 Hz, 1H), 3.02 (td, *J* = 14.4, 5.1 Hz, 1H), 2.69 (dd, *J* = 12.0, 4.8 Hz, 1H), 2.57 (dd, *J* = 18.5, 6.0 Hz, 1H), 2.42 (m, 1H), 2.40 (d, *J* = 6.6 Hz, 2H), 2.29 (dt, *J* = 14.3, 3.1 Hz, 1H), 2.13 (td, *J* = 12.2, 3.8 Hz, 1H), 1.87 (dq, *J* = 5.4, 4.9 Hz, 1H), 1.65 (m, 1H), 1.57 (m, 1H), 0.86 (m, 1H), 0.55 (m, 2H), 0.14 (m, 2H). For ^{13}C NMR see Figure 3.16 (100 MHz, $CDCl_3$): 208.56, 145.04, 142.97, 129.57, 124.95, 119.39, 114.93, 90.44, 70.18, 62.11, 59.24, 56.86, 50.85, 43.63, 36.21, 31.54, 30.73, 22.64, 9.43, 3.99, 3.84. For COSY see Figure 3.18. For HSQC see Figure 3.18. HRMS: $C_{21}H_{26}NO_4$ calc. $[M+H]^+$ = 356.1862 Da; obsd. $[M+H]^+$ = 356.1705 Da.

Synthesis of O-Me Naltrexone-dimethyl ketal

To an oven dried 2-neck 50 mL round bottom flask equipped with a condenser was added O-Me Naltrexone (0.527 g, 1.49 mmol, 1 eq) in 2 mL toluene. After addition, the solvent was removed under vacuum for 2 hours to azeotropically dry the starting material. 15 mL of anhydrous methanol was added to dissolve the resultant material. Once dissolved, trimethyl orthoformate (1.645 mL, 14.86 mmol, 10 eq) was added followed by concentrated sulfuric acid (0.079 mL, 1.49 mmol, 1 eq) and the solution was heated to 75 °C (reflux) and stirred for 18 hours. The reaction was then cooled to ambient temperature and poured into a solution of dilute aqueous NaOH (0.1 M) and extracted three times with DCM. The combined organics were washed once with water and then dried over anhydrous magnesium sulfate, filtered, then dried under vacuum. The material was further purified by preparative HPLC using a method of 30-95% MeCN + 0.1% TFA. Fractions containing the desired product were isolated and lyophilized to yield a tan oil (0.289 g, 48.5% yield). For ^{1}H NMR see Figure 3.19 (400 MHz, $CDCl_3$): δ 6.69

(d, J = 8.2 Hz, 1H), 6.53 (d, J = 8.2 Hz, 1H), 5.16 (s, 1H), 4.56 (s, 1H), 3.89 (s, 3H), 3.37 (s, 3H), 3.08(d, J = 5.9 Hz, 1H), 3.07 (s, 3H), 2.99 (d, J = 18.3 Hz, 1H), 2.61 (m, 1H), 2.57 (dd, J = 18.8, 5.8 Hz, 1H), 2.35 (d, J = 6.6 Hz, 2H), 2.29 (td, J = 12.4, 5.1 Hz, 1H), 2.13 (td, J = 12.1, 3.7 Hz, 1H), 1.93 (td, J = 12.3, 4.2 Hz, 1H), 1.61 (m, 1H), 1.52 (m, 1H), 1.48 (m, 2H), 1.38 (td, J = 11.8, 4.3 Hz, 1H), 0.83 (m, 1H), 0.51 (m, 2H), 0.11 (m, 2H). For ^{13}C NMR see Figure 3.20 (100 MHz, $CDCl_3$): δ 146.58, 141.76, 131.57, 125.40, 117.89, 115.86, 99.92, 91.71, 69.75, 62.53, 59.21, 57.52, 49.21, 47.97, 47.93, 43.97, 32.03, 27.95, 24.79, 22.53, 9.47, 3.96, 3.76. HRMS: $C_{23}H_{32}NO_5$ calc. $[M+H]^+$ = 402.2280 Da; obsd. $[M+H]^+$ = 402.2117 Da.

Synthesis of O-Me Naltrexone-enol-PFPTC

To an oven dried 2-neck 25 mL round bottom flask was added O-Me Naltrexone (128 mg, 0.36 mmol, 1 eq) and approximately 2 mL of toluene. The flask was then placed under vacuum to azeotropically dry the material for 1 hour. Then the flask was cooled to -78 °C in a dry ice and acetone bath. Once cooled, 10 mL of anhydrous DME was added to dissolve the O-Me Naltrexone, then KHMDS (144 mg, 0.72 mmol, 2 eq) was added to the flask to form the enolate and the reaction was stirred under argon for 20 minutes at -78 °C. Meanwhile, in a second identical flask was dissolved pentafluorophenylchlorothionoformate (174 µl, 1.08 mmol, 3 eq) in 5 mL DME under argon and the flask was cooled to -78 °C. The solution of enolate was then cannulated into the solution of the electrophile and stirring was maintained at -78 °C. 5 mL dry DME was used to wash the enolate flask and the entirety of this wash was also cannulated into the second flask containing the electrophile. The combined solution was allowed to continue stirring under argon at -78 °C for 30 minutes and then the reaction was removed from the cold bath and allowed to warm to ambient temperature. The crude reaction mixture was dried under vacuum and then purified via preparative HPLC using a method of 60-95% MeCN + 0.1% TFA.

Fractions containing the desired product were isolated and lyophilized to yield a reddish oil (148 mg, 70.7% yield). For ^{1}H NMR see Figure 3.21 (600 MHz, CD_3CN): δ 7.46 (s, 1H), 6.89 (d, *J* = 8.3 Hz, 1H), 6.79 (d, *J* = 8.3 Hz, 1H), 5.85 (q, *J* = 2.8 Hz, 1H), 5.25 (d, *J* = 1.4 Hz, 1H), 4.07 (d, *J* = 6.7 Hz, 1H), 3.79 (s, 3H), 3.33 (d, *J* = 20.0 Hz, 1H), 3.28 (p, *J* = 7.1 Hz, 1H), 3.21 (dd, *J* = 20.3, 7.0 Hz, 1H), 3.18 (m, 1H), 2.91 (m, 1H), 2.77 (m, 1H), 2.60 (td, *J* = 13.6, 5.0 Hz, 1H), 2.44 (dd, *J* = 18.5, 6.2 Hz, 1H), 2.26 (dt, *J* = 18.5, 2.2 Hz, 1H), 1.81 (dd, *J* = 13.8, 3.1 Hz, 1H), 1.07 (m, 1H), 0.79 (m, 1H), 0.71 (m, 1H), 0.45 (m, 2H). For ^{13}C NMR see Figure 3.22 (125 MHz, CD_3CN): δ 190.22, 159.83, 159.52, 146.67, 144.29, 144.24, 142.16, 142.09, 140.16, 140.13, 140.09, 139.36, 139.25, 137.27, 137.22, 128.56, 127.37, 122.27, 120.35, 119.66, 115.42, 83.80, 70.46, 61.76, 57.92, 56.17, 46.30, 45.83, 31.63, 27.64, 23.54, 5.61, 4.83. For ^{19}F NMR see Figure 3.23 (375 MHz, CD_3CN): δ -154.41 (d, *J* = 17.0 Hz, 2H), -158.21 (t, *J* = 21.0, 1H), -163.92 (dd, *J* = 20.8, 17.2 Hz, 2H). For COSY see Figure 3.24. For HSQC see Figure 3.25. HRMS: $C_{28}H_{25}F_5NO_5S$ calc. $[M+H]^+$ = 582.1374 Da; obsd. $[M+H]^+$ = 582.1249 Da.

Synthesis of CAAK(F)-Naltrexone-enol-thionocarbamate

To a 20 mL glass vial equipped with a stir bar was dissolved the protected peptide CAAK(F) (4.5 mg, 4.6 μmol, 1 eq) in 5 mL MeCN. DIPEA (2.0 μl, 11.5 μmol, 2.5 eq) was then added to the vial followed by Naltrexone-enol-PFPTC (5.3 mg, 9.2 μmol, 2 eq) and the reaction was stirred at 20 °C for 2 hours. The crude reaction mixture was then concentrated under vacuum, redissolved in a 50% MeCN in H_2O, filtered, and purified by semi-preparative HPLC using a method of 50-100% MeCN + 0.1% TFA. Fractions containing the desired product were isolated and lyophilized to yield a white solid (3.5 mg, 54.9% yield). HRMS: $C_{75}H_{94}N_9O_{12}S_2$ calc. $[M+H]^+$ = 1376.6463 Da; obsd. $[M+H]^+$ = 1376.5907 Da. Deprotection was carried out by dissolving the purified peptide in 2 mL of approximately 45:45:5:5 TFA:DCM:triisopropylsilane

(TIPS): H_2O with stirring for 30 minutes. The reaction was concentrated under vacuum, then precipitated into cold 1:1 hexane:diethyl ether to yield a white solid (2.6 mg, quant. yield). HRMS: $C_{51}H_{72}N_9O_{10}S_2$ calc. $[M+H]^+$ = 1034.4844 Da; obsd. $[M+H]^+$ = 1034.4935 Da.

Synthesis of oxycodone (free base)

In a 50 mL conical tube Oxycodone-HCl salt (196 mg, 0.56 mmol) was dissolved in 4 mL H_2O, then 4 mL of a 2 M K_2CO_3 solution was then added dropwise and a white precipitate immediately formed (oxycodone free base). The solid could not be isolated by centrifugation, so the solution was extracted with chloroform (3 x 30 mL) and the combined organics were dried over anhydrous magnesium sulfate, filtered, and the solvent was removed under vacuum to yield the product as a white solid (143 mg, 81.2% yield). For ^{1}H NMR see Figure 3.26 (500 MHz, $CDCl_3$): δ 6.65 (d, *J* = 8.2 Hz, 1H), 6.59 (d, *J* = 8.2 Hz, 1H), 4.90 (s, 1H), 4.61 (s, 1H), 3.84 (s, 3H), 3.11 (d, *J* = 18.6 Hz, 1H), 2.97 (td, *J* = 14.4, 5.1 Hz, 1H), 2.82 (d, *J* = 5.9 Hz, 1H), 2.51 (dd, *J* = 18.7, 6.1 Hz, 1H), 2.40 (m, 1H), 2.37 (m, 1H), 2.36 (s, 3H), 2.24 (dt, *J* = 14.3, 3.1 Hz, 1H), 2.11 (m, 1H), 1.82 (dq, *J* = 13.4, 2.7 Hz, 1H), 1.58 (td, *J* = 14.0, 3.4 Hz, 1H), 1.51 (m, 1H). For ^{13}C NMR see Figure 3.27 (125 MHz, $CDCl_3$): δ 208.56, 144.95, 142.91, 129.37, 124.96, 119.44, 114.84, 90.36, 70.33, 64.55, 56.79, 50.21, 45.22, 42.73, 36.12, 31.40, 30.50, 21.89. HRMS: $C_{18}H_{22}NO_4$ calc. $[M+H]^+$ = 316.1549 Da; obsd. $[M+H]^+$ = 316.1579 Da.

Synthesis of Oxycodone-enol-PFPTC

To an oven dried 2-neck 25 mL round bottom flask was added oxycodone (21 mg, 0.07 mmol, 1 eq) and approximately 2 mL of toluene. The flask was then placed under vacuum to azeotropically dry the material for 2 hours. Then the flask was cooled to -78 °C in a dry ice and acetone bath. Once cooled, 10 mL of anhydrous DME was added to dissolve the oxycodone, then KHMDS (40 mg, 0.20 mmol, 3 eq) was added to the flask to form the enolate and the reaction

was stirred under argon for 20 minutes at -78 °C. Meanwhile, in a second identical flask was dissolved pentafluorophenylchlorothionoformate (64 µl, 0.40 mmol, 6 eq) in 5 mL DME under argon and the flask was cooled to -78 °C. The solution of enolate was then cannulated into the solution of the electrophile and stirring was maintained at -78 °C. 5 mL dry DME was used to wash the enolate flask and the entirety of this wash was also cannulated into the second flask containing the electrophile. The combined solution was allowed to continue stirring under argon at -78 °C for 30 minutes and then the reaction was removed from the cold bath and allowed to warm to ambient temperature. The crude reaction mixture was dried under vacuum and then purified via preparative HPLC using a method of 30-95% MeCN + 0.1% TFA. Fractions containing the desired product were isolated and lyophilized to yield an orange oil (148 mg, 70.7% yield). For ^{1}H NMR see Figure 3.28 (500 MHz, CD_3CN): δ 8.39 (s, 1H), 6.89 (d, J = 8.3 Hz, 1H), 6.80 (d, J = 8.3 Hz, 1H), 5.84 (q, J = 2.8 Hz, 1H), 5.25 (d, J = 1.5 Hz, 1H), 3.82 (d, J = 30.2 Hz, 1H), 3.81 (s, 3H), 3.39 (d, J = 20.2 Hz, 1H), 3.21 (m, 1H), 3.19 (m, 1H), 2.87 (s, 3H), 2.78 (m, 1H), 2.62 (td, J = 13.5, 5.0 Hz, 1H), 2.42 (dd, J = 18.3, 6.2 Hz, 1H), 2.23 (dt, J = 18.3, 2.1 Hz, 1H), 1.79 (dd, J = 13.7, 3.1 Hz, 1H). For ^{13}C NMR see Figure 3.29 (125 MHz, CD_3CN): δ 190.23, 146.65, 144.30, 144.19, 142.18, 140.18, 139.25, 137.25, 128.57, 122.49, 120.33, 119.72, 115.31, 83.82, 70.37, 65.51, 56.16, 46.80, 45.69, 41.19, 31.77, 27.67, 23.60. For ^{19}F NMR see Figure 3.30 (375 MHz, CD_3CN): δ -154.40 (d, J = 17.0 Hz, 2H), -158.25 (t, J = 21.0 Hz, 1H), -163.94 (dd, J = 20.7, 17.4 Hz, 2H). For COSY see Figure 3.31. For HSQC see Figure 3.32. HRMS: $C_{25}H_{21}F_5NO_5S$ calc. $[M+H]^+$ = 542.1061 Da; obsd. $[M+H]^+$ = 542.1112 Da.

Screen to Identify Optimal Reaction Conditions for Synthesis of Oxycodone-enol-PFPTC

20 individual 1 mg oxycodone reactions were performed simultaneously in a combinatorial manner so that each combination of base and electrophile was reacted at the same

concentration using the same molar ratios of oxycodone, base, and electrophile (see Figure 3.7A). Reactions were carried out in previously oven-dried dram vials equipped with stir bars and Teflon caps. Vials were kept under argon using an argon splitter (see Figure 3.7B). The vials were suspended in a -78 °C cold bath (acetone/dry ice) using a modified culture tube rack. All liquid transfers were carried out using anhydrous technique. Bases used in the reaction screen included LiHMDS + TMEDA, LiHMDS, NaHMDS, and KHMDS. Electrophiles used in the reaction screen included acetyl chloride, pentafluorophenylchlorothionoformate, phenylthionochloroformate, thiophosgene, and thionocarbonyldiimidazole + $BF_3 \cdot OEt_2$.

General procedure: Reactions were set up by first adding and dissolving base (48 μmol, 3 eq; and additive if applicable) in 2 mL THF total volume in each of 4 vials, then cooling to -78 °C and stirring for several minutes before addition of 0.5 mL oxycodone as a stock solution (16 μmol per vial) to each reaction vessel. The reactions were then stirred for 30 minutes at -78 °C. Meanwhile, in separate empty vials, electrophiles (10 μmol per vial) were prepared by adding 0.5 mL of the appropriate stock solution to each vial under argon, then cooling to -78 °C. Once all vials were prepared, 0.5 mL of vials containing oxycodone and base were removed via syringe and quickly transferred to the corresponding vials of electrophile (3.2 μmol per electrophile vial). To the leftover enolate in the original vials was added acetyl chloride. After adding all components to each reaction, all reactions were allowed to stir for 30 minutes, then samples were filtered and prepared for HPLC/LCMS analysis. Crude reactions were analyzed first by HPLC using a mobile phase consisting of 10-100% MeCN + 0.1% TFA in water beginning with a 1 min isocratic at 10%, then up to 100% over 10 min in a linear gradient, followed by an isocratic hold at 100% MeCN + 0.1% TFA for 4 min (total time was 15 min). Reaction conversion was assessed by measuring the ratio of oxycodone to product peaks, and these conversions were used

to construct a heat map (Figure 3.7C). Reactions with the highest conversions and minimal side products were further analyzed by LCMS using a similar method, with optimal conditions displayed in see Figure 3.7D; the combination of pentafluorophenylchlorothionoformate and KHMDS was determined to provide the highest reaction conversion with no significant side products.

Synthesis of Griseofulvin-enol-PFPTC and Identification of Double Addition Product

To an oven dried 2-neck 25 mL round bottom flask was added griseofulvin (50.0 mg, 0.14 mmol, 1 eq) and 5 mL anhydrous DME. The flask was then cooled to -78 °C in a dry ice and acetone bath. Once cooled, KHMDS (57.0 mg, 0.28 mmol, 2 eq) was added to the flask to form the enolate and the reaction was stirred under argon for 20 minutes at -78 °C. Meanwhile, in a second identical flask was dissolved pentafluorophenylchlorothionoformate (68.0 µl, 0.43 mmol, 3 eq) in 5 mL DME under argon and the flask was cooled to -78 °C. The solution of enolate was then cannulated into the solution of the electrophile and stirring was maintained at -78 °C. 5 mL dry DME was used to wash the enolate flask and the entirety of this wash was also cannulated into the second flask containing the electrophile. The combined solution was allowed to continue stirring under argon at -78 °C for 30 minutes and then the reaction was removed from the cold bath and allowed to warm to ambient temperature. The crude reaction mixture was dried under vacuum and then purified using a 50 g SNAP KP-SIL Biotage column with a solvent system of 12-100% ethyl acetate in hexanes. Fractions containing the desired product were isolated and lyophilized to yield a yellow solid that was determined to be impure by LCMS (see Figure 3.8B). The crude material was then dissolved in 80% MeCN in H_2O, filtered, and further purified by preparative HPLC using a method of 60-95% MeCN + 0.1% TFA. Fractions containing the desired product were isolated and lyophilized to yield a yellow oil (47.7 mg,

58.2% yield). For ^{1}H NMR see Figure 3.33 (500 MHz, $CDCl_3$): δ 6.16 (s, 1H), 5.83 (s, 1H), 4.87 (d, *J* = 12.6 Hz, 1H), 4.05 (s, 3H), 3.97 (s, 3H), 3.72 (s, 3H), 3.48 (s, *J* = 6.5 Hz, 1H), 1.05 (d, *J* = 6.6 Hz, 3H). For ^{13}C NMR see Figure 3.34 (125 MHz, $CDCl_3$): δ 211.93, 193.66, 192.60, 172.33, 169.67, 165.75, 159.04, 158.70, 158.22, 141.60, 139.58, 139.12, 129.48, 129.44, 128.30, 127.55, 118.13, 117.09, 116.35, 115.86, 113.59, 111.31, 104.57, 103.68, 97.53, 90.05, 89.89, 63.18, 57.46, 57.21, 56.34, 40.85, 12.01. For ^{19}F NMR see Figure 3.35 (375 MHz, $CDCl_3$): δ -150.35 (d, *J* = 18.3 Hz, 2H), -156.27 (d, *J* = 21.6, 1H), -161.87 (dd, *J* = 21.6, 17.5 Hz, 2H). HRMS: $C_{24}H_{17}ClF_5O_7S$ calc. $[M+H]^+$ = 579.0304 Da; obsd. $[M+H]^+$ = 579.0331 Da.

Fractions containing the griseofulvin double addition side product were isolated and lyophilized to yield a yellow oil (17.1 mg, 21.6% yield). For ^{1}H NMR see Figure 3.36 (500 MHz, $CDCl_3$): δ 6.15 (s, 1H), 5.86 (s, 1H), 4.03 (s, 3H), 3.99 (s, 3H), 3.77 (s, 3H), 3.52 (s, *J* = 7.1 Hz, 1H), 1.48 (d, *J* = 7.1 Hz, 3H). For ^{13}C NMR see Figure 3.38 (125 MHz, $CDCl_3$): δ 200.10, 191.41, 185.56, 168.87, 167.70, 165.27, 158.32, 146.21, 132.04, 107.03, 105.05, 97.93, 89.84, 88.74, 57.44, 57.13, 56.36, 43.94, 14.27. For ^{19}F NMR see Figure 3.38 (375 MHz, $CDCl_3$): δ -151.22 (d, *J* = 20.6 Hz, 2H), -154.09 (d, *J* = 20.6 Hz, 2H), -155.08 (t, *J* = 22.6 Hz, 1H), -158.85 (t, *J* = 21.6 Hz, 1H), -161.28 (d, *J* = 22.1, 16.9 Hz, 2H), -161.95 (d, *J* = 21.6, 17.5 Hz, 2H). HRMS: $C_{31}H_{16}ClF_{10}O_8S_2$ calc. $[M+H]^+$ = 804.9815 Da; obsd. $[M+H]^+$ = 804.9841 Da.

3.5 Appendix B

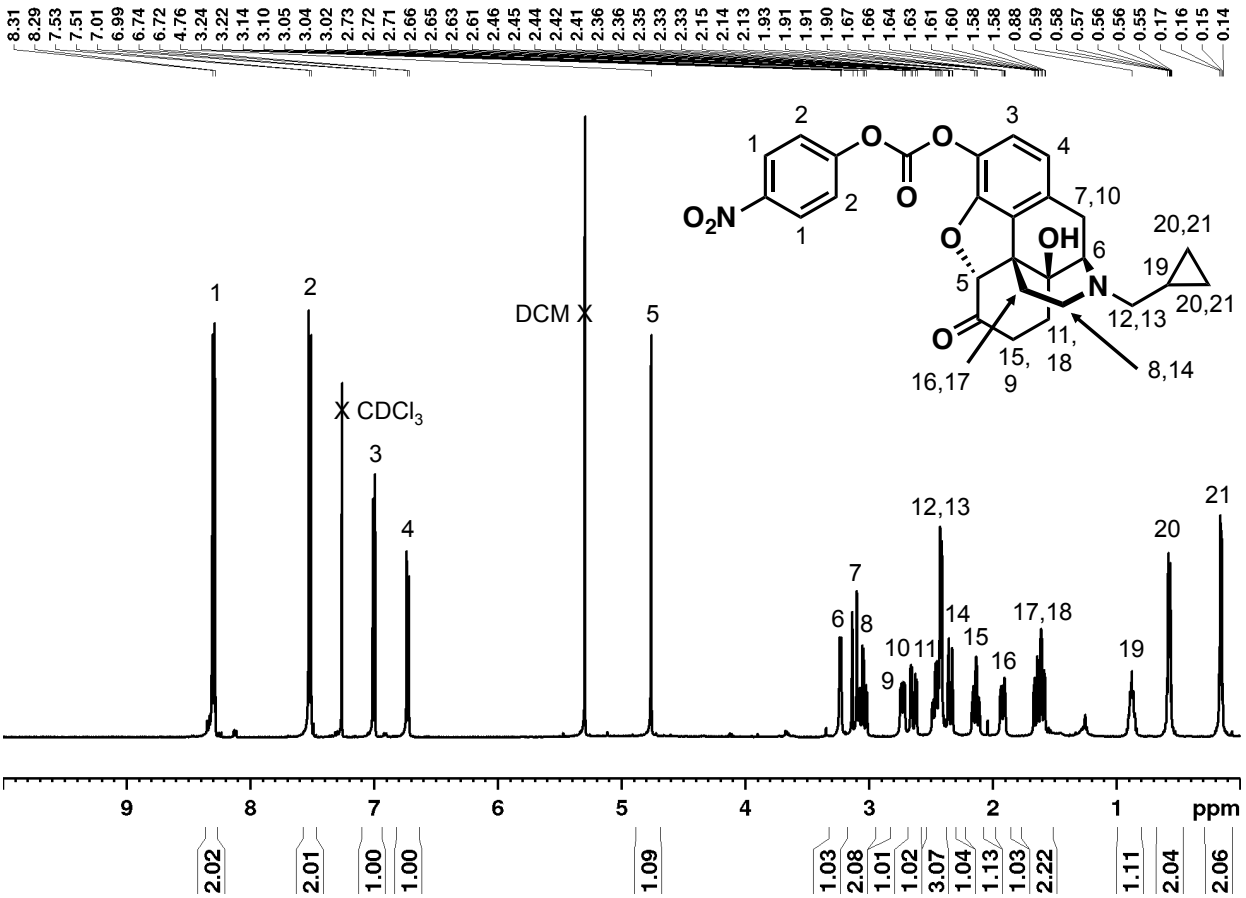

Figure 3.9. ^{1}H NMR of Naltrexone-phenol-NPC in $CDCl_3$.

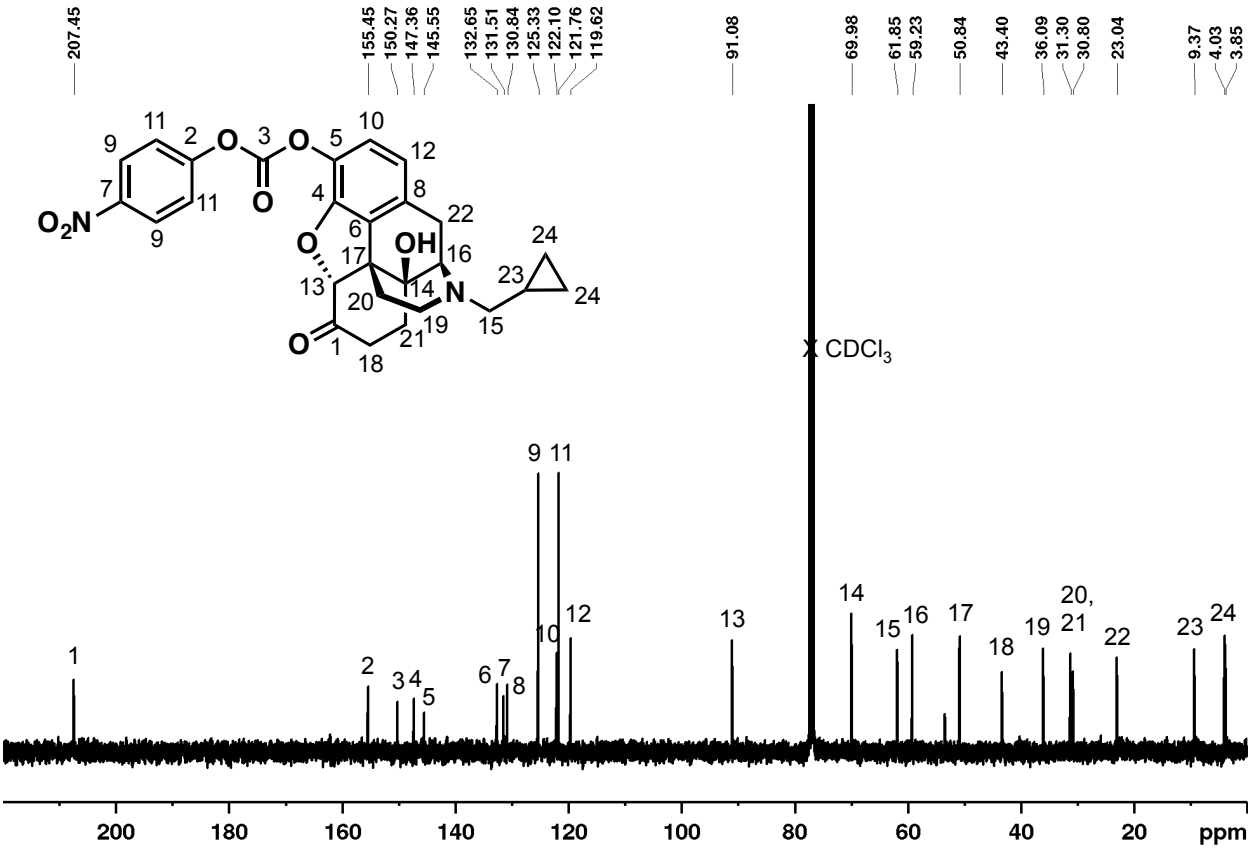

Figure 3.10. ^{13}C NMR of Naltrexone-phenol-NPC in $CDCl_3$.

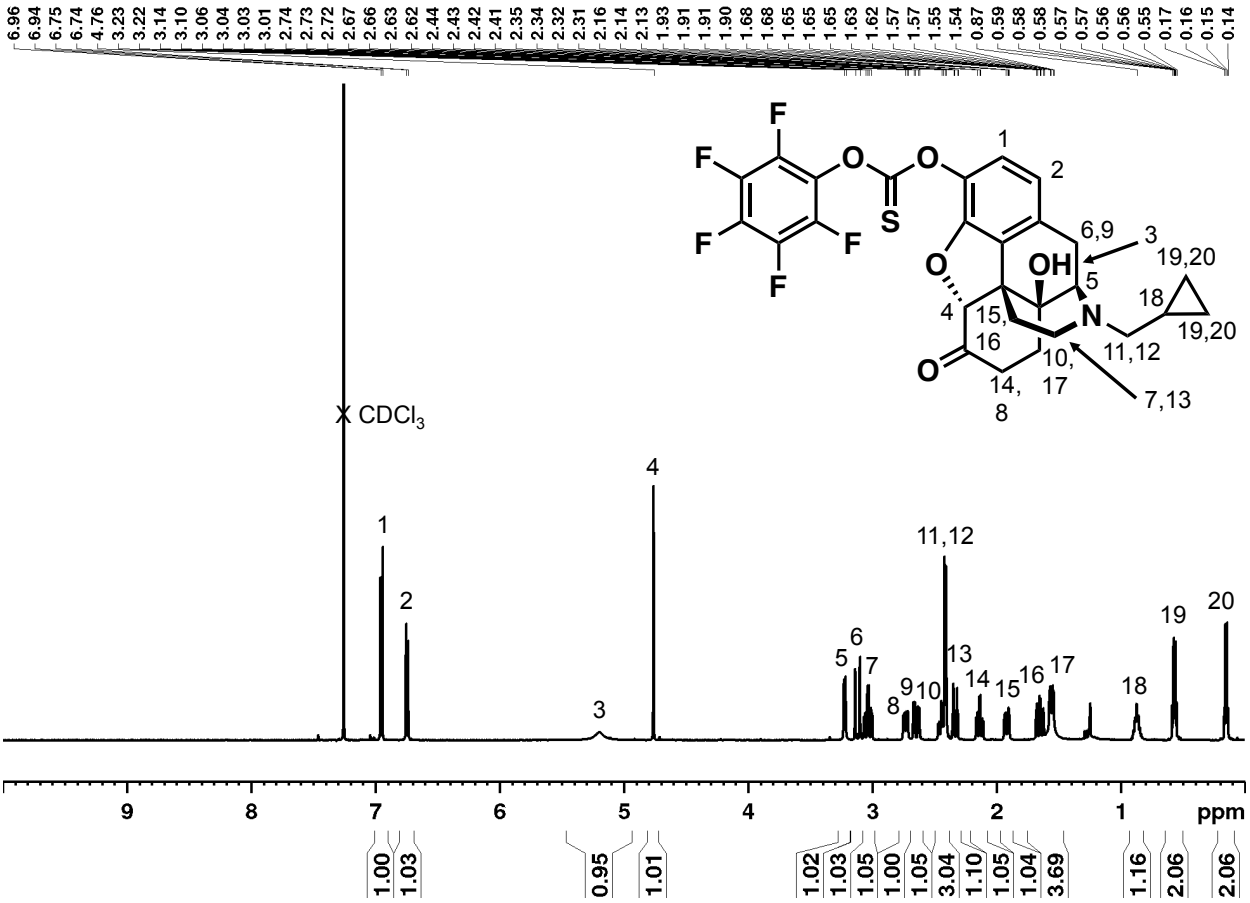

Figure 3.11. ^{1}H NMR of Naltrexone-phenol-PFPTC in $CDCl_3$.

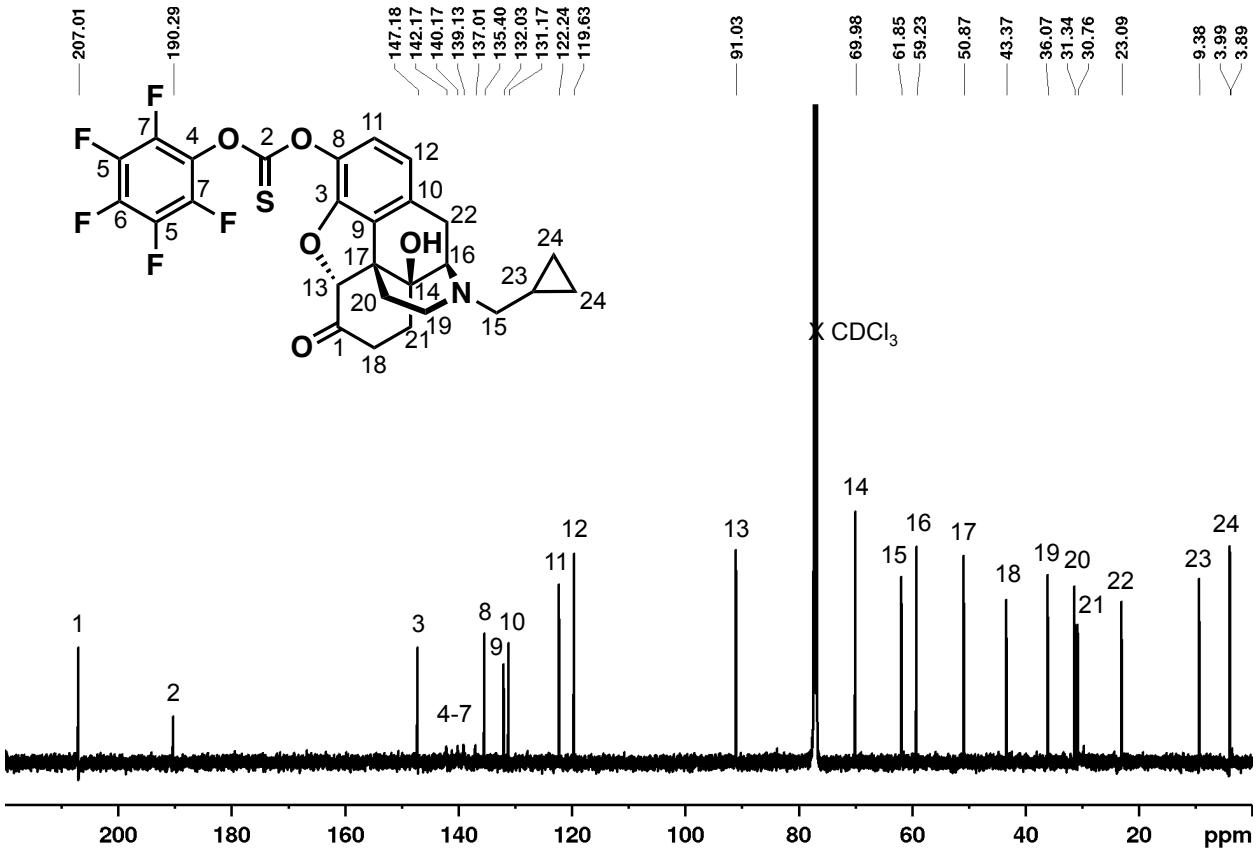

Figure 3.12. ^{13}C NMR of Naltrexone-phenol-PFPTC in $CDCl_3$.

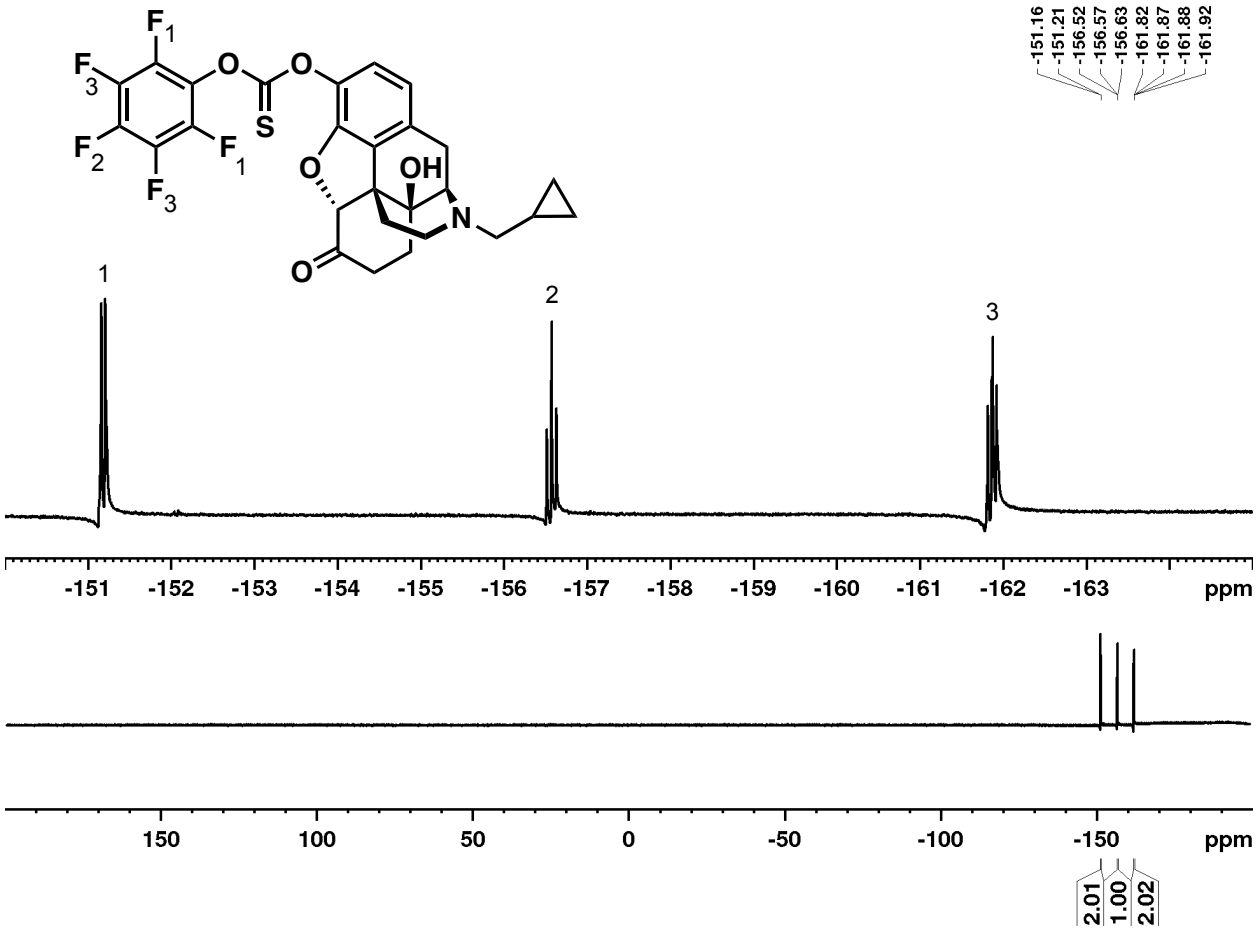

Figure 3.13. ^{19}F NMR of Naltrexone-phenol-PFPTC in $CDCl_3$.

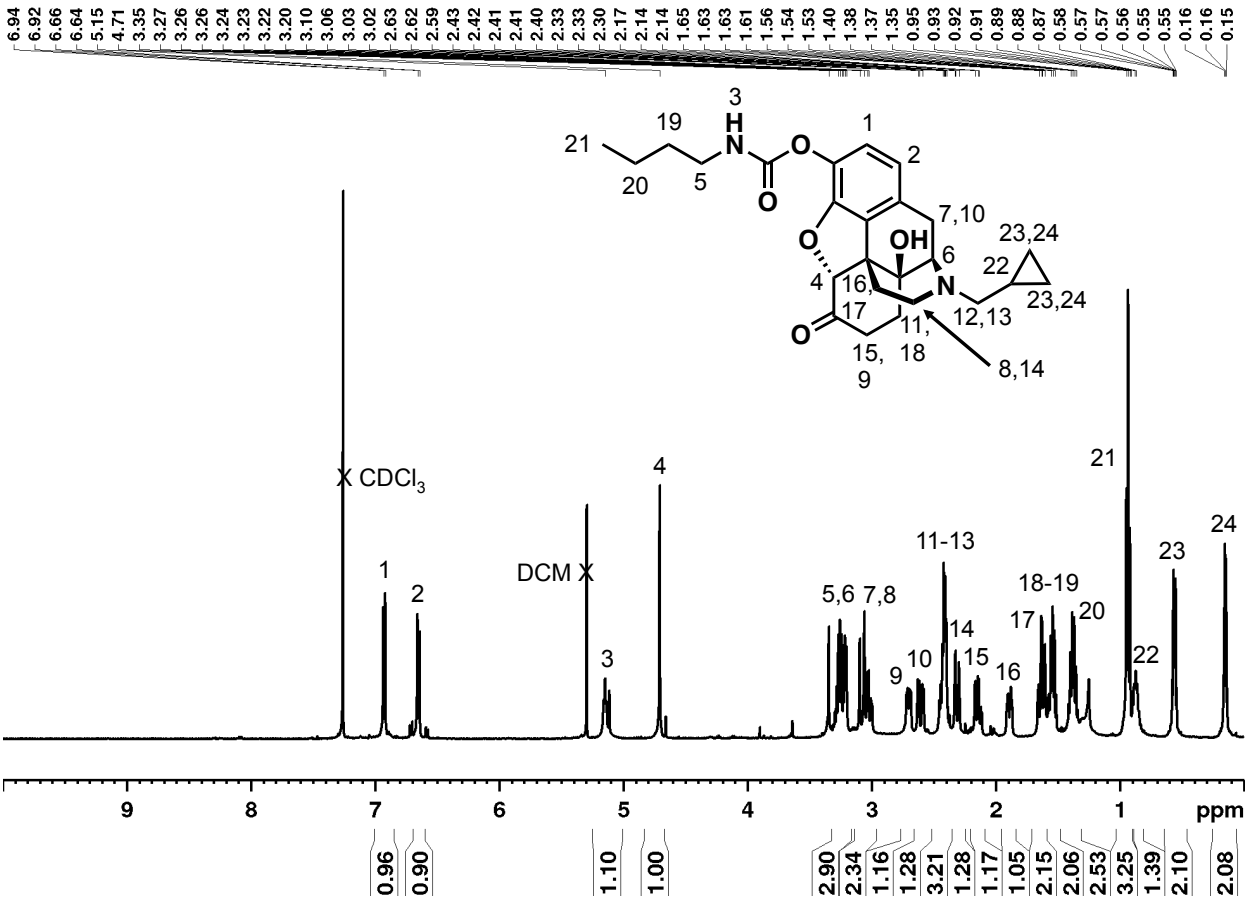

Figure 3.14. ^{1}H NMR of Naltrexone-n-butyl-phenylcarbamate in $CDCl_3$.

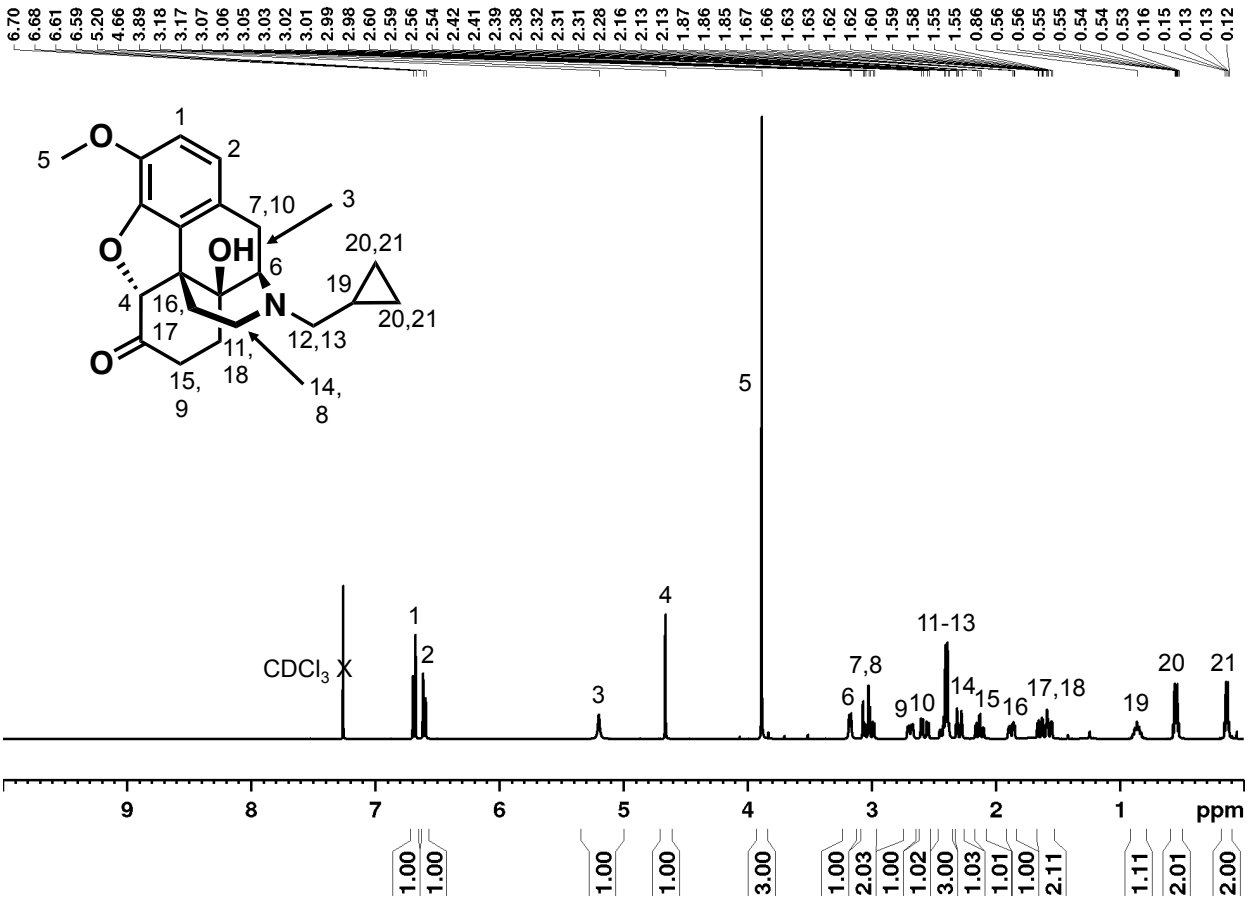

Figure 3.15. ^{1}H NMR of O-Me Naltrexone in $CDCl_3$.

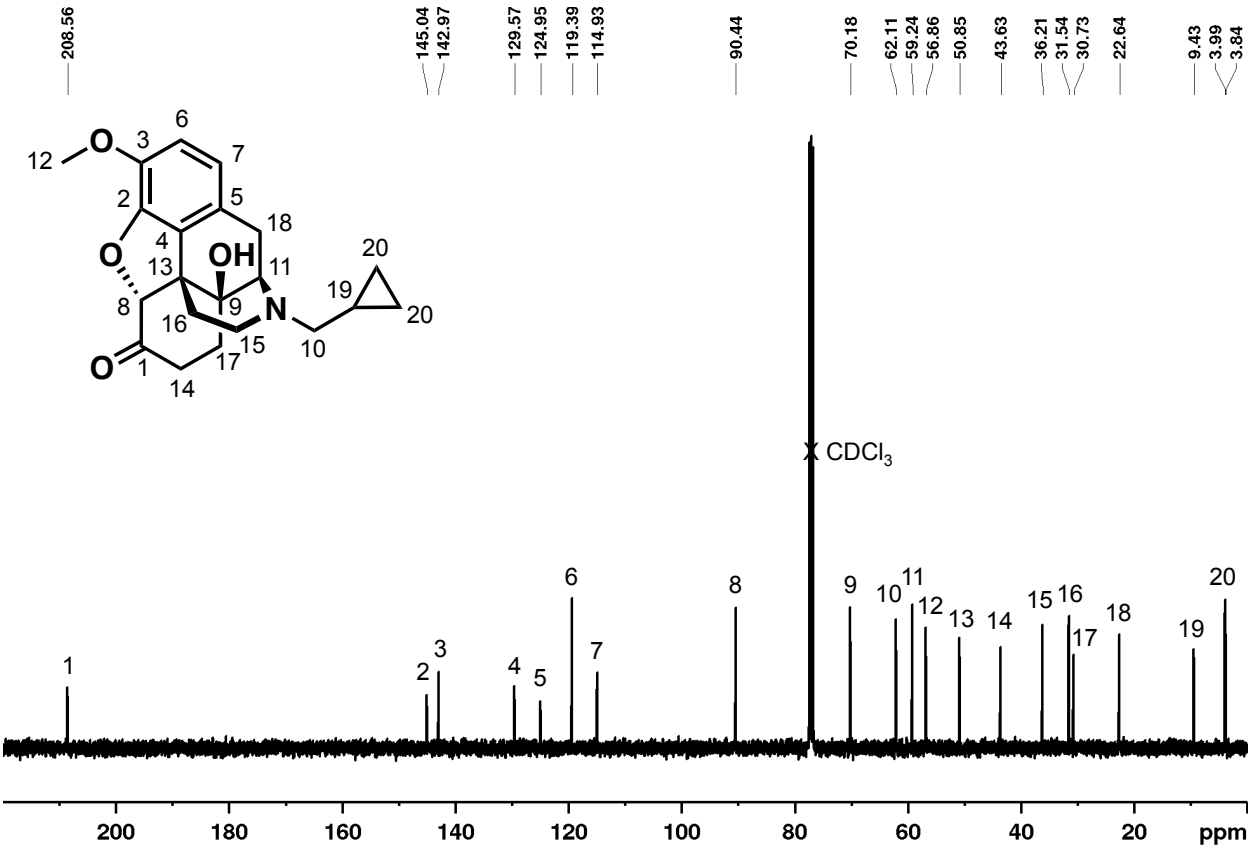

Figure 3.16. ^{13}C NMR of O-Me Naltrexone in $CDCl_3$.

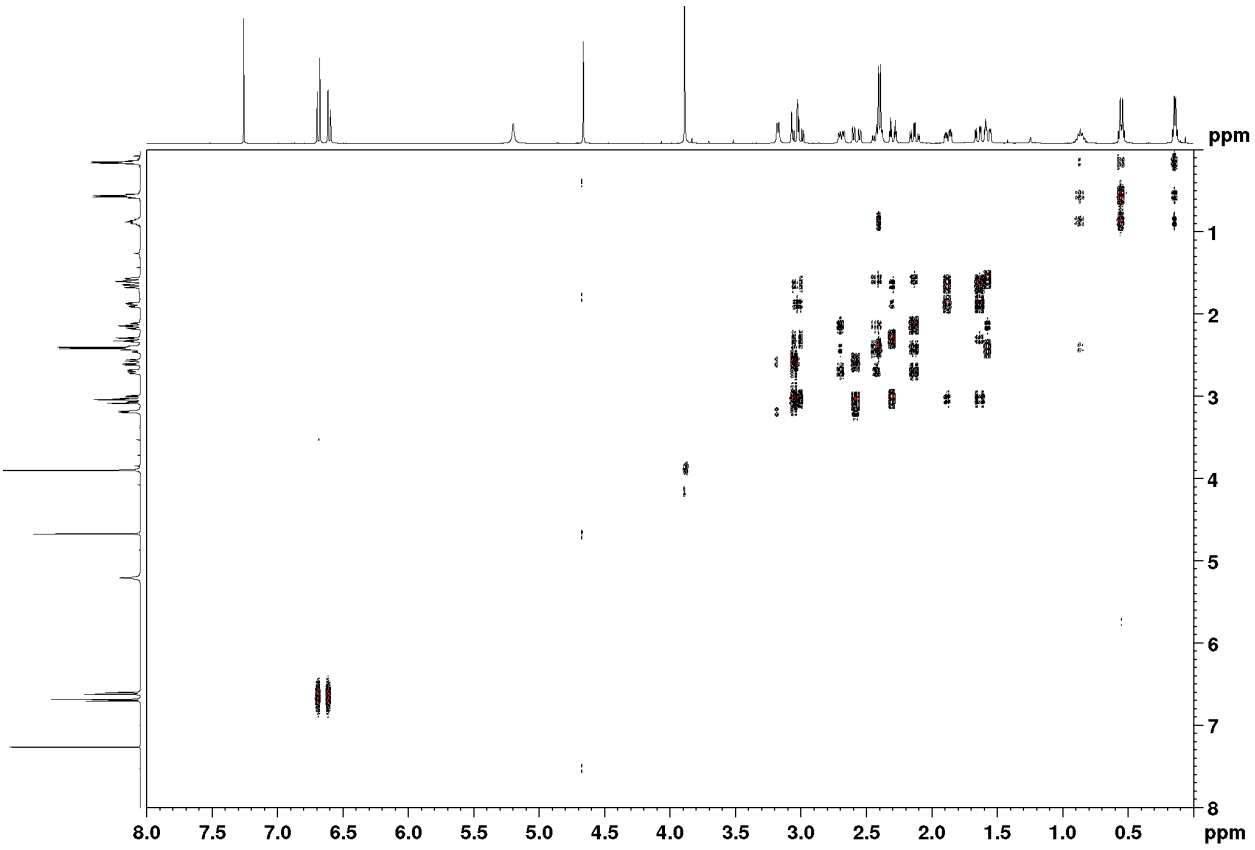

Figure 3.17. COSY of O-Me Naltrexone in $CDCl_3$

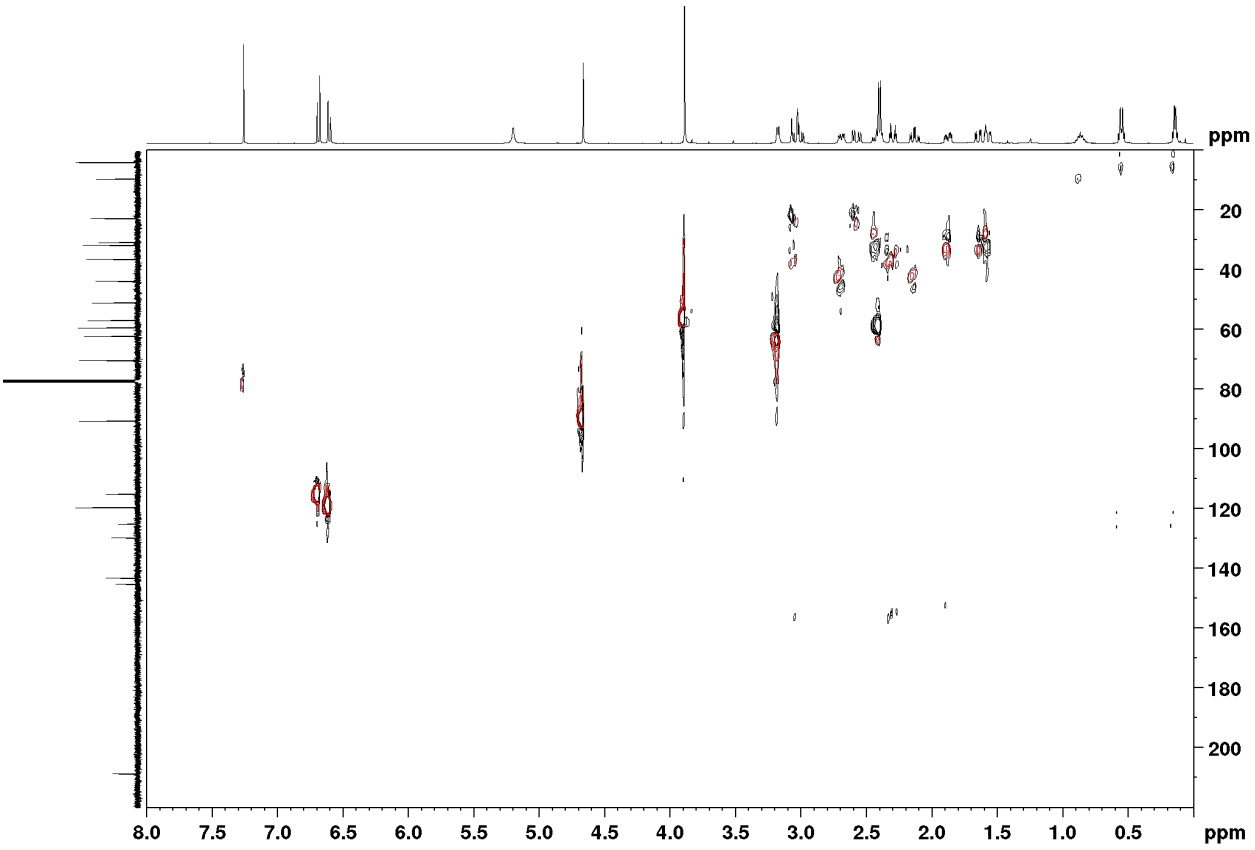

Figure 3.18. HSQC-INEPT135 of O-Me Naltrexone in $CDCl_3$

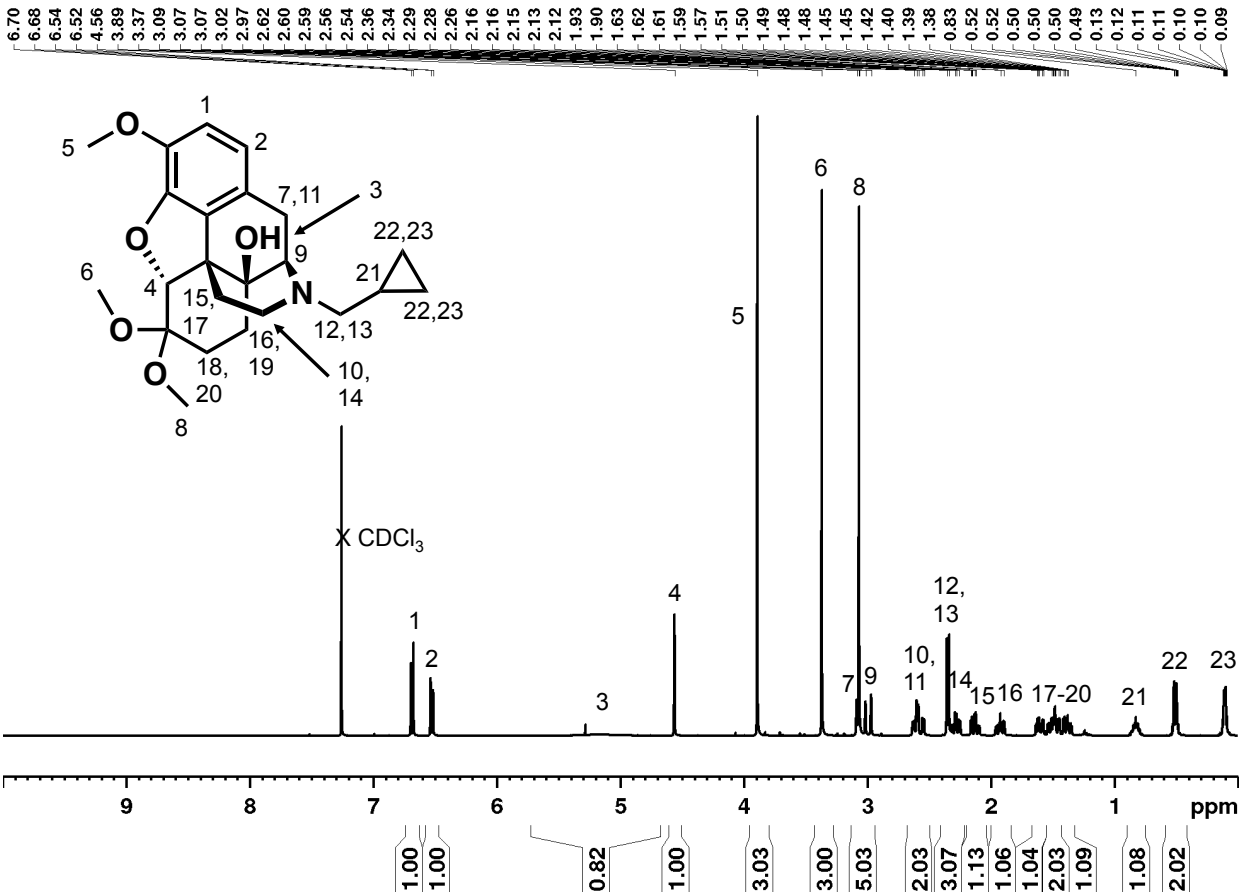

Figure 3.19. ^{1}H NMR of O-Me Naltrexone-dimethyl ketal in $CDCl_3$.

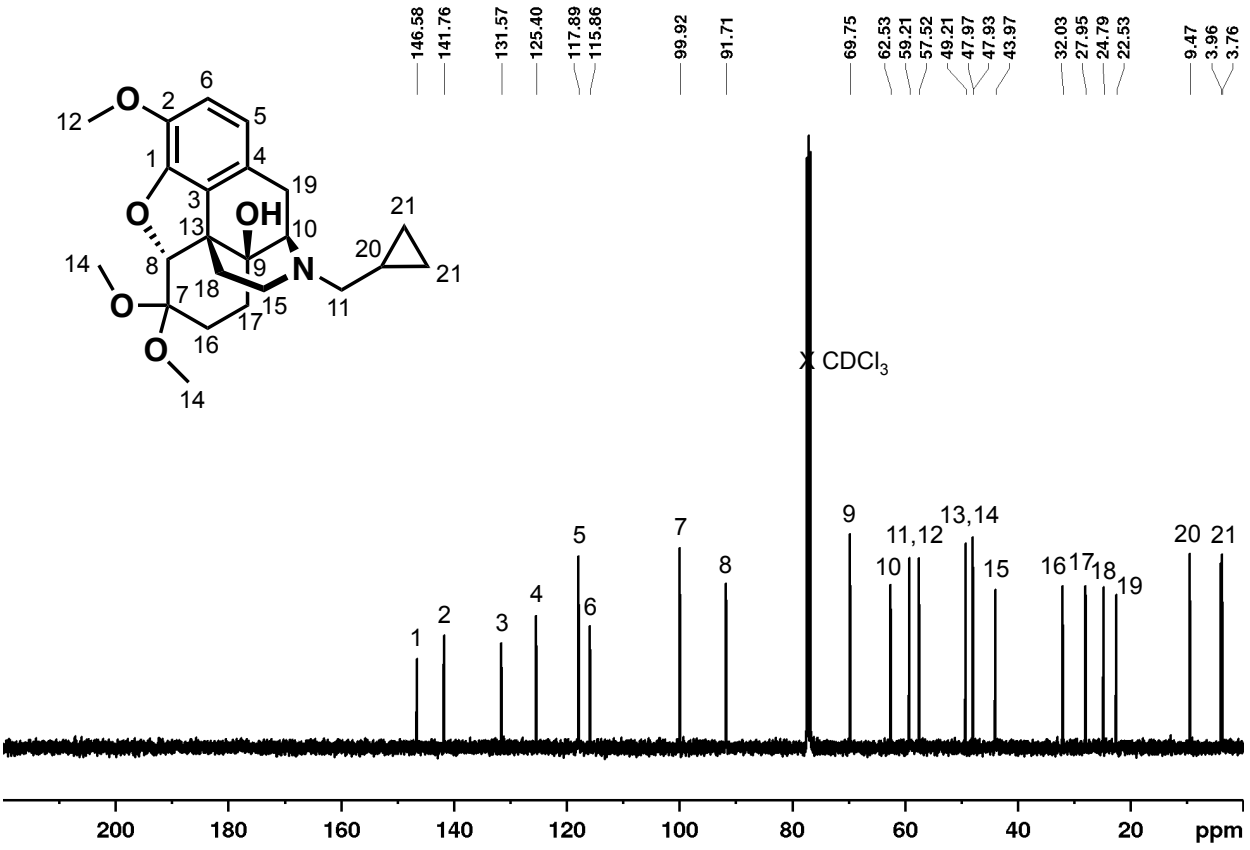

Figure 3.20. ^{13}C NMR of O-Me Naltrexone-dimethyl ketal in $CDCl_3$.

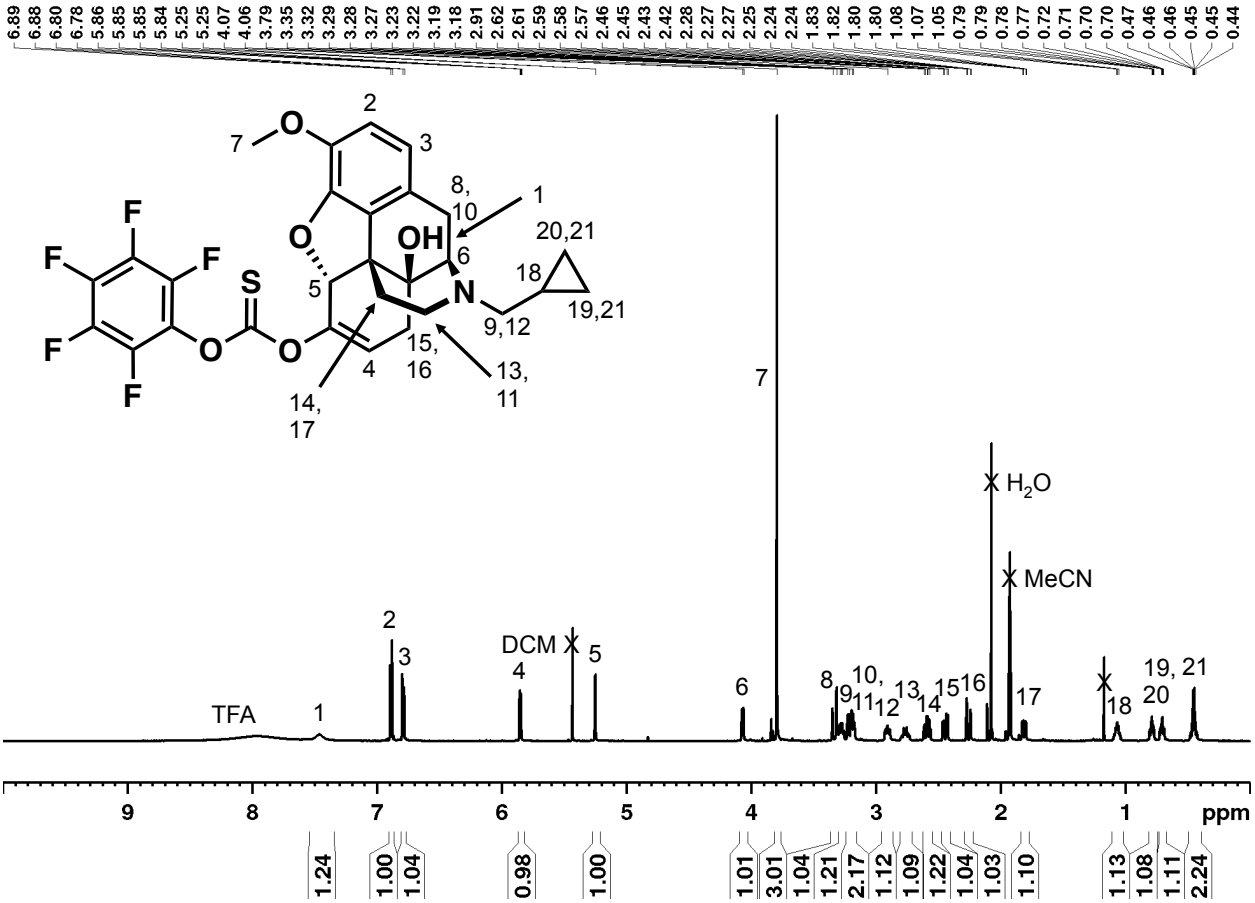

Figure 3.21. ^{1}H NMR of Naltrexone-enol-PFPTC in CD_3CN.

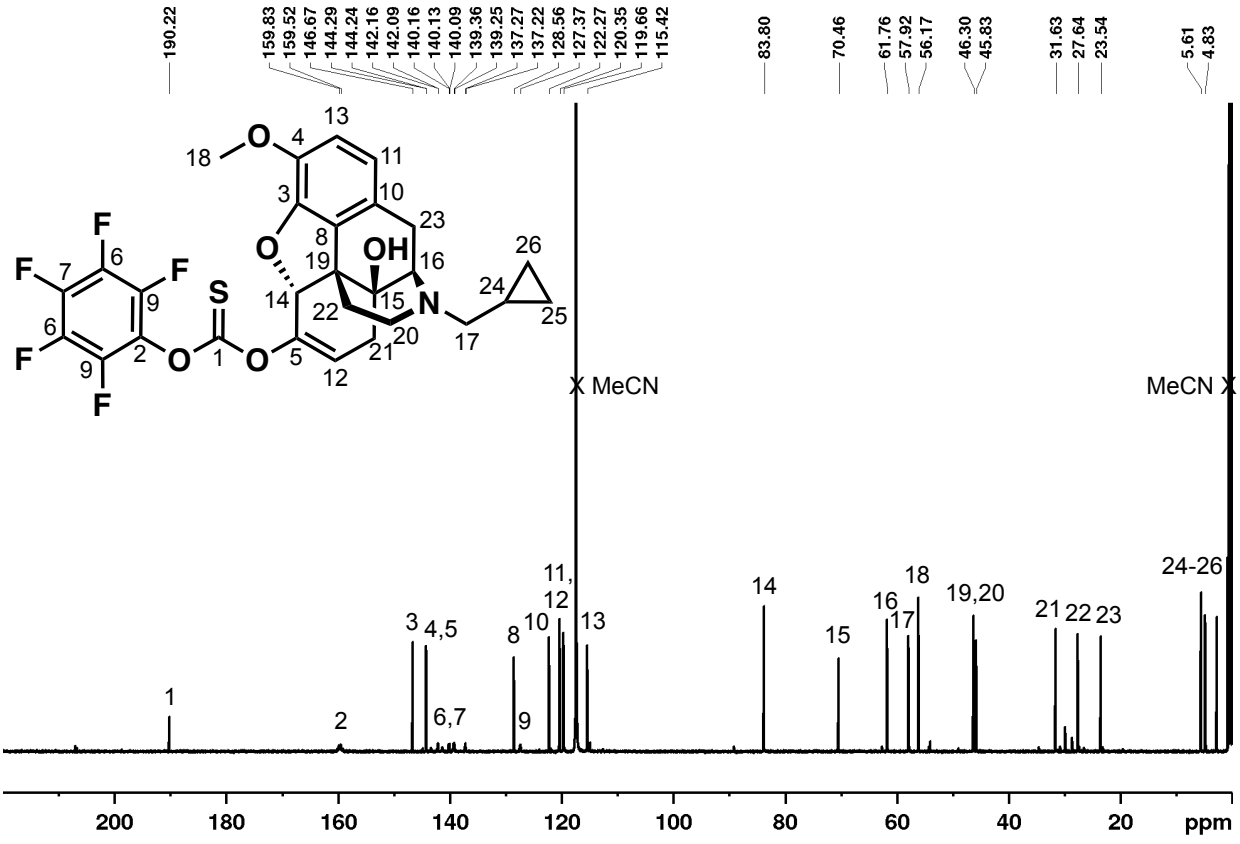

Figure 3.22. ^{13}C NMR of Naltrexone-enol-PFPTC in CD_3CN.

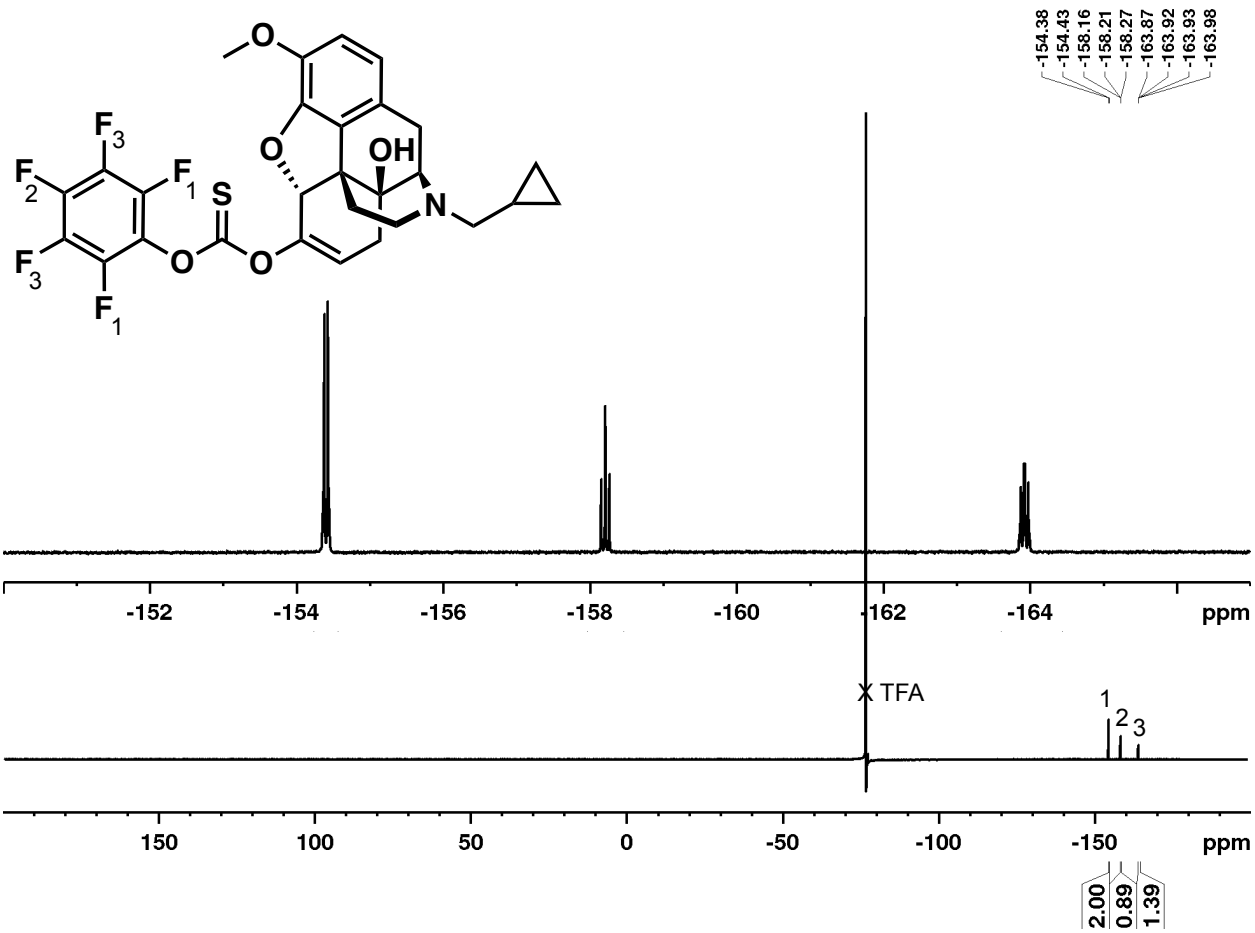

Figure 3.23. ^{19}F NMR of Naltrexone-enol-PFPTC in CD_3CN.

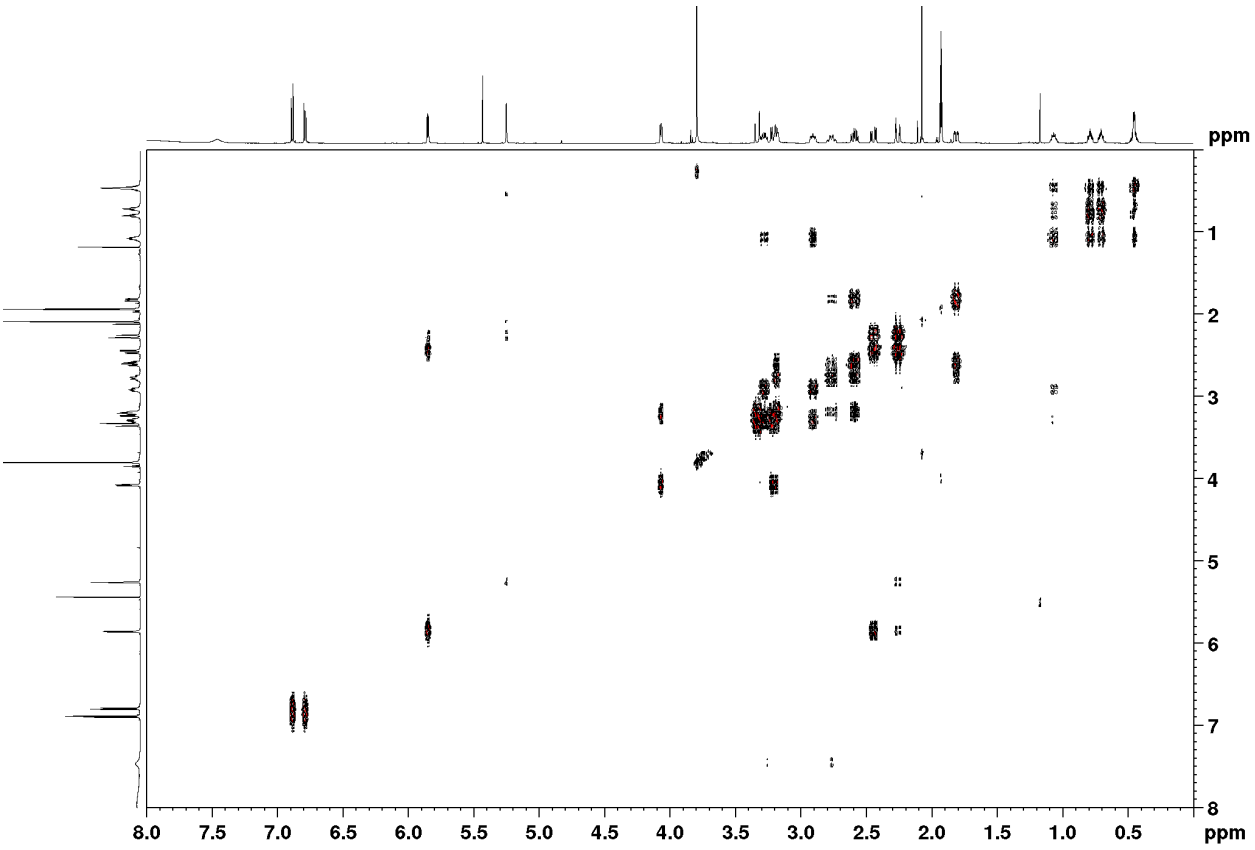

Figure 3.24. COSY of Naltrexone-enol-PFPTC in CD_3CN.

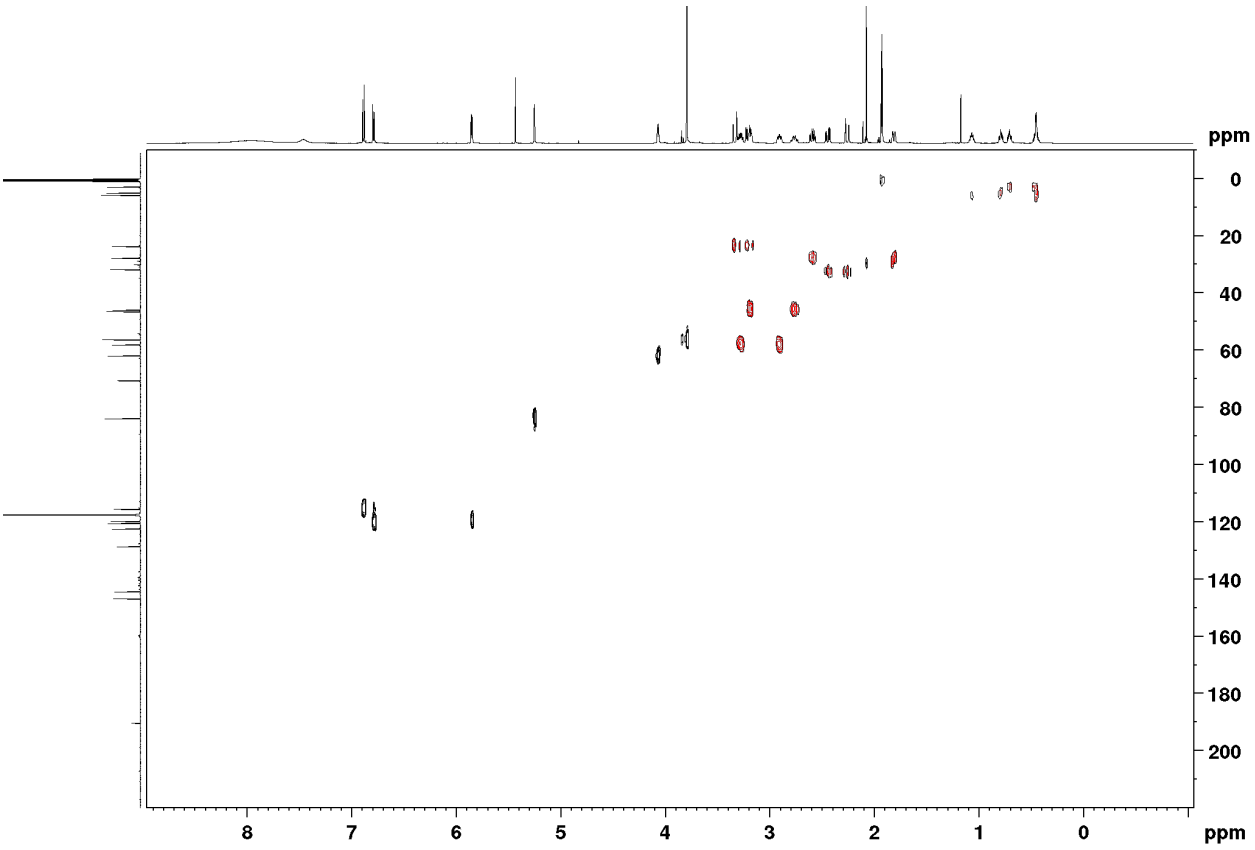

Figure 3.25. HSQC-INEPT135 of Naltrexone-enol-PFPTC in CD_3CN.

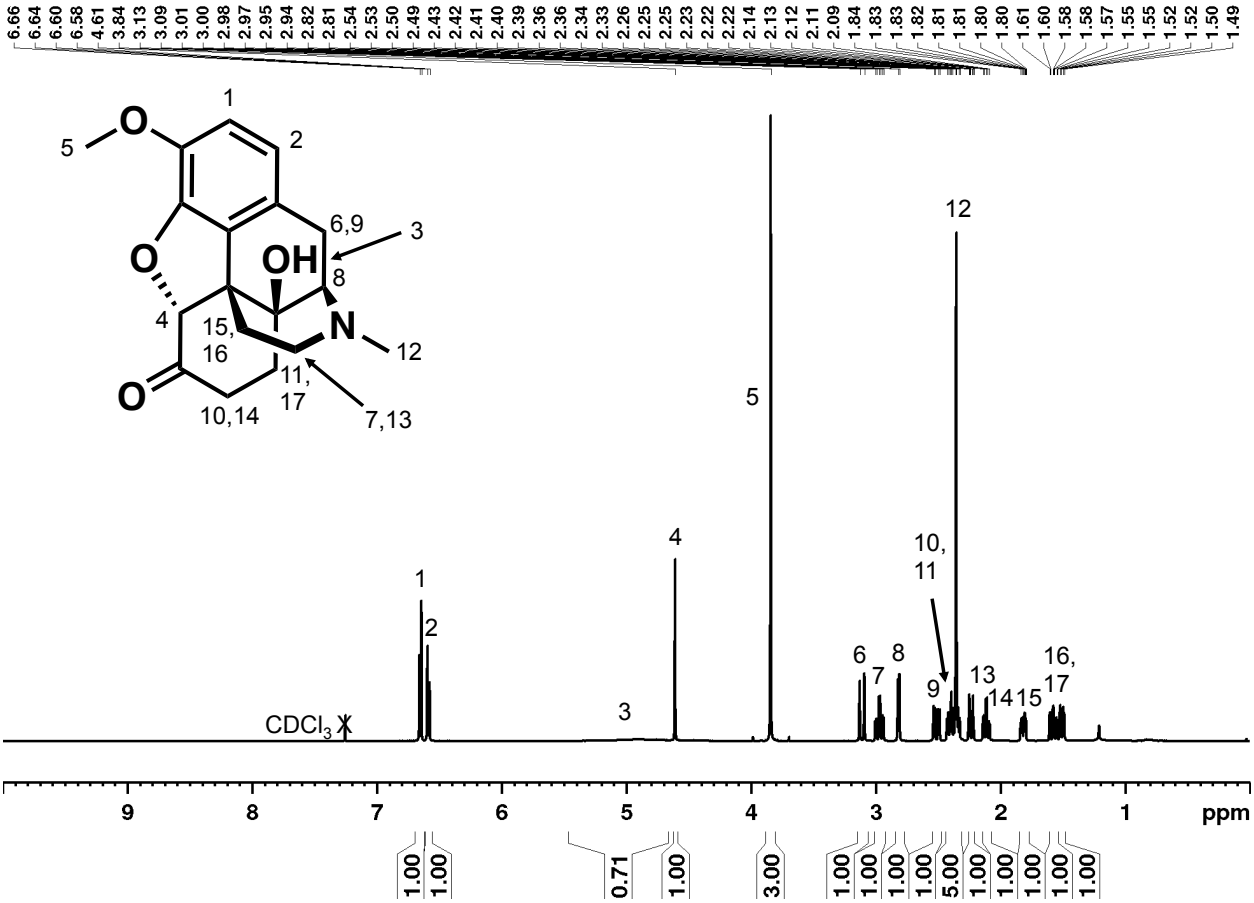

Figure 3.26. ^{1}H NMR of oxycodone (free base) in $CDCl_3$.

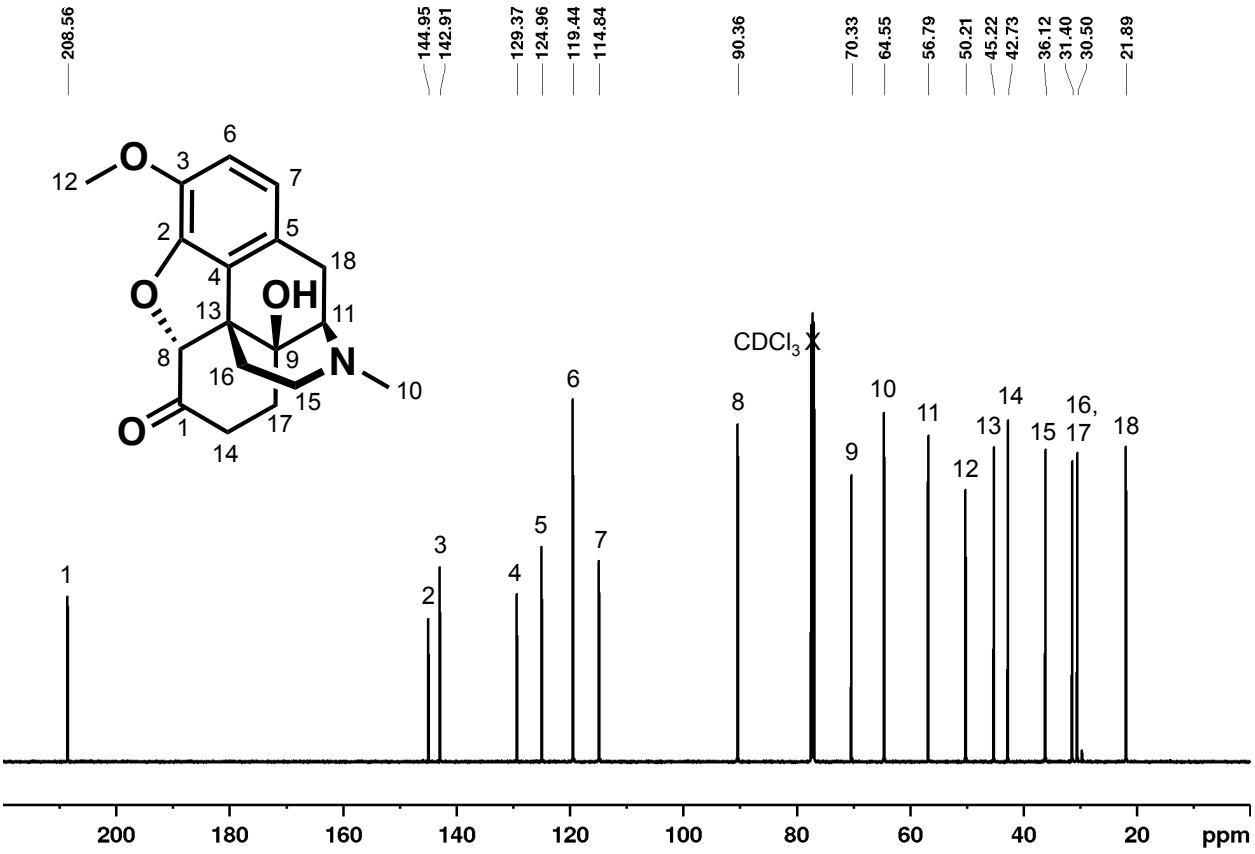

Figure 3.27. ^{13}C NMR of oxycodone (free base) in $CDCl_3$.

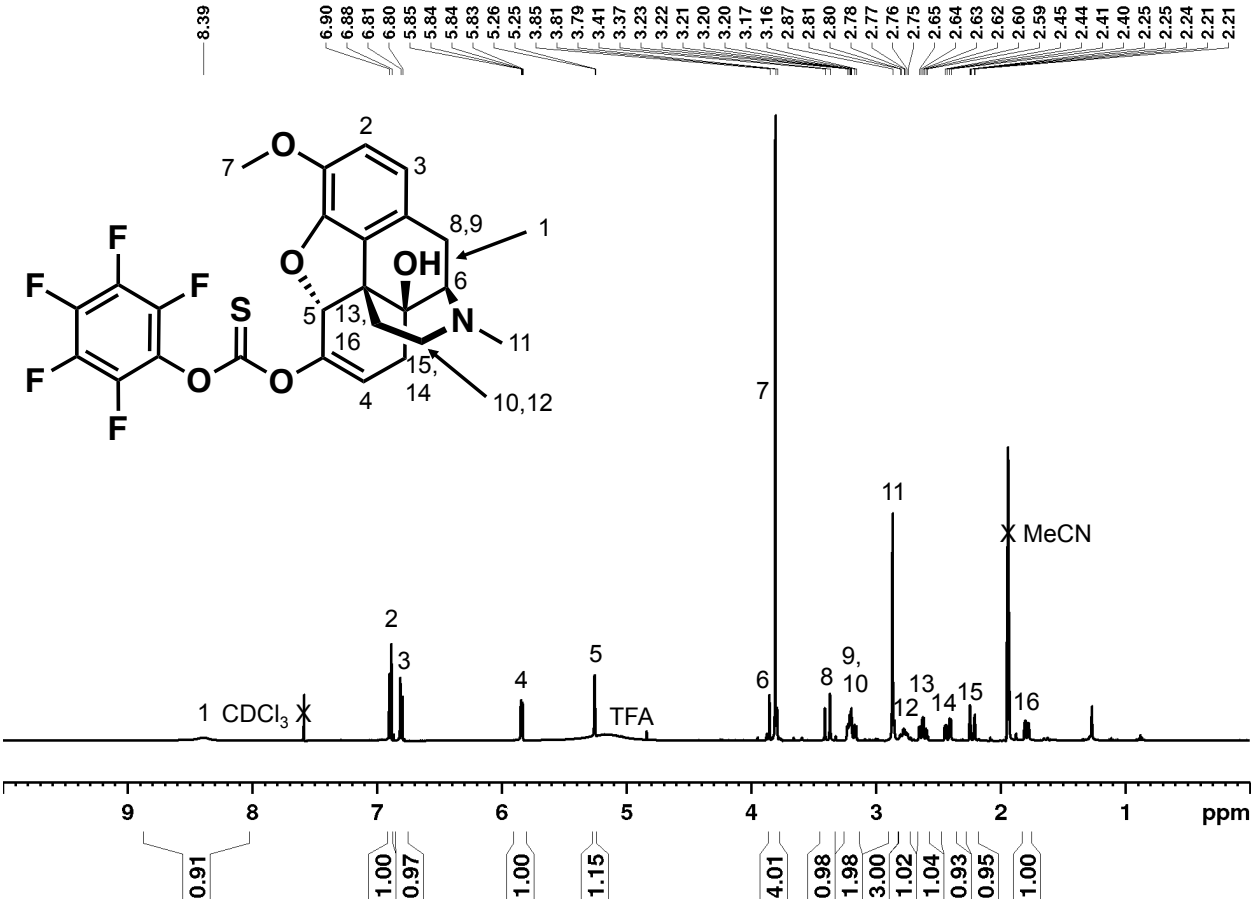

Figure 3.28. ^{1}H NMR of Oxycodone-enol-PFPTC in CD_3CN.

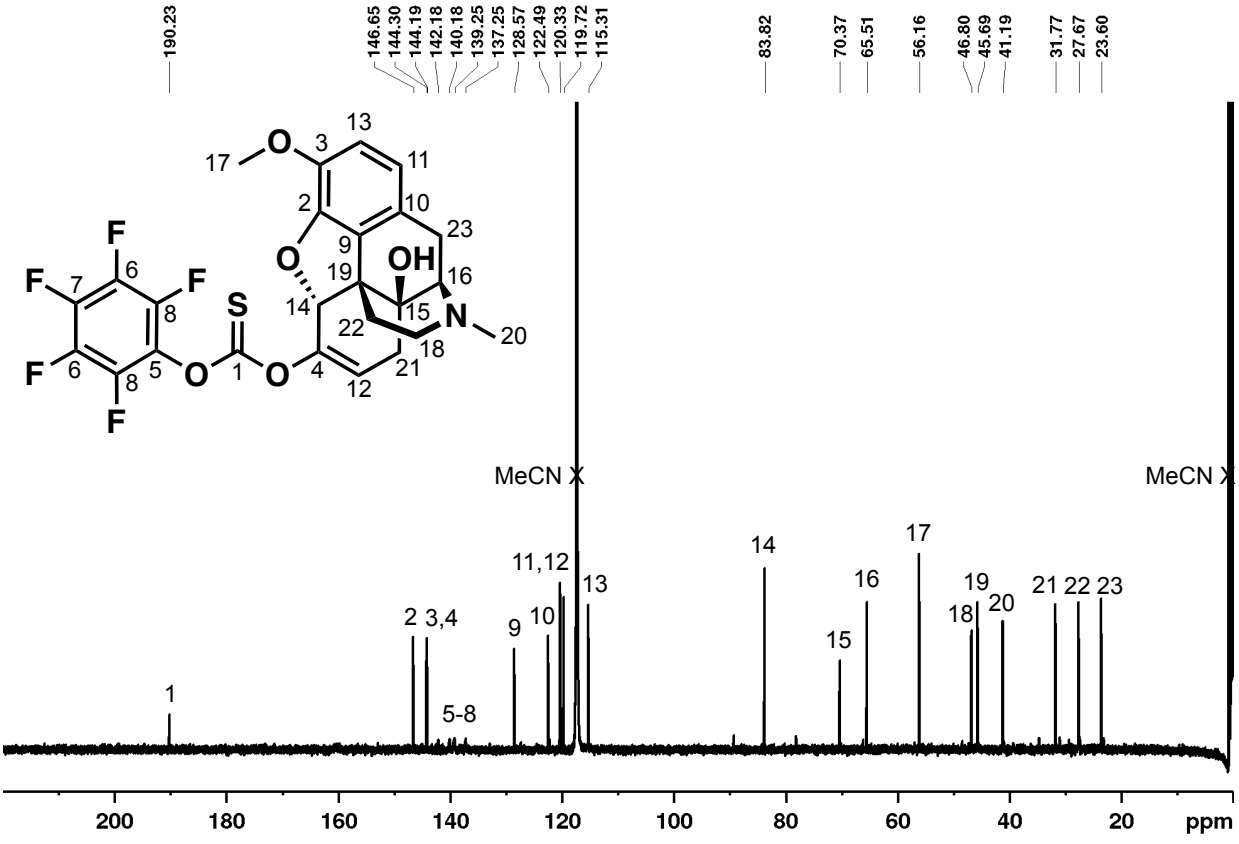

Figure 3.29. ^{13}C NMR of Oxycodone-enol-PFPTC in CD_3CN.

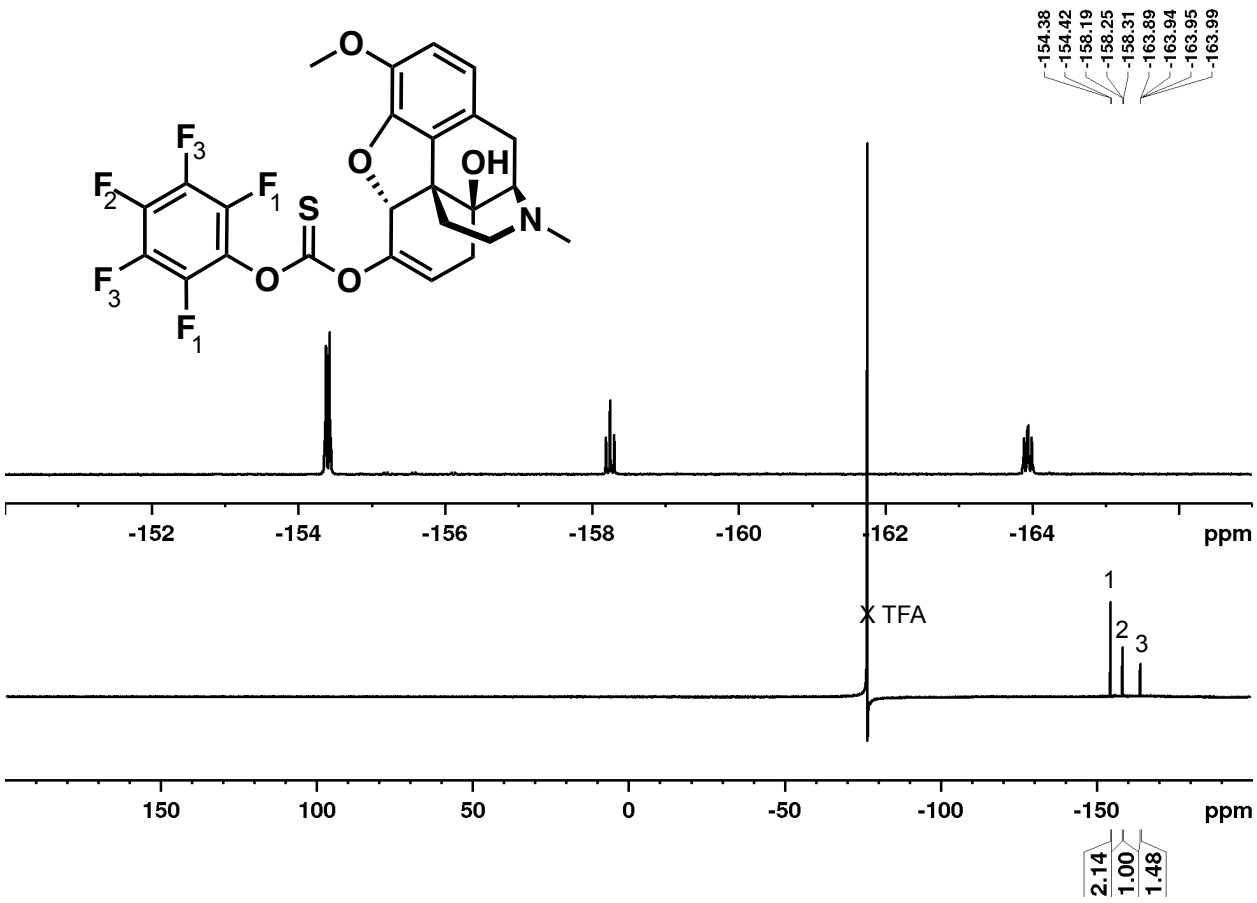

Figure 3.30. ^{19}F NMR of Oxycodone-enol-PFPTC in CD_3CN.

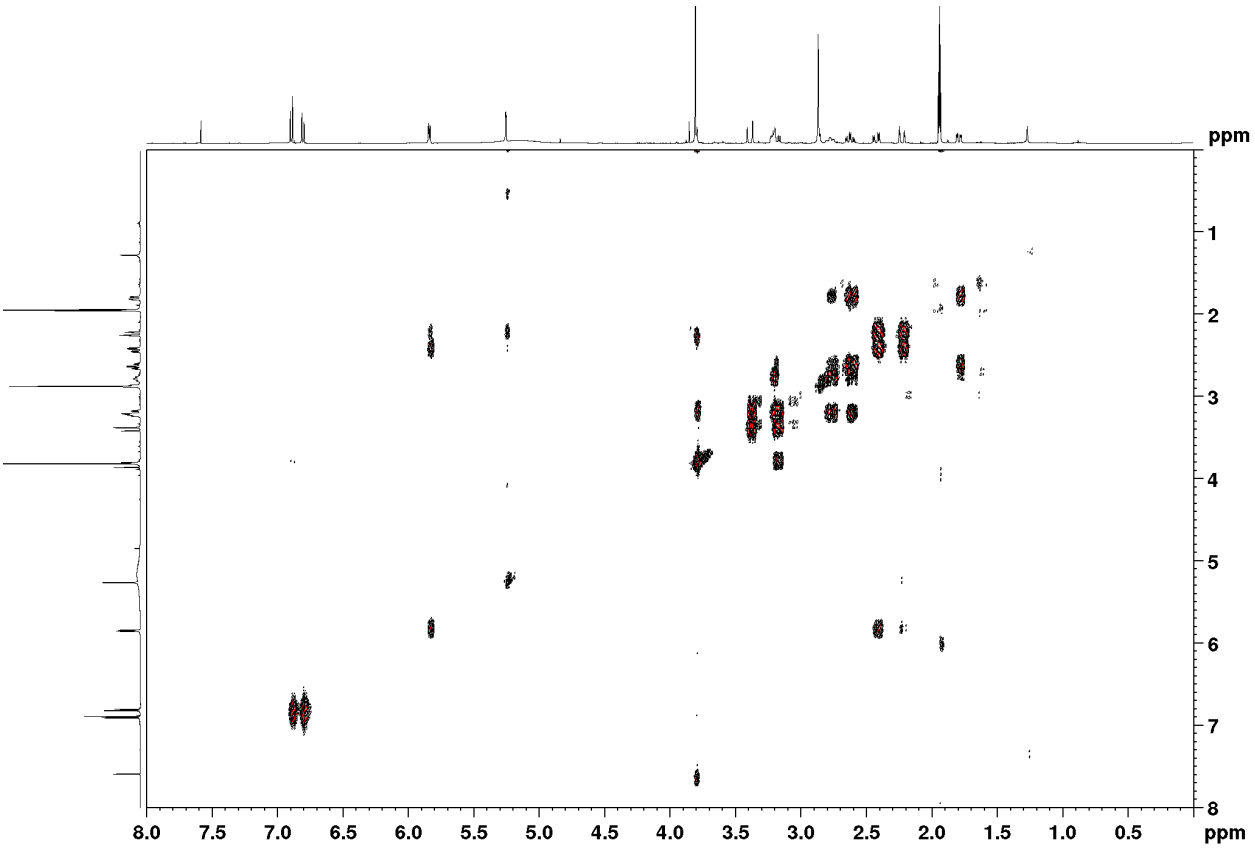

Figure 3.31. COSY of Oxycodone-enol-PFPTC in CD_3CN.

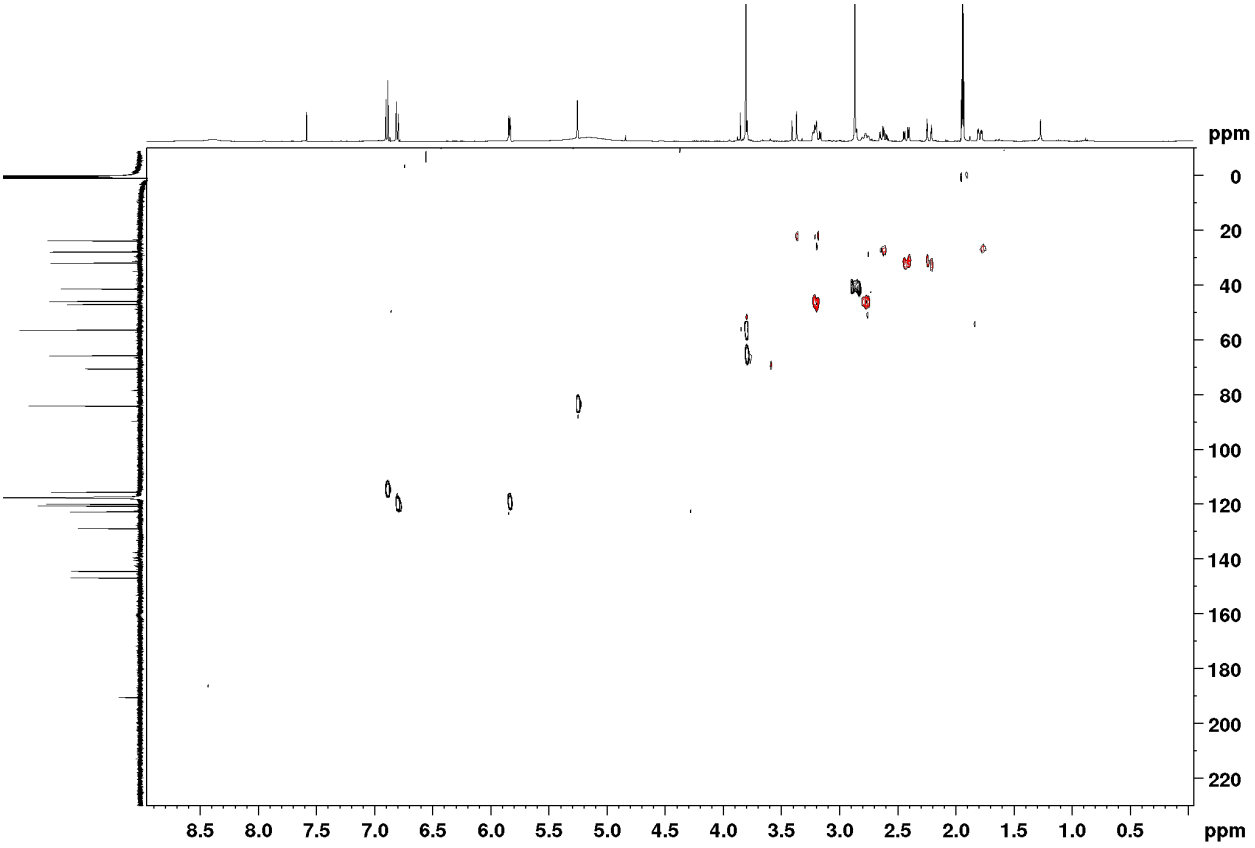

Figure 3.32. HSQC-INEPT135 of Oxycodone-enol-PFPTC in CD_3CN.

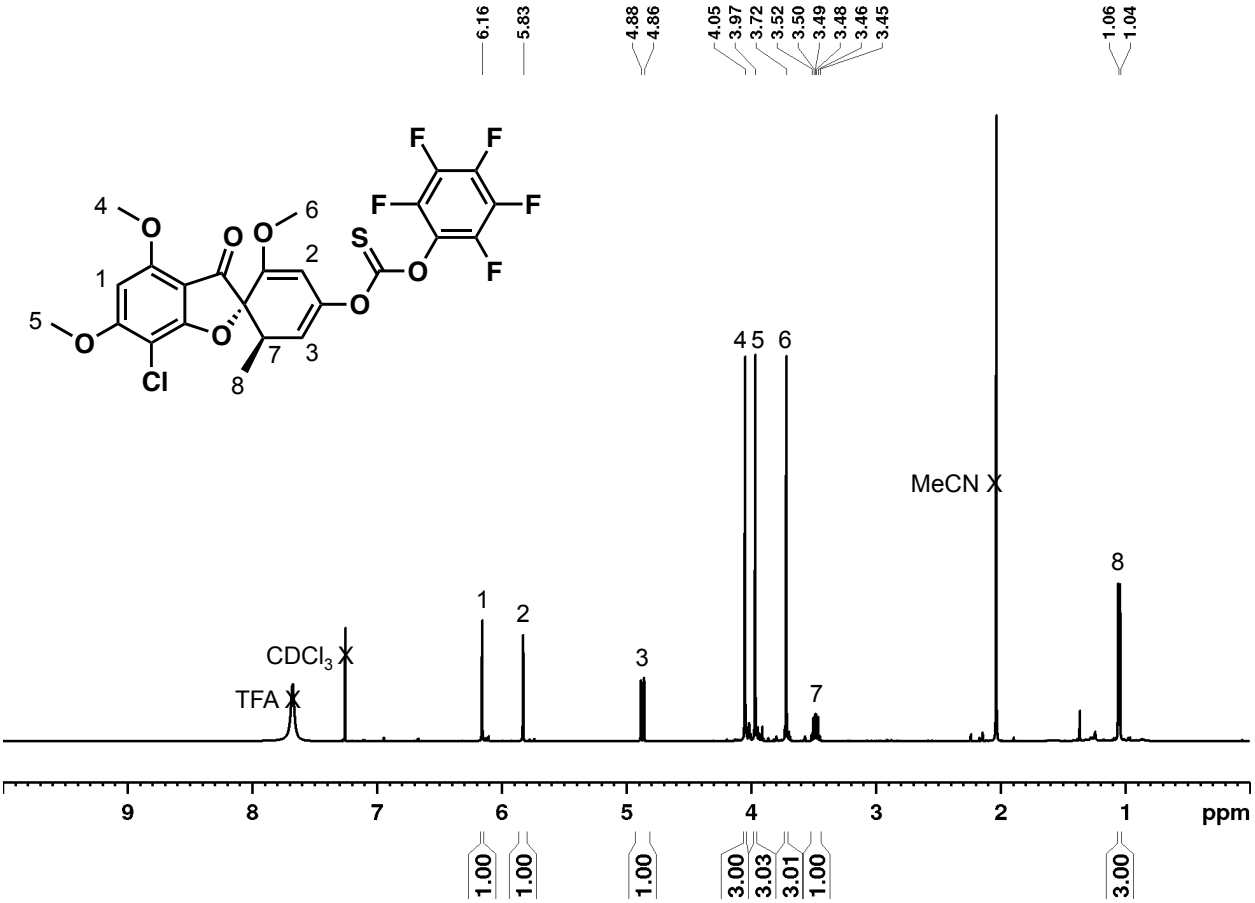

Figure 3.33. ^{1}H NMR of Griseofulvin-enol-PFPTC in $CDCl_3$.

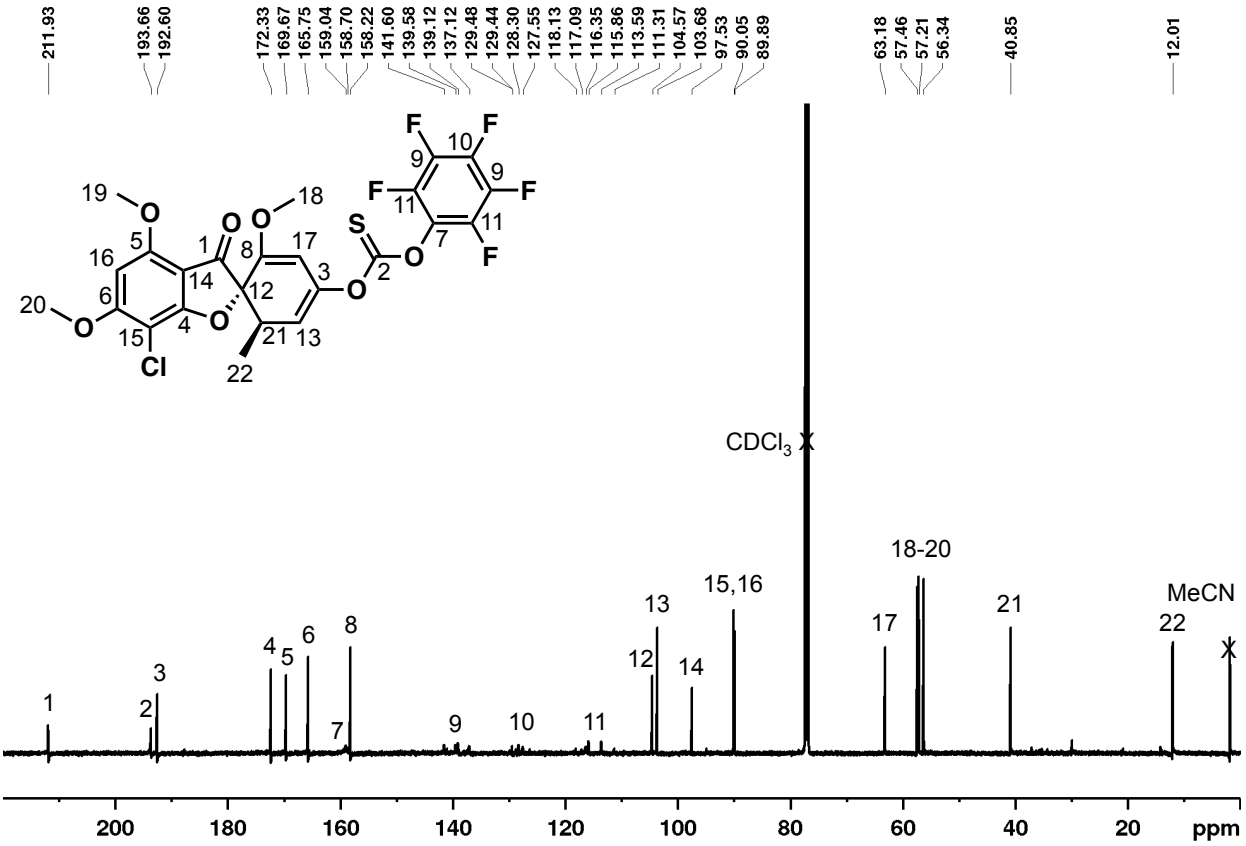

Figure 3.34. ^{13}C NMR of Griseofulvin-enol-PFPTC in $CDCl_3$.

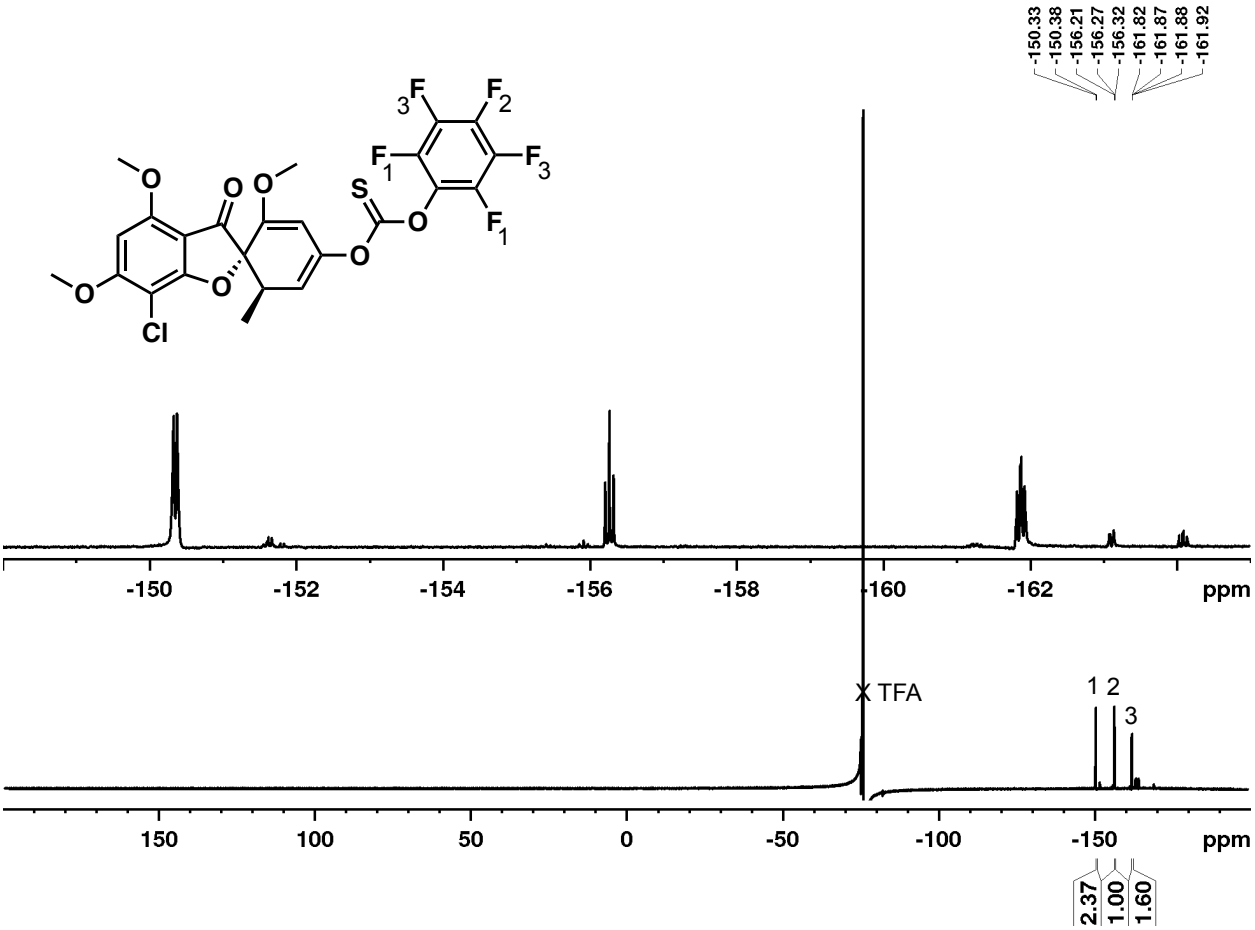

Figure 3.35. ^{19}F NMR of Griseofulvin-enol-PFPTC in $CDCl_3$.

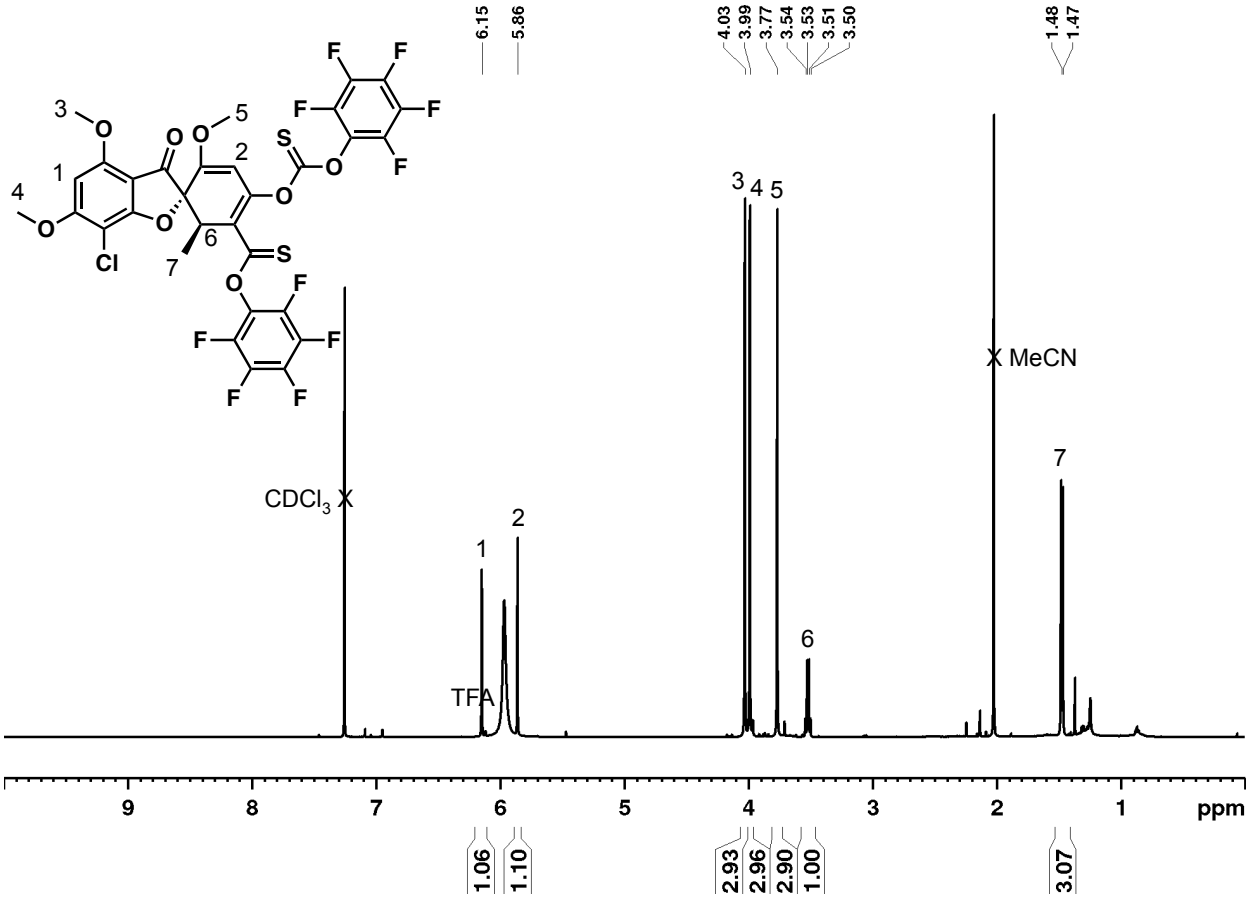

Figure 3.36. ^{1}H NMR of Griseofulvin double addition product in $CDCl_3$.

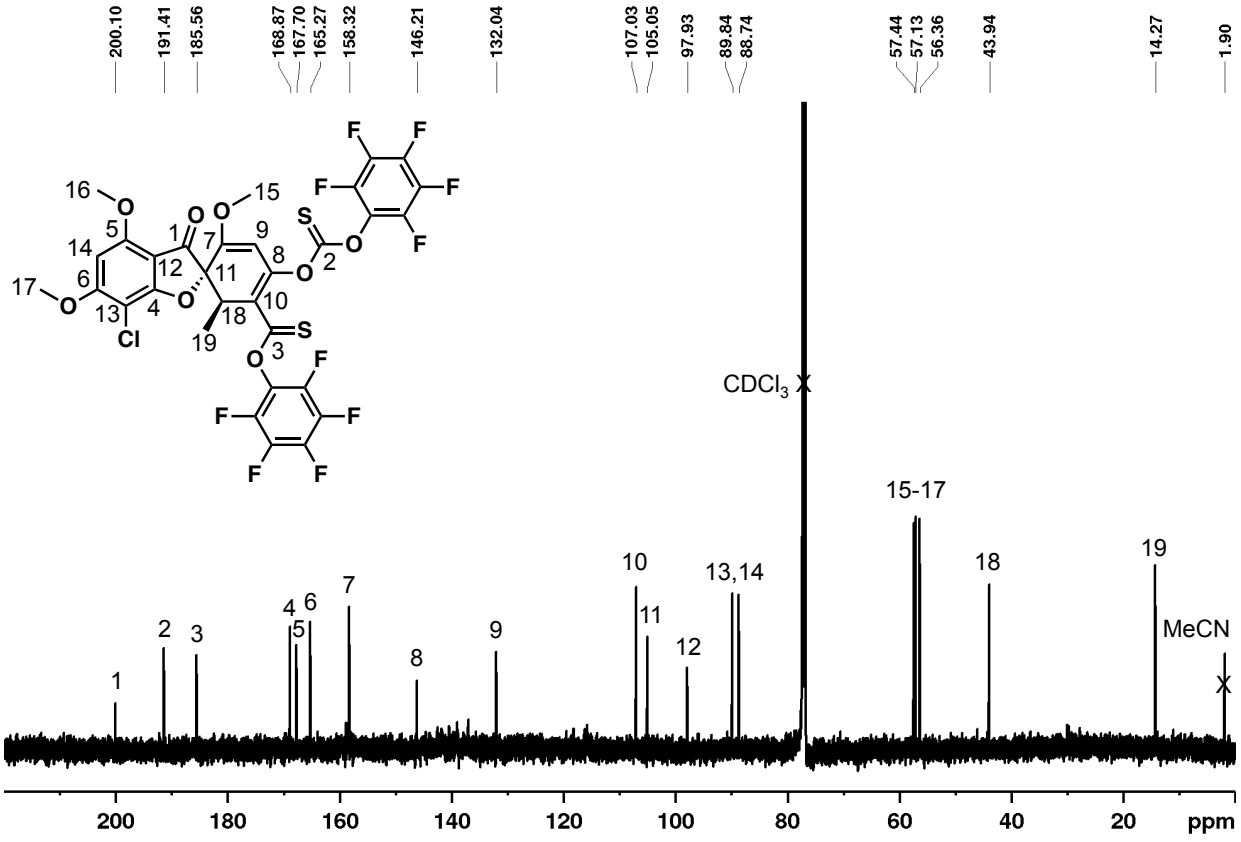

Figure 3.37. ^{13}C NMR of Griseofulvin double addition product in $CDCl_3$. Pentafluorophenyl carbons could not be assigned due to signal broadening.

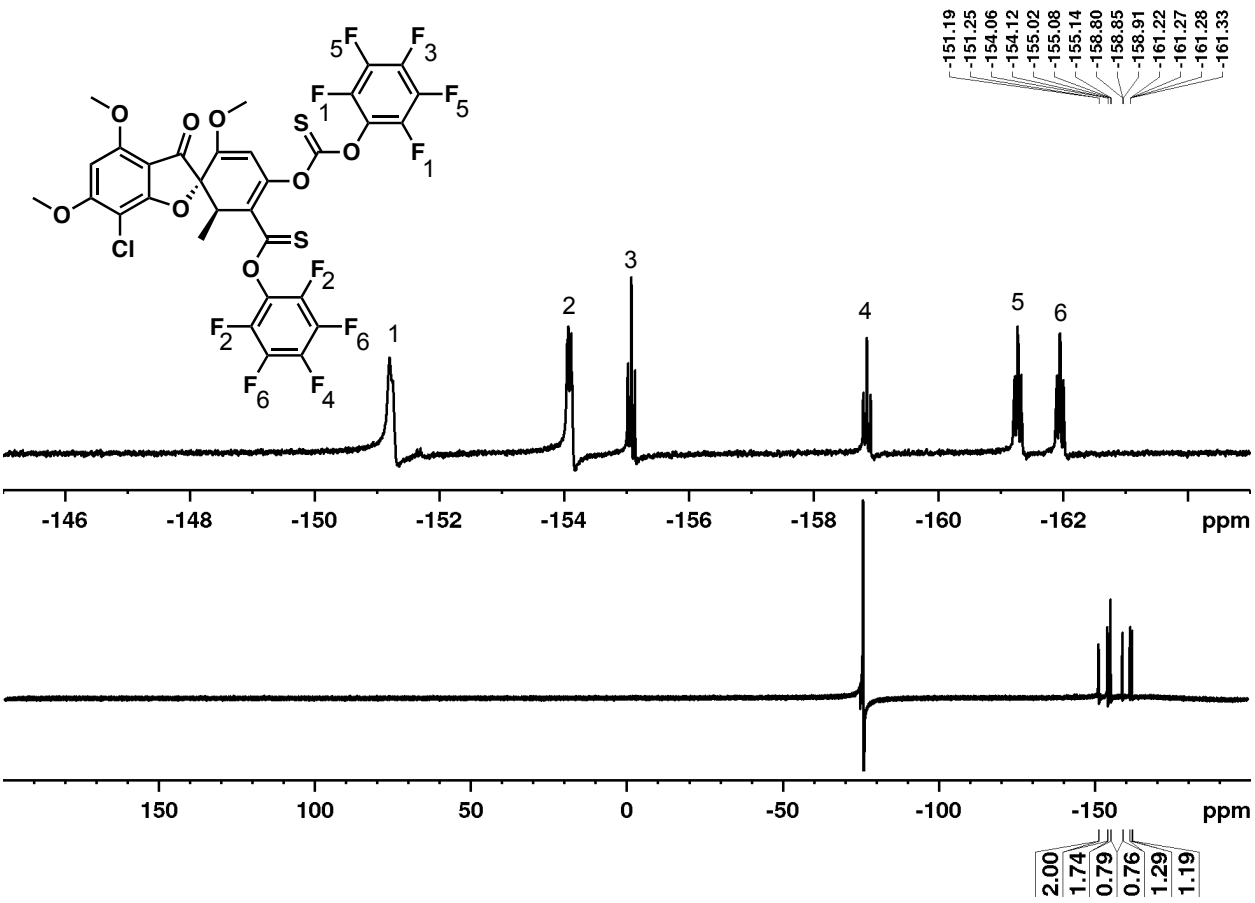

Figure 3.38. ^{19}F NMR of Griseofulvin double addition product in $CDCl_3$.

3.6 References

(1) Johannes, C. B.; Le, T. K.; Zhou, X.; Johnston, J. A.; Dworkin, R. H. (2010) The Prevalence of Chronic Pain in United States Adults: Results of an Internet-Based Survey. *J. Pain 11*, 1230–1239.

(2) *Medicine Use and Spending in the US: A Review of 2018 and Outlook to 2023*; IQVIA Institute for Human Data Science: Parsippany, NJ 07054, 2019; pp 1–60.

(3) Levy, B.; Paulozzi, L.; Mack, K. A.; Jones, C. M. (2015) Trends in Opioid Analgesic–Prescribing Rates by Specialty, U.S., 2007–2012. *Am. J. Prev. Med. 49*, 409–413.

(4) Stoicea, N.; Costa, A.; Periel, L.; Uribe, A.; Weaver, T.; Bergese, S. D. (2019) Current Perspectives on the Opioid Crisis in the US Healthcare System. *Medicine (Baltimore) 98*.

(5) Skolnick, P. (2018) The Opioid Epidemic: Crisis and Solutions. *Annu. Rev. Pharmacol. Toxicol. 58*, 143–159.

(6) Hoots, B. E.; Xu, L.; Kariisa, M.; Wilson, N. O.; Rudd, R. A.; Scholl, L.; Schieber, L.; Seth, P. (2018) 2018 Annual Surveillance Report of Drug-Related Risks and Outcomes -- United States.

(7) Han, B.; Compton, W. M.; Blanco, C.; Crane, E.; Lee, J.; Jones, C. M. (2017) Prescription Opioid Use, Misuse, and Use Disorders in U.S. Adults: 2015 National Survey on Drug Use and Health. *Ann. Intern. Med. 167*, 293–301.

(8) Volkow, N. D.; McLellan, A. T. (2016) Opioid Abuse in Chronic Pain — Misconceptions and Mitigation Strategies. *N. Engl. J. Med. 374*, 1253–1263.

(9) Theisen, K.; Jacobs, B.; Macleod, L.; Davies, B. (2018) The United States Opioid Epidemic: A Review of the Surgeon's Contribution to It and Health Policy Initiatives. *BJU Int. 122*, 754–759.

(10) Kennedy-Hendricks, A.; Gielen, A.; McDonald, E.; McGinty, E. E.; Shields, W.; Barry, C. L. (2016) Medication Sharing, Storage, and Disposal Practices for Opioid Medications Among US Adults. *JAMA Intern. Med. 176*, 1027–1029.

(11) Lipari, R. N.; Hughes, A. *How People Obtain the Prescription Pain Relievers They Misuse*; The CBHSQ Report; Substance Abuse and Mental Health Services Administration, 2017.

(12) Mars, S. G.; Bourgois, P.; Karandinos, G.; Montero, F.; Ciccarone, D. (2014) "Every 'Never' I Ever Said Came True": Transitions from Opioid Pills to Heroin Injecting. *Int. J. Drug Policy 25*, 257–266.

(13) Carlson, R. G.; Nahhas, R. W.; Martins, S. S.; Daniulaityte, R. (2016) Predictors of Transition to Heroin Use among Initially Non-Opioid Dependent Illicit Pharmaceutical Opioid Users: A Natural History Study. *Drug Alcohol Depend. 160*, 127–134.

(14) Compton, W. M.; Jones, C. M.; Baldwin, G. T. (2016) Relationship between Nonmedical Prescription-Opioid Use and Heroin Use. *N. Engl. J. Med. 374*, 154–163.

(15) Jalal, H.; Buchanich, J. M.; Roberts, M. S.; Balmert, L. C.; Zhang, K.; Burke, D. S. (2018) Changing Dynamics of the Drug Overdose Epidemic in the United States from 1979 through 2016. *Science 361*, eaau1184.

(16) *Multiple Cause of Death 1999 - 2018 on CDC WONDER Online Database, Released January, 2020*; National Center for Health Statistics, 2020.

(17) *Substance Abuse and Mental Health Services Administration.* (2019). Key Substance Use and Mental Health Indicators in the United States: Results from the 2018 National Survey on Drug Use and Health (HHS Publication No. PEP19-5068, NSDUH Series H-54).

Rockville, MD: Center for Behavioral Health Statistics and Quality, Substance Abuse and Mental Health Services Administration. Retrieved from https://www.samhsa.gov/data/.

(18) Saha, T. D.; Kerridge, B. T.; Goldstein, R. B.; Chou, S. P.; Zhang, H.; Jung, J.; Pickering, R. P.; Ruan, W. J.; Smith, S. M.; Huang, B.; Hasin, D. S.; Grant, B. F. (2016) Nonmedical Prescription Opioid Use and DSM-5 Nonmedical Prescription Opioid Use Disorder in the United States. *J. Clin. Psychiatry 77*, 772–780.

(19) Pergolizzi, J. V. J.; Raffa, R. B.; Jr, R. T.; Vacalis, S. (2018) Abuse-Deterrent Opioids: An Update on Current Approaches and Considerations. *Curr. Med. Res. Opin. 34*, 711–723.

(20) Gasior, M.; Bond, M.; Malamut, R. (2016) Routes of Abuse of Prescription Opioid Analgesics: A Review and Assessment of the Potential Impact of Abuse-Deterrent Formulations. *Postgrad. Med. 128*, 85–96.

(21) Budman, S. H.; Grimes Serrano, J. M.; Butler, S. F. (2009) Can Abuse Deterrent Formulations Make a Difference? Expectation and Speculation. *Harm. Reduct. J. 6*, 8.

(22) Lankenau, S. E.; Teti, M.; Silva, K.; Bloom, J. J.; Harocopos, A.; Treese, M. (2012) Initiation into Prescription Opioid Misuse amongst Young Injection Drug Users. *Int. J. Drug Policy 23*, 37–44.

(23) Gudin, J. A.; Nalamachu, S. R. (2016) An Overview of Prodrug Technology and Its Application for Developing Abuse-Deterrent Opioids. *Postgrad. Med. 128*, 97–105.

(24) *Abuse-Deterrent Opioids — Evaluation and Labeling*; U.S. Department of Health and Human Services, Food and Drug Administration, Center for Drug Evaluation and Research, 2015.

(25) Maincent, J.; Zhang, F. (2016) Recent Advances in Abuse-Deterrent Technologies for the Delivery of Opioids. *Int. J. Pharm. 510*, 57–72.

(26) *Abuse-Deterrent Formulations of Opioids: Effectiveness and Value*; Institute for Clinical and Economic Review, 2017.

(27) Mickle, T.; Guenther, S.; Mickle, C.; Chi, G.; Kanski, J.; Martin, A. K.; Bera, B. Phenylethanoic Acid, Phenylpropanoic Acid and Phenylpropenoic Acid Conjugates and Prodrugs of Hydrocodone, Method of Making and Use Thereof. US20110002991A1, January 6, 2011.

(28) Shafer, J. A.; Telyatnikov, V. V.; Guo, Z. Compounds and Methods for Lowering the Abuse Potential and Extending the Duration of Action of a Drug. US7230005B2, June 12, 2007.

(29) Jenkins, T. E.; Husfeld, C. O. Opioid Prodrugs with Heterocyclic Linkers. US8685916B2, April 1, 2014.

(30) Boehnke, N.; Maynard, H. D. (2017) Design of Modular Dual Enzyme-Responsive Peptides. *Biopolymers 108*, 1–6.

(31) Ruddick, J. A.; Newsome, W. H.; Nash, L. (1976) Correlation of Teratogenicity and Molecular Structure: Ethylenethiourea and Related Compounds. *Teratology 13*, 263–266.

(32) Litman, R. S.; Pagán, O. H.; Cicero, T. J. (2018) Abuse-Deterrent Opioid Formulations. *Anesthesiol. J. Am. Soc. Anesthesiol. 128*, 1015–1026.

(33) Kreek, M. J.; Reed, B.; Butelman, E. R. (2019) Current Status of Opioid Addiction Treatment and Related Preclinical Research. *Sci. Adv. 5*, eaax9140.

(34) Ossiander, E. M. (2014) Using Textual Cause-of-Death Data to Study Drug Poisoning Deaths. *Am. J. Epidemiol. 179*, 884–894.

(35) Volkow, N. D. America's Addiction to Opioids: Heroin and Prescription Drug Abuse https://archives.drugabuse.gov/testimonies/2014/americas-addiction-to-opioids-heroin-prescription-drug-abuse (accessed Jun 26, 2020).

(36) Staben, L. R.; Koenig, S. G.; Lehar, S. M.; Vandlen, R.; Zhang, D.; Chuh, J.; Yu, S.-F.; Ng, C.; Guo, J.; Liu, Y.; Fourie-O'Donohue, A.; Go, M.; Linghu, X.; Segraves, N. L.; Wang, T.; Chen, J.; Wei, B.; Phillips, G. D. L.; Xu, K.; Kozak, K. R.; Mariathasan, S.; Flygare, J. A.; Pillow, T. H. (2016) Targeted Drug Delivery through the Traceless Release of Tertiary and Heteroaryl Amines from Antibody–Drug Conjugates. *Nat. Chem. 8*, 1112–1119.

(37) Selfridge, B. R.; Wang, X.; Zhang, Y.; Yin, H.; Grace, P. M.; Watkins, L. R.; Jacobson, A. E.; Rice, K. C. (2015) Structure–Activity Relationships of (+)-Naltrexone-Inspired Toll-like Receptor 4 (TLR4) Antagonists. *J. Med. Chem. 58*, 5038–5052.

(38) Muir, W. M.; Ritchie, P. D.; Lyman, D. J. (1966) Acylation. I. The Mechanisms of Enol Ester and 1,3-Diketone Formation in the Reaction of Ketone—Enol Systems with Acyl Halides. *J. Org. Chem. 31*, 3790–3793.

(39) House, H. O.; Auerbach, R. A.; Gall, M.; Peet, N. P. (1973) Chemistry of Carbanions. XXII. C- vs. O-Acylation of Metal Enolates. *J. Org. Chem. 38*, 514–522.

(40) Olofson, R. A.; Cuomo, J.; Bauman, B. A. (1978) An Efficient Synthesis of Enol Carbonates. *J. Org. Chem. 43*, 2073–2075.

(41) Taylor, R. J. K. (1985) Organocopper Conjugate Addition-Enolate Trapping Reactions. *Synthesis 1985*, 364–392.

(42) Trost, B. M.; Xu, J. (2007) The O-Acylation of Ketone Enolates by Allyl 1H-Imidazole-1-Carboxylate Mediated with Boron Trifluoride Etherate: A Convenient Procedure for the Synthesis of Substituted Allyl Enol Carbonates. *J. Org. Chem. 72*, 9372–9375.

Chapter 4

Genetic Code Expansion Enables Site-Specific PEGylation of a Human Growth Hormone Receptor Antagonist through Click Chemistry[†]

4.1 Introduction

Human growth hormone receptor (GHR) antagonists are a class of recombinantly engineered protein therapeutics designed to block human growth hormone (GH) signaling.[1,2] Regulation of GH signaling is important for treatment of acromegaly[3,4] and has also been investigated for use in treatment of GH and insulin-like growth factor 1 (IGF-1)-dependent cancers.[5–9] Acromegaly is a disease characterized by overproduction of GH that can lead to numerous complications if left untreated including diabetes, hypertension, cardiomyopathy, and reduced life expectancy.[3,4] GH signaling also plays a significant role in the development and progression of various cancers, with elevated levels of GH and downstream signaling molecules linked to increased risk of breast cancer, prostate cancer, colon cancer, and others.[4,10–13] In each case, regulation of GH signaling is crucial, and with it, the need for molecules that can most effectively facilitate this regulation.

GH is an important basal pituitary hormone that promotes growth in adolescents and regulates metabolism in adults.[14] Once secreted from the pituitary gland, GH signal transduction occurs upon binding to the GHR located on the surface of cell membranes. Human GH possesses two distinct binding sites that allow it to bind to and promote dimerization of two identical GHR.[15] Following the initial high-affinity binding of one GHR molecule to GH via binding site 1, GH recruits and facilitates dimerization with a second GHR molecule via its lower-affinity binding site 2.[16] While GH acts as an effective GHR agonist, a single mutation from glycine to lysine at residue 120 in GH binding site 2 transforms the protein into an antagonist. This mutant also binds to and facilitates GHR dimerization, but does not promote signal transduction.[17,18] Since this initial discovery, eight additional mutations have been identified and incorporated to improve GHR binding to GH binding site 1,[1,19] ultimately resulting in the GHR antagonist

designated as B2036. As with native GH, B2036 is a small protein of approximately 22 kDa that exhibits rapid blood clearance, with a short half-life in humans of approximately 15 minutes.[20] To extend the half-life of B2036, poly(ethylene glycol) (PEG) with an average molecular weight of 5 kDa was nonspecifically conjugated to 4-6 of the 9 amino groups (8 lysines and the N-terminus) of the protein to generate pegvisomant (Pfizer Inc., USA), which is FDA-approved for acromegaly treatment.

Although multi-PEGylation extended the half-life of B2036 to approximately 74 hours[2,21], its GHR binding and consequent bioactivity were dramatically reduced,[18] likely due to hindered access of the protein to GHR binding sites. This reduction in bioactivity necessitated elevated dosing levels with a recommended dosage range of 10-30 mg injected subcutaneously once daily after a loading dose of 40 mg.[21] While pegvisomant remains an effective treatment for acromegaly, it is also the most expensive treatment option for the disease. Though it is common for protein therapeutics to be expensive, the cost of pegvisomant is particularly high due in part to the high dosing requirements and also likely as a result of the rigorous quality control process that is required for the inherently heterogeneous mixture that results from nonspecific PEGylation.[22,23] One 2009 study applied an economic model to evaluate the cost-effectiveness of pegvisomant treatment compared to standard care and estimated the cost-effectiveness ratio to be approximately £212,000 per life year gained over a 20 year period. The authors ruled that despite the effectiveness of the drug, it could not be deemed good value for its cost compared to standard care.[24] Reduction of the economic burden of pegvisomant is therefore highly desirable.

One strategy with potential to overcome these barriers is to employ site-specific conjugation of PEG to B2036. Controlled attachment of PEG to specific residues distal to the GHR binding regions can reduce blockage of these sites and facilitate improved bioactivity

compared to nonspecific PEGylation. Site-specific protein conjugation strategies are well known and have been reviewed extensively.[25–29] Canonical amino acids within a native protein can be functionalized using a variety of chemical modification strategies, but frequently these methods require extensive optimization to target single residues, and often lack positional specificity in the protein sequence. For example, alkylation of the N-terminal amino group of a protein via reductive amination can be carried out selectively around pH 5 even in the presence of lysine amino groups due to the slight difference in pK_a values between the two types of amino groups. However, competing lysine modification and incomplete protein modification are often observed when employing reductive amination, ultimately diminishing conjugate yields. This approach was used for mono-PEGylation of the N-terminal amino group of B2036 with 20 kDa and 40 kDa PEG chains. Interestingly only the 20 kDa B2036 conjugate demonstrated *in vivo* bioactivity, which the authors speculated to be a result of interference by the larger PEG with GHR binding sites.[30]

Another approach to install a specific reactive site is to express a recombinant protein containing a genetically incorporated cysteine residue. The resulting nucleophilic thiol can be selectively modified with a variety of commercially available reagents such as maleimides or other Michael acceptors.[31] Though these reactions are quite robust and high yielding, expression and purification of the thiol-containing protein can be challenging due to the potential for oxidation of the installed thiol, which can lead to misfolding and dimerization.[27,32] Addition of reducing agents such as dithiothreitol (DTT) or tris(2-carboxyethyl)phosphine (TCEP) have been used to reverse dimerization, but these reagents can lead to global disulfide reduction or disulfide shuffling, which can interfere with protein function and diminish overall conjugate yields.[27,32,29] Nevertheless, this robust approach remains a mainstay in the field of protein engineering, and

several groups, including ours, have reported the preparation of GH and B2036 variants that have demonstrated equivalent bioactivities compared to their native protein using T3C[33] and S144C[34] mutations, respectively. As expected, PEGylation of these variants also led to substantial improvements in bioactivity over the multi-PEGylated pegvisomant.

In more recent years, advances in the field of genetic code expansion have provided alternative opportunities for site-specific protein modifications. Like genetic cysteine incorporation, these amino acids can be substituted into any position in the amino acid sequence, but offer dozens of possible functional handles that can be tailored to meet the specific requirements of a given system. Amber suppression is one of the most common techniques used to site-specifically incorporate unnatural amino acids (UAA) into proteins; it functions by using an amino-acyl tRNA synthetase/tRNA pair that is orthogonal to the host organism's translational machinery, but can effectively be recognized by the host ribosome and facilitate reassignment of the amber-stop codon to a particular UAA.[35] This technique has recently been applied to many proteins including GH to enable site-specific PEGylation. For instance, Cho et al. used amber suppression to prepare twenty site-specifically PEGylated GH variants for receptor binding and evaluated six of the most promising (Y35, F92, Q131, R134, Y143, and K145) for bioactivity, pharmacokinetics, and *in vivo* performance, ultimately identifying tyrosine 35 (Y35) to be the overall best performing PEGylation site.[36] In another report from Wu et al., combinatorial, site-specific PEGylation was explored for three residue positions (Y35, G131, and K145). The authors found that site-specific multi-PEGylated GH variants yielded similar bioactivity as singly-PEGylated GH variants of the same molecular weight, with the multi-PEGylated conjugates additionally exhibiting improved half-lives.[37] While incorporation of multiple UAAs is an attractive option for site-specific multi-PEGylation, it must be noted that presently amber

suppression is inherently less efficient than recoding with canonical amino acids. This results in dramatically reduced yield of full-length protein as more amber codons are added to a protein sequence.[35] Similar to cysteine mutants, protein function must also always be reevaluated following UAA incorporation. Yet, incorporation of artificial amino acids has distinct advantages including orthogonally, and while GH has received significant attention for site-specific PEGylation using genetic code expansion as described above, GHR antagonists such as B2036 have not been extensively investigated.

In the work described herein, we developed a robust, user-friendly platform for preparation of a site-specifically PEGylated GHR antagonist with improved cellular bioactivity compared to pegvisomant. We envisioned that a B2036 variant of equal potency could be prepared in good yield without extensive chromatographic purification by incorporation of the noncanonical amino acid propargyl tyrosine in a region of the protein distal to both GHR binding sites. Reaction of the alkyne-containing protein with azide-containing PEGs via the copper catalyzed cycloaddition reaction efficiently yielded single-polymer conjugates that could be purified by simple anion-exchange chromatography. We evaluated the *in vitro* bioactivity of the resulting conjugates and found each to be significantly more potent than pegvisomant, even at comparable molecular weights. Taken together, this work provides a useful strategy for the preparation of site-specific, bioactive, PEGylated GHR antagonists.

4.2 Results and Discussion

4.2.1 Design and Preparation of a Site-Specifically Modified GHR Antagonist

There are many parameters to consider when using genetic code expansion to site-specifically install an UAA into a protein of interest. First and foremost is the determination of

which UAA to use. One of our primary objectives was to generate a B2036 variant that could be selectively PEGylated at a single residue under mild conditions. Additionally, we sought to use a highly efficient and straightforward conjugation strategy with synthetically accessible reagents, allowing for rapid production of usable protein and conjugates. We also wanted to ensure that the UAA of choice could be incorporated into B2036 with good efficiency in order to obtain usable quantities of the full-length protein. For these reasons, we chose to use propargyl tyrosine (pglY) since its alkyne can react selectively with azides under mild, copper-catalyzed conditions,[38,39] and both pglY and azide-containing reagents can be purchased or prepared with synthetic ease. Furthermore, pglY incorporation relies on the *Methanococcus jannashii* derived amino-acyl tRNA synthetase/cognate amber-suppressing tRNA pair, which is both well established and efficient.[40,41]

Nearly as important as the selection of an UAA is the decision of where to install it. We initially evaluated the reported crystal structure obtained of GH binding with two GHR and identified residues distal to both binding regions.[15] Next, we identified amino acids that were structurally similar to pglY such as tyrosine and phenylalanine so as to minimize structural perturbations following incorporation. Finally, we compared our candidates with literature reports of genetic code expansion applied to structurally similar GH[36,37] and theorized that substitution of tyrosine 35 (Y35) with pglY in GHR antagonist B2036 would provide the most promising candidate (Figure 4.1).

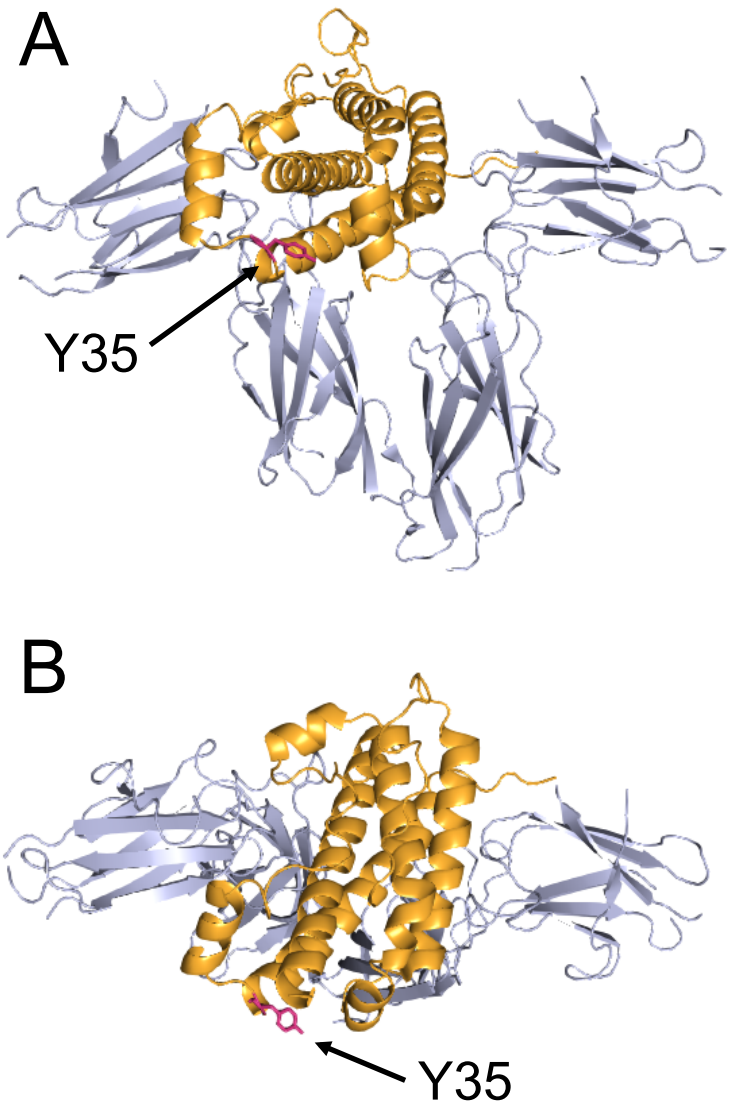

Figure 4.1. Schematic of GH (orange) bound to two GHR (grey) with indicated residue Y35 (red) as viewed side-on (A) and top-down (B). PyMol v.1.8.6.0 was used to render the reported crystal structure (PDB 3HHR).[15]

Expression and purification of B2036 and B2036 Y35pglY (B2036-Alkyne) were then carried out. DNA sequences coding for the mature form of both proteins were genetically fused to an N-terminal tag composed of thioredoxin (TRX) with a hepta-histidine sequence similar to our previously reported construct to promote soluble expression as well as affinity purification.[42]

A tobacco etch virus (TEV) protease recognition sequence was engineered between the TRX-His7 tag and the B2036 sequence for eventual removal of the TRX-His7 tag (Figure 4.7-Figure 4.12). Plasmids for each fusion construct were transformed into *E. coli* Origami B (DE3) competent cells, a strain engineered to help facilitate soluble protein expression. Genetic code expansion machinery was encoded by the previously reported plasmid pDule2-CNF,[40] which was co-transformed only with the B2036-Alkyne expression vector. To ensure that this machinery was selective for pglY incorporation, control expressions were assessed with and without the addition of pglY to the growth medium by sodium dodecyl sulfate polyacrylamide gel electrophoresis (SDS-PAGE) (Figure 4.2A). In the absence of pglY, only a 15 kDa truncation product was observed in the crude cell lysate after induction with isopropyl-β-D-thiogalactopyranoside (IPTG), which corresponds to the expected size of the fusion protein if the amber codon was not suppressed and instead read as a stop codon. In the presence of pglY, a full-length expression band is observed at approximately 33 kDa. Notably, even in the presence of pglY, a significant amount of truncation product was still observed. This is because the cellular machinery used to facilitate incorporation of UAAs is most commonly adapted from other organisms. Imperfect synergy of this non-native machinery with the host cell's translational machinery results in diminished UAA incorporation efficiencies, a byproduct of which is the expression of truncated protein. No observable expression products were observed at 33 kDa in the absence of IPTG.

The fusion protein TRX-B2036-Alkyne was then purified via immobilized metal affinity chromatography (IMAC). As expected, the 15 kDa truncation product, which contained a hepta-histidine tag, bound to and eluted from the Ni-NTA affinity column with the full-length fusion protein (Figure 4.2B). However, following digestion of the fusion protein with Tobacco Etch

Virus (TEV) protease and purification with inverse-IMAC and centrifugal filtration, all byproducts were successfully removed, yielding highly pure B2036-Alkyne (Figure 4.2C). Following TEV digestion, a single N-terminal glycine residue was added to the amino acid sequence of B2036-Alkyne; however, this small change was not expected to perturb structure or activity as our previously reported construct contained a similar, short N-terminal sequence.[42] Expression was approximately 65% efficient for production of B2036-Alkyne compared to B2036 with yields of 8.7 and 13.3 mg/g cell pellet, respectively. Part of this disparity is due to the noted limitations of the adapted machinery, but some portion can also be attributed to the increased metabolic burden associated with the two-plasmid system used to express B2036-Alkyne versus the single-plasmid system for B2036. For our purposes, we found this yield to be satisfactory as approximately 19 mg of high purity B2036-Alkyne could be purified from each liter of growth media.

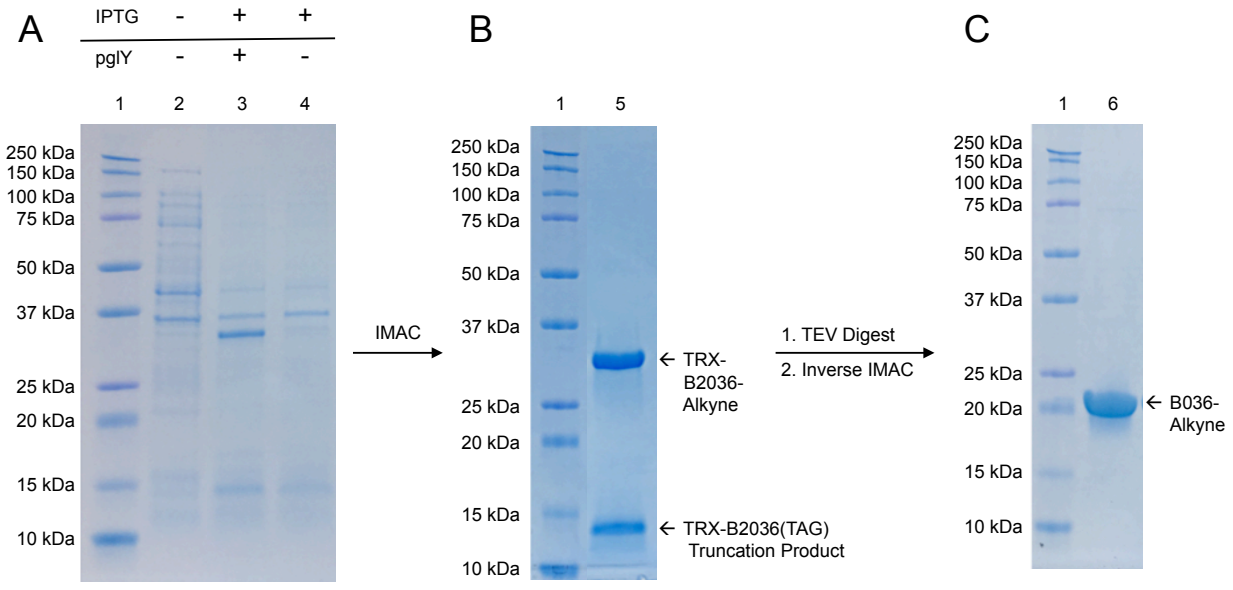

Figure 4.2. Expression and purification of B2036-Alkyne evaluated by SDS-PAGE with Coomassie staining. (A) OD_{600} normalized crude cell lysates were evaluated for full-length expression of TRX-B2036-Y35pglY in the presence or absence of isopropyl-β-D-thiogalactopyranoside (IPTG) and propargyl tyrosine (pglY). (B) TRX-

B2036-Alkyne purified by immobilized metal affinity chromatography (IMAC). (C) Pure B2036-Alkyne following Tobacco Etch Virus (TEV) protease digestion and inverse IMAC. Lanes were loaded as follows: lane 1: protein standards, lane 2: crude cell lysate without IPTG and without pglY, lane 3: crude cell lysate with both IPTG and pglY, lane 4: crude cell lysate with IPTG and without pglY, lane 5: purified TRX-B2036-Alkyne with TRX-B2036 truncation product as indicated, lane 6: pure B2036-Alkyne; loading was normalized to 1.00 OD_{600}/mL for lanes 2-4; expected TRX-B2036-Alkyne MW = 33 kDa and truncation product = 15 kDa.

4.2.2 Evaluation of Structure and *In Vitro* Bioactivity

Having prepared the pure, putative GHR antagonists, we proceeded to confirm the respective sequences of each as well as the incorporation of pglY into the protein by mass spectrometry (MS). We first validated the molecular weight of the proteins via intact MS analysis and found the deconvoluted masses to match the calculated values (Figure 4.3A and Figure 4.13A). We next performed peptide-mapping experiments to confirm the amino acid sequence of each protein and to ensure the site-selectivity of pglY incorporation. Digestion of the pure protein samples with MS-grade trypsin produced peptide fragments that were analyzed by liquid chromatography tandem MS (LC-MS/MS) analysis. Analysis of B2036-Alkyne yielded sequence coverage of 88.5% with coverage for all but the N and C terminal peptide fragments (Figure 4.3B). Importantly, the desired incorporation of pglY in place of tyrosine 35 was confirmed in this experiment as evidenced by the sample tandem mass spectrum of the peptide fragment from residues 18-39 (Figure 4.3C and Table 4.1). A similar analysis was performed for B2036 and 100% sequence coverage was observed (Figure 4.13B). Taken together, these results confirmed the composition and sequence of each GHR antagonist.

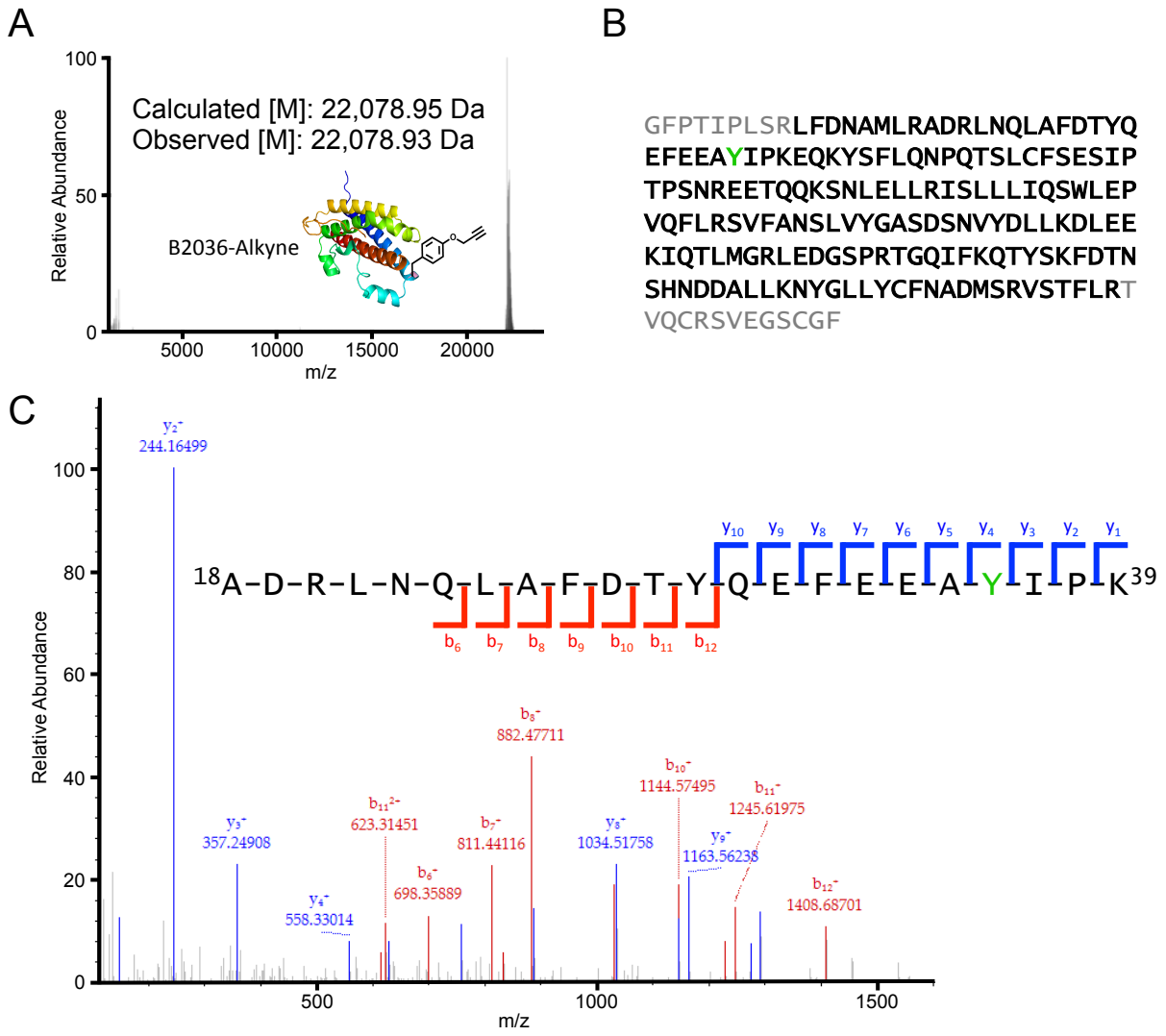

Figure 4.3. Mass spectral analysis of B2036-Alkyne. (A) Deconvoluted intact high-resolution mass spectrum of B2036-Alkyne. (B) Sequence coverage map of B2036-Alkyne was determined following digestion of the purified protein with trypsin and identification of the resulting peptides via LC/ESI/MS/MS. Sequence coverage was determined to be 88.5% (black bolded text) with 100% sequence match and includes coverage of the incorporated noncanonical amino acid propargyl tyrosine (green). (C) Sample tandem mass spectrum of the peptide ADRLNQLAFDTYQEFEEA(pglY)IPK with m/z = 2699.30 in LC/ESI/MS analysis following trypsin digestion of B2036-Alkyne with assigned y- and b- series ions (blue and red, respectively).

Following structural validation, we next evaluated the bioactivity of each protein to ensure that the addition of pglY into B2036-Alkyne did not perturb its function. Bioactivity was

assessed in a resazurin cell viability assay using GH-dependent Ba/F3 cells expressing human GHR developed by the Waters Lab (University of Queensland, St. Lucia, Australia); addition of GHR antagonists blocks GH present in the growth media from binding to GHR and consequently inhibits cellular proliferation in this cell line.[43] By administering serially diluted samples of the antagonists, we generated dose-response curves and determined the half-maximal inhibitory concentration (IC_{50}) for B2036 and B2036-Alkyne to be 16.8 and 17.7 nM, respectively (Figure 4.4). Statistical analysis revealed no significant difference between these values, showing that incorporation of pglY was not deleterious to GHR binding. Having successfully prepared a GHR-antagonist with a nondisruptive, site-specific reaction handle, we next investigated the amenability of B2036-Alkyne to PEGylation and how attachment of a single polymer would affect bioactivity compared to multi-PEGylation.

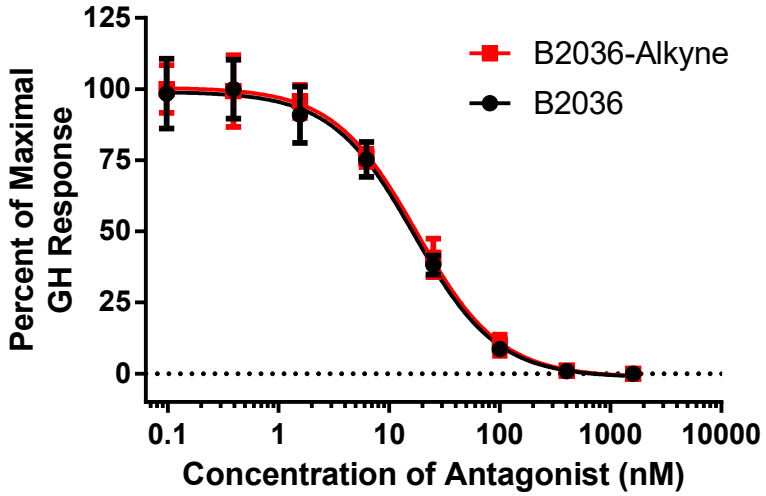

Figure 4.4. Inhibitory bioactivity dose response curves of B2036 (black) and B2036-Alkyne (red) with IC_{50} values of 16.8 and 17.7 nM, with 95% confidence intervals (95% CI) of 14.4-19.6 and 15.5-20.2 nM, respectively, in Ba/F3-GHR cells. No significant difference in bioactivity was observed between B2036 and B2036-Alkyne following comparison by Student's t-test ($p > 0.05$). Data is expressed as mean values with 95% CI of two individual experiments.

4.2.3 Site-Specific PEGylation and Evaluation of Conjugate Bioactivity

We elected to install pglY into B2036 due to the orthogonality, reaction efficiency, and synthetic accessibility of both the alkyne-containing functional group, as well as azide-containing reaction partners. PEG-azides of 5 and 10 kDa were easily prepared in two steps from commercially available methoxy-terminated PEG (mPEG) and the 20 kDa mPEG-azide was purchased. Activation of the terminal alcohol was facilitated by reaction with *p*-toluenesulfonyl chloride in >90% yield, and the azide-terminated mPEG (mPEG-azide) was accessed via subsequent reaction with sodium azide in 78-89% yield. Conjugation of mPEG-azides was carried out starting from well-established procedures for the copper catalyzed azide-alkyne cycloaddition (CuAAC) reaction.[44] However, even when using high-efficiency conjugation reactions such as CuAAC, coupling two macromolecules often requires some level of

optimization. To determine the best conditions for high-efficiency PEGylation of B2036-Alkyne, we varied reaction time, copper concentration, and molar equivalents of PEG-azide. Reaction time had little to no apparent effect on conjugation efficiency for times greater than 2 hours, nor did concentration of copper above a threshold of 0.2 mM (data not shown). Interestingly, the reaction proceeded very slowly below this copper threshold, which was similar to a previous report.[45] Notably, the presence of copper was required for conjugations to proceed, indirectly confirming the site-specificity of the conjugation reaction. Adjustment of the molar ratio of PEG-azide proved critical for reaching high conjugation efficiencies, and for 20 kDa mPEG-azide we found that addition of 10 molar equivalents was necessary to reach a reaction conversion of about 90% (Figure 4.14); addition of extra equivalents failed to further improve conversion.

For this study, we conjugated mPEG-azides of 5, 10, and 20 kDa to B2036-Alkyne via our optimized CuAAC conditions (Figure 4.5A). The reactions were carried out at 20 °C for 2 hours in 100 mM phosphate buffer, pH 7.0 with 0.45 mM B2036-Alkyne, 4.53 mM mPEG-azide, 0.2 mM copper sulfate ($CuSO_4$), 1 mM ligand (2-(4-((Bis((1-(*tert*-butyl)-1*H*-1,2,3-triazol-4-yl)methyl)amino)methyl)-1*H*-1,2,3-triazol-1-yl)acetic acid, or BTTAA), 5 mM aminoguanidine hydrochloride, and 5 mM sodium ascorbate (Figure 4.5A). SDS-PAGE analysis of the crude reaction mixtures revealed that each conjugation proceeded to high conversion and the products were already largely pure with only PEG and minimal unreacted B2036-Alkyne remaining (Figure 4.15). The crude conjugates were easily purified with good peak separation using anion exchange chromatography followed by centrifugal filtration (10 kDa MWCO) of the pooled B2036-PEG fractions to concentrate and remove any remaining small molecules (Figure 4.16). Endotoxin levels were determined to be <0.25 endotoxin units (EU)/mg for conjugates and unmodified protein, which is well below the recommended dosing limit of <5 EU/mg.[46] Purified

conjugates were analyzed by SDS-PAGE stained with Coomassie Brilliant Blue to confirm protein purity and also with 0.1 N iodine solution to confirm removal of excess polymer (Figure 4.5B & Figure 4.5C). Addition of 5, 10, and 20 kDa PEGs to B2036 (22 kDa) would give expected conjugate molecular weights of 27, 32, and 44 kDa, respectively. However, the apparent molecular weights of the conjugates by SDS-PAGE were slightly inflated likely due to the large hydrodynamic radius of PEG, with observed molecular weights of approximately 30, 35, and 50 kDa, respectively. Only one higher molecular weight band was observed for each conjugation reaction, confirming the site-specificity of this approach.

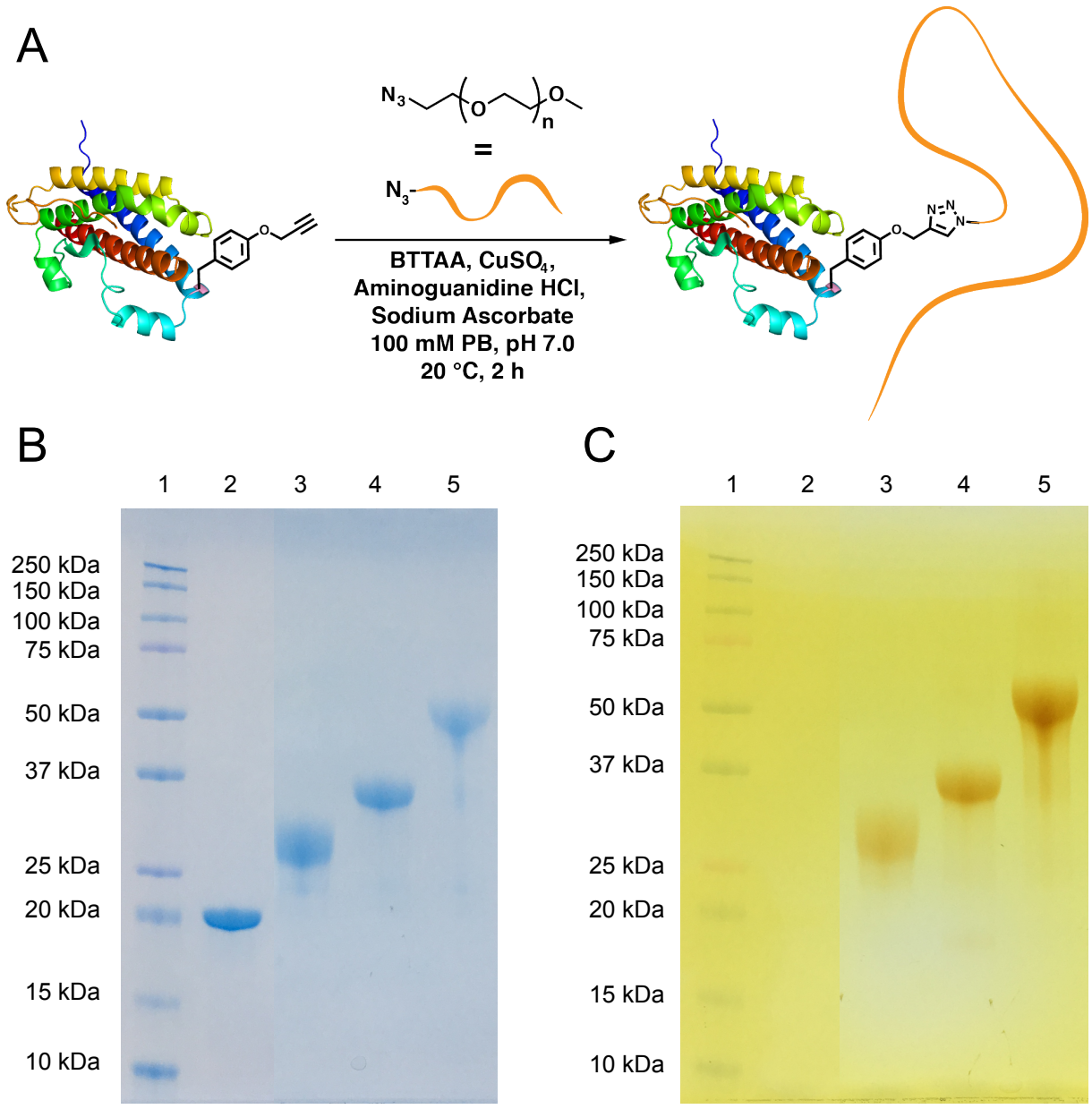

Figure 4.5. Site-specific PEGylation of B2036-Alkyne. (A) Scheme of conjugation of PEG-azide to B2036-Alkyne via CuAAC. SDS-PAGE of purified site-specific B2036-PEG conjugates stained with (B) Coomassie to visualize protein and (C) 0.1 M iodine to visualize PEG. Lane 1: protein standards; lane 2: B2036-Alkyne; lane 3: B2036-5k mPEG; lane 4: B2036-10k mPEG; lane 5: B2036-20k mPEG.

Purified site-specifically PEGylated B2036 conjugates were then evaluated for bioactivity in Ba/F3-GHR cells and compared to pegvisomant and B2036-Alkyne. IC_{50} values

were found to be 17.7, 54.0, 68.8, 103.3, and 1289 nM for B2036-Alkyne, B2036-5k mPEG, B2036-10k mPEG, B2036-20k mPEG, and pegvisomant, respectively (Figure 4.6). These results emphasize the relationship between polymer size and bioactivity, as IC_{50} values increased with conjugation of larger polymers to B2036. Despite the reduction in bioactivity following PEGylation, the B2036-20 kDa mPEG conjugate (~42 kDa) demonstrated only 5.8-fold attenuation of bioactivity compared to a 72.8-fold reduction for multi-PEGylated pegvisomant of similar molecular weight (~42-52 kDa). This difference in IC_{50} cannot fully be explained by the slight differences in molecular weight between the two conjugates, but was rather a result of the specificity of the PEG attachment site.

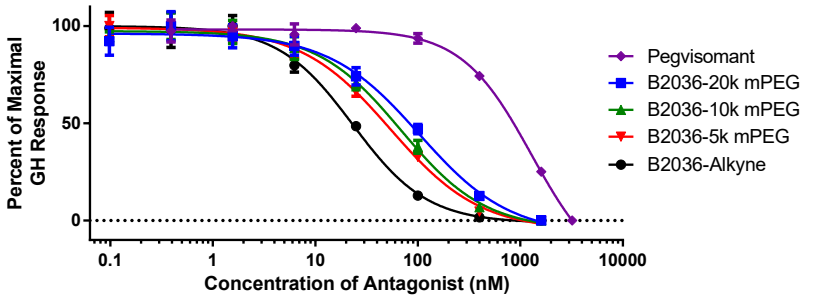

GHR Antagonist	IC_{50} (nM)	95% CI (nM)
Pegvisomant	1289	906.0-1833
B2036-20k mPEG	103.3	81.2-131.3
B2036-10k mPEG	68.8	58.0-81.7
B2036-5k mPEG	54.0	47.8-60.9
B2036-Alkyne	17.7	15.5-20.2

Figure 4.6. Inhibitory bioactivity dose response curves of B2036-Alkyne, site-specifically PEGylated B2036, and the multi-PEGylated pegvisomant in Ba/F3-GHR cells. The IC_{50} values for each GHR antagonist are displayed in the table to the right. All IC_{50} values were determined to be statistically different from each other ($p < 0.05$) except for B2036-5k mPEG and B2036-10k mPEG ($p > 0.05$) using one-way ANOVA with post-hoc analyses (Tukey's multiple comparisons test). Data is expressed as means with 95% confidence intervals (95% CI) of two individual experiments.

We expect that this site-specifically PEGylated B2036 variant will be of significant interest to researchers investigating GH regulation because it offers a number of advantages. First, the incorporation of pglY into B2036 not only retains the protein activity, but also provides access to the highly specific and orthogonal CuAAC click reaction. Neither azides nor alkynes

are cross-reactive with other canonical amino acid functional groups, ensuring that only one polymer can be conjugated to each protein. Additionally, azides and alkynes are stable to the conditions used for protein bioconjugation and these reactions demonstrate excellent conjugation efficiency.[47] This chemistry therefore offers an advantage over other methods where the nucleophile or electrophile is unstable in the aqueous conditions (such as succinimidyl esters). Furthermore, the resultant triazole is stable under biological conditions, whereas certain chemistries are not; for example thiol-maleimide linkages have demonstrated reversibility and may undergo retro-Michael reactions, although this issue has largely been addressed through the design of improved linkers.[47–50] The implementation of CuAAC as the conjugation chemistry also allows B2036-Alkyne to be conjugated to a broad variety of polymers, fluorophores, positron emission tomography probes, or any other azide-containing compound, many of which are either commercially available or synthetically accessible. Accordingly, this work illustrates the value of rational design coupled with click chemistry in the development of modular, site-specific protein-polymer conjugates.

An additional advantage conferred by this approach is the ability to tune the bioactivity of B2036 via modulation of polymer size. In this study, we observed an inverse relationship between polymer molecular weight and bioactivity. As the size of the polymer conjugated to B2036-Alkyne increases, so does its ability to block access to GHR binding sites, consequently reducing the observed bioactivity of the conjugate. Reduced bioactivity may also result from attenuated binding kinetics of B2036 to GHR due to polymer interference. We expect that a combination of these factors is likely responsible for lowering bioactivity for conjugates with larger conjugated polymers. Previous reports have also noted that conjugation of larger PEGs to GH or B2036 tended to reduce bioactivity compared to the unmodified protein, even for site-

specific conjugates.[30,36,37,51] Since proteins tend to exhibit longer circulation times with higher molecular weight PEGs, an inverse relationship between bioactivity and half-life as a function of polymer size is also likely, and has been evidenced with B2036.[30] We therefore expect that our conjugation strategy will be useful in exploring this balance between half-life and bioactivity since the molecular weight of the conjugate can be precisely tuned through addition of a single PEG.

Perhaps most importantly, these site-specific conjugates demonstrated significant improvement of bioactivity compared to the multi-PEGylated pegvisomant. This substantial improvement in bioactivity could contribute to reducing dosing requirements and consequently could help alleviate a portion of the economic burden associated with pegvisomant. Even with the diminished expression yield of B2036-Alkyne of 65% compared to native B2036, we expect the observed 12.5-fold improvement in activity of B2036-20 kDa mPEG over pegvisomant to sufficiently offset this cost. Generally, 65% incorporation efficiency of an unnatural amino acid is relatively high; for example, GH mutants containing a similar unnatural amino acid were prepared in titers ranging from 20-70% compared to the wild type protein depending on the incorporation site.[36] In addition to retaining bioactivity, incorporation of pglY in place of tyrosine 35 also provides B2036-Alkyne in good yield. With these promising results, it must also be acknowledged that improved bioactivity alone is insufficient to reduce dosing regimens if the protein therapeutic is rapidly cleared *in vivo*. Future studies will therefore need to be carried out to determine serum stability and pharmacokinetic parameters for these site-specific conjugates, and these studies are planned in our groups. We expect that the homogeneity of our conjugates as well as the ability to directly modulate protein activity with polymer size will greatly aid efforts toward this research.

4.3 Conclusions

In this work, we report the use of genetic code expansion to prepare a mutant of the GHR antagonist B2036 containing a single alkyne-functionalized residue in a region of the protein distal to its GHR binding domains. This mutation did not affect the bioactivity of B2036 in Ba/F3-GHR cells and facilitated site-specific PEGylation, which demonstrated substantial improvement in bioactivity over the nonspecifically PEGylated pegvisomant. We also established an inverse relationship between the molecular weight of the attached polymer and *in vitro* conjugate bioactivity, which is helpful information for future work focused on balancing bioactivity with pharmacokinetics. Taken together, we expect that our use of rational design and genetic code expansion to generate site-specific protein-polymer conjugates will be of significant interest to others working in the area of GH regulation.

4.4 Materials and Methods

4.4.1 Materials

All chemicals and bioreagents were purchased from Sigma-Aldrich or Fisher Scientific and used as received unless otherwise noted. 20 kDa mPEG-azide was purchased from Jenkem USA and 5 kDa and 10 kDa mPEG were purchased from Sigma-Aldrich and used as received. Boc-L-tyrosine methyl ester was purchased from ChemImpex and used as received. BTTAA was purchased from Click Chemistry Tools and used as received. Dichloromethane (DCM) was distilled over CaH_2 and stored under argon. Tetrahydrofuran (THF) was distilled over sodium/benzophenone and stored under argon. Mouse Ba/F3 cells stably expressing human GHR (Ba/F3-GHR) were obtained from Professor Michael Waters (University of Queensland, Australia). Ba/F3-GHR cells were cultured at 37 °C with 5% CO_2 in RPMI 1640 media (Gibco

RPMI 1640 with L-glutamine, 25 mM HEPES buffer), 5% Fetal Bovine Serum (FBS), 100 U/mL penicillin, 100 μg/mL streptomycin, 1% Glutamax, and 25 ng/mL recombinant human GH. Cells were generally subcultured every three days and split 1:10 into new media. Recombinant human GH was purchased from Dr. A.F. Parlow at the National Hormone and Peptide Program (Harbor-UCLA Medical Center, Torrance, CA) and was resuspended in PBS to 0.5 mg/mL. TEV protease was prepared based on the reported procedure.[52] Plasmids for expression of B2036 fusion constructs were designed by the authors; then the DNA was synthesized and cloned into pET21a expression vectors by Twist Biosciences. The plasmid containing the expanded genetic code machinery for incorporation of propargyl tyrosine via amber suppression was provided by Ryan Mehl (Oregon State University, Corvallis, OR) and is designated as pDule2-CNF (Addgene plasmid #85495).

4.4.2 Analytical Techniques

NMR spectra were obtained on Bruker AV 500 and AV 600 MHz spectrometers with a relaxation delay of 4 seconds for both proton and carbon experiments. Infrared absorption spectra were obtained using a PerkinElmer FT-IR equipped with an attenuated total reflectance (ATR) accessory. High-resolution mass spectra were obtained for small molecules using a Waters Acquity LCT Premier XE equipped with an autosampler and direct injection port. High-resolution mass spectra and peptide mapping were acquired using a Thermo Q Exactive Plus Orbitrap Mass Spectrometer equipped with a direct injection port and switchable UltiMate 3000 nanoLC. Peptide masses were analyzed using Thermo-Fisher Proteome Discoverer software version 1.4. SDS-PAGE was performed using Bio-Rad Any kD Mini-PROTEAN-TGX gels and gels were stained with Coomassie for visualization of protein or 0.1 N iodine for visualization of

PEG. SDS-PAGE protein standards were obtained from Bio-Rad (Precision Plus Protein Pre-stained Standards).

4.4.3 Methods

Plasmid Design

Plasmids were designed based on the previously reported construct[42] for the soluble expression of B2036 as a N-terminally tagged thioredoxin (TRX) fusion protein. For this work, a similar construct was engineered to contain an N-terminal TRX-His7-TEV solubility-enhancing, protease-cleavable tag that was then genetically fused to a codon optimized cDNA sequence encoding B2036 (Figure 4.7-Figure 4.9). To generate a propargyl tyrosine containing B2036 variant (B2036-Alkyne), the amber codon TAG was inserted into the sequence in place of the DNA encoding residue 35 of the original B2036 protein (Figure 4.10-Figure 4.12). Each of these sequences was synthesized and inserted into a pET21a expression vector via restriction cloning between *Bgl*II and *Xho*I sites by Twist Biosciences. These two plasmids were designated pET21a-TRX-B2036 and pET21a-TRX-B2036-Y35TAG for expression of B2036 and B2036-Alkyne, respectively. All plasmid sequences were verified by Sanger sequencing (Eurofins Genomics).

Expression of B2036 and B2036-Alkyne

Plasmids pET21a-TRX-B2036 and pET21a-TRX-B2036-Y35TAG were each transformed into *E. coli* Origami B (DE3) competent cells according to the manufacturer's protocol (Novagen). Plasmid pDule2-CNF, which constitutively expresses an amber-codon suppressing tyrosyl tRNA synthetase and cognate tRNA,[40] was co-transformed with plasmid pET21a-TRX-B2036-Y35TAG in order to provide the genetic code expansion machinery necessary for incorporation of propargyl tyrosine. 5 mL of a saturated overnight culture of each transformant was used to

inoculate 1 L of sterile LB medium in a 2.5 L baffled flask containing 50 μg/mL ampicillin for the single plasmid system (pET21a-TRX-B2036) or 50 μg/mL ampicillin and 50 μg/mL spectinomycin for the two-plasmid system (pET21a-TRX-B2036-Y35TAG and pDule2-CNF). Cells were grown at 37 °C with shaking at 250 rpm to an OD_{600} of 0.4, at which point protein expression was induced with IPTG to a final concentration of 0.1 mM. For the two-plasmid system, propargyl tyrosine was added to a final concentration of 1 mM simultaneous to IPTG addition. Following induction, cells were grown at 18 °C with shaking at 210 rpm for 20 hours then harvested by centrifugation for 15 min at 5,500 g (6,000 rpm; Beckman JA-14 rotor) and stored at -80 °C. Prior to lysis, cells were thawed and resuspended in 30 mL lysis buffer consisting of PBS, pH 7.4 with 150 mM NaCl, 1% Triton X-100, 10% glycerol, and 3 cOmplete Mini Protease Inhibitor Cocktail tablets (Roche). Cell lysis was then carried out by passing cells through an Avestin Emulsiflex C-3 homogenizer two times at 1240 bar with cooling. Crude cell lysates were then clarified via centrifugation for 60 min at 48,300 g (20,000 rpm; Beckman JA-25.50 rotor) and the supernatant was collected for purification.

Purification of B2036 and B2036-Alkyne

Purification was carried out identically for both B2036 and B2036-Alkyne fusion proteins. Supernatant containing protein was filtered through a 0.45 μM syringe filter and then incubated with 5 mL of Ni-NTA resin at 4 °C with gentle rocking for 30 min. The supernatant Ni-NTA slurry was then poured into a gravity column and the flow through was poured back over the column twice to maximize binding. The resin was then washed with 6 column volumes (CV) wash buffer 1 (PBS, pH 7.4, with 150 mM NaCl, 10 mM imidazole, 0.1% Triton X-100, and 10% glycerol), then with 4 CV of wash buffer 2 (PBS, pH 7.4 with 150 mM NaCl, 20 mM imidazole, and 10% glycerol), then the column was eluted with 5 CV elution buffer (PBS, pH 7.4

with 150 mM NaCl, 200 mM imidazole, and 10% glycerol). Fractions were analyzed by SDS-PAGE, and pure fusion protein fractions were combined and buffer exchanged by centrifugal filtration with 30 kDa MW filters into PBS, pH 7.4 with 150 mM NaCl and 10% glycerol. Cleavage of the TRX-His7-TEV tag was then facilitated by incubation of the purified fusion proteins with TEV protease (100:1 mass ratio) for 18 hours at 4 °C. The digested TRX-His7-TEV tag was then removed via reverse Ni-NTA affinity chromatography. Column flow through was collected and pure protein fractions were combined and concentrated by centrifugal filtration with 10 kDa MW filters. Protein concentration was measured using bicinchoninic acid (BCA) assay (Pierce) and protein purity was assessed by SDS-PAGE.

Intact Mass Analysis and Peptide Mapping Analysis

Purified B2036 and B2036-Alkyne were analyzed by intact mass spectrometry and peptide mapping using a Thermo Q Exactive Plus Orbitrap Mass Spectrometer equipped with a direct injection port and switchable UltiMate 3000 nanoLC. For intact mass spectrometry, purified protein samples were desalted by dialyzing overnight against MilliQ ultrapure water, then filtered through 0.22 μM syringe filters, and the masses were determined following continuous direct sample injection at 50 μl/min using an auxilary syringe pump with acquisition over 30 s. Mass deconvolution was performed using the instrument software. To obtain peptide fragments of the purified proteins for peptide mapping, trypsin digests were performed according to the manufacturer's protocol using MS grade trypsin protease (Pierce). Following digestions, samples were desalted and prepared for analysis as previously reported using Empore stage-tips.[53] Following elution from stage-tips, samples were dried using a speed vac then resuspended in 100 μl 0.5% formic acid in ultrapure water to 0.2 μg/μl. 1.0 μl of each sample was injected onto the spectrometer after first passing through an UltiMate 3000 nanoLC equipped with a 75 μm x 2 cm

Acclaim PepMap 100 trap column packed with C18 3 μm bulk resins (Thermo Scientific) and a 75 μm x 15 cm Acclaim PepMap RSLC analytical column packed with C18 2 μm resin (Thermo Scientific) using a method of 3-35% Mobile Phase B over 40 min, then 35-85% Mobile Phase B over 5 min (Mobile Phase A: H_2O with 0.1% formic acid; Mobile Phase B: acetonitrile with 0.1% formic acid; 0.3 μl/min). The spectrometer ESI voltage was set to 1.9 kV with a capillary temperature of 275 °C. Full spectra from m/z 350 - 2000 were acquired in profile mode with resolution 70,000 at m/z 200 with an automated gain control (AGC) target of 3×10^6. The most abundant 15 ions were further fragmented by higher-energy collisional dissociation (HCD) with a normalized collisional energy of 25. MS/MS spectra were acquired in centroid mode with resolution 17,500 at m/z 200. The AGC target for fragment ions are set at 2×10^4 with maximum injection time of 50 ms. Dynamic exclusion was set at 45.0 s. The resultant raw data was then analyzed using Proteome Discoverer software version 1.4 (Thermo Scientific) by searching against a subset of the uniprot human database modified to contain the expected protein sequence using the following parameters: precursor mass tolerance was set to ± 10 ppm, fragment mass tolerance was set to ± 0.02 Th for HCD, false discovery rate was set to 1.0%, up to 2 trypsin miscleavages were allowed, a minimum of 1 peptide was required for protein identification, and variable modifications were set to include methionine oxidation and tyrosine propargylation.

PEGylation of B2036-Alkyne

PEGylation of B2036-Alkyne was carried out according to standard copper-catalyzed azide-alkyne click chemistry conditions.[44] All stock solutions were prepared using 100 mM phosphate buffer and this buffer was added to the reaction solution to achieve a final protein concentration of 1 mg/mL. General procedure: In a 1.5 mL conical tube was added 1 mg (261.1 μl; 3.83 mg/mL stock) B2036-Alkyne, 10 molar equivalents of either 5, 10, or 20 kDa mPEG-azide (113

µl, 226 µl, or 453 µl of a 20 mg/mL stock, respectively), and enough 100 mM phosphate buffer to reach a final reaction volume of 1 mL once all remaining components had been added. Next, a $CuSO_4$ stock solution (20 mM) was premixed with a BTTAA ligand stock solution (50 mM) in a 1:2 ratio of $CuSO_4$:BTTAA before a 30 µl aliquot of this premixed solution was added to the B2036-Alkyne solution to a final concentration of 0.2 mM $CuSO_4$ and 1 mM BTTAA. Aminoguanidine hydrochloride was then added to the reaction solution to a final concentration of 5 mM (50 µl; 100 mM stock). Finally, sodium ascorbate was added to the reaction solution to a final concentration of 5 mM (50 µl; 100 mM stock) and the conical tube was sealed and rocked gently at 20 °C for 2 hours. Reactions were monitored by SDS-PAGE and stained with Coomassie to visualize protein and with 0.1 M iodine to visualize PEG. Conjugates were purified and analyzed by FPLC on a Bio-Rad BioLogic DuoFlow chromatography system equipped with a 1 mL GE Healthcare HiTrap Q HP column using a method of 0 to 1 M NaCl in 10 mM PB, pH 7.4, 10% glycerol (Buffer A: 10 mM PB, pH 7.4, 10% glycerol; Buffer B: 10 mM PB, pH 7.4, 10% glycerol + 1 M NaCl; 0.5 mL/min; 1 mg/0.25 mL injections; 4 CV 0% Buffer B, then 8 CV 0-100% linear gradient Buffer B, then 2 CV 100% Buffer B). Concentration of PEGylated B2036 was determined via BCA assay and protein purity was assessed by SDS-PAGE. Endotoxin levels were measured for all proteins and conjugates using a Pierce LAL Chromogenic Endotoxin Quantification Kit following the manufacturer's recommendations.

Cell Viability Assay

Ba/F3-GHR cells were serum starved for 16 h, then plated at 20,000 cells per well (80 µl) in 5% serum media in the interior wells of a Corning Costar 96-well plate; outer wells were filled with sterile water or media to prevent edge effects. 10 µl of serial dilutions of B2036 variants and conjugates in assay media were added to cells to final protein concentrations ranging from 0-

1,600 nM, and cells were incubated at ambient temperature for 20 min (n=6 replicates per condition). Next, 10 µl of GH solution was added to each well to a final concentration of 20 ng/mL, and cells were incubated at 37 °C with 5% CO_2 for 48 hours. Cell viability was determined by addition of 5 µl resazurin sodium salt (0.5 mg/mL) to each well followed by incubation at 37 °C with 5% CO_2 for 2 hours. Fluorescence measurements were recorded using a Tecan Infinite M1000 Pro automated plate reader system with an excitation wavelength of 560 nm and an emission wavelength of 590 nm. Statistical analysis and non-linear regression analysis of the resulting values were analyzed using GraphPad Prism software version 6.01. Data is expressed as means with 95% CI and data sets were compared using Student's t-test or one-way ANOVA with post-hoc analyses (Tukey's multiple comparisons test) as necessary. *In vitro* assays were repeated at least two times with a representative figure shown. A p-value of <0.05 was used to determine statistical significance. Half-maximal inhibitory concentration (IC_{50}) values of each antagonist were determined by fitting a sigmoidal dose-response model "log (agonist) vs. response-variable slope (four parameters)."

Synthesis of 5 kDa mPEG-Tosylate

To an oven-dried 50 mL 2-neck round bottom flask equipped with a stir bar, septum, and gas adapter was added 20 mL of dichloromethane (DCM) and 5 kDa mPEG (1.000 g, 0.20 mmol, 1 equiv). Once dissolved, tosyl chloride (0.191 g, 1.00 mmol, 5 equiv) was added followed by dropwise addition of triethylamine (0.139 ml, 1.00 mmol, 5 equiv) and the reaction was stirred at 20 °C for 19 h. Anhydrous K_2CO_3 was then added to the reaction and allowed to stir for 10 min before filtering the reaction and concentration under vacuum to a light tan oil. This oil was diluted with minimal DCM and precipitated three times into diethyl ether to yield a white solid (0.945 g, 91.7% yield). See Figure 4.17 for assigned ^{1}H NMR (500 MHz, $CDCl_3$): δ 7.79 (d, J =

8.0 Hz, 2H), 7.33 (d, J = 8.3 Hz, 2H), 4.15 (t, J = 4.9 Hz, 2H), 3.64 (m, 537H), 3.37 (s, 3H), 2.44 (s, 3H).

Synthesis of 10 kDa mPEG-Tosylate

To an oven-dried 25 mL 2-neck round bottom flask equipped with a stir bar, septum, and gas adapter was added 10 mL of DCM and 10 kDa mPEG (0.500 g, 0.05 mmol, 1 equiv). Once dissolved, tosyl chloride (0.095 g, 0.50 mmol, 10 equiv) was added followed by dropwise addition of triethylamine (0.070 mL, 0.50 mmol, 10 equiv) and the reaction was stirred at 20 °C for 24 h. Anhydrous K_2CO_3 was then added to the reaction and allowed to stir for 10 min before filtering the reaction and concentration under vacuum to a light tan oil. This oil was diluted with minimal DCM and precipitated three times into diethyl ether to yield a white solid (0.461 g, 90.8% yield). See Figure 4.18 for assigned ^{1}H NMR (500 MHz, $CDCl_3$): δ 7.78 (d, J = 8.3 Hz, 2H), 7.32 (d, J = 8.0 Hz, 2H), 4.14 (t, J = 4.9 Hz, 2H), 3.63 (m, 537H), 3.36 (s, 3H), 2.43 (s, 3H).

Synthesis of 5 kDa mPEG-Azide

To an oven-dried 2-neck 25 mL round bottom flask equipped with a stir bar, glass stopper, and condenser was added 10 mL of ethanol followed by 5 kDa mPEG-Tosylate (0.500 g, 0.10 mmol, 1 equiv) and sodium azide (0.033 g, 0.50 mmol, 5 equiv). The mixture was heated to 80 °C in an oil bath for 15 h then removed from heat and allowed to cool to room temperature before concentrating the solution under vacuum. The crude material was then dissolved in ethyl acetate and washed twice with water, then the aqueous layer was extracted 3 times with DCM and the combined organics were dried over anhydrous magnesium sulfate and dried under vacuum to yield a colorless oil. This oil was then diluted with minimal DCM and precipitated in diethyl ether 3 times to yield a white solid (0.388 g, 77.7% yield). See Figure 4.19 for assigned ^{1}H NMR (500 MHz, $CDCl_3$): δ 3.63 (m, 527H), 3.38 (t, J = 5.4 Hz, 2H), 3.37 (s, 3H).

Synthesis of 10 kDa mPEG-Azide

To an oven-dried 2-neck 25 mL round bottom flask equipped with a stir bar, glass stopper, and condenser was added 10 mL of ethanol followed by 10 kDa mPEG-Tosylate (0.100 g, 0.01 mmol, 1 equiv) and sodium azide (0.007 g, 0.10 mmol, 10 equiv). The mixture was heated to 80 °C in an oil bath for 19 h then removed from heat and allowed to cool to room temperature before concentrating the solution under vacuum. The crude material was then partitioned between DCM and water and the organic layer was collected. The aqueous layer was then extracted 3 times with DCM and the combined organics were dried over anhydrous magnesium sulfate and dried under vacuum to yield a colorless oil. This oil was then diluted with minimal DCM and precipitated in diethyl ether 3 times to yield a white solid (0.088 g, 89.4% yield). See Figure 4.20 for assigned ^{1}H NMR (600 MHz, $CDCl_3$): δ 3.64 (m, 927H), 3.39 (t, J = 5.1 Hz, 2H), 3.38 (s, 3H).

Synthesis of Boc-L-Propargyl Tyrosine Methyl Ester

To an oven dried 1-neck 100 mL round bottom flask equipped with a stir bar and water condenser was added Boc-L-tyrosine methyl ester (2.000 g, 6.77 mmol, 1 equiv), anhydrous K_2CO_3 (2.808 g, 20.32 mmol, 3 equiv) and 40 mL acetone. The reaction was stirred for several minutes before dropwise addition of propargyl bromide (2.998 mL of 80% solution in toluene, 20.32 mmol, 3 equiv) at ambient temperature. The reaction was then refluxed (72 °C) for 23 hours. After cooling to ambient temperature, the reaction was concentrated under vacuum then partitioned between DCM and water and the organic layer was collected. The aqueous layer was extracted 3 times with DCM. The combined organics were dried over anhydrous magnesium sulfate, filtered, and concentrated under vacuum. The resulting crude oil was then purified via

silica flash column chromatography using a Biotage Isolera One system equipped with a 50 g SNAP KP-Sil cartridge using a method of 5-40% ethyl acetate in hexane and a flow rate of 100 mL/min (R_f = 0.29; 4:1 hexane:ethyl acetate). Fractions containing the desired product were combined and concentrated under vacuum to give an orange oil (yield determined following deprotection steps). See Figure 4.21 for assigned ^{1}H NMR (500 MHz, $CDCl_3$): δ 7.01 (d, J = 8.5 Hz, 2H), 6.85 (d, J = 8.7 Hz, 2H), 5.01 (d, J = 8.1 Hz, 1H), 4.61 (d, J = 2.5 Hz, 2H), 4.50 (q, J = 6.6 Hz, 1H), 3.66 (s, 3H), 3.02 (dd, J_1 = 13.9 Hz, J_2 = 5.7 Hz, 1H), 2.94 (dd, J_1 = 13.9 Hz, J_2 = 6.2 Hz, 1H), 2.49 (t, J = 2.4 Hz, 1H), 1.37 (s, 9H). See Figure 4.22 for assigned ^{13}C NMR (125 MHz, $CDCl_3$): δ 172.4, 156.6, 155.1, 130.3, 129.0, 114.9, 79.8, 78.6, 75.6, 55.8, 54.5, 52.2, 37.4, 28.3. FT-IR: ν 3434, 3386, 3305, 2980, 2935, 2871, 2123, 1738, 1708. HRMS: $C_{18}H_{23}NO_5$ calc. $[M+H]^+$ = 356.1474 Da; obsd. $[M+H]^+$ = 356.1473 Da.

Synthesis of L-Propargyl Tyrosine

Boc-L-propargyl tyrosine methyl ester was dissolved in a mixture of aqueous 1 M NaOH (4 mL) and acetonitrile (4 mL) and stirred for 16 hours at ambient temperature. The solution was then diluted with water, neutralized with citric acid, and extracted 3 times with DCM. The combined organics were dried over anhydrous magnesium sulfate, filtered, and dried under vacuum to yield an orange oil that was immediately taken into the next step. The orange oil was dissolved in 10 mL 45:45:5:5 DCM:TFA:H_2O:TIPS in a 20 mL glass vial and stirred for approximately 10 min before concentrating the solution under vacuum. Once concentrated, the remaining viscous liquid was precipitated twice into 1:1 hexane:diethyl ether to yield a white solid (1.039 g, 70.0% yield over 2 steps) that was determined to be >98% pure by analytical HPLC (Figure S19) and >96% pure by ^{1}H NMR. See Figure 4.23 for assigned ^{1}H NMR (500 MHz, D_2O): δ 7.15 (d, J = 8.6 Hz, 2H), 6.94 (d, J = 8.6 Hz, 2H), 4.68 (s, 2H), 3.84 (dd, J_1 = 7.7 Hz, J_2 = 5.2 Hz, 1H), 3.11 (dd, J_1 =

14.7 Hz, J_2 = 5.2 Hz, 1H), 2.96 (dd, J_1 = 14.7 Hz, J_2 = 7.8 Hz, 1H), 2.82 (t, J = 2.2 Hz, 1H). See Figure 4.24 for assigned ^{13}C NMR (125 MHz, D_2O): δ 173.8, 156.1, 130.6, 128.5, 115.6, 78.7, 76.6, 56.0, 56.0, 35.4. FT-IR: ν 3296, 2997, 2964, 2922, 2866, 2135, 1611, 1555, 1512 cm^{-1}. HRMS: $C_{12}H_{13}NO_3$ calc. $[M+H]^+$ = 220.0974 Da; obsd. $[M+H]^+$ = 220.0932 Da.

4.5 Appendix C

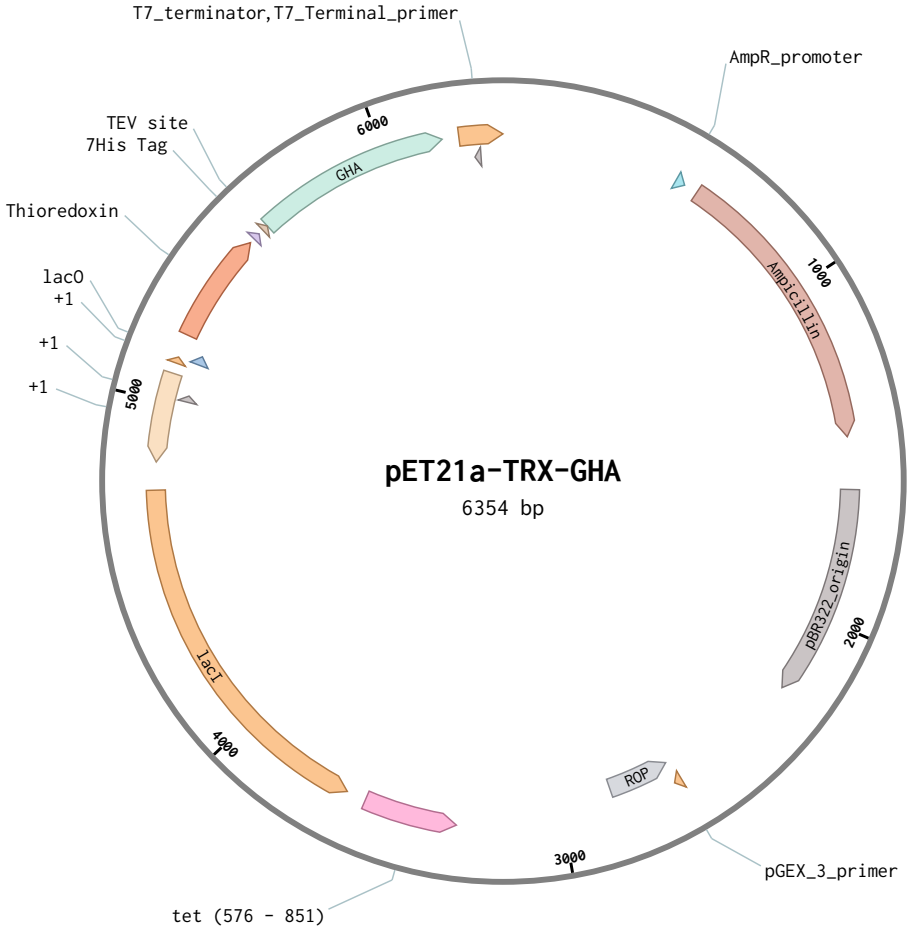

Figure 4.7. Plasmid map of vector used to express TRX-B2036 fusion protein.

ATGAGCGATAAAATTATTCACCTGACTGACGACAGTTTTGACACGGATGTACTCAAAGCGGACG
GGGCGATCCTCGTCGATTTCTGGGCAGAGTGGTGCGGTCCGTGCAAAATGATCGCCCCGATTCT
GGATGAAATCGCTGACGAATATCAGGGCAAACTGACCGTTGCAAAACTGAACATCGATCAAAAC
CCTGGCACTGCGCCGAAATATGGCATCCGTGGTATCCCGACTCTGCTGCTGTTCAAAAACGGTG
AAGTGGCGGCAACCAAAGTGGGTGCACTGTCTAAAGGTCAGTTGAAAGAGTTCCTCGACGCTAA
CCTGGCCGGTTCTGGTTCTGGCCATCACCATCATCATCATCATGGGAGCGGTTCCGGCGAGAAT
CTGTATTTCCAGGGATTCCCGACGATCCCTCTGTCCCGTTTGTTCGATAATGCCATGCTGCGTG
CTGACCGTCTGAATCAACTGGCATTCGATACCTATCAAGAATTTGAAGAGGCGTACATCCCGAA
AGAACAAAAGTATAGCTTTCTGCAGAATCCGCAGACCAGCCTGTGCTTTAGCGAGAGCATCCCG
ACCCCAAGCAACCGTGAGGAAACGCAACAGAAAAGCAACCTGGAATTGTTACGTATTAGCCTGC
TGTTGATTCAGTCTTGGCTGGAACCGGTTCAATTCCTCCGCAGCGTGTTTGCGAACAGCCTGGT
GTACGGCGCAAGCGACAGCAATGTTTACGACCTGTTGAAAGATCTGGAAGAGAAAATTCAGACT
CTGATGGGTCGCCTTGAGGATGGCAGCCCGCGTACCGGTCAGATCTTCAAGCAAACGTACTCTA
AGTTTGACACCAACTCCCACAACGACGATGCGCTGCTGAAGAATTATGGCCTGCTGTACTGTTT
CAACGCCGACATGTCGCGTGTTAGCACCTTCCTGCGCACGGTCCAGTGTCGCAGCGTCGAGGGT
TCCTGCGGTTTT

Figure 4.8. cDNA sequence of TRX-B2036 fusion protein in plasmid pET21a-TRX-B2036. The cDNA has been color coded as follows: TRX (red), spacer regions (black), His7 tag (blue), TEV protease recognition site (orange), and B2036 (green). To facilitate TEV digestion of the translated protein, three additional base pairs (GGA) were added to the sequence of B2036 (green) to encode one additional N-terminal glycine residue.

MSDKIIHLTDDSFDTDVLKADGAILVDFWAEWCGPCKMIAPILDEIADEYQGKLTVAKLNIDQN

PGTAPKYGIRGIPTLLLFKNGEVAATKVGALSKGQLKEFLDANLAGSGSGHHHHHHHGSGSGEN

LYFQGFPTIPLSRLFDNAMLRADRLNQLAFDTYQEFEEAYIPKEQKYSFLQNPQTSLCFSESIP

TPSNREETQQKSNLELLRISLLLIQSWLEPVQFLRSVFANSLVYGASDSNVYDLLKDLEEKIQT

LMGRLEDGSPRTGQIFKQTYSKFDTNSHNDDALLKNYGLLYCFNADMSRVSTFLRTVQCRSVEG

SCGF

Figure 4.9. Amino acid sequence of TRX-B2036 fusion protein. The amino acids have been color coded as follows: TRX (red), spacer regions (black), His7 tag (blue), TEV protease recognition site (orange), and B2036 (green). Following TEV cleavage, one glycine residue is added to the N-terminal sequence of B2036.

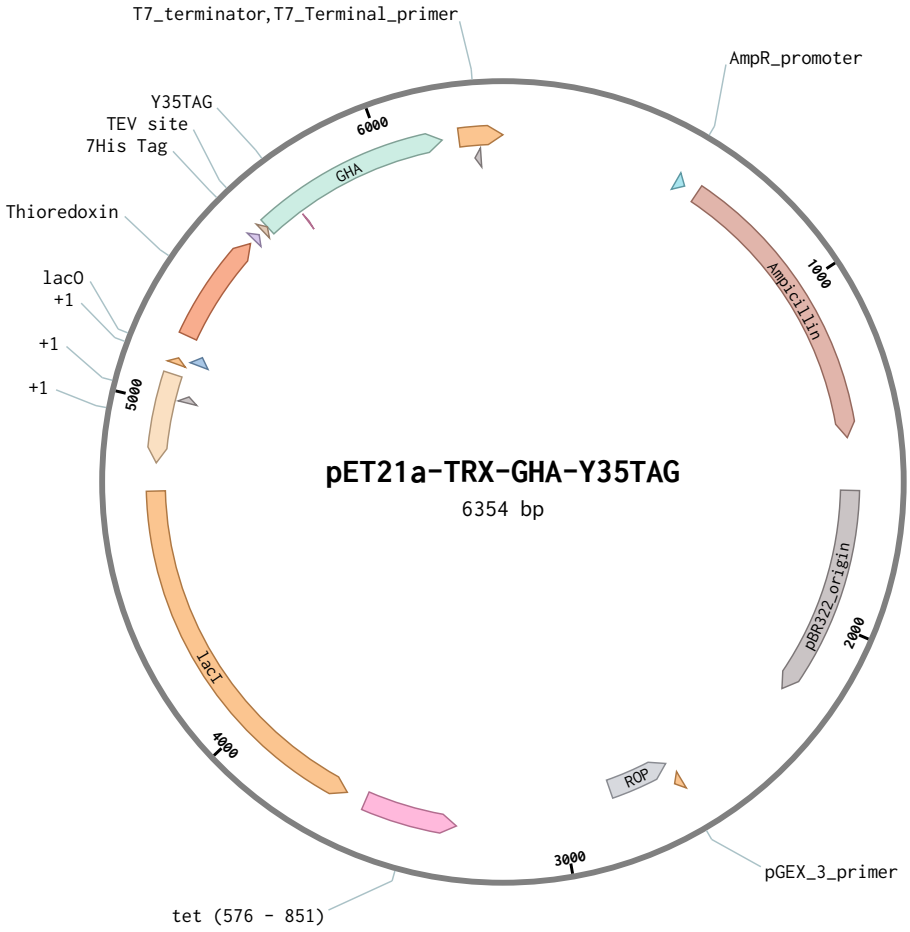

Figure 4.10. Plasmid map of vector used to express TRX-B2036-Alkyne fusion protein.

ATGAGCGATAAAATTATTCACCTGACTGACGACAGTTTTGACACGGATGTACTCAAAGCGGACG

GGGCGATCCTCGTCGATTTCTGGGCAGAGTGGTGCGGTCCGTGCAAAATGATCGCCCCGATTCT

GGATGAAATCGCTGACGAATATCAGGGCAAACTGACCGTTGCAAAACTGAACATCGATCAAAAC

CCTGGCACTGCGCCGAAATATGGCATCCGTGGTATCCCGACTCTGCTGCTGTTCAAAAACGGTG

AAGTGGCGGCAACCAAAGTGGGTGCACTGTCTAAAGGTCAGTTGAAAGAGTTCCTCGACGCTAA

CCTGGCCGGTTCTGGTTCTGGCCATCACCATCATCATCATCATGGGAGCGGTTCCGGCGAGAAT

CTGTATTTCCAGGGATTCCCGACGATCCCTCTGTCCCGTTTGTTCGATAATGCCATGCTGCGTG

CTGACCGTCTGAATCAACTGGCATTCGATACCTATCAAGAATTTGAAGAGGCGTAGATCCCGAA

AGAACAAAAGTATAGCTTTCTGCAGAATCCGCAGACCAGCCTGTGCTTTAGCGAGAGCATCCCG

ACCCCAAGCAACCGTGAGGAAACGCAACAGAAAAGCAACCTGGAATTGTTACGTATTAGCCTGC

TGTTGATTCAGTCTTGGCTGGAACCGGTTCAATTCCTCCGCAGCGTGTTTGCGAACAGCCTGGT

GTACGGCGCAAGCGACAGCAATGTTTACGACCTGTTGAAAGATCTGGAAGAGAAAATTCAGACT

CTGATGGGTCGCCTTGAGGATGGCAGCCCGCGTACCGGTCAGATCTTCAAGCAAACGTACTCTA

AGTTTGACACCAACTCCCACAACGACGATGCGCTGCTGAAGAATTATGGCCTGCTGTACTGTTT

CAACGCCGACATGTCGCGTGTTAGCACCTTCCTGCGCACGGTCCAGTGTCGCAGCGTCGAGGGT

TCCTGCGGTTTT

Figure 4.11. cDNA sequence of TRX-B2036-Alkyne fusion protein in plasmid pET21a-TRX-B2036-Y35TAG. The cDNA has been color coded as follows: TRX (red), spacer regions (black), His7 tag (blue), TEV protease recognition site (orange), and B2036 (green). To facilitate TEV digestion of the translated protein, three additional base pairs (GGA) were added to the sequence of B2036 (green) to encode one additional N-terminal glycine residue. Underlining indicates replacement of Tyrosine 35 codon with amber stop codon.

MSDKIIHLTDDSFDTDVLKADGAILVDFWAEWCGPCKMIAPILDEIADEYQGKLTVAKLNIDQN

PGTAPKYGIRGIPTLLLFKNGEVAATKVGALSKGQLKEFLDANLAGSGSGHHHHHHHGSGSGEN

LYFQGFPTIPLSRLFDNAMLRADRLNQLAFDTYQEFEEAYIPKEQKYSFLQNPQTSLCFSESIP

TPSNREETQQKSNLELLRISLLLIQSWLEPVQFLRSVFANSLVYGASDSNVYDLLKDLEEKIQT

LMGRLEDGSPRTGQIFKQTYSKFDTNSHNDDALLKNYGLLYCFNADMSRVSTFLRTVQCRSVEG

SCGF

Figure 4.12. Schematic and amino acid sequence of TRX-B2036 fusion protein. The amino acids have been color coded as follows: TRX (red), spacer regions (black), His7 tag (blue), TEV protease recognition site (orange), B2036 (green), and Y35pglY mutation (yellow). Following TEV cleavage, one glycine residue is added to the N-terminal sequence of B2036. Underlining indicates replacement of Tyrosine 35 with propargyl Tyrosine.

Table 4.1. Peptide mass table for sample tandem mass spectrum of the peptide ADRLNQLAFDTYQEFEEA(pglY)IPK in LC/ESI/MS analysis following trypsin digestion of B2036-Alkyne with assigned y- and b- series ions (blue and red, respectively).

#1	b^{+}	b^{2+}	b^{3+}	Seq.	y^{+}	y^{2+}	y^{3+}	#2
1	72.04440	36.52584	24.68632	A				22
2	187.07135	94.03931	63.02863	D	2628.26175	1314.63451	876.75877	21
3	343.17247	172.08987	115.06234	R	2513.23480	1257.12104	838.41645	20
4	456.25654	228.63191	152.75703	L	2357.13368	1179.07048	786.38274	19
5	570.29947	285.65337	190.77134	N	2244.04961	1122.52844	748.68805	18
6	698.35805	349.68266	233.45753	Q	2130.00668	1065.50698	710.67374	17
7	811.44212	406.22470	271.15222	L	2001.94810	1001.47769	667.98755	16
8	882.47924	441.74326	294.83126	A	1888.86403	944.93565	630.29286	15
9	1029.54766	515.27747	343.85407	F	1817.82691	909.41709	606.61382	14
10	1144.57461	572.79094	382.19639	D	1670.75849	835.88288	557.59101	13
11	1245.62229	623.31478	415.87895	T	1555.73154	778.36941	519.24870	12
12	1408.68561	704.84644	470.23339	Y	1454.68386	727.84557	485.56614	11
13	1536.74419	768.87573	512.91958	Q	1291.62054	646.31391	431.21170	10
14	1665.78679	833.39703	555.93378	E	1163.56196	582.28462	388.52550	9
15	1812.85521	906.93124	604.95659	F	1034.51936	517.76332	345.51130	8
16	1941.89781	971.45254	647.97079	E	887.45094	444.22911	296.48850	7
17	2070.94041	1035.97384	690.98499	E	758.40834	379.70781	253.47430	6
18	2141.97753	1071.49240	714.66403	A	629.36574	315.18651	210.46010	5
19	2343.05650	1172.03189	781.69035	pglY	558.32862	279.66795	186.78106	4
20	2456.14057	1228.57392	819.38504	I	357.24965	179.12846	119.75473	3
21	2553.19334	1277.10031	851.73596	P	244.16558	122.58643	82.06004	2
22				K	147.11281	74.06004	49.70912	1

A

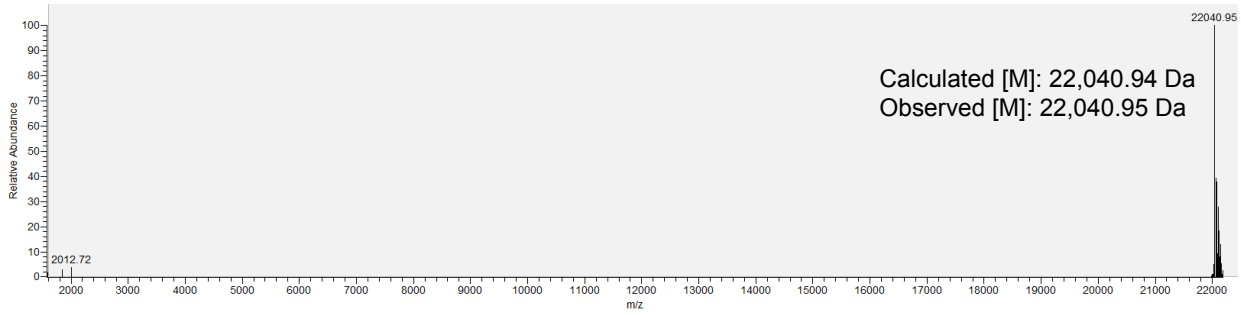

B

GFPTIPLSRLFDNAMLRADRLNQLAFDTYQ
EFEEAYIPKEQKYSFLQNPQTSLCFSESIP
TPSNREETQQKSNLELLRISLLLIQSWLEP
VQFLRSVFANSLVYGASDSNVYDLLKDLEE
KIQTLMGRLEDGSPRTGQIFKQTYSKFDTN
SHNDDALLKNYGLLYCFNADMSRVSTFLRT
VQCRSVEGSCGF

Figure 4.13. Mass spectral analysis of B2036. (A) Deconvoluted intact HR-MS of B2036. (B) Sequence coverage map of B2036-Alkyne was determined following digestion of the purified protein with trypsin and identification of the resulting peptides via LC/ESI/MS/MS. Sequence coverage was determined to be 100% with 100% sequence match.

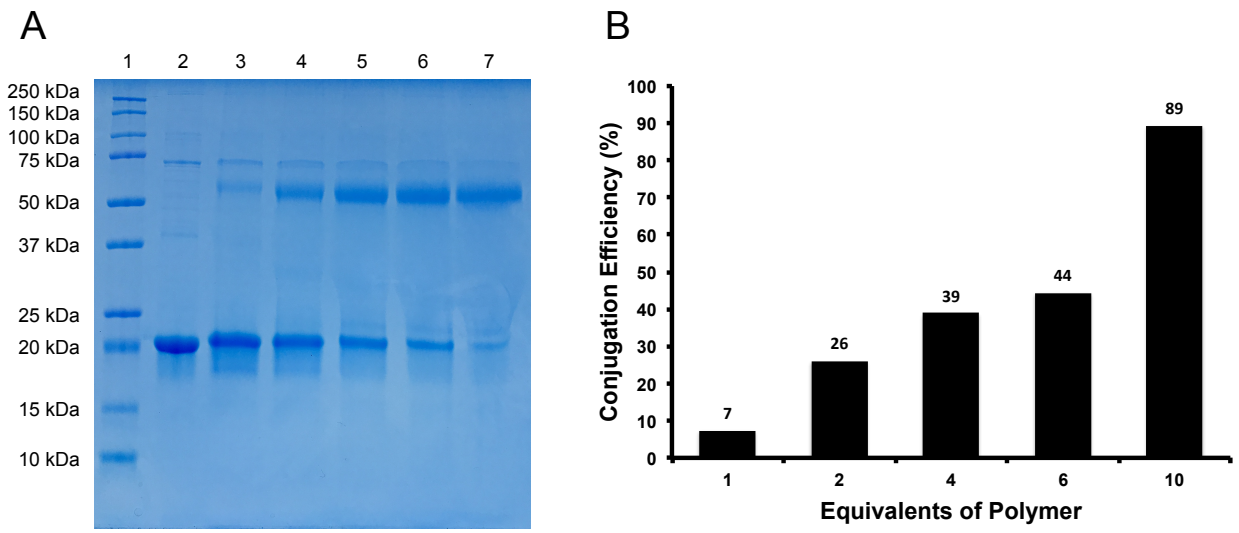

Figure 4.14. Optimization of PEG equivalents for conjugation to B2036-Alkyne. (A) SDS-PAGE of B2036-Alkyne conjugation reactions with 1-10 equivalents of 20 kDa mPEG-azide visualized with Coomassie staining. Lane 1: protein standards; lane 2: B2036-Alkyne; lane 3-7: B2036-Alkyne with 1, 2, 4, 6, and 10 equivalents of 20 kDa mPEG-azide, respectively. (B) Plot of conjugation efficiency against equivalents of PEG per protein estimated using ImageJ software from the Coomassie stained SDS-PAGE.

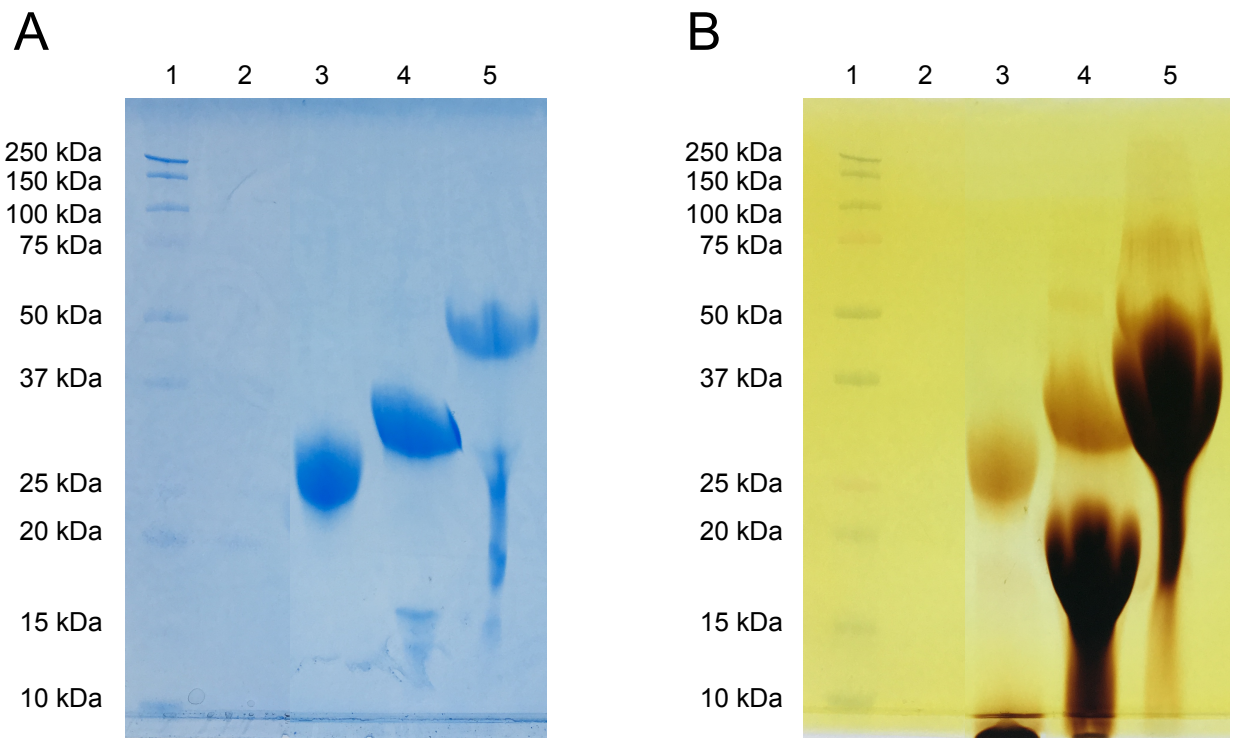

Figure 4.15. SDS-PAGE of crude conjugation reactions to make site-specific B2036-PEG conjugates stained with (A) Coomassie to visualize protein and (B) 0.1 M iodine to visualize PEG. Lane 1: protein standards; lane 2: B2036-Alkyne; lane 3: B2036-5k mPEG; lane 4: B2036-10k mPEG; lane 5: B2036-20k mPEG. For each SDS-PAGE image above, lanes 1-2 were spliced together with lanes 3-5 from the same SDS-PAGE experiment in order to remove extraneous lanes. Cropping was carried out without resizing, recoloring, or making any other alterations to the appearance of the image.

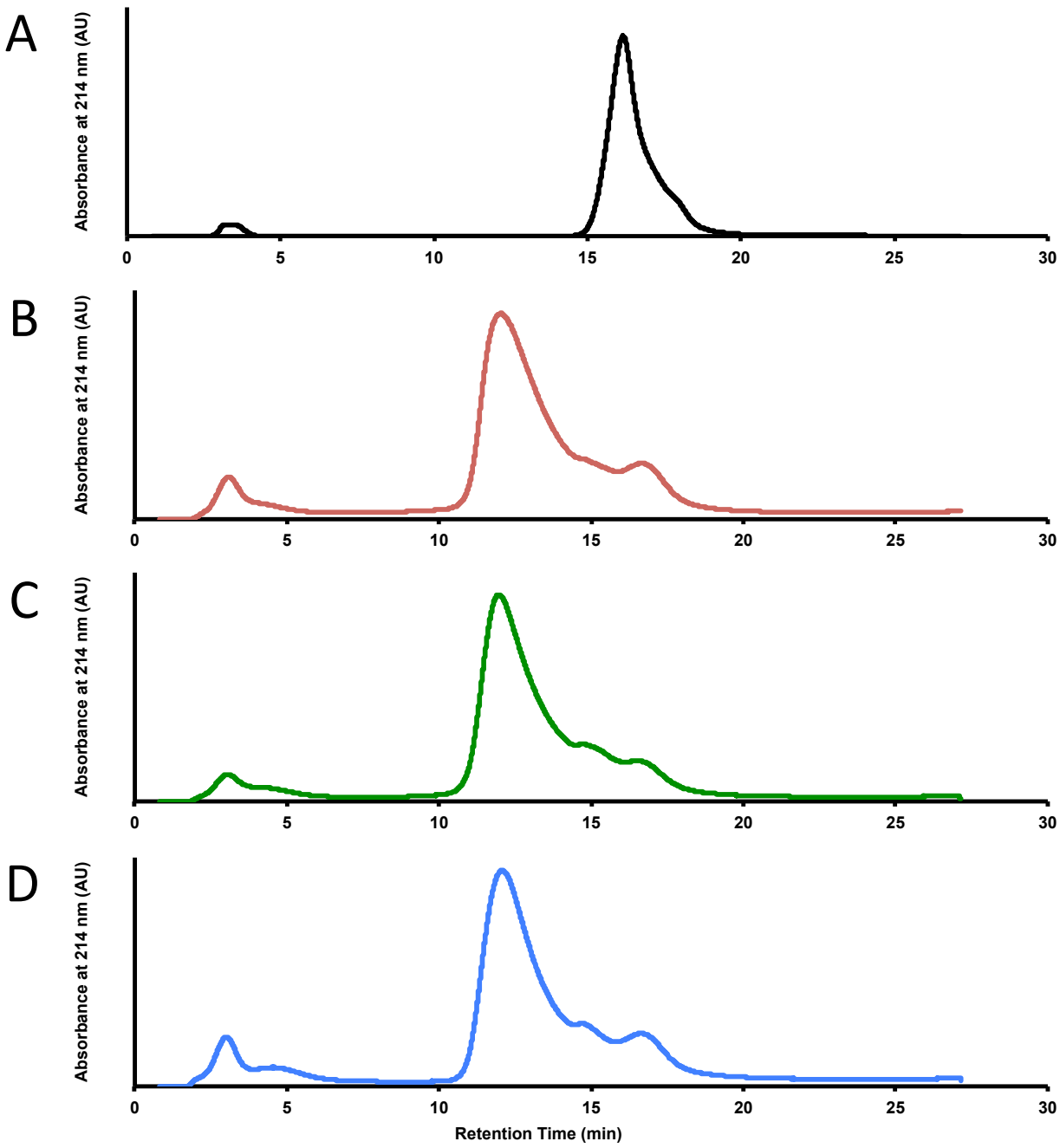

Figure 4.16. FPLC chromatograms of (A) unmodified B2036-Alkyne, (B) B2036-5k mPEG, (C) B2036-10k mPEG, (D) B2036-20k mPEG. PEG elutes with the solvent front at approximately 3 minutes, conjugates elute at approximately 12 minutes, and unmodified B2036-Alkyne elutes at approximately 17 minutes.

Scheme 4.1. Synthesis of mPEG-azide.

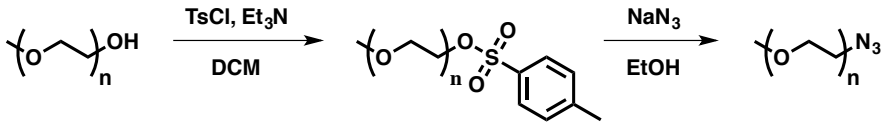

Scheme 4.2. Synthesis of propargyl tyrosine.

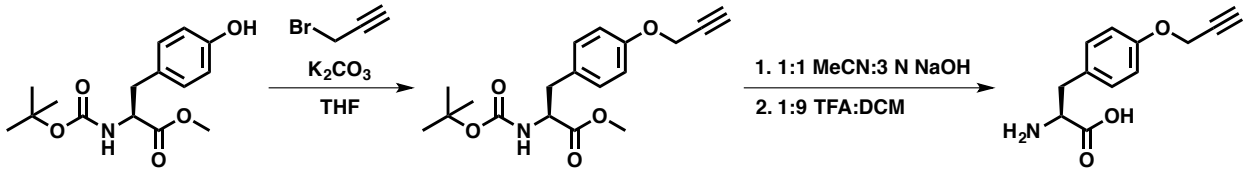

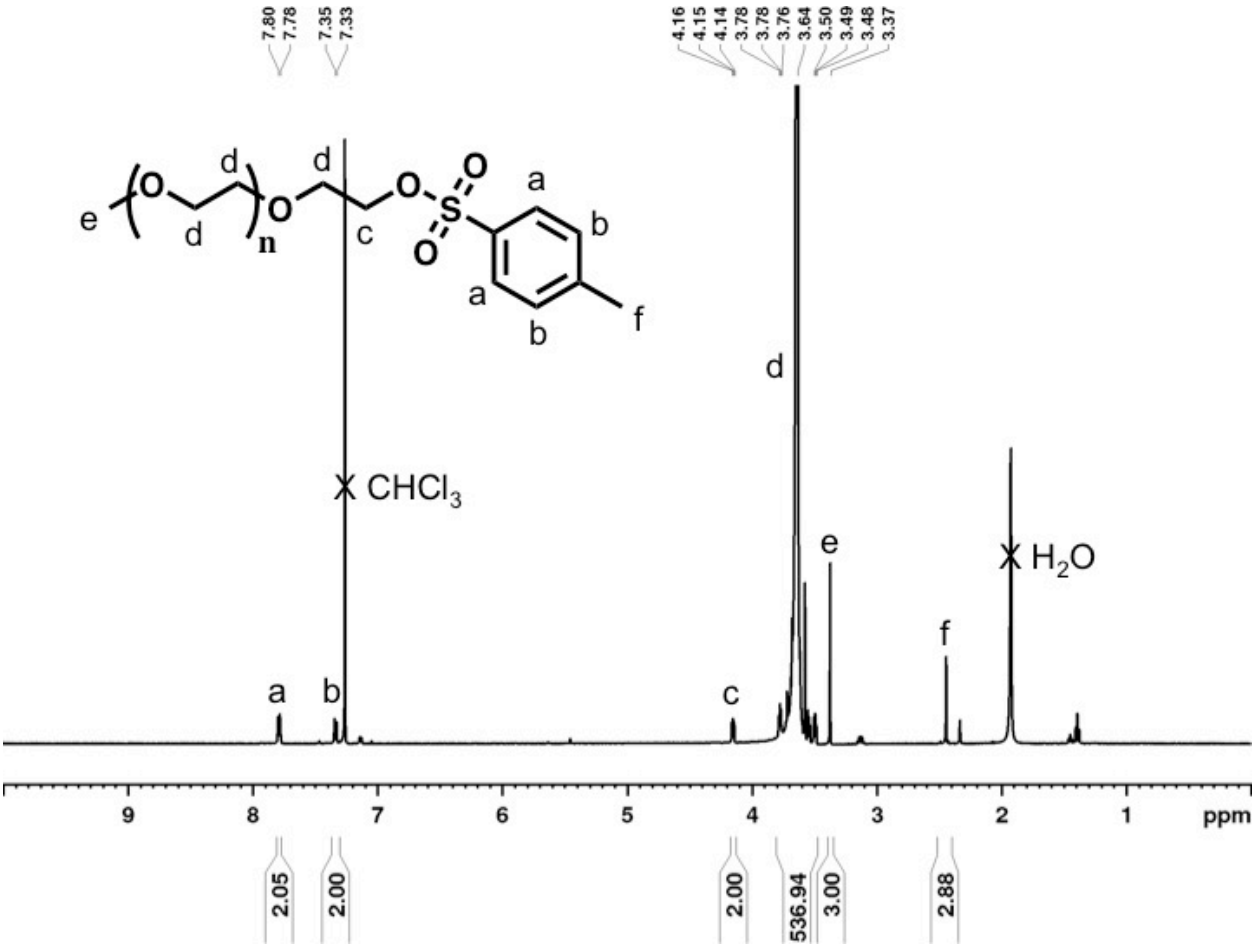

Figure 4.17. ^{1}H NMR spectrum of 5 kDa mPEG-Tosylate (500 MHz, $CDCl_3$). Minor impurity peaks were identified as *p*-toluenesulfonic acid (7.77, 7.14, and 2.33 ppm) and a triethylammonium salt (3.13 and 1.39 ppm). These impurities were carried forward and removed in the following step.

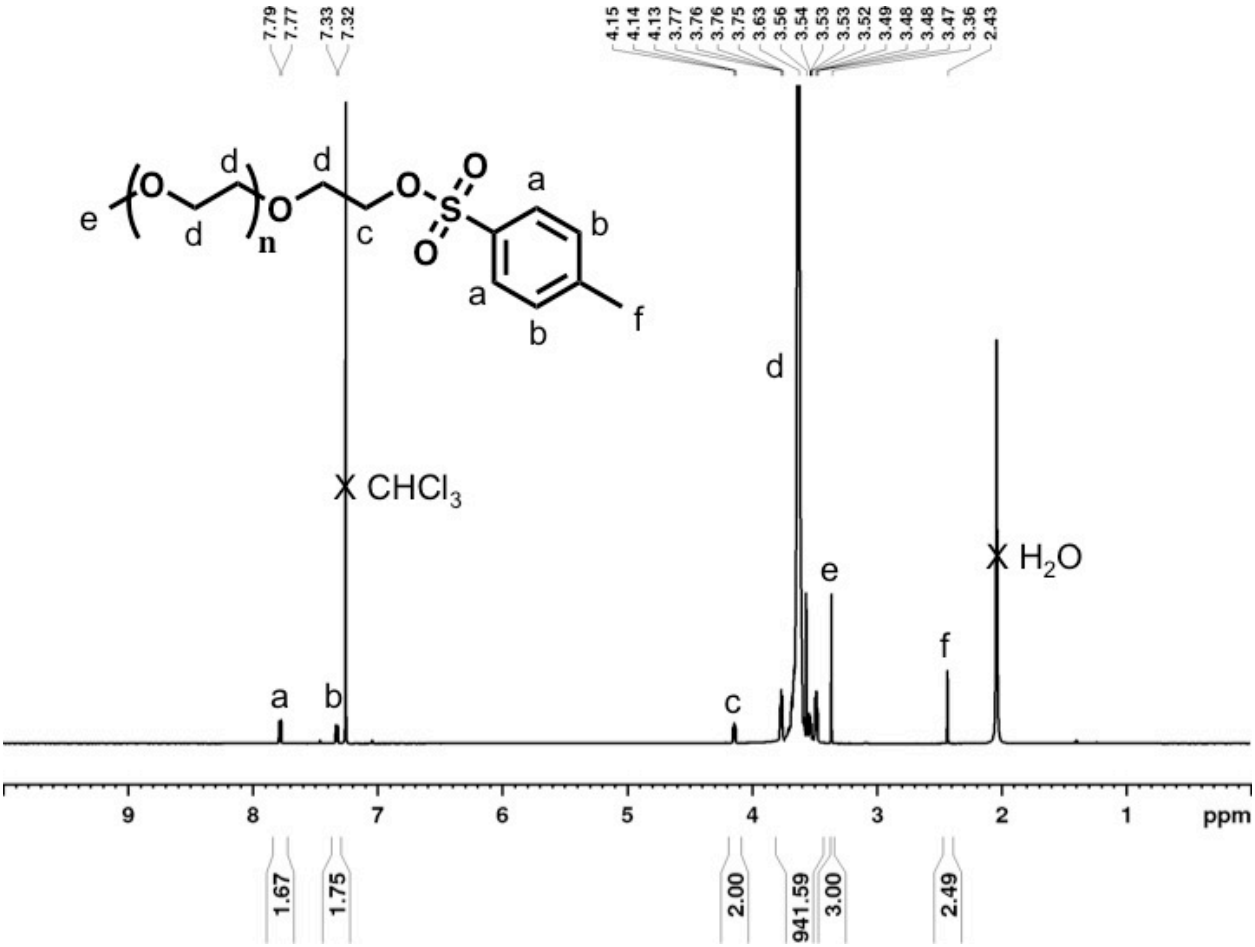

Figure 4.18. ^{1}H NMR spectrum of 10 kDa mPEG-Tosylate (500 MHz, $CDCl_3$).

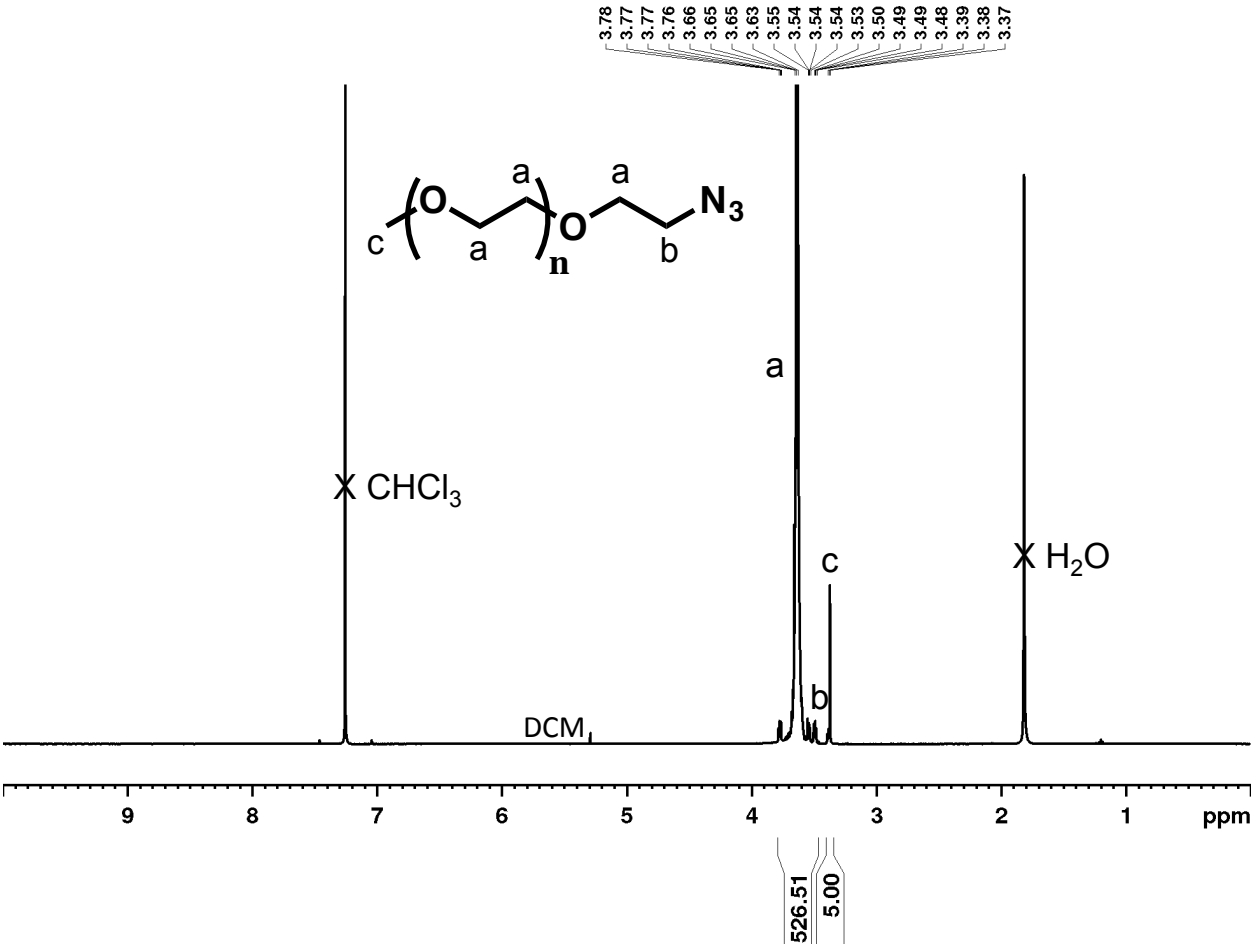

Figure 4.19. ^{1}H NMR spectrum of 5 kDa mPEG-Azide (500 MHz, $CDCl_3$).

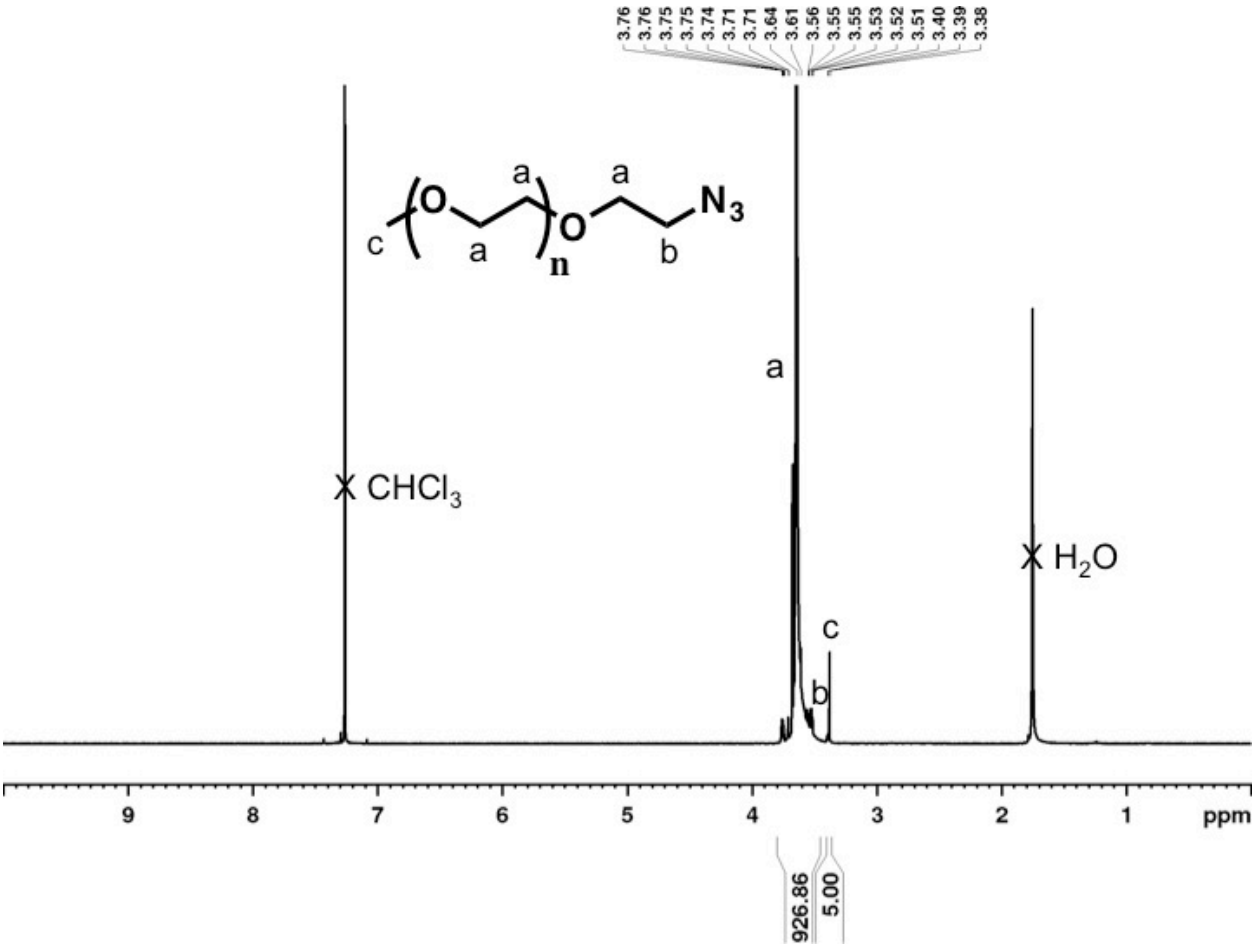

Figure 4.20. ^{1}H NMR spectrum of 10 kDa mPEG-Azide (600 MHz, $CDCl_3$).

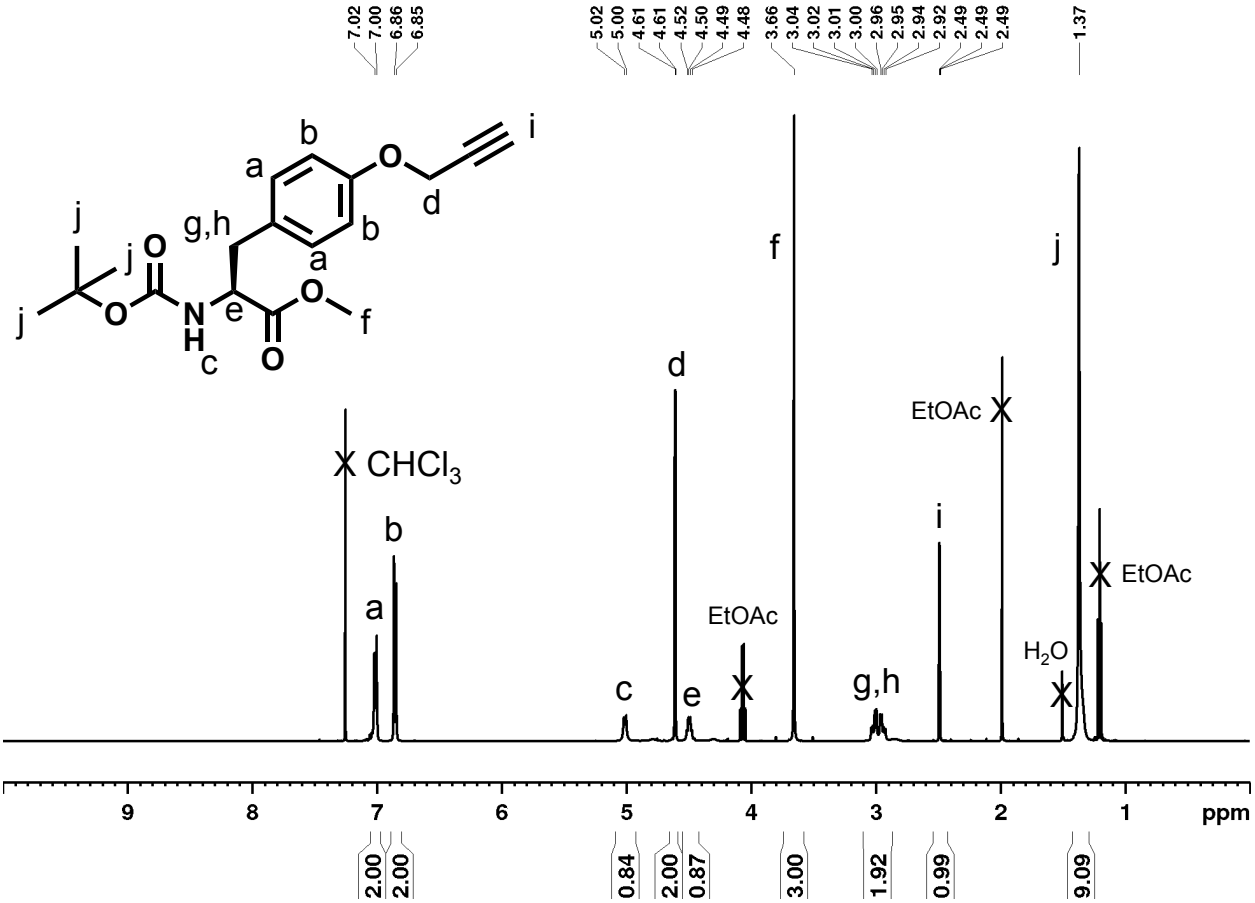

Figure 4.21. ^{1}H NMR spectrum of Boc-L-propargyl tyrosine methyl ester (500 MHz, $CDCl_3$).

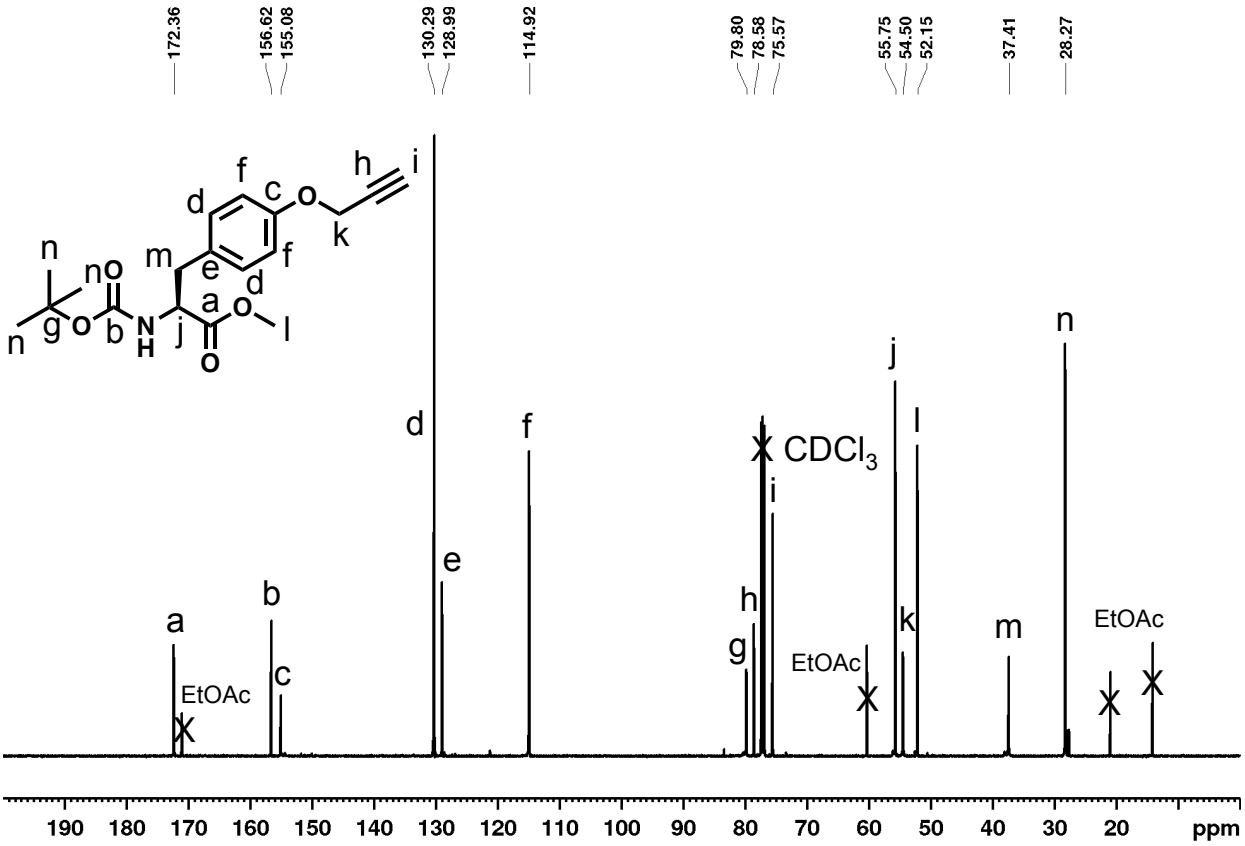

Figure 4.22. ^{13}C NMR spectrum of Boc-L-propargyl tyrosine methyl ester (125 MHz, $CDCl_3$).

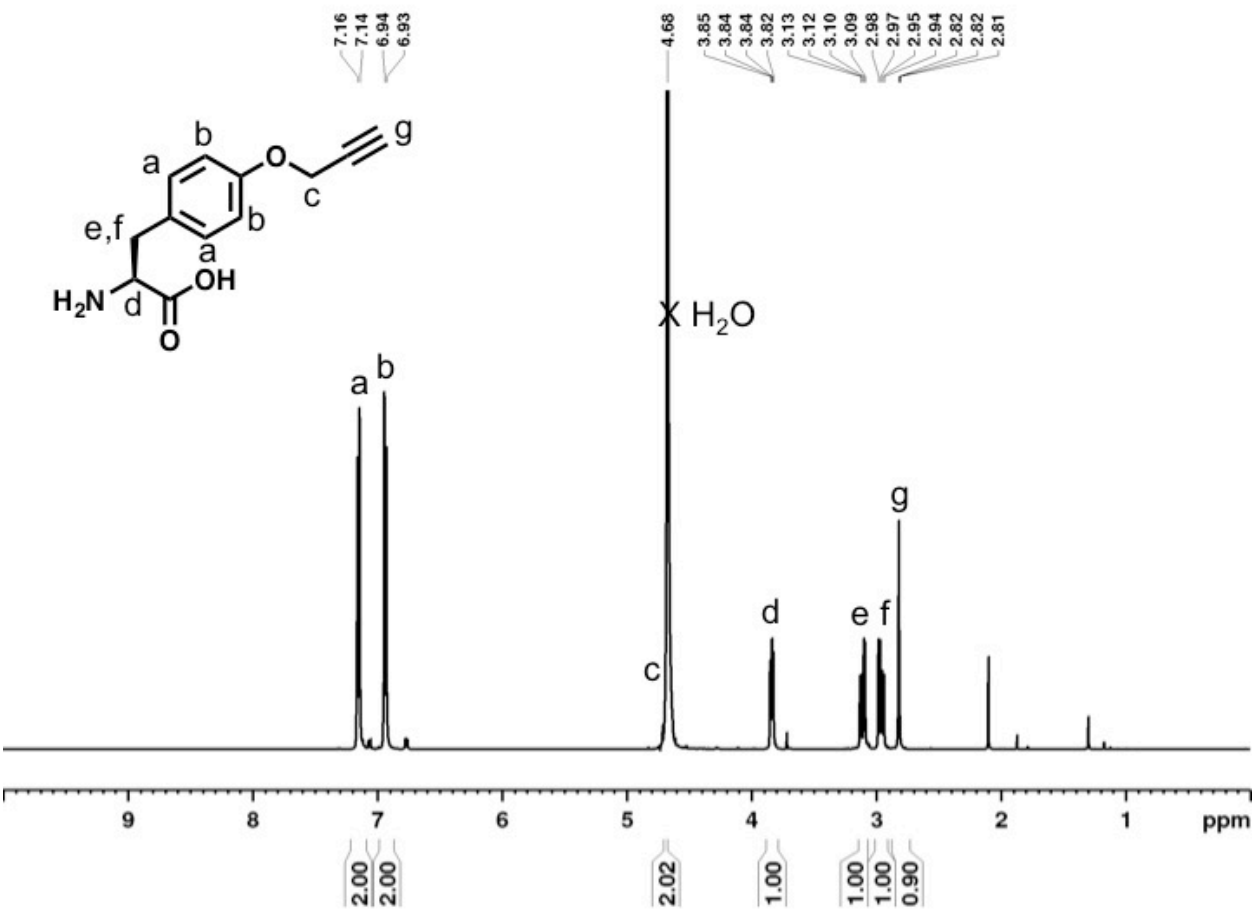

Figure 4.23. ^{1}H NMR spectrum of L-propargyl tyrosine (500 MHz, D_2O).

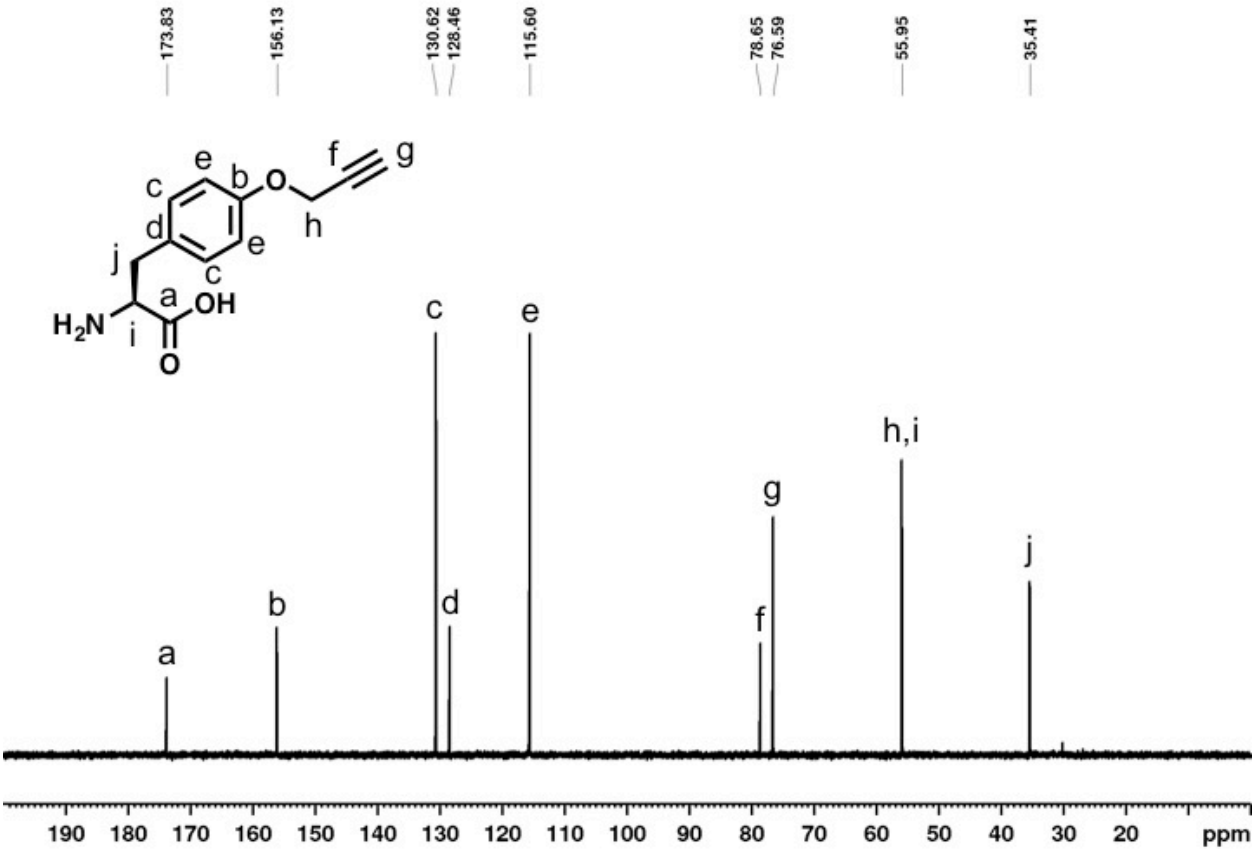

Figure 4.24. ^{13}C NMR spectrum of L-propargyl tyrosine (125 MHz, D_2O).

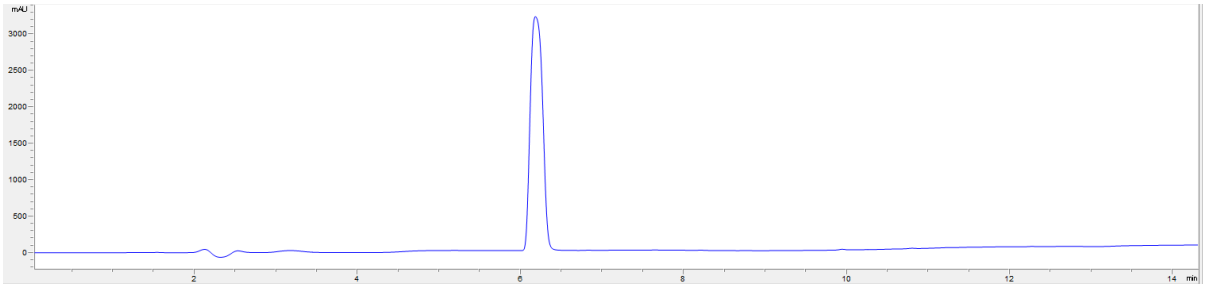

Figure 4.25. Analytical HPLC chromatogram of propargyl tyrosine (>98% pure). Propargyl tyrosine was analyzed using a mobile phase consisting of 10-100% MeCN + 0.1% TFA in water beginning with a 1 min isocratic at 10%, then up to 100% over 10 min in a linear gradient, followed by an isocratic hold at 100% MeCN + 0.1% TFA for 4 min (total time was 15 min; propargyl tyrosine eluted at 6.2 min).

4.6 References

(1) Kopchick, J. J.; Parkinson, C.; Stevens, E. C.; Trainer, P. J. (2002) Growth Hormone Receptor Antagonists: Discovery, Development, and Use in Patients with Acromegaly. *Endocr. Rev. 23*, 623–646.

(2) Muller, A. F.; Kopchick, J. J.; Flyvbjerg, A.; van der Lely, A. J. (2004) Growth Hormone Receptor Antagonists. *J. Clin. Endocrinol. Metab. 89*, 1503–1511.

(3) Colao, A.; Grasso, L. F. S.; Giustina, A.; Melmed, S.; Chanson, P.; Pereira, A. M.; Pivonello, R. (2019) Acromegaly. *Nat. Rev. Dis. Primer 5*, 1–17.

(4) Renehan, A. G.; Brennan, B. M. (2008) Acromegaly, Growth Hormone and Cancer Risk. *Best Pract. Res. Clin. Endocrinol. Metab. 22*, 639–657.

(5) McCutcheon, I. E.; Flyvbjerg, A.; Hill, H.; Li, J.; Bennett, W. F.; Scarlett, J. A.; Friend, K. E. (2001) Antitumor Activity of the Growth Hormone Receptor Antagonist Pegvisomant against Human Meningiomas in Nude Mice. *J. Neurosurg. 94*, 487–492.

(6) Dagnaes-Hansen, F.; Duan, H.; Rasmussen, L. M.; Friend, K. E.; Flyvbjerg, A. (2004) Growth Hormone Receptor Antagonist Administration Inhibits Growth of Human Colorectal Carcinoma in Nude Mice. *Anticancer Res. 24*, 3735–3742.

(7) Divisova, J.; Kuiatse, I.; Lazard, Z.; Weiss, H.; Vreeland, F.; Hadsell, D. L.; Schiff, R.; Osborne, C. K.; Lee, A. V. (2006) The Growth Hormone Receptor Antagonist Pegvisomant Blocks Both Mammary Gland Development and MCF-7 Breast Cancer Xenograft Growth. *Breast Cancer Res. Treat. 98*, 315–327.

(8) Yin, D.; Vreeland, F.; Schaaf, L. J.; Millham, R.; Duncan, B. A.; Sharma, A. (2007) Clinical Pharmacodynamic Effects of the Growth Hormone Receptor Antagonist Pegvisomant: Implications for Cancer Therapy. *Clin. Cancer Res. 13*, 1000–1009.

(9) Evans, A.; Jamieson, S. M. F.; Liu, D.-X.; Wilson, W. R.; Perry, J. K. (2016) Growth Hormone Receptor Antagonism Suppresses Tumour Regrowth after Radiotherapy in an Endometrial Cancer Xenograft Model. *Cancer Lett. 379*, 117–123.

(10) Jenkins, P. J.; Mukherjee, A.; Shalet, S. M. (2006) Does Growth Hormone Cause Cancer? *Clin. Endocrinol. (Oxf.) 64*, 115–121.

(11) Guevara-Aguirre, J.; Balasubramanian, P.; Guevara-Aguirre, M.; Wei, M.; Madia, F.; Cheng, C.-W.; Hwang, D.; Martin-Montalvo, A.; Saavedra, J.; Ingles, S.; et al. (2011) Growth Hormone Receptor Deficiency Is Associated with a Major Reduction in Pro-Aging Signaling, Cancer, and Diabetes in Humans. *Sci. Transl. Med. 3*, 70ra13-70ra13.

(12) Chhabra, Y.; Waters, M. J.; Brooks, A. J. (2011) Role of the Growth Hormone–IGF-1 Axis in Cancer. *Expert Rev. Endocrinol. Metab. 6*, 71–84.

(13) Subramani, R.; Nandy, S. B.; Pedroza, D. A.; Lakshmanaswamy, R. (2017) Role of Growth Hormone in Breast Cancer. *Endocrinology 158*, 1543–1555.

(14) Olarescu, N. C.; Gunawardane, K.; Hansen, T. K.; Møller, N.; Jørgensen, J. O. L. Normal Physiology of Growth Hormone in Adults. In *Endotext*; Feingold, K. R.; Anawalt, B.; Boyce, A.; Chrousos, G.; Dungan, K.; Grossman, A.; Hershman, J. M.; Kaltsas, G.; Koch, C.; Kopp, P.; et al. Eds.; MDText.com, Inc.: South Dartmouth (MA), 2000.

(15) de Vos, A.; Ultsch, M.; Kossiakoff, A. A. (1992) Human Growth Hormone and Extracellular Domain of Its Receptor: Crystal Structure of the Complex. *Science 255*, 306–312.

(16) Pradhananga, S.; Wilkinson, I.; Ross, R. J. M. (2002) Pegvisomant: Structure and Function. *J. Mol. Endocrinol. 29*, 11–14.

(17) Fuh, G.; Cunningham, B. C.; Fukunaga, R.; Nagata, S.; Goeddel, D. V.; Wells, J. A. (1992) Rational Design of Potent Antagonists to the Human Growth Hormone Receptor. *Science 256*, 1677–1680.

(18) Ross, R. J. M.; Leung, K. C.; Maamra, M.; Bennett, W.; Doyle, N.; Waters, M. J.; Ho, K. K. Y. (2001) Binding and Functional Studies with the Growth Hormone Receptor Antagonist, B2036-PEG (Pegvisomant), Reveal Effects of Pegylation and Evidence That It Binds to a Receptor Dimer. *J. Clin. Endocrinol. Metab. 86*, 1716–1723.

(19) Cunningham, B. C.; Wells, J. A. (1989) High-Resolution Epitope Mapping of HGH-Receptor Interactions by Alanine-Scanning Mutagenesis. *Science 244*, 1081–1085.

(20) Veldhuis, J. D.; Bidlingmaier, M.; Anderson, S. M.; Evans, W. S.; Wu, Z.; Strasburger, C. J. (2002) Impact of Experimental Blockade of Peripheral Growth Hormone (GH) Receptors on the Kinetics of Endogenous and Exogenous GH Removal in Healthy Women and Men. *J. Clin. Endocrinol. Metab. 87*, 5737–5745.

(21) Pfizer, Inc. Somavert (Pegvisomant) [Package Insert]. US Food and Drug Administration website December 2013.

(22) Gaberc-Porekar, V.; Zore, I.; Podobnik, B.; Menart, V. (2008) Obstacles and Pitfalls in the PEGylation of Therapeutic Proteins. *Curr. Opin. Drug Discov. Devel. 11*, 242–250.

(23) Payne, R. W.; Murphy, B. M.; Manning, M. C. (2011) Product Development Issues for PEGylated Proteins. *Pharm. Dev. Technol. 16*, 423–440.

(24) Moore, D. J.; Adi, Y.; Connock, M. J.; Bayliss, S. (2009) Clinical Effectiveness and Cost-Effectiveness of Pegvisomant for the Treatment of Acromegaly: A Systematic Review and Economic Evaluation. *BMC Endocr. Disord. 9*, 20.

(25) Pasut, G.; Veronese, F. M. (2012) State of the Art in PEGylation: The Great Versatility Achieved after Forty Years of Research. *J. Controlled Release 161*, 461–472.

(26) Nischan, N.; Hackenberger, C. P. R. (2014) Site-Specific PEGylation of Proteins: Recent Developments. *J. Org. Chem. 79*, 10727–10733.

(27) Dozier, J. K.; Distefano, M. D. (2015) Site-Specific PEGylation of Therapeutic Proteins. *Int. J. Mol. Sci. 16*, 25831–25864.

(28) Wang, Y.; Wu, C. (2018) Site-Specific Conjugation of Polymers to Proteins. *Biomacromolecules 19*, 1804–1825.

(29) Belén, L. H.; Rangel-Yagui, C. de O.; Beltrán Lissabet, J. F.; Effer, B.; Lee-Estevez, M.; Pessoa, A.; Castillo, R. L.; Farías, J. G. (2019) From Synthesis to Characterization of Site-Selective PEGylated Proteins. *Front. Pharmacol. 10*.

(30) Wu, L.; Ho, S. V.; Wang, W.; Gao, J.; Zhang, G.; Su, Z.; Hu, T. (2013) N-Terminal Mono-PEGylation of Growth Hormone Antagonist: Correlation of PEG Size and Pharmacodynamic Behavior. *Int. J. Pharm. 453*, 533–540.

(31) Ravasco, J. M. J. M.; Faustino, H.; Trindade, A.; Gois, P. M. P. (2019) Bioconjugation with Maleimides: A Useful Tool for Chemical Biology. *Chem. – Eur. J. 25*, 43–59.

(32) Gunnoo, S. B.; Madder, A. (2016) Chemical Protein Modification through Cysteine. *ChemBioChem 17*, 529–553.

(33) Cox, G. N.; Rosendahl, M. S.; Chlipala, E. A.; Smith, D. J.; Carlson, S. J.; Doherty, D. H. (2007) A Long-Acting, Mono-PEGylated Human Growth Hormone Analog Is a Potent Stimulator of Weight Gain and Bone Growth in Hypophysectomized Rats. *Endocrinology 148*, 1590–1597.

(34) Wang, Y.; Langley, R. J.; Tamshen, K.; Harms, J.; Maynard, H. D.; Jamieson, S. M. F.; Perry, J. K. (2020) Enhanced Bioactivity of a Human GHR Antagonist by Solid-Phase Site-Specific PEGylation. *Unpubl. Manuscipt*.

(35) Dumas, A.; Lercher, L.; D. Spicer, C.; G. Davis, B. (2015) Designing Logical Codon Reassignment – Expanding the Chemistry in Biology. *Chem. Sci. 6*, 50–69.

(36) Cho, H.; Daniel, T.; Buechler, Y. J.; Litzinger, D. C.; Maio, Z.; Putnam, A.-M. H.; Kraynov, V. S.; Sim, B.-C.; Bussell, S.; Javahishvili, T.; et al. (2011) Optimized Clinical Performance of Growth Hormone with an Expanded Genetic Code. *Proc. Natl. Acad. Sci. 108*, 9060–9065.

(37) Wu, L.; Chen, J.; Wu, Y.; Zhang, B.; Cai, X.; Zhang, Z.; Wang, Y.; Si, L.; Xu, H.; Zheng, Y.; et al. (2017) Precise and Combinatorial PEGylation Generates a Low-Immunogenic and Stable Form of Human Growth Hormone. *J. Controlled Release 249*, 84–93.

(38) Deiters, A.; Schultz, P. G. (2005) In Vivo Incorporation of an Alkyne into Proteins in Escherichia Coli. *Bioorg. Med. Chem. Lett. 15*, 1521–1524.

(39) Bundy, B. C.; Swartz, J. R. (2010) Site-Specific Incorporation of p-Propargyloxyphenylalanine in a Cell-Free Environment for Direct Protein−Protein Click Conjugation. *Bioconjug. Chem. 21*, 255–263.

(40) Miyake-Stoner, S. J.; Miller, A. M.; Hammill, J. T.; Peeler, J. C.; Hess, K. R.; Mehl, R. A.; Brewer, S. H. (2009) Probing Protein Folding Using Site-Specifically Encoded Unnatural Amino Acids as FRET Donors with Tryptophan. *Biochemistry 48*, 5953–5962.

(41) Hammill, J. T.; Miyake-Stoner, S.; Hazen, J. L.; Jackson, J. C.; Mehl, R. A. (2007) Preparation of Site-Specifically Labeled Fluorinated Proteins for 19 F-NMR Structural Characterization. *Nat. Protoc. 2*, 2601–2607.

(42) Wang, Y.; Langley, R. J.; Tamshen, K.; Jamieson, S. M.; Lu, M.; Maynard, H. D.; Perry, J. K. (2020) Long-Acting Human Growth Hormone Receptor Antagonists Produced in E. Coli and Conjugated with Polyethylene Glycol. *Bioconjug. Chem. 31*, 1651–1660.

(43) Conway-Campbell, B. L.; Brooks, A. J.; Robinson, P. J.; Perani, M.; Waters, M. J. (2008) The Extracellular Domain of the Growth Hormone Receptor Interacts with Coactivator Activator to Promote Cell Proliferation. *Mol. Endocrinol. 22*, 2190–2202.

(44) Presolski, S. I.; Hong, V. P.; Finn, M. G. (2011) Copper-Catalyzed Azide–Alkyne Click Chemistry for Bioconjugation. *Curr. Protoc. Chem. Biol. 3*, 153–162.

(45) Nairn, N. W.; Shanebeck, K. D.; Wang, A.; Graddis, T. J.; VanBrunt, M. P.; Thornton, K. C.; Grabstein, K. (2012) Development of Copper-Catalyzed Azide–Alkyne Cycloaddition for Increased in Vivo Efficacy of Interferon β-1b by Site-Specific PEGylation. *Bioconjug. Chem. 23*, 2087–2097.

(46) Malyala, P.; Singh, M. (2008) Endotoxin Limits in Formulations for Preclinical Research. *J. Pharm. Sci. 97*, 2041–2044.

(47) Kenry; Liu, B. (2019) Bio-Orthogonal Click Chemistry for In Vivo Bioimaging. *Trends Chem. 1*, 763–778.

(48) Kim, E.; Koo, H. (2019) Biomedical Applications of Copper-Free Click Chemistry: In Vitro, in Vivo, and Ex Vivo. *Chem. Sci. 10*, 7835–7851.

(49) Alley, S. C.; Benjamin, D. R.; Jeffrey, S. C.; Okeley, N. M.; Meyer, D. L.; Sanderson, R. J.; Senter, P. D. (2008) Contribution of Linker Stability to the Activities of Anticancer Immunoconjugates. *Bioconjug. Chem. 19*, 759–765.

(50) Lyon, R. P.; Setter, J. R.; Bovee, T. D.; Doronina, S. O.; Hunter, J. H.; Anderson, M. E.; Balasubramanian, C. L.; Duniho, S. M.; Leiske, C. I.; Li, F.; Senter, P. D. (2014) Self-Hydrolyzing Maleimides Improve the Stability and Pharmacological Properties of Antibody-Drug Conjugates. *Nat. Biotechnol. 32*, 1059–1062.

(51) Peschke, B.; Zundel, M.; Bak, S.; Clausen, T. R.; Blume, N.; Pedersen, A.; Zaragoza, F.; Madsen, K. (2007) C-Terminally PEGylated HGH-Derivatives. *Bioorg. Med. Chem. 15*, 4382–4395.

(52) Tropea, J. E.; Cherry, S.; Waugh, D. S. Expression and Purification of Soluble His6-Tagged TEV Protease. In *High Throughput Protein Expression and Purification: Methods*

and Protocols; Doyle, S. A., Ed.; Methods in Molecular Biology; Humana Press: Totowa, NJ, 2009; pp 297–307.

(53) Rappsilber, J.; Mann, M.; Ishihama, Y. (2007) Protocol for Micro-Purification, Enrichment, Pre-Fractionation and Storage of Peptides for Proteomics Using StageTips. *Nat. Protoc. 2*, 1896–1906.

Chapter 5

Efforts toward the Synthesis of Degradable and Uniform PEG Analogs[†]

5.1 Introduction

Polyethylene glycol (PEG) is an amphiphilic, biocompatible, synthetic polymer used widely for biomedical applications. PEG is inexpensive, easy to synthesize and functionalize, and has been used in many medical and cosmetic products. Covalent conjugation of PEG to proteins (PEGylation) has been shown to increase solubility and stability of proteins and peptides over a broad range of temperatures and pH. It also confers non-fouling properties to molecules or surfaces upon covalent conjugation. Additionally, PEGylation has been well established to increase *in vivo* circulation times of therapeutic proteins compared to the corresponding unmodified proteins.[1–3] Its efficacy is evidenced by the 15 unique PEGylated proteins currently approved for human use in the United States that are used to treat a wide range of diseases including cancer, hemophilia, and acromegaly.[4,5] Given the widespread utility and broad applicability of PEG in the context of therapeutic protein-polymer conjugates, there is significant interest in the development of structural analogs that offer added functionality while simultaneously retaining the beneficial properties of the polymer. The majority of these efforts have been directed toward two areas: increasing the degradability of PEG and also developing methodology to increase its uniformity. In this chapter, we report and discuss efforts to address both of these challenges.

The most prolific strategy for designing degradable PEG analogs consists of installing distal, but regularly interspaced degradable moieties throughout the polymer backbone. This design ensures minimal structural deviation from PEG so as to retain the polymer's "PEG-like" properties while also facilitating sufficient structural changes to permit degradation. A variety of degradable moieties have been introduced into the backbones of ethylene glycol-based polymers, which respond to a variety of stimuli. For example, hydrolyzable esters have been incorporated

regularly throughout polymer backbones via ring-opening polymerization of oxo-crown ethers[6–9] or by copolymerization of ethylene glycol oligomers with lactides.[10–13] Hydrolytically degradable PEG analogs have also been prepared via installation of vinyl ether moieties following chloride elimination from poly(ethylene oxide-*co*-epichlorohydrin) polymers. In this case, degradation was facilitated by hydration of the vinyl ether groups to form hemiacetals, which could easily be degraded with mild aqueous acid.[14] Acetals and hydrazones have also been directly installed into polymers to facilitate similar acid-catalyzed backbone degradation.[15,16] Reductively degradable analogs have also been prepared by installing disulfides between oligo(ethylene glycol) monomer units.[17,18] Short peptide sequences can also be incorporated between oligo(ethylene glycol) monomer units to prepare enzymatically degradable PEG analogs.[19] As part of our work in this area, we investigated a complementary alternative to these approaches comprising PEG-like polymers with backbone alkenes prepared by ring-opening metathesis polymerization (ROMP) that can undergo metathesis depolymerization.[20]

While numerous creative approaches have been employed toward the synthesis of degradable PEG analogs, the synthesis of uniform PEG-like polymers has remained challenging. Due to the statistical nature of polymer synthesis, all synthetic polymers are composed of a distribution of different molecular weight species. For example, a 3.4 kDa PEG with a dispersity of 1.01 shows at least 28 major peaks by matrix-assisted laser desorption/ionization (MALDI).[21] While this heterogeneity may not be problematic for bulk material applications, it may lead to variability in efficacy when conjugated to therapeutic proteins.[22]

To date, all reported methods of generating uniform PEG utilize variations on a similar strategy known as iterative monomer addition. These routes typically begin with synthesis of either a single heterobifunctional monomer, an A-B monomer, or two homobifunctional

monomers, A-A and B-B monomers, where A and B are mutually reactive functional groups. Monomers are then iteratively coupled together to make longer oligomers. Purification is typically required following addition of each subsequent monomer unit, and most strategies also require the use of protecting groups, both of which result in increased step counts and decreased yields.[23] Building from the efforts of numerous groups,[21,24–33] at the outset of this work the longest reported uniform linear PEG was a 64-mer (2.85 kDa) from the Jiang group.[32] However, most of these strategies suffered from low yield and purification difficulties. For this work, we aimed to develop methodology in which high molecular weight PEG analogs could be synthesized in good yields without extensive purification.

This chapter reports our efforts toward the synthesis and characterization of two types of PEG analogs to address the challenges of degradability or uniformity. Degradability was incorporated by using water-soluble unsaturated PEG analogs that were susceptible to metathesis depolymerization. We previously reported ROMP of unsaturated crown ethers to produce these analogs using Grubbs' first generation catalyst (Grubbs I).[34] Although pendant amino acids could be incorporated into the polymers via copolymerization with unsaturated benzocrown ethers containing amino acids,[35] these polymers lacked protein reactive end groups that could be used for bioconjugation. Previous work from our group performed by Dr. Nic Matsumoto and Dr. Emma Pelegri-O'Day described the ROMP synthesis of PEG analogs (rPEGs) containing ω-aldehyde end-groups.[20] In this chapter, we further describe conjugation of these rPEGs to the model protein lysozyme (Lyz) along with their subsequent depolymerization and finally examine how these modifications affect Lyz activity.

We next report efforts to synthesize high molecular weight uniform PEG analogs while circumventing the typical challenges associated with iterative monomer addition. We envisioned

a strategy whereby heterobifunctional oligo(ethylene glycol)-based monomers could be iteratively coupled using high-efficiency thiol-ene chemistry to produce high molecular weight PEG analogs by solid phase organic synthesis (SPOS). SPOS allows for facile purification, and when combined with high-efficiency "click" reactions, it has the potential to produce sequence-defined, uniform chains. We describe the thiol-ene step-growth polymerization of homobifunctional, dithiol- and divinyl ether-functionalized PEG oligomers to give PEG-like analogs. We next discuss our progress toward the synthesis heterobifunctional, thiol and vinyl ether-functionalized dodecylethylene glycol monomers for SPOS of uniform PEG analogs. Finally, we disclose a useful cationic templation strategy for the efficient synthesis of a dodecylethylene glycol-based macrocyclic sulfite. We expect these preliminary results be useful for synthesis of heterobifunctional PEG-based monomers, which can be applied to preparations of uniform PEG analogs as well as other potential biomedical applications.

5.2 Results and Discussion

5.2.1 PEG Analogs Synthesized by Ring-Opening Metathesis Polymerization for Reversible Bioconjugation

Reversible protein-polymer conjugates can be prepared by direct bioconjugation of polymers with degradable backbones or by using cleavable linkers to bridge proteins and polymers. These conjugates are typically designed to accelerate renal clearance of the polymer after degradation from stimuli such as hydrolysis, reduction, and enzymatic degradation.[17,36–40] While responsiveness to biological triggers has been well studied, development of polymers for bioconjugation that are cleavable by chemoselective, non-bioavailable triggers remains under-investigated. For this work, focused on degradation of polymers containing backbone alkenes via

metathesis depolymerization facilitated by the organometallic reagent, Grubbs third generation catalyst (Grubbs III).

Polymers containing backbone alkenes can readily be prepared by ROMP, a technique that is well-established and functional group tolerant, allowing preparation of functionally diverse and complex polymers.[41,42] Despite the widespread use of ROMP, there are only several examples of the resulting polymers being used for conjugation to proteins.[43–46] Notably, none of these examples reported reversibility of the resulting protein-polymer conjugates. Unsaturated rPEGs were previously reported to undergo depolymerization via lithium-templated backbiting metathesis to reform unsaturated 12-crown-4 monomers in high yields in organic solvents.[34,35] Before adapting these polymers for reversible bioconjugation to proteins, it was first necessary to confirm that rPEGs could be depolymerized in aqueous conditions.

Dr. Nic Matsumoto and Dr. Emma Pelegri-O'Day previously established that rPEGs with aldehyde end-groups could be conjugated to the model protein Lyz and subsequently depolymerized with addition of Grubbs III; however, most of their efforts were directed toward thiol-ene functionalization of the polymer backbone alkenes, and depolymerization conditions for the Lyz-rPEG conjugates had not been fully validated. This work is distinct in that aqueous depolymerization conditions were established and validated for rPEG alone and rPEG Lyz conjugates, and depolymerization was confirmed to be a property exclusive to flexible rPEG polymers versus rigid norbornene-based polymers that are commonly used for ROMP. Additionally, this work optimized the extent of the depolymerization for rPEG-Lyz conjugates, identifying essential reaction components. Furthermore, this work was the first to evaluate the activity of the rPEG-Lyz conjugate before and after depolymerization. This work therefore represents a significant contribution to these overall efforts that have been since reported.[20]

Scheme 5.1. ROMP of unsaturated crown ether **1**, to produce 10 kDa rPEG.

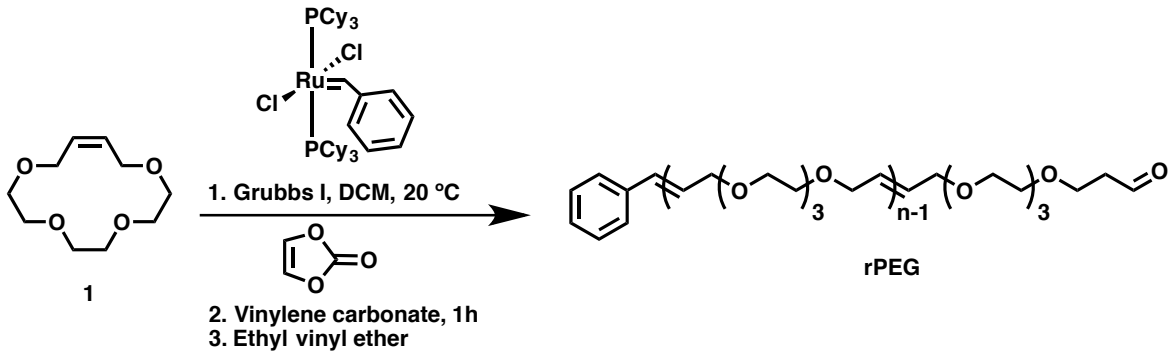

Unsaturated crown ether monomer **1** was polymerized by ROMP using Grubbs I catalyst as reported previously[34] (Scheme 5.1) with a ratio of [Grubbs I]:[monomer **1**] equal to [1]:[50] to produce a polymer of approximately 10 kDa. Once the desired conversion was reached as assessed by ^{1}H NMR, the polymerization was terminated with addition of excess vinylene carbonate to install a ω-aldehyde to make the polymer amenable for conjugation to proteins via standard reductive amination conditions.[42] Aldehyde incorporation was confirmed by ^{1}H NMR via the aldehyde peak at 9.7 ppm (38% conversion) and also the adjacent methylene protons at 2.6 ppm (46% conversion). Slight differences in these peak conversions may be due to hydration of the aldehyde, reducing signal integration at 9.8 ppm, or as a result of side reactions during the reaction. The final polymer was purified via repeated precipitation into cold diethyl ether. As a control for initial depolymerization studies, norbornene-based monomer **2** was also synthesized (Scheme 5.2) and polymerized by ROMP with a ratio of [Grubbs I]:[monomer **1**] equal to [1]:[50] to produce poly(Nor-PEG) of approximately 18 kDa based on the previously reported method (Scheme 5.3).[47] Because this polymer would not be used for bioconjugation, the polymerization was terminated instead with ethyl vinyl ether to provide a terminal alkene end group. Purification was also accomplished by precipitation into cold diethyl ether.

Scheme 5.2. Synthesis of Nor-PEG monomer **2.**

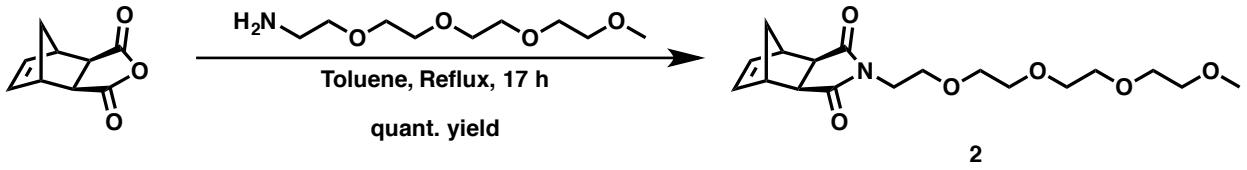

Scheme 5.3. ROMP of Nor-PEG monomer **2**, to produce 20 kDa poly(Nor-PEG)**.**

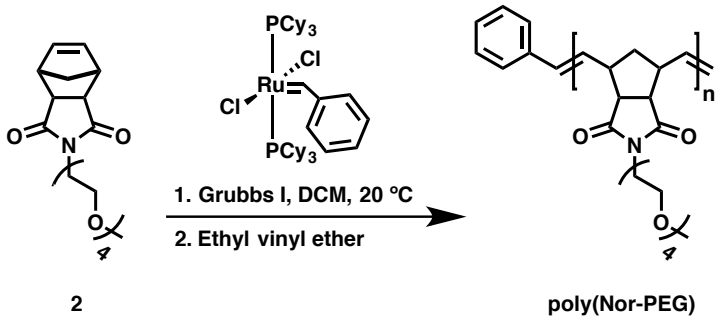

Both rPEG and poly(Nor-PEG) polymers were analyzed by ^{1}H NMR and gel permeation chromatography (GPC). The number average molecular weight (M_n) was determined by ^{1}H NMR via end group analysis by comparing the integrations of the terminal phenyl protons to the backbone alkene protons. For rPEG, M_n = 9.7 kDa (DP = 48), and for poly(Nor-PEG), M_n = 19.9 kDa (DP = 56). ^{1}H NMR analysis was also checked against GPC analysis to assess M_n and dispersity (Đ). rPEG was compared to PEG standards (M_n = 8.6 kDa, M_w = 13.8 kDa, Đ = 1.62), and poly(Nor-PEG) was compared to poly(methyl methacrylate) (PMMA) standards (M_n = 26.2 kDa, M_w = 29.3 kDa, Đ = 1.12). The dispersity for rPEG was much higher than for poly(Nor-PEG) with values of Đ = 1.62 vs. Đ = 1.12, respectively, which was expected for the entropy-driven ROMP of monomer **1** compared to the strain-promoted ROMP of monomer **2**.[48]

Aqueous depolymerizations were then carried out for each polymer based on conditions reported by Davis and coworkers for cross-metathesis on proteins (Scheme 5.4).[49] Typical depolymerizations were carried out by dissolving each polymer into phosphate buffer, pH 8.0

containing 20% *tert*-butyl alcohol (tBuOH), 100 mM $MgCl_2$, and 5 mM Grubbs III, then stirring at 20 °C for 20 hours. Reactions were then quenched via addition of excess ethyl vinyl ether and all solvent was removed under vacuum before redissolving each crude sample in dimethylformamide (DMF) for GPC analysis. Depolymerizations were carried out with or without LiCl. Previous reports of rPEG depolymerization performed in organic solvents detailed the importance of lithium in the backbiting depolymerization process to reform cyclic unsaturated monomers;[34] however, depolymerizations proceeded for rPEG with or without addition of 100 mM LiCl (data not shown).[20] This is most likely due to the weak interaction of the lithium ion with the polymer in water compared to in organic solvents. We also found that the addition of 100 mM $MgCl_2$ was unnecessary to facilitate depolymerization of rPEG alone. Interestingly, 100 mM $MgCl_2$ was necessary for depolymerization of rPEG once conjugated to protein as will be discussed below. Representative GPC chromatograms of depolymerization reactions without addition of LiCl or $MgCl_2$ are shown in Figure 5.1.

Scheme 5.4. Aqueous depolymerization of (A) rPEG and (B) poly(Nor-PEG) with Grubbs III catalyst.

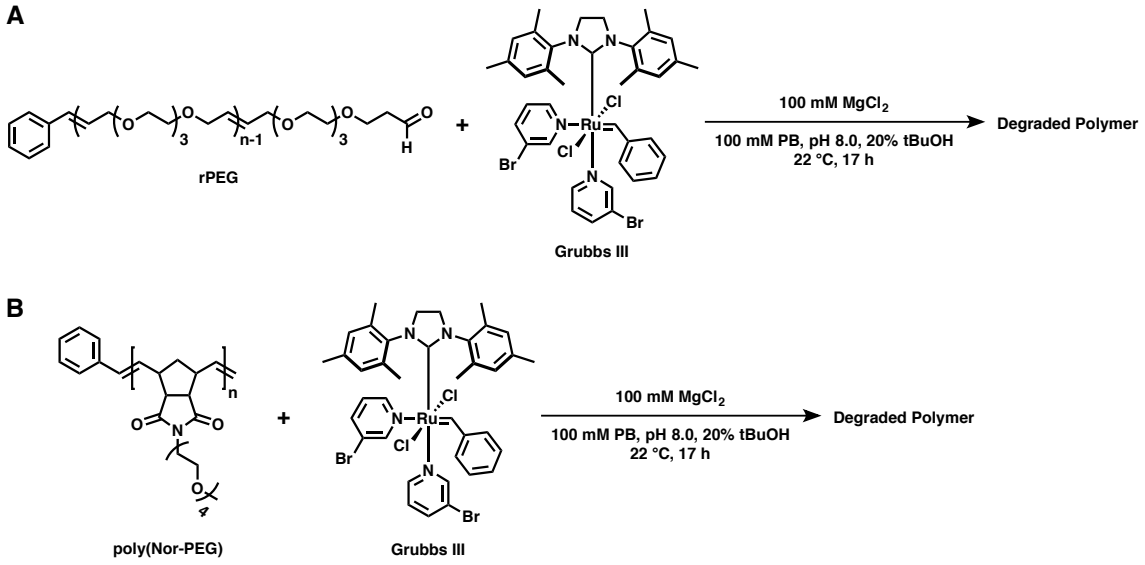

In contrast to rPEG, no reduction in molecular weight was observed in any conditions assessed for poly(Nor-PEG). In fact, GPC analysis following the reaction actually revealed a slight increase in M_n as well as dispersity due to the appearance of a high molecular weight shoulder peak, which may have resulted from chain-end coupling. Since backbiting metathesis is thought to be the mechanism of depolymerization and norbornene monomers are strained and therefore possess a high energy barrier of formation, it was unsurprising that no lower molecular weight peaks were observed via GPC for poly(Nor-PEG). We expected this principle to hold true for depolymerization efforts toward other strained ROMP monomers and therefore limited our focus for this work on developing reversible protein-polymer conjugates to rPEG.

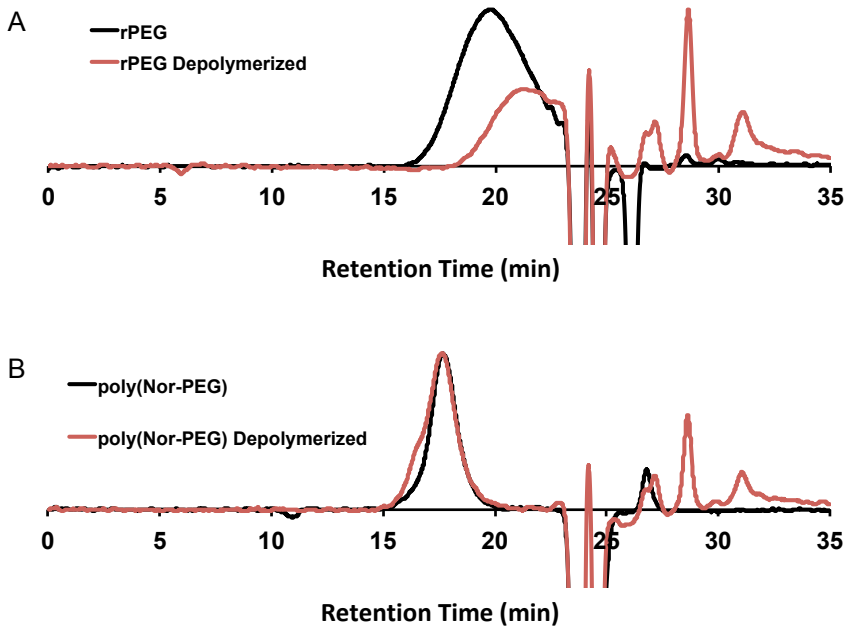

Figure 5.1. Normalized GPC chromatograms of (A) rPEG (M_n = 6.0 kDa, M_w = 10.5 kDa, Đ = 1.74) and (B) poly(Nor-PEG) (M_n = 26.2 kDa, M_w = 29.3 kDa, Đ = 1.12) before and after depolymerization in aqueous conditions with Grubbs III catalyst. After depolymerization, rPEG was observed to decrease in size (M_n = 4.0 kDa, M_w = 4.8 kDa, Đ = 1.21) while poly(Nor-PEG) exhibited a higher molecular weight shoulder with a slight overall increase in molecular weight (M_n = 27.0 kDa, M_w = 33.4 kDa, Đ = 1.24).

We next conjugated the aldehyde-terminated rPEG (M_n = 9.7 kDa) to the model protein Lyz via reductive amination (Figure 5.2A). The reaction was carried out by incubating Lyz and rPEG in 100 mM phosphate buffer, pH 6.0 at 22 °C in a 1:50 molar ratio. The large excess of polymer was added to ensure high conjugation efficiency to the 7 amino groups of Lyz. After 1 hour, sodium cyanoborohydride was added to a final concentration of 20 mM and the reaction was incubated for and additional 26 hours prior to analysis by sodium dodecyl sulfate polyacrylamide gel electrophoreses (SDS-PAGE) (Figure 5.2B). The reaction proceeded to relatively high efficiency as evidenced by the high molecular weight smear in the conjugate lane, and the broadness of the band indicates that the conjugate is a heterogeneous mixture, which was

expected due to nonspecific conjugation to the 7 amines of Lyz. The resulting conjugate was then purified and analyzed using a fast protein liquid chromatography (FPLC) system equipped with a cation exchange column (Figure 5.2C). Unreacted rPEG was easily separated from the rPEG-Lyz conjugate due to its lack of charge. Additionally, conjugation of Lyz to the neutral polymers shifted the retention time of the conjugate significantly compared to the native protein. The absence of unreacted lysozyme in the conjugate trace also suggests high reaction conversion.

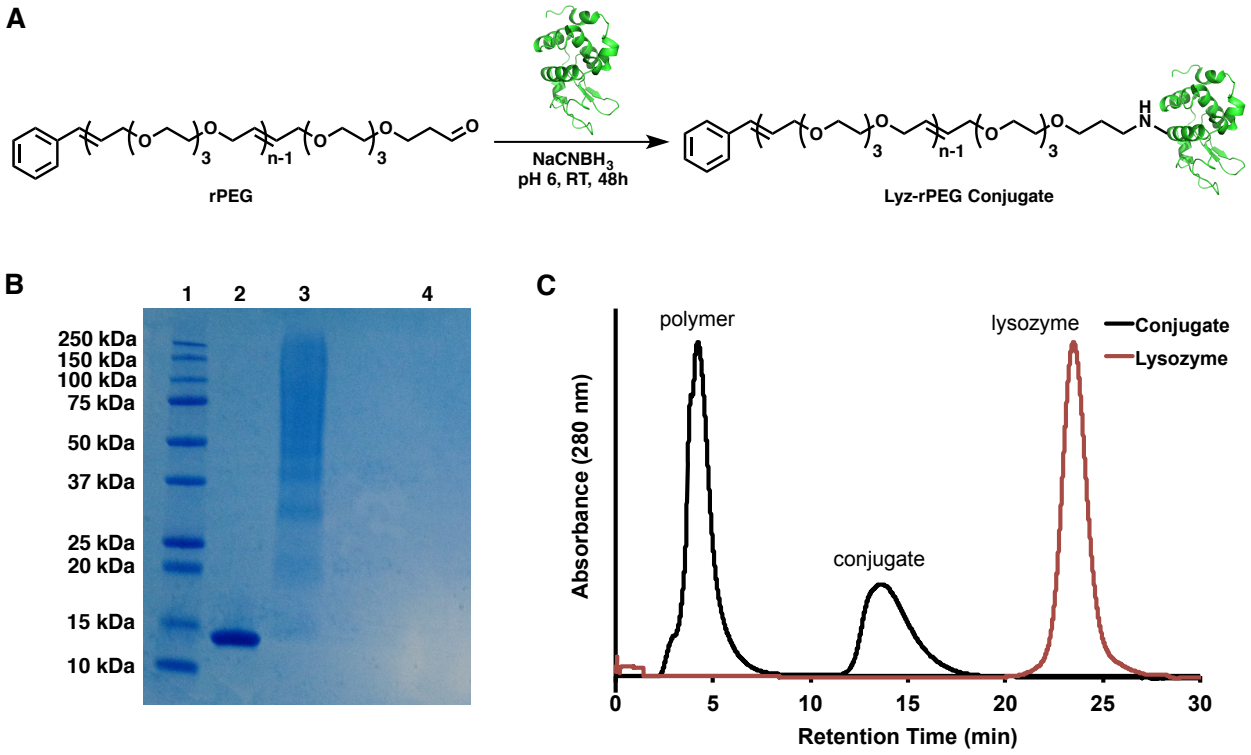

Figure 5.2. Conjugation of 10 kDa rPEG to lysozyme by reductive amination. (A) Reaction scheme of reductive amination for nonspecific conjugation of rPEG to Lyz lysine residues and N-terminus. (B) SDS-PAGE of Lyz and Lyz-rPEG showing the appearance of a high molecular weight smear after treatment with rPEG and $NaCNBH_3$ (lane 1: protein marker; lane 2: Lyz; lane 3: Lyz-rPEG conjugate; lane 4: rPEG 3). (C) FPLC chromatogram of Lyz and Lyz-rPEG conjugate using a cation exchange column. Structure of lysozyme from PDB number 1DPX.

Depolymerization of purified rPEG-Lyz conjugate was carried out using conditions similar to those used for rPEG alone. A typical reaction was carried out by incubating rPEG-Lyz

in phosphate buffer, pH 8.0 with 100 mM $MgCl_2$, 5 mM Grubbs III, and 20% tBuOH for 20 hours at 20 °C. These standard conditions were successful in reducing the molecular weight of the conjugate nearly back to the molecular weight of native Lyz as assessed by SDS-PAGE stained with Coomassie Brilliant Blue to visualize protein and 0.1 N iodine to visualize polymer (Figure 5.3A). Minor adjustments to buffer and tBuOH concentration did not appear to affect the reaction. Interestingly, although the presence of 100 mM $MgCl_2$ was not necessary for the depolymerization of rPEG alone, it was required for depolymerization of the rPEG-Lyz conjugate as evidenced by the lack of shift in conjugate bands in Figure 5.3B. The Davis group observed similar results during ruthenium catalyzed metathesis reactions with protein-tethered allyl sulfides and postulated that this elevated salt concentration may help to disrupt chelation of protein side chains to ruthenium, allowing the catalyst to function as intended.[49] We further discovered that addition of excess allyl alcohol to the reaction also inhibited the depolymerization (Figure 5.3A; lane 6), although it is unclear why this occurred. Finally, we found that replacement of tBuOH with acetonitrile (MeCN) also inhibited depolymerization (Figure 5.3C; lane 5), likely due to coordination to and inactivation of the catalyst. The optimal depolymerization conditions were similar to the above conditions and are depicted in Scheme 5.5 below.

Scheme 5.5. Optimized aqueous depolymerization/degradation of Lyz-rPEG conjugate with Grubbs III catalyst.

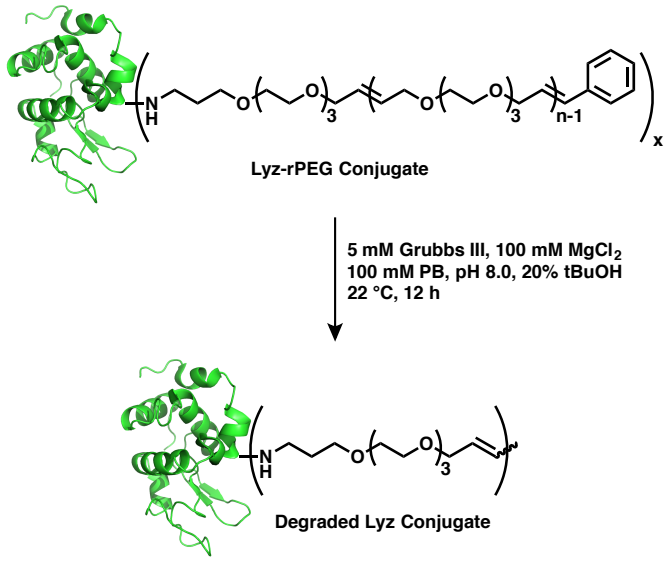

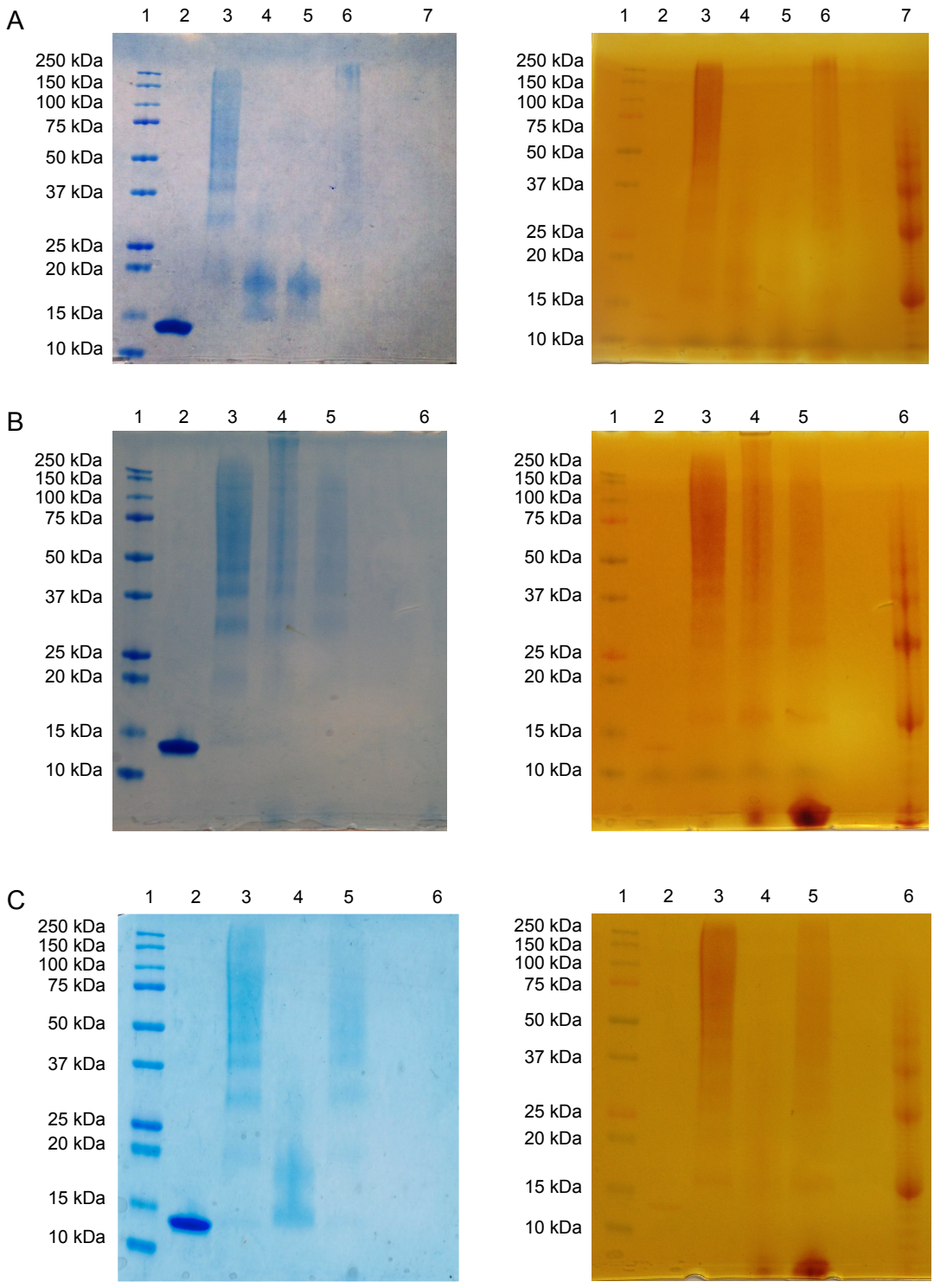

Figure 5.3. Optimization of depolymerization conditions for Lyz-rPEG conjugates in aqueous conditions by Grubbs III catalyst analyzed by SDS-PAGE with differential staining by Coomassie Brilliant Blue and 0.1 N Iodine to visualize protein (left column) and polymer (right column), respectively. Standard reaction conditions were as

follows for (A) and (B): 25 mM phosphate buffer (PB), pH 8.0, 100 mM $MgCl_2$, 5 mM Grubbs III (added as tBuOH stock), 20% tBuOH (V/V); 17 h (A) and 26 h (B) at 20 °C. Standard reaction conditions for (C) were identical to (A) and (B) except that the PB concentration was increased from 25 mM to 100 mM. Deviations from standard conditions are indicated as appropriate with each lane containing 3-5 μg protein. For (A-C), Lane 1: protein standards; lane 2: Lyz; lane 3: Lyz-rPEG conjugate. (A) Lane 4: standard conditions (SC); lane 5: SC with tBuOH raised to 27.3%; lane 6: SC + 1.34 mM allyl alcohol; lane 7: 10 kDa rPEG. (B) Lane 4: SC – $MgCl_2$; lane 5: SC with tBuOH substituted with MeCN – $MgCl_2$; lane 6: 10 kDa rPEG. (C) Lane 4: SC; lane 5: SC with tBuOH substituted with MeCN; lane 6: 10 kDa rPEG.

Having established a robust strategy for synthesis of reversible protein-polymer conjugation, we envisioned that this platform might also provide a useful means for modulation of protein activity. Conjugation of polymers to proteins is typically associated with reduced activity,[1] but previous work from our group suggests that if the polymer length can be reduced from the protein, much of the activity can be recovered.[40] Depolymerization of rPEG-Lyz appears to effectively cleave the bulk of rPEG from the protein, so we therefore expected the depolymerized conjugate to demonstrate regained activity compared to the intact rPEG-Lyz conjugate. Activity of each Lyz species was determined using the commercially available EnzChek Lysozyme Assay Kit (ThermoFisher Scientific) according to the manufacturer's procedure. Freshly dissolved Lyz was used as a positive control to normalize activity values from other conditions. In addition to assessing the activities of Lyz, the rPEG-Lyz conjugate, and the depolymerized rPEG-Lyz conjugate, an additional control condition was assayed that consisted of excipient rPEG with unmodified Lyz that was exposed to the depolymerization reaction conditions. This control was included to ensure that the components of the depolymerization reaction were not responsible for altering Lyz activity and that any change in

activity was a result of the attached rPEG polymers. The relative activities of each Lyz species are provided in Figure 5.4 below.

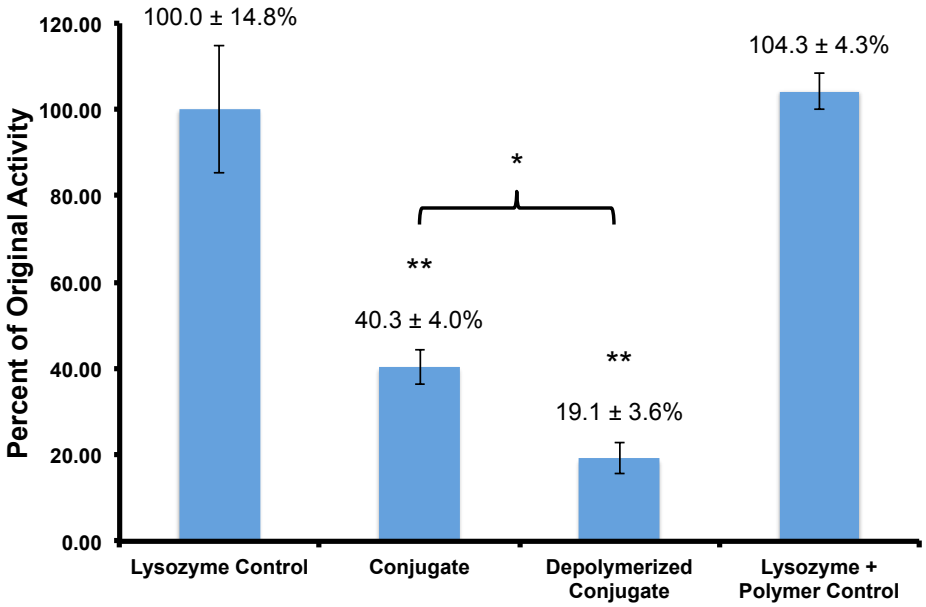

Figure 5.4. Activity of Lysozyme, Lyz-rPEG conjugate, depolymerized Lyz-rPEG conjugate, and Lysozyme with unconjugated polymer after exposure to depolymerization conditions. Data is expressed as means ± standard deviation. Statistical analysis was performed using a one-way ANOVA with post-hoc Tukey HSD tests; * indicates $p < 0.05$; ** indicates $p < 0.01$ (comparison to Lysozyme positive control).

No statistical difference was observed between fresh Lyz and Lyz with excipient polymer following exposure to depolymerization conditions. This result confirmed our hypothesis that the depolymerization reaction did not significantly affect Lyz activity. The rPEG-Lyz conjugate exhibited significantly lower activity (40.3 ± 4.0%) compared to fresh Lyz, which was expected given its attachment to several large polymers that most likely sterically hinder its active site. Surprisingly, we found that depolymerization of rPEG-Lyz not only failed to regain the protein's activity, but actually diminished it significantly further (19.1 ± 3.6%). We next investigated the effects of solvent and catalyst to determine if one of these reaction components was inhibiting the enzyme, but none of these conditions significantly impacted activity (data not shown). Based

on these results, it appears that the remnants of rPEGs that remain covalently linked to Lyz following depolymerization are inhibiting enzymatic activity. These shorter oligomers are slightly more hydrophobic and therefore may perturb the structure of the protein. Alternatively, the Grubbs III catalyst could remain coordinated to the polymer chain ends, with the resulting attachment of the hydrophobic catalyst to the protein interfering with the protein's ability to access or turnover substrate. Because the Lyz control exposed to depolymerization conditions showed no evidence of Lyz inhibition, the presence of metathesis catalyst itself is not causing this lack of activity. Therefore, the decline in activity following depolymerization is likely the result of hydrophobic attachments that disrupting the conformation of the protein and its ability to process substrate.

The results of this study demonstrate that aldehyde-functionalized rPEGs provide promising, degradable analogs of PEG that can be used for reversible protein polymer conjugation. During the course of this work, it was also shown that rPEGs are noncytotoxic up to at least 1 mg/mL in human dermal fibroblasts,[20] suggesting that these polymers may have applications in biotechnology as alternatives to PEG. While not feasible for use in *in vivo* applications, this strategy may have applications in biotechnology in areas such as biosensing or diagnostics. Given that nonspecific conjugation of polymers to proteins often yields heterogeneous products with different numbers of polymers attached to each protein and positional isomers for each of these cases, depolymerization of these polymers to small fragments could facilitate more facile characterization of these aspects. Additionally, the inherent synthetic flexibility of ROMP can facilitate incorporation of higher order functionalities into these polymers by means of copolymerization or end-group functionalization. Furthermore, it may be possible to increase synthetic complexity via functionalization of the backbone alkenes.

Taken together, this work outlines a straightforward method for synthesizing and reversibly conjugating nontoxic, degradable polymers to proteins and therefore provides interesting alternatives to PEG for protein conjugation.

5.2.2 Efforts toward the Generation of Uniform PEG Analogs via Thiol-Ene Chemistry

Currently, all strategies to synthesize uniform PEG or PEG analogs rely on iterative monomer addition, or the repeated, sequential coupling of monomer units to a growing chain. There are four variations of this strategy that have been explored. The first two modes of synthesis involve linear growth resulting from iterative coupling of mono-protected monomers to (1) one end or (2) both ends of an initial bifunctional building block. The other two modes involve exponential growth resulting from functionalization of the growing polymer chain-ends to make either (3) one heterobifunctional or (4) two homobifunctional building blocks that can then be coupled together in processes known as chain doubling and chain tripling, respectively.[27]

Conceptually, the advantage of Modes 1 and 2 include ease of synthesis and precise control of degree of polymerization, and modularity of monomer incorporation, since only one monomer is added at a time to extend the polymer chain. However, because these modes rely on linear growth, reaching high molecular weights is challenging due to compounding effects of suboptimal yields at each coupling step. A good example of a Mode 1 strategy is solid phase organic synthesis (SPOS) to produce compounds such as peptides or oligonucleotides. In these cases, a single protected monomer unit is coupled to an insoluble crosslinked network at a time. Once coupling is complete, a deprotection reaction removes the protecting group from the terminal monomer unit, and addition of the next monomer unit may proceed. SPOS facilitates fast purification by simple filtration and can provide access to virtually any combination of monomer units. However, the overall lengths of polymers of this type are typically limited

because the yield of the final polymer is controlled by the product of the yields of each prior monomer coupling reaction. For example, even with a monomer coupling efficiency of 99%, a polymer containing only 100 monomer units can only reach a theoretical maximum yield of 0.99^{100}, or 36.6% yield. For couplings with lower efficiencies such as 95%, only 0.6% yield would be expected for a 100 monomer unit polymer.

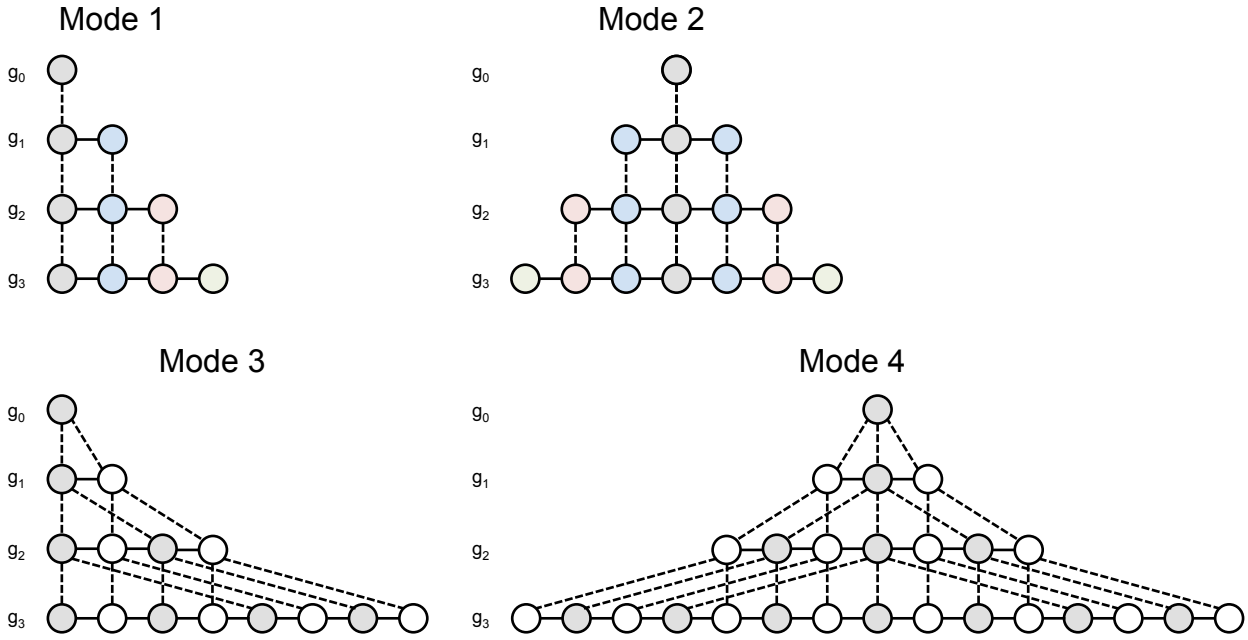

Figure 5.5. Modes of uniform oligomer synthesis strategies. Each circle represents a single monomer unit with dashed lines indicating monomer placement in oligomer in each generations (g_n). Mode 1: unidirectional iterative coupling; Mode 2: bidirectional iterative coupling; Mode 3: chain doubling; Mode 4: chain tripling. Figure redrawn with permission from French, et al.[27] Copyright © 2009 WILEY-VCH Verlag GmbH & Co. KGaA, Weinheim.

Yields of iterative addition products are vastly improved in Modes 3 and 4 because these strategies rely on exponential growth. Instead of adding the same small monomer units iteratively, each coupling step produces the monomer for the next coupling step. For instance, a chain doubling reaction might begin with an (PG_1)A-B monomer and A-B(PG_2) monomer, where A and B are mutually reactive groups and PGs represent orthogonal protecting groups.

After the first coupling step, a new monomer (PG_1)A-B-A-B(PG_2) is generated. Half of this new monomer is then selectively deprotected to give (PG_1)A-B-A-B, and the other half is selectively deprotected to give A-B-A-B(PG_2), and these two new monomers (4-mers) can then be coupled to give a monomer double the length (8-mer) (PG_1)A-B-A-B-A-B-A-B(PG_2). A similar route can be carried out for chain tripling, although more steps are typically required. As noted, Modes 3 and 4 enable rapid, exponential growth of polymer chains and can theoretically produce longer polymers with higher yields than Modes 1 and 2. However, these approaches are limited not only by the number of synthetic steps that must be carried out for each chain extension reaction, but also by the difficulties in purification of large oligomers from smaller oligomers with similar polarities.

PEGs used for therapeutic applications such as protein-polymer conjugates typically fall in the range of 5-40 kDa, or approximately 114-909 monomer units of ethylene glycol (EG).[5] At the outset of this project, the longest reported uniform PEGs consisted of 44,[25] 48,[27] and 62[32] EG units as synthesized by Mode 4, Mode 3, and Mode 3, respectively, the longest being 2850 Da. Though relatively long oligomer chains were produced in these examples, each required a high step count and was ultimately limited by purification difficulties. To bridge the vast disparity in molecular weight between the EG monomer unit and biomedically relevant PEG molecular weights, we devised a strategy that would combine various aspects from each mode of synthesis. Linear growth Modes 1 and 2 are high yielding, but can only be used to prepare low molecular weight oligomers, and exponential growth Modes 3 and 4 are lower yielding, but can facilitate rapid preparation of relatively high molecular weight oligomers. Therefore, we designed a synergistic combination of each mode to exploit the advantages from each approach.

Specifically, we envisioned that chain tripling could first be used to prepare medium length oligomers of PEG containing 12 EG units (PEG12). Beyond this molecular weight, further increases in size result in purification difficulties due to similarities in polarity between smaller and larger oligomer chains. Once the mid-range PEG12 oligomers were prepared, we could then differentially functionalize its end-groups to make a heterobifunctional PEG12 derivative that could be used as a "macro-monomer" for synthesis of high molecular weight PEGs by SPOS. Attachment to an insoluble resin would facilitate purification of the growing polymer chain, and much higher molecular weights could theoretically be reached due to the significantly larger EG-based monomer unit (Figure 5.6; top).

However even with this substantially larger PEG12 monomer, achieving molecular weights of 5 kDa or 20 kDa would require 10 or 38 coupling steps, respectively. The coupling chemistry would therefore need to be highly efficient. In addition, the coupling chemistry should form a linkage that is structurally similar to the polyether backbone of PEG. We therefore elected to use the efficient radical-mediated hydrothiolation reaction between vinyl ethers and thiols, a type of thiol-ene reaction, due to the product resemblance to PEG backbone ethers (Figure 5.6; bottom). Thiol-ene chemistry has been well established as a high-efficiency, atom-economic reaction that has demonstrated broad utility in polymer chemistry.[50] We therefore expected this chemistry to allow us to generate uniform polymers that only differed from PEG in the substitution of one oxygen atom for one sulfur atom every 48 atoms along the polymer backbone. This small structural change was not expected to significantly affect the polymer's "PEG-like" properties.

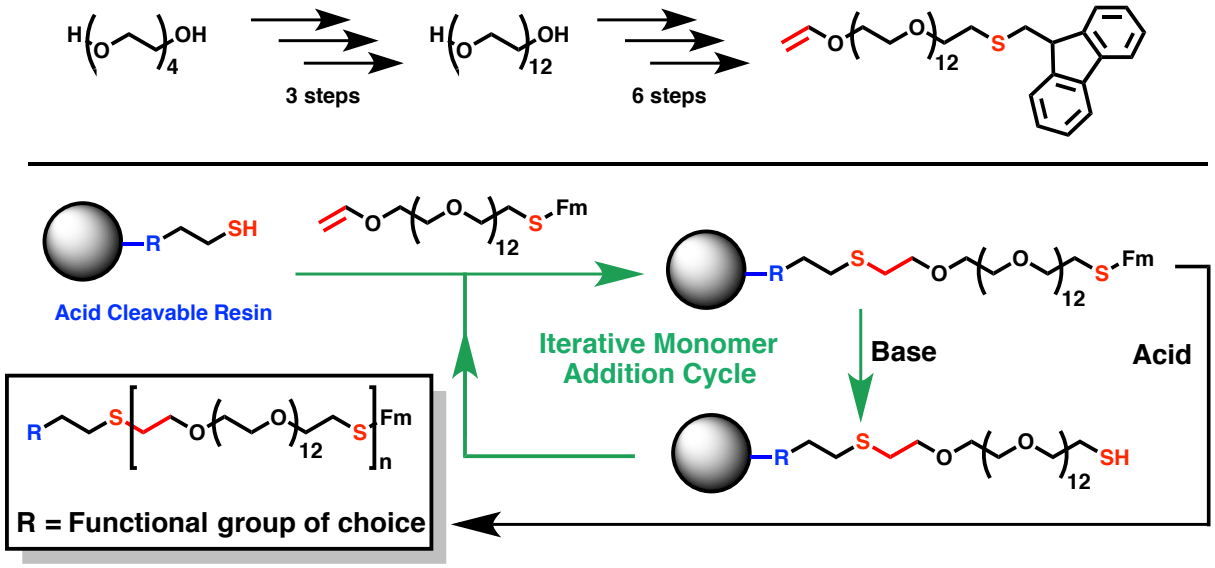

Figure 5.6. Synthetic overview of strategy for generation of uniform PEG analogs via thiol-ene mediated SPOS.

A preliminary objective was to ensure that the polymers produced from this route would be water-soluble. Therefore, we began this work by preparing two homobifunctional monomers, PEG12-dithiol (**4**) and PEG14-divinyl ether (**5**), that could be copolymerized via a thiol-ene step growth polymerization to provide heterogeneous approximations of the desired uniform polymers (sPEG; Scheme 5.6). A small quantity of commercially available dodecylethylene glycol (PEG12) was activated via reaction with tosyl chloride to provide PEG12-ditosylate (**3**) in 95% yield. Disotylate **3** was subsequently reacted with either potassium thioacetate, then 1 M HCl to yield dithiol **4** in 45% yield (over 2 steps), or with ethylene glycol vinyl ether and sodium hydride to yield divinyl ether **5** in 47% yield. Dithiol **4** and divinyl ether **5** monomers were then dissolved in tetrahydrofuran (THF) with photoinitiator dimethoxyphenylacetophenone (DMPA), sparged, and the polymerization initiated with 365 nm light.

Scheme 5.6. Synthesis of sPEG from PEG12-based monomers by step-growth polymerization.

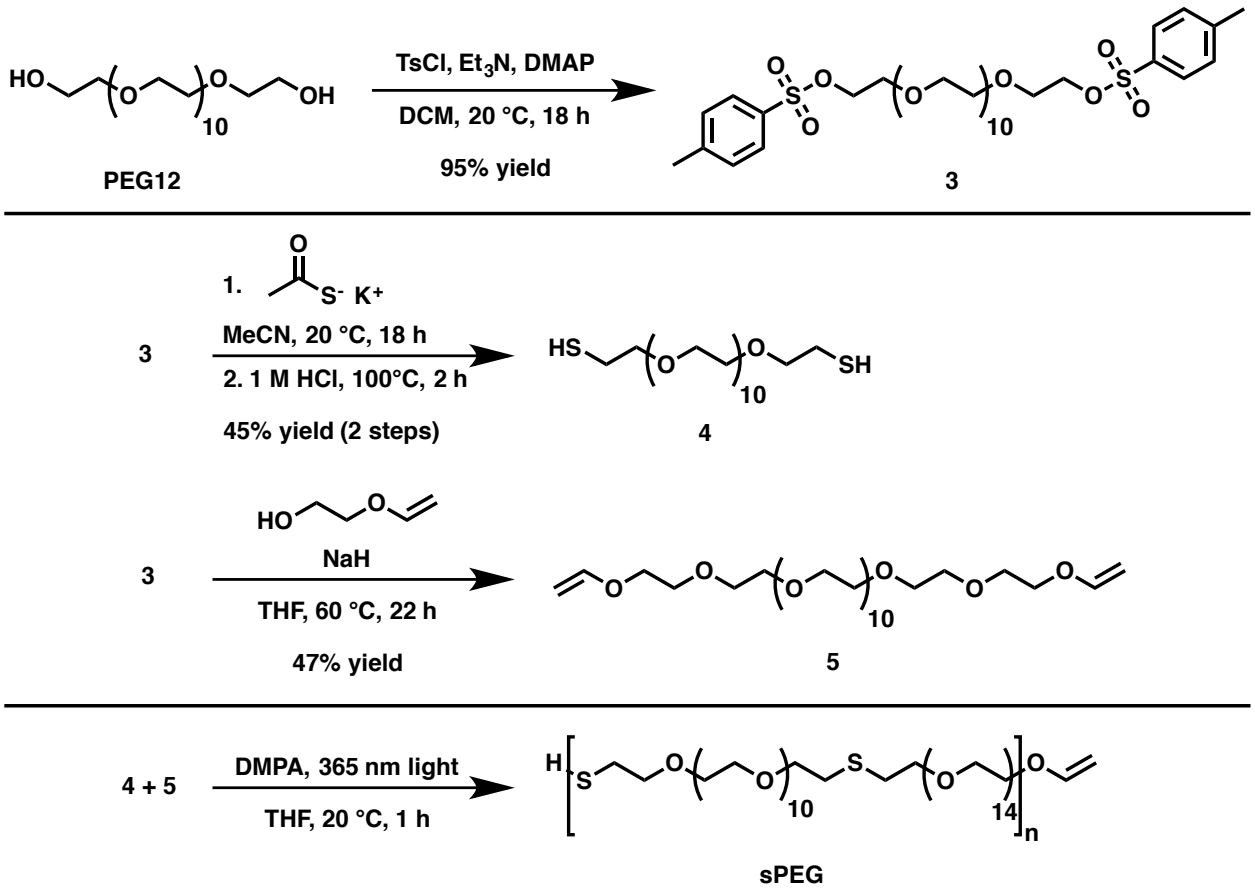

An initial polymerization was carried out using a slight excess dithiol **4**. As observed by ^{1}H NMR (Figure 5.7), the alkene protons were reduced compared to PEG backbone peaks, indicating the formation of thioether products. Addition of further dithiol **4** almost completely reduced the alkene proton peaks (Figure 5.8), suggesting oligomerization of the two monomers. GPC analysis confirmed oligomerization with an observed polymer M_n = 4.5 kDa, and the observed dispersity of 1.68 was also indicative of a low-conversion step-growth polymerization (Figure 5.9). These polymerizations and the resulting short polymers provided insight into how this chemistry could be applied toward uniform PEG analogs; however, the dispersity of the polymers was not desirable, so we continued our pursuit of the uniform polymers.

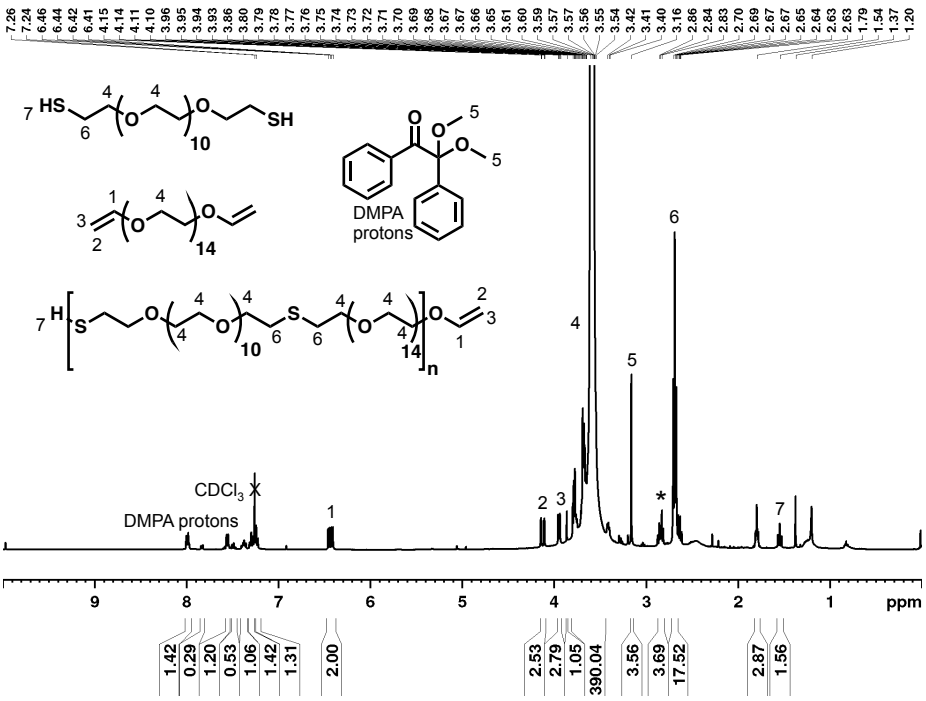

Figure 5.7. ^{1}H NMR of sPEG crude reaction in $CDCl_3$; * indicates methylene protons adjacent to disulfides.

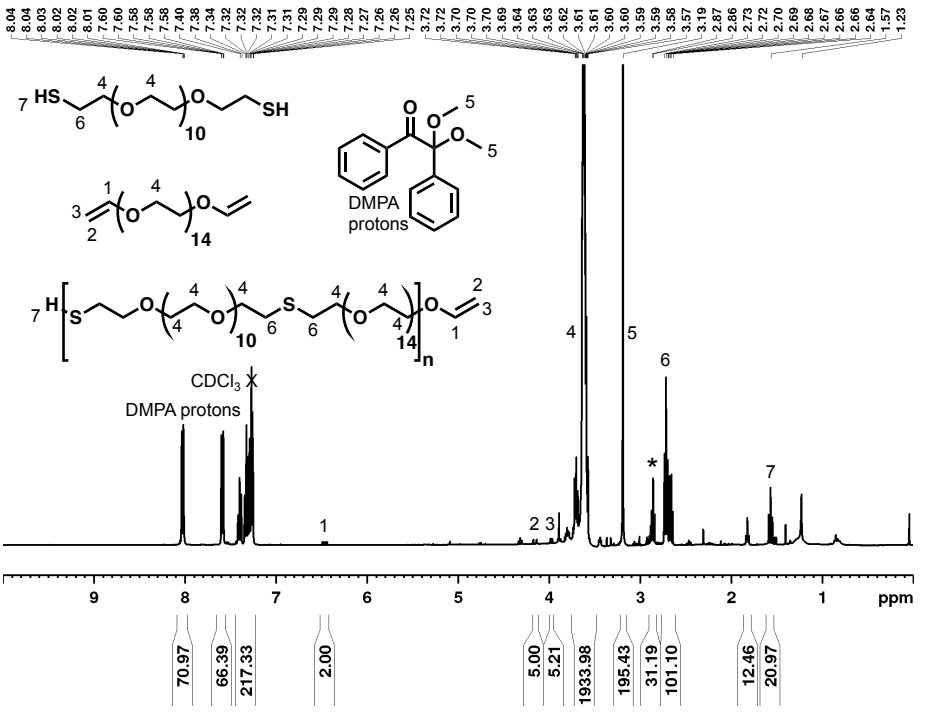

Figure 5.8. ^{1}H NMR of sPEG crude reaction in $CDCl_3$ following addition of more PEG12-dithiol; * indicates methylene protons adjacent to disulfides.

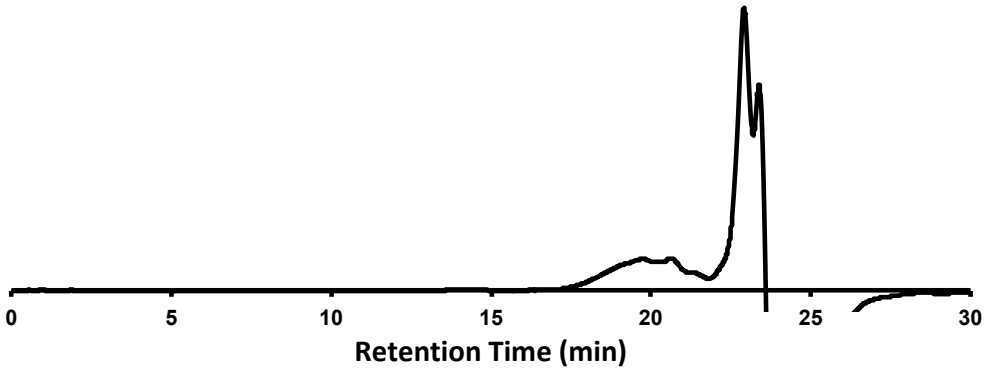

Figure 5.9. GPC chromatogram of sPEG (M_n = 4.5 kDa, M_w = 7.5 kDa, Đ = 1.68) crude reaction. Polymer peaks are observed at a retention time of approximately 20 minutes with monomers, small molecules, and the solvent front eluting from 22-24 minutes.

Importantly, sPEGs were completely water soluble, and further reactions using a water-soluble initiator could even be run directly in water with similar results (data not shown). Moreover, the thiol-ene reaction was observed to be highly efficient with disappearance of alkene peaks observed after only minutes. These preliminary results supported the feasibility of this strategy as applied to the eventual SPOS approach. Shortly after these preliminary studies were carried out, a similar study on step-growth polymerization of tetraethylene glycol (PEG4)-based dithiol and divinyl ether monomers to generate PEG anaologs was reported.[51] These polymers were soluble following polymerization and solubility could be enhanced upon oxidation of the thioethers to sulfoxides or sulfones. Having verified these heterogeneous sPEG analogs possessed the desired PEG-like properties, we next focused our efforts toward the synthesis of heterobifunctional monomers from which we could build uniform PEGs by SPOS.

Given that SPOS of heterobifunctional PEG12 monomers would require at least 10 coupling steps to generate polymers of >5 kDa, it was important to use a scalable process to prepare PEG12 monomer on multigram scale. To this end, we utilized a chain tripling approach based on a previous report of a chromatography-free synthesis of PEG oligomers.[52] We began

the synthesis of PEG12 by bis-tosylation of the inexpensive tetraethylene glycol (PEG4) with tosyl chloride and triethylamine to give 9.7 grams of PEG4-ditosyl (**6**) in 67% yield (Scheme 5.7). Separately, tetraethylene glycol was also mono-tritylated with trityl chloride and triethylamine to provide 19.2 grams of PEG4-monotrityl (**7**) in 82% yield. Compounds **6** and **7** were then coupled in the presence of sodium hydride with heating to provide 12.6 grams of PEG12-ditrityl (**8**) in 63% yield. Finally, PEG12 was obtained in quantitative yield following the deprotection of **8** with trifluoroacetic acid (TFA) with scavengers triisopropylsilane (TIPS) and water and was purified by repeated precipitation in diethyl ether.

Scheme 5.7. Synthesis of PEG12 from tetraethylene glycol.

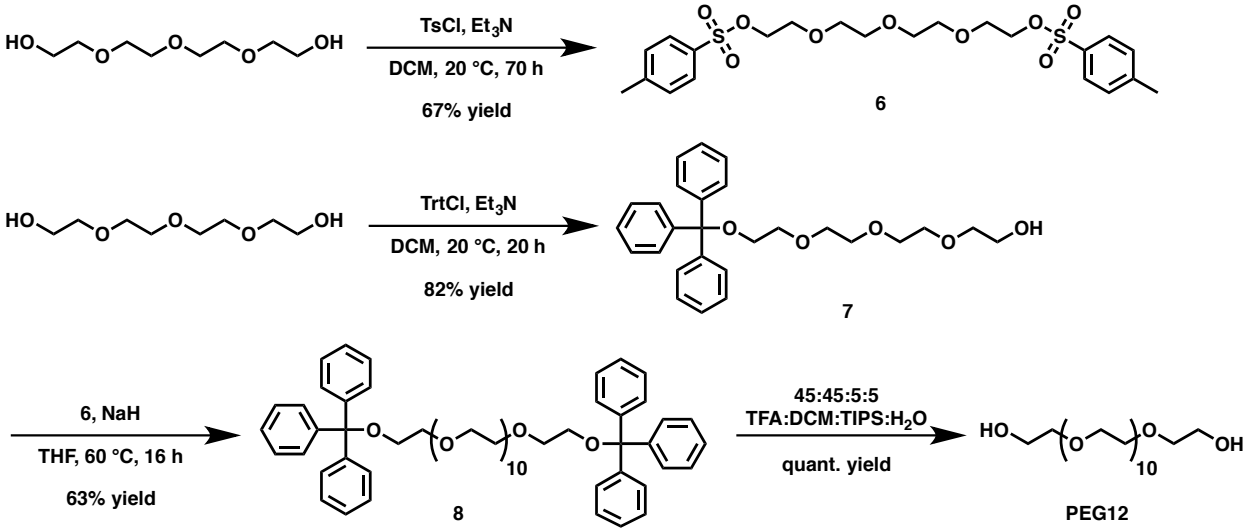

Purification of each of these compounds (and later PEG12 derivatives) was facilitated primarily by washing the organics with water to remove unreacted PEGs as recommended by several literature reports in effort to circumvent column chromatography.[53,54] However, we consistently found that although these aqueous washes could remove unreacted PEG species, there was always a small portion of bis-functionalized PEG remaining in the reaction that could only be separated chromatographically. For all chain coupling steps, monomer purity is of

paramount importance, as small impurities can lead to truncation products and ultimately add heterogeneity to the final polymer chain. For this reason, all synthesized PEG-based compounds were purified using silica gel chromatography, except for PEG12, which was purified by precipitation as noted. Despite reliance on chromatographic purification, 6.7 grams of PEG12 was prepared for further reactions. Notably, although the trityl protecting groups are certainly not atom economical, they were necessary, as other smaller groups were insufficient to shift product polarity and led to purification issues (data not shown).

We next proceeded to differentially convert each of the alcohol end-groups to a protected thiol and vinyl ether. We envisioned a six-step process to carry out these transformations (Scheme 5.8). This synthetic route was designed to result in large changes in polarity after each transformation, improving the chromatographic separation. For example, during initial synthetic routes it was exceedingly difficult to separate monotosylated PEG12 from unmodified PEG12 starting material due to the insufficient difference in polarity between the tosyl and alcohol end-groups. This route also utilized two end-group modifiers to install thiol or vinyl ether functionality. Fluorenylmethanethiol (FmSH) would be used as the thiol source, equipped with a base-cleavable protecting group. Following acidic trityl deprotection, the ethyl vinyl ether electrophile would be installed through coupling with 2-tosylethyl vinyl ether, leading to the hetero bifunctional monomer **13**.

Scheme 5.8. Synthetic route toward preparation of PEG12-based, heterobifunctional monomer 13 for synthesis of uniform PEG analogs by solid-phase iterative addition.

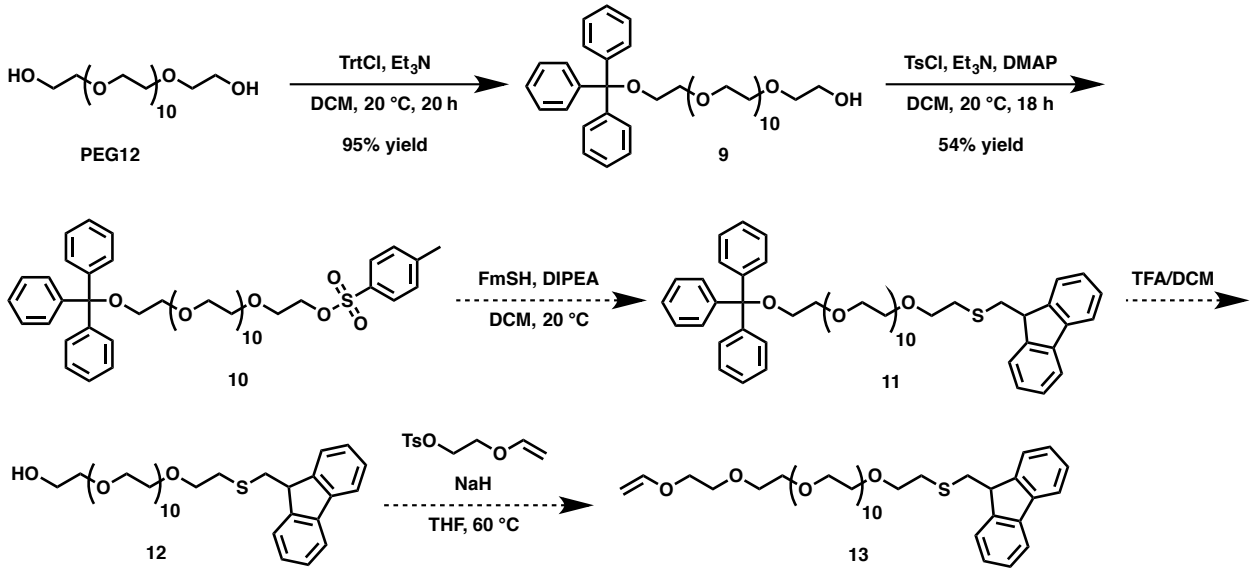

We began the synthesis of heterobifunctional monomer **13** by reaction of PEG12 with trityl chloride and triethylamine to give PEG12-monotrityl (**9**) in 95% yield, using a stoichiometric excess of PEG12 to minimize bifunctionalization. The crude organic reaction solution was washed extensively with water to recover excess PEG12, with 57% of the initially added PEG12 recovered for future use. This strategy was based on literature precedent for chromatography-free purification of monofunctional EG oligomers.[53,54] Compound **9** was then reacted with tosyl chloride and triethylamine to give monotosyl-PEG12-monotrityl (**10**) in 54% yield. As previously mentioned, purification was negatively impacted by the insufficient shift in polarity of **9** compared to **10**. Even following preparative HPLC purification of **10**, several minor impurities tended to persist as observed by ^{1}H NMR and analytical HPLC. These impurities included residual **9** as well as PEG12-ditrityl.

Scheme 5.9. Synthesis of 2-tosylethyl vinyl ether.

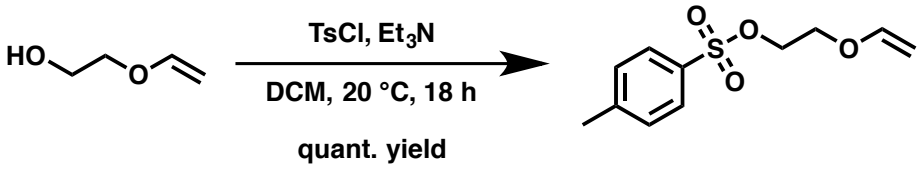

Our synthetic approach utilized two PEG12 end-group modifiers to install the desired vinyl ether and thiol reactive end-groups. Synthesis of the electrophilic ethylene glycol vinyl ether building block was easily obtained from reaction of ethylene glycol vinyl ether with tosyl chloride and triethylamine to give 2-tosylethyl vinyl ether in in quantitative yield (Scheme 5.9). However, synthesis of FmSH, proved more challenging. Several strategies were attempted to access this compound; however, none were able to generate FmSH in sufficient yields despite literature precedent. We first attempted to synthesize FmSH directly via reaction of potassium thioacetate with the standard protecting group reagents fluorenylmethyloxycarbonyl chloride and fluorenylmethyloxycarbonyl succinimidyl ester,[55–57] but these reactions only produced fluorenylmethanol (FmOH) as formed via elimination followed by hydration. We next attempted two more conservative, alternative strategies. The first consisted of a Mitsunobu reaction between thioacetic acid and FmOH. The desired product was observed, but removal of the resulting triphenylphosphine and diisopropyl hydrazidodicarboxylate side products resulted in reduced yield after purification, providing fluorenylmethylthioacetate (FmSAc) in only 20% yield (Scheme 5.10; top). Higher yields were initially obtained following a literature route[58] that first tosylated FmOH to make fluorenylmethyltosylate in 48% yield, but subsequent reactions with a variety of thiolate nucleophiles such as potassium thioacetate and tritylthiol returned only starting materials (Scheme 5.10; bottom). During these reactions, it also became clear that the fluorenylmethyl group was more prone to elimination and deprotection than originally

anticipated, making it ultimately unsuitable for use in synthesis of monomer **13**. This realization forced us to reevaluate our synthetic plan to make a heterobifunctional monomer for SPOS.

Scheme 5.10. Efforts toward the synthesis of fluorenylmethanethiol (FmSH).

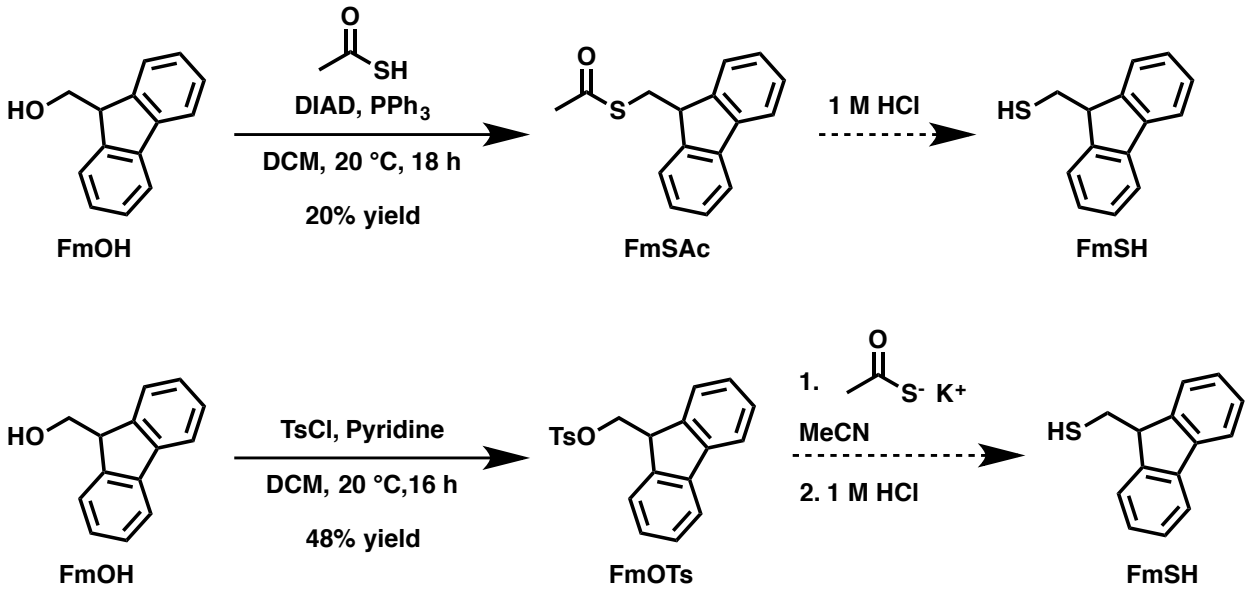

To improve purification and potentially lower the step count for the synthesis of monomer **13**, we took inspiration from a literature report from the Jiang group that used a unique strategy to differentiate between symmetrical PEG diols.[32] The Jiang group found that reaction of thionyl chloride with PEG diols of various lengths facilitated macrocyclization to form the PEG-based macrocyclic sulfites. This was followed by *in situ* oxidation with catalytic ruthenium tetroxide to produce the corresponding PEG macrocyclic sulfates, which could be ring-opened and desymmetrized with a variety of nucleophiles. This strategy had the advantage of increasing yield by improving desymmetrization, and we predicted that this route might also facilitate more facile purifications of longer EG oligomers.

One of the notable disadvantages of this report was the low reaction concentrations that were required to favor macrocyclization over oligomerization. For example, the reported

macrocyclization of PEG12 to the sulfite was carried out at a concentration of only 5 mM (2.73 g/L) with a yield of 63%, and the yield decreased to 59% when the concentration was increased to 10 mM (5.47 g/L).[32] Given our prior experience with crown ethers, we envisioned that templating the PEG chains with the appropriate alkali metal cation would increase the concentration at which these reactions could be run as well as the overall yield. This strategy has been well established for crown ether synthesis in general, and it has been reported that cesium cations in particular are particularly amenable to complexation with 36-crown-12 ethers, which closely resembles PEG12-macrocyclic sulfite.[59,60]

We therefore began synthesizing PEG12-macrocyclic sulfite with the goal of using this platform as an alternative route toward monomer **13**. Macrocyclization of PEG12 was carried out using the reported conditions, with the addition of 5 molar equivalents of cesium iodide to template the macrocyclization. Additionally, the reaction was carried out at a concentration of 40 mM, which was at least 4-fold higher than the literature report (Scheme 5.11). The reaction was carried out by stirring together PEG12, diisopropylethylamine, and cesium iodide in dichloromethane at 0 °C in an ice bath followed by addition of thionyl chloride in portions every 10 minutes for 60 minutes to ensure slow addition and low concentrations of thionyl chloride. After chromatographic purification, PEG12-macrocyclic sulfite was obtained in 75% yield. This offered a significant improvement over the literature yield of 59% for the same compound and at a 4-fold higher concentration. Purification of this compound was achieved by running three successive silica-gel columns. As noted previously, significant shifts in polarity are required for facile separation of large PEG-based oligomers, and although the macrocyclization shifted polarity of PEG12 enough for purification, clean separation of products remained challenging.

While purification was still time-consuming, the slight increase in yield and decrease in step count was a promising methodology for preparation of monomer **13**.

Scheme 5.11. Synthesis of PEG12 macrocyclic sulfite.

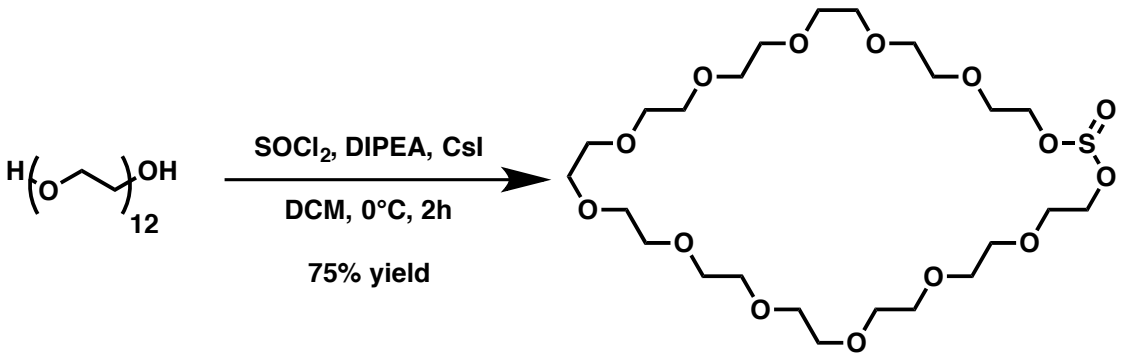

As we were in the process of preparing more PEG12-macrocyclic sulfite, the Jiang group published a manuscript in which they successfully prepared a series of uniform PEGs with molecular weights up to 10 kDa.[61] Their report contained a very similar approach to ours with only minor differences in chemistry. Instead of using thiol-ene as the efficient coupling chemistry, they elected to use carboxylic acid-amine coupling methodology to iteratively couple EG oligomers of similar lengths, leading to uniform PEGs as large as 10 kDa with excellent purity. The group has since published several more interesting reports of these uniform PEGs as applied to various applications.[62–64] Given these results, we discontinued our efforts toward thiol-ene based synthesis of uniform PEGs. However, the use of an alkali metal cation to template the formation of macrocyclic sulfites and sulfates may prove useful for others preparing uniform polymers. We expect that these macrocycles will come to represent an important synthetic building blocks in the field of polymer chemistry and therefore believe that the ability to carry out PEG macrocyclization reactions at higher concentrations with higher yields via simple addition of an appropriate alkali metal cation will prove invaluable for future efforts in this area.

5.3 Conclusions

As the field of protein-polymer conjugates has advanced, so has the demand for biocompatible polymers with higher order functionalities. While PEG exemplifies the gold standard in this field, it lacks chain degradability and uniformity. This work addresses these modern synthetic challenges in polymer chemistry by detailing an approach to prepare degradable PEG analogs by ROMP that can be conjugated to proteins and subsequently degraded from the protein by metathesis depolymerization. We additionally report our novel strategy and efforts toward synthesis of uniform PEG analogs by thiol-ene iterative monomer coupling of PEG12 "macro-monomers." The synthesis of degradable or uniform PEG analogs denotes an important development not only for PEG related applications, but for other biomedical polymers that could be precisely engineered using this methodology. We therefore expect that the work presented herein will be of significant interest to other scientists pursuing next-generation polymers for biomedical applications.

5.4 Experimental

5.4.1 Materials

All chemicals were purchased from Sigma-Aldrich, Fisher Scientific, and Acros and used as received unless otherwise noted. Lyz was obtained from Sigma-Aldrich and used as received. Dodecylethylene glycol (PEG12) was purchased from Jenkem USA. Dichloromethane (DCM) was distilled over CaH_2 and stored under argon. Tetrahydrofuran (THF) was distilled over sodium/benzophenone and stored under argon. Unsaturated crown ether **1** was prepared by Dr. Emma Pelegri-O'Day as previously described,[34] ruthenium catalyst was removed as described,[65] and the monomer was distilled under reduced pressure before use. Polymerizations were carried

out in a Vacuum Atmospheres Genesis stainless steel glove box under nitrogen atmosphere unless otherwise noted. All other reactions were carried out under an argon atmosphere unless otherwise noted.

5.4.2 Analytical Techniques

NMR spectra were obtained on Bruker AV400, AV500 or DRX500 MHz spectrometers. Proton NMR spectra were acquired with a relaxation delay of 4 s for small molecules and 30 s for all polymers. GPC was conducted on one of two systems. System one is a Shimadzu HPLC system equipped with a refractive index detector RID-10A, one Polymer Laboratories PLgel guard column, and two Polymer Laboratories PLgel 5 μm mixed D columns with a column oven set at 40 °C and LiBr (0.1 M) in DMF as an eluent (flow rate: 0.60 mL/min). Calibration was performed using near-monodisperse PEG standards from Polymer Laboratories. System two is a Shimadzu HPLC system with a refractive index detector RID-10A, one Tosoh TSKGel guard column, and one Tosoh TSKGel G4000PW column. Eluent was 0.3 M NaNO3 + 20 mM phosphate buffer pH 7 + 20% MeCN at 25 °C (flow rate 0.7 mL/min). Calibration was performed using near-monodisperse PEG standards from Polymer Laboratories. SDS-PAGE was performed using Bio-Rad Any kD Mini-PROTEAN-TGX gels. SDS-PAGE protein standards were obtained from Bio-Rad (Precision Plus Protein Pre-stained Standards). For SDS-PAGE analysis, approximately 5 μg of protein was loaded into each lane. Conjugates were purified and analyzed by FPLC on a Bio-Rad BioLogic DuoFlow chromatography system equipped with a 1 mL GE Healthcare HiTrap Heparin HP column (used as a cation exchange column) using a method of 0 to 1 M NaCl in 10 mM PB, pH 6.0 (Buffer A: 10 mM PB, pH 6.0; Buffer B: 10 mM PB, pH 6.0 + 1 M NaCl; 0.4 mL/min; 3x 0.33 mL injections; 2 CV 0% Buffer B, then 8 CV 0-100% Buffer B, then 2 CV 100% Buffer B). Bicinchoninic acid assays for determination of

protein concentration were carried out using a Pierce BCA Protein Assay Kit (ThermoFisher Scientific) according to the manufacturer's protocol and absorbance was read at 562 nm using a Tecan Infinite M1000 Pro automated plate reader system. ESI mass spectra were obtained using either a Waters Acquity LCT Premier XE equipped with an autosampler and direct injection port or an Agilent 6530 QTOF-ESI with a 1260 Infinity LC with autosampler. Infrared absorption spectra were obtained using a PerkinElmer FT-IR equipped with an ATR accessory. Normal phase flash column chromatography was carried out using a Biotage Isolera One Flash Purification Chromatography system. Analytical reverse phase high performance liquid chromatography (HPLC) was carried out on a Agilent 1260 Infinity II HPLC system equipped with an autosampler and a UV detector using a Poroshell 120 2.7 μm C18 120 Å column (analytical: 2.7 μm, 4.6 × 100 mm) with monitoring at λ = 220 and 280 nm and with a flow rate of 0.8 mL/min. Preparatory reverse phase HPLC was carried out on a Shimadzu high performance liquid chromatography system equipped with a UV detector using a Luna 5 μm C18 100 Å column (preparatory: 5 μm, 250 × 21.2 mm) with monitoring at λ = 215 and 254 nm and with a flow rate of 20 mL/min.

5.4.3 Methods

ROMP polymerization of monomer 1 to synthesize rPEG

In a nitrogen-filled glovebox, Grubbs I (8 mg, 0.01 mmol, 1 eq) was dissolved in DCM (495 μl) and added to a dram vial containing monomer **1** (100 mg, 0.49 mmol, 50 eq) and a stir bar. The polymerization solution was stirred rapidly at room temperature for 6 hours before addition of vinylene carbonate (75 μl, 1.24 mmol, 125 eq) and stirring for an additional 60 minutes. The reaction vial was then removed from the glovebox and any residual active catalyst was further quenched with ethyl vinyl ether (150 μl, 1.48 mmol, 150 eq) and stirred for an

additional 75 minutes. The polymer was then precipitated twice into cold ether (20 mL) and dried under vacuum to yield a tan oil (65 mg, 65% yield). M_n (^{1}H NMR) = 9.7 kDa, M_n (GPC) = 8.6 kDa, M_w (GPC) = 13.8 kDa, Đ = 1.62; see Figure 5.11 for GPC chromatogram. See Figure 5.10 for ^{1}H NMR (500 MHz, CD_3CN) δ: 9.67 (t, J = 2.0 Hz, 1H), 7.42 (d, J = 7.8 Hz, 2H), 7.31 (t, J = 7.6 Hz, 2H), 7.24 (t, J = 7.3 Hz, 1H), 6.61 (d, J = 15.9 Hz, 1H), 6.32 (m, 1H), 5.84−5.60 (m, 111H), 4.18−3.86 (m, 225H), 3.71−3.34 (m, 691H), 2.57 (m, 2H).

Synthesis of Nor-PEG monomer 2

Synthesis of monomer **2** was based on the previously reported procedure.[47] To a previously oven-dried 1-neck 50 mL round bottom flask equipped with a stir bar and water condenser was added cis-5-Norbornene-exo-2,3-dicarboxylic anhydride (500 mg, 3.05 mmol, 1 eq), 2,5,8,11-tetraoxatridecan-13-amine (MeO-PEG4-NH_2; 689 µl, 3.65 mmol, 1.2 eq), and 20 mL toluene. The solution was heated to reflux and stirred for 17 hours under Argon. The solution was then cooled to ambient temperature, diluted with DCM, then washed 3 times with a mixture of water and saturated sodium bicarbonate solution, once with a mixture of water and 1 M HCl, then once more with a mixture of water and saturated sodium bicarbonate solution. The combined organics were dried over anhydrous magnesium sulfate and then concentrated under vacuum to yield a colorless oil (1.087 grams; quant. yield). See Figure 5.12 for ^{1}H NMR (500 MHz, $CDCl_3$) δ: 6.25 (t, *J* = 1.8 Hz, 2H), 3.66-3.50 (m, 16H), 3.34 (s, 3H), 3.23 (m, 2H), 2.65 (d, *J* = 1.4 Hz, 2H), 1.45 (dt, *J* = 9.9, 1.4 Hz, 1H), 1.33 (dt, *J* = 9.9, 1.4 Hz, 1H). See Figure 5.13 for ^{13}C NMR (125 MHz, $CDCl_3$) δ: 177.99, 137.82, 71.92, 70.59 (2C), 70.54, 70.51, 69.85, 66.87, 59.03, 47.80, 45.26, 42.71, 37.72. HRMS: $C_{18}H_{28}NO_6$ calc. $[M+H]^+$ = 354.1917 Da; obsd. $[M+H]^+$ = 354.1960 Da.

ROMP polymerization of monomer 1 to synthesize poly(Nor-PEG)

In a nitrogen-filled glovebox, Grubbs I (6 mg, 0.007 mmol, 1 eq) was dissolved in DCM (495 µl) and added to a dram vial containing monomer **1** (127 mg, 0.358 mmol, 50 eq) and a stir bar. The polymerization solution was stirred rapidly at room temperature for 80 minutes. The reaction vial was then removed from the glovebox and any residual active catalyst was quenched with ethyl vinyl ether (100 µl, 1.052 mmol, 150 eq) and stirred for an additional 75 minutes. The polymer was then precipitated thrice into cold ether (20 mL) and dried under vacuum to yield a brown oil (135 mg, quant. yield). M_n (^{1}H NMR) = 19.9 kDa, M_n (GPC) = 26.2 kDa, M_w (GPC) = 29.3 kDa, Đ = 1.12; see Figure 5.15 for GPC chromatogram. See Figure 5.14 for ^{1}H NMR (500 MHz, $CDCl_3$) δ: 6.38 (m, 2H), 7.30 (m, 2H), 7.22 (m, 1H), 6.54 (d, *J* = 16.2, 1H), 6.31 (dd, *J* = 15.8, 7.0 Hz, 1H), 5.80-5.40 (m, 112H), 5.20 (d, *J* = 17.0 Hz, 1H), 5.11 (d, *J* = 10.4 Hz, 1H), 3.84-3.51 (m, 910H), 3.44-3.34 (m, 168H), 3.31-3.18 (m, 18H), 3.17-2.89 (m, 117H), 2.86-2.58 (m, 95H), 2.32-1.97 (m, 58H), 1.69-1.52 (m, 54H).

Representative aqueous depolymerization of rPEG and poly(Nor-PEG)

rPEG (M_n = 6.1 kDa calculated by GPC, 1.7 mg, 0.28 µmol) and poly(Nor-PEG) (M_n = 26.2 kDa calculated by GPC, 3.0 mg, 0.11 µmol) were weighed into separate 3 mL vial and dissolved in 900 µl of 50 mM PB, pH 8.0. A 50 mM saturated stock solution of Grubbs III was prepared in *tert*-butyl alcohol and 100 µl of the catalyst solution was added to the polymer solution. The final concentration of catalyst in the reaction was 5 mM. A magnetic stir bar was added and the solution was sealed under argon. The reaction was stirred for 18 h at 20 °C. After 18 h, the reaction was stopped with the addition of 100 µl ethyl vinyl ether and stirred for 30 min. The ethyl vinyl ether was removed under vacuum, and the crude reaction was lyophilized to remove water. After the water was removed, the remaining solids and oils were dissolved in DMF and analyzed by GPC.

Conjugation of rPEG to Lyz

Lyz (1.0 mg, 0.07 μmol) was dissolved in pH 6.0 100 mM PB (0.50 mL) in a 1.5 mL LoBind tube. rPEG (Mn = 9.7 kDa, 35.0 mg, 3.50 μmol) was dissolved in pH 6.0, 100 mM PB (0.40 mL) in a separate 1.5 mL tube. The polymer solution was then added to the Lyz solution and placed on a laboratory rocker for 1 h at 23 °C. A 200 mM stock solution of sodium cyanoborohydride was prepared in pH 6.0, 100 mM PB, and 0.10 mL of the sodium cyanoborohydride solution was added to the solution containing Lyz and the polymer for a total volume of 1 mL. The reaction was gently rocked for 26 h at 23 °C. The crude reaction was then filtered through a 0.22 μm syringe filter and purified by FPLC to obtain the conjugate.

Representative aqueous depolymerization of Lyz-rPEG conjugate

100 μl of 200 mM $MgCl_2$ in 200 mM PB, pH 8.0 was added to a 1.5 mL LoBind tube containing 100 μl of Lyz-rPEG conjugate (0.51 μg/μl; 51 μg). Next, A saturated solution of Grubbs III catalyst was prepared in tBuOH (1.1 mg in 50 μl tBuOH; 25 mM stock) and the entire catalyst suspension was added to the tube, bringing the concentration of catalyst to approximately 5 mM and the concentration of tBuOH to 20% for a total reaction volume of 250 μl. The reaction mixture was then incubated for 17 hours at 23 °C. After 17 hours, any precipitate in the solution was pelleted by centrifugation and discarded. The remaining crude mixture was analyzed by SDS-PAGE using 0.1 N Iodine stain to visualize polymer, then by Coomassie stain to visualize protein.

Lysozyme Activity Assays

Activity of Lyz, Lyz-rPEG conjugates and depolymerized Lyz-rPEG conjugates were carried out using EnzChek Lysozyme Assay Kit (ThermoFisher Scientific) following the manufacturer's procedure. All standards and experimental samples were prepared in triplicate in

a 96-well plate and measured using a Molecular Devices Flexstation II fluorescent plate with an excitation wavelength of 485 nm and an emission wavelength of 530 nm. Statistical analysis of the resulting activity values was analyzed using a one-way ANOVA with post-hoc analyses using Tukey's test. A p-value of <0.05 was used to determine statistical significance.

Synthesis of PEG12-ditosylate (3)

To a previously oven dried 25 mL 2-neck round bottom flask was added dodecylethylene glycol (PEG12) (500 mg, 0.91 mmol, 1 eq) and 2 mL of toluene. The flask that was then placed under vacuum for 2 hours to azeotropically remove water. Once dry, the flask was placed under Argon and DCM (20 mL) was added and stirred to dissolve the PEG12. Next, DMAP (40 mg, 0.37 mmol, 0.4 eq) was added was added and the flask was placed in an ice bath. After several minutes, tosyl chloride (420 mg, 2.20 mmol, 2.4 eq) was added. Finally, triethylamine (0.51 mL, 3.66 mmol, 4.0 eq) was added dropwise with a syringe. The reaction proceeded for 18 hours, then solvent was removed under vacuum. Once dry, a small amount of H_2O was added and washed three times with hexanes followed by extraction of the aqueous layer with DCM. The organic layer was then washed once with brine, then once with a small volume of 0.1 M HCl before drying over anhydrous $MgSO_4$. Solvent was removed solvent under vacuum to yield a light tan oil. Product **3** was further purified using a 25g SNAP Ultra Biotage column using DCM with a gradient of 2-20% MeOH. Solvent was removed under vacuum to give a light yellow oil (640 mg, 91.4% yield). See Figure 5.16 for ^{1}H NMR (400 MHz, $CDCl_3$): δ 7.79-7.77 (d, J = 8.32 Hz, 4H), 7.34-7.32 (d, J = 7.96 Hz, 4H), 4.16-4.13 (t, 4H), 3.70-3.55 (m, 44H), 2.44 (s, 6H). HRMS: $C_{38}H_{62}O_{17}S_2Na$ calc. $[M+Na]^+$ = 877.01 Da; obsd. $[M+Na]^+$ = 877.34 Da.

Synthesis of PEG12-dithiol (4)

To a previously oven dried 25 mL two-neck round bottom flask, **3** (320 mg, 0.37 mmol, 1 eq) was dried azeotropically from 2 mL toluene for 2 hours. Next, dry acetonitrile was added to dissolve **3** after purging the flask with Argon. Potassium thioacetate (94 mg, 0.82 mmol, 2.2 eq) was added. The solution immediately turned red/orange and the potassium tosylate salt byproduct quickly began crashing out of solution. The reaction was left stirring at room temperature for 18 hours after which it was filtered and dried under vacuum to provide a red oil. Flash column chromatography was performed using a 25 g SNAP KP-SIL Biotage column with a solvent system of a gradient of 2-20% MeOH in DCM as a solvent system. Fractions containing product (PEG12-dithioacetate) were collected and dried under vacuum to yield a light red oil (137 mg, 55% yield). See Figure 5.17 for ^{1}H NMR (400 MHz, $CDCl_3$): δ 3.75-3.55 (m, 44H), 3.10-3.07 (t, J = 6.46 Hz, 4H), 2.33 (s, 6H). Deprotection of PEG12-dithioacetate was carried our by dissolving the resulting material in 10 mL of 1 M HCl and refluxing for 2 hours. The solution was then neutralized with 1 M NaOH, then the solution was washed once with hexanes, then extracted three times with DCM. The combined organics were then dried over anhydrous $MgSO_4$, filtered, and dried under vacuum to yield product **4** as a red oil (102 mg; 47% yield over 2 steps). See Figure 5.18 for ^{1}H NMR (400 MHz, $CDCl_3$): δ 3.75-3.55 (m, 44H), 2.88-2.85 (t, J = 6.72 Hz, 0.46H) 2.71-2.65 (q, J = 7.96 Hz, 3.3H) 1.60-1.56 (t, J = 8.18 Hz, 1.77H); HRMS: $C_{24}H_{50}O_{11}S_2Na$ calc. $[M+Na]^+$ = 601.27 Da; obsd. $[M+Na]^+$ = 601.29 Da.

Synthesis of PEG14-divinyl ether (5)

To a previously oven dried 25 mL 2-neck round bottom flask, **3** (PEG12-ditosylate, 320 mg, 0.37 mmol, 1 eq) was dissolved in 2 mL of toluene and was azeotropically dried for 2 hours. To a separate flame dried 25 mL 2-neck round bottom, 6 mL of dry THF was added under Argon and stirring was initiated. NaH (60% dispersion in mineral oil, 150 mg, 3.74 mmol, 10 eq) was

then added to the flask and the flask was placed in an ice bath. After the NaH dissolved, ethylene glycol vinyl ether (336 µl, 3.74 mmol, 10 eq) was added dropwise. 5 mL of dry THF was then added to the flask containing **3** and the solution was added dropwise over 5 minutes to the flask with NaH and ethylene glycol vinyl ether. The flask was then heated in an oil bath under Argon to 60 °C for 18 hours. Unreacted NaH was quenched with MeOH and then solvent was removed under vacuum. The resulting oil was diluted with a small amount of water and washed three times with hexanes and extracted with chloroform. The organic layer was dried over anhydrous $MgSO_4$ and filtered before removing solvent under vacuum to yield a viscous yellow oil. The product was further purified by high performance liquid chromatography (HPLC) using a gradient of 60-95% MeOH in water. Solvent was removed under vacuum to yield a light yellow oil (0.1219g, 47% yield). See Figure 5.19 for ^{1}H NMR (400 MHz, $CDCl_3$): δ 6.50-6.45 (dd, J = 14.32, 6.80 Hz, 2H), 4.19-4.15 (dd, J = 12.24, 2.12 Hz, 2H), 4.00-3.98 (dd, J = 6.80, 2.12 Hz, 2H), 3.84-3.82 (dd, J = 6.40, 5.24 Hz, 4H), 3.75-3.55 (m, 52H). HRMS: $C_{32}H_{62}O_{15}Na$ calc. $[M+Na]^+$ = 709.40 Da; obsd. $[M+Na]^+$ = 709.41 m/z.

Representative thiol-ene step growth polymerization with monomers 4 and 5

Monomers **4** and **5** (0.03 mmol each), DMPA (0.14 mmol), and THF were added to a small scintillation vial and degassed with Argon for 30 min. After degassing, the reaction was started with stirring and UV initiation using a handheld UV lamp at 365 nm. The reaction proceeded for 1 hour. Solvent was removed under vacuum and ^{1}H NMR was taken in $CDCl_3$. The reaction mixture was subsequently dried and dissolved in THF and excess dodecylethylene glycol dithiol was added. The reaction was again reinitiated and run for an additional hour before drying under vacuum. M_n (GPC) = 4.5 kDa, M_w (GPC) = 7.6 kDa, Đ = 1.68; see Figure 5.9 for GPC chromatogram. See Figure 5.7 and Figure 5.8 for assigned ^{1}H NMR (400 MHz, $CDCl_3$).

Additional experiments were carried out in water with initiator I2959 with similar results indicating that the polymers were water-soluble. Similar experiments monitoring the kinetics of the reaction also confirmed that the reaction reached full conversion in a matter of minutes in either THF or water.

Synthesis of PEG4-ditosylate (6)

To a previously oven dried 250 mL 2-neck round bottom flask was added 100 mL DCM, tetraethylene glycol (5.00 mL, 29.0 mmol, 1 eq), and triethylamine (9.69 mL, 69.5 mmol, 2.4 eq). Finally, tosyl chloride (13.25 g, 69.5 mmol, 2.4 eq) was added to the flask, and the reaction was stirred vigorously for 70 hours at 20 °C. The reaction solution was then washed 4 times with a mixture of saturated bicarbonate solution and water. The organic layer was then dried over anhydrous $MgSO_4$, filtered, and concentrated under vacuum to provide a crude yellow oil that was purified using a 100 g SNAP KP-SIL Biotage column with a solvent system of 50-100% ethyl acetate in hexanes. Fractions containing the desired product were isolated and solvent was removed under vacuum to give a pale yellow oil (9.74 grams, 66.9% yield). R_f = 0.4 (2:1 ethyl acetate:hexanes). See Figure 5.20 for ^{1}H NMR (400 MHz, CD_3CN): δ 7.76 (d, *J* = 8.3 Hz, 4H), 7.41 (d, *J* = 8.0 Hz, 4H), 4.08 (t, *J* = 4.4 Hz, 4H), 3.57 (t, *J* = 4.4 Hz, 4H), 3.44 (m, 8H), 2.41 (s, 6H). See Figure 5.21 for ^{13}C NMR (100 MHz, CD_3CN): δ 145.37, 132.86, 130.02, 127.78, 70.16, 70.04, 69.97, 68.20, 20.66. HRMS: $C_{22}H_{31}O_9S_2$ calc. $[M+H]^+$ = 503.1410 Da; obsd. $[M+H]^+$ = 503.1441 Da.

Synthesis of PEG4-monotrityl (7)

To a previously oven dried 500 mL 3-neck round bottom flask equipped with an addition funnel was added 100 mL DCM and tetraethylene glycol (92.90 mL, 538.1 mmol, 10 eq). The flask was then cooled to 0 °C in an ice bath and triethylamine (22.51 mL, 161.4 mmol, 3 eq) was

added. Trityl chloride (15.00 g, 53.8 mmol, 1 eq) was then dissolved in 20 mL DCM and added dropwise via addition funnel to the reaction over 30 minutes and the reaction was stirred at 20 °C for 9 days. The reaction solution was then washed 5 times with a mixture of saturated bicarbonate solution and water. The organic layer was then dried over anhydrous $MgSO_4$, filtered, and concentrated under vacuum to provide an orange oil that was purified using a 100 g SNAP Ultra Biotage column (multiple runs) with a solvent system of 2-20% MeOH in DCM. Fractions containing the desired product were isolated and solvent was removed under vacuum to give an orange oil (19.20 g, 81.7% yield). See Figure 5.22 for ^{1}H NMR (400 MHz, CD_3CN): δ 7.45 (d, J = 7.1 Hz, 6H), 7.31 (t, J = 7.4 Hz, 6H), 7.24 (t, J = 7.2 Hz, 3H), 3.61-3.54 (m, 12H), 3.47 (m, 2H), 3.13 (t, J = 4.8 Hz, 2H), 2.76 (t, J = 5.8 Hz, 1H). See Figure 5.23 for ^{13}C NMR (100 MHz, CD_3CN): δ 144.30, 128.58, 127.84, 127.06, 86.39, 72.34, 70.46, 70.31, 70.28, 70.16, 70.12, 63.42, 61.00. HRMS: $C_{27}H_{32}O_5Na$ calc. $[M+Na]^+$ = 459.2147 Da; obsd. $[M+Na]^+$ = 459.2083 Da.

Synthesis of PEG12-ditrityl (8)

To a previously oven dried 250 mL 2-neck round bottom flask was added **6** (PEG4-ditosylate, 9.74 g, 19.4 mmol, 1 eq), **7** (PEG4-monotrityl, 19.21 g, 44.0 mmol, 2.27 eq), and 10 mL of toluene. The flask was then placed under vacuum for 1 hour to azeotropically dry the contents. The reaction was then placed under Argon and the mixture was dissolved in 100 mL THF. NaH (60% dispersion in mineral oil, 3.02 g, 50.4 mmol, 2.6 eq) was then added to the flask and the reaction was heated to 60 °C and stirred vigorously for 16 hours. The reaction was then cooled to ambient temperature, filtered, and concentrated under vacuum. The crude material was then diluted with DCM, filtered again, and washed 4 times with a mixture of saturated bicarbonate solution and water. The organic layer was then dried over anhydrous $MgSO_4$,

filtered, and concentrated under vacuum to provide a crude oil that was purified using a 100 g SNAP Ultra Biotage column (multiple runs) with a solvent system of 0-6% MeOH in ethyl acetate. Fractions containing the desired product were isolated and solvent was removed under vacuum to give an orange oil (12.62 g, 63.1% yield). R_f = 0.28 (97.5:2.5 ethyl acetate:methanol). See Figure 5.24 for ^{1}H NMR (500 MHz, CD_3CN): δ 7.46 (d, *J* = 7.5 Hz, 12H), 7.32 (t, *J* = 7.5, 12H), 7.25 (t, *J* = 7.3 Hz, 6H), 3.61-3.52 (m, 44H), 3.14 (t, *J* = 4.8 Hz, 4H). See Figure 5.25 for ^{13}C NMR (125 MHz, CD_3CN): δ 144.30, 128.58, 127.86, 127.08, 86.37, 70.49, 70.30, 70.28, 70.24, 70.19, 70.17, 63.44. HRMS: $C_{62}H_{78}O_{13}Na$ calc. $[M+Na]^+$ = 1053.5340 Da; obsd. $[M+Na]^+$ = 1053.5500 Da.

Synthesis of PEG12

To a 250 mL 1-neck round bottom flask was added **8** (PEG12-dityrityl, 12.62 g, 12.2 mmol, 1 eq) and 30 mL DCM. Once dissolved, trifluoroacetic acid (9.36 mL, 122.3 mmol, 10 eq) was added dropwise with a small amount of triisopropylsilane, methanol, and water as scavengers. The reaction was stirred for 30 minutes, then as much of the solvent as possible was removed under vacuum. The remaining crude material was precipitated 3 times in hexanes, then dried under vacuum to yield a tan oil (6.68 g, 99.8% yield). See Figure 5.26 for ^{1}H NMR (500 MHz, $CDCl_3$): δ 4.48 (m, 2H), 3.79-3.75 (m, 4H), 3.67-3.61 (m, 44H). See Figure 5.27 for ^{13}C NMR (125 MHz, $CDCl_3$): δ 72.20, 70.71, 70.53, 70.53, 70.50, 70.45, 70.41, 70.40, 70.38, 70.36, 70.33, 70.13, 68.15, 66.94, 61.54. HRMS: $C_{24}H_{51}O_{13}$ calc. $[M+H]^+$ = 547.3330 Da; obsd. $[M+H]^+$ = 547.3403 Da.

Synthesis of PEG12-monotrityl (9)

To a previously oven dried 100 mL 2-neck round bottom flask was added PEG12 (5.88 g, 10.8 mmol, 4 eq) and 4 mL toluene. The flask was then placed under vacuum for 3 hours to

azeotropically dry the material. The flask was then placed under Argon and 50 mL DCM was added to dissolve the material. Trityl chloride (0.75 g, 2.7 mmol, 1 eq) was then added to the flask. Once dissolved, triethylamine (0.56 mL, 4.0 mmol, 1.5 eq) was added dropwise over 5 minutes and the reaction was stirred at 20 °C for 20 hours. The reaction solution was then washed 4 times with a mixture of saturated bicarbonate solution and water. The organic layer was then dried over anhydrous $MgSO_4$ and concentrated under vacuum to yield a tan oil (2.02 g, 95.3% yield). Aqueous washes were combined and extracted with DCM followed by drying of the combined organics over anhydrous $MgSO_4$, filtering, and concentration under vacuum to recover unreacted PEG12 (2.51 g, 56.8% recovery). See Figure 5.28 for ^{1}H NMR (400 MHz, CD_3CN): δ 7.46-7.44 (d, J = 7.25 Hz, 6H), 7.33-7.30 (t, J = 7.53 Hz, 6H), 7.26-7.23 (t, J = 7.30 Hz, 3H), 3.80-3.35 (m, 46H), 3.14-3.12 (t, J = 4.90, 2H), 2.78 (s, 1H). See Figure 5.29 for ^{13}C NMR (100 MHz, CD_3CN): δ 144.29, 128.57, 127.84, 127.07, 86.38, 72.36, 70.48, 70.29, 70.28, 70.24, 70.19, 70.08, 63.44, 61.00. HRMS: $C_{43}H_{64}O_{13}Na$ calc. $[M+Na]^+$ = 811.4245 Da; obsd. $[M+Na]^+$ = 811.4824 Da.

Synthesis of monotosyl-PEG12-monotrityl (10)

To a previously oven dried 100 mL 2-neck round bottom flask was added **9** (PEG12-monotrityl, 2.00 g, 2.5 mmol, 1 eq) and 8 mL toluene. The flask was then placed under vacuum for 2 hours to azeotropically dry the material. The flask was then placed under Argon and 40 mL DCM was added to dissolve the material. Tosyl chloride (1.16 g, 6.1 mmol, 2.4 eq) was then added to the flask. Once dissolved, DMAP (0.06 g, 0.5 mmol, 0.2 eq) was added followed by dropwise triethylamine (0.71 mL, 5.1 mmol, 2 eq) and the reaction was stirred at 20 °C for 18 hours. The reaction solution was then concentrated under vacuum then diluted with water. The aqueous solution was then washed three times with hexanes, then extracted three times with

DCM, dried over anhydrous $MgSO_4$, filtered, and concentrated under vacuum to yield a tan oil. The crude material was futher purified via preparative HPLC (1.30 g, 54.2% yield). See Figure 5.30 for ^{1}H NMR (400 MHz, CD_3CN): δ 7.79 (d, *J* = 8.3 Hz, 2H), 7.45 (d, *J* = 7.4 Hz, 6H), 7.33 (d, *J* = 8.1 Hz, 2H), 7.28 (t, *J* = 7.3 Hz, 6H), 7.21 (t, *J* = 7.2 Hz, 3H), 4.15 (t, *J* = 4.9 Hz, 2H), 3.66-3.57 (m, 44H), 3.22 (t, *J* = 5.2 Hz, 2H), 2.43 (s, 3H). See Figure 5.31 for ^{13}C NMR (100 MHz, CD_3CN): δ 145.36, 144.29, 132.89, 130.03, 128.57, 127.84, 127.79, 127.07, 86.37, 70.47, 70.28, 70.27, 70.22, 70.17, 70.03, 69.98, 68.21, 63.43, 20.68. HRMS: $C_{50}H_{70}O_{15}SNa$ calc. $[M+Na]^+$ = 965.4333 Da; obsd. $[M+Na]^+$ = 965.5081 Da.

Synthesis of 2-tosylethylvinyl ether

To a previously oven dried 100 mL 2-neck round bottom flask was added 25 mL DCM followed by ethylene glycol vinyl ether (EGVE, 2.00 g, 22.3 mmol, 1 eq). Once dissolved, triethylamine (9.33 mL, 66.9 mmol, 3 eq) was added to the flask, followed shortly by DMAP (0.27 g, 2.2 mmol, 0.1 eq). The reaction was then cooled to 0 °C in an ice bath and tosyl chloride (5.10 g, 26.8 mmol, 1.2 eq) was added. The reaction was stirred on ice for 30 minutes, then at room temperature for 18 hours. The reaction solution was then diluted with DCM, and washed 3 times with a mixture of water and saturated sodium bicarbonate solution, then once with water and 1 M HCl, and then twice more with water and saturated sodium bicarbonate solution. The combined organics were then dried over anhydrous $MgSO_4$, filtered, and concentrated under vacuum to yield a yellowish oil (5.75 g, quant. yield). R_f = 0.5 (9:1 hexane:ethyl acetate). See Figure 5.32 for ^{1}H NMR (400 MHz, $CDCl_3$): δ 7.79 (d, *J* = 8.3 Hz, 2H), 7.34 (d, *J* = 8.0 Hz, 2H), 6.35 (q, *J* = 7.0 Hz, 1H), 4.23 (t, *J* = 4.7 Hz, 2H), 4.11 (dd, *J* = 14.3, 2.4 Hz, 1H), 4.01 (dd, *J* = 6.8, 2.4 Hz, 1H), 3.86 (t, *J* = 4.7 Hz, 2H), 2.44 (s, 3H). See Figure 5.33 for ^{13}C NMR (100 MHz, $CDCl_3$): δ 151.05, 144.98, 132.85, 129.88, 128.01, 87.42, 68.02, 65.28, 21.65.

Efforts toward synthesis of 9-fluorenylmethanethiol (FmSH)

Method 1: To a previously oven dried 50 mL 2-neck round bottom flask was added 9-fluorenylmethanol (500 mg, 2.55 mmol, 1 eq) and 20 mL DCM. Next, thioacetic acid (237 µl, 3.31 mmol, 1.3 eq) and triphenylphosphine (869 mg, 3.31 mmol, 1.3 eq) were added, causing the solution to turn yellow and cloudy. The reaction was then cooled to 0 °C in an ice bath. Diisopropyl azodicarboxylate (DIAD, 652 µl, 3.31 mmol, 1.3 eq) was added in 4 aliquots of 163 µl each with about 1 min in between additions. The solution immediately turned amber, then gradually more yellow again as DIAD was consumed. The reaction stirred for 1 hour in the ice bath, then for 18 hours at 20 °C. The reaction mixture was then concentrated under vacuum and purified using a 50 g SNAP KP-SIL Biotage column with a solvent system of 2-20% ethyl acetate in hexanes. Fractions containing the desired product were isolated and solvent was removed under vacuum to give an off white solid (129 mg, 20.0% yield). R_f = 0.5 (9:1 hexanes:ethyl acetate). See Figure 5.34 for ^{1}H NMR (400 MHz, $CDCl_3$): δ 7.75 (d, *J* = 7.5 Hz, 2H), 7.65 (d, *J* = 7.5 Hz, 2H), 7.40 (t, *J* = 7.4 Hz, 2H), 7.32 (dt, *J* = 7.4, 1.2 Hz, 2H), 4.17 (t, *J* = 5.9 Hz, 1H), 3.53 (d, *J* = 5.9 Hz, 2H), 2.28 (s, 1H). See Figure 5.35 for ^{13}C NMR (100 MHz, $CDCl_3$): δ 195.43, 145.46, 141.10, 127.73, 127.14, 124.66, 119.91, 46.70, 32.50, 30.68.

Method 2: To a previously oven dried 250 mL 2-neck round bottom flask was added 9-fluorenylmethanol (3.00 g, 15.3 mmol, 1 eq) and 40 mL DCM. The reaction was then cooled to 0 °C in an ice bath, then tosyl chloride (3.50 g, 18.3 mmol, 1.3 eq) dissolved in pyridine (2.46 mL, 30.6 mmol, 2 eq) was added dropwise over 5 minutes. After addition, the reaction was warmed to ambient temperature and stirred for 16 hours. The reaction mixture was then washed twice with 1 M HCl, twice with saturated bicarbonate, and twice with brine/water. The organics were then dried over anhydrous $MgSO_4$, filtered, and concentrated under vacuum. The resulting

material was purified using a 100 g SNAP KP-SIL Biotage column with a solvent system of 2-20% ethyl acetate in hexanes. Fractions containing the desired product were isolated and solvent was removed under vacuum to give a white, crystalline solid (2.56 g, 47.9% yield). See Figure 5.36 for ^{1}H NMR (400 MHz, $CDCl_3$): δ 7.76 (d, *J* = 8.4 Hz, 2H), 7.73 (d, *J* = 7.6 Hz, 2H), 7.53 (dd, *J* = 7.5, 0.7 Hz, 2H), 7.39 (dt, *J* = 7.5, 0.6 Hz, 2H), 7.29 (dd, *J* = 8.5, 0.6 Hz, 2H), 7.28 (dt, *J* = 7.5, 1.1 Hz, 2H), 4.25 (m, 3H), 2.42 (s, 3H). See Figure 5.37 for ^{13}C NMR (100 MHz, $CDCl_3$): δ 144.88, 142.51, 141.27, 140.10, 129.89, 128.09, 127.95, 127.23, 125.19, 120.10, 71.89, 46.72, 21.64. HRMS: [2 × ($C_{21}H_{18}O_3S$) + Na] calc. $[2M+Na]^+$ = 723.1851 Da; obsd. $[2M+Na]^+$ = 723.1933 Da.

Synthesis of PEG12-macrocyclic sulfite

Synthesis of PEG12-macrocyclic sulfite was based on the previously reported procedure.[32] To a previously oven dried 100 mL 2-neck round bottom flask was dissolved PEG12 (1.00 g, 1.83 mmol, 1 eq) in 5 mL toluene. The flask was then placed under vacuum for 1.5 hours to azeotropically dry the material. The flask was then placed under Argon and 45.7 mL DCM was added to dissolve the material at a concentration of 40 mM. Cesium iodide (2.38 g, 9.15 mmol, 5 eq) and diisopropylethylamine (1.53 mL, 8.78 mmol, 4.8 eq) were then added to the solution and the reaction was cooled to 0 °C in an ice bath. Thionyl chloride (0.27 mL, 3.66 mmol, 2 eq) was then added in 44 µl portions each 10 minutes over 60 minutes, then the reaction was warmed to ambient temperature and stirred for 21 hours. The reaction was quenched by pouring into brine, then the mixture was extracted twice with DCM. The combined organics were then washed once with 1:1 brine: 1 M HCl, then dried over anhydrous $MgSO_4$, filtered, and concentrated under vacuum. The resulting material was purified using a 50 g SNAP KP-SIL Biotage column with a solvent system of 2-20% MeOH in DCM. Fractions containing the

desired product were isolated and solvent was removed under vacuum to give a brown oil (808 mg, 74.5% yield). R_f = 0.6 (9:1 DCM:MeOH). See Figure 5.38 for ^{1}H NMR (400 MHz, $CDCl_3$): δ 4.16 (m, 4H), 3.73 (m, 4H), 3.65 (m, 40H). See Figure 5.39 for ^{13}C NMR (100 MHz, $CDCl_3$): δ 70.75, 70.72, 70.68, 70.65, 69.60, 61.47. HRMS: $C_{24}H_{49}O_{14}S$ calc. $[M+H]^+$ = 593.2843 Da; obsd. $[M+H]^+$ = 593.2825 Da. FT-IR: ν = 2869, 1460, 1350, 1246, 1206, 1107 cm^{-1}.

5.5 Appendix D

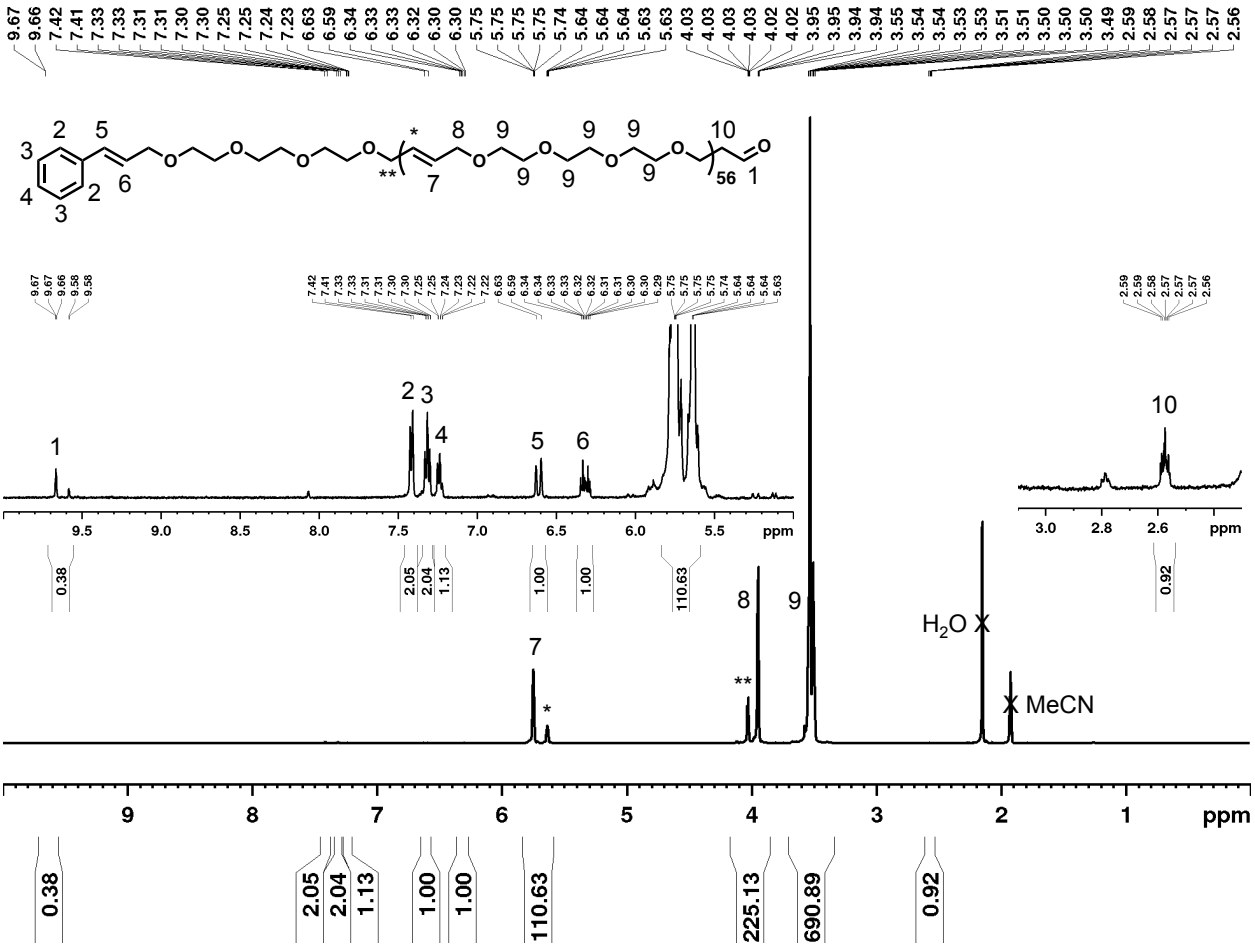

Figure 5.10. ^{1}H NMR of 10 kDa rPEG in CD_3CN. * indicates protons corresponding to *cis* backbone alkenes. ** indicates protons corresponding to methylene protons adjacent to *cis* alkenes.

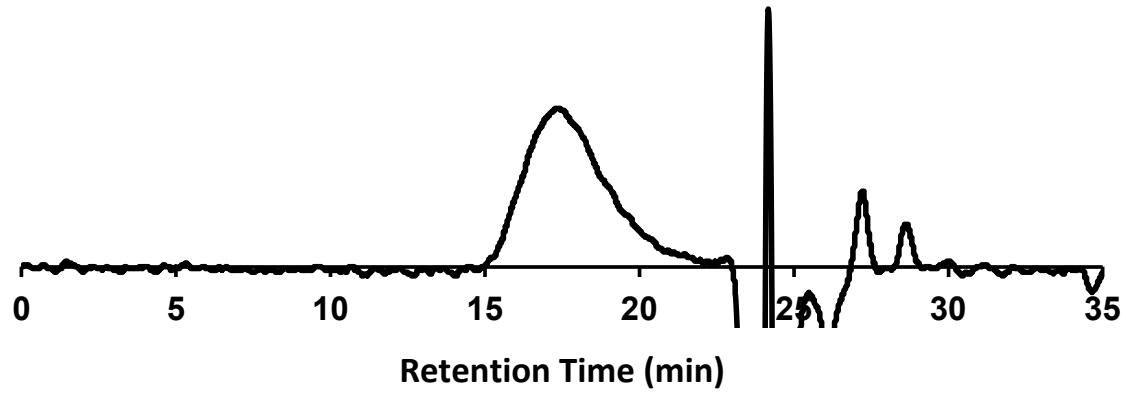

Figure 5.11. GPC chromatogram of rPEG (M_n = 8.6 kDa, M_w = 13.8 kDa, Đ = 1.62).

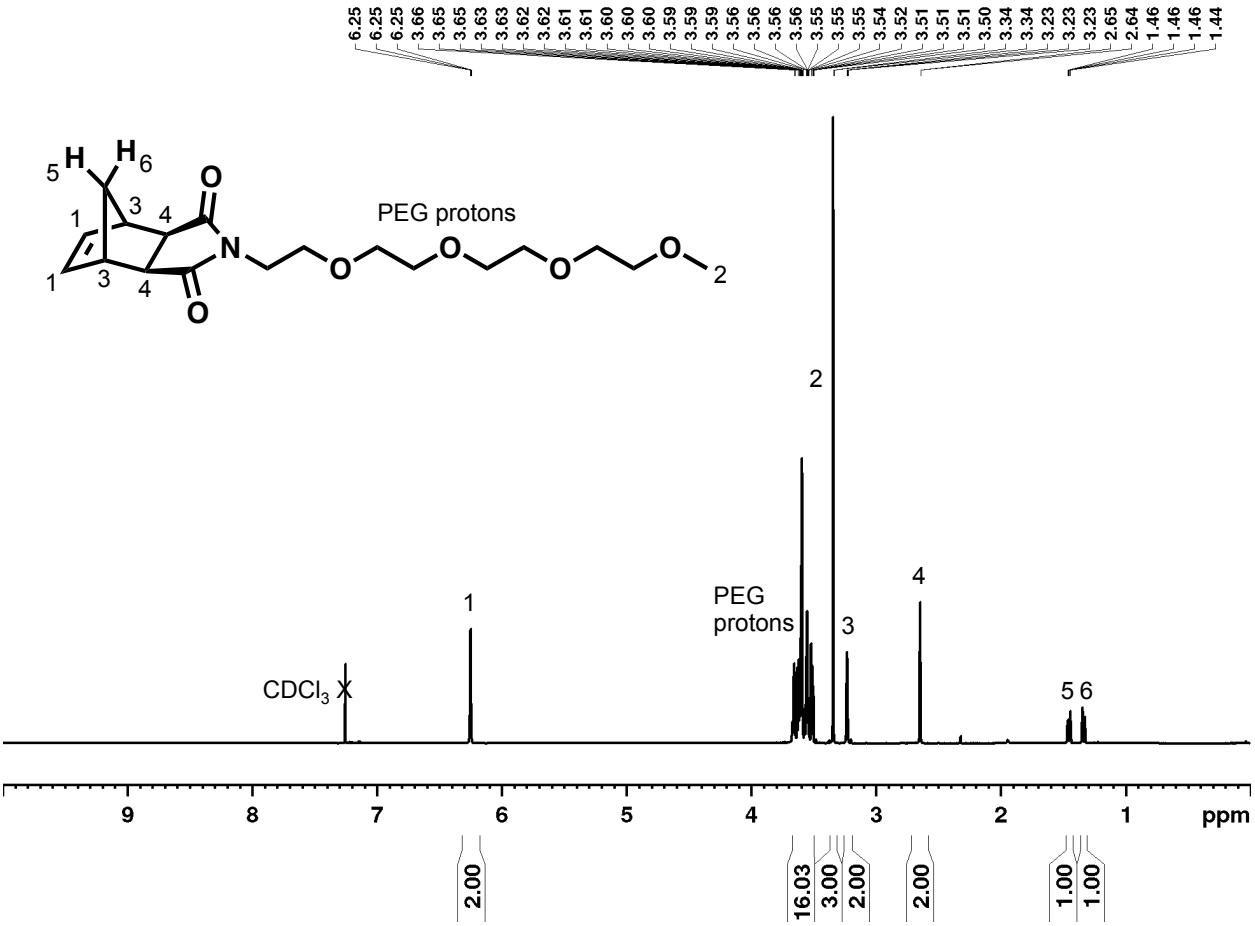

Figure 5.12. ^{1}H NMR of Nor-PEG monomer 2 in $CDCl_3$.

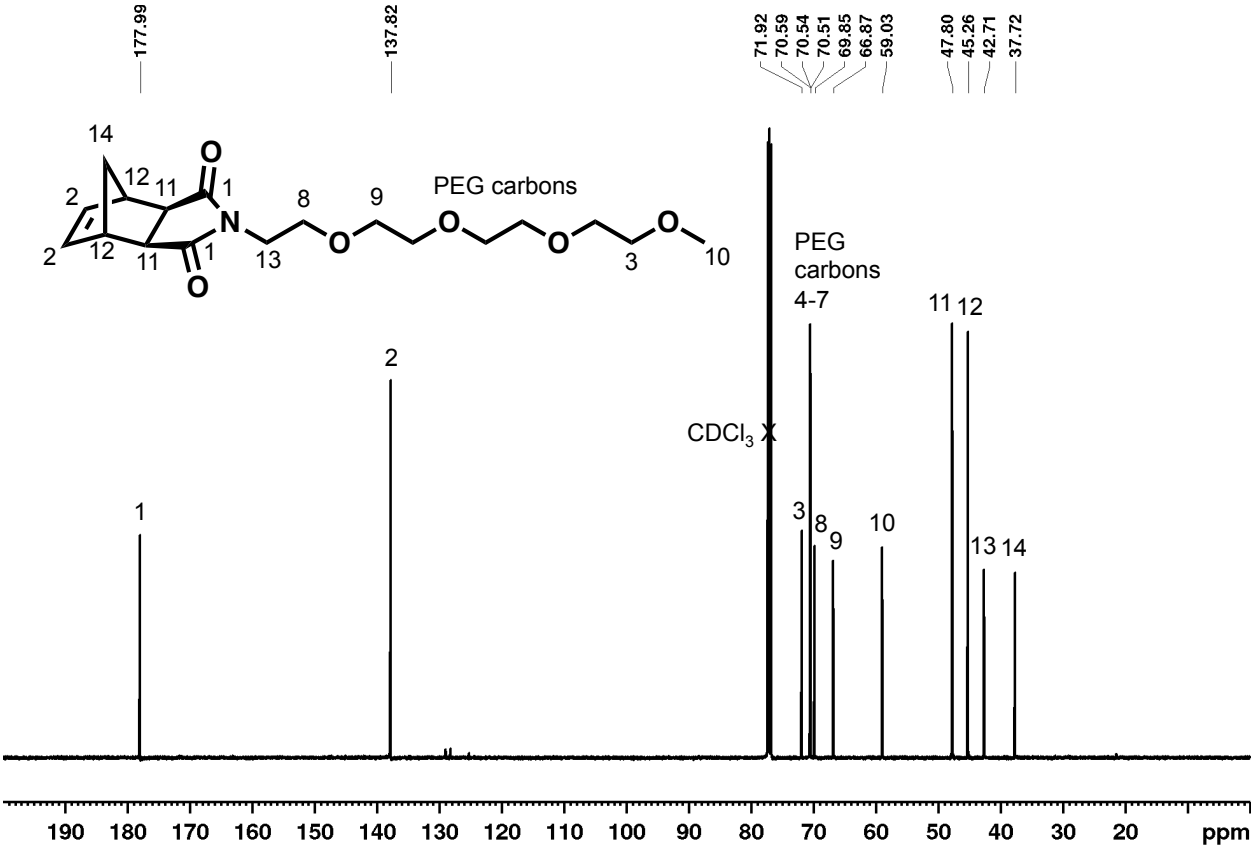

Figure 5.13. ^{13}C NMR of Nor-PEG monomer 2 in $CDCl_3$.

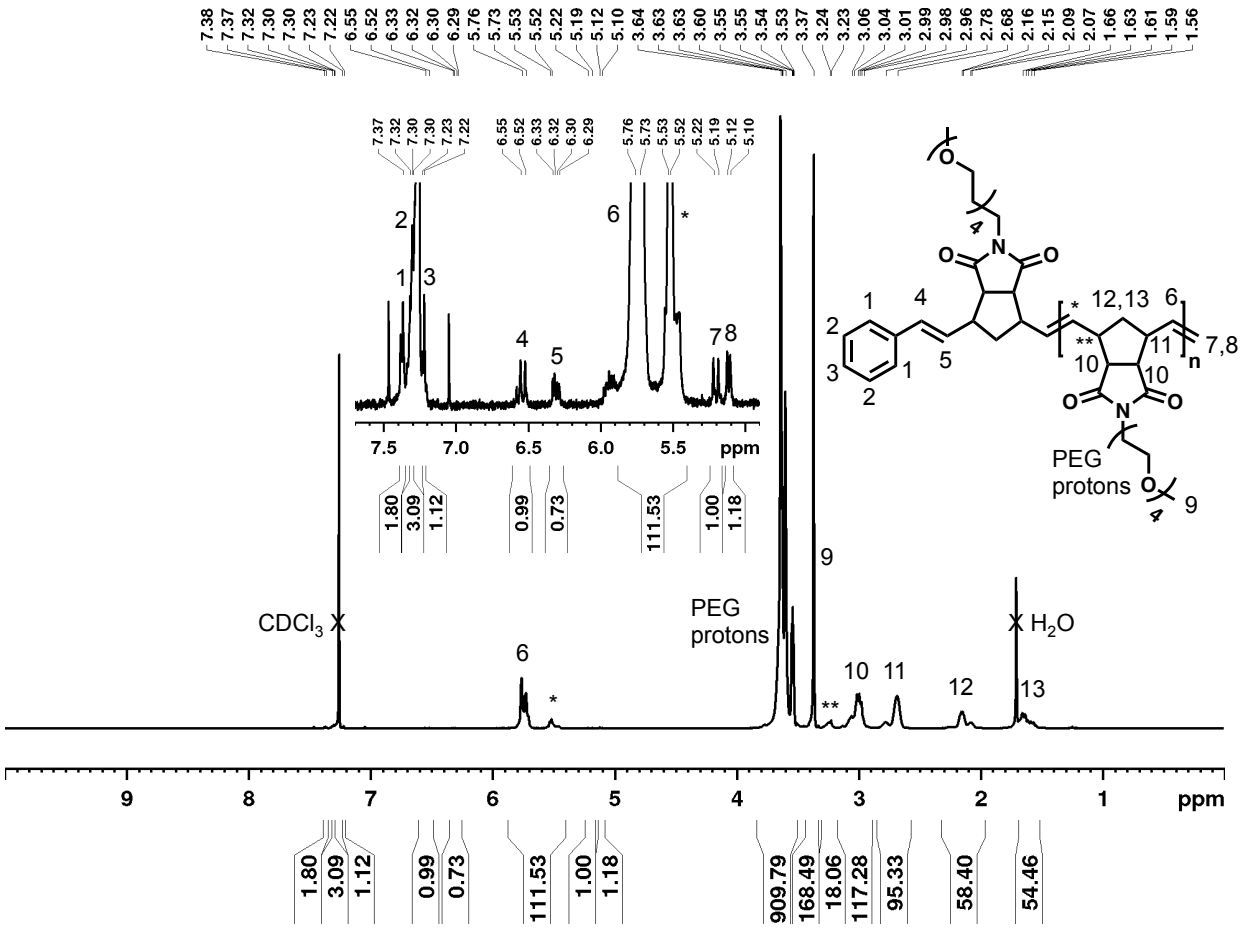

Figure 5.14. ^{1}H NMR of 20 kDa poly(Nor-PEG) in $CDCl_3$. * indicates protons corresponding to *cis* backbone alkenes. ** indicates protons corresponding to methyne protons adjacent to *cis* alkenes.

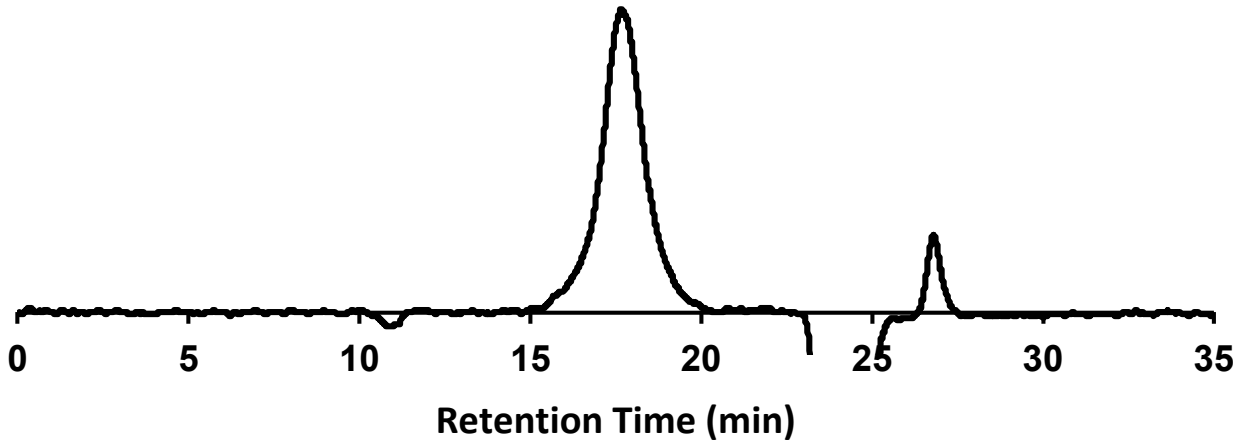

Figure 5.15. GPC chromatogram of poly(Nor-PEG) (M_n = 26.2 kDa, M_w = 29.3 kDa, Đ = 1.12).

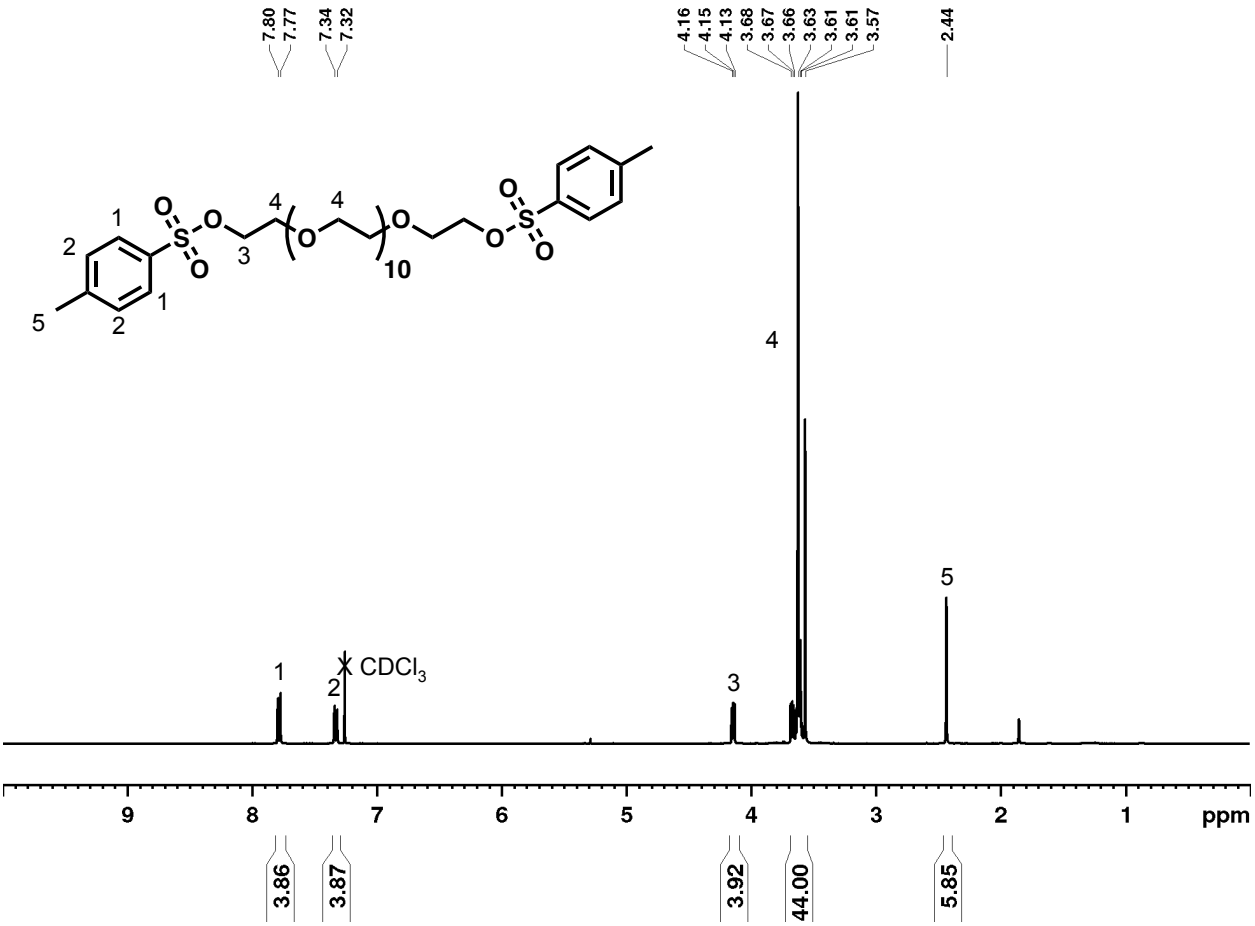

Figure 5.16. ^{1}H NMR of PEG12-ditosylate (3) in $CDCl_3$.

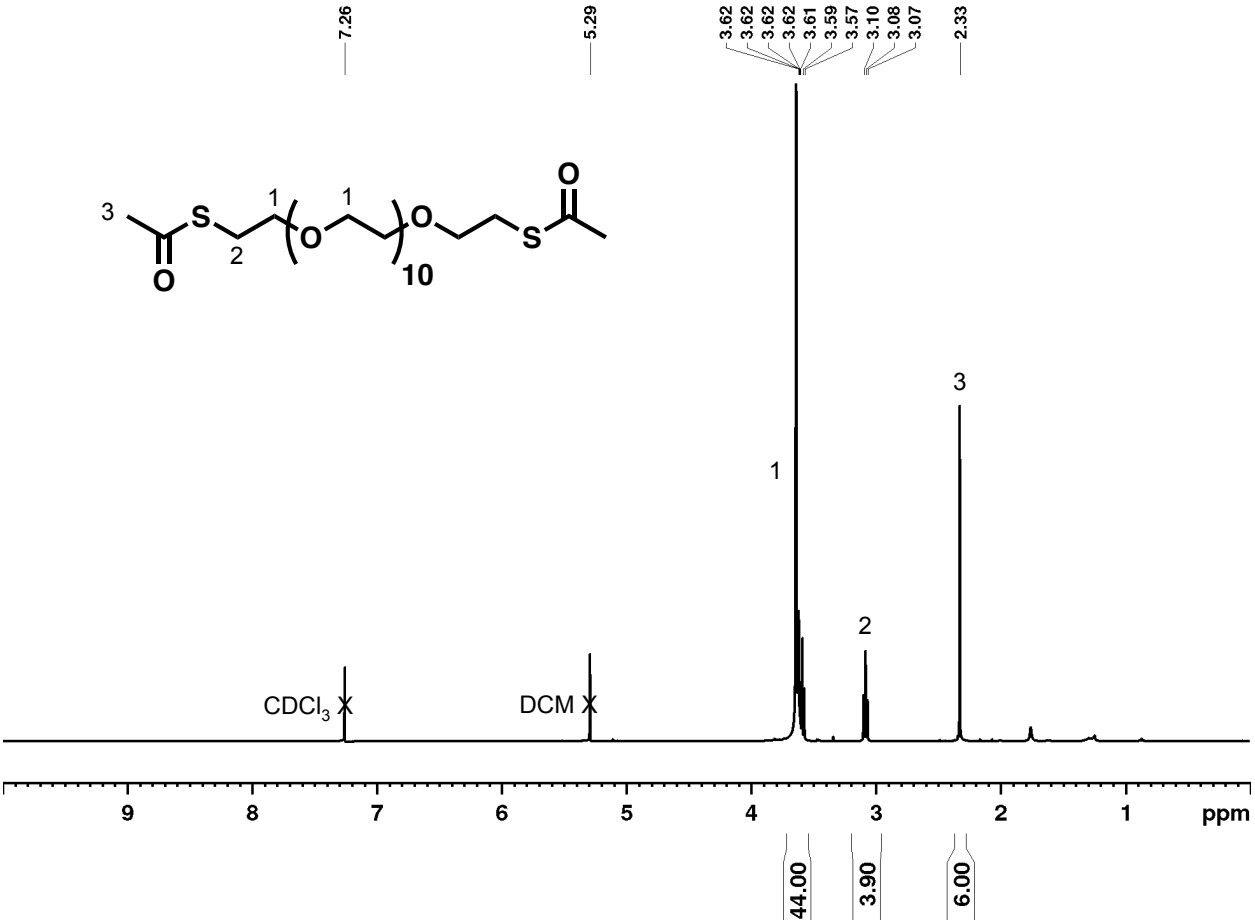

Figure 5.17. ^{1}H NMR of PEG12-dithioacetate in $CDCl_3$.

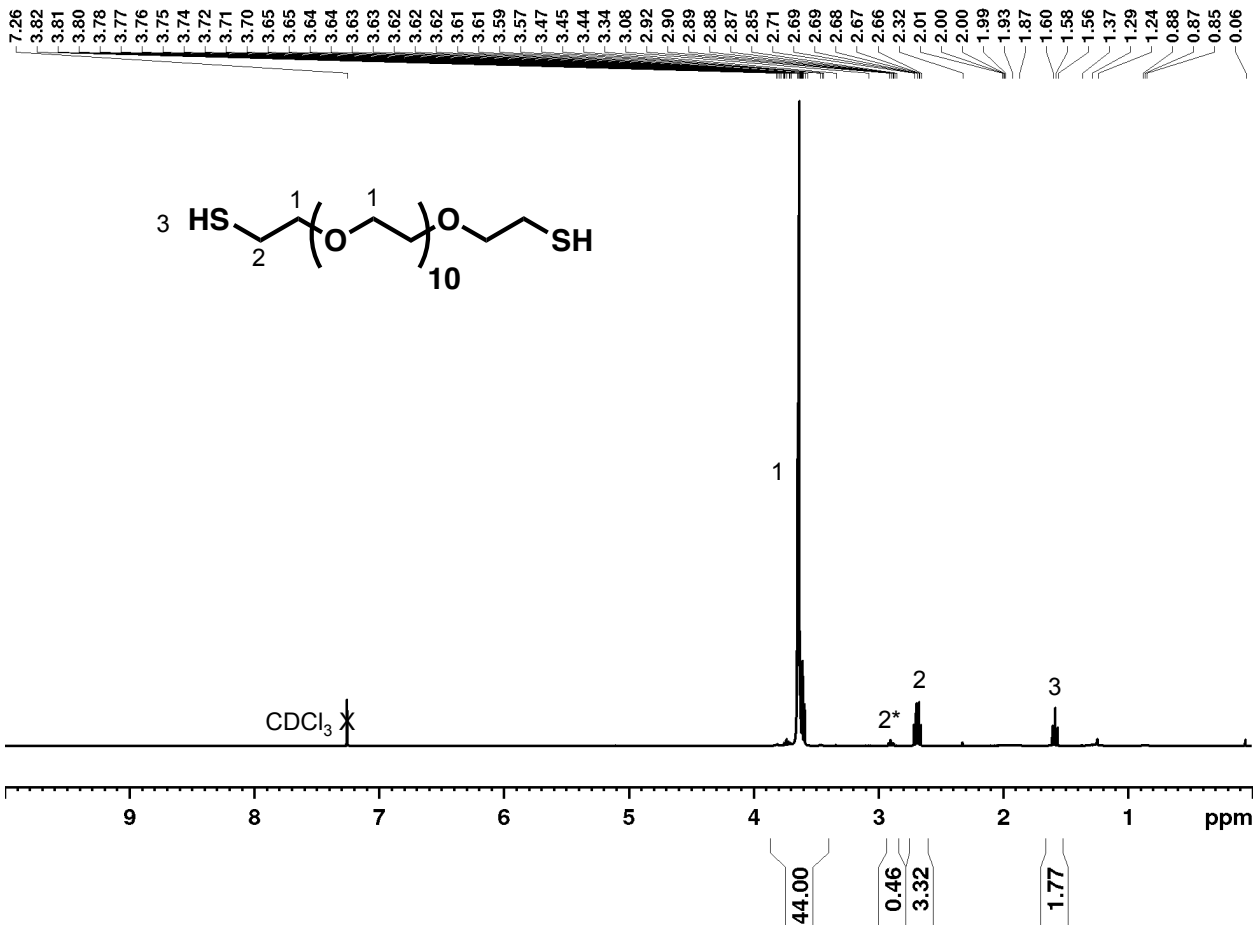

Figure 5.18. ^{1}H NMR of PEG12-dithiol (4) in $CDCl_3$.

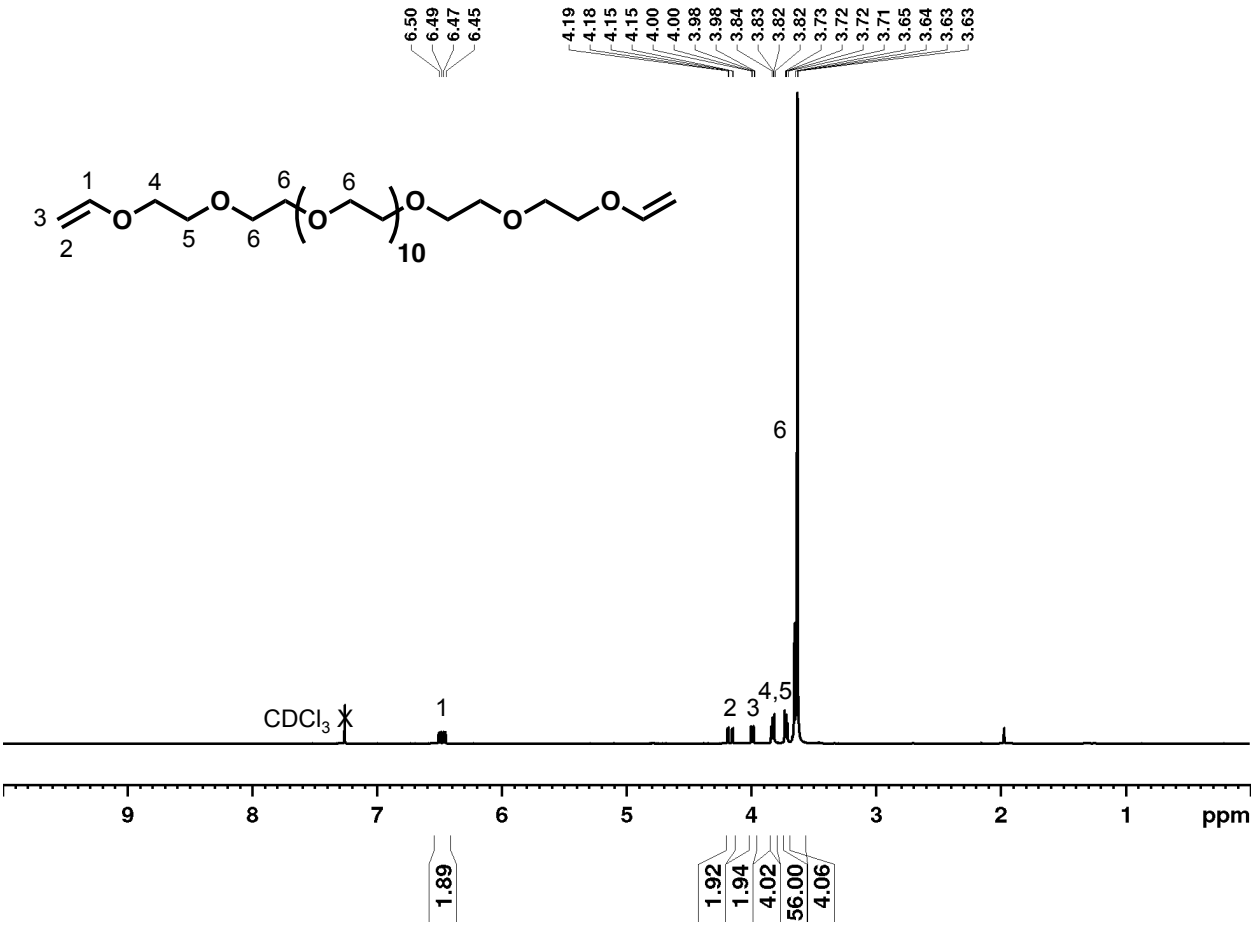

Figure 5.19. ^{1}H NMR of PEG14-divinyl ether (5) in $CDCl_3$.

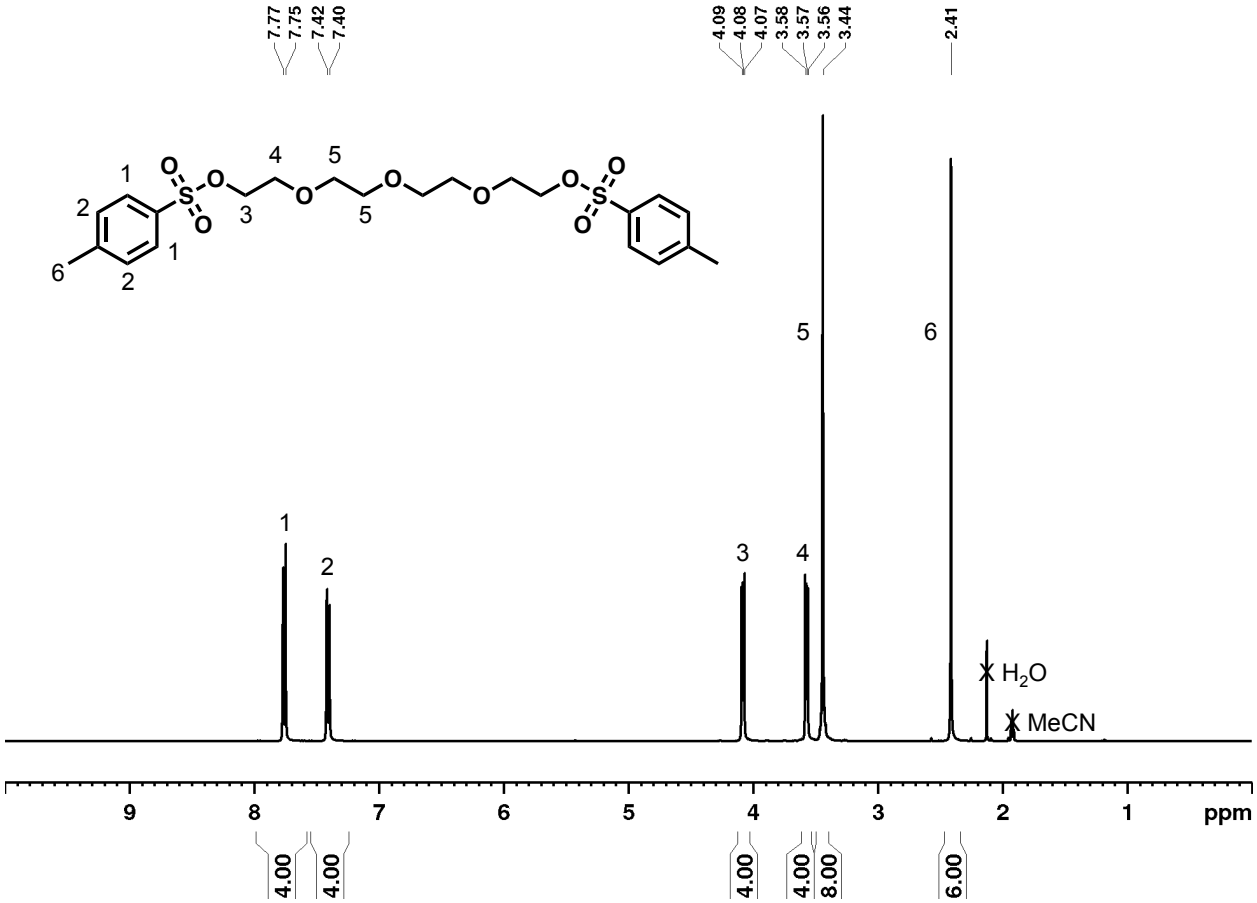

Figure 5.20. ^{1}H NMR of PEG4-ditosylate (6) in CD_3CN.

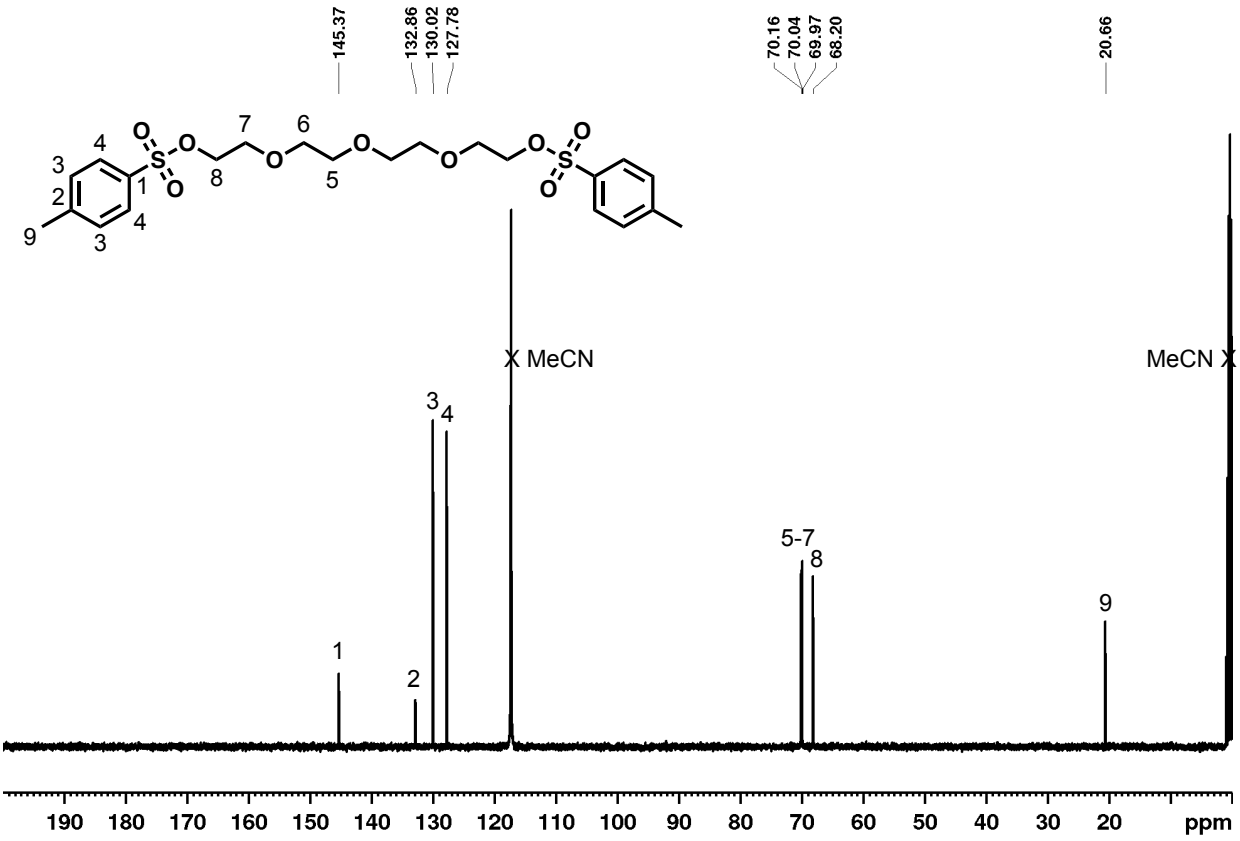

Figure 5.21. ^{13}C NMR of PEG4-ditosylate (6) in CD_3CN.

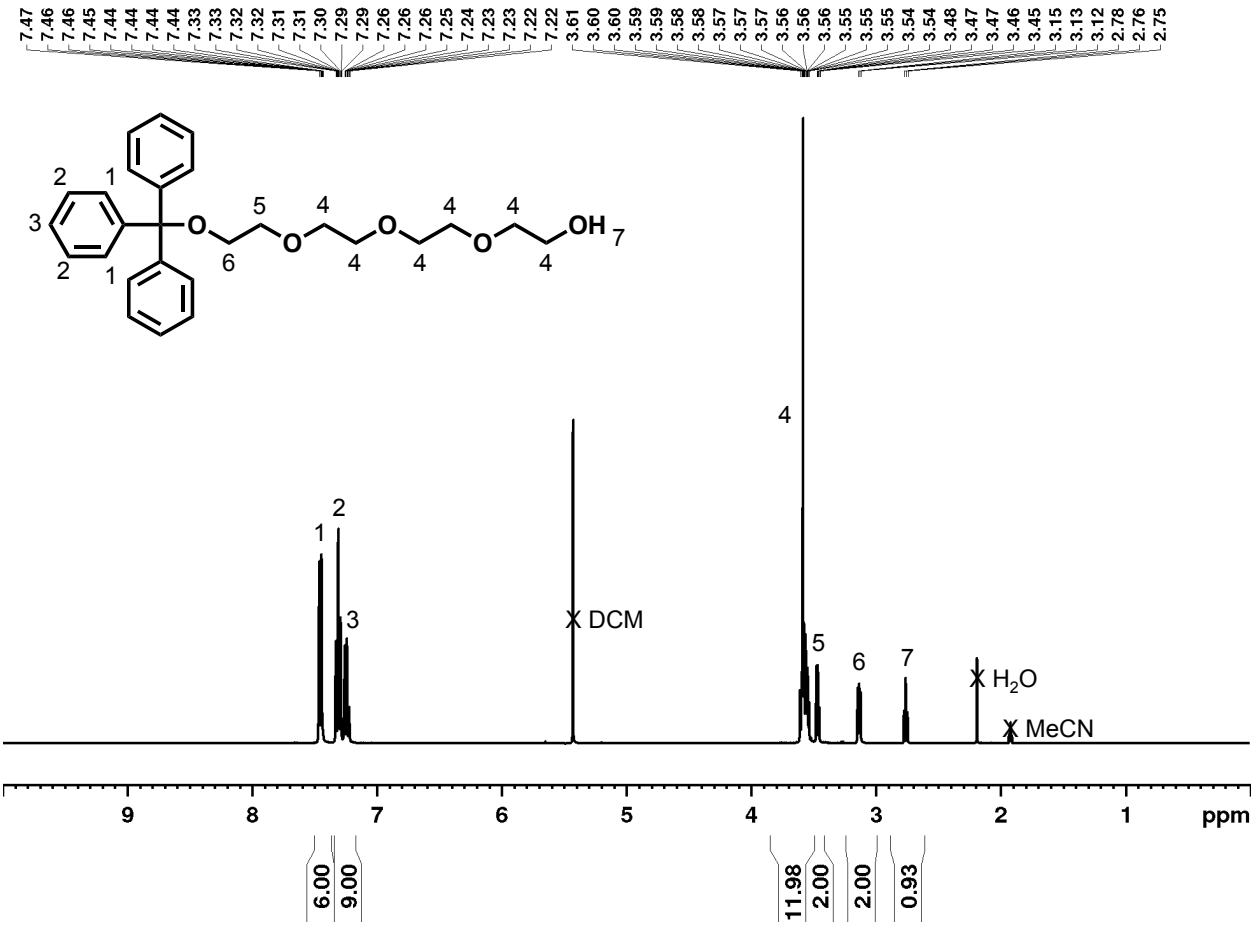

Figure 5.22. ^{1}H NMR of PEG4-monotrityl (7) in CD_3CN.

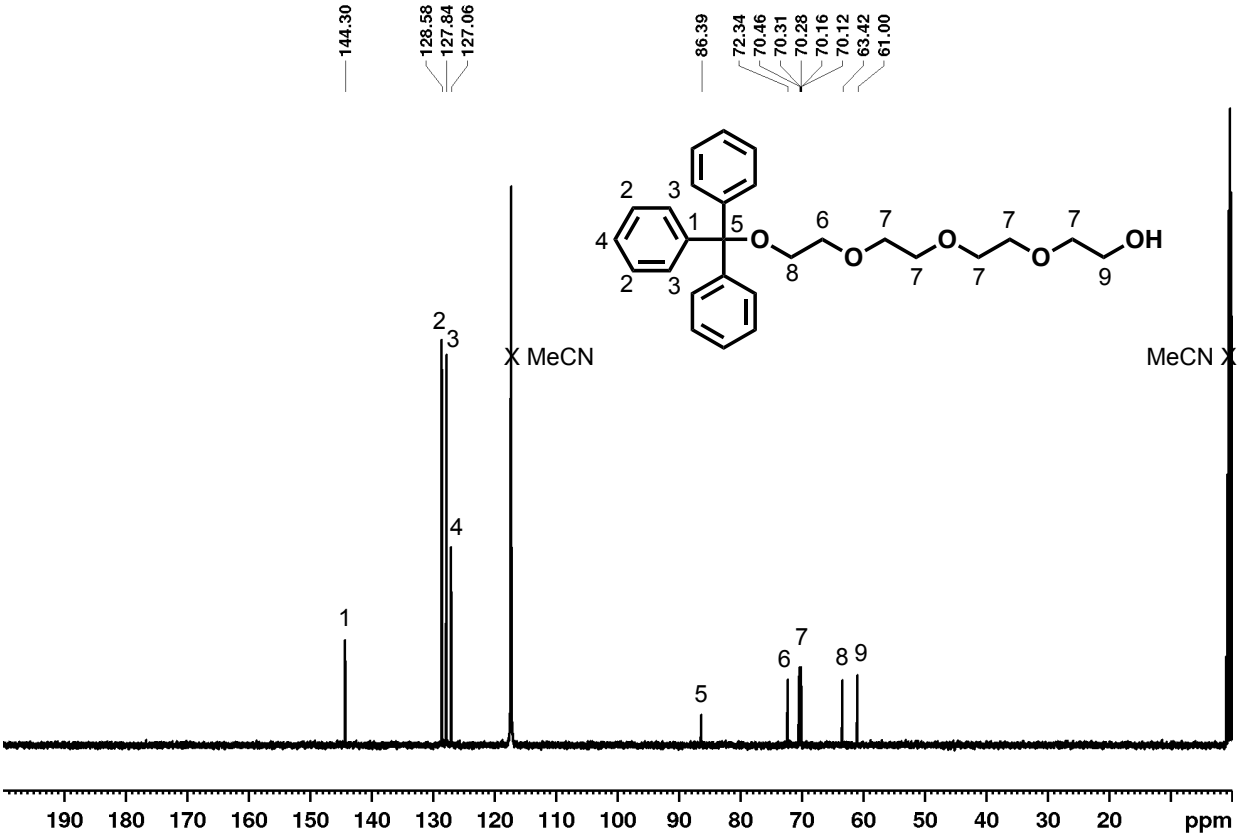

Figure 5.23. ^{13}C NMR of PEG4-monotrityl (7) in CD_3CN.

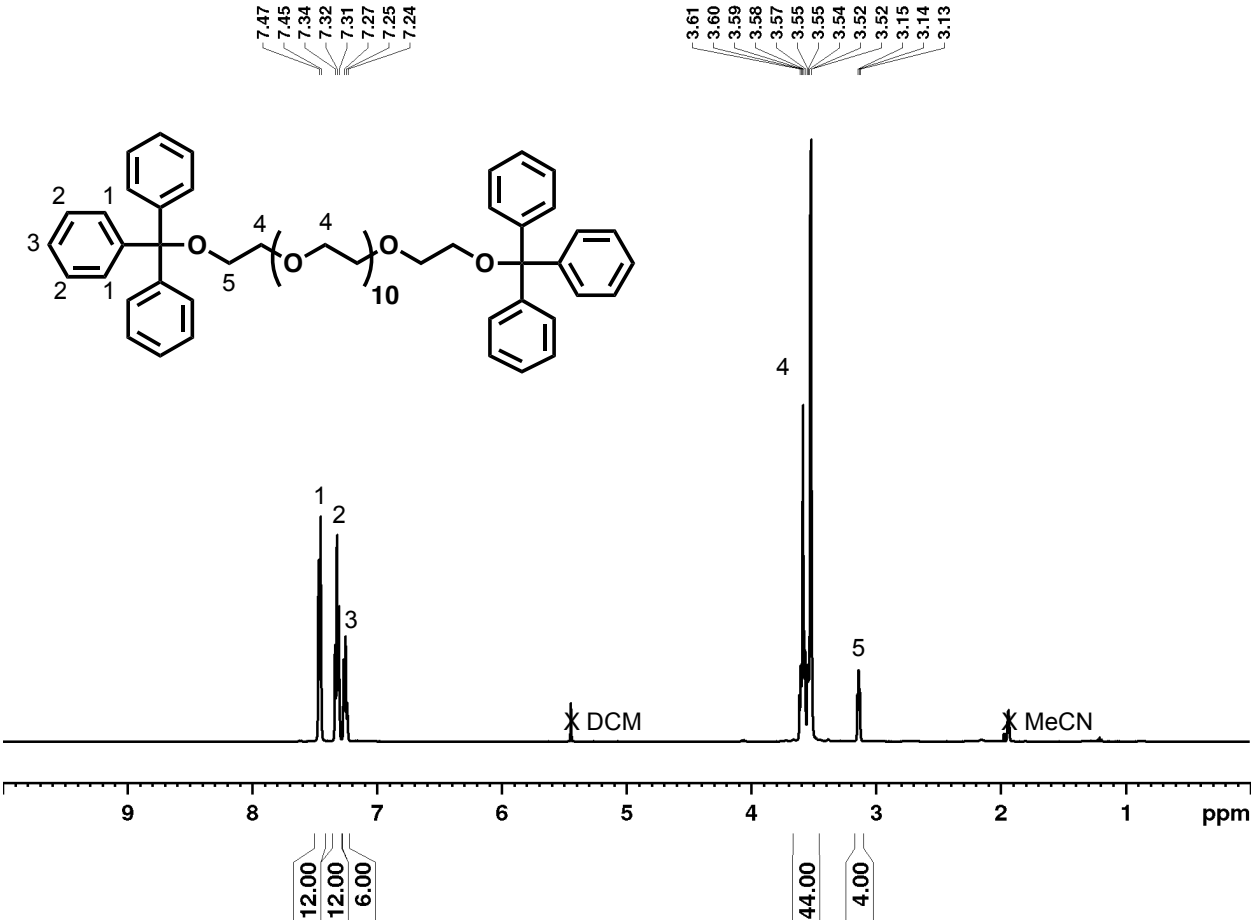

Figure 5.24. ^{1}H NMR of PEG12-dityrityl (8) in CD_3CN.

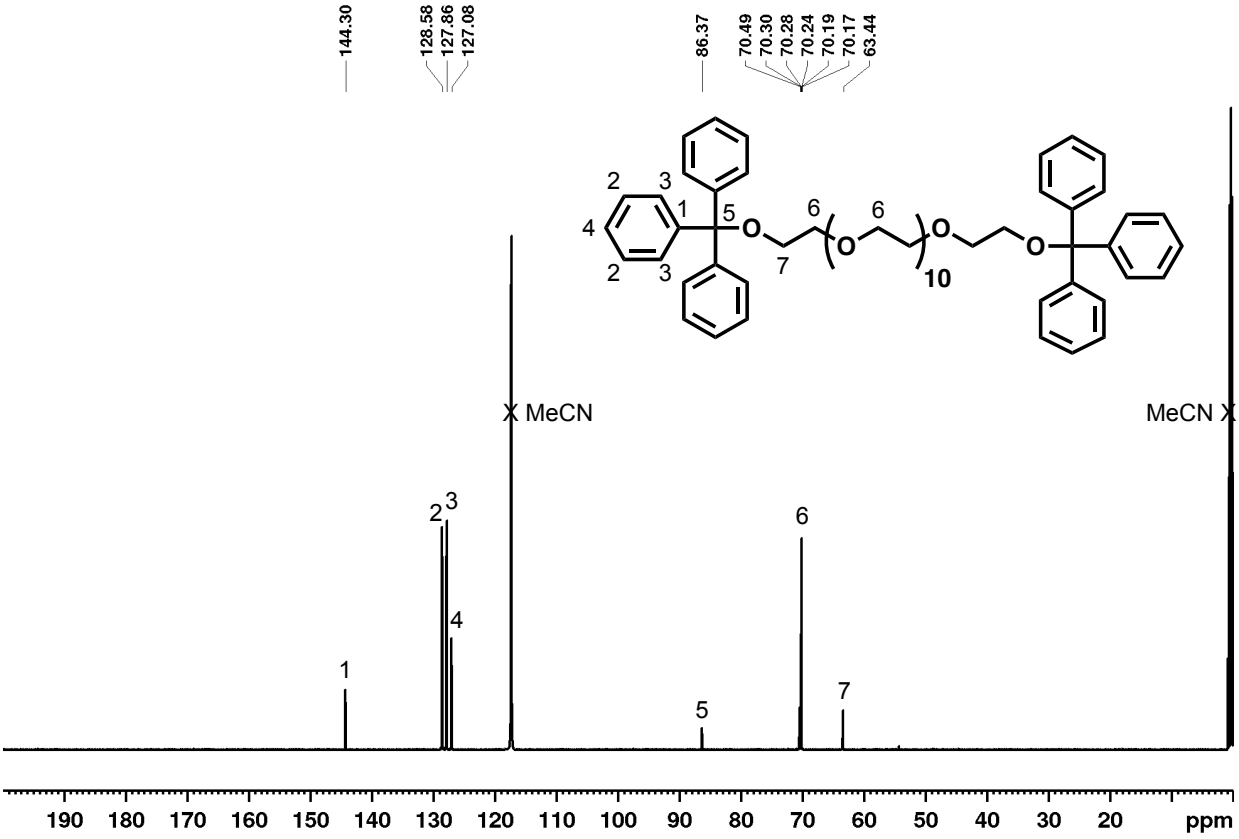

Figure 5.25. ^{13}C NMR of PEG12-ditrityl (8) in CD_3CN.

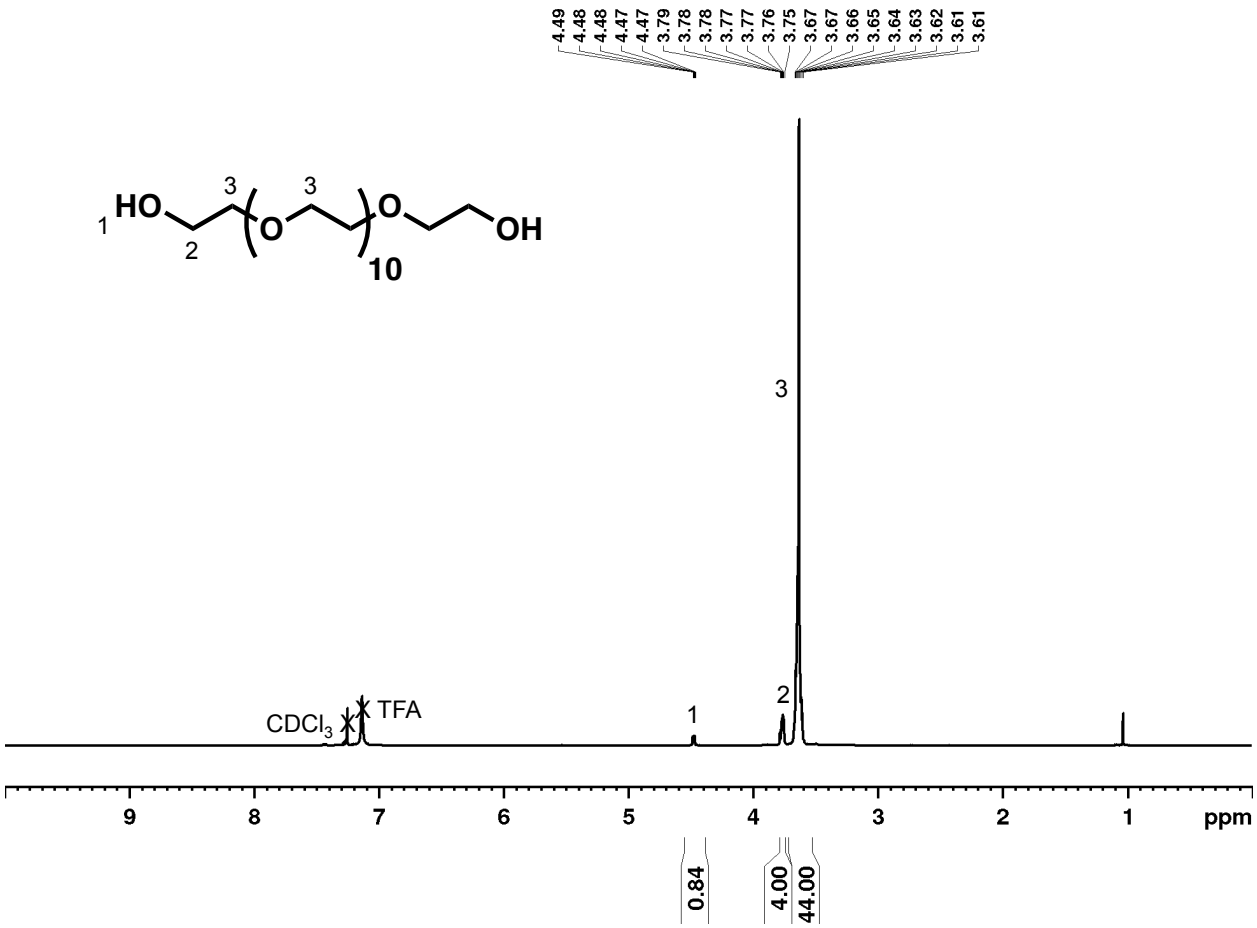

Figure 5.26. ^{1}H NMR of PEG12 in $CDCl_3$. Peak 1 is broadened by presence of TFA and integrates to < 2.00.

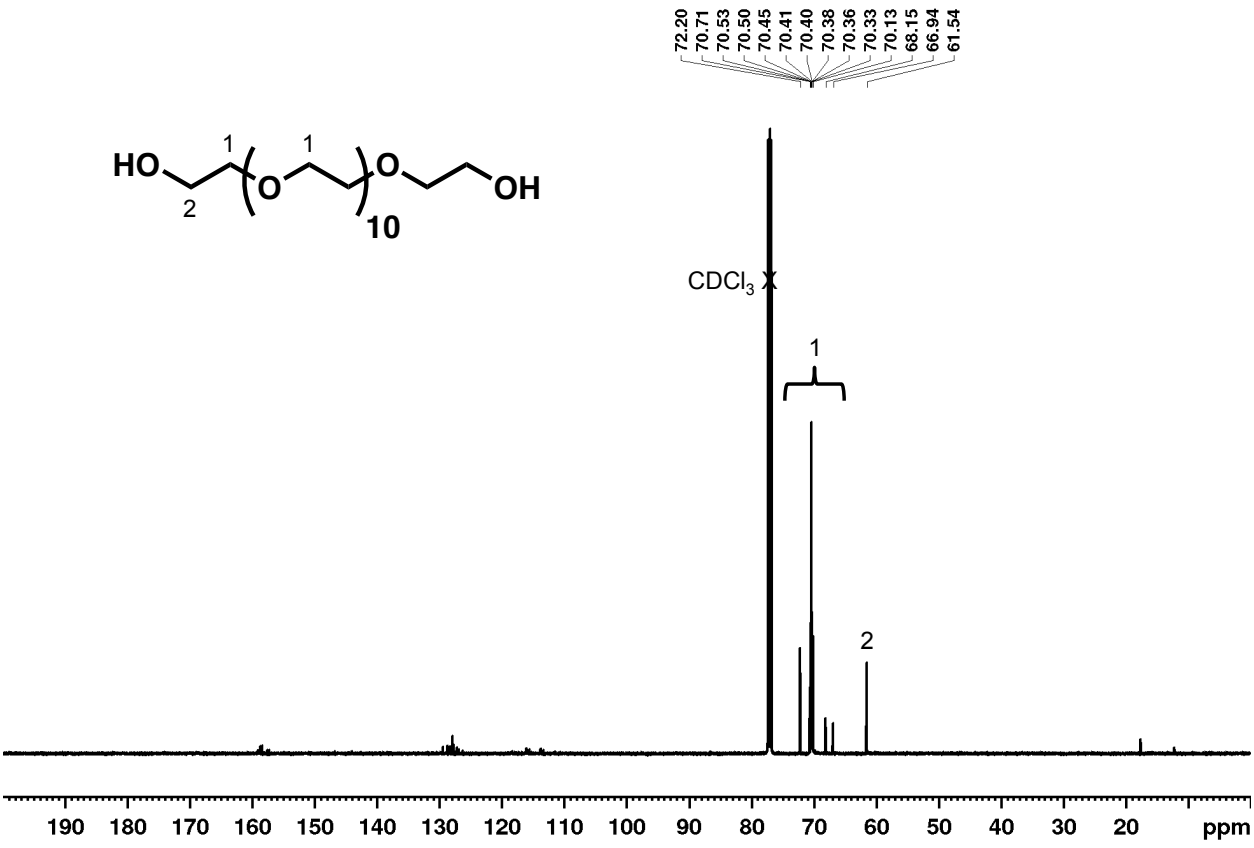

Figure 5.27. ^{13}C NMR of PEG12 in $CDCl_3$. Peaks above 110 ppm reflect the presence of minor trityl impurities.

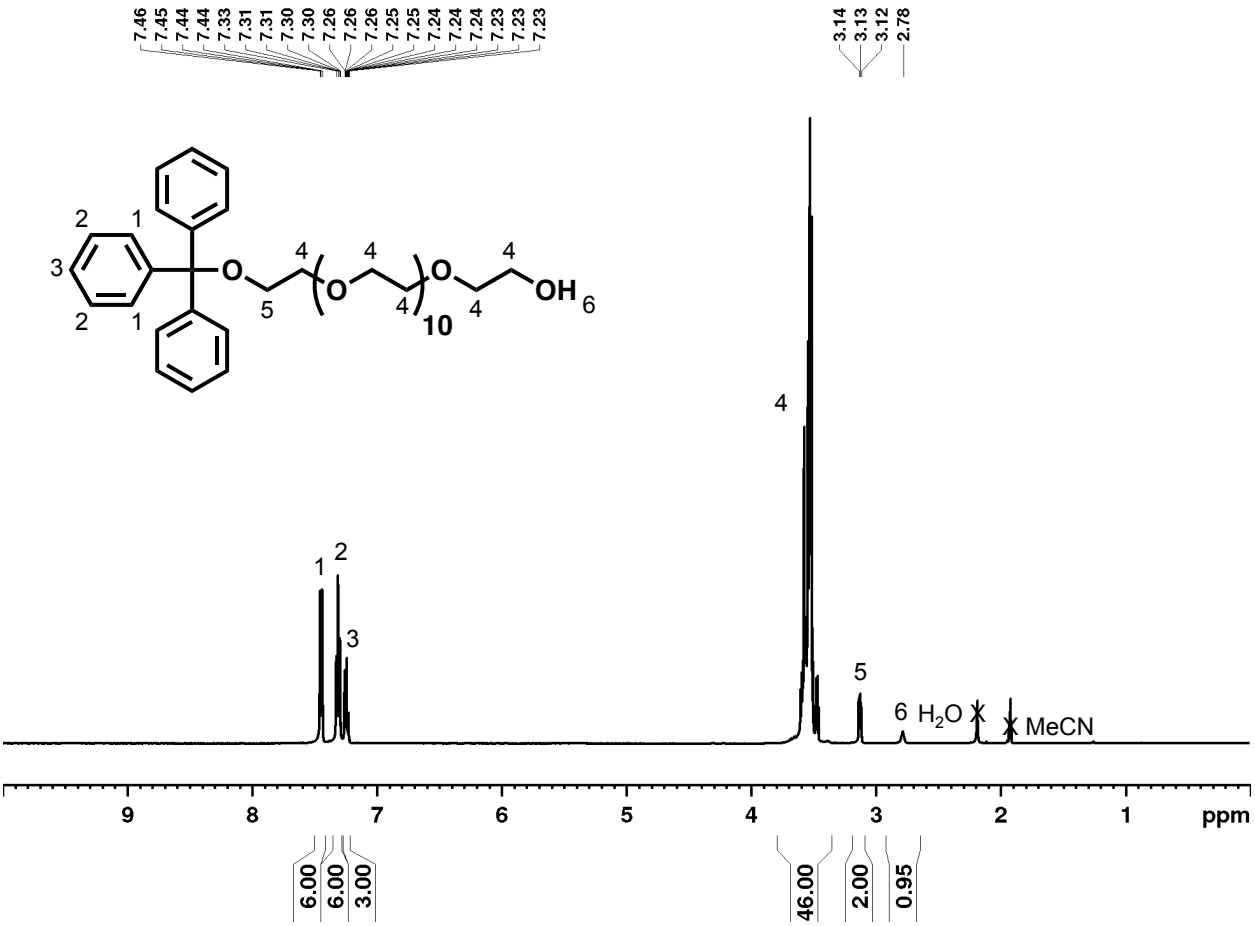

Figure 5.28. ^{1}H NMR of PEG12-monotrityl (9) in CD_3CN.

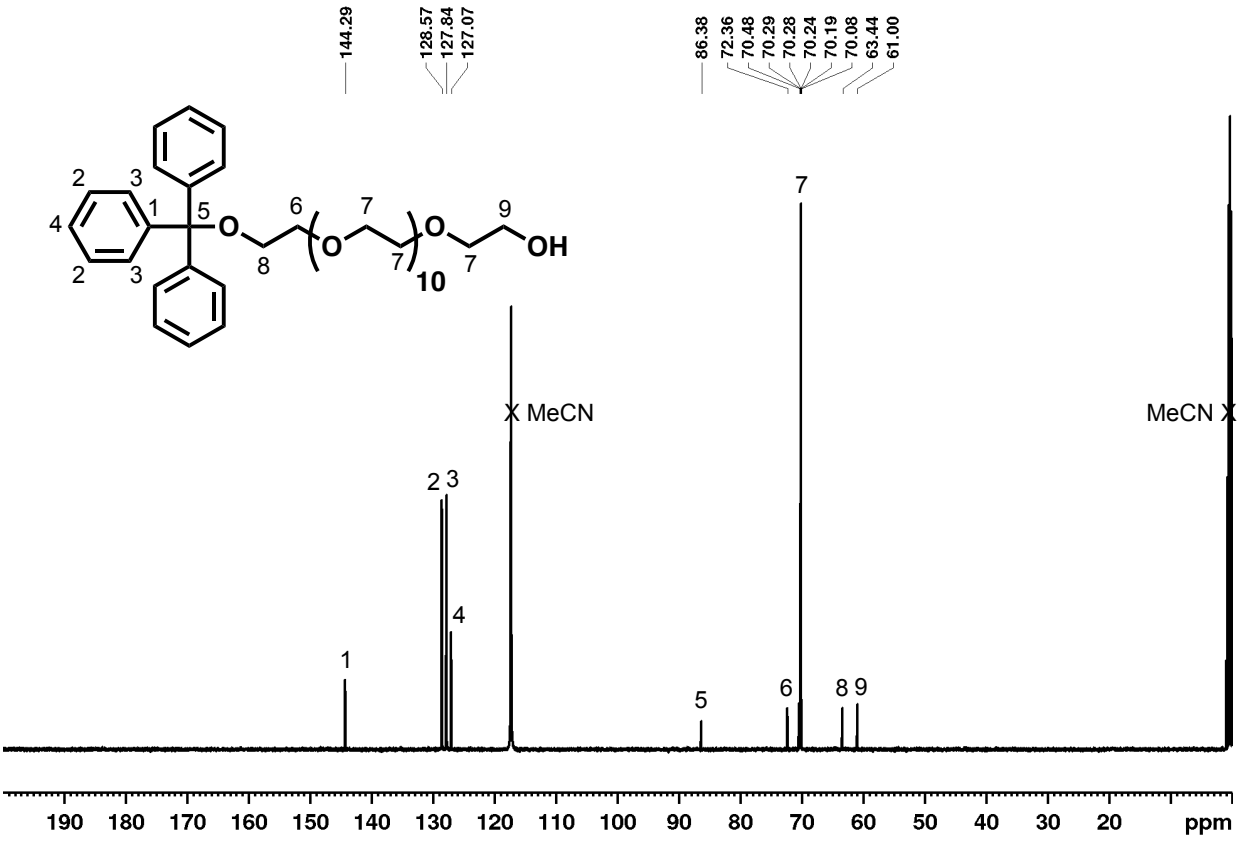

Figure 5.29. ^{13}C NMR of PEG12-monotrityl (9) in CD_3CN.

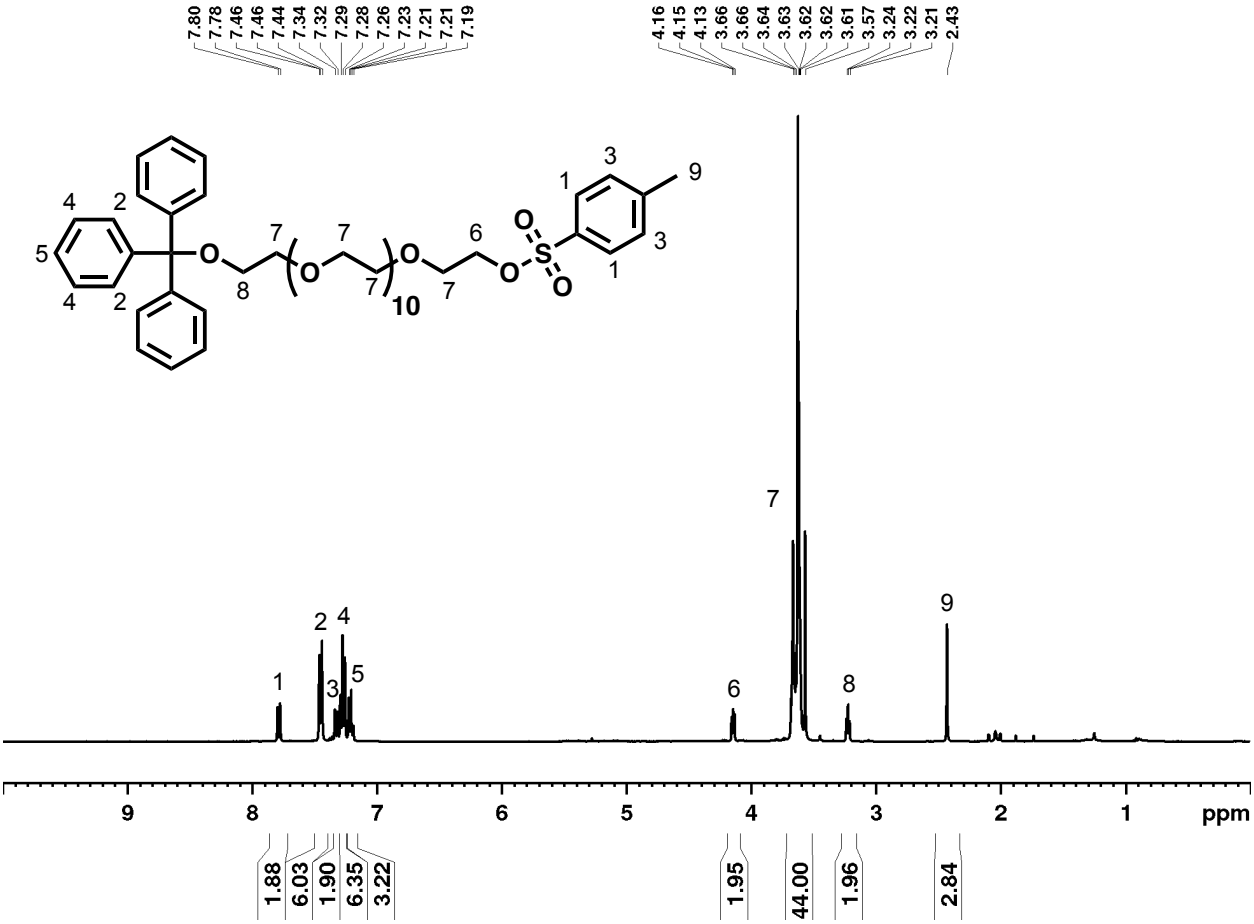

Figure 5.30. ^{1}H NMR of monotosyl-PEG12-monotrityl (10) in CD_3CN.

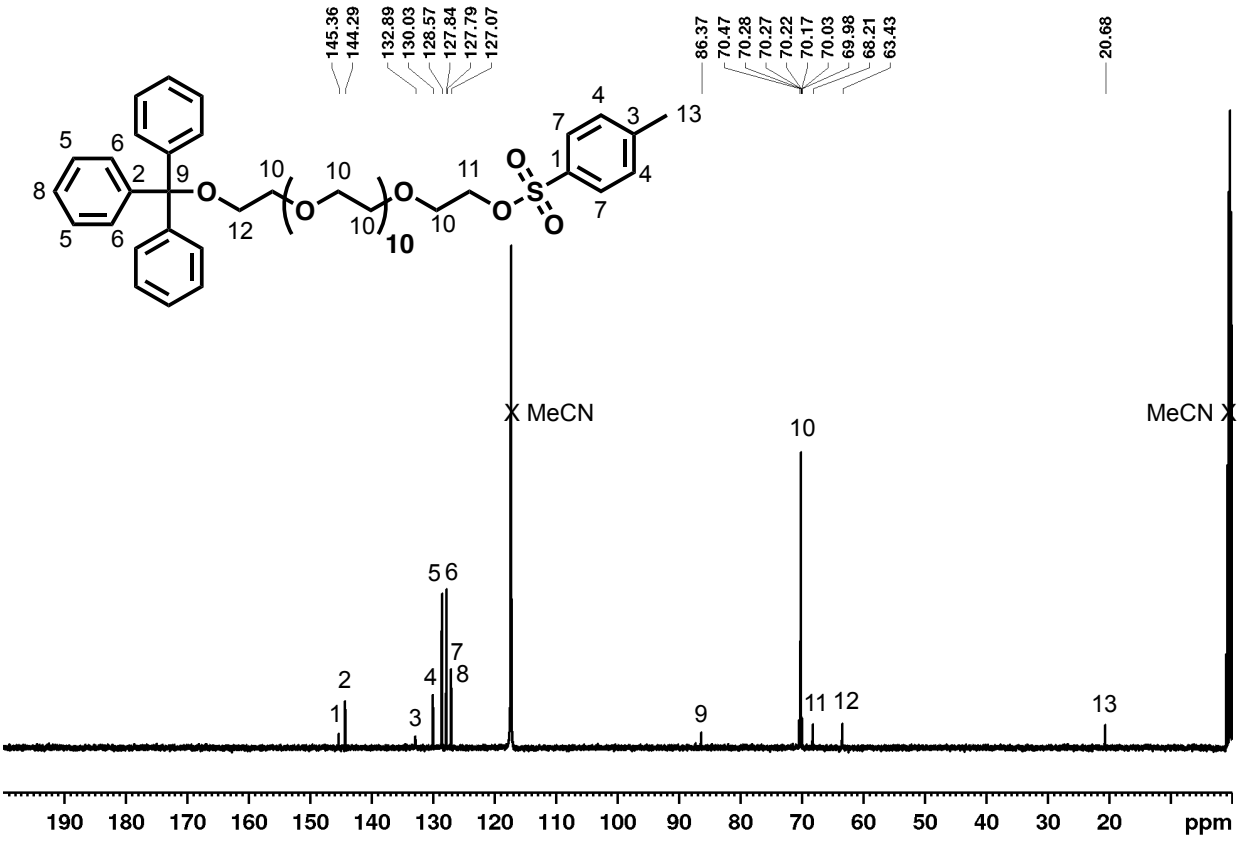

Figure 5.31. ^{13}C NMR of monotosyl-PEG12-monotrityl (10) in CD_3CN.

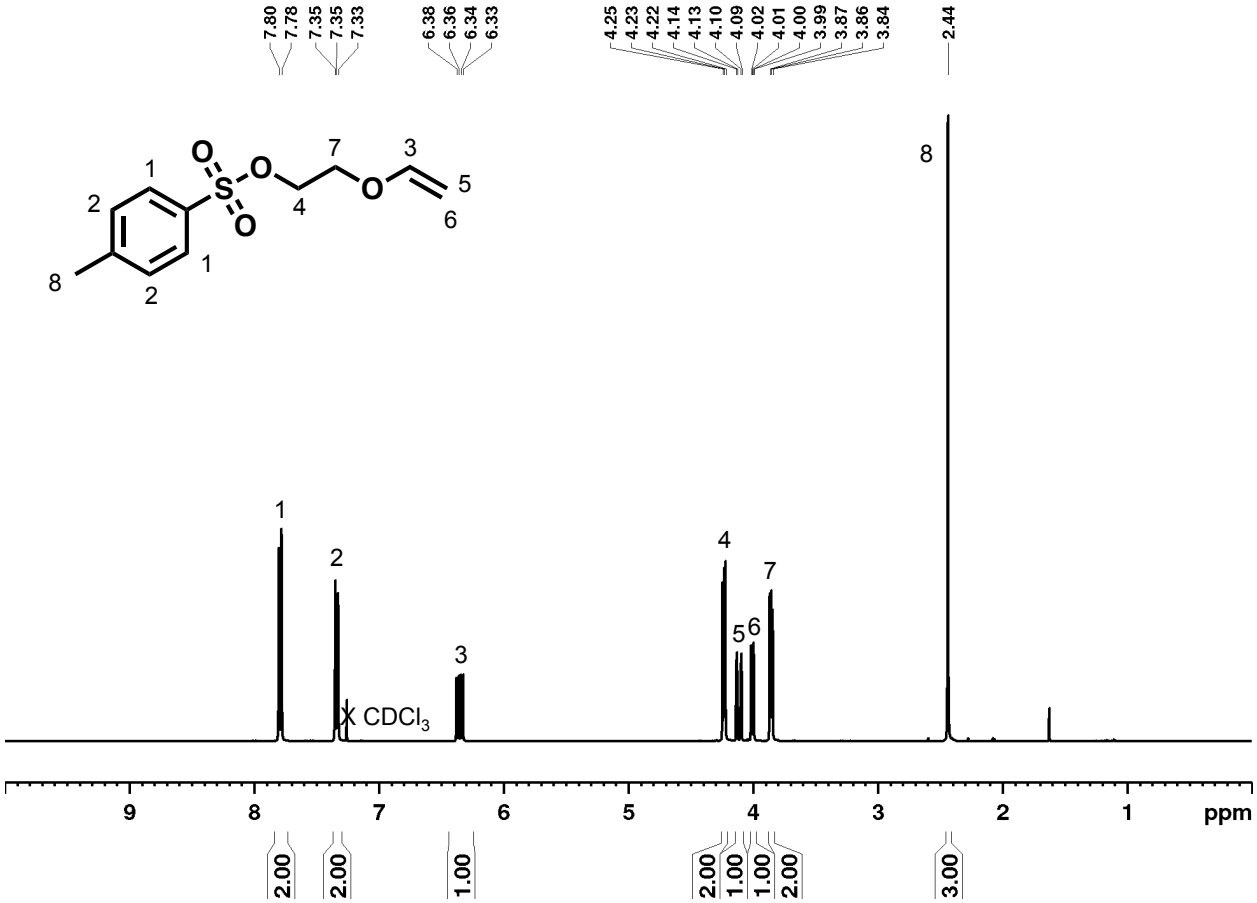

Figure 5.32. ^{1}H NMR of 2-tosylethyl vinyl ether in $CDCl_3$.

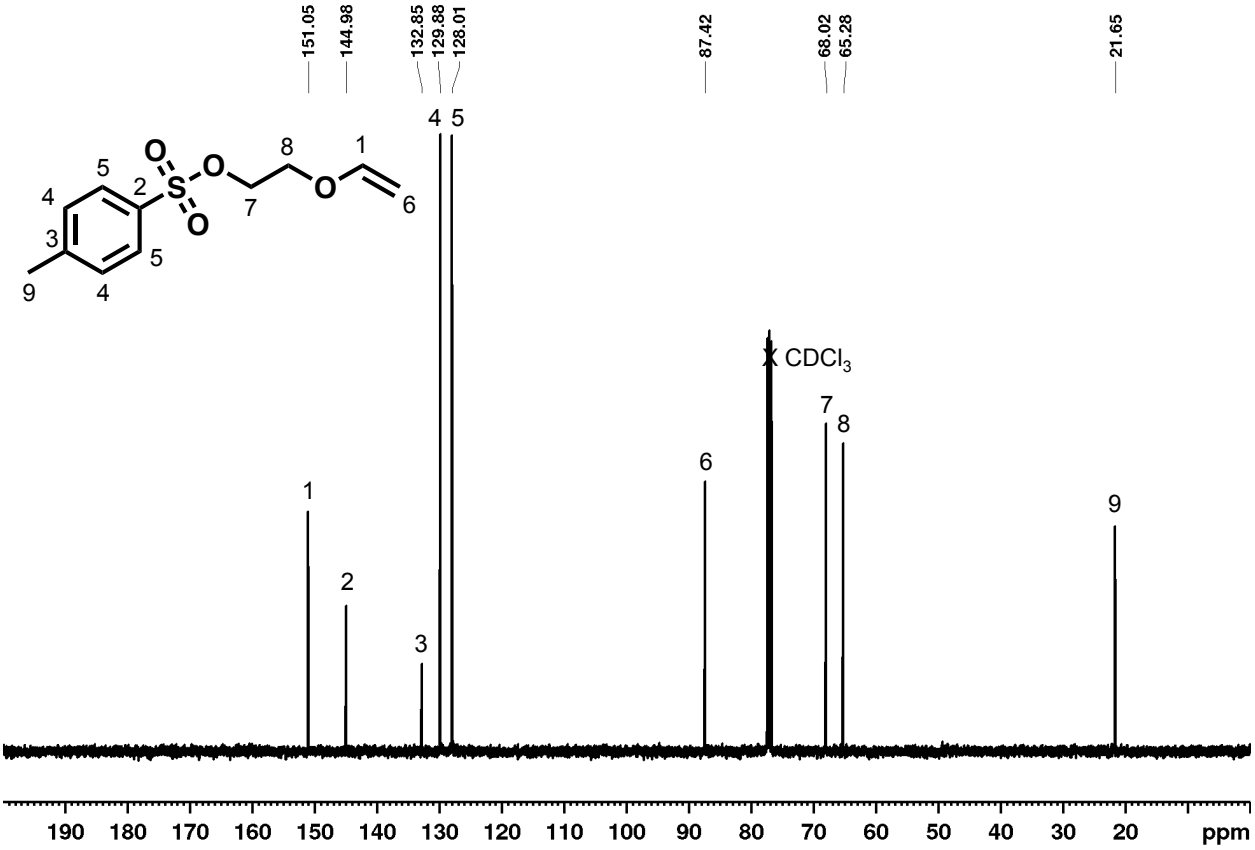

Figure 5.33. ^{13}C NMR of 2-tosylethyl vinyl ether in $CDCl_3$.

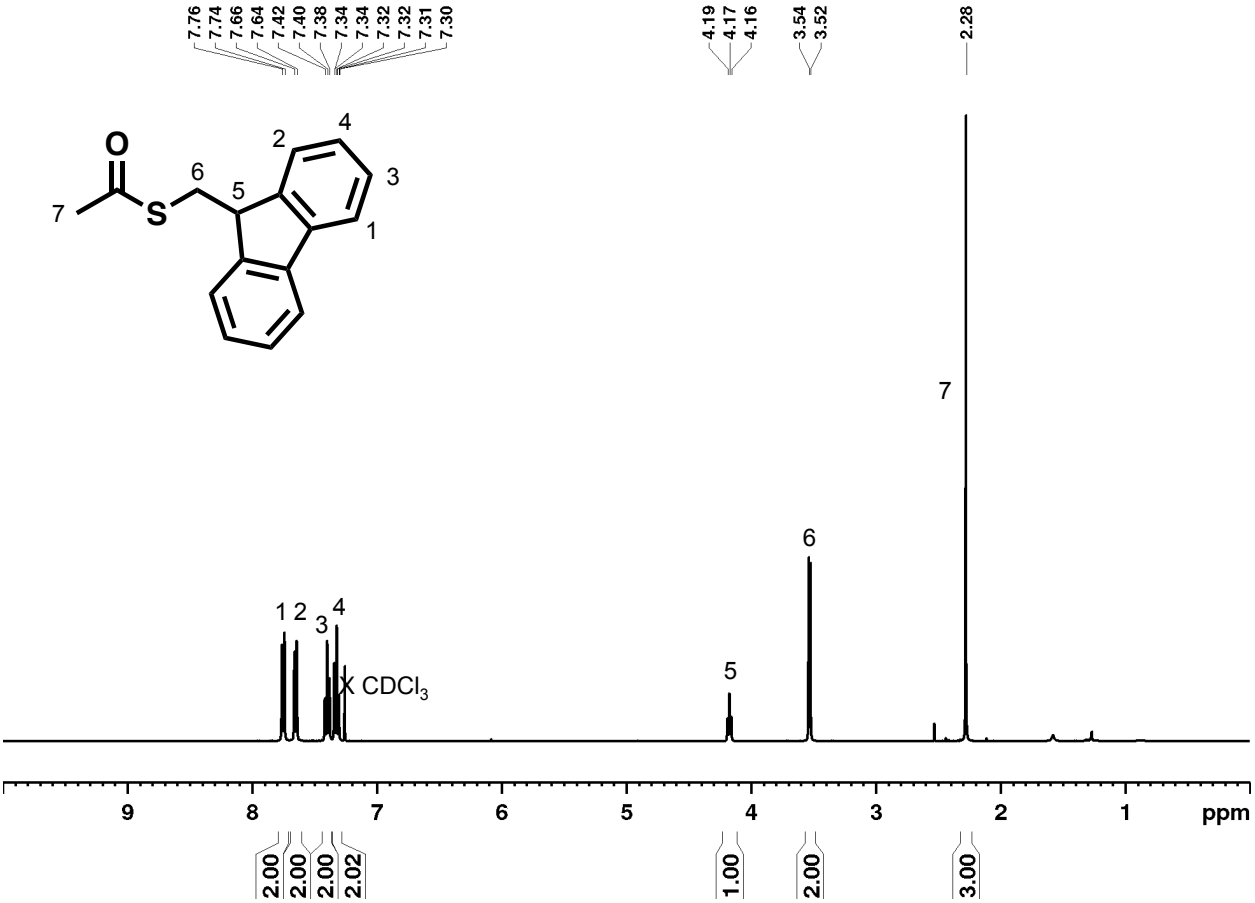

Figure 5.34. ^{1}H NMR of FmSAc in $CDCl_3$.

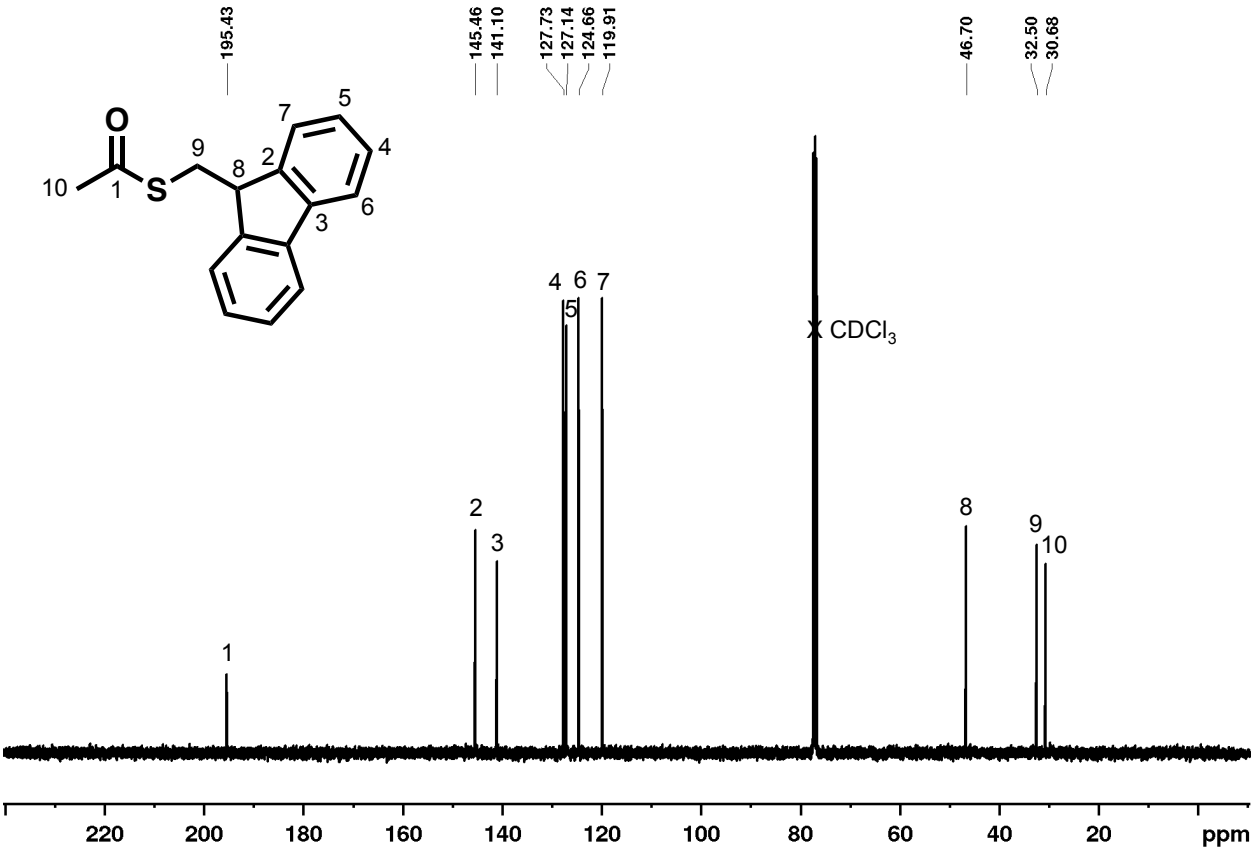

Figure 5.35. ^{13}C NMR of FmSAc in $CDCl_3$.

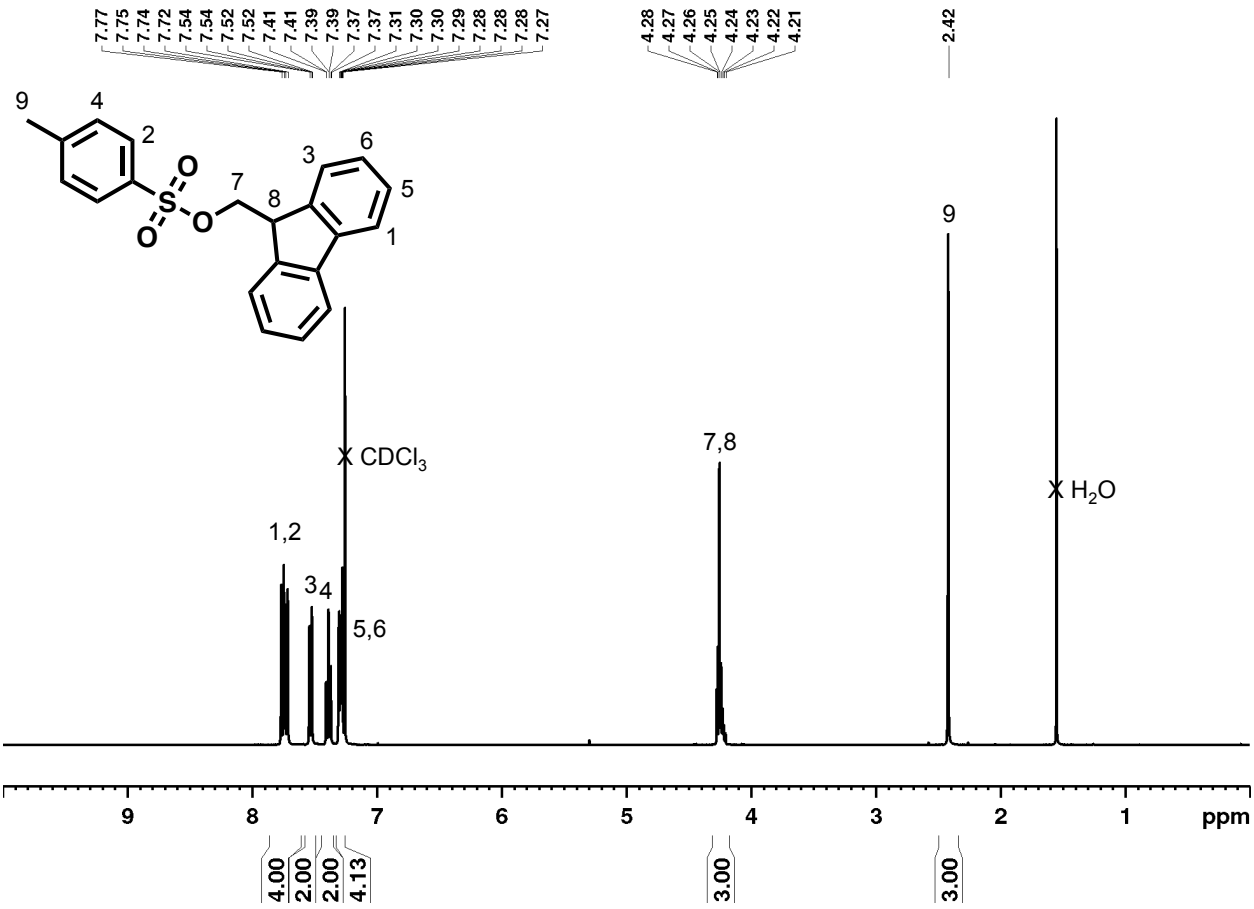

Figure 5.36. ^{1}H NMR of FmOTs in $CDCl_3$.

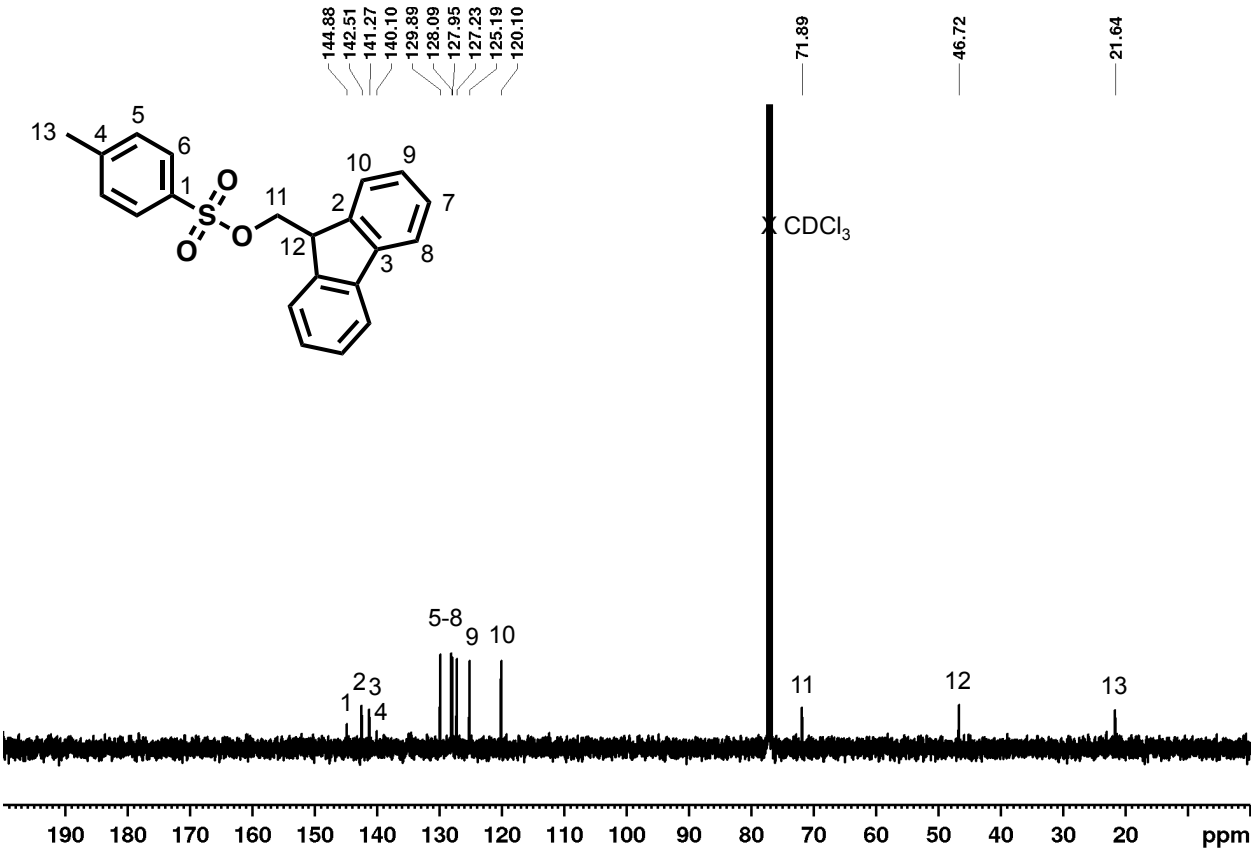

Figure 5.37. ^{13}C NMR of FmOTs in $CDCl_3$.

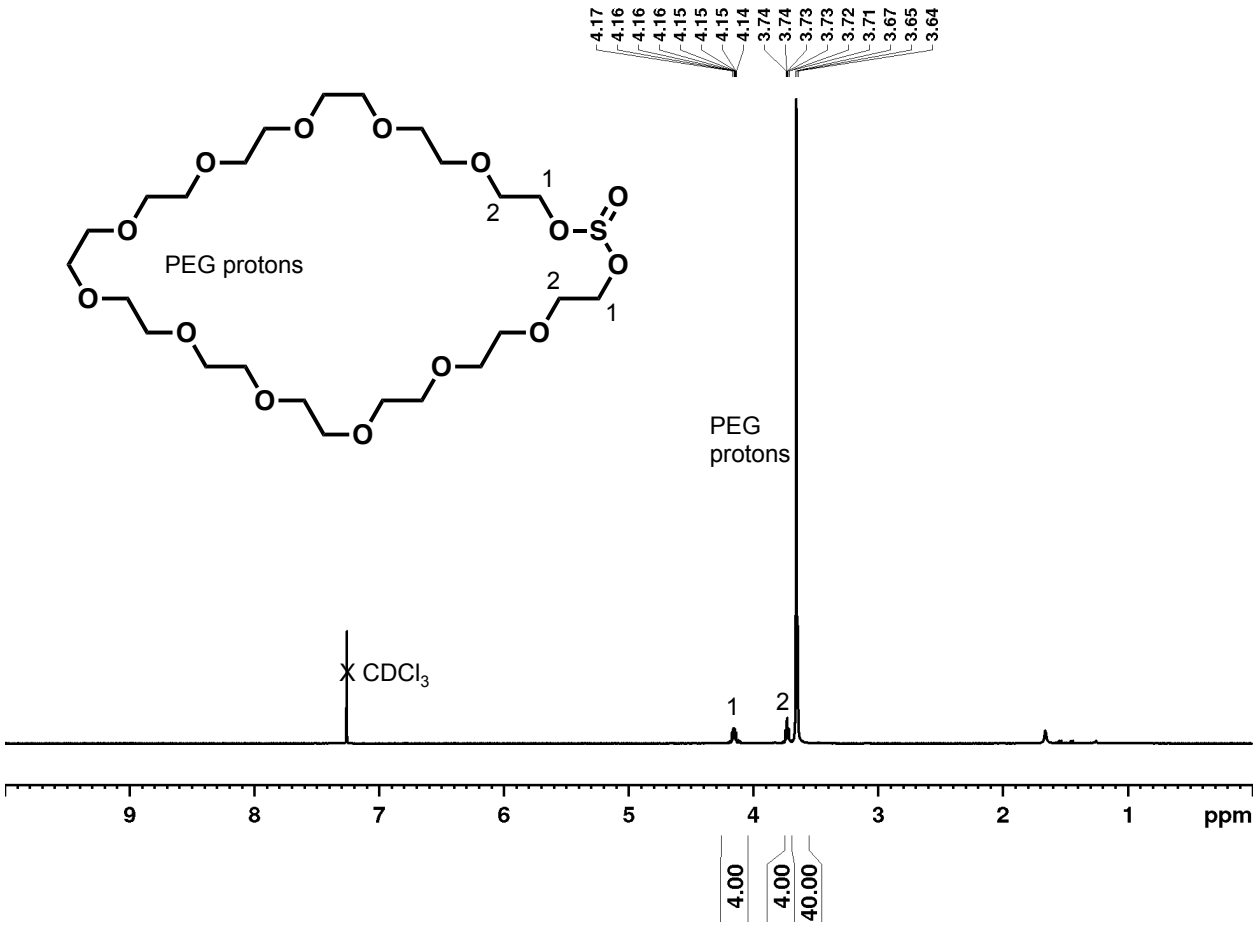

Figure 5.38. ^{1}H NMR of PEG12-macrocyclic sulfite in $CDCl_3$.

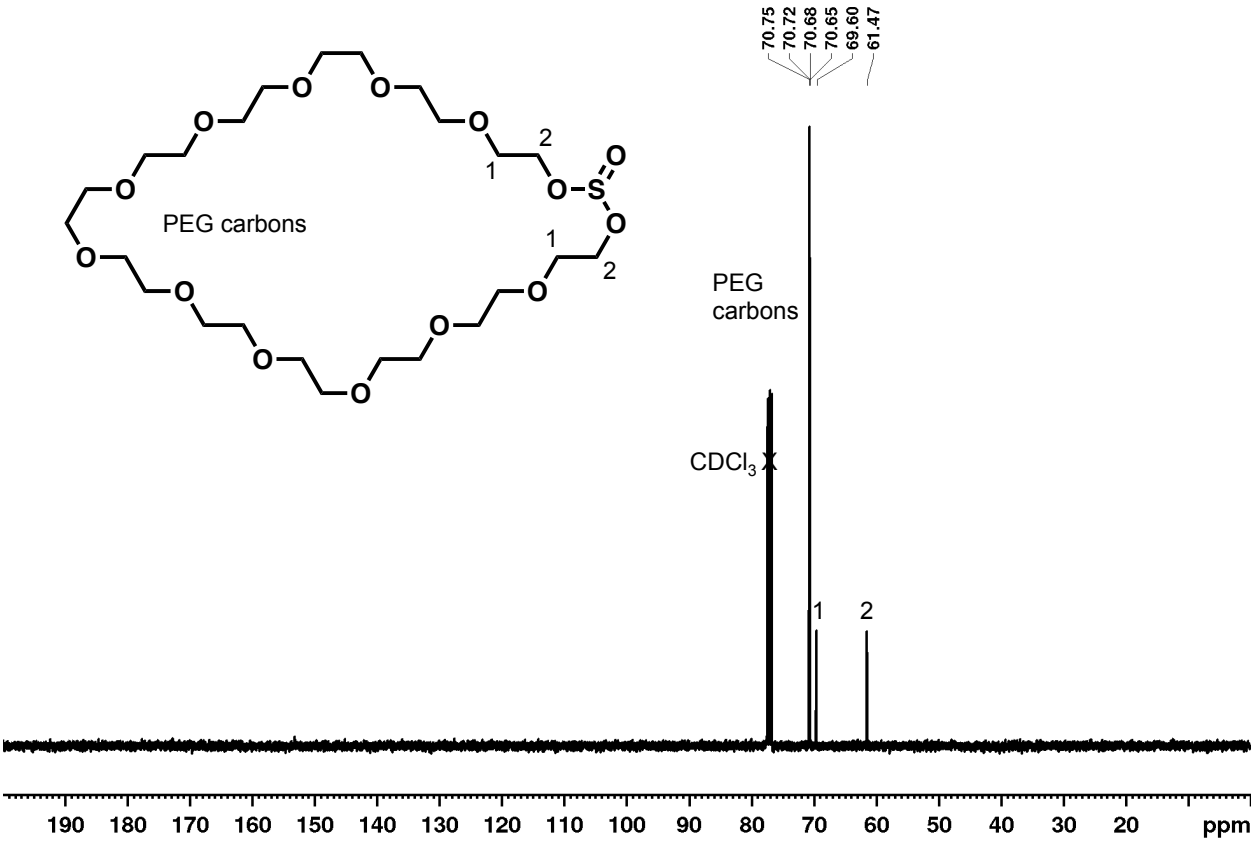

Figure 5.39. ^{13}C NMR of PEG12-macrocyclic sulfite in $CDCl_3$.

5.6 References

(1) Harris, J. M.; Chess, R. B. (2003) Effect of Pegylation on Pharmaceuticals. *Nat. Rev. Drug Discov. 2*, 214–221.

(2) Fishburn, C. S. (2008) The Pharmacology of PEGylation: Balancing PD with PK to Generate Novel Therapeutics. *J. Pharm. Sci. 97*, 4167–4183.

(3) Knop, K.; Hoogenboom, R.; Fischer, D.; Schubert, U. S. (2010) Poly(Ethylene Glycol) in Drug Delivery: Pros and Cons as Well as Potential Alternatives. *Angew. Chem. - Int. Ed. 49*, 6288–6308.

(4) Elsadek, N. E.; Abu Lila, A. S.; Ishida, T. 5 - Immunological Responses to PEGylated Proteins: Anti-PEG Antibodies. In *Polymer-Protein Conjugates*; Pasut, G., Zalipsky, S., Eds.; Elsevier, 2020; pp 103–123.

(5) Mora, J. R.; White, J. T.; DeWall, S. L. (2020) Immunogenicity Risk Assessment for PEGylated Therapeutics. *AAPS J. 22*, 35.

(6) Peeters, E.; Janssen, H. M.; Zundert, M. F. van; Genderen, M. H. P. van; Meijer, E. W. (1996) The Synthesis and Polymerization of Oxo-Crown Ethers. *Acta Polym. 47*, 485–491.

(7) Janssen, H. M.; Peeters, E.; Zundert, M. F. van; Genderen, M. H. P. van; Meijer, E. W. (1997) Unconventional Amphiphilic Polymers Based on Chiral Polyethylene Oxides. *Angew. Chem. Int. Ed. Engl. 36*, 122–125.

(8) Janssen, H. M.; Peeters, E.; van Zundert, M. F.; van Genderen, M. H. P.; Meijer, E. W. (1997) Unconventional, Amphiphilic Polymers Based on Chiral Poly(Ethylene Oxide) Derivatives. I. Synthesis and Characterization. *Macromolecules 30*, 8113–8128.

(9) Illy, N.; Taylan, E.; Brissault, B.; Wojno, J.; Boileau, S.; Barbier, V.; Penelle, J. (2013) Synthesis and Anionic Ring-Opening Polymerization of Crown-Ether-like Macrocyclic Dilactones: An Alternative Route to PEG-Containing Polyesters and Related Networks. *Eur. Polym. J. 49*, 4087–4097.

(10) Zhu, K. J.; Xiangzhou, L.; Shilin, Y. (1990) Preparation, Characterization, and Properties of Polylactide (PLA)–Poly(Ethylene Glycol) (PEG) Copolymers: A Potential Drug Carrier. *J. Appl. Polym. Sci. 39*, 1–9.

(11) Sawhney, A. S.; Pathak, C. P.; Hubbell, J. A. (1993) Bioerodible Hydrogels Based on Photopolymerized Poly(Ethylene Glycol)-Co-Poly(.Alpha.-Hydroxy Acid) Diacrylate Macromers. *Macromolecules 26*, 581–587.

(12) Li, S. M.; Rashkov, I.; Espartero, J. L.; Manolova, N.; Vert, M. (1996) Synthesis, Characterization, and Hydrolytic Degradation of PLA/PEO/PLA Triblock Copolymers with Long Poly(l-Lactic Acid) Blocks. *Macromolecules 29*, 57–62.

(13) Metters, A. T.; Anseth, K. S.; Bowman, C. N. (2000) Fundamental Studies of a Novel, Biodegradable PEG-b-PLA Hydrogel. *Polymer 41*, 3993–4004.

(14) Lundberg, P.; Lee, B. F.; van den Berg, S. A.; Pressly, E. D.; Lee, A.; Hawker, C. J.; Lynd, N. A. (2012) Poly[(Ethylene Oxide)-Co-(Methylene Ethylene Oxide)]: A Hydrolytically Degradable Poly(Ethylene Oxide) Platform. *ACS Macro Lett. 1*, 1240–1243.

(15) Knorr, V.; Ogris, M.; Wagner, E. (2008) An Acid Sensitive Ketal-Based Polyethylene Glycol-Oligoethylenimine Copolymer Mediates Improved Transfection Efficiency at Reduced Toxicity. *Pharm. Res. 25*, 2937–2945.

(16) Boehnke, N.; Cam, C.; Bat, E.; Segura, T.; Maynard, H. D. (2015) Imine Hydrogels with Tunable Degradability for Tissue Engineering. *Biomacromolecules 16*, 2101–2108.

(17) Lee, Y.; Koo, H.; Jin, G. W.; Mo, H.; Cho, M. Y.; Park, J. Y.; Choi, J. S.; Park, J. S. (2005) Poly(Ethylene Oxide Sulfide): New Poly(Ethylene Glycol) Derivatives Degradable in Reductive Conditions. *Biomacromolecules 6*, 24–26.

(18) Sun, K. H.; Sohn, Y. S.; Jeong, B. (2006) Thermogelling Poly(Ethylene Oxide-b-Propylene Oxide-b-Ethylene Oxide) Disulfide Multiblock Copolymer as a Thiol-Sensitive Degradable Polymer. *Biomacromolecules 7*, 2871–2877.

(19) Ulbrich, K.; Strohalm, J.; Kop, J. (1986) Poly(Ethylene Glycol)s Containing Enzymatically Degradable Bonds. *Makromol. Chem. 187*, 1131–1144.

(20) Pelegri-O'Day, E. M.; Matsumoto, N. M.; Tamshen, K.; Raftery, E. D.; Lau, U. Y.; Maynard, H. D. (2018) PEG Analogs Synthesized by Ring-Opening Metathesis Polymerization for Reversible Bioconjugation. *Bioconjug. Chem. 29*, 3739–3745.

(21) Niculescu-Duvaz, D.; Getaz, J.; Springer, C. J. (2008) Long Functionalized Poly (Ethylene Glycol) s of Defined Molecular Weight : Synthesis and Application in Solid-Phase Synthesis of Conjugates. *Bioconjug. Chem. 19*, 973–981.

(22) Gaberc-Porekar, V.; Zore, I.; Podobnik, B.; Menart, V. (2008) Obstacles and Pitfalls in the PEGylation of Therapeutic Proteins. *Curr. Opin. Drug Discov. Devel. 11*, 242–250.

(23) Solleder, S. C.; Schneider, R. V.; Wetzel, K. S.; Boukis, A. C.; Meier, M. A. R. (2017) Recent Progress in the Design of Monodisperse, Sequence-Defined Macromolecules. *Macromol. Rapid Commun. 38*, 1600711.

(24) Loiseau, F. A.; Hii, K. K.; Hill, A. M. (2004) Multigram Synthesis of Well-Defined Extended Bifunctional Polyethylene Glycol (PEG) Chains. *J. Org. Chem. 69*, 639–647.

(25) Ahmed, S. A.; Tanaka, M. (2006) Synthesis of Oligo (Ethylene Glycol) toward 44-Mer. No. 6, 9884–9886.

(26) Berna, M.; Dalzoppo, D.; Pasut, G.; Manunta, M.; Izzo, L.; Jones, A. T.; Duncan, R.; Veronese, F. M. (2006) Novel Monodisperse PEG-Dendrons as New Tools for Targeted Drug Delivery: Synthesis, Characterization and Cellular Uptake. *Biomacromolecules 7*, 146–153.

(27) French, A. C.; Thompson, A. L.; Davis, B. G. (2009) High-Purity Discrete PEG-Oligomer Crystals Allow Structural Insight. *Angew. Chem. - Int. Ed. 48*, 1248–1252.

(28) Székely, G.; Schaepertoens, M.; Gaffney, P. R. J.; Livingston, A. G. (2014) Iterative Synthesis of Monodisperse PEG Homostars and Linear Heterobifunctional PEG. *Polym. Chem. 5*, 694.

(29) Li, Y.; Guo, Q.; Li, X.; Zhang, H.; Yu, F.; Yu, W.; Xia, G.; Fu, M.; Yang, Z.; Jiang, Z. X. (2014) Fluorous Synthesis of Mono-Dispersed Poly(Ethylene Glycols). *Tetrahedron Lett. 55*, 2110–2113.

(30) Maranski, K.; Andreev, Y. G.; Bruce, P. G. (2014) Synthesis of Poly(Ethylene Oxide) Approaching Monodispersity. *Angew. Chem. Int. Ed. 53*, 6411–6413.

(31) Li, Y.; Qiu, X.; Jiang, Z.-X. (2015) Macrocyclic Sulfates as Versatile Building Blocks in the Synthesis of Monodisperse Poly(Ethylene Glycol)s and Monofunctionalized Derivatives. *Org. Process Res. Dev. 19*, 800–805.

(32) Zhang, H.; Li, X.; Shi, Q.; Li, Y.; Xia, G.; Chen, L.; Yang, Z.; Jiang, Z. X. (2015) Highly Efficient Synthesis of Monodisperse Poly(Ethylene Glycols) and Derivatives through Macrocyclization of Oligo(Ethylene Glycols). *Angew. Chem. - Int. Ed. 54*, 3763–3767.

(33) Khanal, A.; Fang, S. (2017) Solid Phase Stepwise Synthesis of Polyethylene Glycols. *Chem. – Eur. J. 23*, 15133–15142.

(34) Marsella, M. J.; Maynard, H. D.; Grubbs, R. H. (1997) Template-Directed Ring-Closing Metathesis: Synthesis and Polymerization of Unsaturated Crown Ether Analogs. *Angew. Chem. Int. Ed. Engl. 36*, 1101–1103.

(35) Maynard, H. D.; Grubbs, R. H. (1999) Synthesis of Functionalized Polyethers by Ring-Opening Metathesis Polymerization of Unsaturated Crown Ethers. *Macromolecules 32*, 6917–6924.

(36) Gong, Y.; Leroux, J.-C.; Gauthier, M. A. (2015) Releasable Conjugation of Polymers to Proteins. *Bioconjug. Chem. 26*, 1172–1181.

(37) Dingels, C.; Müller, S. S.; Steinbach, T.; Tonhauser, C.; Frey, H. (2013) Universal Concept for the Implementation of a Single Cleavable Unit at Tunable Position in Functional Poly(Ethylene Glycol)s. *Biomacromolecules 14*, 448–459.

(38) Luo, Y.-L.; Nan, Y.-F.; Xu, F.; Chen, Y.-S.; Zhao, P. (2010) Degradation Behavior and Biocompatibility of PEG/PANI-Derived Polyurethane Co-Polymers. *J. Biomater. Sci. Polym. Ed. 21*, 1143–1172.

(39) Hardwicke, J.; Ferguson, E. L.; Moseley, R.; Stephens, P.; Thomas, D. W.; Duncan, R. (2008) Dextrin–RhEGF Conjugates as Bioresponsive Nanomedicines for Wound Repair. *J. Controlled Release 130*, 275–283.

(40) Decker, C. G.; Maynard, H. D. (2015) Degradable PEGylated Protein Conjugates Utilizing RAFT Polymerization. *Eur. Polym. J. 65*, 305–312.

(41) Trnka, T. M.; Grubbs, R. H. (2001) The Development of L2X2RuCHR Olefin Metathesis Catalysts: An Organometallic Success Story. *Acc. Chem. Res. 34*, 18–29.

(42) Hilf, S.; Kilbinger, A. F. M. (2009) Functional End Groups for Polymers Prepared Using Ring-Opening Metathesis Polymerization. *Nat. Chem. 1*, 537–546.

(43) Carrillo, A.; Gujraty, K. V.; Rai, P. R.; Kane, R. S. (2005) Design of Water-Soluble, Thiol-Reactive Polymers of Controlled Molecular Weight: A Novel Multivalent Scaffold. *Nanotechnology 16*, S416–S421.

(44) Chen, B.; Metera, K.; Sleiman, H. F. (2005) Biotin-Terminated Ruthenium Bipyridine Ring-Opening Metathesis Polymerization Copolymers: Synthesis and Self-Assembly with Streptavidin. *Macromolecules 38*, 1084–1090.

(45) Isarov, S. A.; Pokorski, J. K. (2015) Protein ROMP: Aqueous Graft-from Ring-Opening Metathesis Polymerization. *ACS Macro Lett. 4*, 969–973.

(46) Isarov, S. A.; Lee, P. W.; Pokorski, J. K. (2016) "Graft-to" Protein/Polymer Conjugates Using Polynorbornene Block Copolymers. *Biomacromolecules 17*, 641–648.

(47) Hahn, M. E.; Randolph, L. M.; Adamiak, L.; Thompson, M. P.; Gianneschi, N. C. (2013) Polymerization of a Peptide-Based Enzyme Substrate. *Chem. Commun. 49*, 2873–2875.

(48) Xue, Z.; Mayer, M. F. (2009) Entropy-Driven Ring-Opening Olefin Metathesis Polymerizations of Macrocycles. *Soft Matter 5*, 4600–4611.

(49) Lin, Y. A.; Chalker, J. M.; Floyd, N.; Bernardes, G. J. L.; Davis, B. G. (2008) Allyl Sulfides Are Privileged Substrates in Aqueous Cross-Metathesis: Application to Site-Selective Protein Modification. *J. Am. Chem. Soc. 130*, 9642–9643.

(50) Lowe, A. B. (2010) Thiol-Ene "Click" Reactions and Recent Applications in Polymer and Materials Synthesis. *Polym. Chem. 1*, 17–36.

(51) Sarapas, J. M.; Tew, G. N. (2016) Thiol-Ene Step-Growth as a Versatile Route to Functional Polymers. *Angew. Chem. Int. Ed.* 15860–15863.

(52) Gothard, C. M.; Grzybowski, B. A. (2012) A Cost-Effective, Column-Free Route to Ethylene Glycol Oligomers EG 6, EG 10, and EG 12. *Synthesis 44*, 717–722.

(53) Wawro, A. M.; Muraoka, T.; Kato, M.; Kinbara, K. (2016) Multigram Chromatography-Free Synthesis of Octa(Ethylene Glycol) p-Toluenesulfonate. *Org Chem Front* 1524–1534.

(54) Wawro, A. M.; Muraoka, T.; Kinbara, K. (2016) Chromatography-Free Synthesis of Monodisperse Oligo(Ethylene Glycol) Mono-p-Toluenesulfonates and Quantitative Analysis of Oligomer Purity. *Polym Chem 7*, 2389–2394.

(55) Amblard, M.; Fehrentz, J.-A.; Martinez, J.; Subra, G. (2006) Methods and Protocols of Modern Solid Phase Peptide Synthesis. *Mol. Biotechnol. 33*, 239–254.

(56) Behrendt, R.; White, P.; Offer, J. (2016) Advances in Fmoc Solid-phase Peptide Synthesis. *J. Pept. Sci. 22*, 4–27.

(57) West, C. W.; Estiarte, M. A.; Rich, D. H. (2001) New Methods for Side-Chain Protection of Cysteine. *Org. Lett. 3*, 1205–1208.

(58) Crich, D.; Sana, K. (2009) Solid-Phase Synthesis of Peptidyl Thioacids Employing a 9-Fluorenylmethyl Thioester-Based Linker in Conjunction with Boc Chemistry. *J. Org. Chem. 74*, 7383–7388.

(59) Gokel, G. W.; Korzeniowski, S. *Macrocyclic Polyether Syntheses*; Reactivity and Structure: Concepts in Organic Chemistry; Springer-Verlag: Berlin Heidelberg, 1982.

(60) Inoue, Y.; Liu, Y.; Tong, L.-H.; Ouchi, M.; Hakushi, T. (1993) Complexation Thermodynamics of Crown Ethers. Part 3. 12-Crown-4 to 36-Crown-12: From Rigid to Flexible Ligand. *J. Chem. Soc. Perkin Trans. 2* No. 10, 1947–1950.

(61) Wan, Z.; Li, Y.; Bo, S.; Gao, M.; Wang, X.; Zeng, K.; Tao, X.; Li, X.; Yang, Z.; Jiang, Z.-X. (2016) Amide Bond-Containing Monodisperse Polyethylene Glycols beyond 10 000 Da. *Org. Biomol. Chem. 14*, 7912–7919.

(62) Yu, Z.; Bo, S.; Wang, H.; Li, Y.; Yang, Z.; Huang, Y.; Jiang, Z.-X. (2017) Application of Monodisperse PEGs in Pharmaceutics: Monodisperse Polidocanols. *Mol. Pharm. 14*, 3473–3479.

(63) Deng, T.; Mao, X.; Li, Y.; Bo, S.; Yang, Z.; Jiang, Z.-X. (2018) Monodisperse Oligoethylene Glycols Modified Propofol Prodrugs. *Bioorg. Med. Chem. Lett. 28*, 3502–3505.

(64) Deng, T.; Mao, X.; Xiao, Y.; Yang, Z.; Zheng, X.; Jiang, Z.-X. (2019) Monodisperse Oligoethylene Glycols Modified Camptothecin, 10-Hydroxycamptothecin and SN38 Prodrugs. *Bioorg. Med. Chem. Lett. 29*, 581–584.

(65) Maynard, H. D.; Grubbs, R. H. (1999) Purification Technique for the Removal of Ruthenium from Olefin Metathesis Reaction Products. *Tetrahedron Lett. 40*, 4137–4140.